

**Please cite the Published Version**

Owda, Amani Yousef (2018) Medical applications of microwave and millimetre-wave Imaging. Doctoral thesis (PhD), Manchester Metropolitan University.

Downloaded from: <https://e-space.mmu.ac.uk/622096/>

Usage rights:  Creative Commons: Attribution-Noncommercial-No Derivative Works 4.0

**Enquiries:**

If you have questions about this document, contact [openresearch@mmu.ac.uk](mailto:openresearch@mmu.ac.uk). Please include the URL of the record in e-space. If you believe that your, or a third party's rights have been compromised through this document please see our Take Down policy (available from <https://www.mmu.ac.uk/library/using-the-library/policies-and-guidelines>)

**Medical Applications of Microwave and Millimetre-Wave  
Imaging**

**Amani Yousef Owda**

A thesis submitted in partial fulfilment of the requirements of the Manchester Metropolitan University for the degree of Doctor of Philosophy.

School of Engineering

Department of Electrical and Electronic Engineering

Manchester Metropolitan University

November 2018

## **Abstract**

This thesis presents a feasibility study of using microwave and millimetre wave radiations to assess burn wounds and the potential for monitoring the healing process under dressing materials, without their removal. As interaction of these types of radiations with the human body is almost exclusively with the skin, there is potential in others areas of medicine such as early skin cancer detection and the diagnosis of skin conditions such as eczema and psoriasis. This study involves developments of experimental methodologies, electromagnetic modelling, and measurements conducted on human skin (in vivo from 150 healthy participants), porcine skin samples (ex vivo from 20 fresh samples), and dressing materials (20 samples). Radiometric measurements obtained from the human skin over the frequency band (80-100) GHz show that the emissivity of the skin varies consistently over different regions of the hand and forearm, with gender, ethnicity, body mass index, age, and hydration level of the skin. A half space electromagnetic model of human skin has been developed and simulations using this model indicate that the human skin can be modelled as a single layer over the band 30 GHz to 300 GHz. The model also indicates that the band could be used to detect burns and a range of medical conditions associated with the skin. Experimental data collected from samples (human and porcine) have been measured by passive and active imaging systems and the results analysed in terms of the emissivity and the reflectivity of the skin. The major outcomes of the thesis are that microwave and millimetre wave radiations are capable of discriminating burn-damaged skin from healthy tissue and these measurements can be made through bandages without the sensor making any physical contact with the skin or the bandage.

## **Acknowledgements**

*“Every moment, thank God.”*

I would like to offer my special thanks to my Director of Studies Dr. Neil Salmon for his help, support, guidance, encouragement, discussion, and patience throughout my PhD studentship. Without his help, I would never be where I am now. I also would like to thank my second supervisor Dr. Nacer-Ddine Rezgui for his help and technical guidance. As members of my supervision team, I would like to thank Professor Nicholas Bowring, Professor Stuart Harmer, and Dr. Mamta Shah for providing the funding and making my PhD possible.

In addition, special thanks for our research collaborator Professor Sergiy Shylo from the Usikov Institute of Radiophysics and Electronics at the National Academy of Sciences of Ukraine, in kharkiv, for his dedication, help, and discussion throughout my PhD studentship.

Moreover, I would like to offer big thanks to Dr. Keeley Crockett for her help in reading my PhD thesis and providing me with valuable comments.

I am also grateful for the School of Engineering at Manchester Metropolitan University for their financial support, especially to the Head of Electrical and Electronic Engineering Division Mrs. Margaret Fowler.

Finally and importantly, I would like to thank my husband (Dr. Majdi Owda), my little son (Ibrahim Owda), and my little daughter (Lara Owda) for their patience and support throughout my PhD. Thanks also goes to my great family members, especially my father (Mr. Yousef Abubaha), my mother (Mrs. Naima Abubaha), my sisters, and my brothers. I love you all.

# Table of Contents

<b>Abstract</b> .....	<b>I</b>
<b>Acknowledgements</b> .....	<b>II</b>
<b>List of Figures</b> .....	<b>XIV</b>
<b>List of Tables</b> .....	<b>XXVI</b>
<b>List of Abbreviations</b> .....	<b>XXVIII</b>
<b>Chapter 1</b> .....	<b>1</b>
<b>Introduction</b> .....	<b>1</b>
1.1 Overview .....	1
1.2 Thesis Aim and Objectives.....	4
1.3 Contributions to Knowledge .....	5
1.4 List of Publications and Awards .....	8
1.5 Thesis Structure .....	10
<b>Chapter 2</b> .....	<b>13</b>
<b>Literature Review and Medical Background</b> .....	<b>13</b>
2.1 Electromagnetic Spectrum.....	14
2.2 History of the Millimetre Wave Radiation.....	15
2.3 Key Features of the Millimetre Wave Radiation.....	16
2.4 Interaction of Millimetre Wave Radiation with the Human Body.....	17
2.5 Exposure Limits for Millimetre Wave Radiation.....	20
2.6 Dielectric Properties of the Human Skin.....	22

2.7 Methods for Measuring the Relative Complex Permittivity .....	23
2.8 Relative Complex Permittivity Theoretical Models.....	25
2.9 Dielectric Properties of the Human Skin in the MMW Band .....	28
2.10 Review of Dielectric Properties in Medical Applications.....	30
2.10.1 Dielectric Properties of Healthy Skin and Skin with Basal Cell Carcinoma .....	30
2.10.2 Dielectric Properties of Healthy Skin and Skin with Burns .....	31
2.10.3 Relative Complex Permittivity for Skin with Differing Water Contents	32
2.10.4 Relative Complex Permittivity of Dry and Wet Skin.....	33
2.11 Thermal Emission and Blackbody Radiation.....	34
2.12 Reflection and Refraction Index.....	37
2.13 Human Skin Structure .....	39
2.14 Functions of the Human Skin.....	40
2.15 Skin Conditions and Diseases .....	41
2.15.1 Psoriasis .....	41
2.15.2 Eczema.....	42
2.15.3 Melanoma .....	43
2.15.4 Basal Cell Carcinoma .....	44
2.15.5 Burn Wound.....	45
2.16 Technologies for Assessing Burn Wound and Skin Cancer.....	47
2.16.1 Terahertz Imaging.....	47
2.16.2 Optical Coherence Tomography.....	49

2.16.3 Ultrasound Imaging .....	50
2.16.4 Infrared Imaging .....	51
2.16.5 Microwave and Millimetre Wave Imaging.....	52
2.17 Conclusions .....	54
<b>Chapter 3 .....</b>	<b>56</b>
<b>The Half Space Electromagnetic Model.....</b>	<b>56</b>
3.1 Background .....	56
3.2 The Half Space Electromagnetic Model.....	58
3.3 Simulation Results from the Half Space Model.....	61
3.3.1 Skin with Differing Water Contents (Psoriasis, Normal Healthy Skin, and Malignancy).....	62
3.3.2 Skin Mutated with Basal Cell Carcinoma .....	64
3.3.3 Dry and Wet Human Skin Samples over the Band (90 -100) GHz.....	65
3.3.4 Skin after the Application of Aqueous Gel (30-100) GHz.....	67
3.3.5 Burned and Unburned Porcine Skin Samples (30-40) GHz .....	68
3.4 Model Comparison: Half Space versus Three-Layer Model.....	70
3.5 Comparison of Skin Emissivity with Another Study .....	71
3.6 Discussion .....	73
3.7 Conclusions .....	75
<b>Chapter 4 .....</b>	<b>76</b>
<b>In Vivo Measurements for the Human Skin Emissivity .....</b>	<b>76</b>
4.1 Millimetre Wave Radiometry.....	76

4.2 Radiometric Calibration .....	79
4.3 Antenna Parameters.....	82
4.4 Experiment 1: Radiometric Measurements at 95 GHz.....	84
4.4.1 Participants and Ethical Approval .....	84
4.4.2 Selection of Frequency .....	85
4.4.3 Experimental Method for Measuring the Human Skin Emissivity .....	86
4.4.4 Experimental Setup for Measuring the Human Skin Emissivity.....	88
4.4.5 Experimental Results .....	92
4.4.5.1 Experimental Results from the Whole Sample .....	92
4.4.5.2 Experimental Results from Female Measurements.....	93
4.4.5.3 Experimental Results from Male Measurements .....	95
4.4.6 Discussion.....	97
4.5 Experiment 2: Radiometric Measurements (80-100) GHz.....	99
4.5.1 The First Group of Healthy Participants.....	100
4.5.2 Selection of the Millimetre Wave Band .....	100
4.5.3 Choice of Measurement Locations .....	101
4.5.4 Experimental Setup.....	102
4.5.5 Calibration and Initial Measurements.....	104
4.5.6 Methodology for Measuring the Human Skin Emissivity.....	106
4.5.7 Methodology of Data Processing.....	108
4.5.8 First Group of Healthy Participants Experimental Results.....	109

4.5.8.1 Female Emissivity Measurements.....	109
4.5.8.2 Male Emissivity Measurements .....	114
4.5.8.3 Comparison in Emissivity between Male and Female Participants ..	117
4.5.8.4 Skin Emissivity for Participants Having Normal and High Body Mass Index.....	118
4.5.8.5 Skin Emissivity for Participants Having Asian and European Ethnicities .....	122
4.5.8.6 Emissivity of Male and Female Skin in Dry and Wet State .....	126
4.5.9 Second Group of Healthy Participants Experimental Results .....	130
4.5.9.1 Male Emissivity Measurements for Different Age Groups .....	130
4.5.9.2 Female Emissivity Measurements for Different Age Groups.....	133
4.5.10 Discussion.....	135
4.6 Conclusions .....	139
4.7 Possible New Applications Highlighted by this Research .....	140
4.7.1 Radiometry in Medical Applications.....	140
4.7.2 Skin Signature in Security Screening .....	141
<b>Chapter 5 .....</b>	<b>143</b>
<b>Passive Millimetre Wave Sensing Through Dressing Materials Using Porcine Skin Samples.....</b>	<b>143</b>
5.1 Introduction .....	143
5.2 Selection of Porcine Skin and Ethical Approval .....	146
5.3 Three Layer Model for Dressed Burn Wound.....	147

5.4 Experimental Work .....	149
5.4.1 Experimental Description for Calibration and Dressing Materials .....	150
5.4.2 Experimental Setup for Porcine Skin Measurements .....	152
5.5 Methodologies Applied on Porcine Skin Samples .....	156
5.5.1 Methodology 1: Skin without Burns.....	156
5.5.2 Methodology 2: Skin without Burns and with Dressing Materials .....	156
5.5.3 Methodology 3: Skin after the Application of Water and Cream.....	157
5.5.4 Methodology 4: Skin with Burns.....	157
5.5.5 Methodology 5: Skin with Different Burn Depth.....	158
5.6 Experimental Results.....	158
5.6.1 Dressing Materials Measurements.....	159
5.6.2 Porcine Skin Measurements .....	161
5.6.2.1 Experiment 1: Porcine Skin Measurements without Burns .....	161
5.6.2.2 Experiment 2: Porcine Skin Measurements with Burns .....	165
5.7 Discussion .....	173
5.8 Conclusions .....	176
<b>Chapter 6 .....</b>	<b>177</b>
<b>Active Millimetre Wave Radar for Sensing and Imaging Through Dressing Materials .....</b>	<b>177</b>
6.1 Technical Background for Radar.....	177
6.1.1 Principle of Operation of a Monostatic Pulsed Radar System.....	180
6.1.2 Radar Range Equation .....	181

6.1.3 Radar Clutter.....	183
6.1.4 Radar Resolution .....	184
6.1.4.1 Range Resolution .....	184
6.1.4.2 Spatial Angular Resolution .....	185
6.1.5 Scattering Parameters and Vector Network Analyser .....	185
6.1.6 Fourier Transform.....	188
6.1.7 Radar Range.....	189
6.2 Experiment 1: Sensing and Imaging Through Dressing Materials .....	190
6.2.1 Selection of the Frequency Band 15-40 GHz .....	190
6.2.2 Experimental Description .....	191
6.2.3 Methodology of Data Processing.....	193
6.2.4 Experimental Results .....	195
6.2.4.1 Radar Spatial Resolution Measurements .....	195
6.2.4.2 Calibration Measurements .....	197
6.2.4.3 Propagation Path Length Measurements for Rigid Samples.....	199
6.2.4.4 Measurements Applied on Dressing Materials .....	203
6.2.4.4.1 Gauze Burn Dressing Materials in Dry State .....	203
6.2.4.4.2 Gauze Burn Dressing Materials with Sudocrem .....	204
6.2.4.4.3 Gauze Burn Dressing Materials with Flamazine Cream .....	206
6.2.4.4.4 Gauze Burn Dressing Materials with Water.....	207
6.2.4.4.5 Light Support Bandage with Savlon Cream.....	208

6.2.4.4.6 Light Support Bandage with Sudocrem .....	209
6.2.4.4.7 Hand Support Cast Sample.....	210
6.2.5 Data Validation .....	212
6.3 Experiment 2: Attenuation in Different Types of Cream.....	215
6.3.1 Selection of Creams .....	215
6.3.2 Experimental Description .....	215
6.3.3 Methodology of Data Processing.....	218
6.3.4 Experiment 2: Experimental Results .....	219
6.4 Discussion .....	222
6.5 Conclusions .....	224
<b>Chapter 7 .....</b>	<b>226</b>
<b>Passive and Active Millimetre Wave Scanners for Burn Wound Diagnostics .</b>	<b>226</b>
7.1 Introduction .....	226
7.2 Imaging Radiometer .....	227
7.2.1 Lenses and Mirrors .....	227
7.2.2 Depth of Field and the Field of View .....	228
7.2.3 Near Field and Far Field Regions .....	230
7.2.4 Diffraction Limits and Resolution .....	231
7.3 Synthetic Aperture Radar .....	233
7.3.1 Active Imaging Reconstruction Criteria .....	234
7.3.2 Cross Range Resolution.....	235

7.3.3 Clutter and Speckle in Radar Imaging.....	237
7.4 Experiment 1: In Vivo Passive Sensing and Imaging Using the ThruVision 250 GHz Imager .....	240
7.4.1 Frequency Band (232-268) GHz .....	240
7.4.2 Participants .....	240
7.4.3 Experimental Setup and Description .....	241
7.4.4 Methodology of Conducting the Experimental Work .....	242
7.4.4.1 Methodology 1: Normal Skin.....	242
7.4.4.2 Methodology 2: Wet Skin .....	242
7.4.4.3 Methodology 3: Skin with Cream.....	243
7.4.5 Data Processing.....	243
7.4.6 Experimental Results .....	244
7.4.6.1 Initial Measurements.....	244
7.4.6.2 Images for the Human Skin at Different States .....	245
7.4.6.2.1 Normal Skin and Wet Skin.....	245
7.4.6.2.2 Normal Skin and Skin with Creams .....	248
7.4.6.2.3 Passive Imaging for Detecting Missing Parts.....	252
7.5 Experiment 2: Burn Detection Using the ThruVision 250 GHz Imager .....	253
7.5.1 Porcine Skin Samples .....	253
7.5.2 Methodologies Applied on Porcine Skin Samples .....	253
7.5.2.1 Methodology 1: Skin without Burns .....	253
7.5.2.2 Methodology 2: Skin with Burns .....	254

7.5.3 Data Processing .....	255
7.5.4 Porcine Skin Measurements .....	255
7.5.4.1 Skin without Burns.....	255
7.5.4.2 Skin with Single and Multiple Burns .....	257
7.5.4.3 Skin with Burns and Dressing Materials.....	259
7.6 Experiment 3: Burn Wound Diagnostics Using Active Microwave Scanner	261
7.6.1 Frequency Band (15-40) GHz .....	261
7.6.2 Porcine Skin Samples .....	261
7.6.3 Experimental Setup.....	262
7.6.4 Methodology of Conducting the Measurements.....	263
7.6.5 Data Processing .....	264
7.6.6 Experimental Results .....	265
7.6.6.1 Skin without Burns.....	265
7.6.6.2 Skin with Dressing Materials .....	267
7.6.6.3 Skin with Burns.....	269
7.6.6.4 Skin with Burns and Dressing Materials.....	271
7.7 Discussion .....	274
7.8 Conclusions .....	278
<b>Chapter 8 .....</b>	<b>279</b>
<b>Conclusions and Future Work.....</b>	<b>279</b>
8.1 Thesis Summary and Conclusions .....	279

8.2 Future Work .....	285
<b>References .....</b>	<b>287</b>
<b>Appendix A: Ethical Approval for Human Skin Emissivity Measurements....</b>	<b>307</b>
<b>Appendix B: Ethical Approval for Porcine Skin Measurements .....</b>	<b>316</b>
<b>Appendix C: Publications and Best Student Award Certificate.....</b>	<b>320</b>
<b>Appendix D: Matlab Codes .....</b>	<b>384</b>

## List of Figures

Figure 1.1: Visual inspection for assessing bandage wound (burn wound) [2].	1
Figure 1.2: A block diagram shows the detailed structure of the thesis.	10
Figure 2.1: Electromagnetic spectrum frequency ranges, wavelengths, and penetrations [6].	14
Figure 2.2: Penetration depth of the millimetre wave radiation in the human skin as a function of frequency using different skin models [28].	18
Figure 2.3: The inverse relationship between the time limits of continues exposure and the frequency as determined by IEEE, ICNIRP and CENELEC organisations.	21
Figure 2.4: Radiation intensity of the blackbody versus the wavelength at different absolute temperatures [66].	35
Figure 2.5: Reflection and refraction in mediums having different dielectric properties.	37
Figure 2.6: Schematic for human skin structure and its' derivatives (sweat glands, oil glands, nails, hair, and hair follicles) [74]. Radiation in the lower frequency portion of the millimetre wave band penetrates down into the dermis layer of the skin.	39
Figure 2.7: Illustration of chronic plaque psoriasis from less to more severe [78].	41
Figure 2.8: A schematic illustrates eczema and different signs appeared on the affected part of the human skin [77].	42
Figure 2.9: Illustration of different types of melanoma; a) a spreading melanoma and b) an amelanotic melanoma [79].	43
Figure 2.10: Illustration of shapes, sizes and colours of basal cell carcinoma [77].	44
Figure 2.11: Illustration of different depth of invasion for burn injury [80, 81].	45
Figure 3.1: The half space model for calculating the emissivity of the skin.	58

Figure 3.2: Simulations of the emissivity of the skin having different water contents. .....	62
Figure 3.3: Simulations of the emissivity of healthy skin and skin with BCC.....	64
Figure 3.4: Simulations of the emissivity of samples of dry and wet human skin. ...	66
Figure 3.5: The simulated emissivity of healthy skin before and after it has been moistened by the application of an aqueous gel.....	67
Figure 3.6: Emissivity of unburned and burn damaged porcine skin samples.....	69
Figure 3.7: Comparison between the half space and the three-layer models.....	70
Figure 4.1: A block diagram shows the basic components of a single channel radiometer. ....	77
Figure. 4.2: General schematic for a radiometer collecting uniform thermal emissions from a blackbody (foam absorber). The horn antenna collects the emission and generates a fluctuating voltage, and the receiver amplifies and detects the emission. .....	79
Figure 4.3: Schematic for the Y- factor method with hot and cold calibration loads [140].....	81
Figure. 4.4: In the experimental setup radiometric emission at 95 GHz is collected by a moveable horn antenna (3) at positions: A to measure a hot calibration source (1), B to measure the skin (5) and C to measure the cold calibration source (2), a thermocouple (4) is used to measure the thermodynamic temperature of the skin, a digital voltmeter (8) is used to measure the output voltage of the calibration sources and the skin. The horn antenna connected through a waveguide circulator (6) to a radiometer (7) that consists of a low noise amplifier and detector. ....	88
Figure 4.5: Mean emissivity values for a sample of 12 female participants.....	94
Figure 4.6: Mean emissivity values for a sample of 18 male participants.....	96

Figure 4.7: Locations on the arm where the emissivity of the skin is measured. ....	101
Figure 4.8: The main elements of the experimental work: A horn antenna connected to MMIC detector (consisting of a two-stage low noise amplifier; zero bias diode detector and buffer amplifier). A wall of carbon loaded absorbing foam surrounds the majority of the system. ....	102
Figure 4.9: Illustrations of the experimental setup inside the walls (blue-grey) of the anechoic chamber, showing the hot (a) and the cold (b) calibration procedures and the measurement of the skin (c). ....	107
Figure 4.10: A methodology of data processing applied in experiment 2. ....	108
Figure 4.11: Mean emissivity for the palm of the hand and the back of the hand skin for a sample of 24 female participants. The participants' ages are as follows: 1) 22, 2) 23, 3) 23, 4) 24, 5) 24, 6) 24, 7) 25, 8) 26, 9) 27, 10) 29, 11) 29, 12) 30, 13) 31, 14) 32, 15) 32, 16) 33, 17) 33, 18) 35, 19) 36, 20) 42, 21) 44, 22) 45, 23) 45, 24) 54. .	111
Figure 4.12: Mean emissivity for the outer and the inner wrist skin for a sample of 24 female participants. The participants' ages are identified in Figure 4.11. ....	112
Figure 4.13: Mean emissivity for the dorsal surface and the volar side skin for a sample of 24 female participants. The participants' ages are identified in Figure 4.11. ....	113
Figure 4.14. Mean emissivity for the palm of the hand and the back of hand skin for a sample of 36 male participants. The participants' ages are as follows: 1) 20, 2) 20, 3) 21, 4) 22, 5) 22, 6) 22, 7) 23, 8) 23, 9) 23, 10) 24, 11) 24, 12) 25, 13) 26, 14) 26, 15) 26, 16) 26, 17) 27, 18) 28, 19) 29, 20) 29, 21) 30, 22) 31, 23) 31, 24) 32, 25) 34, 26) 35, 27) 37, 28) 37, 29) 40, 30) 40, 31) 42, 32) 42, 33) 45, 34) 52, 35) 58 , 36) 67. .	115
Figure 4.15: Mean emissivity for the outer wrist and the inner wrist skin for a sample of 36 male participants. The participants' ages are identified in Figure 4.14. ....	116

Figure 4.16: Mean emissivity for the dorsal surface and the volar side skin for a sample of 36 male participants. The participants' ages are identified in Figure 4.14.....	116
Figure 4.17: Mean emissivity for a sample of 10 male participants having normal and high body mass index on: 1) the palm of the hand, 2) the back of the hand, 3) the inner wrist, 4) the outer wrist, 5) the volar side, and 6) the dorsal surface of the forearm. .....	118
Figure 4.18: Mean emissivity for a sample of 10 female participants having normal and high body mass index at six locations identified in Figure 4.17. ....	120
Figure 4.19: Mean emissivity of 24 male participants having Asian and European ethnicities at six measurement locations identified in Figure 4.17. ....	122
Figure 4.20: Mean emissivity of 24 female participants having Asian and European ethnicities at six measurement locations identified in Figure 4.17. ....	124
Figure 4.21: Mean emissivity for a sample of 10 male participants before and after the application of water. ....	127
Figure 4.22: Mean emissivity for a sample of 6 female participants before and after the application of water. ....	129
Figure 4.23: Mean emissivity values for the dorsal surface and the volar side skin for a sample of 35 male participants. ....	131
Figure 4.24: Mean emissivity values for the outer wrist and the inner wrist skin for a sample of 35 male participants. ....	132
Figure 4.25: Mean emissivity values for the dorsal surface and the volar side skin for a sample of 25 female participants. ....	133
Figure 4.26: Mean emissivity values for the outer wrist and the inner wrist skin for a sample of 25 female participants. ....	134

Figure 5.1: Three-layer model for dressed burn wound comprising of: a semi-infinite layer of air, finite thickness layer of dressing materials, and a semi-infinite layer of burn-damaged skin.....	147
Figure 5.2: Radiometric emission centred at 90 GHz is collected by a moveable horn antenna at positions: A to measure a hot calibration source (1) (carbon loaded foam absorber; type: Eccosorb AN-73) stabilized at a temperature $\sim 54$ °C using a digital hotplate (3) placed in a polystyrene foam bucket (4), B to measure the cold calibration source (2) (carbon loaded foam absorber; type: Eccosorb AN-73) in thermodynamic equilibrium with air temperature $\sim 20$ °C, and C to measure the emission from dressing materials samples (5).....	150
Figure 5.3: The experimental setup for the emissivity measurements of the porcine skin samples. A digital voltmeter is used to measure the output voltage level of the samples and a thermocouple and an infrared thermometer are used to measure the thermodynamic temperature of the samples. ....	152
Figure 5.4: A wall of carbon loaded absorbing foam (length 1200 mm x width 2400 mm) surrounded the instrumentation. ....	153
Figure 5.5: Samples of porcine skin used in the experimental work of this research. ....	154
Figure 5.6: A digital hotplate used for heating and stabilising the surface temperature of the porcine skin samples (a) and a heat control device with (50 mm x 50 mm) metal plate used for performing burns on the porcine skin samples (b).....	155
Figure 5.7: Mean emissivity values and standard deviation bars for porcine skin samples A, B, C, and D was taken from the back region of the same animal. ....	162
Figure 5.8: Mean emissivity values and standard deviation bars for porcine skin without and with dressing materials. The samples A, B, C, and D represent skin	

without dressing materials, A1, B1, C1, and D1 represent skin with 4-layer gauze burn bandage, and A2, B2, C2, and D2 represent skin with a light support bandage..... 163

Figure 5.9: Mean emissivity values and standard deviation bars for porcine skin samples before and after the application of water and cream. Samples A, B, C, and D represent normal skin, A3: represents skin with Sudocrem, B3: represents skin with Flamazine cream, C3: represents skin with Savlon cream, and D3: represents skin with water..... 164

Figure 5.10: Mean emissivity values and standard deviation bars for porcine skin samples (obtained from the same animal) before and after the application of localised heat treatment. Samples X, Y, Z, and W represent normal skin. X1 represents skin with burns after 10 seconds of heat treatment, Y1 represent skin with burns after 60 seconds of heat treatment. Z1 represents skin with burns after 120 seconds of heat treatment, and W1 represents skin with burns after 180 seconds of heat treatment. X2, Y2, Z2, and W2 represent skin with burns and dressing (6-layer gauze burn dressing). X3, Y3, Z3, and W3 represent skin with burns and 1-layer light support bandage. 166

Figure 5.11: Mean emissivity values and standard deviation bars for porcine skin samples (obtained from different animals) before and after different applications of localised heat treatments. Samples a, b, c, and d represent normal skin; a1, b1, c1 and d1 represent skin with burns after 10 seconds of heat treatment (first degree burn); a2, b2, c2, and d2 represent skin with burns after 60 seconds of extra heat treatment (second degree burn); a3, b3, c3, and d3 represent skin with burns after 120 seconds of extra heat treatment (third degree burn). ..... 168

Figure 5.12: Mean emissivity values and standard deviation bars for porcine skin sample before and after different applications of localised heat treatments. Sample L represents the normal skin; L1 represents skin with burns and exudates after 10

seconds of heat treatment, L2 represents skin with burns and without exudates after 60 seconds of extra heat treatment, L3 represents skin with burns and without exudates after 120 seconds of extra heat treatment.....	170
Figure 5.13: Mean emissivity values and standard deviation bars for porcine skin samples before and after different applications of localised heat treatments. Samples m and f represent normal skin; m1 and f1 represent skin with burns after 10 seconds of localised heat treatment, m2 and f2 represent skin with burns after 60 seconds of extra heat treatment, m3 and f3 represent skin with burns after 120 seconds of extra application of heat treatment, and m4 and f4 represent skin with burns after 60 seconds of extra application of heat treatment.....	171
Figure 6.1: A block diagram shows the basic elements of the monostatic radar system [205].	179
Figure 6.2: Synchronisation between the transmitter and the receiver of the monostatic radar system [219].	180
Figure 6.3: Scattering parameters as function of incident and reflected voltage of the two ports network.....	185
Figure 6.4: Two ports vector network analyser device used for measuring the magnitude and the phase of the scattering parameters.....	187
Figure 6.5: Representations of impulse function in both time and frequency domains. .....	188
Figure 6.6: Illustration of the experimental apparatus used to make measurements of the propagation path length and the attenuation of the dressing materials using radar. .....	191
Figure 6.7: A block diagram summarises the methodology of data processing. ....	194

Figure 6.8: The minimum resolvable distance between the two metal plates is ~8.0 mm (a) a further decreases in this distance results in a combination of the two peaks into a single peak (b). .....	196
Figure 6.9: The reflected signal from a flat metal plate background (length=1200 mm, and width= 660 mm). .....	197
Figure 6.10: The reflected signal from a wall of foam absorber background. ....	198
Figure 6.11: The reflected signal from a 50.0 mm thick polyethylene cylinder located in free space between the horn antenna and the metal plate background. ....	200
Figure 6.12: The reflected signal from a 10.0 mm thick polyethylene flat plate located in free space between the horn antenna and the metal plate background. ....	201
Figure 6.13: The reflected signal from an 80.0 mm thick wax candle located in free space between the horn antenna and the metal plate background. ....	202
Figure 6.14: The reflected signal from a 10.0 mm thick bandage located in free space between the horn antenna and the metal plate. The solid red line shows the signal from the bandage and the metal plate and the broken blue line when the metal plate only is present. ....	203
Figure 6.15: The reflected signal from a ~25.0 mm thick bandage with Sudocrem. The bandage was attached directly to the metal plate. ....	205
Figure 6.16: The reflected signal from a ~10.0 mm thick bandage coated with Flamazine cream. The bandage was attached directly to the metal plate. ....	206
Figure 6.17: The reflected signal from a ~10.0 mm thick wet bandage. The bandage was attached directly to the metal plate. ....	207
Figure 6.18: The reflected signal from a ~25.0 mm thick light support bandage with Savlon cream. The bandage was attached directly to the metal plate. ....	208

Figure 6.19: The reflected signal from a ~40.0 mm thick light support bandage with Sudocrem. The bandage was attached directly to the metal plate.....	209
Figure 6.20: The reflected signal from a 90.0 mm wide hand cast located in free space between the horn antenna and the metal plate background.....	210
Figure 6.21: A methodology of data processing applied on different types of cream. ....	218
Figure 6.22: The attenuation in the MMW radiation caused by Flamazine cream. .	219
Figure 6.23: The attenuation in the MMW radiation caused by Savlon cream. ....	220
Figure 6.24: The attenuation in the MMW radiation caused by Sudocrem. ....	220
Figure 7.1: Illustration of the field of view and the angle of view for an imaging system [229]......	229
Figure 7.2: Illustration of the near and the far field regions of the EM radiation [230]. ....	230
Figure 7.3: Different resolution limits identified by Rayleigh, Abbe, and Sparrow. The resolution limit can also be defined as a full width at half maximum (FWHM) or a $1/e^2$ width [234]......	231
Figure 7.4: illustration of cross range resolutions in x, y, and z directions in polar coordination [238]......	235
Figure 7.5: Different sources of clutter and anomalies in radar imaging system [241]. ....	237
Figure 7.6: A ThruVision 250 GHz passive imager comprises a TS4 unit, a CCTV camera, a thermal imaging window, and a laptop with a ThruViewer software. ....	241
Figure 7.7: Measurements for the depth of the field of the imager using a cup of hot water ~70 °C; a) represents an image in the depth of field region, and b) represents an image out the depth of the field region. ....	245

Figure 7.8: MMW images for the palm of the hand skin in normal and wet state for a female participant at 250 GHz; a) represents normal skin without dressing materials, b) represents normal skin with dressing materials, c) represents wet skin without dressing materials, and d) represents wet skin with dressing materials. ....246

Figure 7.9: MMW images for the palm of the hand skin of a female participant at 250 GHz; a) represents normal skin without dressing materials, b) represents normal skin with dressing materials, c) represents skin with Savlon cream, and d) represents skin with both Savlon cream and dressing materials. ....249

Figure 7.10: MMW images for the palm of hand skin for the female participant at 250 GHz; a) represents normal skin without dressing materials, b) represents normal skin with dressing materials, c) represents skin with Sudocrem, and d) represents skin with both Sudocrem and dressing materials. ....251

Figure 7.11: MMW images from the palm of the hand skin for a male participant; a) represents the hand without dressing materials, and b) represents the hand with a light support bandage. ....252

Figure 7.12: MMW images for porcine skin sample at 250 GHz; a) represents the skin without dressings, b) represents the skin with one layer light support bandage, c) represents the skin with 10-layers white gauze burn bandage, and d) represents the skin with 4-layers blue gauze burn bandage. ....256

Figure 7.13: MMW images for porcine skin samples at 250 GHz; a) represents the skin with one burn, b) represents the skin with two burns, c) represents the skin with three burns, and d) represents the skin with four burns. ....258

Figure 7.14: MMW images for porcine skin samples at 250 GHz; images in (a) and (c) represent the skin with burns and without dressing materials. Whereas, images in

(b) and (d) represent the skin with burns and 10-layer gauze burn dressing materials. .....	260
Figure 7.15: The front view of the active microwave scanner (a) and the bottom view of the scanner (b). The scanner has 6.0 mm theoretical range resolution, 25.0 GHz bandwidth, and 256 frequency steps. ....	262
Figure 7.16: A methodology applied to obtain an image from the active scanner [244]. .....	264
Figure 7.17: Microwave images for unburned skin over the band 15-40 GHz; case (a) represents SAR microwave image 32 x 30 pixels for unburned skin obtained from the amplitude of $S_{11}$ , (b) represents the sample photo, (c) represents SAR microwave image with interpolation 249 x 233 pixels obtained from the amplitude of $S_{11}$ , and (d) represents SAR microwave image with interpolation 249 x 233 pixels obtained from the phase of $S_{11}$ .....	266
Figure 7.18: Microwave images for the skin with dressing materials over the band 15- 40 GHz; case (a) represents SAR microwave image 32 x 30 pixels for the skin with dressings obtained from the amplitude of $S_{11}$ , (b) represents SAR microwave image with interpolation 249 x 233 pixels obtained from the amplitude of $S_{11}$ , (c) represents SAR microwave image with interpolation 249 x 233 pixels obtained from the phase of $S_{11}$ , and (d) represents the skin photo. ....	268
Figure 7.19: Microwave images for burn-damaged skin over the band 15-40 GHz; case (a) represents SAR microwave image 32 x 30 pixels for the skin with burns obtained from the amplitude of $S_{11}$ , (b) represents the skin with burns photo, (c) represents SAR microwave image with interpolation 249 x 233 pixels for the skin with burns obtained from the amplitude of $S_{11}$ , and (d) represents SAR microwave image	

with interpolation 249 x 233 pixels for the skin with burns obtained from the phase of  $S_{11}$ .....270

Figure 7.20: Microwave images for the skin with burns and dressing materials over the band 15-40 GHz; case (a) represents SAR microwave image 32 x 30 pixels for the skin with burns and dressings obtained from the amplitude of  $S_{11}$ , (b) represents SAR microwave image with interpolation 249 x 233 pixels obtained from the amplitude of  $S_{11}$ , (c) represents SAR microwave image with interpolation 249 x 233 pixels obtained from the phase of  $S_{11}$ , and (d) represents the skin with burns photo. ....272

## List of Tables

Table 2.1: Exposure limits for protecting the human body from active millimetre wave radiations [36, 37, 38].	20
Table 2.2: The relative complex permittivities measurements of the human skin.	28
Table 2.3: Predicted relative complex permittivity of the human skin (30-100) GHz.	29
Table 2.4: Effect of changing the water content on the dielectric properties of the human skin [42].	31
Table 2.5: The relative complex permittivity of the skin with different water content.	32
Table 2.6: An overview of the main characteristics and features of the burn wound.	46
Table 3.1: Characteristics and parameters of the skin with differing water contents.	63
Table 3.2: The simulated and the calculated emissivity of the palm of the hand skin.	72
Table 4.1: Statistical analysis of the data for a sample of 30 healthy participants.	92
Table 4.2: Statistical analysis of the data for a sample of 12 female participants.	95
Table 4.3: Statistical analysis of the data for a sample of 18 male participants.	96
Table 4.4: Statistical analysis of the data for a sample of 24 female participants.	110
Table 4.5: Statistical analysis of the data for a sample of 36 male participants.	114
Table 4.6: Statistical analysis of the data for male and female participants.	117
Table 4.7: The standard deviation for a sample of 10 male participants having normal and high body mass index.	119
Table 4.8: Standard deviation for a sample of 10 female participants having normal and high BMI.	121

Table 4.9: Standard deviation for Asian and European males at six locations. ....	123
Table 4.10: Standard deviation for Asian and European females at six locations. ...	125
Table 4.11: Statistical analysis of the dry and the wet skin for a sample of 10 males. .....	128
Table 4.12: Statistical analysis of the dry and the wet skin for a sample of 6 females. .....	128
Table 4.13: An overview of the statistical analysis of the human skin emissivity. .	138
Table 5.1: Measurements conducted on various types of dressing materials used in the treatment of burn wound. ....	160
Table 5.2: Mean emissivity values for porcine skin samples before and after different applications of localised heat treatments.....	169
Table 6.1: Summary of the measured samples dielectric properties and dimensions. .....	199
Table 6.2: Propagation path length measurements obtained from experiment 1.....	212
Table 6.3: Propagation path length measurements obtained from experiment 2.....	212
Table 6.4: Propagation path length measurements obtained from experiment 3.....	213
Table 7.1: Key features and properties of passive and active MMW imaging systems. .....	277
Table 8.1: An overview of the thesis objectives that have been achieved. ....	284

## List of Abbreviations

<b>MMW</b>	Millimetre Wave
<b>PMMW</b>	Passive Millimetre Wave
<b>EM</b>	Electromagnetics
<b>IEEE</b>	The Institute of Electrical and Electronics Engineers
<b>ICNIRP</b>	The International Commission on Non-ionising Radiation Protection
<b>CENELEC</b>	The European Committee for Electrotechnical Standardization
<b>BCC</b>	Basal Cell Carcinoma
<b>UV</b>	Ultraviolet
<b>THz</b>	Terahertz
<b>TPI</b>	Terahertz Pulse Imaging
<b>SC</b>	Stratum Corneum
<b>THz-TDS</b>	Terahertz Time-Domain Spectroscopy
<b>MRI</b>	Magnetic Resonance Imaging
<b>TWC</b>	Tissue Water Content
<b>OCT</b>	Optical Coherence Tomography
<b>PS-OCT</b>	Polarisation Sensitive Optical Coherence Tomography
<b>S-OCT</b>	Spectroscopic Optical Coherence Tomography
<b>RF</b>	Radio Frequency
<b>LN<sub>2</sub></b>	Liquid Nitrogen
<b>SD</b>	Standard Deviation
<b>MMIC</b>	Monolithic Millimetre Wave Integrated Circuit
<b>LNA</b>	Low Noise Amplifier

<b>BMI</b>	Body Mass Index
<b>FASS</b>	Future Aviation Security Solutions Programme
<b>JSaRC</b>	The Joint Security and Resilience Centre
<b>EPSRC</b>	Engineering and Physical Sciences Research Council
<b>CW</b>	Continuous Wave
<b>RADAR</b>	Radio Detection and Ranging
<b>IF</b>	Intermediate Frequency
<b>PRT</b>	Pulse Repetition Time
<b>PRF</b>	Pulse Repetition Frequency
<b>RCS</b>	Radar Cross Section
<b>VNA</b>	Vector Network Analyser
<b>DFT</b>	Discrete Fourier Transform
<b>IDFT</b>	Inverse Discrete Fourier Transform
<b>PPL</b>	Propagation Path Length
<b>SUT</b>	Sample Under Test
<b>IFFT</b>	Inverse Fast Fourier Transform
<b>DoF</b>	Depth of Field
<b>AFoV</b>	Angular Field of View
<b>SFoV</b>	Spatial Field of View
<b>SAR</b>	Synthetic Aperture Radar
<b>SEM</b>	Standard Error in the Mean
<b>SNR</b>	Signal to Noise Ratio
<b>NHS</b>	The National Health Service

# Chapter 1

## Introduction

*This chapter presents an overview of the research problem, the thesis aim and objectives, a list of contributions to knowledge, and a list of publications arising from this research.*

### 1.1 Overview

Burns are a very common cause of injury with over a quarter of a million people requiring treatment a year in the UK and costing the National Health Service (NHS) millions of pounds [1]. Globally, this figure is far greater. The current management of burn wounds i.e. (visual inspection) involves the removal of dressing materials for monitoring the wound healing progress and detecting the signs of infection, as illustrated in Figure 1.1.

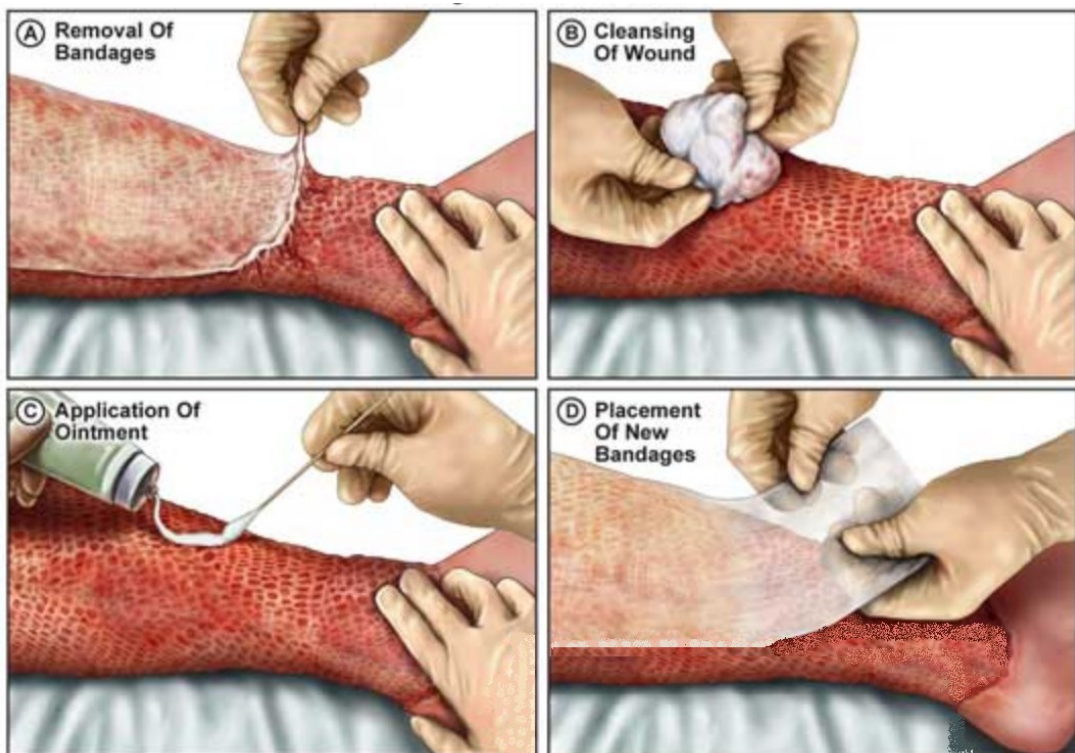


Figure 1.1: Visual inspection for assessing bandage wound (burn wound) [2].

The removal of dressing materials causes pain, anxiety and discomfort for the patients, particularly for children. In addition, it also causes distress to the parents/carers, and the frequent visits to hospital results in loss of person-hours from work. Furthermore, frequent exposure and handling of the wounds for washing during dressing changes could potentially cause damage to the neo-epithelium covering the wound bed and increase the risk of infection.

Currently, there are no methods for effectively assessing the wound healing progress without removing the dressing materials. A technique that could identify the healing state of a burn wound under dressing material is of great interest to patients, healthcare professionals, the National Health Service, and the private healthcare industry. It would reduce the pain, anxiety and distress caused by wound dressing changes, as well as reducing healthcare interventional time. Because electromagnetic radiation at microwave and millimetre wave frequencies can propagate through typical dressing materials with little attenuation (less than 0.85 dB for both Ka and W bands) [3], these bands of the electromagnetic spectrum are promising for assessing bandaged wounds. Several other clinical scenarios would also benefit from such a technique. Patients who have sustained fractures will require plaster casts for prolonged periods of time. Often these patients may also have cutaneous wounds that would require periodic inspection to determine the wound healing status. This inevitably requires the plaster cast to be removed or a window placed in the cast overlying the wound. The mechanics of this interfere with the healing of the underlying fractured bone. Hence, if a system were available to inspect the healing state of the wound through the plaster cast and the dressings, it would be possible to reduce the frequency of plaster cast changes.

Another group of patients to benefit would be patients who have relatively clean venous leg ulcers with minimal exudates requiring the prolonged wearing of

compression bandages [3]. In this case, the technique will be very useful as it can monitor the wound healing process without the dressings removal as the removal might delay the healing of the wounds for those patients.

## **1.2 Thesis Aim and Objectives**

The aim of this thesis is to investigate the feasibility of using radiation in the microwave/millimetre wave region (30-300) GHz to assess and monitor changes to the burns wound under dressing materials without the necessity of dressings removal. This capability might be useful in the monitoring of the wound healing process under dressing materials. To meet this aim, the following objectives are defined:

1. Develop a model for diagnosing the contrast between natural skin and damaged skin i.e. (skin with burns, skin mutated by basal cell carcinoma, and skin with different water contents).
2. Assess the variation in emissivity between individuals and locations on the arm.
3. Demonstrate how passive millimetre wave (PMMW) imaging systems can be used for monitoring changes in emissivity under dressing materials.
4. Determine the feasibility of using active millimetre wave radar systems to penetrate dressing materials and provide information about the propagation path length through dressing materials i.e. (thickness of the dressings).
5. Determine the feasibility of sensing and imaging burns under dressing materials using both passive and active imaging systems.

### **1.3 Contributions to Knowledge**

The major outcome of this thesis is that it is possible to discriminate a burn wound from a healthy skin under dressing materials using microwave and millimetre wave (MMW) radiation. This highlights the opportunity that the healing of burn wounds may be assessed and monitored without the removal of dressing materials. This has been assessed using measurements performed on human skin (*in vivo*) and fresh porcine skin samples (*ex vivo*) using both active and passive imaging systems. Other novel and unique contributions that have been achieved in this research are addressed as follows:

- The half space model presented in chapter 3 is used for calculating the emissivity of healthy and damaged skin in the MMW region of the electromagnetic spectrum. The model indicates a well-defined contrast in the emissivity between healthy skin and damaged or diseased skin. This contrast can be measured experimentally without touching or making contact with the human body using radiometry. Non-contact screening methods are often desirable in medical applications as they are quick and less painful. The half-space model, therefore, introduces a novel means to analyse the performance of radiometry as a new non-contact diagnostic tool. To the best of the author's knowledge, there is no available data in the open literature about the emissivity of healthy and damaged skin in the MMW band. Therefore, modelling of the emissivity of human skin at MMW lengths is required to bridge this gap, to help assess the feasibility of non-invasive (non-contact) diagnosis of diseased or damaged skin where the disease or the damage changes the water content of the skin.

- Human skin emissivity measurements presented in chapter 4 indicate that there is a signature for the human skin. The key innovation in this is in recognising that signatures from the human body enable regions of the body to be identified as skin. These signature variations from the skin are small (down to tens of milliKelvin), with changes taking place on scale lengths of a centimetre. This has been overlooked until now, as the sensitivities of existing PMMW imagers are typically in the region of a few Kelvin and with spatial resolutions greater than one centimetre. Consequently, anyone who would have looked would not have observed these subtle effects of the skin. The development of a precisely calibrated radiometer having a radiometric sensitivity of 5.0 mK with a centimetre spatial resolution on the skin has enabled new measurements of the human skin to be made, for exploitation in the fields of medicine and security screening.
- A development of an experimental setup and different methodologies for measuring the emissivity of porcine skin samples in chapter 5 reveal that there is a signature for the burn that can be detected using a 90 GHz calibrated radiometer. This signature is observed through dressing materials. These findings are unique and they suggest that MMW radiometry might be used as a new type of medical diagnostic, potentially to monitor burn wound healing under dressing materials or identify unusually high or low levels of emissivity values, which may indicate a deviation from a normal healing process.

- The development of an experimental setup and data processing methodology combined with a deconvolution technique to generate high-quality images from the radar is presented in chapter 6. The images obtained, prove for the first time the capability of the pulse synthesis radar system to provide information about the propagation path length of the dressing materials, and the attenuating effect of the bandages and medicinal creams. This capability might be used to detect and monitor burn wound healing under dressing materials in non-contact with the human body.
- Experimental images obtained from porcine skin samples in chapter 7 confirm the feasibility of detecting burns and features of the skin under dressing materials using passive (non-coherent) and active (coherent) imaging scanners. These unique findings enable microwave and MMW radiation to be used for evaluating the wound healing progress under dressing materials as they show edges, irregularities, burns and variation in the reflectance of the samples.

## 1.4 List of Publications and Awards

This thesis contains material that has been published in the following journals and conferences:

1. A. Y. Owda, N. Salmon and N.-D. Rezgui, “Electromagnetic Signatures of Human Skin in the Millimeter Wave Band 80–100 GHz,” *Progress In Electromagnetics Research B*, vol. 80, pp. 79-99, 2018.
2. A. Y. Owda, N. Salmon, S. W. Harmer, S. Shylo, N. J. Bowring, N. D. Rezgu and M. Shah, “Millimeter-wave emissivity as a metric for the non-contact diagnosis of human skin conditions,” *Bioelectromagnetics*, vol. 38, no. 7, pp. 559-569, 2017.
3. S. W. Harmer, S. Shylo, M. Shah, N. J. Bowring and A. Y. Owda, “On the feasibility of assessing burn wound healing without removal of dressings using radiometric millimetre-wave sensing,” *Progress In Electromagnetics Research M*, vol. 45, pp. 173-183, 2016.
4. A. Y. Owda, N. Salmon, D. Andrews and N.-D. Rezgui, “Active millimeter-wave radar for sensing and imaging through dressing materials,” in *IEEE SENSORS*, Glasgow, 2017.
5. A. Y. Owda, N. Salmon, N.-D. Rezgui and S. Shylo, “Millimetre wave radiometers for medical diagnostics of human skin,” in *IEEE SENSORS*, Glasgow, 2017.
6. A. Y. Owda, N.-D. Rezgui and N. Salmon, “Signatures of human skin in the millimeter wave band (80-100) GHz,” in *SPIE Europe Security+Defence, Millimetre Wave and Terahertz Sensors and Technology X*, Warsaw, 2017.

7. A. Y. Owda and N. Salmon, "On the feasibility of monitoring the wound healing under dressing materials using non-contact active millimetre wave imaging system," in *Tissue and Cell Engineering Society Annual Conference*, Manchester, 2017.
8. A. Y. Owda and N. Salmon, "Assessment of Human Skin Emissivity using Passive Millimetre-Wave Sensing," in *Science & Engineering Research Symposium*, Abstract, Manchester, 2017.
9. A. Y. Owda and N. Salmon, "Active Millimetre-Wave Imaging for Monitoring the Wound Healing Progress," in *the 9th MMU Postgraduate Research Conference 'CHANGING LIVES'*, Abstract, Manchester, 2017.
10. A. Y. Owda, S. W. Harmer, N. J. Bowring "Millimetre-Wave Radiometer in Medical Applications," in *Science & Engineering Research Symposium*, Abstract, Manchester, 2016.
11. Best student paper award in *SPIE Europe Security+Defence, Millimetre Wave and Terahertz Sensors and Technology X*, Warsaw, 2017. Paper title "Signatures of human skin in the millimeter wave band (80-100) GHz.

## 1.5 Thesis Structure

The overall structure of the thesis is outlined as illustrated in Figure 1.2.

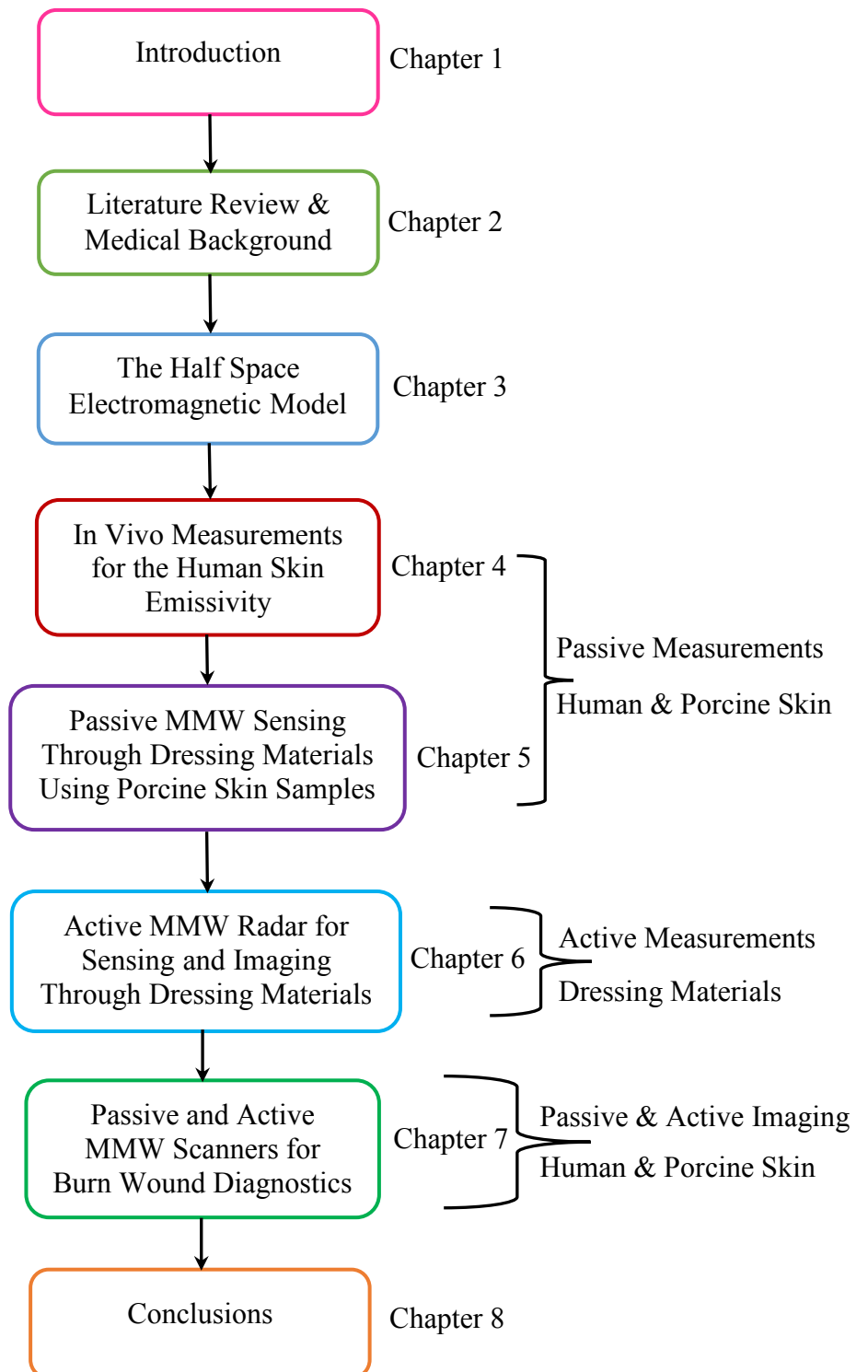


Figure 1.2: A block diagram shows the detailed structure of the thesis.

**Chapter 2** presents two phases of literature reviews; phase one reviews the MMW and the dielectric properties of the healthy and diseased human skin, whilst phase two provides a medical background and reviews potential technologies for use in assessing burn wound and skin cancer.

**Chapter 3** introduces the half space electromagnetic model. Different types of skin are modelled, namely: healthy skin, skin with burn injuries, dry and wet skin, skin mutated by basal cell carcinoma, and skin with different water contents.

**Chapter 4** presents in vivo measurements for the human skin emissivity. The measurements were conducted on two phases; phase one presents measurements conducted on 30 healthy participants at four measurement locations on the arm at 95 GHz, and phase two presents measurements conducted on two groups of healthy participants over the band 80 GHz to 100 GHz (group 1 six measurement locations on the arm, group 2 four measurements locations on the arm, and there were 60 participants in each group).

**Chapter 5** describes and discusses emissivity measurements conducted on 15 fresh porcine skin samples. The measurements were performed on samples with and without dressing materials and before and after the application of localised heat treatments.

**Chapter 6** presents the propagation path length measurements obtained from the hand support cast and the dressing materials samples having varying moisture contents and various medicinal creams using a radar system.

**Chapter 7** provides images obtained from three separate experiments and applied on human hands and porcine skin samples using both a passive MMW imager (centre frequency ~250 GHz) and active synthetic aperture radar (centre frequency ~27 GHz).

**Chapter 8** provides the conclusions of the thesis and plans for future research.

## Chapter 2

### Literature Review and Medical Background

*This chapter presents a literature review and a medical background about millimetre wave and other technologies used in the assessment of burn wound and skin cancer diagnostics. In the first part of this chapter, the dielectric properties of the human skin are presented and discussed. The second part of the chapter presents problems associated with the human skin from a medical diagnostic perspective and overviews emerging technologies being evaluated for assessing burn wounds and skin cancer such as terahertz imaging, optical coherence tomography, magnetic resonance imaging, infrared imaging, ultrasound imaging, and microwave and millimetre wave imaging.*

## 2.1 Electromagnetic Spectrum

The electromagnetic (EM) spectrum is defined as the ranges of frequencies and wavelengths of the radiation from radio waves to gamma ray. In 1873, James Clerk Maxwell [4, 5] formulated the concept of electromagnetic waves as a combination of electric and magnetic fields resulting in a propagation of energy at the speed of the light. EM waves can be characterised by their frequency, amplitude, and wavelength. These factors are important in the identification of the penetration capabilities and possible applications of the waves. The diagram in Figure 2.1 shows the inverse relationship between the frequency ranges and the wavelengths of the EM radiations from radio waves to gamma ray.

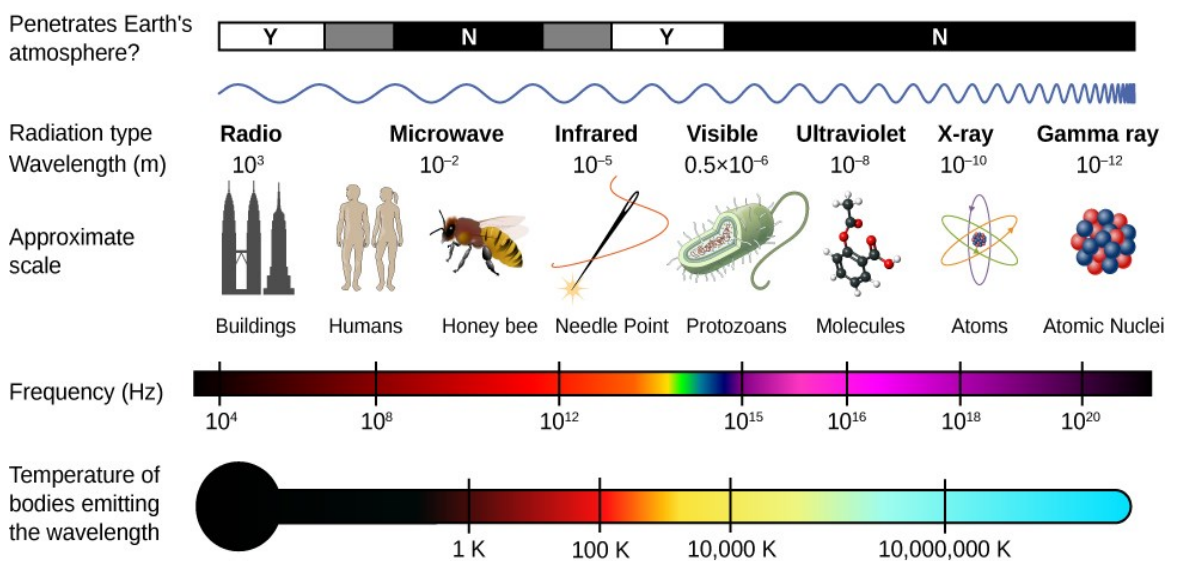


Figure 2.1: Electromagnetic spectrum frequency ranges, wavelengths, and penetrations [6].

## **2.2 History of the Millimetre Wave Radiation**

The millimetre wave (MMW) band is the electromagnetic region between the microwave and terahertz, covering the frequency ranges (30-300) GHz [7, 8, 9]. Radiation in this band is known as a millimetre wave since the wavelength of this radiation lies between 10 mm and 1.0 mm [9]. In the 1890's, a German physicist Heinrich Hertz [10] initiated the first experimental investigation into MMW radiation, recording a wavelength of 66.0 cm in his experiments. Then in 1895, the Russian Peter Lebedew [11] repeated the Hertz experiment with a resonator and recorded a wavelength of 6.0 mm. This was followed with the experimental work conducted by Bose [12] that recorded a wavelength of 5.0 mm, confirming the short wavelength of the MMW radiation. These achievements were then followed by the discovery of X-ray radiation by Röntgen [13]. Arkadiewa [14] conducted further experiments on MMWs measuring a wavelength of 11.0 mm. In 1923, the first American contribution to MMW research is achieved by Nichols and Tear [15], they identified the MMW band as the region between the infrared and the radio wave band (as investigated by Tesla and Marconi [16]) where they conducted experiments at a wavelength ranging from 2.0 mm to 0.2 mm. The discovery of the laser [17] made a huge contribution to the development of MMW research and the coherent electromagnetic wave energy. These achievements are led to a growing interest and huge developments in the MMW technology in many applications including the developed of landmark systems such as MMW radar and passive and active imaging systems.

## 2.3 Key Features of the Millimetre Wave Radiation

The key features of the radiation in the MMW band are as follows:

- Spatial resolution sufficient to identify features down to scale lengths of  $\sim 1.0$  mm in a diffraction limited system. This is due to the relative short wavelength of the MMW radiation. This allows discrimination between different objects [8] and means MMW band is suitable for use in military, remote sensing, and automotive radar applications.
- Good penetration capability through dielectric materials such as clothing and textiles [3, 18, 19]. This makes MMW radiation suitable for the purposes of security screening and non-destructive testing and evaluation.
- Large bandwidth and high data rate [20]. This feature makes MMW radiation suitable for use in communication systems.
- MMW radiation is non-ionising and is believed to be harmless to humans and animals at intensity levels  $< 1.0$  mW/cm<sup>2</sup> compared with X-ray and Gamma-ray [21, 22]. It, therefore, is ideal for potential medical applications.

This thesis is concerned with the medical applications of MMW radiation and more specifically, assessing the feasibility of using MMW radiation for detecting burns under dressing materials and for non-invasive diagnosis of diseased skin. Therefore, the review in this chapter will focus on these areas.

## 2.4 Interaction of Millimetre Wave Radiation with the Human Body

Millimetre wave radiation interacts significantly with the human skin and eyes since they can be exposed directly to the MMW radiation [23]. Any radiation, which is incident on the skin, is absorbed within a short distance [24, 25]. The penetration depth of the MMW radiation is defined as the distance in the tissue over which the magnitude of the electric field reduces to a fraction of  $1/e$  (or  $1/e^2$  of the transmitted power). In human skin, the penetration depth of the MMW radiation is reported to be 0.782-0.23 mm over the frequency band 30-300 GHz [24]. The short penetration depth of the MMW radiation in the human skin is due to the attenuating effects arising mainly due to the presence of water. Such losses in a media are quantified by a loss tangent, which for water is given in [26]. The penetration depth of radiation in a dielectric medium,  $\delta$  can be calculated using Equations (2.1) and (2.2) [27].

$$\delta = \frac{1}{\alpha} \quad (2.1)$$

$$\alpha = \omega \sqrt{\frac{\mu \epsilon_0 \epsilon'_r}{2} \left( \sqrt{1 + \left( \frac{\sigma}{\omega \epsilon_0 \epsilon'_r} \right)^2} - 1 \right)} \quad (2.2)$$

Where,  $\alpha$  is the attenuation factor measured in nepers per metre,  $\omega = 2\pi f$  is the angular frequency measured in radians per second,  $\epsilon'_r$  is the dielectric constant of the medium (in this research skin) measured in Farads per metre,  $\epsilon_0$  is the free space permittivity ( $\epsilon_0 = 8.854191 \times 10^{-12}$  F/m),  $\sigma$  is the conductivity of the medium measured in siemens per metre, and  $\mu$  is the permeability of the medium measured in Henries per metre.

Equation (2.2) indicates that the interaction of the MMW radiation with the human skin depends on the dielectric properties of the skin (relative complex permittivity), and the frequency range. Figure 2.2 illustrates the relationship between the frequency band and the penetration depth of the MMW radiation using different skin models.

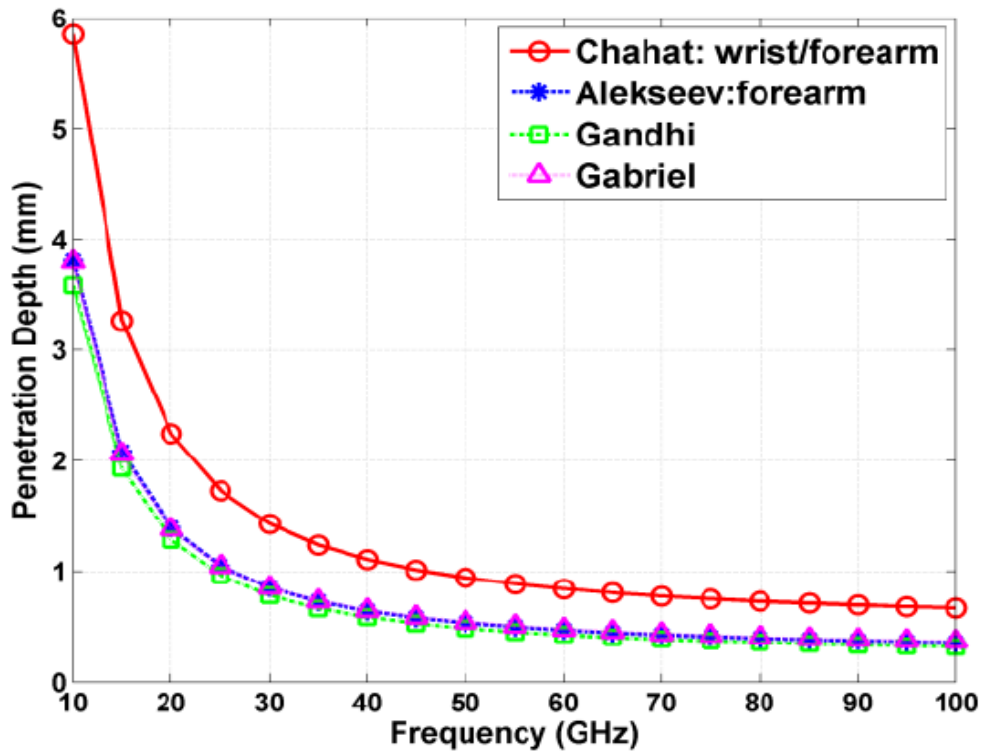


Figure 2.2: Penetration depth of the millimetre wave radiation in the human skin as a function of frequency using different skin models [28].

Millimetre wave radiation can penetrate through clothing and textiles [18]. Many researchers have investigated the interaction of the MMW radiation with different types of clothing such as fleece, leather, and denim [18, 25, 29, 30, 31]. These studies reveal that an existing layer of clothing in direct contact with the human skin enhances the transmission between the air- skin interfaces since it acts as an impedance match. This interaction depends on the thickness of the clothing layer, the smoothness of the clothing surface, and the type of textiles.

As MMW radiation is absorbed near to the skin surface, the main concern associated with this radiation is its heating effect. The in vivo measurements conducted by Gustrau and Bahr [32] on the human skin at 77 GHz reveal that MMW radiation with an incident power density of 10 mW/cm<sup>2</sup> increases the skin surface temperature by 0.7°C. However, when the incident power density decreases to 1.0 mW/cm<sup>2</sup>, the skin surface temperature increases by less than 0.1°C. This is also confirmed in the study conducted by Zhadobov et al [25], who revealed an incident power density of 1.0 mW/cm<sup>2</sup> at 60 GHz increases the skin surface temperature by 0.1°C. Furthermore, the Alabaster thermal model [33] reveals that the maximum increase in the skin surface temperature at 60 GHz, 77 GHz and 94 GHz due to an exposure to MMW radiation for thirty-second with an incident power density of 10 mW/cm<sup>2</sup> is less than 0.25°C.

Studies in microwave and MMW indicate that high exposure (above the recommended level of the incident power density that will discuss in section 2.5) to these radiations might cause cataract in human and animals eyes [34, 35]. This might occur when the temperature of the eyes is raised above the threshold of 41°C [23]. As a result of this, the interaction of the MMW radiation with the human and animal tissues is based on the following [23]:

- The strength of the electric and the magnetic fields.
- The operating frequency.
- The thermal conductivity of the tissue.
- The time duration of the exposure.
- The type of the exposure (continuous or discrete).
- The incident power density of the radiation.

## 2.5 Exposure Limits for Millimetre Wave Radiation

The Institute of Electrical and Electronics Engineers (IEEE) [36], the International Commission on Non-ionising Radiation Protection (ICNIRP) [37] and the European Committee for Electrotechnical Standardization (CENELEC) [38] provide limits for public and occupational exposure for protecting the human body. These standards provide recommendation and restriction for exposing the human body to MMW radiation. The restriction provided by these institutions for occupational and general public areas are summarised in Table 2.1. These restrictions are specified for surface areas of 100 cm<sup>2</sup> (the whole body), 20 cm<sup>2</sup> (adult human eye), and 1.0 cm<sup>2</sup> (cornea).

Institution	Frequency (GHz)	Area Type	Power density (mW/cm <sup>2</sup> )	Area (cm <sup>2</sup> )& time (min)	
IEEE	(30-300)	Occupational	10	100	$\frac{25.24}{f(GHz)^{(0.476)}}$
			100	1	
	(30-100)	General	1	100	
			100	1	
ICNIRP	(10-300)	Occupational	5	20	$\frac{68}{f(GHz)^{(1.05)}}$
			100	1	
		General	1	20	
			20	1	
CENELEC	(2-300)	Occupational	5	20	$\frac{68}{f(GHz)^{(1.05)}}$
			100	1	
		General	1	20	
			20	1	

Table 2.1: Exposure limits for protecting the human body from active millimetre wave radiations [36, 37, 38].

Table 2.1 indicates that the recommendation of the CENELEC standard is agreed with the ICNIRP standard for occupational workers and the general public. However, IEEE provides less restriction for the maximum permissible exposure values for the general public and occupational areas. Simulation in Figure 2.3 indicates that the mean time limit for IEEE standard is varied between 5.0 minutes at 30 GHz to 1.67 minutes at 300 GHz, whereas the time limit for CENELEC and ICNIRP standards is between 2.0 minutes and 10.0 seconds over the band (30-300) GHz for an average area of 1.0 cm<sup>2</sup>.

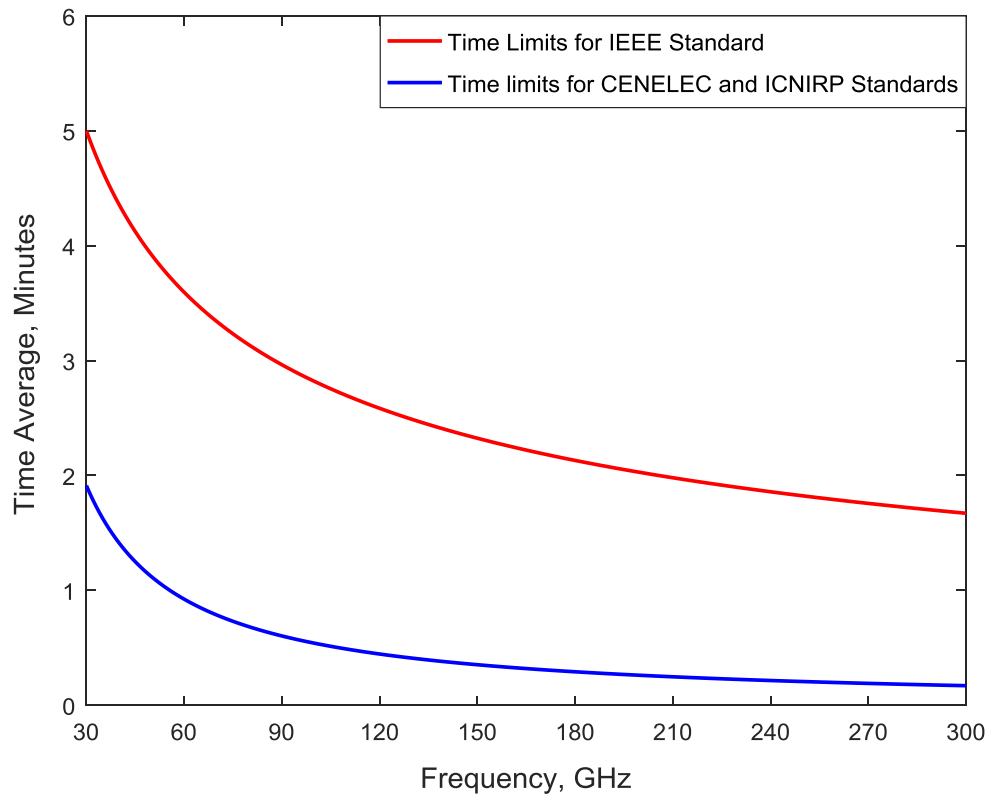


Figure 2.3: The inverse relationship between the time limits of continues exposure and the frequency as determined by IEEE, ICNIRP and CENELEC organisations.

## 2.6 Dielectric Properties of the Human Skin

The interaction of the electromagnetic radiations with dielectric materials including the human skin is determined by the electrical parameters of the materials and specifically the complex permittivity [33]. The complex permittivity of the material can be expressed in terms of the free space permittivity,  $\epsilon_0 = 8.85 \times 10^{-12}$  F/m and the relative complex permittivity,  $\epsilon_r$  as [39, 40]:

$$\epsilon = \epsilon_0 \epsilon_r \quad (2.3)$$

The relative complex permittivity of a material is a complex quantity that consists of a real part and an imaginary part and it is a measure of the phase and electric field amplitude changes relative to those in free space [39, 40], specifically given by:

$$\epsilon_r = \epsilon_r' - j\epsilon_r'' = \epsilon \left[ 1 - \frac{j\sigma}{\omega\epsilon} \right] \quad (2.4)$$

The real part of the relative permittivity,  $\epsilon_r'$ , represents the dielectric constant of the material (in this research the skin), and it is a measure of the energy stored in the material due to an external applied electric field. Whereas, the imaginary part,  $\epsilon_r''$ , represents the loss factor of the material and is a measure of the energy loss from the material due to the external electric field. Measurements of the relative complex permittivity of the human skin indicate that the complex permittivity of the skin varies with the frequency [39, 40] and the thermodynamic temperature of the skin [33]. The ratio between the loss factor and the dielectric constant of the relative complex permittivity is called the loss tangent and it is expressed as:

$$\tan \theta = \frac{\epsilon_r''}{\epsilon_r'} = \frac{\sigma}{\omega\epsilon} \quad (2.5)$$

Where  $\omega$  is the angular frequency measured in radians per seconds, and  $\sigma$  is the conductivity of the skin measured in Siemens per meter, and  $\epsilon$  is the complex permittivity of the skin measured in Farad per meter.

## **2.7 Methods for Measuring the Relative Complex Permittivity**

The relative complex permittivity of different types of materials, samples, and biological tissue (in vivo and in vitro) are measured experimentally using the following methods [41]:

- Transmission/reflection line method.
- Open-ended coaxial probe method.
- Free space method.
- Resonant method.

In the microwave and the MMW frequency bands, the most common methods used for measuring the relative complex permittivity of the biological tissue (human and animals) are the open-ended coaxial probe method [26, 42, 43, 44, 45] and the free space method [33, 46].

The open-ended coaxial probe method is fast, and easy to apply over a large number of samples after the system is calibrated. However, the relative complex permittivity measurements are subject to changes if the sample and the coaxial probe are not in close contact. This is due to the varying size of the air gap between the two and this affects the measured relative complex permittivity [41]. In addition, the diameter of the probe should be chosen to be less than the wavelength of the radiation in the skin, if accurate measurements are to be achieved [42] and the thickness of the sample under test should be greater than the diameter of the probe [43]. This means that the open-ended coaxial probe can perform measurements over a specific frequency band. Also,

different frequency bands required different probes with different diameters and characteristics. Furthermore, the power level of the microwave and the MMW radiation should be chosen within the safety limits [21] according to the recommendations of the IEEE, ICNIRP, and CENELEC organizations [36, 37, 38].

The second method is the free space method. The main advantages of this method over the open-ended coaxial probe method are the ability to measure both the electric ( $\epsilon_r$ ) and the magnetic ( $\mu_r$ ) properties of the sample over a wide range of frequencies without making any physical contact with the subject being measured. However, the free space method is more appropriate for planer samples that achieve the following properties [33, 41]:

- The sample size should be large enough to fill the beam of the horn antenna and to reduce the diffraction at the edge of the sample.
- The sample thickness should be the same over the full surface area.
- The sample surface should be smooth and flat.
- The sample should be aligned properly as the system is very sensitive to the alignment.

These properties make the free space method suitable for limited and specific types of samples, and this might justify the wide usage of the open-ended coaxial probe for measuring the relative complex permittivity of the human skin in vivo over the microwave and the MMW frequency bands, as it is more accurate due to lower sources of error [33].

## 2.8 Relative Complex Permittivity Theoretical Models

The frequency dependence of the relative complex permittivity of the biological tissue is modelled over the microwave and the MMW bands using different models such as the single relaxation Debye model, the multiple dispersion Debye model, the Cole-Cole model, and the multiple dispersion Cole-Cole model [33, 46, 47, 48, 49, 50, 51]. The relative complex permittivity of the tissue can be estimated using the single relaxation Debye equation as [47]:

$$\epsilon_r = \epsilon_\infty + \frac{\epsilon_s - \epsilon_\infty}{1 + j\omega\tau} \quad (2.6)$$

Where,  $\epsilon_s$  is the static relative complex permittivity ( $\omega\tau \ll 1$ ),  $\epsilon_\infty$  is the infinite frequency relative permittivity ( $\omega\tau \gg 1$ ),  $\omega$  is the angular frequency,  $\tau$  is the relaxation time constant, and  $j = \sqrt{-1}$ .

The complex permittivity of the biological tissue can be characterized by three relaxation regions  $\alpha, \beta$ , and  $\gamma$ . These regions are associated with low frequency, medium frequency, and high frequency bands respectively [48]. In 1985, Debye [51] developed a multiple dispersion (five terms) expression for estimating the relative complex permittivity of muscle tissue. This expression can be described as:

$$\epsilon_r(\omega) = \epsilon_\infty + \sum_{n=1}^5 \frac{\Delta\epsilon_n}{1 + j\omega\tau_n} + \frac{\sigma_i}{j\omega\epsilon_o} \quad (2.7)$$

Where,  $\Delta\epsilon_n = \epsilon_s - \epsilon_\infty$  is the magnitude of the dispersion,  $\sigma_i$  is the static conductivity, and  $\epsilon_o$  is the free space permittivity.

Cole-Cole [49, 50] have developed an empirical expression that considers the broadening of the dispersion in the relative complex permittivity of the biological tissue. This expression is known as the Cole-Cole expression and it can be expressed in terms of a spread parameter alpha  $\{0 < \alpha < 1\}$  as:

$$\epsilon_r(\omega) = \epsilon_\infty + \frac{\epsilon_s - \epsilon_\infty}{1 + (j\omega\tau)^{(1-\alpha)}} \quad (2.8)$$

Due to the complexity of the biological tissue, the multiple terms in the Cole-Cole expression suggests it is a more appropriate expression for predicting the relative complex permittivity of the biological tissue and it can be expressed as [48]:

$$\epsilon_r(\omega) = \epsilon_\infty + \sum_n \left( \frac{\Delta\epsilon_n}{1 + (j\omega\tau_n)^{(1-\alpha_n)}} \right) + \frac{\sigma_i}{j\omega\epsilon_o} \quad (2.9)$$

These models have been developed due to the limited measured in vivo data of the relative complex permittivity of the human tissue over the microwave and the MMW bands. This is due to many reasons, these being essentially:

- The technical difficulty in making calibrated measurements when there are instrument alignment difficulties [33].
- Both methods (open-ended coaxial probe and free space methods) used for measuring the dielectric properties of the biological tissue or human body require exposing the human body to microwave and MMW radiations. These radiations are artificial man-made radiations generated typically by a vector network analyser (VNA), requiring the power level of these radiations to be within the safety limits and the recommendations of IEEE, ICNIRP, and CENELEC standards [36, 37, 38]. This makes getting participants in these studies a difficult task. As alternatives, researchers conduct measurements on

animal tissue as in [33, 48] or they use models for predicting the relative complex permittivity of the tissue.

- Microwave and MMW devices are expensive and some of these devices only work over a limited frequency band and therefore conducting measurements over different frequency bands required different devices such as an open-ended coaxial probe, horn antennas, high frequency cables, and a VNA. Therefore, researchers conduct measurements over limited frequency bands based on using available resources.

## 2.9 Dielectric Properties of the Human Skin in the MMW Band

It is a known fact that the electromagnetic interaction of the biological tissue over the MMW bands is dominated by its free water content [21, 25, 45]. The relative complex permittivities measurements conducted on the human skin over the microwave and the MMW bands are summarised in Table 2.2.

Location/Skin	Sample Type	Frequency Band	Method /Source
The palm of the hand The back of the hand Wet and dry skin	In vivo	(30-40) GHz	Open-ended coaxial probe [42]
Forearm skin The palm of the hand	In vivo	(37-74) GHz	Open-ended waveguide [26, 45]
Dry (normal skin) Wet (skin with gel)	Dry skin in vivo Wet skin in vitro	10Hz to 20 GHz	Open-ended coaxial probes [48, 52]
The palm of the hand Wrist of the hand skin	In vivo	(0.5-110) GHz	Open-ended coaxial probes [43]
The palm of the hand Forearm skin Wrist of the hand skin	In vivo	(10-60) GHz	Coaxial slim probe [44]
The palm of the hand	In vivo	(26.5-60) GHz	Waveguide technique [53]
Dry (normal skin) Wet (skin with water)	In vitro	(57-100) GHz (90-100) GHz	Free space method [33, 46]

Table 2.2: The relative complex permittivities measurements of the human skin.

The studies discussed in Table 2.2 indicate that the relative complex permittivity values of the human skin are measured in specific frequency bands and measurement locations. Therefore, many researchers have conducted measurements over a specific frequency band and extracted the parameter of the theoretical models (discussed in section 2.8) to predict and estimate the relative complex permittivity of the skin over the rest of the MMW band. As an example of this is the estimated relative complex permittivity of the skin that is presented in Table 2.3.

Frequency (GHz)	Gabriel [48] Cole-Cole	Gandhi [24] Debye	Alekseev [26, 45] Palm	Alekseev [26, 45] Forearm	Hwang [43] Palm	Hwang [43] Wrist
30	15.5-j16.2	18-j19.2	14.6-j13.9	15.9-j16.3	7.4-j3.6	10.4-j5.3
40	11.7-j14.3	13.5-j17	11.3-j12.4	11.9-j14.5	6.8-j3.1	9.3-j4.9
50	9.4-j12.5	10.7-j15	9.3-j10.9	9.6-j12.7	6.4-j2.8	8.6-j4.5
60	7.9-j10.9	8.8-j13.2	8.0-j9.5	8.1-j11.1	6.1-j2.5	8.1-j4.1
70	7.0-j9.7	7.7-j11.7	7.2-j8.5	7.1-j9.9	5.9-j2.3	7.7-j3.8
80	6.4-j8.6	6.9-j10.4	6.6-j7.6	6.5-j8.8	5.8-j2.1	7.3-j3.6
90	5.9-j7.8	6.3-j9.4	6.2-j6.8	5.9-j7.9	5.7-j1.9	7.1-j3.4
100	5.6-j7.1	5.9-j8.6	5.9-j6.2	5.6-j7.3	5.6-j1.8	6.9-j3.2

Table 2.3: Predicted relative complex permittivity of the human skin (30-100) GHz.

The dielectric permittivity data presented in Table 2.3 indicates that the relative complex permittivity of the skin is frequency dependent as the real and the imaginary parts of the complex permittivity decrease with the frequency. The data also show differences in the relative complex permittivity values of the skin from model to model. These differences are assumed to be due to model assumptions, measurement techniques, and sample type (in vivo or in vitro) [22, 53].

## **2.10 Review of Dielectric Properties in Medical Applications**

The relative complex permittivity and the reflectivity of the skin over the microwave, the MMW and the terahertz bands are significantly affected by the water content of the skin. Therefore, the dielectric permittivity and the reflectivity of healthy skin and diseased skin (skin with basal cell carcinoma, skin with burns, dry and wet skin, skin cancer, and skin with differing water content) are measured and predicted over the MMW bands for the purpose of non-invasive diagnostics of skin diseases [33, 42, 48, 54, 55, 56, 57, 58, 59, 60].

### ***2.10.1 Dielectric Properties of Healthy Skin and Skin with Basal Cell***

#### ***Carcinoma***

The relative complex permittivity of healthy skin and skin with basal cell carcinoma (BCC) are calculated using a two pole Debye model over the frequency band (100-300) GHz by Pickwell et al [58, 59]. The parameters of the model are extracted from measurements performed on five patients having BCC. The studies indicate that the relative complex permittivity of the skin with BCC is higher than that of healthy skin as the water content of the skin with BCC is higher than that of healthy skin [61].

The in vivo study conducted by Taeb et al [56] shows a well-defined contrast in the real and the imaginary parts of the relative complex permittivity of healthy skin (11.5-j14.3) and skin with BCC (15.0-j20.5) at 42 GHz. This contrast suggested that radiation in microwave and MMW bands might be useful for early detection of BCC.

### ***2.10.2 Dielectric Properties of Healthy Skin and Skin with Burns***

The complex reflection coefficient of unburned and burned porcine skin was measured experimentally using an open-ended rectangular waveguide probe over the frequency band (30-40) GHz by Gao and Zoughi [62]. The measurements show that the reflectance of unburned skin is higher than that of burned damaged skin. However, the in vivo study conducted on the human subject over the frequency band (30-40) GHz [42] indicates different trends as the relative complex permittivity of the burned skin is ~10% higher than that of unburned skin. Based on this result, the in vivo study suggested possible trends for the dielectric properties of the skin with the level of water content illustrated in Table 2.4.

Level of water content	Dielectric permittivity	Penetration depth	Emissivity
High level	Increase	Decrease	Decrease
Low level	Decrease	Increase	Increase

Table 2.4: Effect of changing the water content on the dielectric properties of the human skin [42].

### 2.10.3 Relative Complex Permittivity for Skin with Differing Water Contents

The relative complex permittivity of the skin with differing water contents, 50%, 75%, and 95% is calculated in the frequency band (30-100) GHz using the general second order dispersion model [63]. The parameters of the model are estimated from measurements conducted on skin phantoms using an in-contact waveguide probe. The relative complex permittivity of the skin with different water content shows well define differences in the real and imaginary part of the relative complex permittivity of the skin with different water content illustrated in Table 2.5.

Frequency (GHz)	Dielectric permittivity (Skin cancer 95%)	Dielectric permittivity (Normal skin 75%)	Dielectric permittivity (Dry skin 50%)
30	28- j34	18- j16	12- j8.0
40	20- j28	14- j14	10- j8.0
60	12- j22	10- j9.0	8.0- j6.0
80	8.0- j17	7.8- j7.5	7.6- j4.0
100	7.6- j13.7	7.3- j5.7	6.86- j3.3

Table 2.5: The relative complex permittivity of the skin with different water content.

Another study conducted by Aminzadeh et al [57] on healthy skin with 65% and 70% water content and malignant skin tissue with 81.6% water content in the frequency band (30-100) GHz indicates significant differences between healthy skin (65% and 75% water content) and malignant lesion tissue (81.6% water content). These differences are due to the different water content of healthy skin and malignant tissue. The percentage of the water content in the epidermis and dermis layers of healthy skin has been reported to be 65%-70% [45], compared to 81%-82% in malignant skin [64].

#### ***2.10.4 Relative Complex Permittivity of Dry and Wet Skin***

Over the MMW bands, the dielectric permittivity of dry and the wet skin are measured experimentally in [33, 42, 48]. In general, dry skin is representative of normal skin, whereas wet skin is representative of skin that has recently be moistened. These definitions are used in most cases in this thesis unless dry and wet skin are identified differently.

Measurements conducted on dry and wet skin by Gabriel et al [48] show that the relative complex permittivity of wet skin (moistened with aqueous gel) is higher than that of dry skin over the frequency band (30-100) GHz; this is due to the gel increasing the hydration level of the skin and this raises the relative complex permittivity of the wet skin. This study is supported with another in vivo study conducted on the palm of the hand and the back of the hand skin in a dry and wet state (skin with water) over the frequency band (30-40) GHz [42]. The study shows that the relative complex permittivity of the wet skin is higher than that of dry skin for all measurement locations. The measurements also indicate that the imaginary part of the dielectric permittivity of the wet palm of hand skin is ~50% higher than that of the dry skin.

## 2.11 Thermal Emission and Blackbody Radiation

When radiation is incident on an object, part of the radiation is reflected and the remainder will penetrate inside the object. Depending on the type of the object, either the radiation will be absorbed inside the object (internal energy) or they might be transmitted outside the object as in the case of glass that transmitted visible radiation. A so-called blackbody is an ideal absorber and emitter. It absorbs all incident radiation and re-radiates emission in all directions at a level set by the Planck radiation law. [65]. It is called a blackbody since good absorbers for visible light have the colour black. What appears black in the visible band may not indeed be “black” in the MMW band and vice versa. In reality, few materials can be used as an approximation to the blackbody such as carbon black, gold black, and platinum black. These materials can be used as reference samples for the purposes of calibration as they have closed properties to the blackbody. The key features of the blackbody are addressed as follows [65]:

- A blackbody is a perfect emitter, this means that blackbody is emitting and absorbing the same amount of radiation and this is valid under thermal equilibrium (Prevost’s law).
- Blackbody radiation is isotropic; this means that radiations emitted from the blackbody are independent of the blackbody location and orientation.
- The intensity of the blackbody radiation,  $B_{\lambda}(T)$  is expressed by Plank’s function as:

$$B_{\lambda}(T) = \frac{2hc^2}{\lambda^5 \left( e^{\left(\frac{hc}{kT\lambda}\right)} - 1 \right)} \quad (2.10)$$

Where,  $h$  is the Planck's constant ( $6.626 \times 10^{-34}$  J.S),  $k$  is the Boltzmann's constant ( $1.38 \times 10^{-23}$  J K<sup>-1</sup>),  $c$  is the speed of the light ( $3.0 \times 10^8$  m/s), and  $T$  is the absolute temperature of the blackbody measured in Kelvin.

When the wavelength  $\lambda$  goes to infinity, the intensity of the blackbody radiation is expressed by Raleigh Jean's distribution as [65]:

$$B_{\lambda}(T) = \frac{2kcT}{\lambda^4} \quad (2.11)$$

The peak of the blackbody radiation goes to higher intensities at shorter wavelengths when the absolute temperature increases. Figure 2.4 illustrates how the wavelength and the intensity of the blackbody radiations vary with the absolute temperature.

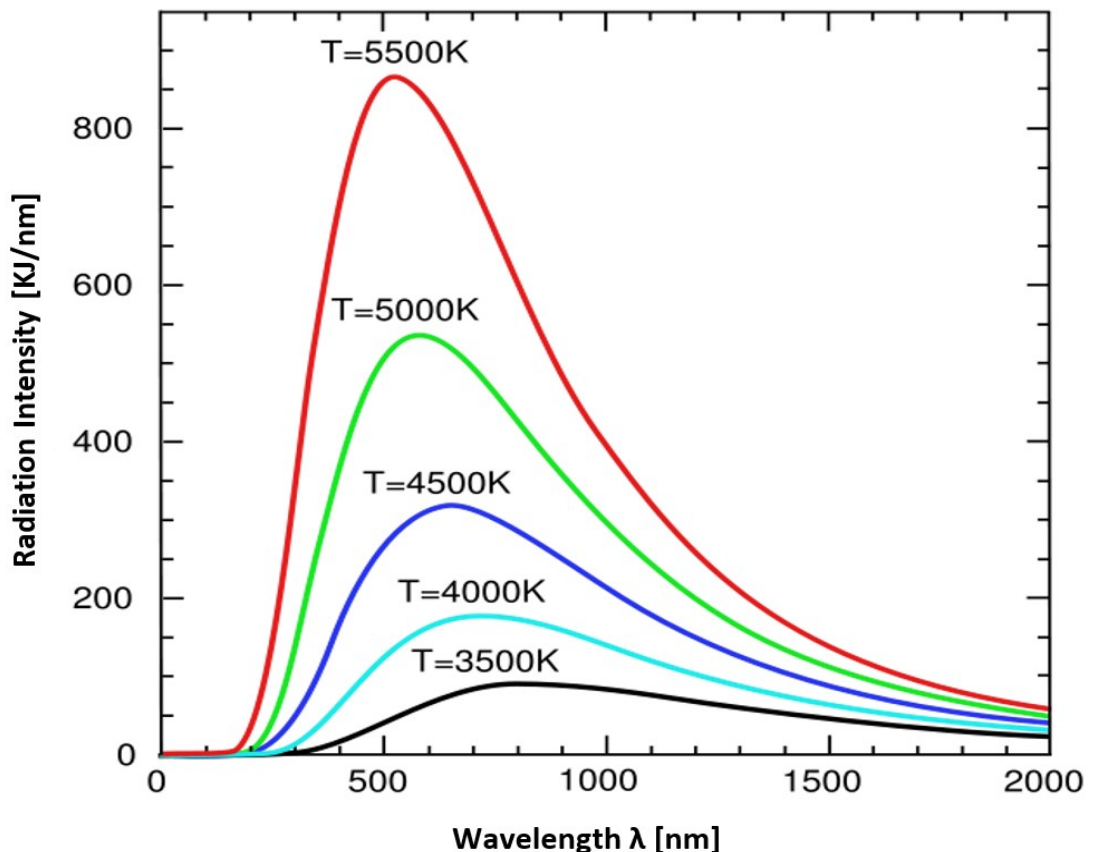


Figure 2.4: Radiation intensity of the blackbody versus the wavelength at different absolute temperatures [66].

The power of the blackbody radiation per unit area is directly proportioned with the fourth power of the blackbody thermodynamics temperature, and it can be expressed by the Stefan's Boltzmann law as [65]:

$$P(Wm^{-2}) = T^4 \sigma_B \quad (2.12)$$

Where,  $\sigma_B$  is Stefan's Boltzmann constant and it is  $5.67 \times 10^{-8} Wm^{-2} K^{-4}$ .

The wavelength of the blackbody at the peak intensity of the radiation is inversely proportional to the absolute temperature of the blackbody and it is described by Wien's displacement law as [65]:

$$\lambda_{peak_{radiation}} (\mu m) = \frac{\sigma_w}{T} \quad (2.13)$$

Where  $\sigma_w$  is Wien's displacement constant and it is equal to  $2897 K \mu m$ .

- A blackbody is emitting radiation in each direction and at every wavelength, this is to maintain the thermal equilibrium. If radiation is absorbed coming from all directions at different wavelengths, it should radiate the same to maintain thermal equilibrium.
- The blackbody radiation intensity is proportional to the thermodynamic temperature of the medium.

## 2.12 Reflection and Refraction Index

Electromagnetic radiation propagates at the speed of the light in free space. However, when the radiation facing or hitting a surface or target object having different optical properties (refractive index); radiation will be reflected and refracted at the boundary of the two mediums as illustrated in Figure 2.5.

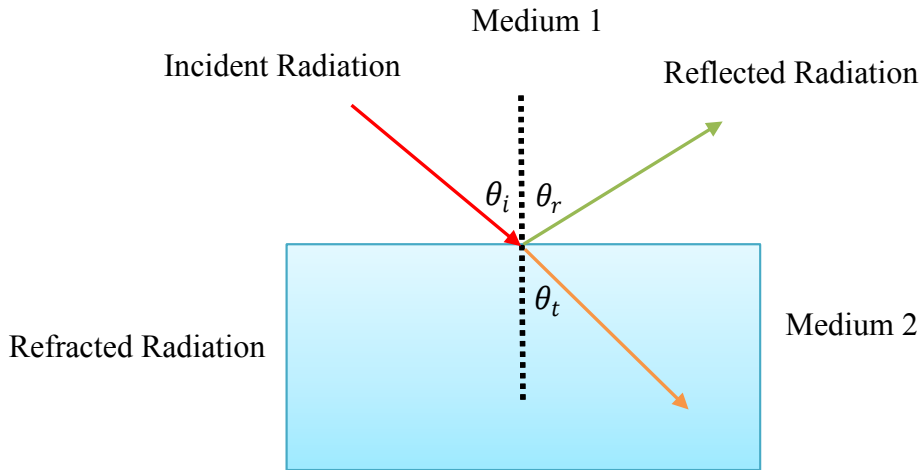


Figure 2.5: Reflection and refraction in mediums having different dielectric properties.

The reflected radiation has a similar angle to that of incident radiation as they are travelling in the same medium. However, the relationship between the incident angle,  $\theta_i$  and the refraction angle,  $\theta_t$  is determined by Snell's law as [67]:

$$n_1 \sin(\theta_i) = n_2 \sin(\theta_t) \quad (2.14)$$

Where,  $n_1$  is the refractive index of medium 1, and  $n_2$  is the refractive index of medium 2.

Refractive index,  $n(\omega)$  of a medium is a complex quantity that is a measure of the ratio of the speed of the light in the free space to that in the medium. This quantity varies with frequency and it can be expressed as [68]:

$$n(\omega) = n'(\omega) + i\kappa(\omega) \quad (2.15)$$

Where,  $n'(\omega)$  is the real part of the refractive index and it represents the phase speed,  $\kappa(\omega)$  is the imaginary part of the refractive index and it represents the loss in the electromagnetic radiation, and  $\omega$  is the angular frequency.

The refractive index for the dielectric materials and the biological tissue (lossy dielectric) over the MMW band can be characterised by the relative complex permittivity of the materials,  $\epsilon_r(\omega)$  as:

$$n(\omega) = \sqrt{\epsilon_r(\omega)} = \sqrt{(\epsilon'_r(\omega) + j\epsilon''_r(\omega))} \quad (2.16)$$

Where,  $\epsilon'_r(\omega)$  is the dielectric constant, and  $\epsilon''_r(\omega)$  is the loss factor of the dielectric materials.

For a low loss dielectric material;  $\epsilon''_r(\omega) \ll 1$ , the refractive index of the material is given by the real part of the relative complex permittivity as:

$$n(\omega) = \sqrt{\epsilon'_r(\omega)} \quad (2.17)$$

This section reviewed the interaction of the MMW radiation with the skin and the dielectric properties of the human skin (healthy and diseased skin). The following sections will review some of the problems associated with the human skin from a medical diagnostic perspective and emerging technologies being evaluated for assessing burn wounds and skin cancer disease.

## 2.13 Human Skin Structure

Human skin has a layered structure comprising, the epidermis (outer protective layer), the dermis (inner connective layer), and the hypodermis (subcutaneous fat layer); as illustrated in Figure 2.6. For adults, skin covers a total surface area of  $\sim 1.7 \text{ m}^2$  and constitutes  $\sim 15\%$  of the total body weight [69, 70]. Skin thickness varies with location over the body, sex, and age of the individual [71]. Based on the thickness of the skin layers, human skin is classified into two types [72, 73]:

- Thin hairy skin that is covered the majority of the human body. This skin has a thickness range of 1.0 mm to 3.0 mm.
- Thick hairless skin that is covered the palm of the hand and the soles of the feet and its' thickness is in the range of 4.0 mm to 5.0 mm.

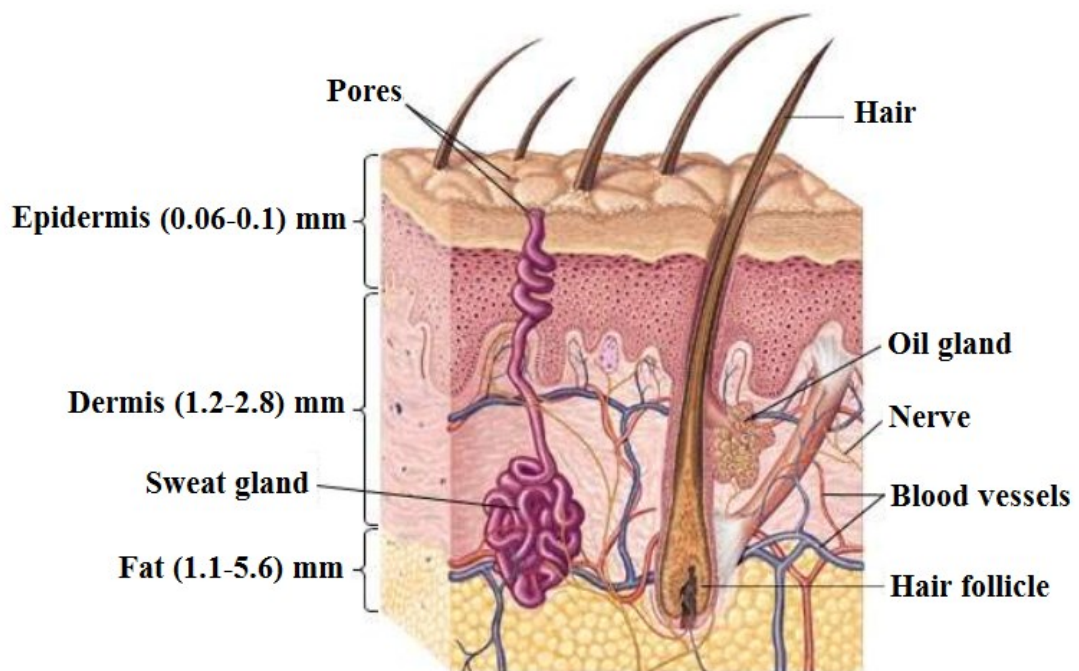


Figure 2.6: Schematic for human skin structure and its' derivatives (sweat glands, oil glands, nails, hair, and hair follicles) [74]. Radiation in the lower frequency portion of the millimetre wave band penetrates down into the dermis layer of the skin.

The epidermis layer is the outer layer of the skin that is responsible for providing a waterproof barrier and it produces the skin colour as it consists the melanocytes cells. This layer consists of five layers from dermis to the outer layer; 1) stratum basale, 2) stratum spinosum, 3) stratum granulosum, 4) stratum lucidum, and 5) stratum corneum (SC). The dermis layer is the second layer of the skin that is responsible for the sense of feeling and the generation of sweat. This layer contains sweat glands, oil glands, nerve endings, blood vessels, and hair follicles. The hypodermis is the fat layer of the skin and it is responsible for controlling the skin temperature and attaching the skin with muscles and bones [72, 73].

## **2.14 Functions of the Human Skin**

Human skin is the largest multifunctional organ of the human body. Its main function is protecting the human body from viruses, bacteria, dehydration (by maintaining water balance), and ultraviolet radiation damage as it provides a barrier between the human body and the external environment. Human skin is also responsible for temperature and thermal regulations, generation of vitamin D formation, destruction of microorganism, and sensation of pain, temperature (warm and cold), and mechanical sensation (pressure and touch) [72, 73, 75].

Human skin is different compared with other organs as it presents our interface to the external world, and it is the first part of the human body that can be seen by others and it provides an indication about the state of health of the human body through the appearance of the skin [76]. It is essential that human beings have healthy skin. During the cycle of life, human skin is affected by many factors such as the age, the environment, the interaction with different types of radiation, genetic defects, and accidents. These factors might cause diseases, temporal skin conditions, and permanent disorders.

## 2.15 Skin Conditions and Diseases

This section discusses different types of skin conditions and diseases as they will be considered in the half space model; these are 1) psoriasis, 2) eczema, 3) skin cancer (including malignant melanoma and basal cell carcinoma), and 4) burn wound.

### 2.15.1 Psoriasis

Psoriasis (chronic plaque psoriasis) is a chronic inflammatory disorder that has a genetic basis. This disorder makes the human skin red, itchy, painful, sore, flaky, produce a burning sensation, and it also makes crusty patches appear on the skin surface as illustrated in Figure 2.7. Psoriasis is usually developed in adulthood from both genders and it is affected around 2% of the UK population [77] and has a genetic basis. Stress, smoking, sunlight, and variation in hormones levels might trigger and increase its severity. Topical creams, phototherapy, oral therapies, and injected medicines can be used to reduce the severity of the condition [72, 73, 77].

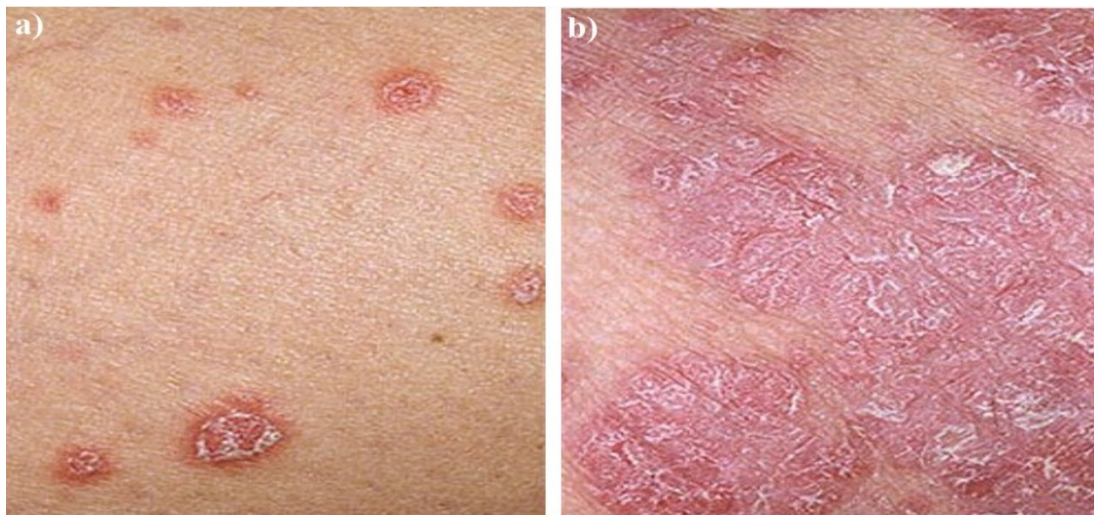


Figure 2.7: Illustration of chronic plaque psoriasis from less to more severe [78].

### 2.15.2 Eczema

Eczema (atopic eczema) is an inflammation combined with blisters. This condition makes the human skin itchy, cracked, dry, and red as illustrated in Figure 2.8. These signs usually appear on the hands, wrists, the face, inside the elbow, and on the back of the knee of both genders. Eczema is usually developed in childhood and it is caused and triggered by many factors such as genetic defect (expected to be the primary cause), diets, allergies to dust, family history, sweating, pollution, stress, and infection. Moisturising treatments and topical corticosteroids are applied to the skin when it is required to reduce the severity of eczema by reducing the dryness and the itchiness of the skin. Oral therapies and phototherapy are also used in the treatments of severe non-responsive cases. However, there is no cure for eczema. Nevertheless, treatment can be used to control eczema and this can be supported by self-treatment using emollients and bath oil [72, 73, 77].

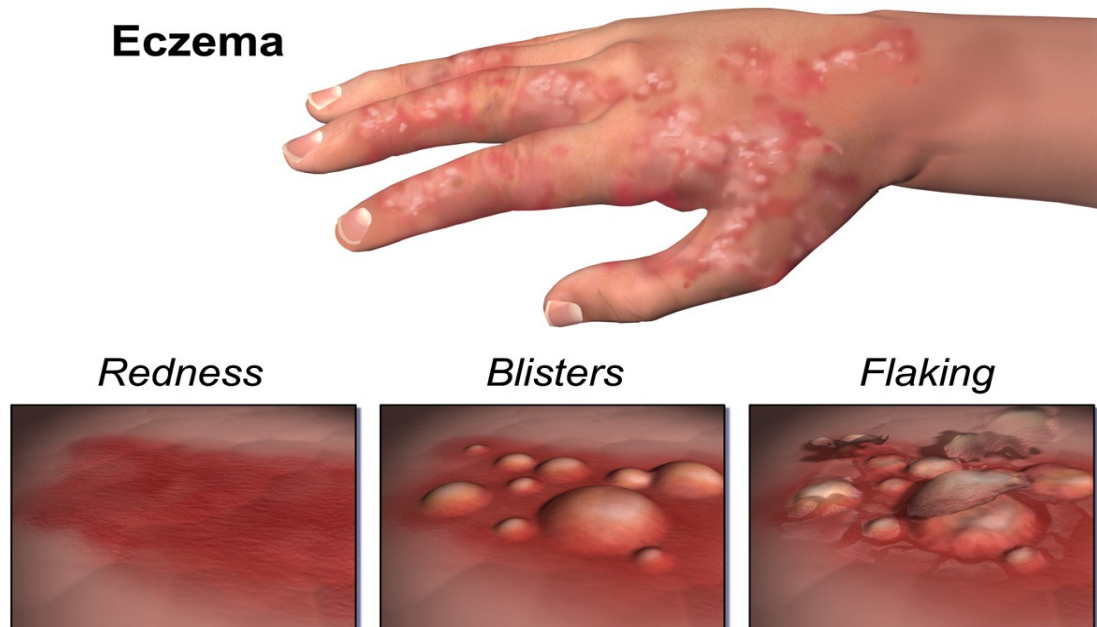


Figure 2.8: A schematic illustrates eczema and different signs appeared on the affected part of the human skin [77].

### 2.15.3 Melanoma

Melanoma illustrated in Figure 2.9 is a malignant skin cancer that affects the epidermal melanocytes and can spread quickly to other organs of the human body. Melanoma might appear either in an existing mole or in a newly developed mole that might be itchy, bleeding, and has an irregular shape. The main features of melanoma can be identified by the “**A**symmetrical shape, **B**order irregularity, **C**olour irregularity, **D**iameter > 6mm, and **E**volution of lesion. This is known as ABCDE symptoms rule” [77]. In the UK, about 2,000 people die annually from melanoma [79]. The main cause of melanoma is the exposure to ultraviolet (UV) radiation from the sun. Melanoma typically develops on the legs and trunk, appearing at any region on the body that is not protected from the exposure to the sun. Based on the patient circumstances melanoma can be treated mainly using surgery and radiotherapy. In addition, oral medication might be given to the patient to enhance the immune system and slow down the spread of the melanoma [72, 77].

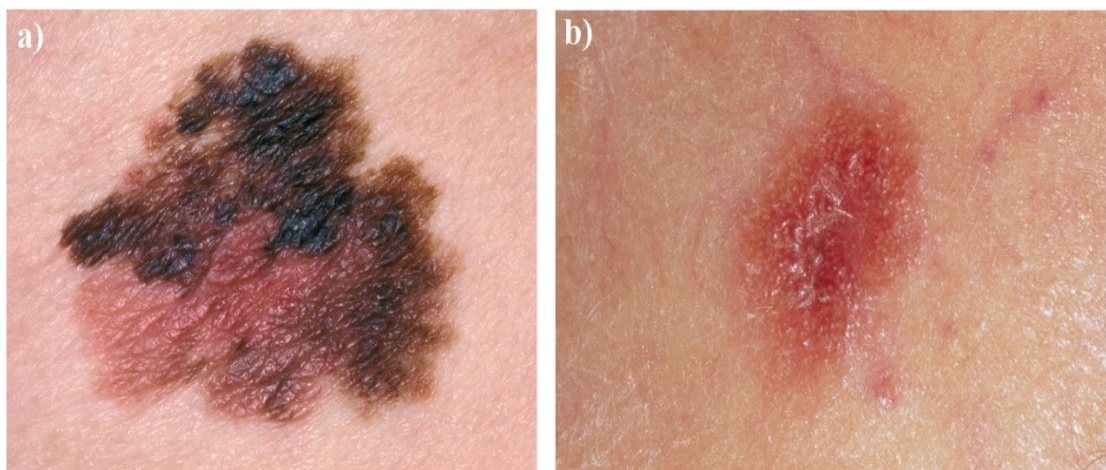


Figure 2.9: Illustration of different types of melanoma; a) a spreading melanoma and b) an amelanotic melanoma [79].

#### **2.15.4 Basal Cell Carcinoma**

Basal Cell Carcinoma (BCC) is the most common type of non-melanoma skin cancer that develops slowly in the epidermis layer of the skin as illustrated in Figure 2.10. BCC develops in the uncovered areas of the human body that are exposed directly to the UV radiation from the sunlight such as the neck, the face, and the head. Although UV radiation is the main cause of BCC cancer, other factors such as history of skin cancer, and sunburn might increase the chance of getting BCC. This disease can be diagnosed by taking part of the affected skin region and looking for characteristic signatures under magnification. This process is called a biopsy and it is widely used in the diagnostics of the skin conditions and diseases [72, 77]. BCC can be treated by either removing the affected part of the skin using a surgery or it can be treated using radiotherapy when the surgery is not appropriate. Although, around 90% of the patients having BCC are cured [77], regular monitoring of the skin is required as discovering the BCC in early stages reduces the chance of skin cancer development and increases the chance of patient recovery. BCC has different sizes, colours, and shapes (nodular, cystic, pigmented, and superficial).

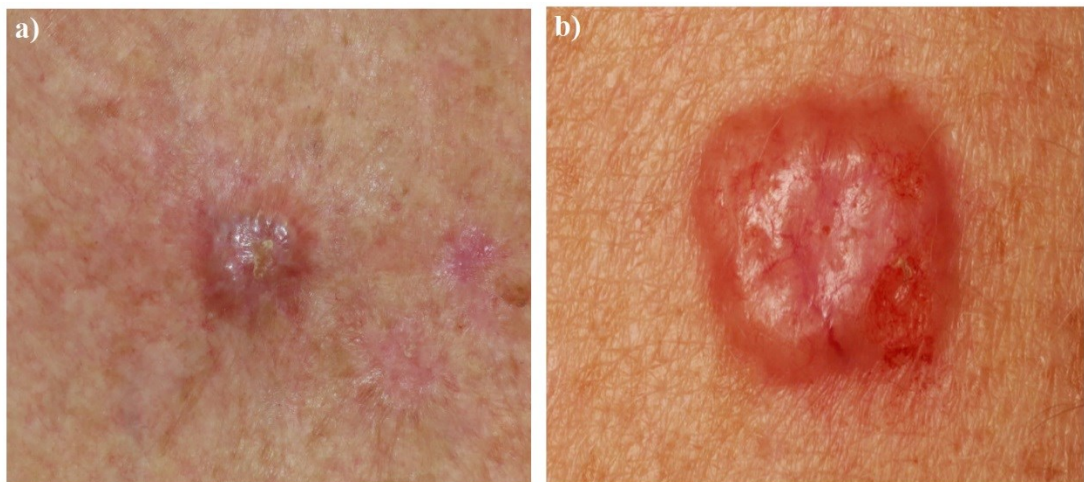


Figure 2.10: Illustration of shapes, sizes and colours of basal cell carcinoma [77].

### 2.15.5 Burn Wound

A burn is a thermal injury or damage caused by chemical, electrical, thermal traumas, and excessive sun exposure. Based on the depth of invasion, burns are classified into partial thickness (first and second degree) and full thickness (third and fourth degree) [72]; as illustrated in Figure 2.11. In medical practice, the treatments of burn injury are based on the degree of the burn, the severity of the burn, and the medical circumstances of the patient. As an example of this, the first-degree burn that can be treated using cold water, pain relief, creams, and bandages. Alternatively, the third and the fourth degrees burns required different treatments that might include surgery (surgical excision and grafting), rehabilitation, physical therapy, and lifelong assisted care.

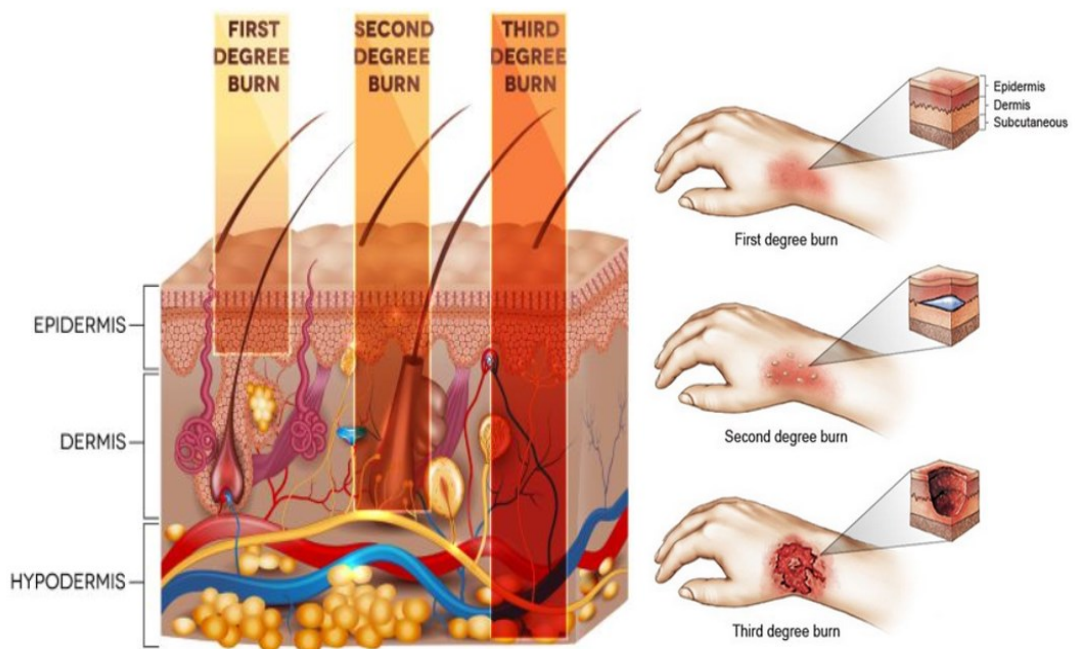


Figure 2.11: Illustration of different depth of invasion for burn injury [80, 81].

Human skin is a self-healing organ that can go through complex dynamic processes to re-establish and repair the damaged areas. During the healing progress, a wound goes through many phases and these are; 1) haemostasis, 2) inflammation, 3) proliferation, and 4) tissue maturation [72, 82]. There are variations in the healing process and these are dependent on the degree of the burn, the interaction of the human body with the burn, and the age of the patient. The skin might be repaired either successfully or it might fail to repair and this results in disorders and mortality. Characteristics and features for partial and full thickness burns are summarised in Table 2.6 [62, 72, 83].

Degree of burn	Depth of invasion	Signs	Degree of pain
First degree or Superficial	Epidermis	Looks red without blisters and scars.	Painful
Second degree or Superficial dermal	Papillary dermis	Looks red with swelling, blisters, moist, and scars.	Severe pain
Third degree or Deep dermal	Reticular dermis	Looks dry with pink and white colour and severe scarring.	Pain & sensitivity are minima.
Fourth degree or Full thickness	The tissue under the skin (fat layer and beyond)	Looks dry with white, brown or black colour and serious scarring.	No pain and no sensitivity because of nerve ending destruction.

Table 2.6: An overview of the main characteristics and features of the burn wound.

## **2.16 Technologies for Assessing Burn Wound and Skin Cancer**

Visual inspection is the current medical practice for assessing burn wound whereas skin biopsy is used for assessing skin cancer [3, 84]. Visual inspection involves the removal of dressing materials that might be uncomfortable and painful to the patient [3], and skin biopsy (shave, punch, and excisional) which is invasive as it involves partial removal of the affected part of the skin [84]. As an alternative to the current medical practice, technologies are emerging to enhance the medical assessment of burn wound and skin cancer [85, 86, 87, 88, 89, 90, 91, 92]. These technologies are; terahertz imaging [59, 85, 86, 87, 93, 94], optical coherence tomography [88, 89, 95, 96, 97, 98, 99], ultrasound imaging [90, 91, 100, 101, 102, 103], infrared imaging [92, 104, 105, 106], and microwave and millimetre wave sensing [55, 56, 57, 107], the latter is the subject of the research in this thesis.

### ***2.16.1 Terahertz Imaging***

The dependence of reflection and emission of terahertz radiation ( $\text{THz} > 300 \text{ GHz}$ ) to variation in water content in biological tissue makes terahertz imaging feasible for non-invasive diagnosis of skin cancer and burn wounds [59, 85, 86, 87, 93, 94]. The terahertz pulse imaging (TPI) results obtained from BCC tissue and scars burns in the study conducted by Woodward et al [85] indicate that BCC provides a positive contrast. Whereas, scar tissue provides a negative contrast compared with healthy tissue. TPI study applied on five patients and 18 ex vivo tissue having BCC by Wallace et al [108] indicates that the contrast between healthy tissue and BCC tissue is sufficient to identify tumour margins. Furthermore, the in vivo measurements of the refractive index and the absorption coefficient of healthy skin and skin with BCC conducted by Pickwell et al [58] indicate that normal skin has lower refractive index

and absorption coefficient than skin having BCC. A further in vivo study of TPI applied to the palm of the hand skin and the fingertips conducted by Cole et al [94] indicates the capability of terahertz radiation to distinguish between different hydration levels of a stratum corneum layer of the skin.

The terahertz time-domain spectroscopy (THz-TDS) introduced by Arbab et al [109] was used to obtain in vivo images from second and third degree burn wounds from rats. This study indicates a possible capability for THz-TDS to differentiate between partial thickness and full thickness burn wounds. The in vivo reflectivity measurements conducted by Arbab et al [110], indicate that the reflectivity of the burned skin is higher than that of the unburned skin. This can be supported by other in vivo terahertz images obtained from the rats' skin by Tewari et al [87]. This study shows dynamic variations in skin reflectivity following the burning process, an increase in the skin reflectivity was observed in the burned skin as a result of increased the water concentration due to the post-injury inflammatory response, whereas, lower reflectivity was observed in the surrounding unburned tissue. Although, terahertz imaging seems to be a promising technology for skin cancer, burn wound, and cancer margin detection, the low penetration depth in the human body of THz radiation are the main limitations.

Due to the limited penetration capability of THz radiation, magnetic resonance imaging (MRI) has been used with THz imaging to assess the burn wound as it can provide comprehensive information about the tissue water content (TWC) and the dynamic behaviour of the water in burn wound over a depth greater than 258  $\mu\text{m}$  [111, 112]. The clinical scanner of MRI penetrating the whole body has an in vivo spatial resolution of  $\sim 1.0$  mm [113]. The work conducted by Lohmann et al [114] indicates that the spatial resolution of the MRI can be enhanced in the range of  $(0.2 \times 0.2 \times 2.0$

mm<sup>3</sup>) to (0.328 x 0.328 x 0.6 mm<sup>3</sup>) using magnetic field strength of 7.0 Tesla and various imaging protocols. Although MRI can provide useful information to assess the severity of burns, there are limited measurements conducted in this area and this might be due to the very high cost of this technology. Therefore, it is still early to assess how much MRI might be useful for assessing the severity of the burn wound.

### ***2.16.2 Optical Coherence Tomography***

Optical coherence tomography (OCT) is a high-resolution (~10 μm) in vivo surface imaging that is suggested for use in medical applications and in the non-invasive diagnosis of burn depth [88, 95, 96, 97, 98], and skin cancer margin detection [89, 99]. The in vivo study conducted on female rats by Srinivas et al [95] suggests that polarization-sensitive optical coherence tomography (PS-OCT) might be feasible to assess the burn wound depth in the first two days only as increasing the water content and exudates due to edema formation present the main limitation. The high-resolution cross-sectional images obtained from the high-speed fiber-based PS-OCT by Park et al [96], indicate that the detectable amount of collagen content in the burn surface might be useful to assess the degree of the burn as severe burns have higher collagen content compared with superficial burns. The in vivo study applied on two human patients having superficial and full thickness burn wound by Kim et al [97] indicates that the three-dimensional images obtained from PS-OCT can characterise the burn wound based on vasculature and birefringence. Although, the in vivo study applied in a mouse model conducted by Zhao et al [88] indicates that spectroscopic optical coherence tomography (SOCT) shows significant differences in the spectra associated with the depth of the burn. However, this approach is not sufficient to assess the deep burns, as the penetration capability is only a few hundred microns from the skin

surface [88]. The conventional OCT has a spatial resolution of  $\sim 10 \mu\text{m}$  recorded at a penetration depth of 1.0 mm of the tissue [113]. According to Rayleigh [115, 116] scattering is inversely proportional to the wavelength and this makes the phase reconstruction of an image at depth, through the overlying tissue difficult.

As a plan for clinical usage, an efficient OCT system should be designed to have the following components and specifications; 1) a high-speed scanner that is capable of scanning the target area of the human body within a reasonable period of time combined with a high power source to illuminate the target area of the human body, and 2) the system should be able to display the images in real time [98]. When these considerations are met, OCT might be adapted clinically for assessing the burn wound.

### ***2.16.3 Ultrasound Imaging***

Ultrasound waves are high-frequency sound waves above the human hearing (typically greater than 20 KHz). These waves are used to generate images of the internal tissue and organs of the human body by using the reflected pulse echoes. The basic elements of the traditional ultrasound scanner are; a transducer (a hand-held probe) that is located and moved manually to scan the target area of the human body, and a water-based gel that is used to enhance the coupling between the probe and the human body [117]. Ultrasound imaging has been used in the diagnostics of skin cancer [90, 91, 100], in measuring the skin thickness [118, 119], and in the assessment of burn wounds [101, 102, 103]. The spatial resolution of the Ultrasound imaging is  $\sim 150 \mu\text{m}$  [113]. The study conducted by Rippon et al [101] indicates that ultrasound imaging at 20 MHz can visualise porcine skin (in vivo) and human tissue (cadaver) to a depth of 25.0 mm and therefore, it has been suggested as an alternative to biopsy in medical practice.

The in vivo study conducted on six Yorkshire pigs by Gnyawali et al [102] indicates that ultrasound imaging combined with a laser speckle might be an effective tool for the non-invasive diagnosis of wound healing progress. In addition, ultrasound imaging seems to be an efficient tool for providing qualitative information about the burn depth [120] and the collagen content [101]. Although non-contact ultrasound imaging has been developed to assess the burn depth [121], it has not been adapted clinically [103]. The main limitations of the ultrasound imaging are artefacts and clutter generated from unwanted reflected echoes [102].

#### ***2.16.4 Infrared Imaging***

Over the Infrared frequency band, a thermogram analyser (infrared camera) was used to examine the healing progress of the burn wound by estimating the surface area of the burn based on temperature detection [104]. In vivo thermographic images obtained from 65 patients having burns injury by Liddington and Shakespeare [92] indicate that thermography might be used to assess the burn depth within 72 hours post of injury, as deep burns expressed a significant variation in the temperature after 48 hours to 72 hours after the burn injury. The results presented in this study is in a good agreement with the results obtained from other studies conducted on two female pigs by Miccio et al [105]. Furthermore, the study conducted by Ruminski et al [106] introduces the active dynamic infrared thermal imaging as a technique to assess the burn depth. Although infrared imaging has been introduced as a non-invasive technique for assessing burn wound, it has not been adapted clinically due to the following limitations:

- Infrared imaging relies on variation in thermodynamics temperature and this might be measured in error due to the presence of exudates and blood flow.
- Infrared radiation has a very low penetration capability. Therefore, it provides information about the surface area of the skin only.

### ***2.16.5 Microwave and Millimetre Wave Imaging***

Microwave and MMW radiations are both non-ionising radiation that is capable of providing highly localised measurements. Therefore, they have been used in medical trials aimed at applications such as skin cancer detection [55, 56, 57], breast cancer detection [122, 123], non-invasive diagnosis of diseased skin [21], pain relief, and diabetes [26].

Microwave and MMW radiation techniques are very sensitive to the variations in water content in biological tissues. Since burn wounds cause significant variations in the water content of the tissue, as an immediate response to burn injury (that produces blood and lymph fluid), the radiation may be useful for assessing bandaged wounds [42, 107]. This idea initiated originally by Essen et al [107] as they were scanning in vivo images of the healing of the scars under the plaster of Paris using in-contact active scanner operating at 94 GHz. This work was followed by emissivity measurements conducted by Harmer et al [3] on a phantom chicken after the application of localised heat treatment. These measurements indicate that changes in surface emissivity of the skin samples are observable through dressing materials, indicating the feasibility of the MMW imaging to map changes in tissue emissivity for monitoring the state of burn wounds non-invasively and without the removal of dressing materials. Meanwhile, Gao and Zoughi [60, 62] conducted measurements on pigskin samples. These measurements suggested that MMW reflectometry could be used as a non-

invasive in-contact technique to distinguish between unburned and burned skin having different degrees of burn injuries; and more importantly, this study indicates the potential of using synthetic aperture radar (SAR) imaging to detect burn wound under dressing materials. As non-contact screening is desirable in medical applications, a half space electromagnetics model has been constructed and developed by Owda et al [124]. This model suggested the potential of using radiometry as a non-contact technique to distinguish between healthy skin and diseased skin (skin cancer, burn injury, and dry skin conditions). This is followed by another two studies conducted by Owda et al [125, 126]. These studies introduce active MMW radar for sensing and imaging through dressing materials over the band (15-40) GHz and radiometry as a non-invasive technique for assessing diseased skin.

## 2.17 Conclusions

This chapter has reviewed 1) the MMW radiation and its interaction with the human body, 2) the dielectric properties of the human skin, and 3) different technologies and methodologies that are proposed for assessing burn wound and skin diseases. Based on this review, the following challenges have been addressed in this thesis:

Although, human skin is the largest multifunctional organ in the human body, to date, no detailed investigations of a statistical nature have been carried out on the emissivity and the reflectance of the human skin. This research redresses this balance by analysing the emissivity of the skin at different locations of the hand and forearm, for subjects of different gender, ethnicity, age, body mass index, and for the skin in a wet and normal state, over the MMW band (80-100) GHz. These results will provide foundational measurements to support medical applications as discussed in chapter 4.

The relative complex permittivity measurements conducted on human skin in the literature survey indicate a well-defined difference between healthy skin and diseased skin. However, using a probe in contact with the human body and exposing the human body to man-made radiation are the main challenges that are needed to be considered. As an alternative; radiometry as a non-contact technique is suggested for a non-invasive diagnosis of skin diseases as illustrated in chapters 3, 4, and 5.

In the literature survey, different technologies are suggested for assessing burn wounds such as terahertz imaging, optical coherence tomography, magnetic resonance imaging, infrared imaging, and ultrasound imaging. Although the results obtained from these technologies are promising, none of these technologies successfully assesses the wound healing progress without the removal of dressing materials. As microwave and MMW radiation can penetrate dressing materials, this research will

assess the feasibility of using the microwave and MMW radiation for assessing bandaged wounds. This will be discussed in details using both passive and active microwave and MMW imaging systems in chapters 5, 6, and 7.

The following chapter discusses the half space electromagnetic model and the potential of using radiometry as a non-contact technique for the diagnostics of diseased skin.

## Chapter 3

### The Half Space Electromagnetic Model

*This chapter introduces the half space model and explains the structure of this model. Simulation results associated with healthy skin, skin with differing water contents, skin mutated by basal cell carcinoma, dry skin, wet skin, skin after the application of aqueous gel, and burn-damaged skin are presented and discussed in details.*

#### 3.1 Background

Skin is the largest organ of the human body, playing important roles in temperature and water regulation. In contact with the environment, it suffers a variety of damage: cancer arising from exposure to UV radiation; thermal burns from sources of heat; psoriasis and eczema from exposure to chemicals and through allergies. However, in response to this damage, the skin presents signatures, which can be measured using non-contact MMW sensors that could indicate the degree and the type of the damage. Radiation in the MMW band (30 GHz to 300 GHz) [9, 127] is ideally suited to measuring the skin as it interacts strongly and only with the skin layers of the human body [21, 24, 25, 45], thus enabling the potential for highly localised measurements.

It is well known that the level of water in the human skin changes as a result of damage. Water levels rise as a result of vascularisation around tumours and exudates from burns, while levels fall as a result of eczema or psoriasis [82]. Conveniently, water molecules has a very high dipole moment (1.85 Debye; 1 Debye =  $3.33 \times 10^{-30}$  coulomb. meter) [128], resulting in a high dielectric permittivity in the MMW band [24, 25, 45], which generates a large signature that can be measured using sensors in this band. Furthermore, the permittivity changes with frequency over the band

meaning lower frequencies can probe deeper into the skin layers, whilst higher frequencies can measure the surface of the skin.

Although the relative complex permittivity of the human skin can be measured easily using open-ended coaxial probes [42], such a device must be in contact with the sample under measurement. This requirement prevents use in scenarios where contact is not desirable or not possible. As non-contact screening is often desirable in medical applications and since coaxial probes are unable to provide measurements over large areas without being repeatedly placed in contact with the skin, a radiometric approach is a more appropriate solution.

A convenient metric to describe the condition of the human skin is the emissivity (fraction of the incident radiation that is absorbed), as this can be measured relatively easily using active (radar) and passive (radiometry) techniques [129, 130]. A half space electromagnetic model of the human skin is therefore developed to determine the emissivity of healthy skin and skin having a variety of medical conditions using either the relative complex permittivity or the complex reflectivity measurements of the skin over the MMW band.

The complex reflection coefficient for unburned and burned porcine skin samples have been taken over the band 30 GHz to 40 GHz from [62] with open-ended coaxial probes data from [48, 56, 63, 131]. Permittivity data were used from the parametric models such as the Cole-Cole model and Debye model [48, 52, 58, 59, 108].

### 3.2 The Half Space Electromagnetic Model

A half space electromagnetic model has been constructed to determine the emissivity of the human skin directly from measurements or calculations of either the relative complex permittivity or the complex reflectivity of human or animal tissue. In the half space model, the first half is a semi-infinite layer of air (incident medium), and the second half is a semi-infinite layer of skin (absorbing medium), as illustrated in Figure 3.1.

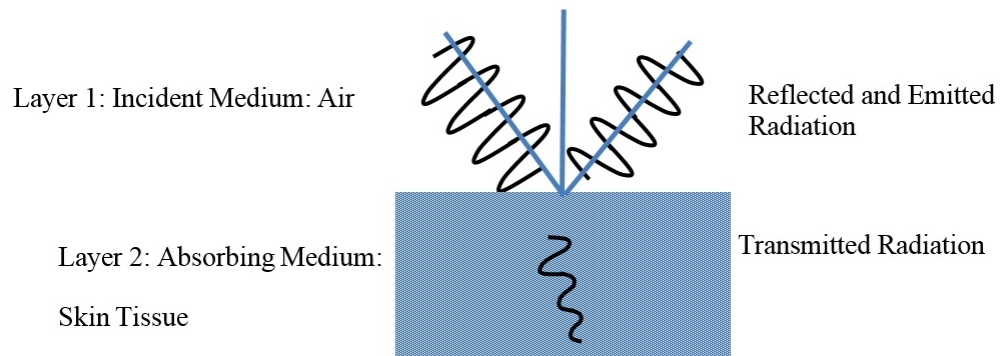


Figure 3.1: The half space model for calculating the emissivity of the skin.

In the half space model, the two layers are isotropic and homogenous and they can be described by their relative complex permittivity values. Conservation of electromagnetic energy in the model gives the relationship between the reflectance  $R$ , the transmittance  $T$ , and the emissivity  $\eta$ , at the skin surface as:

$$R + T + \eta = 1 \quad (3.1)$$

The relationship between the reflectance and the reflectivity (fraction of incident complex field amplitude reflected),  $\Gamma$ , can be expressed as:

$$R = |\Gamma|^2 \quad (3.2)$$

The relationship between the transmittance and the transmissivity (fraction of complex field amplitude transmitted),  $t$ , can be expressed as:

$$T = |t|^2 \quad (3.3)$$

In this model, it is assumed that skin is a specular reflector, which is reasonable, as the surface roughness of the skin (13.7 $\mu\text{m}$  to 66.0  $\mu\text{m}$  depending on the age) [132] is considerably less than the wavelength of the radiation. Therefore, in this half space model the normal and the parallel polarisation reflectivities of the skin can be determined by the Fresnel equations [67], which are:

$$\Gamma_n = \frac{\sqrt{\epsilon_1} \cos(\theta_i) - \sqrt{\epsilon_2} \cos(\theta_t)}{\sqrt{\epsilon_1} \cos(\theta_i) + \sqrt{\epsilon_2} \cos(\theta_t)} \quad (3.4)$$

$$\Gamma_p = \frac{\sqrt{\epsilon_2} \cos(\theta_i) - \sqrt{\epsilon_1} \cos(\theta_t)}{\sqrt{\epsilon_2} \cos(\theta_i) + \sqrt{\epsilon_1} \cos(\theta_t)} \quad (3.5)$$

Where,  $\theta_i$  is the angle of incidence,  $\theta_t$  is the angle of transmission,  $\epsilon_1$  is the relative complex permittivity of medium 1, and  $\epsilon_2$  is the relative complex permittivity of medium 2.

The normal and the parallel polarisation transmissivities (likewise from the Fresnel equations) are [67]:

$$t_n = \frac{2\sqrt{\epsilon_1} \cos(\theta_i)}{\sqrt{\epsilon_1} \cos(\theta_i) + \sqrt{\epsilon_2} \cos(\theta_t)} \quad (3.6)$$

$$t_p = \frac{2\sqrt{\epsilon_1} \cos(\theta_i)}{\sqrt{\epsilon_2} \cos(\theta_i) + \sqrt{\epsilon_1} \cos(\theta_t)} \quad (3.7)$$

The penetration depth of the MMW radiation in the human skin is 0.782-0.23 mm over the frequency band 30-300 GHz [24]. The short penetration depth is mainly due to the attenuating effects of water in the human body [26]. A consequence of this is that an

accurate electromagnetic model of the skin may be realised without knowledge of deeper tissue properties. This property also enables highly localised measurements to be made of skin which cannot be obtained in the visible region of the spectrum, and so potentially constitute the basis for a new viable non-contact diagnostic tool.

For an object that transmits no radiation ( $T=0$ ), the emissivity is equal to the fraction of the incident radiation that is absorbed, which becomes  $(1-R)$  as indicated by Equation (3.1). In a half space model, therefore, the emissivity can be calculated by integrating  $(1-R)$  over the air-side hemisphere. The reflectance is a function of polarisation and angle of incidence and thus integration over all angles and polarisation states is required to calculate the emissivity. The power incident over an area,  $dS$ , of skin is:

$$dP_{\text{incident}} = IdS \int_{2\pi} \cos(\theta)d\Omega \quad (3.8)$$

Where,  $d\Omega$  is the solid angle which defines the direction of propagation of the radiation relative to the normal to the area  $dS$ , and  $I$  is the power density from the incident isotropic sources in units of Watts per unit area, per steradian. Integration over the air-side hemisphere gives;

$$dP_{\text{incident}} = I\pi dS \quad (3.9)$$

The fraction of this incident power absorbed by the skin is then;

$$\begin{aligned} dP_{\text{absorbed}} &= IdS \int_{2\pi} (1 - R(\theta))\cos(\theta)d\Omega \\ &= I\pi dS \left( 1 - \int_0^{\pi/2} R(\theta) \sin(2\theta)d\theta \right) \end{aligned} \quad (3.10)$$

The emissivity  $\eta$  is the fraction of the incident radiation that is absorbed, hence, from Equation (3.9) and Equation (3.10) this is:

$$\eta = 1 - \int_0^{\pi/2} R(\theta)\sin(2\theta)d\theta \quad (3.11)$$

In the case of unpolarised sources, the reflectance  $R(\theta)$  must be replaced by the average of the normal and the parallel polarisation reflectances as:

$$R(\theta) = \frac{1}{2}(R_n(\theta) + R_p(\theta)) \quad (3.12)$$

Equation (3.11) provides a relationship between the emissivity and the complex permittivity of the sample. The integral in Equation (3.11), is not easily evaluated analytically and so a numerical approach developed by the author, implemented in Matlab, is used to compute the emissivity values.

The uncertainties in the simulated emissivity values can be determined by error propagation of uncertainties in the relative complex permittivity values through Equations (3.2 to 3.11). Given that, the uncertainty in the permittivity from the single relaxation Debye model is  $\pm 0.05$  [48, 133, 134, 135], error propagation indicates that the uncertainty in the emissivity of the skin is  $\pm 0.006$  unless otherwise stated; this is the case throughout this chapter.

### **3.3 Simulation Results from the Half Space Model**

Simulations of human skin emissivity are made using the half space model described by Equations (3.2 to 3.11); the model is used to predict the emissivity for the skin with differing water contents, skin mutated by basal cell carcinoma, dry skin, wet skin, skin after the application of aqueous gel, and burn-damaged skin.

### 3.3.1 Skin with Differing Water Contents (Psoriasis, Normal Healthy Skin, and Malignancy)

The relative complex permittivity of the skin with different water content is calculated from the measurement of the complex reflection coefficients of the skin over the frequency band of 30 GHz to 100 GHz [63]. From the relative complex permittivity data, the emissivity of the skin with different water content is calculated using the model discussed in section 3.2. The simulations of the emissivity of the skin for the three different water contents namely: 50%, 75%, and 95%, shown in Figure 3.2, correspond to water content that is representative of dry skin, normal healthy skin, and skin with malignant lesions respectively [45, 64, 136, 137].

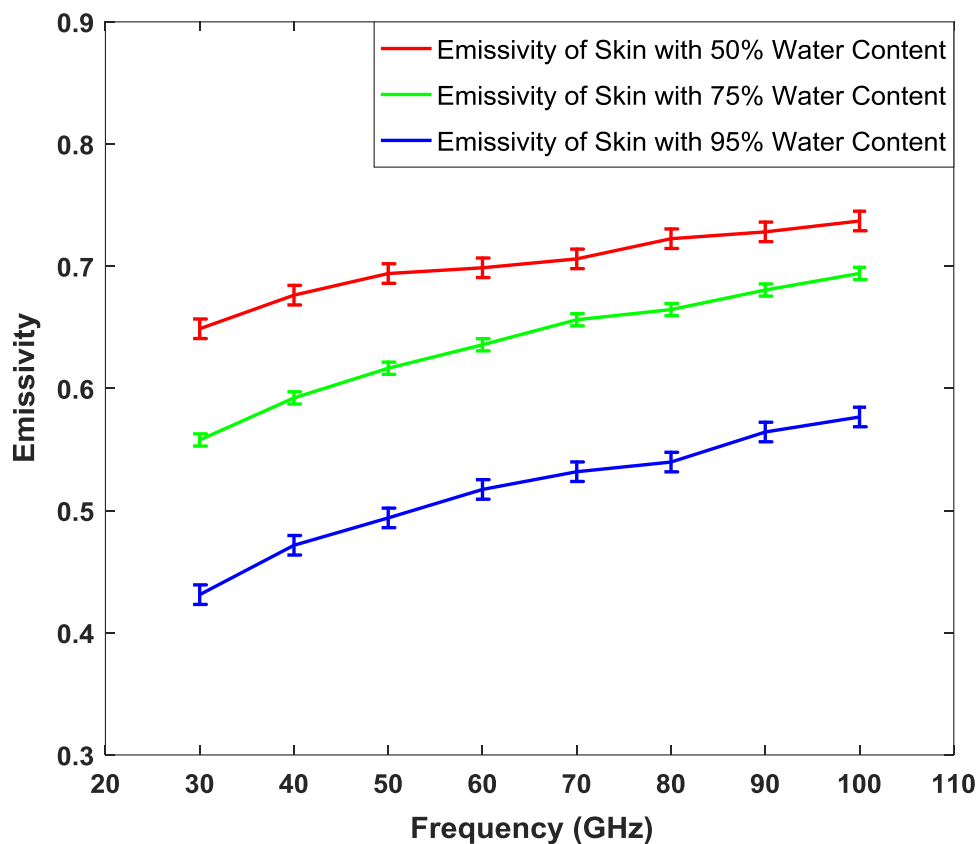


Figure 3.2: Simulations of the emissivity of the skin having different water contents.

The results presented in Figure 3.2 show that the emissivity of the skin with 50% free water content is higher than that of skin with 75% and 95% free water contents. The results also show how the emissivity of the skin rises with the frequency and falls with the skin water content. These results indicate that the emissivity of the skin with a 95% water content is lower by  $\sim 0.12$  than that of the normal healthy skin with a water content of 75%. This difference is due to high water content that strongly affects the relative complex permittivity and consequently the emissivity. Increasing the water content increases the magnitude of the relative complex permittivity and makes the skin more reflective, and as a result, the emissivity decreases. The properties and the characteristics of the skin with differing water content are summarised in Table 3.1.

Parameters	Skin type	Sources
Skin with 50% water content		
Skin condition	Dry: eczema & psoriasis	[136]
Return loss ( $S_{11}$ )	-9.22 dB at 100 GHz	[63]
Complex permittivity	6.86 - j3.33 at 100 GHz	[63]
Skin with 75% water content		
Skin condition	Healthy Skin	[45]
Return loss ( $S_{11}$ )	-8.59 dB at 100 GHz	[63]
Complex permittivity	7.34 - j5.71 at 100 GHz	[63]
Skin with 95% water content		
Skin condition	Skin with malignant lesion	[64]
Return loss ( $S_{11}$ )	-5.81 dB at 100 GHz	[63]
Complex permittivity	7.55 - j13.72 at 100 GHz	[63]

Table 3.1: Characteristics and parameters of the skin with differing water contents.

### 3.3.2 Skin Mutated with Basal Cell Carcinoma

The relative complex permittivity of healthy skin and skin with BCC is calculated in the frequency band 100-300 GHz using a two pole Debye model [58, 59, 108]. The parameters of the model were extracted from measurements performed on five patients [59, 108]. From the relative complex permittivity data, the emissivity of healthy skin and skin with BCC is calculated using the model discussed in section 3.2; and the simulation results are illustrated in Figure 3.3.

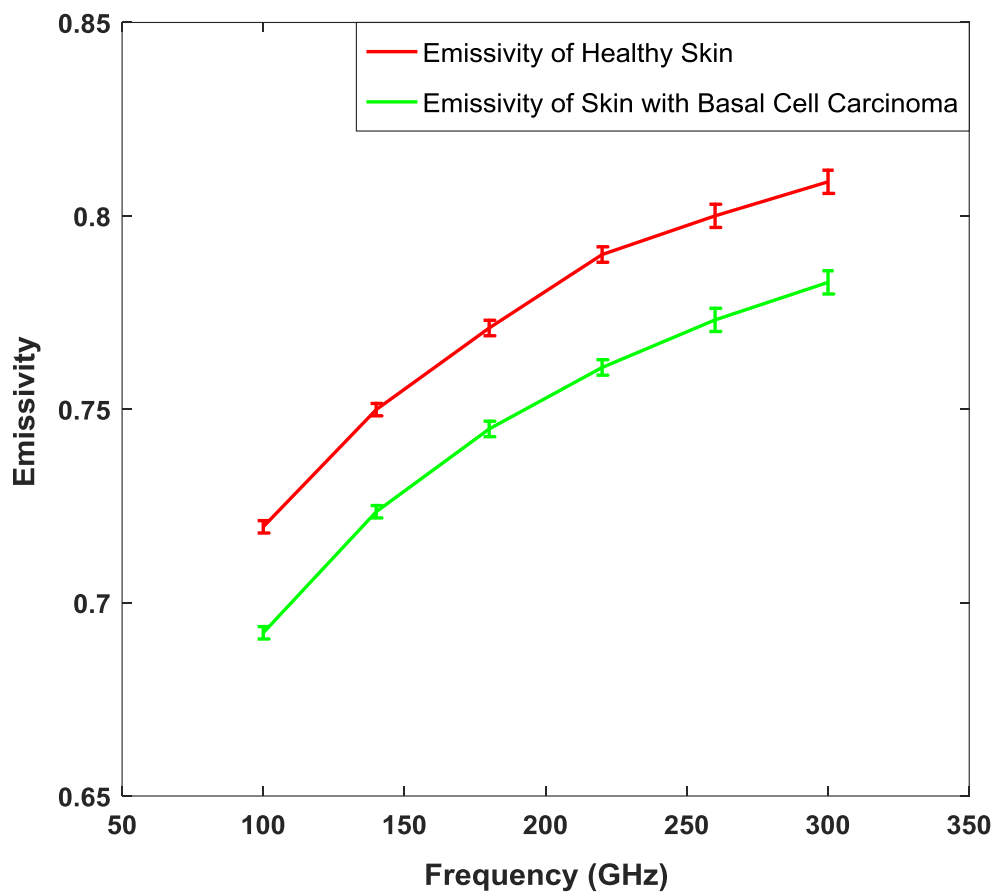


Figure 3.3: Simulations of the emissivity of healthy skin and skin with BCC.

The simulation results in Figure 3.3 indicate that the emissivity of the skin with BCC is  $\sim 0.03$  lower than that of normal healthy skin, the simulation indicates also that the emissivity rises with the frequency over the band (100 GHz - 300 GHz). The uncertainties in the simulated emissivity values over the frequency band are  $\pm 0.0016$  (100 GHz - 140 GHz),  $\pm 0.002$  (150 GHz - 220 GHz), and  $\pm 0.003$  (230 GHz-300 GHz), estimated by error propagation analysis through Equation (3.11).

Another study of skin with BCC using in vivo reflectivity measurements [56] has estimated the relative permittivity to be  $15.0-j20.5$  at 42 GHz, and that of healthy skin to be  $11.5-j14.3$ . Using these permittivity values in the half space model gives emissivity values of 0.52 and 0.57 for skin with BCC and healthy skin respectively. These results indicate that the emissivity of skin with BCC is  $\sim 0.05$  lower than that of normal healthy skin. These results indicate that radiometry might be used as a non-contact viable technique for early detection of BCC.

### ***3.3.3 Dry and Wet Human Skin Samples over the Band (90 -100) GHz***

In this simulation, a comparison is made between the emissivity of wet and dry skin samples taken from a human cadaver. The wet samples were taken from a 10% formaldehyde solution, rinsed in water and then measured, whereas the dry samples were dried for a 4.0 hours period prior to the measurements [46]. Measurements of the relative complex permittivity were made over the frequency band 90 GHz to 100 GHz [46] using the free-space method of the transmission and reflection coefficients, and these measurements were taken and used in the half space model to calculate the emissivity values of wet and dry skin, these being presented in Figure 3.4.

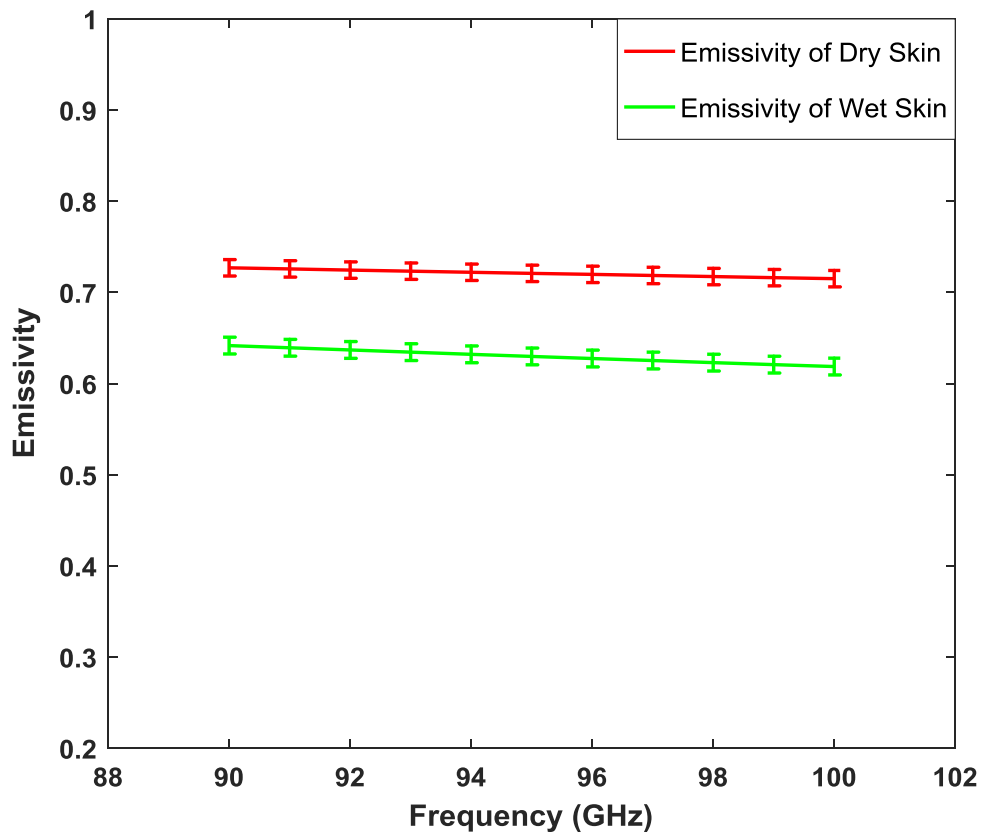


Figure 3.4: Simulations of the emissivity of samples of dry and wet human skin.

The simulation results in Figure 3.4 show higher emissivity values for dry skin, with the difference between dry and wet skin being  $\sim 0.09$  across the frequency band (90-100) GHz. This difference might be useful for the non-invasive diagnosis of skin diseases, where the disease significantly alters the water content of the skin. The results show also a slight decrease in the emissivity with the frequency and this is due to systematic uncertainty in the relative complex permittivity measurements obtained from the free space method (as discussed in chapter 2, section 2.7). The uncertainties on the skin emissivity values are estimated to be  $\pm 0.009$  over the frequency band 90 GHz to 100 GHz by error propagation analysis through Equation (3.11).

### 3.3.4 Skin after the Application of Aqueous Gel (30-100) GHz

In this section, a comparison is made between the emissivity of normal healthy skin and skin after the application of an aqueous gel (a mixture that consists mainly of water with a thickener, such as Ultrasound scan gel). This simulation uses the relative complex permittivity of in vivo skin [48]. The simulated emissivity rises over the frequency band from 30 GHz to 100 GHz, as illustrated in Figure 3.5:

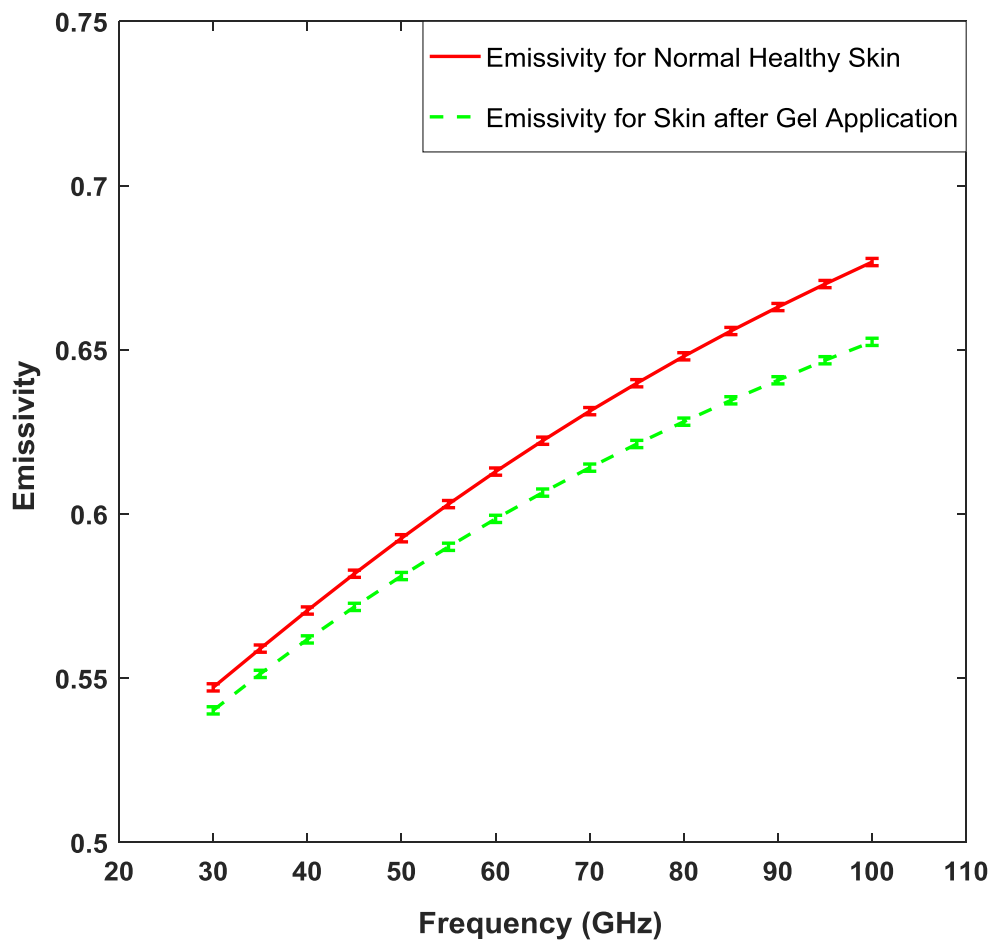


Figure 3.5: The simulated emissivity of healthy skin before and after it has been moistened by the application of an aqueous gel.

The simulation results in Figure 3.5 indicating that the emissivity of moistened skin is lower than that of the normal skin by an average value of 0.016 over the band (30-100) GHz. At 100 GHz, this difference in emissivity rises to  $\sim 0.025$ , with error propagation analysis indicating the uncertainty is  $\pm 0.0011$ .

Aqueous gel is used in the relative complex permittivity measurements to achieve good contact between the open-ended coaxial probes and the human skin. Adding gel to the human skin increases the hydration level of the stratum corneum layer of the skin and reduces the inhomogeneity of the skin [48, 134]. This improved the contact between the probe and the skin and reduces the systematic uncertainties in the dielectric permittivity measurements arising from the otherwise varying coupling between the probe and the skin. Furthermore, the gel that consists mainly of water can be used in the measurements of the dielectric properties of the skin in a wet state as it can stay adhered to the skin surface longer than the water. As there are complex logistics and ethical issues associated with performing measurements on patients [3] this type of modelling is convenient means for a first evaluation of damage effects on the skin tissue.

### ***3.3.5 Burned and Unburned Porcine Skin Samples (30-40) GHz***

Simulation of the emissivity of burned and unburned porcine skin is made using the complex reflection coefficient measurements conducted on the skin samples over the frequency band 30 GHz to 40 GHz [62]. The skin samples were taken after the animals had been slaughtered. The complex reflection coefficient measurements are used for calculating the emissivity of the skin as illustrated in Figure 3.6.

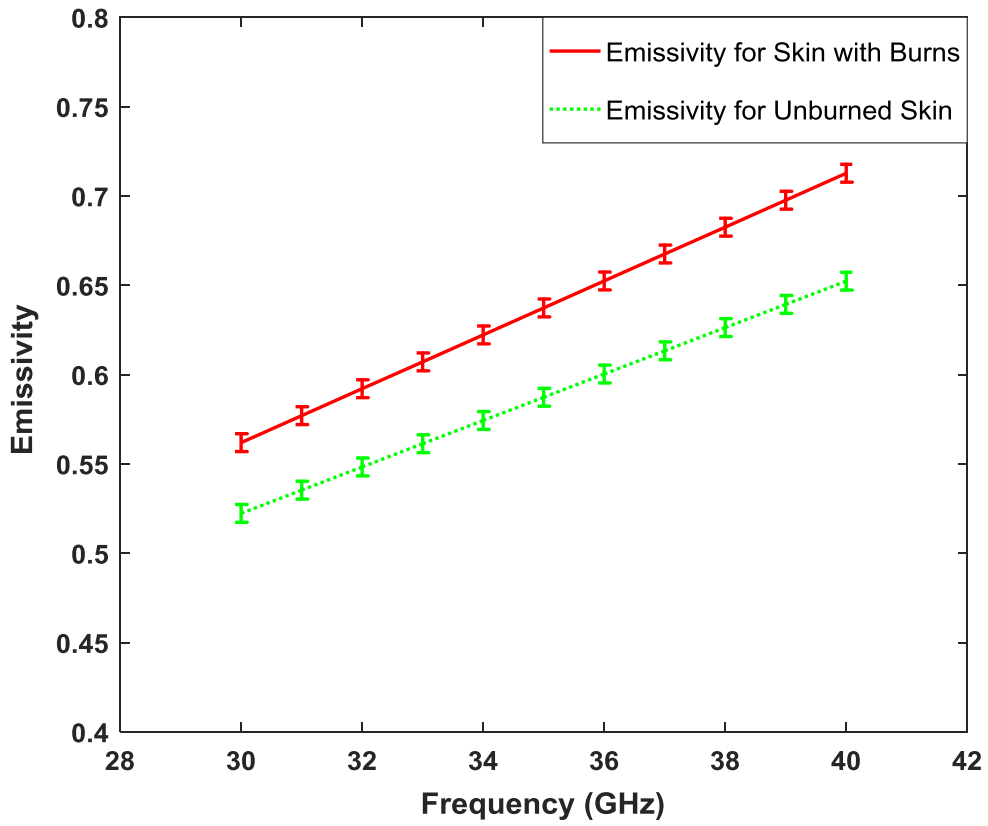


Figure 3.6: Emissivity of unburned and burn damaged porcine skin samples.

The simulation results in Figure 3.6 show a rise in emissivity with frequency and the results indicate that the burned skin has an emissivity of  $\sim 0.05$  higher than that of unburned skin. This increase is due reduced the water content in the skin, a direct result of the burning process. The absolute uncertainty in the measured emissivity is estimated to be  $\pm 0.005$  from error propagation analysis through Equation (3.11).

### 3.4 Model Comparison: Half Space versus Three-Layer Model

This section investigates the effects of possible reflections from deeper inner layers of tissue under the skin; a comparison is made between the half space model and the more complex three-layer model developed by the author [3]. The three-layer model comprises a semi-infinite layer of air, 1.44 mm layer of skin, and a semi-infinite layer of fat. The relative complex permittivity of skin is calculated from the measurement of reflection coefficients of skin [63], whilst the relative complex permittivity of fat tissue is calculated using Gabriel model [48]. The comparison between the two models is made for the skin with different water contents as shown in Figure 3.7.

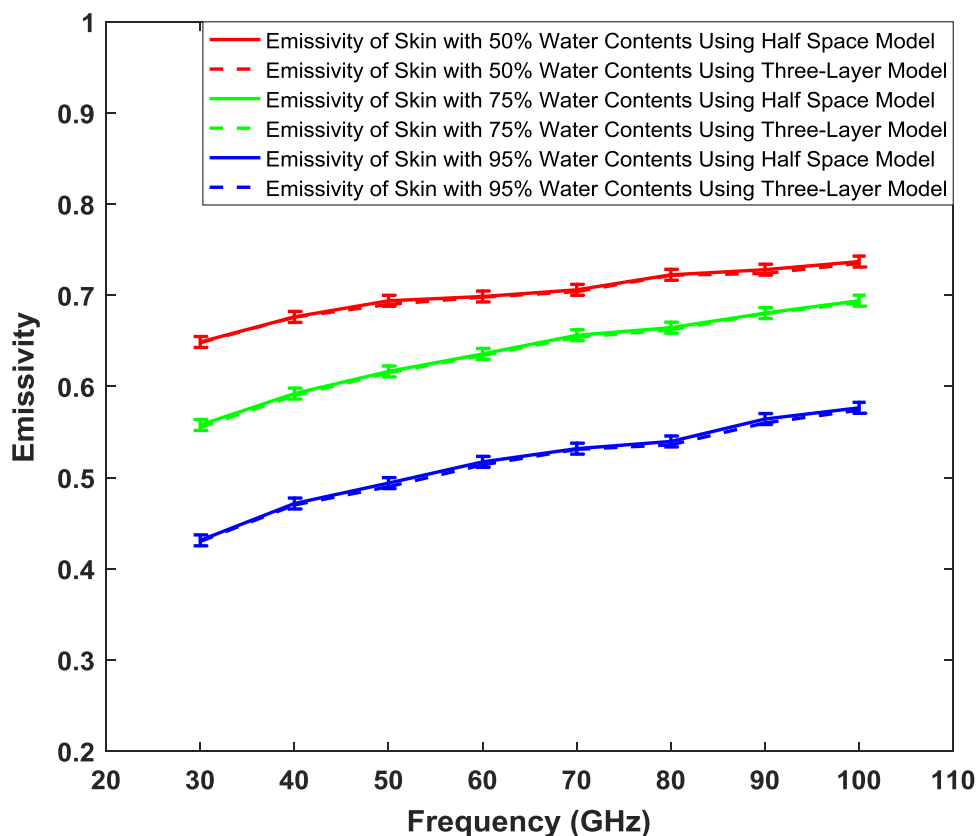


Figure 3.7: Comparison between the half space and the three-layer models.

The comparison between the half space model and the three-layer model in Figure 3.7 shows that the results from the half space model are the same as those for the three-layer model over the frequency band (30-100) GHz. This means that the deeper layers of tissue under the skin, consisting usually of fat doesn't change the emissivity of the skin in the MMW band. This means that the half space model is sufficient for use over the whole MMW bands as the penetration depths fall with increasing the frequency. The three-layer model was found to be redundant as discussed in [124]. For this reason, further results are discussed with reference to the simpler half space model.

### **3.5 Comparison of Skin Emissivity with Another Study**

The relative complex permittivity of healthy skin was measured experimentally over the band (20-37) GHz [131]. In this study, the mean value of the relative complex permittivity was used and converted into emissivity using the assumption that the human skin is a lossy dielectric and the reflection from inner layers is neglected. In the half space model, the emissivity of the skin is calculated over the band (30-37) GHz using the relative complex permittivity data in [131] and then compared with the emissivity values reported in [131] as shown in Table 3.2.

Frequency (GHz)	Emissivity calculated in [131]	Emissivity from the half- space model
30	0.61	0.59
31	0.62	0.61
32	0.63	0.61
33	0.64	0.62
34	0.65	0.62
35	0.66	0.63
36	0.67	0.64
37	0.68	0.65

Table 3.2: The simulated and the calculated emissivity of the palm of the hand skin.

The comparison in Table 3.2 shows a consistent rise in emissivity with frequency, with values from the half space model being 2.0% lower. This difference may be accounted for by the two slightly different ways in which the total reflectance is calculated. The study described in this chapter (using the half space model) is a refinement on the other study [131], integrating emission over the air-side hemisphere, which includes reflectance at all angles from normal to glancing incidence, whereas the other study [131] assumes a plane wave normal to the skin surface.

### 3.6 Discussion

Simulations of the emissivity of skin with varying water contents (50%, 75%, and 95%) in Figure 3.2 over the band 30 GHz to 100 GHz show that the emissivity rises with frequency but falls with the skin water content. This is due to the electromagnetic properties of water dominating the electromagnetic properties of the skin, providing a potentially viable, non-contact method to assist in the diagnosis of medical conditions where the skin water content is affected, such as eczema, malignancy, and psoriasis [55, 122].

Simulations of the emissivity of human skin with BCC over the band 100 GHz to 300 GHz indicate values are 0.03 lower than that of healthy tissue (as illustrated in Figure 3.3). This is consistent with the interpretation that BCC increases the local vascularisation, which through increased the blood flow, raises the water content of the tissue and resulting in reduced emissivity at the site. This indicates the potential opportunities of the technique for the initial detection of the basal cells, which may not easily be observed in the visible band of the spectrum due to the opacity of the epidermis.

Simulations of samples of wet and dry human skin indicate that the emissivity over the band 90 GHz to 100 GHz is lower for wet skin than for dry skin by  $\sim 0.09$  (as illustrated in Figure 3.4). The lower value for the wet skin is consistent with the high relative permittivity of water resulting in higher reflectance and therefore, lowers emissivity.

Simulations of the emissivity of human skin over the 30 GHz to 100 GHz band (illustrated in Figure 3.5), before and after the application of an aqueous gel indicate

that the gel reduces the emissivity at all frequencies on average over the band by  $\sim 0.016$ .

Simulations of the emissivity of porcine skin indicate that the burned samples have an emissivity of  $\sim 0.05$  higher than unburned samples (as illustrated in Figure 3.6). The interpretation here is that the burning process removes water from the skin, thereby reducing the reflectance and increasing the emissivity. For living organisms, however, a burn would result in exudates (mainly water) being introduced around the wound which would reduce the emissivity of the wound site. Knowledge of this and the transparency of bandages in the MMW region has led Essen et al [107] to investigate the feasibility of using MMW radiation to monitor the wound healing under plaster and hand support cast.

As simulated emissivities from the half space and the three-layer model of the human skin (illustrated in Figure 3.7) are identical (within the simulation uncertainty), radiation from the skin must originate from the layer not deeper than  $\sim 1.44$  mm, as that was the upper layer of the skin thickness in the three-layer model. This is consistent with the statement from Gandhi and Riazi [24] that radiation over the band 30 GHz to 300 GHz is absorbed within a distance of 0.782 mm to 0.238 mm from the surface of the skin. It also means that the simulation model of human skin using the half space model described in this chapter is valid over the whole frequency band 30 GHz to 300 GHz. These results also show a rise in the emissivity of skin with frequency, which is a behaviour that results directly from the decrease in the magnitude of the relative complex permittivity of water over this frequency band. As with other authors [21, 25], the author concludes that the water content of skin dominates the electromagnetic behaviour of the skin in the MMW band.

### **3.7 Conclusions**

Simulation results from the half space electromagnetic model show that emissivity of human skin rises from 0.43 to 0.81 over the 30 GHz to 300 GHz band and this behaviour is consistent with the fall in the magnitude of the complex dielectric permittivity of water over this region. Simulations show that the emissivity of the skin varies with the water content and this could be used as a metric to detect and monitor malignancy, eczema, psoriasis, and burn healing in skin. Simulations indicate that interaction of the MMWs is in the region from the skin surface to ~1.0 mm below the surface, with greater (or less) penetration at the lower (or higher) frequencies over the 30 GHz to 300 GHz band, suggesting opportunities for highly localised and selective skin layer measurements.

Simulations indicate that the emissivity of the skin could be exploited potentially for the diagnosis of a range of medical conditions. Research continues in this area to understand how and why the emissivity of the skin varies on samples of healthy participants as illustrated in chapter 4.

## Chapter 4

### **In Vivo Measurements for the Human Skin Emissivity**

*This chapter discusses the development of an experimental setup used to measure the human skin emissivity in vivo. Radiometers centred at 95 GHz and 90 GHz are calibrated and characterised for measuring the human skin emissivity. The measurements made on a sample of 30 healthy participants and two groups of 120 healthy participants (60 participants in each group) are presented and discussed in two separate experiments. Variation in emissivity over different regions on the hand and forearm, with age, gender, body mass index, ethnicity, and hydration level of the skin are presented and discussed.*

#### **4.1 Millimetre Wave Radiometry**

A radiometer is a device that is used to measure the thermal (Planck) radiation which looks like a thermal noise in character [138] and for radiation frequencies below the mid-infrared band ( $hf < kT$ ) the intensity of the emission is directly proportional to the thermodynamic temperature of the object, enabling calibration in degrees Kelvin [139]. Radiometers can be either a single channel or multiple channels (imaging radiometers). This chapter will discuss a single channel radiometer and chapter 7 will discuss the imaging radiometer.

The in vivo measurements of the MMW emission from the human body were made using a single channel radiometer. Such an instrument comprises of a receiving horn antenna (which collects the radiation), an amplifier, radio frequency filters, a detector (a square law detector that uses for generating an output voltage proportional to the input noise power), further video amplifiers, an integrator (which uses for averaging and smoothing the fluctuating voltage of the detector), and a data-recording device as illustrated in Figure 4.1.

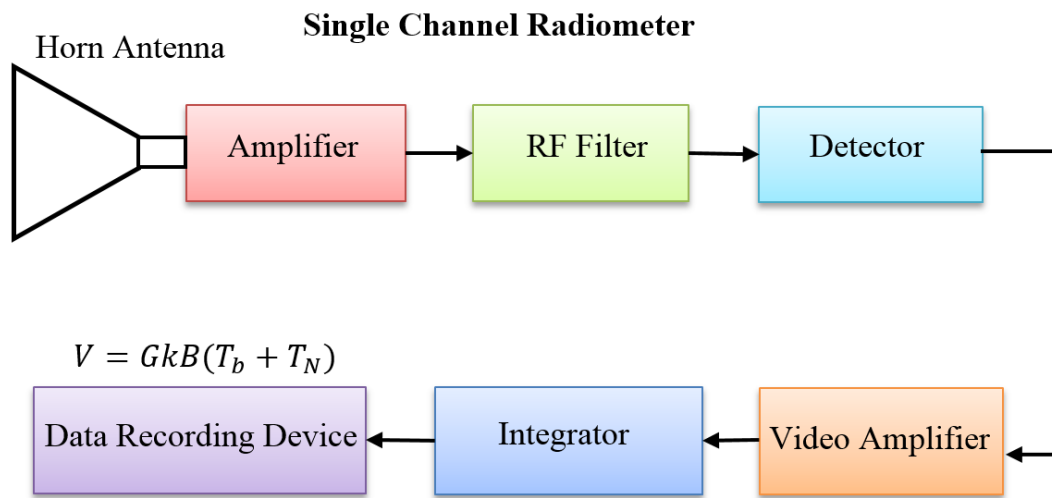


Figure 4.1: A block diagram shows the basic components of a single channel radiometer.

The minimum detectable radiation temperature variation  $\Delta T_{min}$  for a radiometer (thermal sensitivity) is given by the radiometer equation, namely [130, 139, 140]:

$$\Delta T_{min} = \frac{T_A + T_R}{\sqrt{B t}} \quad (4.1)$$

Where,  $t$  is the post-detection integration time,  $T_R$  is the receiver noise temperature,  $B$  is the receiver bandwidth, and  $T_A$  is the antenna radiation temperature, effectively the radiation temperature of the source in front of the antenna [140]. This constitutes the random uncertainty in the measurements for radiometers of this type.

From Equation (4.1) it can be seen that radiometric sensitivity can be enhanced either by increasing the integration time or the receiver bandwidth. However, a single channel radiometer and an imaging radiometer need to meet different scenario requirements so normally there is some compromise between the radiometric sensitivity, the rate at which images are generated and the cost and the size of the components.

In the general radiometric measurement scenario of a single channel radiometer, the horn antenna collects thermal radiation from a target, a general descriptor for the object under investigation. In this case, the target is the human skin and in these experiments, the area of skin to be measured is larger than the antenna pattern at the skin.

Materials in the MMW band have certain reflectance ranging from almost zero for highly absorbing materials to unity for metals. The level of reflectance is dependent on the dielectric properties of the materials and is described by the Fresnel equations (described in chapter 3, section 3.2). The skin also has a reflectance and as such measurement will include emission from the skin but also emission from the surroundings which becomes reflected from the skin into the radiometer antenna. The horn antenna is directed toward radiating thermal emissions from a target object, collects the emission, and generates a fluctuation voltage (the fluctuating voltage is a result of the radiometer equation (Equation 4.1)). Then the voltage level is amplified and detected through the receiver [138].

In radiometry, the total amount of radiation includes radiation from the target, radiation from the radiometer, and radiation from the environment; as illustrated in Figure 4.2. This radiation is dependent on the architecture of the radiometer and it is an essential requirement to distinguish between two types of received radiations; 1) the noise power received from the target source, and 2) the unwanted noise generated by the receiver (the noise temperature of the radiometer) [138].

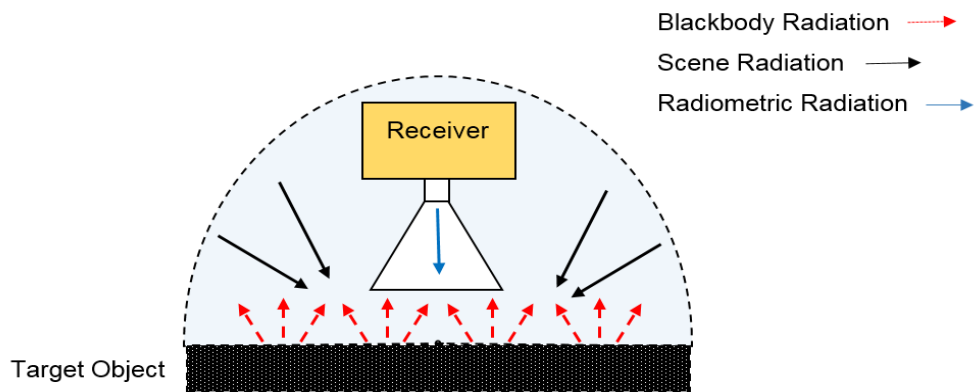


Figure. 4.2: General schematic for a radiometer collecting uniform thermal emissions from a blackbody (foam absorber). The horn antenna collects the emission and generates a fluctuating voltage, and the receiver amplifies and detects the emission.

## 4.2 Radiometric Calibration

Radiometric calibration is based on comparing the measured data of a known sample with its known standard value. In fact, this process is required for achieving a high quality of measurements with an acceptable level of uncertainty since the accuracy of the measuring devices reduces over the time due to frequent usage, electrical and mechanical factors and environmental effects [141]. Microwave radiometer can be calibrated using different methods namely; 1) liquid Nitrogen calibration (LN<sub>2</sub>), 2) tipping curve calibration technique, and 3) noise diode calibration [142, 143].

The LN<sub>2</sub> calibration method is the most common radiometric calibration method, as it is easy to apply and it provides accurate measurements. For precise and accurate LN<sub>2</sub> calibration, the following conditions should be met [142, 144]:

- A well-known reference sample should be used in the calibration measurements with a known standard emissivity value close to unity.
- The dimensions of the reference sample should be chosen to fill the beam pattern of the horn antenna.
- The temperature of the reference sample should be uniform, constant and known across the whole area.
- A large difference in temperature between the hot and the cold load calibration sources is required for achieving a predictable behaviour of the radiometer.
- Repetition of the calibration process is required for achieving long-term stable measurements and drifts corrections.

In radiometry, the external noise is introduced to the system through the receiving horn antenna. The sources of the external noise include lighting, gas discharge lamp and wireless devices. However, the internal noise or thermal noise is generated internally due to the motion of electrons. The power level of the thermal noise,  $P$  can be expressed in terms of the system bandwidth,  $B$  measured in Hertz, the absolute temperature,  $T$  in Kelvin, and Boltzmann's constant,  $k=1.38 \times 10^{-23}$  Joule/Kelvin as [138, 140]:

$$P = kTB \tag{4.2}$$

In microwave devices, the overall system noise can be identified by one parameter namely; the equivalent noise temperature or the effective noise temperature,  $T_N$  that can be measured using the Y-factor method illustrated in Figure 4.3:

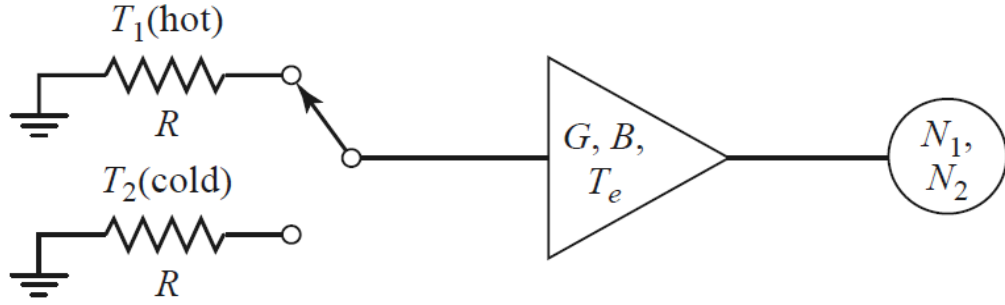


Figure 4.3: Schematic for the Y- factor method with hot and cold calibration loads [140].

The output noise power from the hot load  $N_1$  is a combination of the noise power from the hot load and the noise power from the amplifier [140]:

$$N_1 = GkT_1B + GkT_NB = GkB(T_1 + T_N) \quad (4.3)$$

Where,  $G$  is the amplifier gain and  $T_1$  is the hot load temperature in Kelvin.

The output noise power from the cold load  $N_2$  likewise is [140]:

$$N_2 = GkT_2B + GkT_NB = GkB(T_2 + T_N) \quad (4.4)$$

Where,  $T_2$  is the cold load temperature in Kelvin and it is less than  $T_1$ .

The Y-factor is defined as the ratio of the receiver output noise power when measuring the hot load source to that of measuring the cold load source [140]:

$$Y = \frac{N_1}{N_2} = \frac{T_1 + T_N}{T_2 + T_N} \quad (4.5)$$

Using the measured Y-factor, and the known temperatures for the hot and the cold load sources, the equivalent noise temperature can be calculated as [140]:

$$T_N = \frac{T_1 - YT_2}{Y - 1} \quad (4.6)$$

The noise figure is used for characterising the noise in the microwave devices, and it is defined as the ratio between the input signal to noise ratio,  $S_i/N_i$  to that of the output signal to noise ratio,  $S_o/N_o$  as [140]:

$$NF = \frac{S_i/N_i}{S_o/N_o} = \frac{N_o}{GN_i} = \frac{(T_o + T_N)}{T_o} \quad (4.7)$$

Equation (4.7) indicates that the noise figure, NF of an instrument is directly proportioned to the equivalent noise temperature,  $T_N$  and it is inversely proportional to the ambient temperature,  $T_o$ .

### 4.3 Antenna Parameters

The antenna is a system component that collects inward coming electromagnetic radiation, from one or a number of directions, and direct this, via transitions and transmission lines, to a receiver as in radiometry. Operating the other way around, it may direct radiation from a source outwards to an object, to illuminate it as in a radar system (that will be discussed in chapters 6 and 7). However, different frequency bands require different types of antennas that can be described and characterised by the following parameters [27]:

- Antenna pattern: is a three-dimensional graphical representation that measured the radiated field strength of the antenna using either rectangular or polar representations.
- Antenna radiation efficiency ( $E_f$ ): is measured how much input power radiated by an antenna. Usually, antennas with high efficiency radiate most of the input power whereas antennas with low efficiency absorb or reflect most of the input power.

$$E_f = \left( \frac{P_{rad}}{P_{in}} \right) \quad (4.8)$$

- Antenna bandwidth ( $B$ ): is the frequency range at which the antenna operates within an acceptable level of performance. The bandwidth of the antenna can be calculated as:

$$B = F_H - F_L \quad (4.9)$$

Where,  $F_H$  is the highest frequency, and  $F_L$  is the lowest frequency.

- Antenna gain ( $G$ ): is measured the ability of the antenna to direct radio frequency (RF) energy in a specific direction or pattern. An antenna with high gain is more efficient than that of low gain as it is capably to direct most of the RF energy toward a specific direction rather than all direction. The gain of the antenna can be expressed in terms of antenna directivity,  $D$  and antenna radiation efficiency,  $E_f$  as:

$$G = D \times E_f \quad (4.10)$$

- Polarisation: is defined by the orientation of the electric field within the electromagnetic wave. Antenna polarisation can be classified into a linear polarisation (either vertical or horizontal), a circular polarisation (either right or left-handed), and an elliptical polarisation (combination of linear and circular polarisation).
- Radiation intensity: is the ratio of the total radiated power of the antenna per unit of the solid angle.
- Antenna directivity ( $D$ ): is the ratio between the maximum radiation intensity of the antenna at a specific direction and the average radiation intensity of an isotropic antenna. The directivity of the antenna can be enhanced by using focusing components such as a mirror or lens. Although, this component enhance the directivity of the antenna. However, it increases the weight and the size of the antenna.

## **4.4 Experiment 1: Radiometric Measurements at 95 GHz**

The objective of this experiment is to study how the emissivity of the human skin varies between individuals and locations on the arm. This experiment represents the initial investigation about the emissivity of the human skin over the MMW band. In this experiment, the measurements were conducted at a centre frequency of 95 GHz on a sample of 30 healthy participants [124]. The measurements were made at four locations and these were: 1) the outer wrist, 2) the inner wrist, 3) the dorsal surface of the forearm, and 4) the volar side of the forearm. The measurement locations are illustrated in Figure 4.7.

### ***4.4.1 Participants and Ethical Approval***

Thirty healthy participants (18 males and 12 females) with no history of skin disease were measured in this experiment. The participants have ages ranging from 23 to 65 years. The study was approved by the ethics committee of Manchester Metropolitan University (ethics reference no: SE151630CA1). Written consent form was obtained from all participants before performing the measurements and all participants were informed that no skin care products were applied to the measured sites. The ethical approval for this study is attached in Appendix A.

#### ***4.4.2 Selection of Frequency***

The motivations for using the 95 GHz centre frequency are as follows:

- The 95 GHz frequency was chosen, as indications are that radiation at this frequency interacts mostly with the top 0.4 mm layer of the skin [21], and so is ideally suited to the measurements of the epidermis and the dermis layers of the human skin. The penetration depth of the millimetre wave radiation in the human skin as a function of frequency is illustrated in Figure 2.2 (chapter 2, section 2.4).
- Millimetre wave devices (radiometers, radars, low noise amplifiers, and detectors) are widely available and developed at 95 GHz as this transmission window provides a balance between the spatial resolution and the atmospheric absorption [8, 145].

#### ***4.4.3 Experimental Method for Measuring the Human Skin Emissivity***

The emissivity of the sample is defined as the fraction of thermal electromagnetic (Planck) radiation relative to the thermal blackbody radiation for a source at the same thermodynamic temperature [129]. Human skin emissivity can be measured using a radiometer, the output of such a device is a voltage  $V$  in volts, expressed as [3, 140]:

$$V = \alpha(T_b + T_N) \quad (4.11)$$

Where,  $T_b$  is the radiation temperature of the source (in this case the skin) expressed in Kelvin,  $\alpha$  is the receiver responsivity in Volts per Kelvin, and  $T_N$  is the receiver noise temperature in Kelvin. However, the radiation temperature of the source can also be expressed in terms of the source emissivity  $\eta$ , the skin thermodynamic (or physical) temperature  $T_s$ , and the background illumination radiation temperature  $T_0$  [146] as:

$$T_b = (1 - \eta)T_0 + T_s\eta \quad (4.12)$$

Calibration of this radiometer can be done using two blackbody radiator sources, one at a low temperature  $T_C$  and the other at a high temperature  $T_H$  [130, 140, 147]. This process calibrates the receiver responsivity and the receiver noise temperature, both of which are assumed to be constant, or alternatively, the system response is assumed to be linear. If the measurements are done indoors in an anechoic environment (where there is no radiometric emission from people or lower emissions from outdoors), the low temperature calibration source is a foam absorber at ambient temperature  $T_C$ . Under these circumstances, the output voltage when measuring the low temperature calibration source  $V_C$  becomes [140]:

$$V_C = \alpha(T_C + T_N) \quad (4.13)$$

and when measuring the high temperature calibration source  $V_H$ , the high temperature calibration source is a piece of foam absorber heated and stabilised at 53.8 °C, it is:

$$V_H = \alpha(T_H + T_N) \quad (4.14)$$

From this calibration procedure the receiver responsivity is:

$$\alpha = \frac{(V_H - V_C)}{(T_H - T_C)} \quad (4.15)$$

and the output voltage for the human skin target  $V_S$  is:

$$V_S = \alpha(T_b + T_N) \quad (4.16)$$

Using Equations (4.12, 4.15 and 4.16), and equating  $T_0$  to  $T_C$  the emissivity of the skin becomes:

$$\eta = \frac{(V_S - V_C)(T_H - T_C)}{(V_H - V_C)(T_s - T_C)} \quad (4.17)$$

Equation (4.17) indicates that the emissivity of the skin can be measured experimentally by measuring the output voltage and the thermodynamic temperature of the calibration sources (hot and cold) and the target area of the skin.

#### 4.4.4 Experimental Setup for Measuring the Human Skin Emissivity

A radiometer sensitive at 95 GHz was used for the measurements of the human skin emissivity. The equipment for measurement and calibration comprises a horn antenna connected through a circulator to a radiometer, two pieces of carbon loaded foam absorbers acting as hot and cold calibration sources (foam absorber type: Eccosorb AN-73), and the subject tissue to be measured, as illustrated in Figure 4.4.

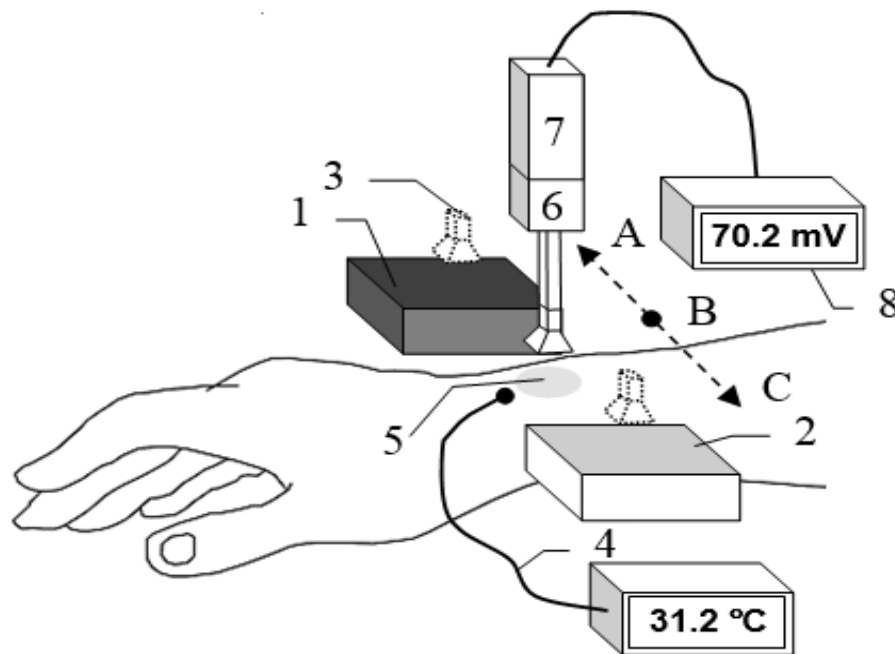


Figure. 4.4: In the experimental setup radiometric emission at 95 GHz is collected by a moveable horn antenna (3) at positions: A to measure a hot calibration source (1), B to measure the skin (5) and C to measure the cold calibration source (2), a thermocouple (4) is used to measure the thermodynamic temperature of the skin, a digital voltmeter (8) is used to measure the output voltage of the calibration sources and the skin. The horn antenna connected through a waveguide circulator (6) to a radiometer (7) that consists of a low noise amplifier and detector.

The radiometer (type: direct detector radiometer, manufacturer: Millitech) is essentially a low noise, high gain amplifier, followed by a detector, with sufficient sensitivity to detect the thermal (Planck) emission from ambient temperature sources over the frequency band (94-96) GHz. Radiometers have the performance metric of noise temperature measured in Kelvin; the lower the figure the more sensitive the system. The noise temperature of the radiometer was measured in the course of this research to be 430.5 K (using Equations 4.5 and 4.6), which represents a good performance for this application.

A circulator (model number: CR-10/95/2, manufacturer: ELVA-1) operating over the frequency band (94-96) GHz was placed between the horn antenna and the receiver. This device prevents radiation that has passed into the radiometer from being reflected back out of the system, which may be reflected from the subject back into the radiometer. Its function in the system is to minimise the effects of spurious signals which would otherwise arise from these retro-reflections. In trials to identify spurious signals, by reflecting emissions from the radiometer back into the receiver, none were found.

The complete system except for an opening for the subject to be measured was enclosed in an anechoic region made by surrounding the majority of the radiometer and antenna with carbon loaded absorbing foam (type: anechoic pyramidal absorber and dimensions per each piece are; length= 600 mm x width= 600 mm). This prevented radiation from external sources, be it from the outdoors or other people in the environment, getting into the system to corrupt signals.

A horn antenna (model number: 27240-20, manufacturer: Flann Microwave) has a rectangular aperture ( $20 \times 15 \text{ mm}^2$ ) and a nominal gain of 20 dBi, effective over the frequency band (90-100) GHz. During the experiment, the horn antenna was moved laterally by the hand to measure emission from the subject and from the hot and cold calibration sources in relatively quick succession. It typically takes about 1.0 min to complete this measurement process, allowing for a settling time, which minimises systematic errors associated with drift. The horn antenna during these measurements is located approximately  $\sim 10.0 \text{ mm}$  away from the sources and the antenna beam pattern on the skin is approximately 20.0 mm across.

The hot calibration source is stabilised at a temperature of  $53.8 \text{ }^\circ\text{C}$  with a precision that is smaller than a fraction of a degree by using a heat control metal plate (model number: SP2230-280H, manufacturer: SciQuip Ltd). The foam absorber was placed on the metal plate after the metal plate is heated and located in a polystyrene foam bucket that transparent to MMW radiation. The cold calibration source remains at the ambient temperature of  $23.0 \text{ }^\circ\text{C}$ , as maintained by the building central heating system. The carbon loaded foam absorbers used in this experiment (type: Eccosorb AN-73, manufacturer: Laird) have measured emissivity values greater than 0.99 as reported in [148, 149], thus they behave as good approximations to a black body emitter.

Regions of the human body measured by this method were areas on the wrist and forearm. A standard thermocouple (model number: L812, manufacturer: Leaton) was used to measure the skin surface temperature in these regions directly, before and after the measurement. The temperature is indicated via a digital readout with a  $\pm 0.5 \text{ }^\circ\text{C}$  absolute measurement uncertainty and  $0.1 \text{ }^\circ\text{C}$  step size. An infrared thermometer (model number: N85FR, manufacturer: Maplin) was used to measure the thermodynamic temperatures of the calibration sources and had an absolute

measurement uncertainty of  $\pm 1.5$  °C. The devices are cross-calibrated by measuring the temperature of the same source, so the relative uncertainty of the measurement is much smaller, typically less than 0.1 °C. The typical voltage measurements were up to 100 mV with a precision of 0.1 mV. Error propagation through Equation (4.17) indicates the uncertainty on the measured emissivity is  $\pm 0.002$ .

#### ***4.4.5 Experimental Results***

The emissivity of the human skin was measured experimentally using the calibrated radiometer of Figure 4.4 and Equation (4.17). The measurements were performed at a centre frequency of 95 GHz on a sample of 30 healthy participants. The measurements were repeated five times at each location to grade against the systematic errors. The mean emissivity values were calculated and represented for all participants, as illustrated in Figures (4.5 and 4.6).

##### ***4.4.5.1 Experimental Results from the Whole Sample***

Statistical analysis of the measurements of the human skin emissivity of a sample of 30 healthy participants are summarised in Table 4.1 as:

Location	Mean emissivity ( $\mu$ )	Standard deviation ( $\sigma$ )	Standard error in the mean ( $\sigma/\sqrt{30}$ )
The outer wrist	0.417	0.0598	0.0109
The inner wrist	0.357	0.0616	0.0112
The dorsal surface	0.476	0.0957	0.0175
The volar side	0.400	0.0950	0.0174
All locations	0.413	0.091	0.0166

Table 4.1: Statistical analysis of the data for a sample of 30 healthy participants.

Experimental results in Table 4.1 indicate that there are differences in the mean emissivity values between different locations on the arm. The sample mean of the differences in the mean emissivity values between the outer and inner wrist locations is 0.06 with a sample standard deviation in the differences of 0.035, generating an error in the mean ( $\sigma/\sqrt{n}$ , where  $n$  is the number of samples) of 0.0064. This difference is 9.3 times the standard error, indicating consistent differences in the mean emissivity values between the outer wrist and the inner wrist locations.

The sample mean of the differences in the mean emissivity values between the dorsal and the volar side of the forearm is 0.076 with a sample standard deviation in the differences of 0.041, generating an error in the mean of 0.0075. This difference is 10.1 times the standard error, indicating consistent differences in the mean emissivity values between the dorsal surface and the volar side of the forearm skin. Upon closer inspection, these differences are related to the thickness of the skin layers.

#### ***4.4.5.2 Experimental Results from Female Measurements***

Measurements of human skin emissivity for a sample of 12 female participants show consistent variations in the mean emissivity values between individuals and at different locations on the arm of individuals. The measurements in Figure 4.5 show that the mean emissivity values for the dorsal surface and the outer wrist locations are higher than the volar side and the inner wrist locations.

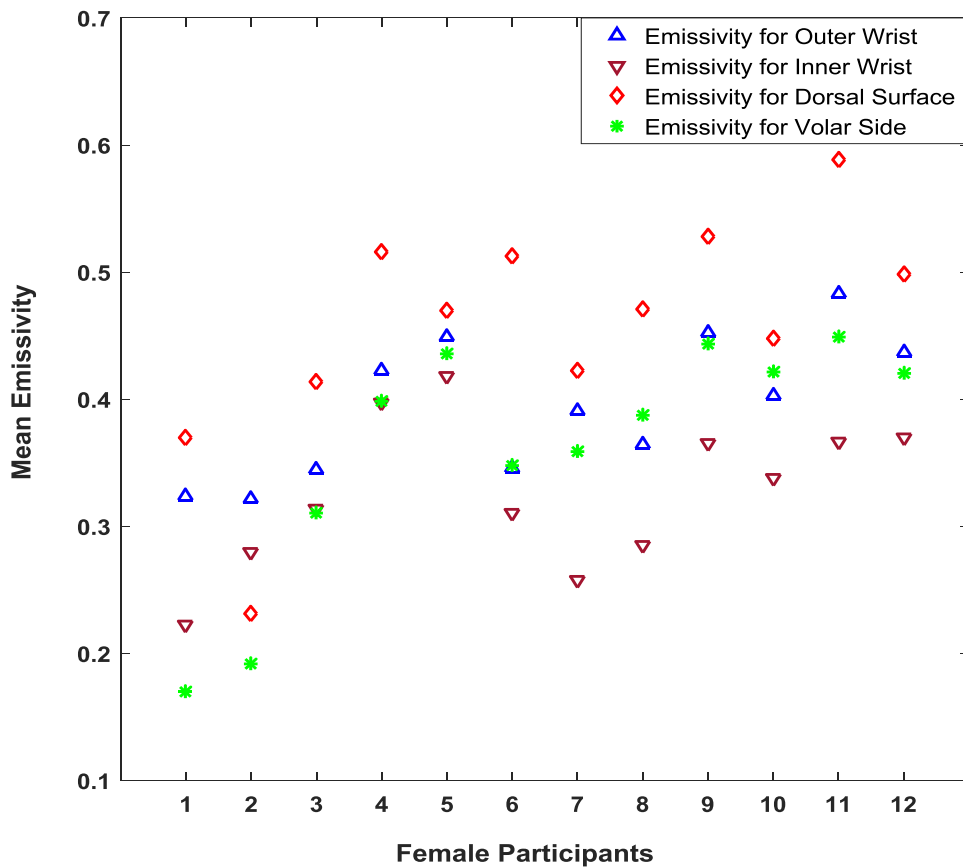


Figure 4.5: Mean emissivity values for a sample of 12 female participants.

Measurements in Figure 4.5 indicate that females have a sample mean emissivity of 0.3846 with a sample standard deviation of 0.0877, generating a standard error in the mean of 0.0253. Statistical analysis indicates that the mean differences in the emissivity values between the outer and the inner wrist, and the dorsal and the volar regions are 0.0678 and 0.0948 with a sample standard deviation in the differences of 0.0365 and 0.0535 respectively. These differences are significant as the  $p$ -values i.e (the  $p$ -value for the inner and the outer wrist locations is  $49 \times 10^{-6}$  and the  $p$ -value for the dorsal and volar regions is  $73 \times 10^{-6}$ ) obtained from the paired t-tests are less than the critical significance level of 0.05. An overview of the statistical analysis for the human skin measured emissivity values over a sample of 12 female participants are summarised in Table 4.2 as:

Location	Mean emissivity ( $\mu$ )	Standard deviation ( $\sigma$ )	Standard error in the mean ( $\sigma/\sqrt{12}$ )
The outer wrist	0.395	0.0524	0.0151
The inner wrist	0.327	0.0565	0.0163
The dorsal surface	0.456	0.0878	0.0254
The volar side	0.361	0.0899	0.0259

Table 4.2: Statistical analysis of the data for a sample of 12 female participants.

#### ***4.4.5.3 Experimental Results from Male Measurements***

The emissivity measurements from 18 male participants in Figure 4.6 show a similar trend to that of females in terms of the differences in the mean emissivity values between the thicker skin region (outer wrist and dorsal surface of the forearm) and the thinner skin region (inner wrist and volar side of the forearm). The results obtained from the paired t-tests of male participants indicate significant differences in the mean emissivity values between the inner and the outer wrist locations ( $p$ -value =  $4.0 \times 10^{-6}$ ) and the dorsal and volar regions ( $p$ -value =  $1.104 \times 10^{-8}$ ). The measurements indicate that males have a sample mean emissivity of 0.431 with a sample standard deviation of 0.0878, generating a standard error in the mean of 0.0207. Although the sample mean of the emissivity values of the male participants are higher by 0.0464 than those of the female participants. However, the results obtained from the unpaired t-test indicate that these differences are insignificant as the  $p$ -value (0.2433) is greater than the critical significance level of 0.05. This is due to the small number of human subjects that involved in this study (18 males and 12 females).

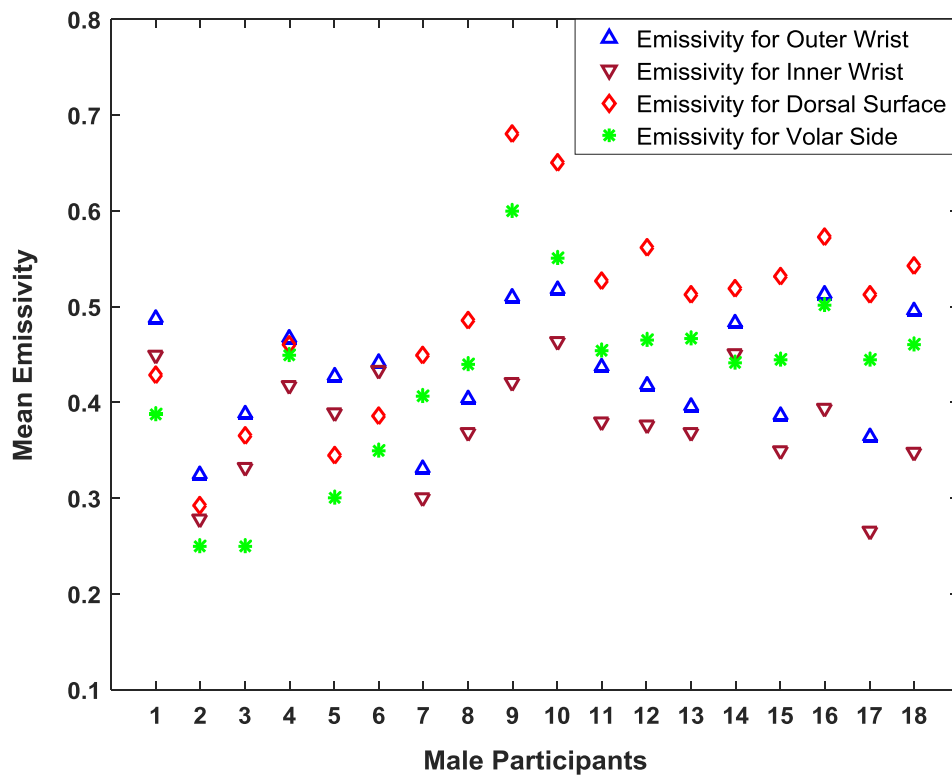


Figure 4.6: Mean emissivity values for a sample of 18 male participants.

An overview of the statistical analysis for the human skin measured emissivity values over a sample of 18 male participants are summarised in Table 4.3 as:

Location	Mean emissivity ( $\mu$ )	Standard deviation ( $\sigma$ )	Standard error in the mean ( $\sigma/\sqrt{18}$ )
The outer wrist	0.432	0.0596	0.0141
The inner wrist	0.377	0.0565	0.0133
The dorsal surface	0.490	0.0982	0.0232
The volar side	0.426	0.0894	0.0211

Table 4.3: Statistical analysis of the data for a sample of 18 male participants.

#### ***4.4.6 Discussion***

Radiometric measurements made on a sample of 30 healthy participants at 95 GHz indicate that there is a scatter over the range from 0.2 to 0.7 with experimental measurements uncertainty of  $\pm 0.002$ . Calculating the sample mean emissivity values for the 18 males and the 12 females separately over all measurement locations indicates that the sample mean of the males are higher by 0.0464 than those of females. This finding is consistent with the skin of males being thicker than that of females [150, 151, 152].

Radiometric measurements of the human skin emissivity indicate variation in the mean emissivity values of the skin between individuals and locations. It is likely that these variations are due to the water content and the skin thicknesses that varies between individuals and locations on the arm. This capability could potentially be exploited for the diagnosis of a range of medical conditions and this is strongly supported by the simulation results obtained from the half space model in chapter 3.

Measurements of the differences in the mean emissivity values between the inner and the outer wrist, and between the dorsal and the volar regions of the forearm of all 30 participants are in the range of 0.06 to 0.076. These differences being approximately 10 times the standard errors in the mean and they are likely to be due to the much thicker skin on the outer wrist and the dorsal area of the forearm. The thinner skin on the inner wrist and volar regions [82, 153] means that radiation is more readily reflected from the blood vessels [154] and this increases the reflectance of the skin and reduces the emissivity. These measurements indicate the potential for a non-contact method of diagnosing a variety of skin conditions using MMW radiometers.

Based on the results presented herein, it is recommended that further measurements be made on larger and more varied groups of individuals to investigate possible links between variations in emissivity and other factors such as the body mass index, the gender, the age, and the ethnicities of the participants and also the hydration level of the skin. This will be discussed in details in the following section (experiment 2).

## **4.5 Experiment 2: Radiometric Measurements (80-100) GHz**

A radiometer, integrating the emission over the frequency band 80 GHz to 100 GHz, was used for measuring the human skin emissivity. The measurements were conducted on two groups of healthy participants and there were 60 participants in each group.

The objectives of this experiment are summarised as follows:

- Assess variations in emissivity between individuals and locations on the arm.
- Assess variation in emissivity between males and females participants.
- Assess variation in emissivity between participants having normal and high body mass index from both genders.
- Assess variation in emissivity between participants having Asian and European ethnicities from both genders.
- Assess variations in emissivity between normal and wet skin from both genders.
- Assess variations in emissivity between different age groups from both genders.

#### ***4.5.1 The First Group of Healthy Participants***

Sixty healthy adult participants (36 males and 24 females) having a variety of ethnicities, ages, and body mass index were measured in this experiment. The participants have ages ranging from 20 to 67 years. The participants have a mean and a standard deviation ( $\pm$ SD) in mass:  $72.5 \pm 13.92$  kg, and height:  $1.66 \pm 0.099$  m. The male group comprised: 12 Europeans (UK), 12 Asians (Middle Eastern), and 12 others of different ethnicities. The female group consisted of 12 Europeans (UK) and 12 Asians (Middle Eastern). The ethics of the study was approved by the ethics committee of Manchester Metropolitan University and a written consent form was obtained from each participant (ethics reference no: SE151630CA1). The ethical approval for this study is attached in Appendix A.

#### ***4.5.2 Selection of the Millimetre Wave Band***

The millimetre wave band offers a higher spatial resolution measurement capability than the microwave band, with a spatial resolution down to approximately half wavelength and a penetration in the skin of up to around 1.0 millimetre it offers a deeper probing capability than the terahertz ( $>300$  GHz) systems [21] and as such it is ideal for measuring the epidermis and the dermis layer of the skin. The penetration depth of the millimetre wave radiation in the human skin as a function of frequency is illustrated in Figure 2.2 (chapter 2, section 2.4).

### 4.5.3 Choice of Measurement Locations

In the first group of 60 healthy participants, the measurements were made at six locations on the arm and these were: 1) the palm of the hand, 2) the back of the hand, 3) the inner wrist, 4) the outer wrist, 5) the volar side of the forearm (50 mm from the inner elbow), and 6) the dorsal surface of the forearm (50 mm from the outer elbow) as illustrated in Figure 4.7. These locations were chosen as they provide variations in skin thickness and water content all of which vary with age, gender, ethnicity, body mass index, and location on the body [71, 150, 151, 155, 156, 157, 158]. To identify possible variation in human skin emissivity due to the presence of hair, the emissivities for the dorsal surface skin were measured before and after shaving the hair. These measurements were conducted on a female participant and the results obtained indicate that the mean emissivity value of the skin is  $(0.5 \pm 0.005)$  for both hairy and hairless dorsal surface skin. These measurements confirm that there is no effect of the hair on the emissivity of the skin over the frequency band (80-100) GHz.

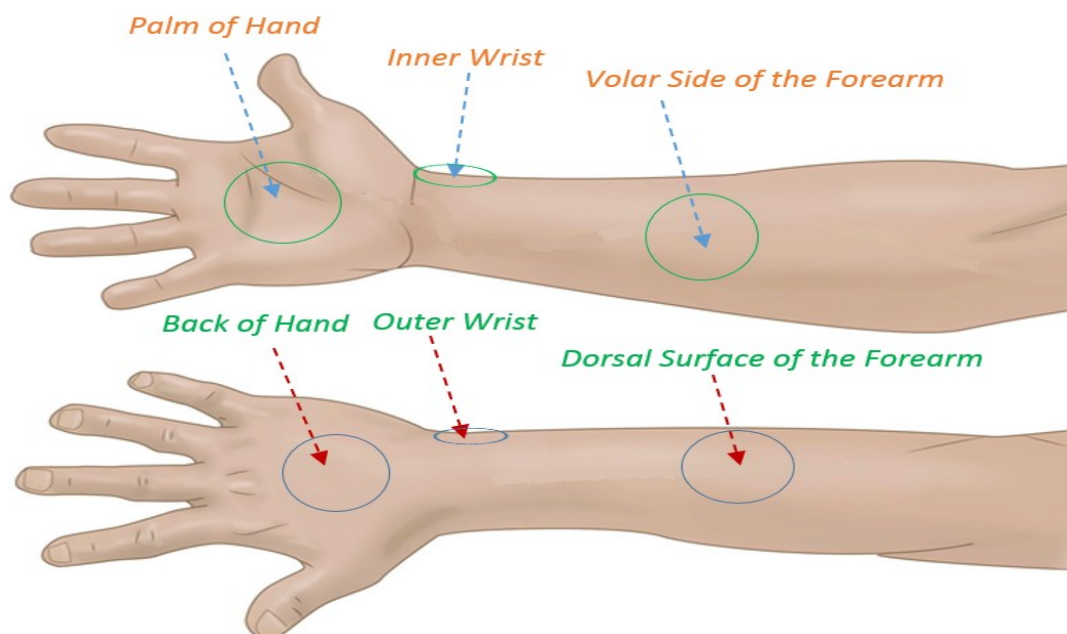


Figure 4.7: Locations on the arm where the emissivity of the skin is measured.

#### 4.5.4 Experimental Setup

A direct detection radiometer sensitive over the frequency band (80-100) GHz was used for measuring the emissivity of the human skin. The equipment for measurement consists of a W-band horn antenna connected directly to the millimetre wave monolithic integrated circuit (MMIC) detector. The output of the detector was connected through a coaxial cable to a digital voltmeter and through wires to a DC power supply, as illustrated in Figure 4.8.

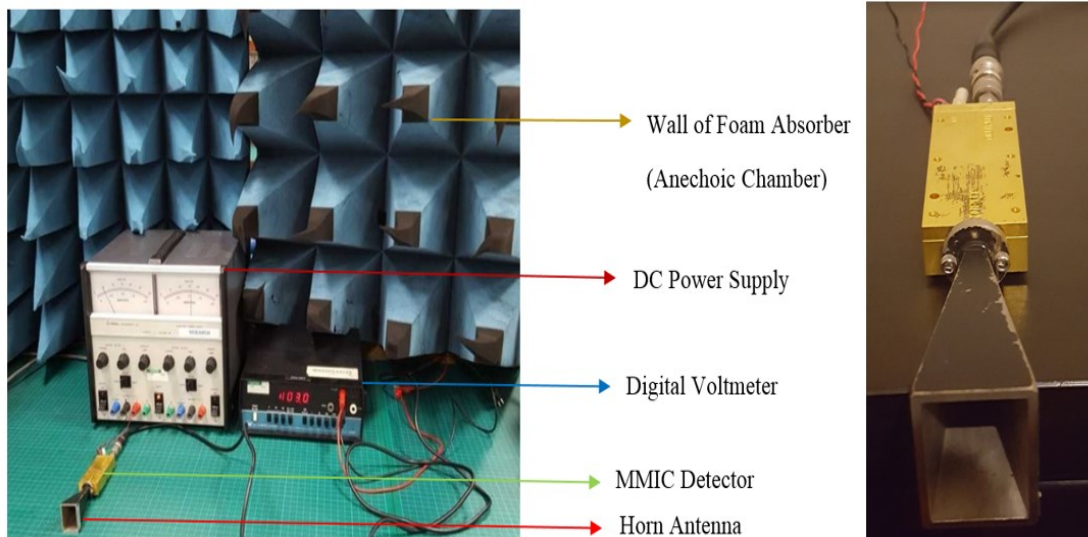


Figure 4.8: The main elements of the experimental work: A horn antenna connected to MMIC detector (consisting of a two-stage low noise amplifier; zero bias diode detector and buffer amplifier). A wall of carbon loaded absorbing foam surrounds the majority of the system.

The horn antenna (model number: AS4341, manufacturer: Atlan Tec RF) has a rectangular aperture (30 mm x 25 mm) and a nominal gain of 20 dBi over the frequency band 80-100 GHz. During the experiment, the horn antenna was fixed to measure emission from the subject and from the hot and the cold calibration sources.

The MMIC detector consists of a two-stage low noise amplifier (type: monolithic millimetre wave integrated circuit (MMIC) LNA, gain: 20 dB), zero bias diode detector (type: MMIC wideband ZBD, power 10.0  $\mu$ W) and buffer amplifier (type: MMIC wideband buffer amplifier, power: 20 dBm, and voltage: 5.0 V). The complete system except for an opening for the subject to be measured was enclosed in an anechoic region made by surrounding the detector and the horn antenna with a wall of carbon loaded absorbing foam (type: anechoic pyramidal absorber and dimensions per each piece are; length= 600 mm, and width= 600 mm).

#### ***4.5.5 Calibration and Initial Measurements***

The radiometer was calibrated by comparing the measured data from subjects with the emission levels from known standard sources [130, 140, 142, 147]. The standard sources were carbon loaded foam absorbers at liquid Nitrogen (77.0 K) and ambient temperature (293.0 K), as illustrated in Figure 4.9. A standard thermocouple and an infrared thermometer (described in section 4.4.4) were used to measure the thermodynamic temperatures of the target area of the skin and the calibration sources. The results obtained from the two thermometers were the same with a relative uncertainty of the measurement less than 0.1 °C, and as the infrared thermometer can measure the thermodynamic temperature of the skin in non-contact with the human body, it was chosen to measure the thermodynamic temperature of the skin.

The carbon foam absorbers (type: Eccosorb AN-73, manufacturer: Laird) had a rectangular shape and dimensions (length=170 mm, width=150 mm, and thickness 10 mm). These dimensions were chosen to fill the beam pattern of the horn antenna, thereby minimising systematic uncertainties. The measured emissivity values of the foam absorbers are greater than 0.99 over the frequency band 80-100 GHz [148, 149], thus they behave as good approximations to a black body emitter. The difference in temperature between the hot and the cold load is ~216 K, this large difference reducing the systematic uncertainties in the emissivity measurements to a minimum. The calibration Y-factor was measured to be 1.408 (using Equation 4.5). These measurements were taken from ten separate experiments and repeated 5-10 times at each experiment, the calibration measurements were repeated 5-10 times and they were consistent. This indicates that the radiometer had a long-term measurement

stability. The noise temperature and the noise figure for the system were measured to be 453.7 K and 2.55 respectively (using Equations 4.6 and 4.7).

The amount of self-emission reflected back from subjects was investigated by placing a metal plate perpendicular to a beam distance of 1.0 cm from the horn antenna beam. The mean level of self-emission reflected back from the metal plate (100% reflective surface) was measured to be in the range of 294-295 K with a standard deviation of  $\pm 1.0$  K. These results show that the radiation temperature from the metal plate is approximately the same as the ambient temperature, meaning there is no spurious emission from the radiometer to corrupt the measurements [159].

It is a well-known fact that the fluorescent lighting generates a low level (few Kelvin) of MMW radiation, modulated at 100 Hz, the second harmonic of the frequency of the mains electricity supply [159]. Millimetre wave emission emitted from a fluorescent light located  $\sim 5.0$  cm from the horn antenna (where the measurements are conducted) was found to increase the radiation temperature measured by the radiometer by an amount of 62 K to 74 K; a mean value of 67.5 K with a standard deviation of  $\pm 4.0$  K. When the fluorescent light was located directly in the beam of the horn antenna (where the maximum increase in radiation temperature is observed), the radiation temperature was found to increase by an amount of 80 K to 100 K; a mean value of 84.3 K with a standard deviation of  $\pm 8.0$  K. For this reason, all fluorescent lights were turned off in the laboratory during the measurements.

#### ***4.5.6 Methodology for Measuring the Human Skin Emissivity***

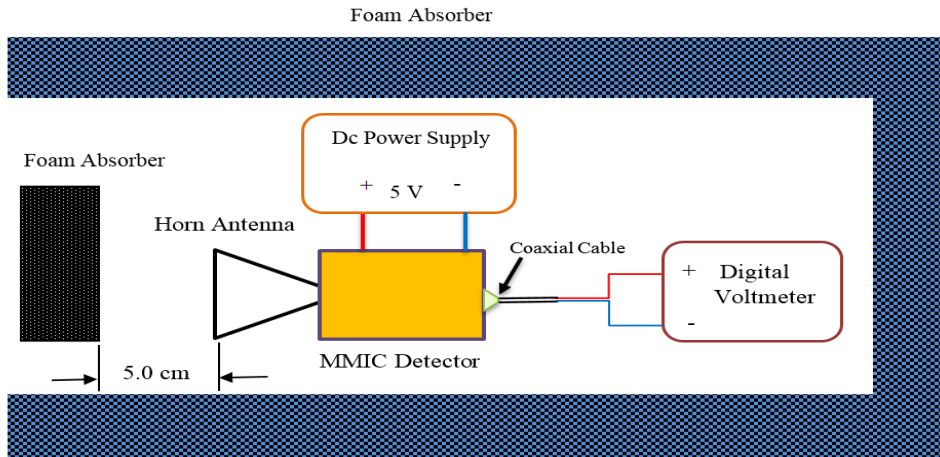
The horn antenna was located at a distance  $\sim 5.0$  cm from three different radiation sources: 1) ambient temperature source calibration (Figure 4.9 a), 2) liquid Nitrogen source calibration (Figure 4.9 b), and 3) the human skin (Figure 4.9 c). The distance 5.0 cm has been chosen as an optimal distance for an existing measurements system. This distance is chosen for convenience, to minimize the chances of subjects accidentally touching and moving the measurement apparatus. A greater distance between the measured subject and the horn antenna would lead to measurements having poorer spatial resolution. Using Equations (4.12, 4.15 and 4.16), and equating  $T_0$  to  $T_H$  the emissivity of the skin becomes [126]:

$$\eta = \frac{(V_s - V_H)(T_H - T_C)}{(T_s - T_H)(V_H - V_C)} \quad (4.18)$$

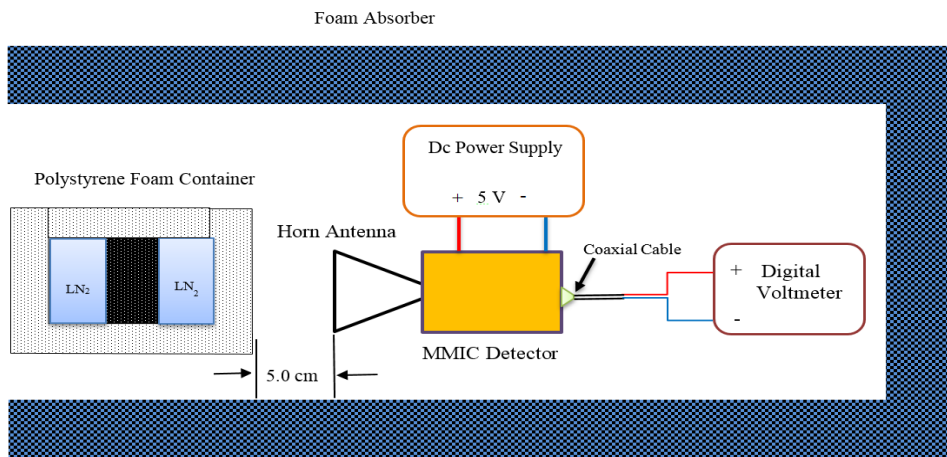
A digital voltmeter with 0.1 mV resolution was used to measure the output voltage for the target area of the skin  $V_s$  and the calibration sources ( $V_H$  and  $V_C$ ), and an infrared thermometer with absolute accuracy 0.01 °C was used to measure the skin surface temperature  $T_s$ , and the thermodynamics temperature of the calibration sources ( $T_H$  and  $T_C$ ).

Error propagation through Equation (4.18) indicates that the systematic uncertainty is  $\pm 0.005$ , whereas error propagation from Equation (4.1) indicates that the random error in the minimum detectable radiation temperature is 5.0 mK.

a) Hot Load, Ambient Temperature Source Calibration



b) Cold Load, Liquid Nitrogen Source Calibration (LN<sub>2</sub>)



c) Human Skin Measurements

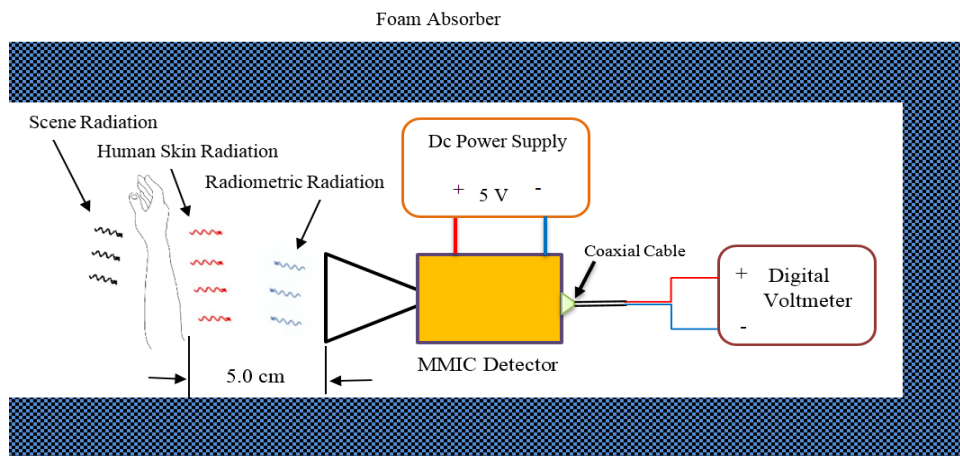


Figure 4.9: Illustrations of the experimental setup inside the walls (blue-grey) of the anechoic chamber, showing the hot (a) and the cold (b) calibration procedures and the measurement of the skin (c).

### 4.5.7 Methodology of Data Processing

The following block diagram summarises the methodology of data processing for the measurements conducted in experiment 2:

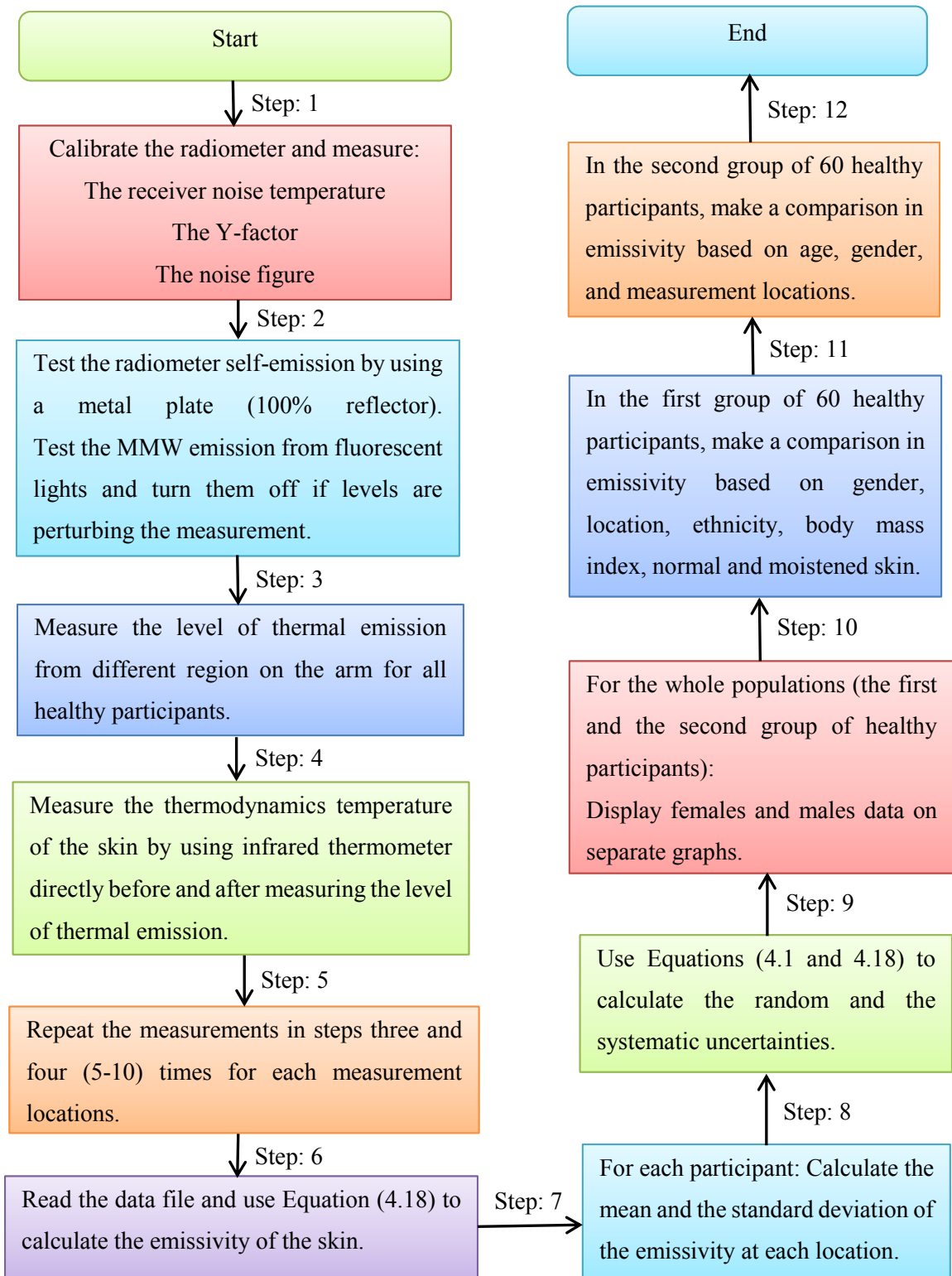


Figure 4.10: A methodology of data processing applied in experiment 2.

#### ***4.5.8 First Group of Healthy Participants Experimental Results***

The emissivity of the human skin was measured experimentally using the calibrated radiometer of Figure 4.8 and Equation (4.18). In this part, the measurements were performed over the band 80 GHz to 100 GHz on a sample of 60 healthy participants from both genders (first group of healthy participants; 36 males and 24 females).

##### ***4.5.8.1 Female Emissivity Measurements***

The measurements in Figures (4.11, 4.12 and 4.13) represent the mean emissivity for a sample of 24 female participants, with error bars representing the systematic uncertainty. The measurements show variation in the mean emissivity values between individuals and locations on the arm. These variations are due to the differences in skin thickness and the number of blood vessels (which raises the water content) which varies from location to another and between individuals [71, 153]. The mean emissivity of the sample overall measurement locations is 0.383 with a standard deviation of 0.0839 and experimental measurements uncertainty of  $\pm 0.005$ . Table 4.4 shows the mean, the standard deviation, and the standard error in the mean for a sample of 24 female participants at six measurement locations:

Location	Mean emissivity ( $\mu$ )	Standard deviation ( $\sigma$ )	Standard error in the mean ( $\sigma/\sqrt{24}$ )
The palm of hand	0.430	0.0951	0.0194
The back of hand	0.371	0.0865	0.0177
The outer wrist	0.378	0.0654	0.0134
The inner wrist	0.313	0.0620	0.0127
The dorsal surface	0.438	0.0659	0.0135
The volar side	0.365	0.0549	0.0112

Table 4.4: Statistical analysis of the data for a sample of 24 female participants.

In general, the lower values of emissivity are results of measuring particularly thin skin on the back of the hand, the inner wrist, and the volar side of the forearm [153], whereas the higher values of emissivity are results of measuring thick skin on the palm of the hand, the outer wrist, and the dorsal surface of the forearm [82].

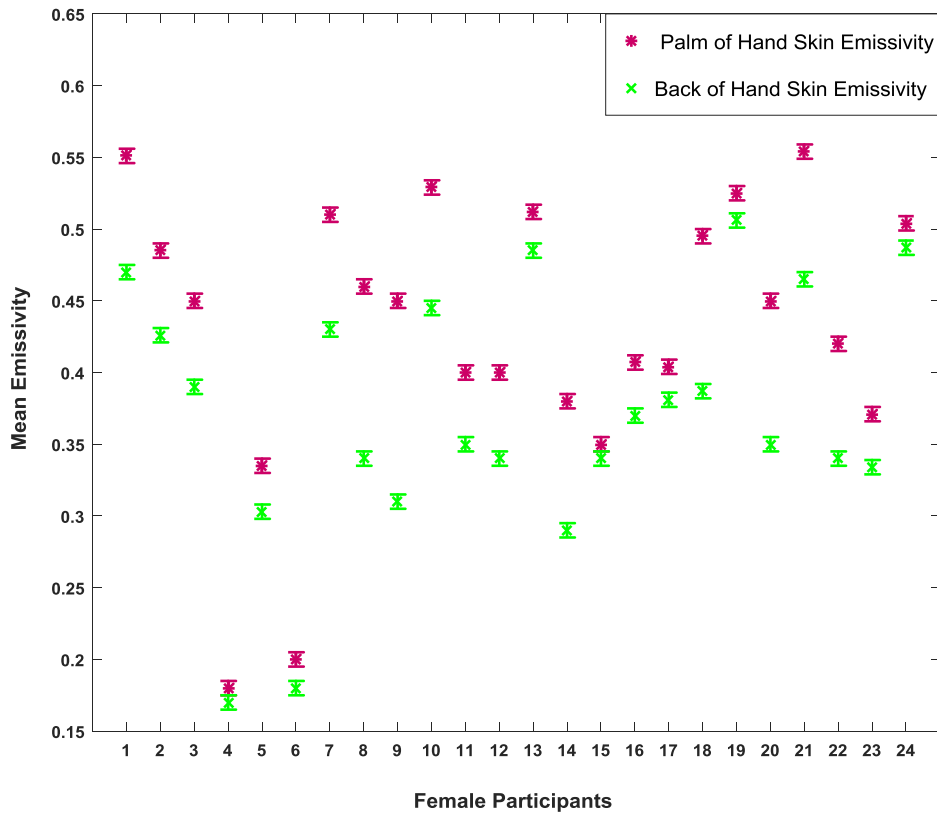


Figure 4.11: Mean emissivity for the palm of the hand and the back of the hand skin for a sample of 24 female participants. The participants' ages are as follows: 1) 22, 2) 23, 3) 23, 4) 24, 5) 24, 6) 24, 7) 25, 8) 26, 9) 27, 10) 29, 11) 29, 12) 30, 13) 31, 14) 32, 15) 32, 16) 33, 17) 33, 18) 35, 19) 36, 20) 42, 21) 44, 22) 45, 23) 45, 24) 54.

Measurements in Figure 4.11 show that the mean emissivity for the palm of the hand skin is higher than that of the back of the hand skin for all female participants. Statistical analysis of the data indicates that the mean differences in the emissivity values between the palm of the hand and the back of the hand is 0.0589 with a sample standard deviation in the differences of 0.0375. These differences are significant as the  $p$ -value ( $6.014 \times 10^{-8}$ ) obtained from the paired t-test is lower than the critical significance level of 0.05.

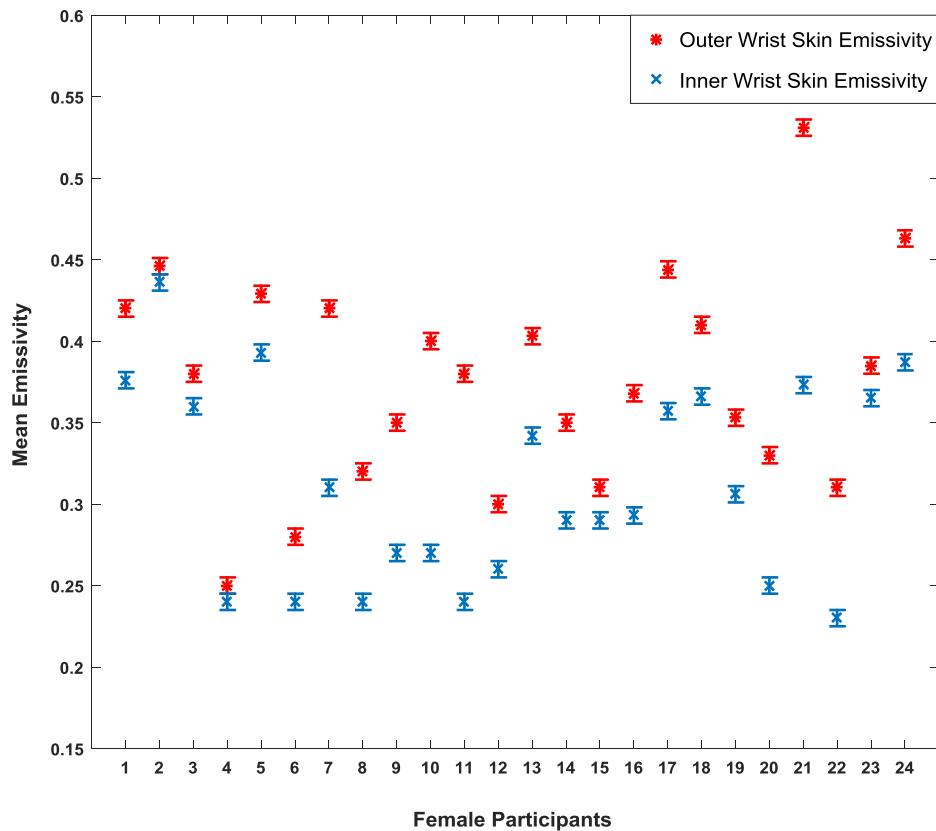


Figure 4.12: Mean emissivity for the outer and the inner wrist skin for a sample of 24 female participants. The participants' ages are identified in Figure 4.11.

Measurements in Figure 4.12 show that the mean emissivity for the outer wrist is higher than that of the inner wrist for all female participants. Statistical analysis of the data indicates that the mean differences in the emissivity values between the outer and the inner wrist is 0.0646 with a sample standard deviation in the differences of 0.0394. These differences are significant as the  $p$ -value ( $6.37 \times 10^{-8}$ ) obtained from the paired t-test is lower than the critical significance level of 0.05.

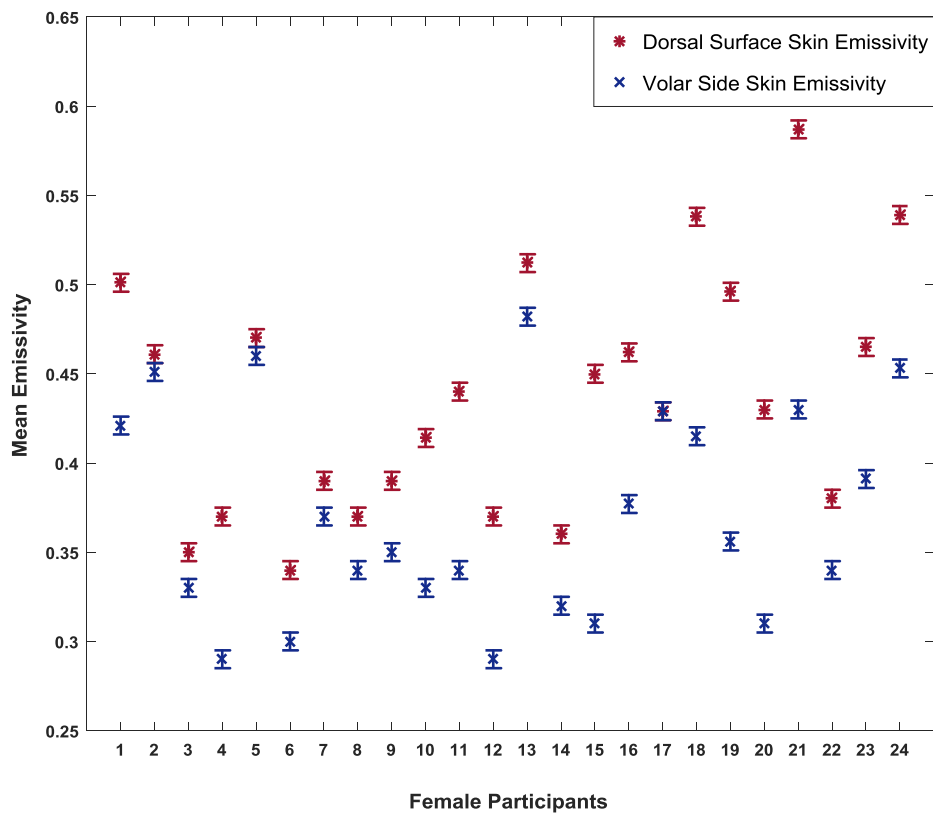


Figure 4.13: Mean emissivity for the dorsal surface and the volar side skin for a sample of 24 female participants. The participants' ages are identified in Figure 4.11.

The measurements in Figure 4.13 show that the mean emissivity for the dorsal surface is higher than that of the volar side for all female participants. Statistical analysis of the data indicates that the mean differences in the emissivity values between the dorsal and the volar regions is 0.0729 with a sample standard deviation in the differences of 0.0449. These differences are significant as the  $p$ -value ( $2.22 \times 10^{-7}$ ) obtained from the paired t-test is lower than the critical significance level of 0.05.

#### 4.5.8.2 Male Emissivity Measurements

The measurements in Figures (4.14, 4.15 and 4.16) represent the mean emissivity for 36 male participants, with error bars representing the systematic uncertainty. The emissivity from males was found to range from 0.18 to 0.68, with mean and standard deviation for all measurement locations being 0.401 and 0.0865 respectively. Table 4.5 shows the mean, the standard deviation, and the standard error in the mean for a sample of 36 male participants at six measurement locations:

Location	Mean emissivity ( $\mu$ )	Standard deviation ( $\sigma$ )	Standard error in the mean( $\sigma/\sqrt{36}$ )
The palm of hand	0.451	0.0997	0.0166
The back of hand	0.385	0.0844	0.0140
The outer wrist	0.396	0.0606	0.0101
The inner wrist	0.343	0.0639	0.0106
The dorsal surface	0.449	0.0778	0.0129
The volar side	0.381	0.0725	0.0121

Table 4.5: Statistical analysis of the data for a sample of 36 male participants.

The measurements in Figures (4.14, 4.15 and 4.16) show a similar trend to that of the females in terms of differences in the mean emissivity values between the thicker skin region and the thinner skin region. Statistical analysis on a sample of 36 male participants indicates that the mean differences in the emissivity values between the outer and the inner wrist, the palm of the hand and the back of the hand, and the dorsal and the volar regions are: 0.0529, 0.0658 and 0.0675 with a sample standard deviation

in the differences of 0.0345, 0.0531 and 0.0319 respectively. These differences are due to the skin thickness and the water content that varies with location and between individuals [71, 153]. The thinner skin regions with blood vessels closed to the skin surface makes the skin more reflective and this results in higher reflectance ( $R$ ) and lower emissivity ( $\eta = 1 - R$ ). The results obtained from the paired t-tests indicate significant differences in the mean emissivity values between the palm of the hand and the back of the hand ( $p$ -value= $2.13 \times 10^{-12}$ ), the outer and the inner wrist ( $p$ -value= $3.99 \times 10^{-11}$ ), and the dorsal and the volar regions ( $p$ -value= $1.91 \times 10^{-14}$ ) since the  $p$ -values are much lower than the critical significance level of 0.05.

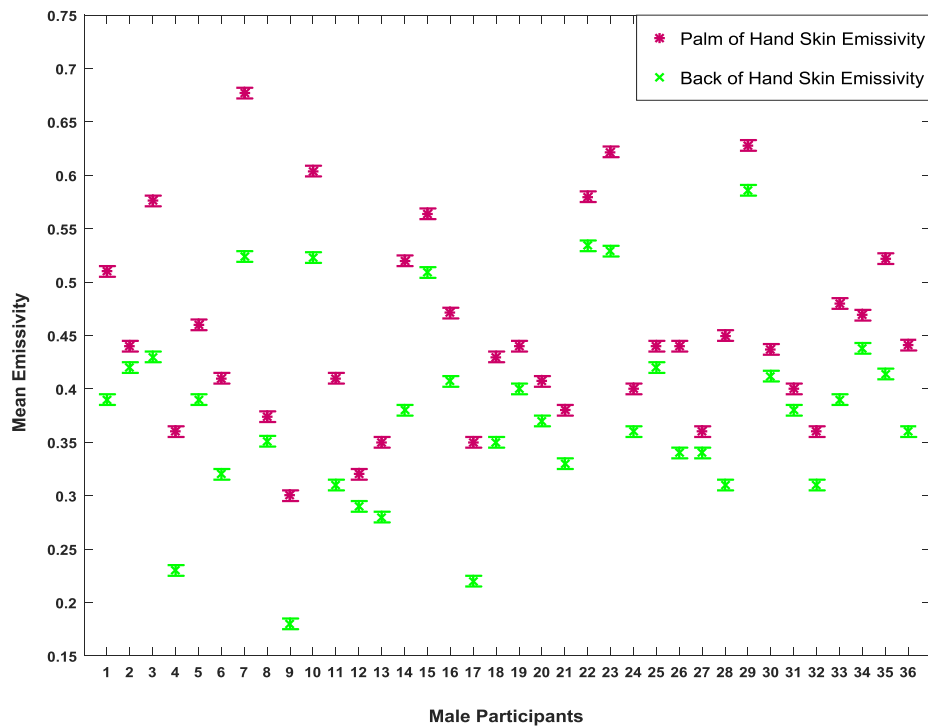


Figure 4.14. Mean emissivity for the palm of the hand and the back of hand skin for a sample of 36 male participants. The participants' ages are as follows: 1) 20, 2) 20, 3) 21, 4) 22, 5) 22, 6) 22, 7) 23, 8) 23, 9) 23, 10) 24, 11) 24, 12) 25, 13) 26, 14) 26, 15) 26, 16) 26, 17) 27, 18) 28, 19) 29, 20) 29, 21) 30, 22) 31, 23) 31, 24) 32, 25) 34, 26) 35, 27) 37, 28) 37, 29) 40, 30) 40, 31) 42, 32) 42, 33) 45, 34) 52, 35) 58, 36) 67.

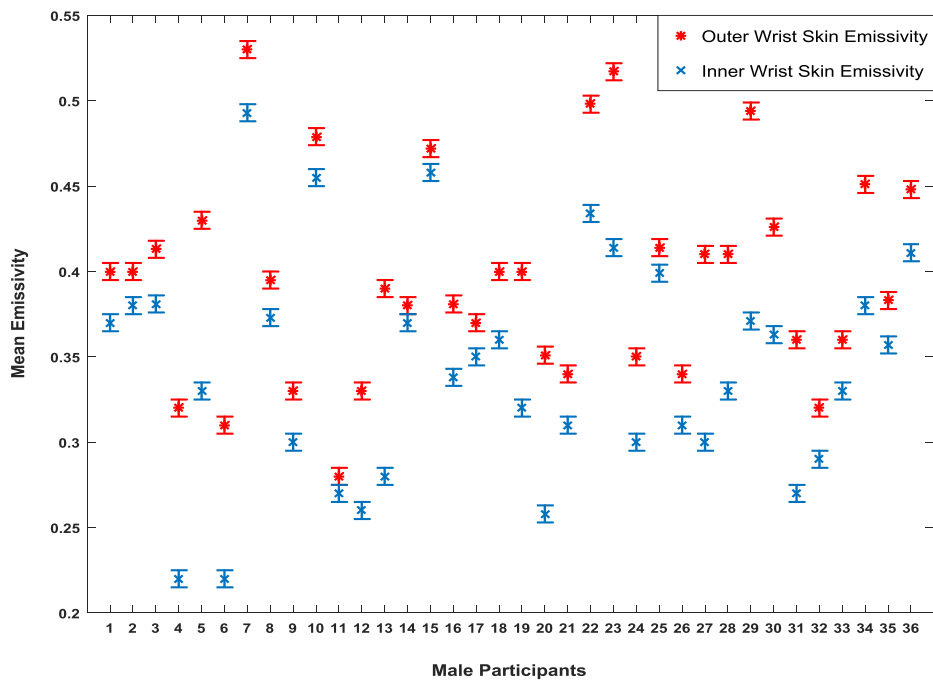


Figure 4.15: Mean emissivity for the outer wrist and the inner wrist skin for a sample of 36 male participants. The participants' ages are identified in Figure 4.14.

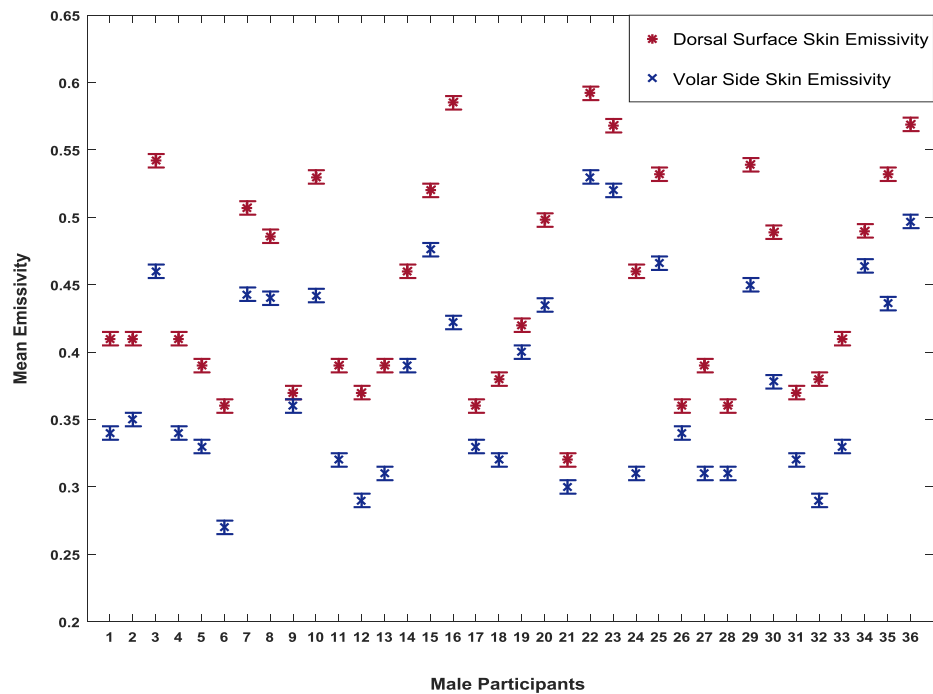


Figure 4.16: Mean emissivity for the dorsal surface and the volar side skin for a sample of 36 male participants. The participants' ages are identified in Figure 4.14.

#### 4.5.8.3 Comparison in Emissivity between Male and Female Participants

Measurements of human skin emissivity of 36 male and 24 female participants are presented in Table 4.6. The measurements show that the mean emissivity of male participants is higher than that of the females overall measurement locations. Estimating the sample mean emissivity values for the 36 males and the 24 females separately for all measurement locations indicates that the difference between male and female emissivity is  $\sim 0.02$ . This finding is consistent with the skin of males being thicker than that of females for all ages [150, 151, 152]. Although the sample mean of the emissivity values of the male participants are higher by 0.02 than those of the female participants. However, the results obtained from the unpaired t-test indicate that these differences are insignificant since the  $p$ -value (0.488) is greater than the critical significance level of 0.05.

Location	Mean Emissivity Males	SD Males ( $\sigma$ )	Mean Emissivity Females	SD Females ( $\sigma$ )
Palm of hand	0.451	0.0997	0.430	0.0951
Back of hand	0.385	0.0844	0.371	0.0865
Outer wrist	0.396	0.0606	0.378	0.0654
Inner wrist	0.343	0.0639	0.313	0.0620
Dorsal surface	0.449	0.0778	0.438	0.0659
Volar side	0.381	0.0725	0.365	0.0549

Table 4.6: Statistical analysis of the data for male and female participants.

#### 4.5.8.4 Skin Emissivity for Participants Having Normal and High Body Mass

##### Index

Human skin becomes thicker with increasing the body mass index (BMI) for both genders at any age [155], so variability in the emissivity of the skin from suitably selected participants was investigated. The measurements were performed on 20 participants (10 males and 10 females) having normal and high body mass index. For the purpose of this study, participants with BMI ranging between (18.5-24.9) kg/m<sup>2</sup> were classified as having normal BMI, whereas participants with BMI ranging between (25.0-29.9) kg/m<sup>2</sup> were classified as having high BMI [160]. The measurements of the mean emissivity values of males with high and normal BMI are shown in Figure 4.17, with similar plots for females shown in Figure 4.18, with the corresponding values of the standard deviations shown in Tables (4.7 and 4.8).

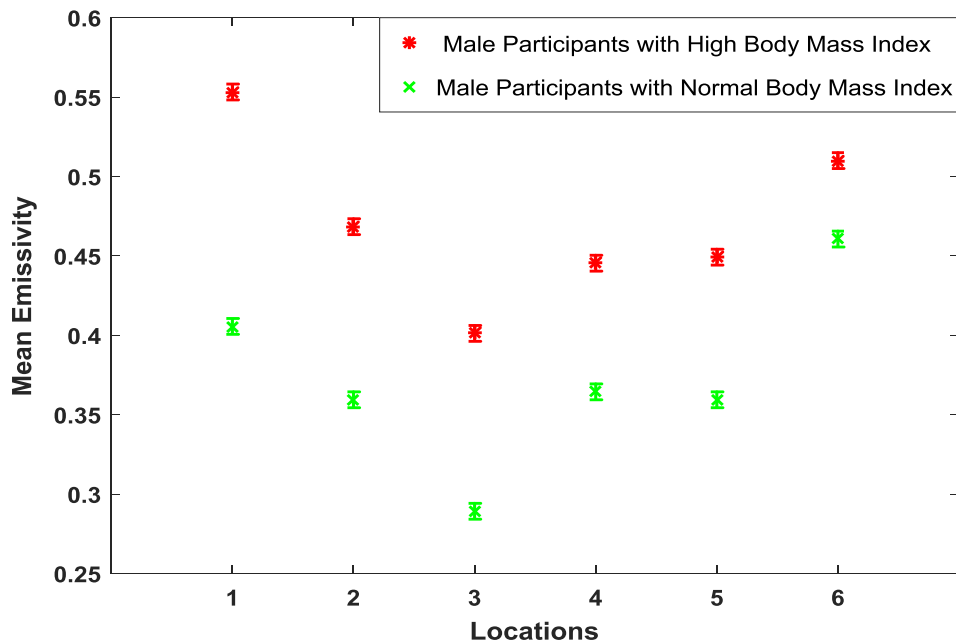


Figure 4.17: Mean emissivity for a sample of 10 male participants having normal and high body mass index on: 1) the palm of the hand, 2) the back of the hand, 3) the inner wrist, 4) the outer wrist, 5) the volar side, and 6) the dorsal surface of the forearm.

The measurements in Figure 4.17 indicate that males with high BMI have on average an emissivity  $\sim 0.0981$  higher than those with normal BMI, with differences in the mean emissivity values across the different locations varying from  $\sim 0.05$  to  $\sim 0.15$ . These differences are consistent with the fact that human skin is getting thicker with increasing the BMI [155], a consequence of this being that blood vessels are further from the surface of the skin. The results obtained from the unpaired t-tests indicate that these differences are significant for the palm of the hand ( $p$ -value=0.0017), the back of the hand ( $p$ -value=0.0322), and the inner wrist ( $p$ -value=0.0047) locations since the  $p$ -values are lower than the critical significance level of 0.05. However, the mean differences in emissivity values are insignificant for the outer wrist ( $p$ -value=0.062), the dorsal surface ( $p$ -value=0.365), and the volar side ( $p$ -value=0.102) regions as the  $p$ -values are higher than the critical significance level of 0.05.

Location	Standard deviation for males with normal BMI	Standard deviation for males with high BMI
The palm of the hand	$\pm 0.039$	$\pm 0.049$
The back of the hand	$\pm 0.043$	$\pm 0.069$
The inner wrist	$\pm 0.028$	$\pm 0.046$
The outer wrist	$\pm 0.0136$	$\pm 0.064$
The volar side of forearm	$\pm 0.0567$	$\pm 0.077$
The dorsal surface	$\pm 0.078$	$\pm 0.067$

Table 4.7: The standard deviation for a sample of 10 male participants having normal and high body mass index.

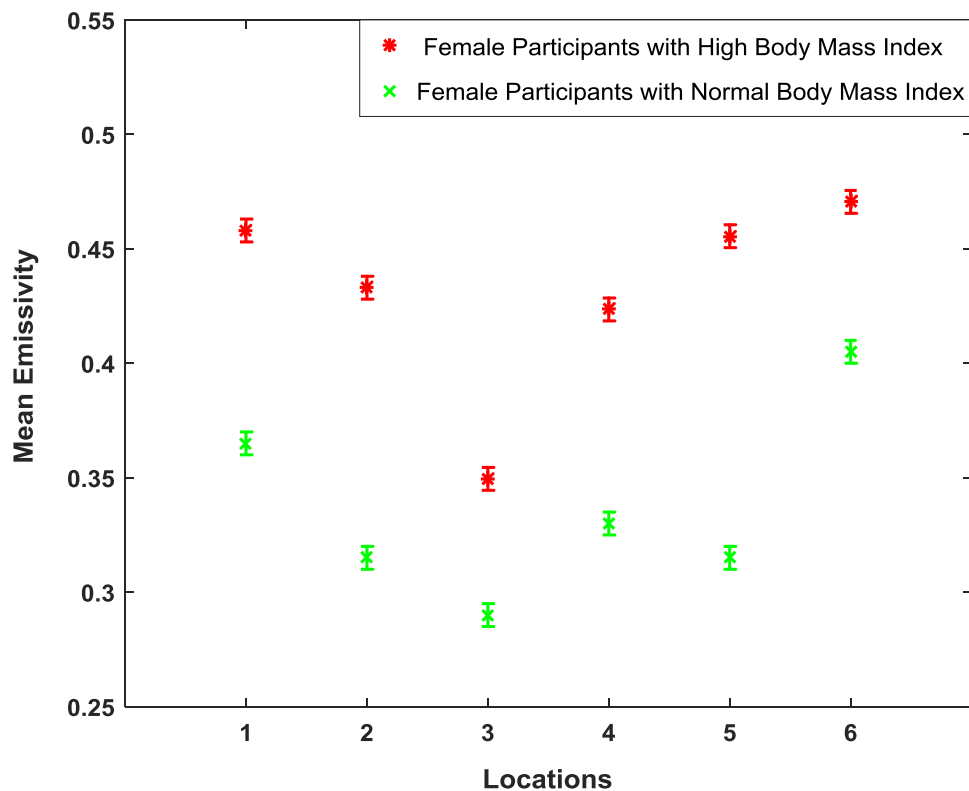


Figure 4.18: Mean emissivity for a sample of 10 female participants having normal and high body mass index at six locations identified in Figure 4.17.

The measurements in Figure 4.18 indicate that females with high BMI have on average an emissivity  $\sim 0.095$  higher than those with normal BMI, with differences in the mean emissivity values across the different arm locations varying from  $\sim 0.06$  to  $\sim 0.14$ , a result similar to the male group. However, the measurements of male emissivity indicate a larger scatter, this being 0.29 and 0.553 for those of normal and high BMI respectively. The corresponding scatters in the female group are 0.29 and 0.47 for normal and high BMI of the individuals. As with previous measurements, these also indicate that the emissivity of males is  $\sim 0.038$  higher than those of females. The results obtained from the unpaired t-test indicate that the differences in the mean emissivity values between male and female groups are insignificant since the  $p$ -value (0.191) is greater than the critical significance level of 0.05.

The results obtained from the unpaired t-tests for female participants having normal and high body mass index at six locations indicate that the differences in the mean emissivity values between the two groups are significant for the back of the hand ( $p$ -value=0.005) and the volar side of the forearm locations ( $p$ -value=0.002) since the  $p$ -values for these locations are lower than the critical significance level of 0.05. However, these differences are insignificant for the palm of the hand ( $p$ -value=0.095), the outer wrist ( $p$ -value=0.082), the inner wrist ( $p$ -value=0.397), and the dorsal surface ( $p$ -value=0.079) regions as the  $p$ -values for these regions are higher than the critical significance level of 0.05.

Location	Standard deviation for females with normal BMI	Standard deviation for females with high BMI
The palm of the hand	$\pm 0.015$	$\pm 0.054$
The back of the hand	$\pm 0.025$	$\pm 0.052$
The inner wrist	$\pm 0.005$	$\pm 0.008$
The outer wrist	$\pm 0.02$	$\pm 0.021$
The volar side	$\pm 0.005$	$\pm 0.027$
The dorsal surface	$\pm 0.045$	$\pm 0.042$

Table 4.8: Standard deviation for a sample of 10 female participants having normal and high BMI.

#### 4.5.8.5 Skin Emissivity for Participants Having Asian and European Ethnicities

The measurements presented in this section are from 48 participants having two different ethnicities; European (UK) and Asian (Middle Eastern) from both genders (24 male (12 European and 12 Asian), and 24 female (12 European and 12 Asian)). The measurements in Figures (4.19 and 4.20) represents the mean emissivity for male and female groups with error bars representing the systematic uncertainty.

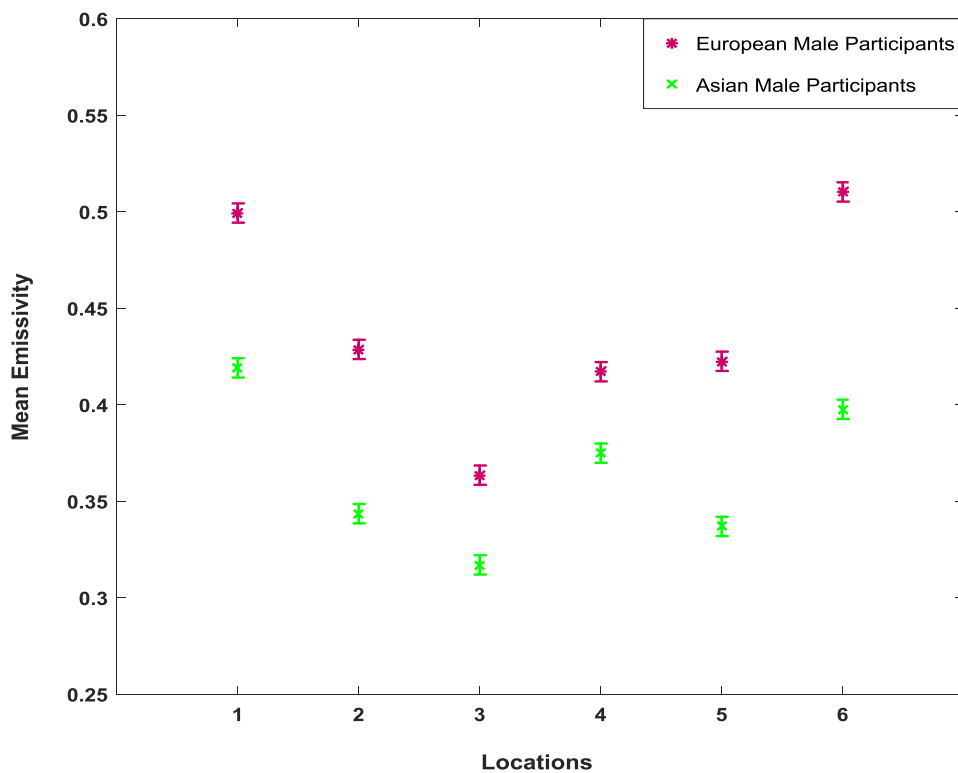


Figure 4.19: Mean emissivity of 24 male participants having Asian and European ethnicities at six measurement locations identified in Figure 4.17.

The measurements in Figure 4.19 indicate that the mean emissivity for the sample of Asian males is lower than that of European males at all measurement locations. The mean values of the differences in emissivity between Asian and European males were calculated to be  $\sim 0.04$  for the inner wrist and the outer wrist locations,  $\sim 0.085$  for the palm of the hand, the back of the hand and the volar side locations, and  $\sim 0.11$  for the

dorsal surface location. These differences are likely to arise due to Asian skin being thinner than that of European skin and the hydration levels and the water contents of the Asian skin being higher than that of European skin [161, 162, 163]. This makes Asian skin more reflective compared to European skin and as a result the mean emissivity of Asian participants is lower than that of European participants at all measurement locations. The results obtained from the unpaired t-tests indicate that these differences are significant for the palm of the hand ( $p$ -value=0.0255), the back of the hand ( $p$ -value=0.0015), the volar side ( $p$ -value=0.006), and the dorsal surface ( $p$ -value=0.00025) locations as the  $p$ -values for these locations are lower than the critical significance level of 0.05. However, these differences are insignificant for the outer wrist ( $p$ -value=0.105) and the inner wrist ( $p$ -value=0.0899) regions as the  $p$ -values are higher than the critical significance level of 0.05. The standard deviations for Asian and European male participants are summarised in Table 4.9 as follows:

Location	Standard deviation for Asian males	Standard deviation for European males
The palm of the hand	±0.081	±0.080
The back of the hand	±0.089	±0.073
The inner wrist	±0.047	±0.074
The outer wrist	±0.054	±0.064
The volar side	±0.041	±0.081
The dorsal surface	±0.051	±0.068

Table 4.9: Standard deviation for Asian and European males at six locations.

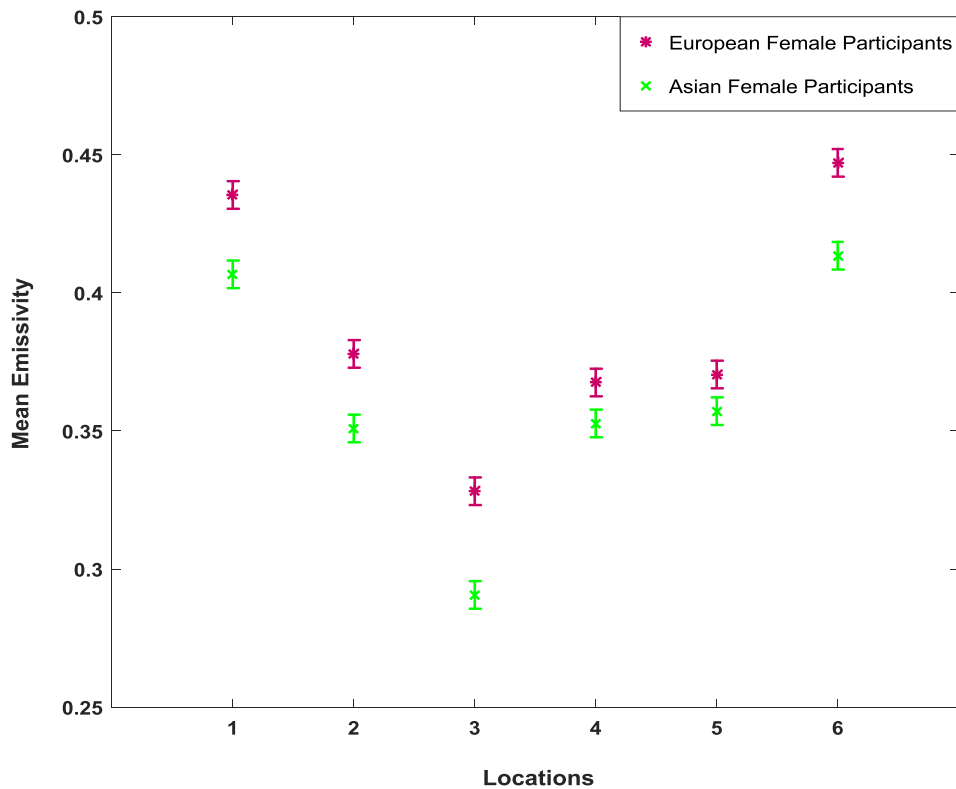


Figure 4.20: Mean emissivity of 24 female participants having Asian and European ethnicities at six measurement locations identified in Figure 4.17.

The measurements in Figure 4.20 indicate that there are differences in the mean emissivity values of the skin between the Asian and the European female samples, the measurements showing a similar trend to that of the males. However, the mean differences in the emissivity values between the two female groups were calculated to be in the range of 0.014 to 0.038 for all measurement locations. These differences are lower than that of the male groups. The results obtained from the unpaired t-tests for female participants having Asian and the European ethnicities at six locations indicate that the differences in mean emissivity values between the two groups are insignificant since the  $p$ -values for the palm of the hand (0.497), the back of the hand (0.492), the inner wrist (0.193), the outer wrist (0.502), the volar side of the forearm (0.599), and the dorsal surface (0.209) regions are higher than the critical significance level of 0.05.

The standard deviation for Asian and European female groups is calculated and summarised in Table 4.10.

Location	Standard deviation for Asian females	Standard deviation for European females
The palm of the hand	$\pm 0.072$	$\pm 0.103$
The back of the hand	$\pm 0.065$	$\pm 0.097$
The inner wrist	$\pm 0.054$	$\pm 0.065$
The outer wrist	$\pm 0.045$	$\pm 0.048$
The volar side	$\pm 0.053$	$\pm 0.054$
The dorsal surface	$\pm 0.050$	$\pm 0.060$

Table 4.10: Standard deviation for Asian and European females at six locations.

#### ***4.5.8.6 Emissivity of Male and Female Skin in Dry and Wet State***

This experiment investigates the ability of the radiometer to identify and sense water (H<sub>2</sub>O) on the skin surface and to distinguish between normal skin and skin saturated with water. Wet skin in this experiment describes skin which has been saturated with water but contains no surface water. It is a known fact that the electromagnetic properties of water dominate the electromagnetic properties of the skin over the MMW bands [21, 25, 26, 55, 122]. Therefore, measurements were made to quantify this statement at 90 GHz. The measurements were applied on 16 participants (10 males and 6 females) and on two measurement locations; the palm of the hand and the back of the hand skin. Firstly, emissivity measurements of normal clean skin on the palm and the back of the hand were made. Then these areas of the skin were covered with water, and the methodology of measuring the emissivity of wet skin are summarised as follows:

- The target area of the skin was placed in a bowl of water for one minute.
- The hand was located on a flat surface (table) with the measurement location facing upwards; to avoid water dropping for a period of 2-4 minutes until the water is absorbed.
- The wet skin was wiped using clean and dry wipes.
- The measurements were made and repeated five times directly; to obtain a mean value.

The mean emissivity values of the palm of the hand and the back of the hand skin before and after the application of water for males and females are illustrated in Figures (4.21 and 4.22) respectively, with the corresponding statistical analysis overall measurement location is shown in Tables (4.11 and 4.12).

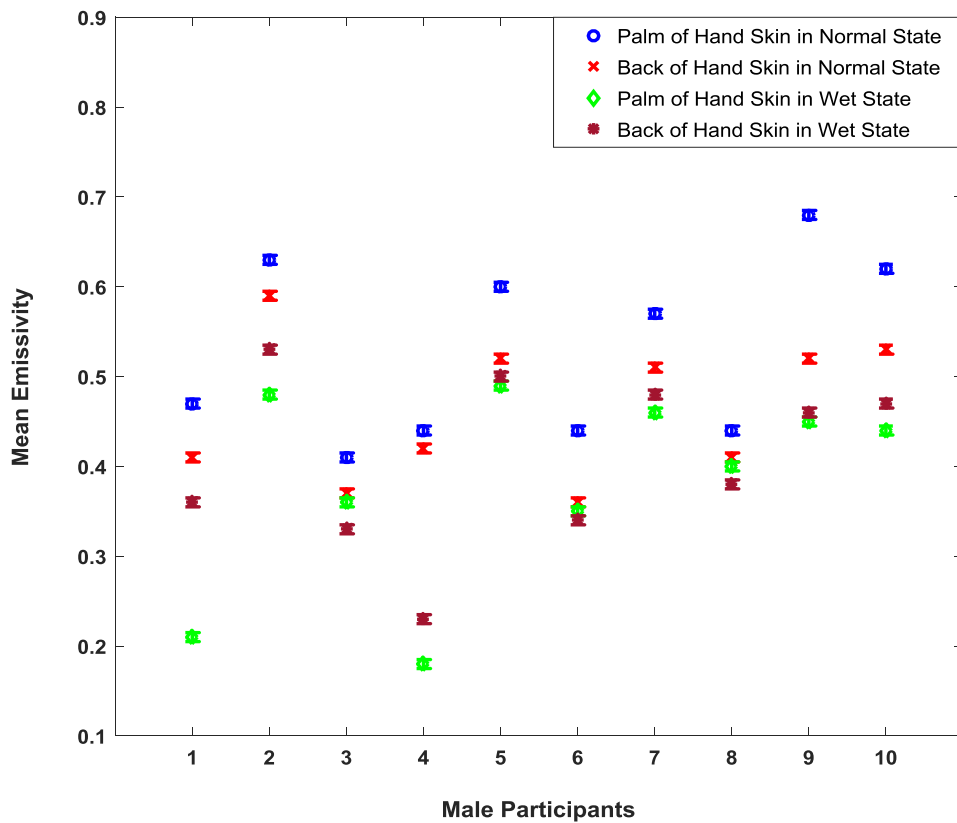


Figure 4.21: Mean emissivity for a sample of 10 male participants before and after the application of water.

The measurements for a sample of 10 male participants in Figure 4.21 indicate that the mean emissivity values for the palm of the hand skin and the back of the hand skin after the application of water are significantly lower than the mean emissivity of the skin in a normal state for the two measurements locations. Statistical analysis of the data indicates that the mean difference in emissivity for the palm of the hand skin before and after moistening with water is  $\sim 0.148$  with a sample standard deviation in the differences of  $\sim 0.0776$ . The mean difference in the emissivity for the back of the hand skin before and after adding water is  $\sim 0.056$  with a standard deviation in the differences of  $\sim 0.047$ . It is reasonable to assume that these differences are due to the water that increases the hydration level of the skin; this increases the reflectance of the skin [164], and as a result the emissivity of the skin becomes lower.

The results obtained from the paired t-tests indicate that the differences in the mean emissivity values between the normal and the wet palm of the hand ( $p$ -value = 0.0033), and the normal and the wet back of the hand skin ( $p$ -value = 0.006) are significant since the  $p$ -values for these locations are lower than the critical significance level of 0.05.

Location	Mean emissivity ( $\mu$ )	Standard deviation ( $\sigma$ )	Standard error in the mean( $\sigma/\sqrt{10}$ )
Dry palm of hand	0.53	0.0946	0.0299
Dry back of hand	0.464	0.0749	0.0237
Wet palm of hand	0.382	0.1037	0.0328
Wet back of hand	0.408	0.0898	0.0284

Table 4.11: Statistical analysis of the dry and the wet skin for a sample of 10 males.

Location	Mean emissivity ( $\mu$ )	Standard deviation ( $\sigma$ )	Standard error in the mean( $\sigma/\sqrt{6}$ )
Dry palm of hand	0.478	0.0308	0.0126
Dry back of hand	0.435	0.0461	0.0188
Wet palm of hand	0.350	0.0516	0.0211
Wet back of hand	0.352	0.0682	0.0278

Table 4.12: Statistical analysis of the dry and the wet skin for a sample of 6 females.

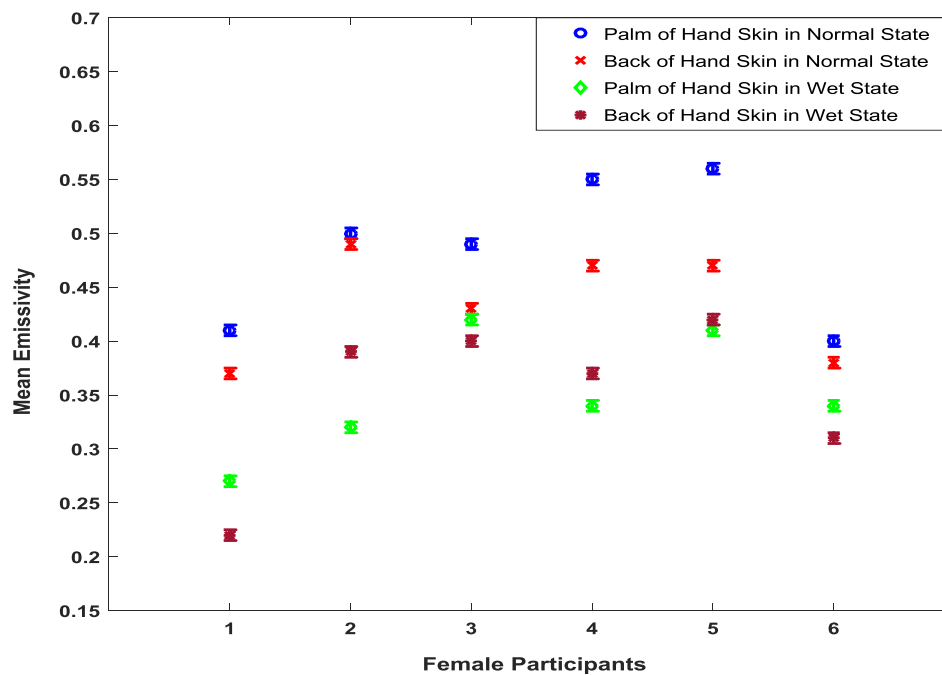


Figure 4.22: Mean emissivity for a sample of 6 female participants before and after the application of water.

The measurements for a sample of 6 female participants in Figure 4.22, show that the mean emissivity for the palm of the hand skin and the back of the hand skin after moistening with water is lower than that of the palm of the hand and the back of the hand skin before adding water by mean values of 0.128 and 0.0833 and standard deviations of the differences of 0.04 and 0.039 respectively. The differences between the wet and the normal palm of hand skin are more significant than that of the back of the hand skin for both males and females participants, and this is due to thick stratum corneum (SC) layer that can retain water and make the hydration level for the palm of the hand skin significantly higher in a wet state compared with a normal state [164]. The results obtained from the paired t-tests confirm that these differences are significant since the  $p$ -values (0.0026 and 0.0049 for the palm of the hand and the back of the hand skin before and after the application of water respectively) are lower than the critical significance level of 0.05.

#### ***4.5.9 Second Group of Healthy Participants Experimental Results***

The objective of this experiment is to study how the emissivity of the human skin varies with age for both gender. For this purpose, a new sample of 60 healthy participants (second group); 35 males and 25 females with ages ranging from 20 to 60 years were recruited and measured [126]. For the purpose of this experiment, participants were divided into four age groups: 20-30, 30-40, 40-50, and 50-60 years. There were 5-10 subjects in each age group and the measurements were conducted at four locations: 1) the dorsal surface of the forearm, 2) the volar side of the forearm, 3) the outer wrist, and 4) the inner wrist. The emissivity of the human skin was measured experimentally using the calibrated radiometer of Figure 4.8 and Equation (4.18). In this experiment, the measurements were performed over the band 80 GHz to 100 GHz on the second group of healthy participants.

##### ***4.5.9.1 Male Emissivity Measurements for Different Age Groups***

The measurements in Figures (4.23 and 4.24) represent the mean emissivity values for the male age groups, with error bars representing the standard error in the mean (SEM). The measurements show significant and consistent variations in emissivity at different locations of the hand for different age groups. Emissivity for dorsal surface and outer wrist locations are higher than that of volar side and inner wrist locations. The results also suggest two age-related trends: 1) a possible slight decrease in the mean emissivity values in the age groups between 20-40 years. This decrease is consistent with the fact that male skin thickness decreases gradually with the age [154, 165], and 2) an increase in the mean emissivity values in the age groups between 40-60 years. This increase is consistent with the fact that water content and skin hydration level decrease with the age [156, 166] and this makes aged skin drier compared with young skin [165].

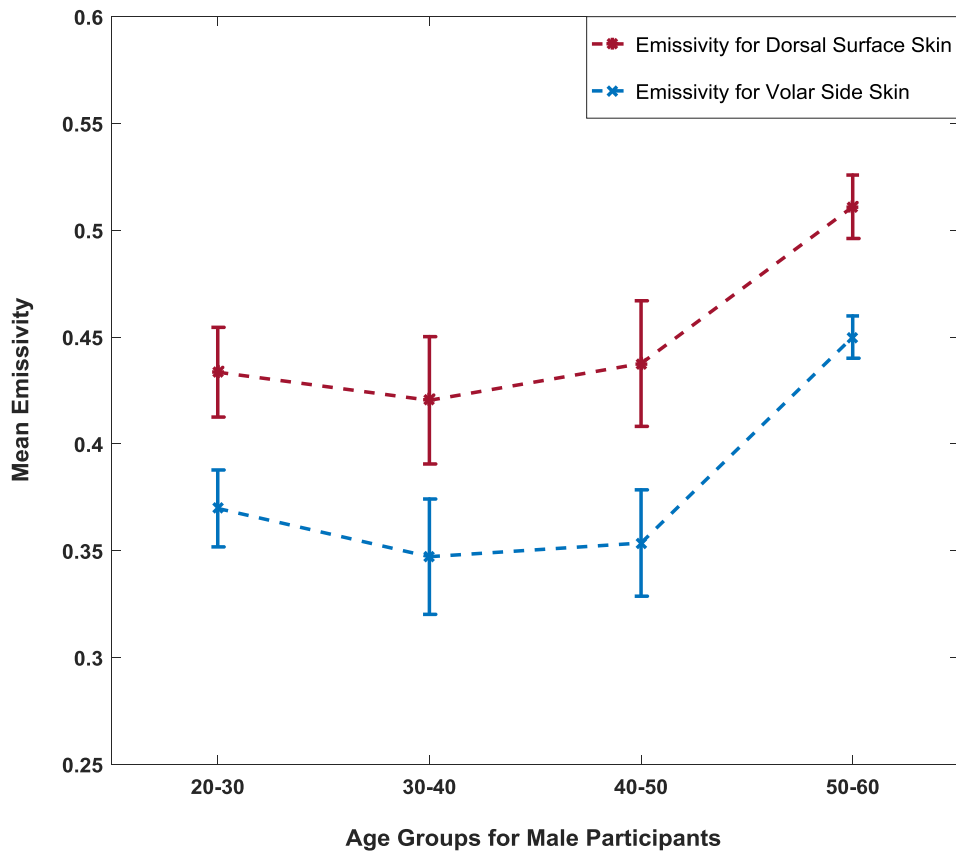


Figure 4.23: Mean emissivity values for the dorsal surface and the volar side skin for a sample of 35 male participants.

The statistical analysis of the male samples in Figure 4.23 indicates that the sample mean of the differences in the mean emissivity values between the dorsal and the volar side of the forearm is 0.0675 with a sample standard deviation in the differences of 0.0319. These differences are significant as the  $p$ -value (0.00087) obtained from the paired t-test is lower than the critical significance level of 0.05.

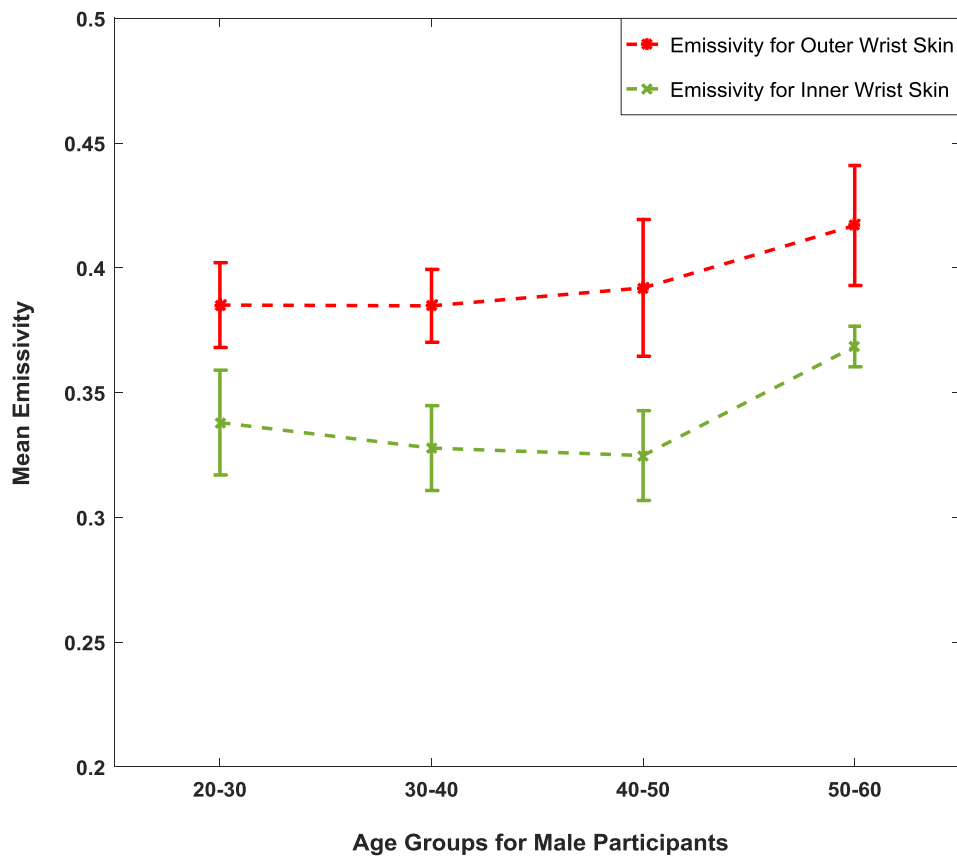


Figure 4.24: Mean emissivity values for the outer wrist and the inner wrist skin for a sample of 35 male participants.

The statistical analysis of the male samples in Figure 4.24 indicates that the sample mean of the differences in the mean emissivity values between the inner and the outer wrist is 0.0535 with a sample standard deviation in the differences of 0.0336. These differences are significant as the  $p$ -value (0.0013) obtained from the paired t-test is lower than the critical significance level of 0.05. These results indicating a very consistent difference between the emissivity of different locations on the arm.

#### 4.5.9.2 Female Emissivity Measurements for Different Age Groups

The measurements in Figures (4.25 and 4.26) show that the mean emissivity of the dorsal surface skin and the outer wrist skin are higher than that of the volar side and the inner wrist skin for all female groups. The measurements also suggest two age-related trends: 1) relatively unchanged mean emissivity values in the age groups 20-50 years with a slight increase in the dorsal surface skin emissivity, and 2) significant decreases in the mean emissivity values in the age group 50-60 years. These trends are consistent with the fact that females skin maintain the same thickness up to the age of 50 and then beyond this the skin thickness gets significantly thinner, probably due to decreased oestrogen levels after menopause [165].

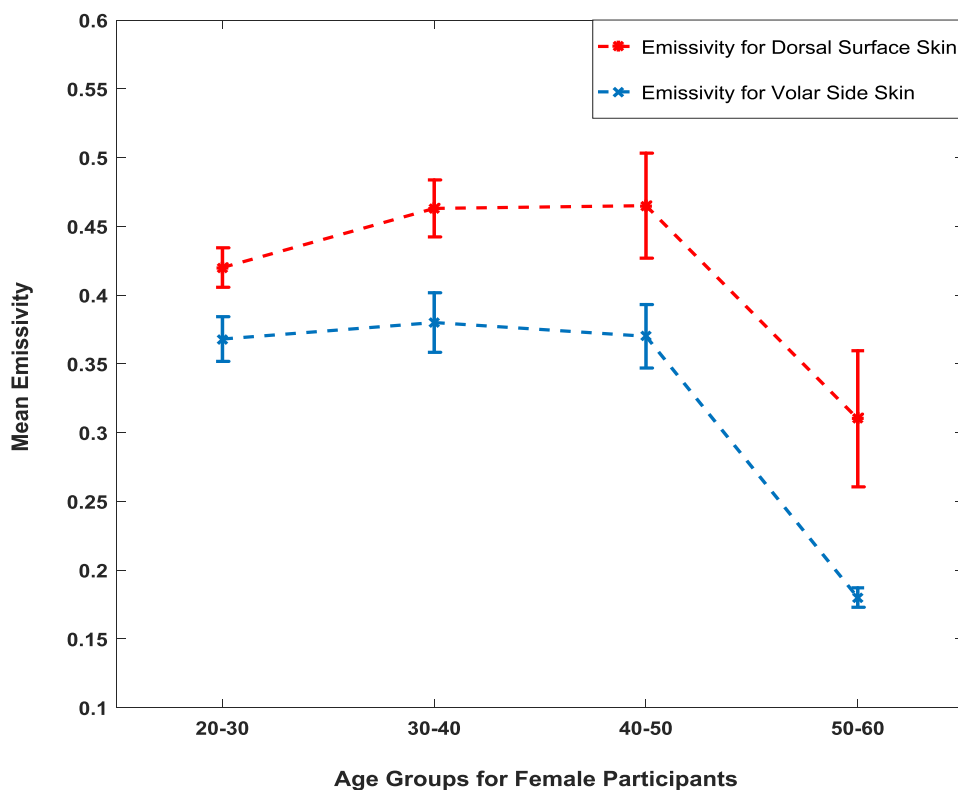


Figure 4.25: Mean emissivity values for the dorsal surface and the volar side skin for a sample of 25 female participants.

The statistical analysis of the female sample in Figure 4.25 indicates that the sample mean of the differences in the mean emissivity values between the dorsal surface and the volar side locations is 0.0678 with a sample standard deviation in the differences of 0.0439. These differences are significant as the  $p$ -value (0.011) obtained from the paired t-test is lower than the critical significance level of 0.05.

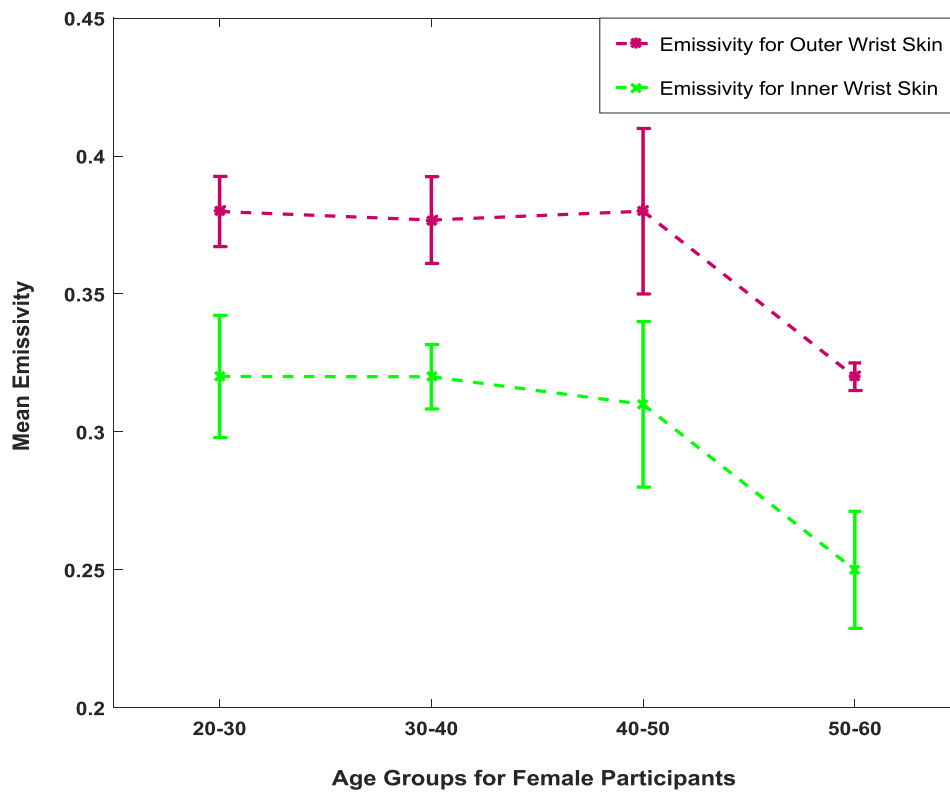


Figure 4.26: Mean emissivity values for the outer wrist and the inner wrist skin for a sample of 25 female participants.

The statistical analysis of the data in Figure 4.26 indicates that the sample mean of the differences in the mean emissivity values between the inner and the outer wrist location is 0.0645 with a standard deviation in the differences of 0.0387. These differences are significant as the  $p$ -value (0.0003) obtained from the paired t-test is lower than the critical significance level of 0.05.

#### ***4.5.10 Discussion***

A radiometer effective over the frequency band 80-100 GHz has been investigated and characterised for measuring the human skin emissivity of two samples of healthy participants. The system was calibrated absolutely using liquid Nitrogen and ambient temperature sources. These measurements were used to characterise self-emission and MMW radiation from a metal plate and fluorescent lights. The mean level of the self-emission reflected back from a metal plate was typically  $\pm 1.0$  K above the background. MMW emission emitted from a fluorescent light was found to increase the radiation temperature of the radiometer in the range of 62.0 K to 74.0 K with a standard deviation of  $\pm 4.0$  K.

Radiometric measurements made on the first group of 60 healthy participants over the 80 GHz to 100 GHz band indicate that there is a scatter in emissivity measurements over a range 0.17 to 0.68, and this is much greater than the experimental measurement uncertainty of  $\pm 0.005$ . The measurements show that the levels of thermal emission (emissivity and reflectance) varies consistently over different regions of the hand and forearm, with age, gender, ethnicity, body mass index, and hydration level of the skin. In general, the lower values of the mean emissivity are a result of measuring particularly thin skin on the inner wrist, the volar side and the back of the hand, whereas the higher values of the mean emissivity are results of measuring thick skin on the outer wrist, the dorsal surface and the palm of the hand. The measurements also show variation in emissivity from person to person, and at different locations on the hand. These variations are due to the differing water content and skin thicknesses of the participants. Calculating the sample mean emissivity values for the 36 males and 24 females separately for all measurement locations indicates that the mean difference

between male and female emissivity is  $\sim 0.02$ . This finding is consistent with the skin of males being thicker than that of females [150, 151, 152].

Measurements of a sample of 36 male participants indicate that the mean differences in the emissivity values between the palm of the hand and the back of the hand, the dorsal and the volar regions of the forearm, and the inner and the outer wrist locations are: 0.0658, 0.0675 and 0.0529 with a sample standard deviation in the differences of 0.0531, 0.0319 and 0.0345 respectively. For a sample of 24 female participants, the sample mean of the differences in the emissivity values between the thinner and the thicker skin regions were found to be: 0.0589, 0.0729 and 0.0646 respectively with a standard deviation in the differences of 0.0375, 0.0449, and 0.0394. These measurements indicate significant differences in the mean emissivity values between the thinner and the thicker skin regions.

Measurements of a sample of 20 healthy participants from both genders having normal and high body mass index show that male and female groups with high BMI have higher mean emissivity values at all measurement locations compared with those having normal BMI. The mean differences in the emissivity values between the two male groups are calculated to be in the range of 0.05 to 0.15 for all measurement locations, these differences are also similar between the two females group. These measurements confirm a strong correlation between the human skin emissivity and the BMI, the latter being directly proportional to the skin thickness [155].

Measurements of the mean emissivity of a sample of 24 male participants having Asian and European ethnicities show that the mean emissivity of male participants having Asian ethnicity is lower than that of male participants having European ethnicity overall measurement locations. The mean differences in emissivity values

between Asian and European male participants were calculated to be in the range of 0.04 to 0.11. These differences are likely to be due to higher hydration level and thinner skin of Asian male participants [161, 162, 163].

Measurements of the mean emissivity of a sample of 24 female participants having Asian and European ethnicities show that the mean emissivity of female participants having Asian ethnicity is lower than that of female participants having European ethnicity overall measurement locations. The mean differences in emissivity values between Asian and European female participants were calculated to be in the range of 0.014 to 0.038. Again, it is likely that these differences are due to thinner skin and higher hydration levels of female participants having Asian ethnicity compared with Europeans [161, 162, 163].

Measurements of a sample of 16 participants (10 males and 6 females) indicate that the mean differences in the emissivity values between the normal and wet palm of hand, and normal and wet back of hand skin are 0.141, and 0.067 with a sample standard deviation in the differences of 0.066, and 0.046 respectively. This indicates a strong correlation between the human skin emissivity and the hydration level of the skin. The differences between the wet and the normal palm of hand skin are more significant than that of the back of hand skin, and this is due to the thick SC layer that can retain water and make the hydration level for the palm of hand skin significantly higher in a wet state compared with a normal state [164]. These results confirm that radiometry can distinguish between normal healthy skin and wet skin in tens of seconds in non-contact with the human body.

Measurements obtained from the second group of 60 healthy participants suggest a trend in the mean emissivity values with age and gender, which might be due to variations of skin thickness, water content, and blood circulation, these factors having some dependency on the age, the gender, and the state of health of the participants. An overview of the statistical analysis of the human skin measured emissivity obtained from the first group of 60 healthy participants are summarises in Table 4.13.

Locations or group	Differences in emissivity ±SD males participants	Differences in emissivity ±SD females participants
Palm and back of the hand	0.0658±0.0531	0.0589±0.0375
Inner and outer wrist	0.0529±0.0345	0.0646±0.0394
Dorsal and volar side	0.0675±0.0319	0.0729±0.0449
Dry and wet palm of hand	0.148±0.0776	0.128±0.04
Dry and wet back of hand	0.056±0.047	0.0833±0.039
Normal and high BMI	Differences: 0.05-0.15 SD normal BMI:±0.0704 SD high BMI: ±0.0797 For all six locations	Differences: 0.06 to 0.14 SD normal BMI:±0.0446 SD high BMI: ±0.0549 For all six locations
Asian and European participants	Differences: 0.04-0.11 SD for Asian: ±0.0726 SD for European: ±0.098 For all locations	Differences: 0.014-0.038 SD for Asian: ±0.0723 SD for European:±0.0875 For all locations

Table 4.13: An overview of the statistical analysis of the human skin emissivity.

## 4.6 Conclusions

Radiometric measurements made on a sample of 30 healthy participants at 95 GHz show that the mean emissivity values of males are higher than that of females by 0.0464. The results obtained from the unpaired t-test indicate that these differences are insignificant since the  $p$ -value (0.2433) is greater than the critical significance level of 0.05. This is due to the small number of human subjects that involved in this study.

Measurements of human skin emissivity of a sample of 60 healthy participants (36 males and 24 females) over the frequency band 80-100 GHz show that the mean emissivity of males skin is higher than that of females by  $\sim 0.02$ . This difference is insignificant since the  $p$ -value (0.488) obtained from the unpaired t-test is greater than the critical significance level of 0.05. The measurements also show the emissivity of thick layers of skin in the human hand and forearm, such as the palm of the hand, the outer wrist and the dorsal surface of the forearm is significantly higher (as obtained from the paired t-tests) than those of the back of the hand, the inner wrist and the volar side of the forearm for both genders.

The results obtained from radiometric measurements presented and discussed in this chapter (from samples of 30 healthy participants, the first group of 60 healthy participants, and the second group of 60 healthy participants) show the quantitative variations in the skin emissivity between locations, gender, individuals, body mass index, different age groups, and ethnicity. The study reveals that these variations are related to the skin thickness, water content, and hydration level of the skin. These measurements indicate that the emissivity of the human skin in the MMW band is rich in information, a capability that may enable radiometry to be used as a non-contact technique to detect and monitor skin conditions.

## **4.7 Possible New Applications Highlighted by this Research**

The main advantages of the technique presented in this chapter are: 1) human skin signatures (emissivity) can be measured without exposing the human body to any type of artificial or man-made radiation, 2) radiometric sensitivity is sufficient to identify surfaces attached to the human skin such as liquid, metallic and non-metallic objects. Furthermore, materials intentionally attached to the skin, having dielectric properties identical with the human skin will be identified by their differential radiation temperatures, something which an active system cannot achieve, 3) the measurements can be made in tens of seconds using a non-contact sensor with high precision, and 4) the system is free from artefacts of speckle effects and multipath problems since spatially incoherent emission is used [167, 168]. These properties make radiometry good technique to be used for the purposes of medical applications and security screening portals.

### ***4.7.1 Radiometry in Medical Applications***

The measurements presented in this chapter show a strong correlation between the skin emissivity, thickness and the water content. As an imaging sensor, radiometry can deliver spatial resolutions down to around half of the wavelength of the radiation used, which can be  $\sim 1.0$  mm for the MMW band (Abbes' microscope resolution limit) [169, 170]. This property enables highly localized, non-contact measurements to be made just below the skin surface. This indicates that radiometry could be used as a non-contact viable technique to detect and monitor skin disease or damage, where the disease or the damage alters the water content or the skin thickness. It may complement established methods on the optical band that have difficulty in measuring the dermis and the ultrasound techniques which measure different physical properties

in the skin. Developing this goes part way to satisfying the recommendations of the Engineering and Physical Sciences Research Council (EPSRC) funded Teranet programme which would like to see greater penetration capabilities of terahertz technologies into the skin for medical applications [171]. These findings are consistent with the simulation results of the half space electromagnetics model [124].

#### ***4.7.2 Skin Signature in Security Screening***

Variation in the mean emissivity values presented in this chapter opens a new window of research in security screening, this being the identification of boundaries and limits for the emissive and the reflective properties of different parts of the human body, as a means to anomaly identification [172]. The implications of having model emissivities for different regions of the human body and different genders, ethnicities and age groups, is that security screening of persons can become more of an automated process. As radiometry is used in the estimation of emissivity, any attempts at deception, by substituting a human skin surrogate over the body will be recognised as it will not fit the expected characteristics. This is because the emissivity is derived from the amount of radiation emitted by the body, not just from its reflection properties. This means skin surrogates will be recognised even if they have exactly the same electrical properties as human skin. An active (coherent wave) illumination system will not have this capability, as it measures reflectivity directly. In a walk-through portal screening system, a machine would process in a matter of seconds the radiometric measured emissivity from all regions of the human body together with a profile of the individual derived from gender, age and ethnicity. This will increase the detection probabilities and reduce the false alarm rates in security screening portals, a capability that is being demanded internationally by governments and in the UK by

the Home Office Future Aviation Security Solutions (FASS) programme and the Joint Security and Resilience Centre (JSaRC) [173].

The following chapter discusses the feasibility of using radiometry as a non-contact technique for detecting the signature of the burn of the porcine skin samples with and without dressing materials and before and after the application of localised heat treatments.

## Chapter 5

### Passive Millimetre Wave Sensing Through Dressing

#### Materials Using Porcine Skin Samples

*This chapter presents the development of an experimental setup for measuring the emissivity of porcine skin samples over the band (80-100) GHz. The measurements were conducted on samples with and without dressing materials and before and after the application of localised heat treatments. Different methodologies were developed and applied on fresh porcine skin samples. The experimental results reveal that radiometry is capable of detecting burns under dressing materials without their removal.*

#### 5.1 Introduction

In England and Wales, around 13 000 patients with burn injuries are admitted to burn services department annually [174]. According to 2003-2011 statistics, males accounted for 63% of those patients whereas females 37% with a total in-hospital mortality of ~1.51% [174]. The severity of the burn can range from minor (erythema or redness) to extremely severe (full thickness). This characterised by the extent of the skin affected, the depth of damage, the age of the patient, the anatomical site, and the presence of disorders [96, 174]. Burn is classified by depth into; first degree, second degree, third degree, and fourth degree [175]; as discussed in chapter 2 (section 2.15.5).

Burn wound requires treatment for the purposes of preventing fluid and protein loss, reducing the risk of infection, and preventing the hypothermia [176, 177]. Wound healing is a complex dynamic process of tissue regeneration and growing that requires a good environment to heal successfully [178]. Dressing materials are used in the treatments of burn wound since 1) it absorbs the exudates, 2) it provides a barrier against bacteria and organism that causes infection and prolong the period of healing, 3) it maintains appropriate temperature and moist environment, 4) it allows gas exchange between the environment and the wound site and 5) it enhances the blood flow. Visual inspection is the current protocol for monitoring the burn wound healing progress [175, 179, 180]. This protocol gives an excellence indicator about the state of the wound and the healing progress, and more importantly, it can detect signs of infections such as exudates, redness, swelling, heat, functionality of the infected part and pus draining [181]. However, visual inspection requires the removal of dressing layers. This practice consumes time, money, and it is definitely uncomfortable and painful to the patient especially in the cases where the dressing materials are being moistened and become adherent to the wound bed [3, 178].

Although many signs can help the experienced burn surgeon to identify the depth of the burn, making a distinction between the second and the third degree burns visually is a difficult task. The accuracy of this assessment is around 64% to 76% [182, 183] and it can fall to 50% if the burn is assessed by inexperienced surgeons [182, 184]. False assessments of burn depth prolong the time required for burn wound to heal and make the patient faces unnecessary surgery [182]. Therefore, many techniques have been developed for assessing the wound healing progress and the degree of the burn such as the optical coherence tomography [96, 185, 186, 187], the thermography (including the active dynamics thermography and the infrared thermography) [188, 189, 190,

191], and the ultrasound (including the pulse-echo ultrasound, the pulse-wave Doppler ultrasound, and the laser Doppler ultrasound) [120, 192, 193, 194]. Although some of the results obtained from these technologies are promising as discussed in chapter 2 (section 2.16), none of these techniques can monitor the wound healing progress and the depth of the burn without the removal of the dressing materials. A technique that could penetrate dressings and identify the healing status of the burn wounds would be extremely beneficial to both patients and healthcare professionals.

It is unethical to expose the human skin to a high temperature source that might damage or burn the skin. Therefore, an animal's model in close mimic with the human skin is a more appropriate solution. Although ex vivo model of porcine skin might not be perfect as ex vivo tissue of animal can't be full manner imitator of in vivo skin because of the absence of capillary blood flow. However, a standardisation of the method, passive sensing and imaging, for detecting burn wound and burn depth under dressing materials would be a great practical utility.

## **5.2 Selection of Porcine Skin and Ethical Approval**

A motivation for measuring the skin of pigs (porcine skin) is that it has structural and functional similarities to the human skin [176, 195]. Porcine and human skin have similar percentages of collagen and elastic fibers in their extracellular matrix [176]. The thickness of the epidermis layer for porcine skin varies depending on the location in the range of 30-140  $\mu\text{m}$ , whereas the thickness of the epidermis layer for the human skin varies in the range of 50-120  $\mu\text{m}$  [176, 196]. In addition, human and porcine skin have resemblances in elastic components [176], thermal sensitivity [197], type of keratins [198], vascularization [176], and stratum corneum thickness [198].

In this research, 15 porcine skin samples were purchased from an abattoir and the measurements were conducted on these for a time of up to no longer than four hours after the slaughter. The samples were taken from pigs having ages ranging from six to eight months and average weights from 55 kg to 60 kg. The samples were taken from the back region of nine healthy animals. This region is chosen since it is free from hair follicle and sweat glands.

The study was approved by the ethics committee of Manchester Metropolitan University (ethics reference no: SE1617114C). A copy of the ethical approval is attached in Appendix B.

### 5.3 Three Layer Model for Dressed Burn Wound

A three-layer model has been constructed and developed to determine the emissivity of the dressed burn-damaged skin; in this model, the first layer is a semi-infinite layer of air, the second layer is a finite thickness dressing materials, and the third layer is a semi-infinite layer of skin, as illustrated in Figure 5.1.

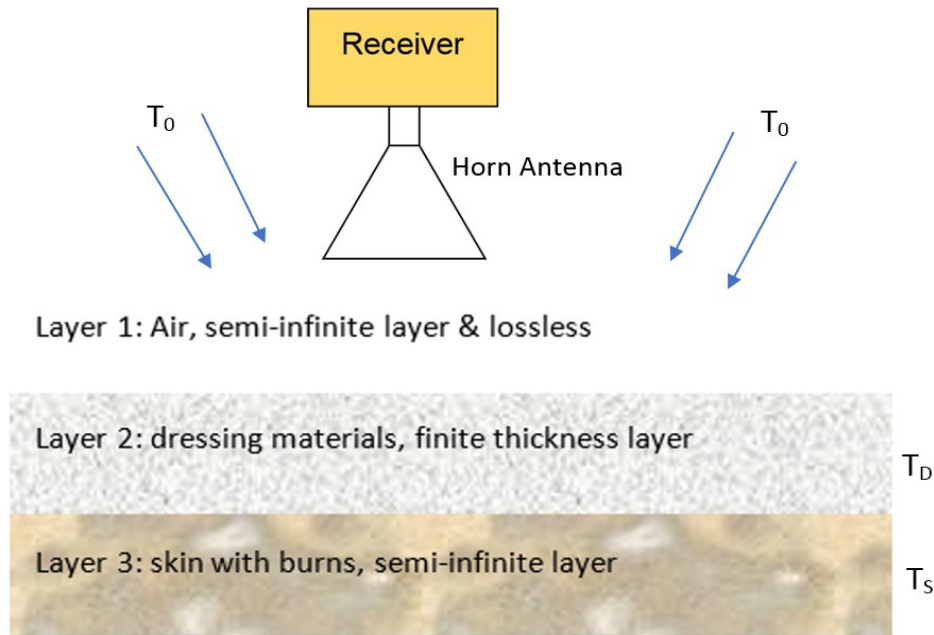


Figure 5.1: Three-layer model for dressed burn wound comprising of: a semi-infinite layer of air, finite thickness layer of dressing materials, and a semi-infinite layer of burn-damaged skin.

In the model radiation from the surrounding environment, having a radiation temperature  $T_0$ , illuminates the dressing materials, whilst radiometric emission from the skin having a physical temperature  $T_S$  illuminates from the opposite direction. As the dressing material, at a physical temperature  $T_D$  has finite absorption, these are also radiating. The radiation temperature of the sample (dressed burn-damaged skin) as measured by the radiometer can, therefore, be expressed [199] as:

$$T_b = T_0 R(1 - b) + T'_N R b + T_D A + T_S \eta \quad (5.1)$$

Where  $T'_N$ , is the receiver noise intensity of the noise that is injecting to the antenna feeder from the input circuit of the first active element,  $R$  is the reflectance of the dressed skin,  $A$  is the absorptance of the dressing layer, and  $\eta$  is the emissivity of the skin. The parameter  $b$  is the fraction of the total radiation blocked from being reflected from the sample by the antenna, the value of  $b$  depends upon the antenna and its proximity to the sample. Law of conservation of energy applied on the system gives [140]:

$$1 = R + A + \eta \quad (5.2)$$

A wave-guide circulator was placed between the horn antenna and the receiver and this makes,  $T'_N = T_0$ . For a very low loss dressing materials,  $A \approx 0$ , this means the radiation temperature of the sample in Equation (5.1) can be expressed in terms of the sample emissivity, the sample thermodynamic (or physical) temperature, and the background illumination radiation temperature as:

$$T_b = (1 - \eta)T_0 + T_s\eta \quad (5.3)$$

Using Equation (5.3), the receiver output voltage (discussed in chapter 4, section 4.4.3) can be written in terms of the 3-layer system's radiation temperature as:

$$Vs = \alpha\{T_0(1 - \eta) + T_s\eta + T_N\} \quad (5.4)$$

Where,  $T_N$  is the receiver noise temperature in Kelvin. Using Equation (4.14) in chapter 4 (section 4.3.3). The receiver noise temperature can be expressed in terms of the receiver responsivity  $\alpha$  and the hot load calibration parameters ( $V_H$  and  $T_H$ ) as:

$$\alpha T_N = V_H - \alpha T_H \quad (5.5)$$

Using Equation (4.15) in chapter 4 (section 4.3.3) and Equations (5.4 and 5.5), and equating  $T_0$  to  $T_C$  as the cold load is a foam absorber at ambient temperature; the emissivity of the sample becomes:

$$\eta = \frac{(V_S - V_C)(T_H - T_C)}{(V_H - V_C)(T_S - T_C)} \quad (5.6)$$

Where,  $V_S$ ,  $V_H$ , and  $V_C$  are the voltage levels in Volts for the sample, the hot and the cold calibration loads respectively.  $T_S$ ,  $T_H$ , and  $T_C$  are the thermodynamic temperature of the sample, and the hot and the cold calibration loads respectively in Kelvin.

## 5.4 Experimental Work

The objectives of the experimental work presented in this chapter are highlighted as follows:

- To develop an experimental setup for measuring the emissivity of porcine skin samples.
- To measure the transmission and the loss in different types of dressing materials samples that have different thicknesses and textiles.
- To assess the feasibility of using the 90 GHz calibrated radiometer to obtain information about the signature of the skin under dressing materials in normal and burn-damaged states.
- To assess the feasibility of using the 90 GHz calibrated radiometer as a non-contact technique to distinguish between normal and burn-damaged skin with and without the presence of dressing materials.

The experimental work presented in this chapter is divided into three parts; 1) calibration measurements of the 90 GHz radiometer, 2) measurements of emissivity, transmission and loss for different types of dressing materials samples, and 3) measurements of porcine skin emissivity before and after the applications of localised heat treatments with and without the presence of dressing materials.

#### 5.4.1 Experimental Description for Calibration and Dressing Materials

A radiometer effective over the frequency band (80-100) GHz was calibrated and used for measuring the emissivity of the dressing materials; as illustrated in Figure 5.2, this radiometer is described in details in chapter 4 (section 4.5.4).

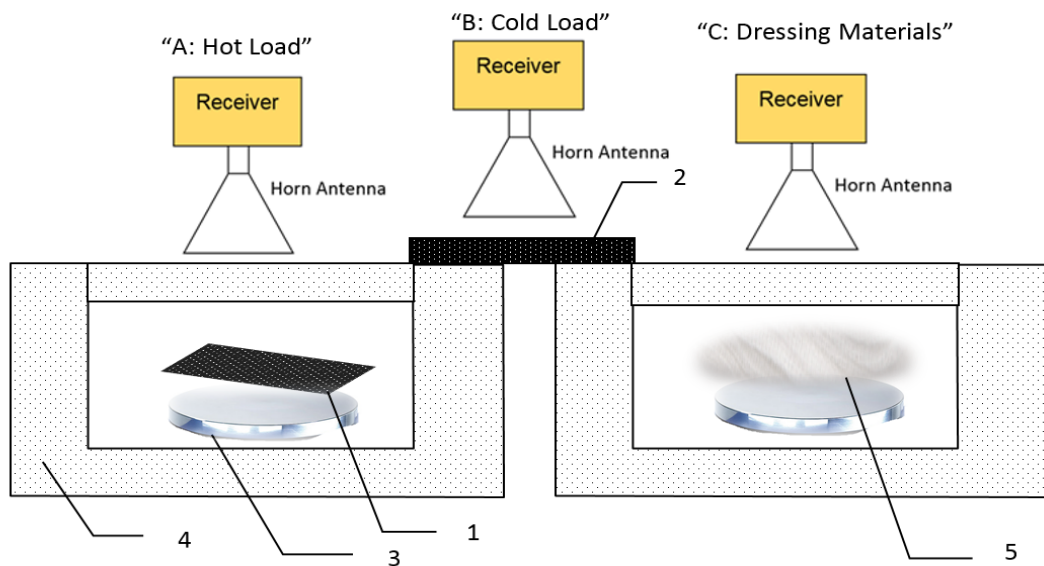


Figure 5.2: Radiometric emission centred at 90 GHz is collected by a moveable horn antenna at positions: A to measure a hot calibration source (1) (carbon loaded foam absorber; type: Eccosorb AN-73) stabilized at a temperature  $\sim 54$  °C using a digital hotplate (3) placed in a polystyrene foam bucket (4), B to measure the cold calibration source (2) (carbon loaded foam absorber; type: Eccosorb AN-73) in thermodynamic equilibrium with air temperature  $\sim 20$  °C, and C to measure the emission from dressing materials samples (5).

All measurements presented in Figure 5.2 were made over a distance of ~5.0 cm from the horn antenna to minimize the chances of subjects touching the measurement apparatus. When the dressing materials are directly placed on the digital hotplate, the temperature of the sample becomes:

$$T_s = T_H \quad (5.7)$$

Using Equation (5.6) and equating  $T_s$  to  $T_H$ , the emissivity of the dressing materials alone becomes:

$$\eta_D = \frac{(V_D - V_C)}{(V_H - V_C)} \quad (5.8)$$

Where  $V_D$  is the voltage level of the thermal radiation emitted from the dressing materials.

#### 5.4.2 Experimental Setup for Porcine Skin Measurements

The 90 GHz calibrated radiometer is used for measuring the mean emissivity values of the porcine skin samples before and after the applications of localised heat treatments. The samples were located over a digital hotplate and they were covered with dressing materials when it is required as illustrated in Figure 5.3.

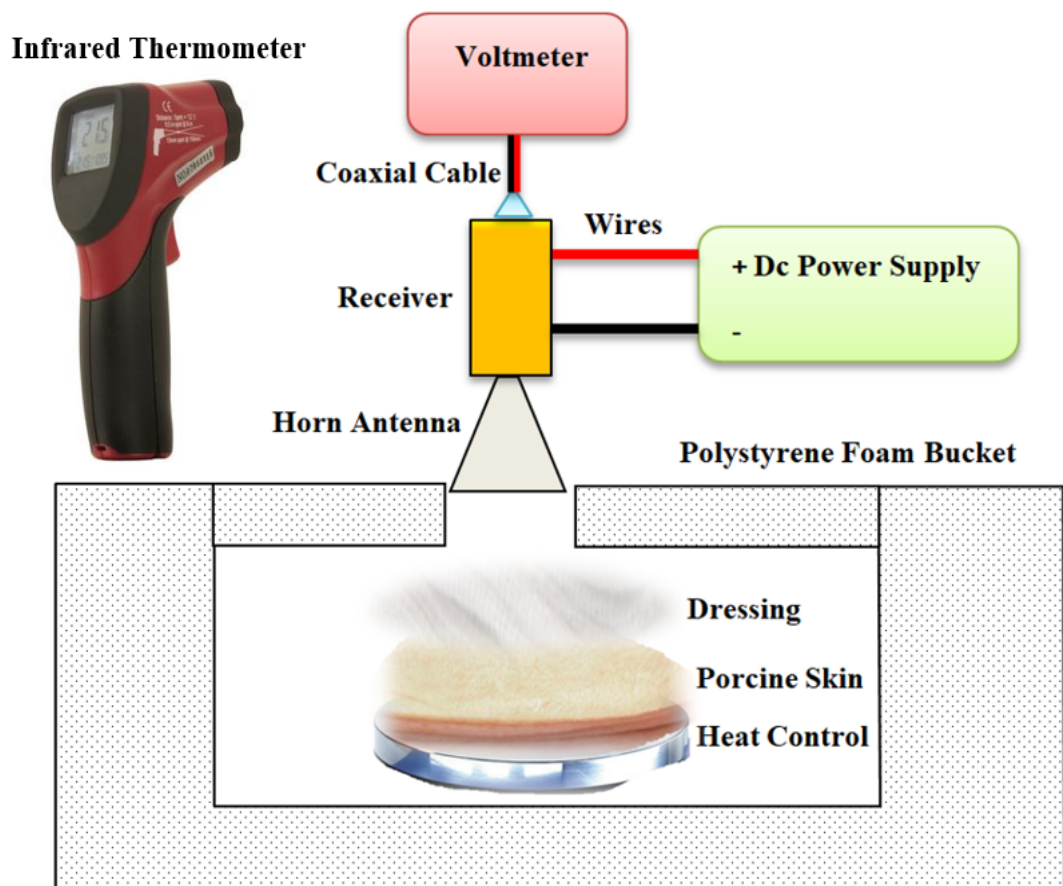


Figure 5.3: The experimental setup for the emissivity measurements of the porcine skin samples. A digital voltmeter is used to measure the output voltage level of the samples and a thermocouple and an infrared thermometer are used to measure the thermodynamic temperature of the samples.

The horn antenna was moved by hand to measure emission from the porcine skin samples in normal and burn damaged state with and without the presence of the dressing materials. The measurements were performed in an anechoic region, this achieved by surrounding the lab with a wall of carbon loaded absorbing foam as illustrated in Figure 5.4.



Figure 5.4: A wall of carbon loaded absorbing foam (length 1200 mm x width 2400 mm) surrounded the instrumentation.

Fifteen fresh porcine skin samples were taken from the back regions of nine animals to be used in this research. In general, the samples have a rectangular shape and average dimensions (length=100 mm, width=80 mm, and thickness=5.0-10.0 mm); all samples were chosen to be free from the hair follicles. The samples were taken directly after the animal was slaughtered and before the skin is washed. Figure 5.5 shows some of the samples that used in this research.

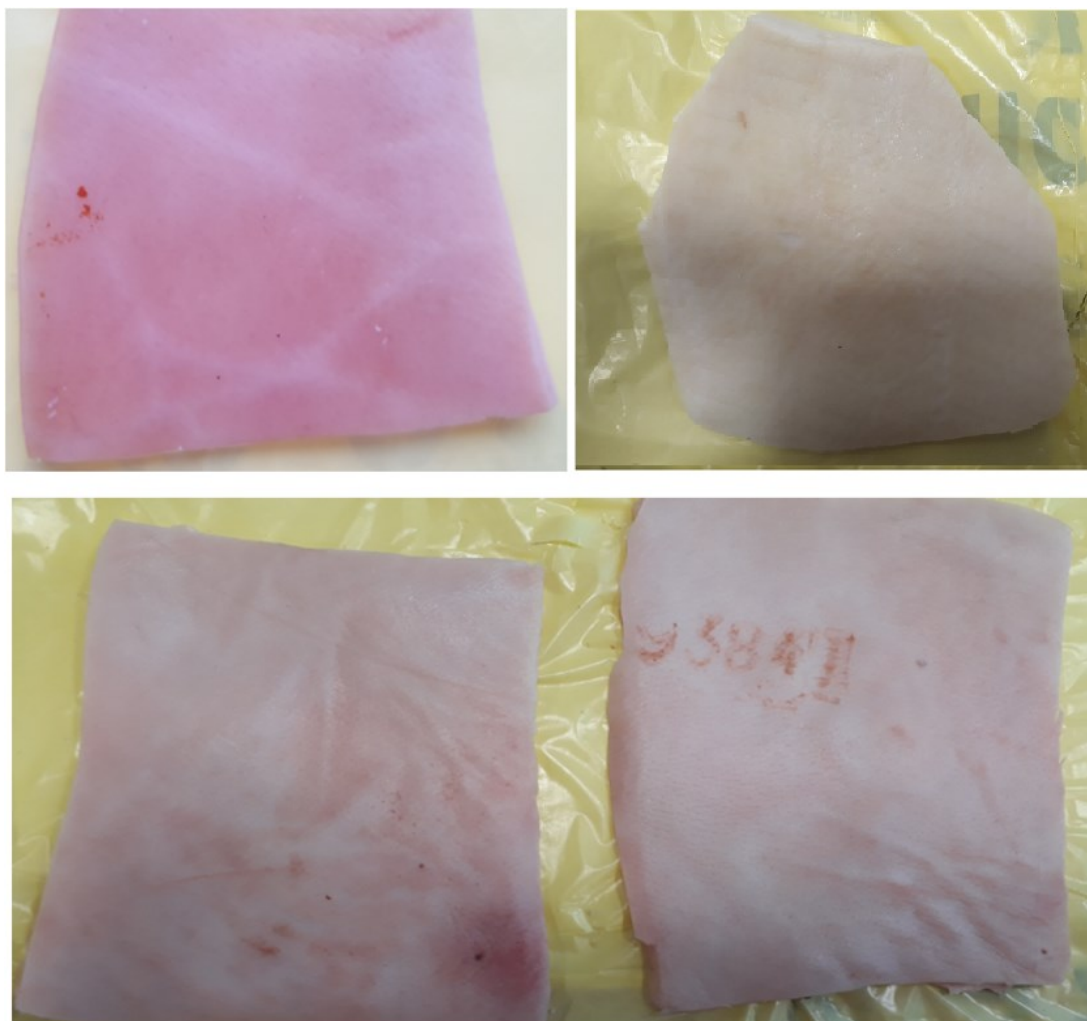


Figure 5.5: Samples of porcine skin used in the experimental work of this research.

A digital hotplate (type: LED digital hotplate magnetic stirrer, manufacturer: SciQuip Ltd) with a temperature range of 280 °C was located inside a polystyrene foam bucket and used to heat the samples and to stabilise the skin surface temperature to  $\sim 37$  °C as illustrated in Figure 5.6a. This temperature is chosen since it is closed to the in vivo surface temperature of the porcine skin  $\sim 35$  °C [195, 200].

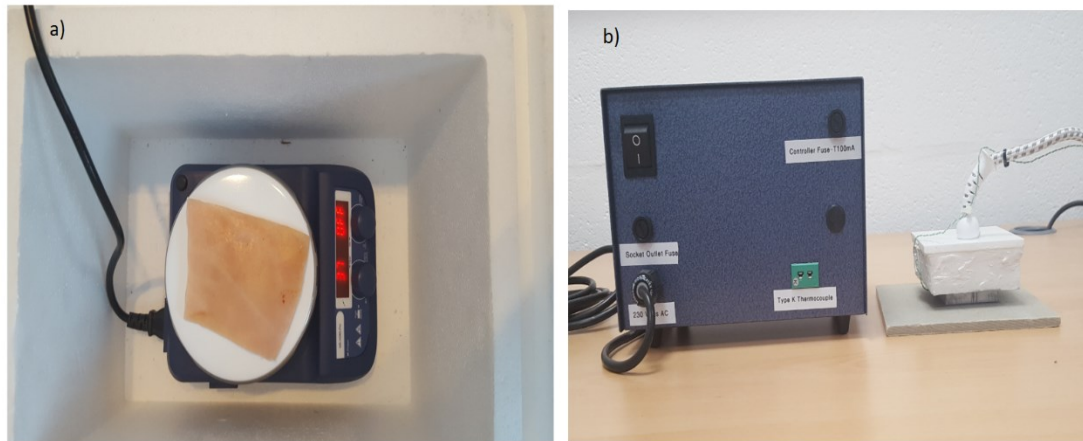


Figure 5.6: A digital hotplate used for heating and stabilising the surface temperature of the porcine skin samples (a) and a heat control device with (50 mm x 50 mm) metal plate used for performing burns on the porcine skin samples (b).

A thermocouple and an infrared thermometer (type: N85FR, manufacturer: Maplin) with a temperature range  $-50\text{ }^{\circ}\text{C}$  to  $+550\text{ }^{\circ}\text{C}$  and resolution of  $0.1\text{ }^{\circ}\text{C}$  were used to measure the skin surface temperature. A digital voltmeter (type: digital voltmeter, manufacturer: Keysight Technologies) with  $0.1\text{ mV}$  step size was used to measure the voltage level of the thermal emission of the porcine skin samples.

The heat control metal plate shown in Figure 5.6 b consists of a temperature controller, thermocouple, and a square metal plate (50 mm x 50 mm). During the experimental work, the device was used to apply a contact burn after the plate was heated in the range of  $100\text{ }^{\circ}\text{C}$  to  $140\text{ }^{\circ}\text{C}$  and placed on the skin surface with a constant pressure for different periods of time ranging from 10 seconds to 180 seconds. These periods were chosen to achieve different degrees of burn and different burn depths. Dressing materials (type: gauze burn dressing and light support bandage) were placed over the skin sample when it is required.

## **5.5 Methodologies Applied on Porcine Skin Samples**

This section discusses different methodologies developed and applied on porcine skin samples for measuring the emissivity of the skin before and after the applications of localised heat treatments with and without the presence of dressing materials.

### ***5.5.1 Methodology 1: Skin without Burns***

The samples were located over a digital hotplate and left to be heated and stabilised to 37.0 °C. Then the calibrated radiometer of Figure 5.3 was used to measure the voltage level of the thermal emission emitted from the samples and a thermocouple and an infrared thermometer were used to measure the skin surface temperature. The measurements were repeated five times and processed using Equation (5.6).

### ***5.5.2 Methodology 2: Skin without Burns and with Dressing Materials***

The samples were located over a digital hotplate and left to be heated and stabilised to 37.0 °C. Then dressing materials (4-layer Gauze burn bandage, and 1-layer light support bandage) were placed separately over the samples. After that, the calibrated radiometer of Figure 5.3 and an infrared thermometer were used to measure the voltage level and the thermodynamic temperature of the samples respectively. These measurements were repeated five times and processed using Equation (5.6).

### ***5.5.3 Methodology 3: Skin after the Application of Water and Cream***

The samples were located over a digital hotplate and left to be heated and stabilised to 37.0 °C. A thin layer of water was placed on the skin surface for a period of time ranging from 2.0 minutes to 4.0 minutes until the water is just absorbed (but not evaporated). Then emissivity measurements were conducted directly and quickly using the calibrated radiometer of Figure 5.3 and Equation (5.6).

For the cream, a thin layer of different types of cream (uses in the treatments of burns and injuries such as Savlon, Sudocrem, and Flamazine) was placed on the skin surface for a period of time ranging from 2.0 minutes to 4.0 minutes until the cream is absorbed. Then emissivity measurements were conducted directly and quickly using the calibrated radiometer of Figure 5.3 and Equation (5.6).

### ***5.5.4 Methodology 4: Skin with Burns***

The samples were located over the digital hotplate and left to be heated and stabilised to 37.0 °C. Then contact burns were applied using a heat control metal plate. The plate was heated to 140 °C and placed directly on the skin surface for a period of time ranging from 10 seconds to 180 seconds with a constant pressure. Then emissivity measurements for the burn-damaged skin were obtained and repeated five times using the calibrated radiometer of Figure 5.3 and Equation (5.6).

Then dressing materials were placed over the burn-damaged skin and the emissivity of the sample was measured using the calibrated radiometer of Figure 5.3.

### ***5.5.5 Methodology 5: Skin with Different Burn Depth***

The samples were located over the digital hotplate and left to be heated and stabilised to 37.0 °C. The emissivities of the samples were obtained using the calibrated radiometer. Then contact burns were applied using a heat control metal plate heated to 100 °C and placed directly on the skin surface for a different period of time; start from 10 seconds (first degree burn), then 60 seconds (second degree burn) and finally 120 seconds (third degree burns). The emissivities of the samples after each application of localised heat treatments were obtained using the calibrated radiometer of Figure 5.3.

## **5.6 Experimental Results**

The 90 GHz radiometer was calibrated and used to measure the emissivity of the dressing materials and the porcine skin samples. The calibration measurements (receiver noise temperature 453.0 K) are similar to that obtained using the ambient and the liquid Nitrogen calibration sources applied to the same radiometer in chapter 4 (section 4.5.5). This indicates that the radiometer has consistent and long-term stable measurements.

### ***5.6.1 Dressing Materials Measurements***

It is a known fact that MMW radiation is minimally attenuated by textiles used in clothing [3, 201]. This section investigates the transparency of the dressing materials used in the treatment of burn injuries, as there is little available information for these materials. The measurements were made over the band 80 GHz to 100 GHz using the calibrated radiometer of Figure 5.2 and Equation (5.8). The measurements were made on different types of samples having different thicknesses as illustrated in Table 5.1. Dressing materials were purchased from the pharmacy and they were dry and removed from protective packaging prior to the measurements. The measurements were repeated (5-10) times and they were conducted at ambient temperature of ~ 20 °C. The reflectance of the gauze burn bandage samples consist of 2 to 20 layers were assumed to be in the range of 0.05 to 0.1, whereas the reflectance of the light support bandage was assumed to be 0.05 [125].

Dressing materials Type	Thickness	Emissivity	Transmission%	Loss in dB $10 \log_{10}(T)$
White gauze burn bandage (20 layers)	8-10 mm	0.1	80	0.969
White gauze burn bandage (4 layers )	1.0 mm	0.05	90	0.458
White gauze burn bandage (2 layers)	< 1.0 mm	0.02	93	0.315
White gauze burn bandage (1 layer)	<< 1.0 mm	0.01	99	0.0436
Light support cotton stretch bandage type 2 (1 layer)	1.0 mm	0.07	88	0.555
Light support cotton stretch bandage type 2 (2 layers)	2.0 mm	0.13	82	0.862
Non-adherent wound dressing (Tefla™) (1 layer)	<< 1.0 mm	0.01	99	0.0436
Temporary wound dressing (Biobrane®) (1 layer)	<< 1.0 mm	0.01	99	0.0436

Table 5.1: Measurements conducted on various types of dressing materials used in the treatment of burn wound.

The measurements in Table 5.1 indicate that dressing materials are highly transparent over the band (80-100) GHz. The measurements also indicate that the thickness of the bandage is an important factor to consider as increasing the thickness of the dressing materials is decreasing the transmission and increasing the loss and the emissivity of the sample as expected.

### ***5.6.2 Porcine Skin Measurements***

This section presents emissivity measurements made on porcine skin samples using the calibrated radiometer of Figure 5.3 and Equation (5.6). These measurements were obtained from two separate experiments over the band 80 GHz to 100 GHz.

#### ***5.6.2.1 Experiment 1: Porcine Skin Measurements without Burns***

The objectives of this experiment are as follows:

- To measure the mean emissivity values of porcine skin samples without burns.
- To investigate the ability of the 90 GHz calibrated radiometer to penetrate dressing materials and provide information about the signature of the skin under dressing materials without the dressings removal.
- To investigate the ability of the radiometer to sense variation in water content and hydration level of the skin by measuring the mean emissivity values of the samples before and after the application of water and cream.

In this experiment, the mean emissivity values of the porcine skin samples were measured experimentally using methodology 1 described in section 5.5.1. The measurements were made on four fresh samples taken from the same animal. The measurements were repeated five times on each sample. The mean and the standard deviation of the measurements are illustrated in Figure 5.7.

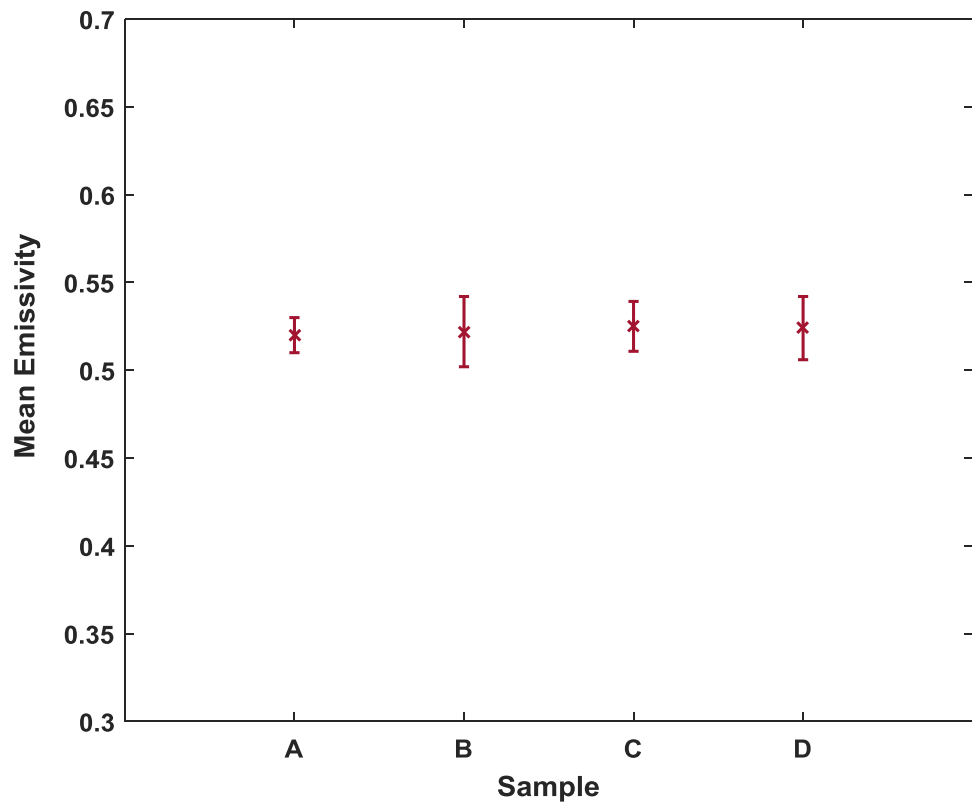


Figure 5.7: Mean emissivity values and standard deviation bars for porcine skin samples A, B, C, and D was taken from the back region of the same animal.

The measurements in Figure 5.7 indicate that the mean emissivity value of the samples A, B, C, and D is  $\sim 0.52$  with experimental measurements uncertainty of  $\pm 0.005$ . The standard deviations of the samples were calculated to be in the range of  $\sim 0.01$  to  $\sim 0.02$ . It is reasonable to obtain the same mean emissivity value for all the samples as they were taken from the back region of the same animal.

The capability of the 90 GHz calibrated radiometer to detect the signature of the porcine skin under dressing materials was investigated and measured using methodology 2 described in section 5.5.2. The methodology was applied on the samples A, B, C, and D. The mean emissivity values of the samples were obtained before and after the dressing materials were placed as illustrated in Figure 5.8.

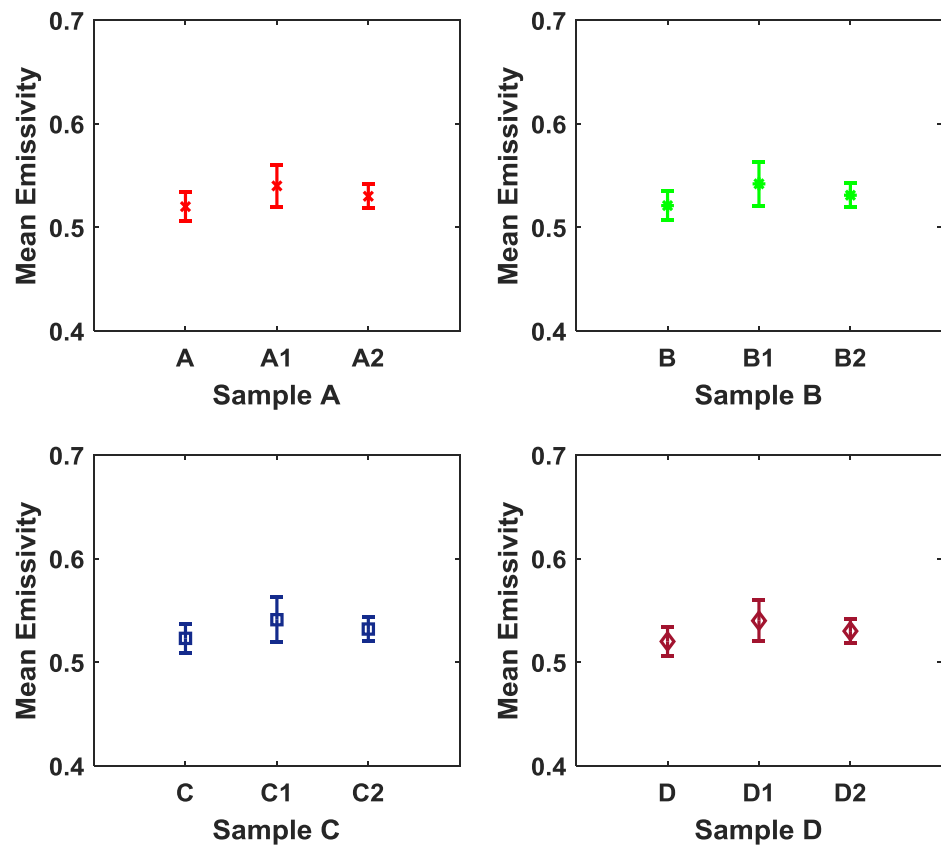


Figure 5.8: Mean emissivity values and standard deviation bars for porcine skin without and with dressing materials. The samples A, B, C, and D represent skin without dressing materials, A1, B1, C1, and D1 represent skin with 4-layer gauze burn bandage, and A2, B2, C2, and D2 represent skin with a light support bandage.

The measurements in Figure 5.8 indicate that the differences in the mean emissivity values between the undressed and the dressed samples are in the range of  $\sim 0.01$  to  $\sim 0.02$  for all measured samples. These results confirm that the signature of the skin is seen through the 4-layer gauze burn bandage and the light support bandage as the mean emissivity values of the dressed samples are very close to that of undressed samples.

The mean emissivity values for porcine skin samples before and after the application of water and cream were investigated and measured experimentally using methodology 3 described in section 5.5.3. The methodology was applied on samples A, B, C, and D as illustrated in Figure 5.9.

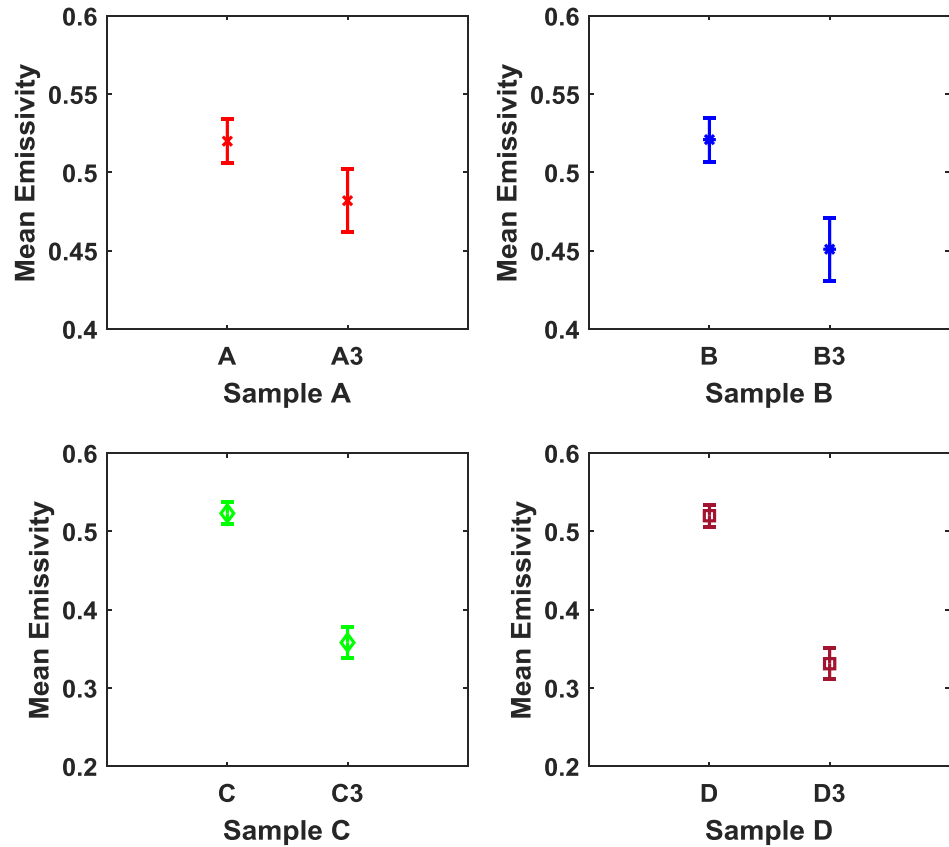


Figure 5.9: Mean emissivity values and standard deviation bars for porcine skin samples before and after the application of water and cream. Samples A, B, C, and D represent normal skin, A3: represents skin with Sudocrem, B3: represents skin with Flamazine cream, C3: represents skin with Savlon cream, and D3: represents skin with water.

The measurements in Figure 5.9 indicate that there is a well define contrast in the mean emissivity values of the skin before and after the application of water and cream. The differences in the mean emissivity values of the skin before and after the application of cream and water are ranging from  $\sim 0.04$  to  $\sim 0.19$ . The mean emissivity values of the porcine skin samples after the application of Savlon cream (that includes of Cetostearyl alcohol, liquid paraffin, perfume, and purified water) and Flamazine cream (that includes of Silver Sulfadiazine, cetyl alcohol, liquid paraffin, and purified water) are lower than that of Sudocream (that includes of purified water, liquid paraffin, and paraffin wax). These differences are due to the dielectric properties of the cream, the percentage of water content in the cream, the interaction of the porcine skin samples with different types of creams, and the ingredients that vary from cream to cream. These differences indicate that radiometric sensitivity is sufficient to sense and detect variation in the skin water content and hydration level.

#### ***5.6.2.2 Experiment 2: Porcine Skin Measurements with Burns***

The objectives of this experiment are as follows:

- To assess the feasibility of using the 90 GHz calibrated radiometry to distinguish between the signature of the skin before and after the application of localised heat treatments (unburned and burn-damaged skin).
- To assess the feasibility of using the 90 GHz calibrated radiometer to detect the signature of the burn under dressing materials.
- To assess the feasibility of using the 90 GHz calibrated radiometer to predict the degree of the burn (or the burn depth).

The signature of burn-damaged skin after the application of localised heat treatments was measured experimentally using methodology 4 described in section 5.5.4. The

methodology was applied on four samples X, Y, Z, and W. These samples were taken from the back region of the same animal. The measurements were conducted before and after the dressings were applied on the samples. The measurements were repeated five times and the mean emissivity values were obtained as illustrated in Figure 5.10.

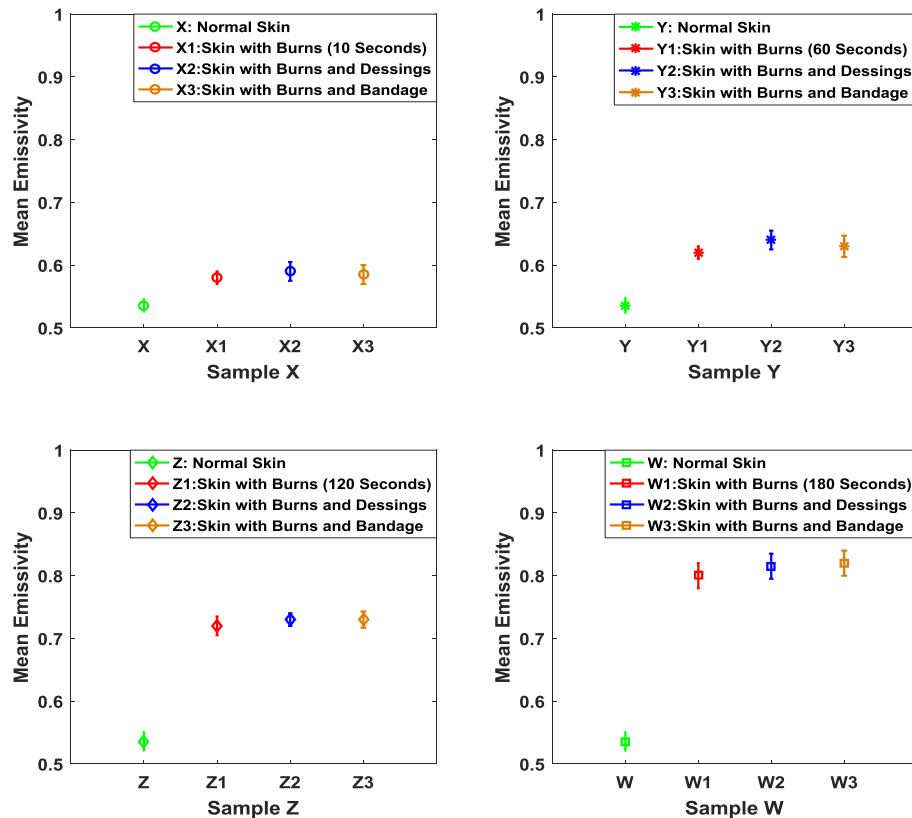


Figure 5.10: Mean emissivity values and standard deviation bars for porcine skin samples (obtained from the same animal) before and after the application of localised heat treatment. Samples X, Y, Z, and W represent normal skin. X1 represents skin with burns after 10 seconds of heat treatment, Y1 represent skin with burns after 60 seconds of heat treatment. Z1 represents skin with burns after 120 seconds of heat treatment, and W1 represents skin with burns after 180 seconds of heat treatment. X2, Y2, Z2, and W2 represent skin with burns and dressing (6-layer gauze burn dressing). X3, Y3, Z3, and W3 represent skin with burns and 1-layer light support bandage.

The measurements in Figure 5.10 indicate that the differences in the mean emissivity values between the unburned and the burned skin are: 0.044, 0.084, 0.184, and 0.264 for samples X, Y, Z, and W respectively. These differences confirm that there is a clear signature for the burn that can be detected using radiometry. The measurements also show that the signature of the burn is observed through the 6-layer gauze burn bandage and the light support bandage, as the mean emissivity values of the dressed burn are slightly higher than the undressed burn in the range of  $\sim 0.01$  to 0.02. The measurements also indicate that there is a direct proportionality between the mean emissivity values of the burn-damaged skin and the period of time for the localised heat treatment as it is significantly increased the burn depth.

It is a well-known fact that the depth of the burn is proportional to the length of time of the localised heating [200, 202]. The capability of the 90 GHz calibrated radiometer to distinguish between different burns depths was investigated using methodology 5 described in section 5.5.5. The methodology was applied on seven different samples taken from the back region of seven different animals. Different applications of heat treatments were applied on the same samples and the mean emissivity values of the samples were measured before and after different applications of heat treatments as shown in Figures (5.11, 5.12 and 5.13).

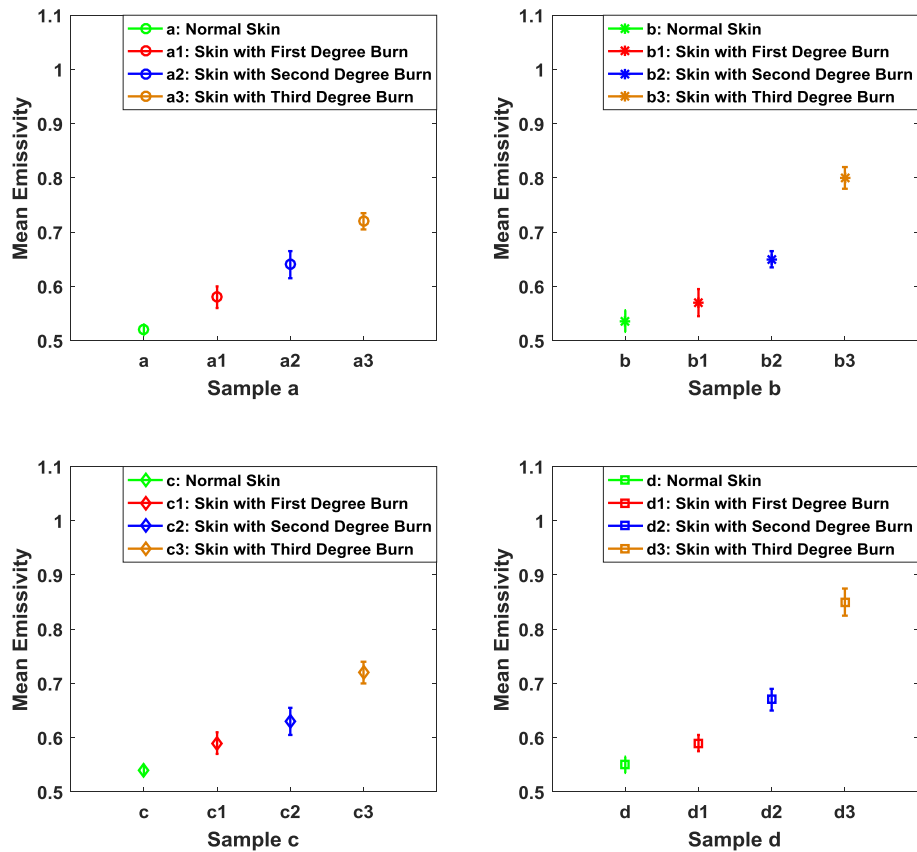


Figure 5.11: Mean emissivity values and standard deviation bars for porcine skin samples (obtained from different animals) before and after different applications of localised heat treatments. Samples a, b, c, and d represent normal skin; a1, b1, c1 and d1 represent skin with burns after 10 seconds of heat treatment (first degree burn); a2, b2, c2, and d2 represent skin with burns after 60 seconds of extra heat treatment (second degree burn); a3, b3, c3, and d3 represent skin with burns after 120 seconds of extra heat treatment (third degree burn).

The measurements in Figure 5.11 indicate that the mean emissivity values for the four samples before the application of heat treatments are in the range of 0.52 to 0.55. It is reasonable to find differences in the mean emissivity value of the skin as the samples were taken from different animals in which each animal has different skin thickness and different dielectric properties [157, 203]. The measurements also reveal that

biological tissue is responding similarly to the application of heat treatment as the mean emissivity values increase after each application of heat treatment for all samples as summarised in Table 5.2. However, the mean emissivity values for burn-damaged skin are different from sample to sample and this might be due to the resistivity and the conductivity of the skin that varies from animal to animal [134, 157, 203]. The measurements presented in Figure 5.11 confirm that radiometry can distinguish between different burn depths as it provides different mean emissivity values after each application of localised heat treatment.

The time period for heat treatment (in seconds)	Sample (a)	Sample (b)	Sample (c)	Sample (d)
0	0.52	0.536	0.54	0.55
10	0.58	0.57	0.59	0.59
60	0.64	0.65	0.63	0.67
120	0.72	0.8	0.72	0.85

Table 5.2: Mean emissivity values for porcine skin samples before and after different applications of localised heat treatments.

Heat treatment alters the chemistry and the structure of the biological tissue and more importantly cauterises parts of the tissue. This process produces exudates around the wound site. Although for *ex vivo* tissue, it is difficult to observe exudates with the absence of blood circulation. However, during the experimental work, one of the samples produces exudates and as a result, the effect of exudates around the burn wound has been measured and investigated as illustrated in Figure 5.12.

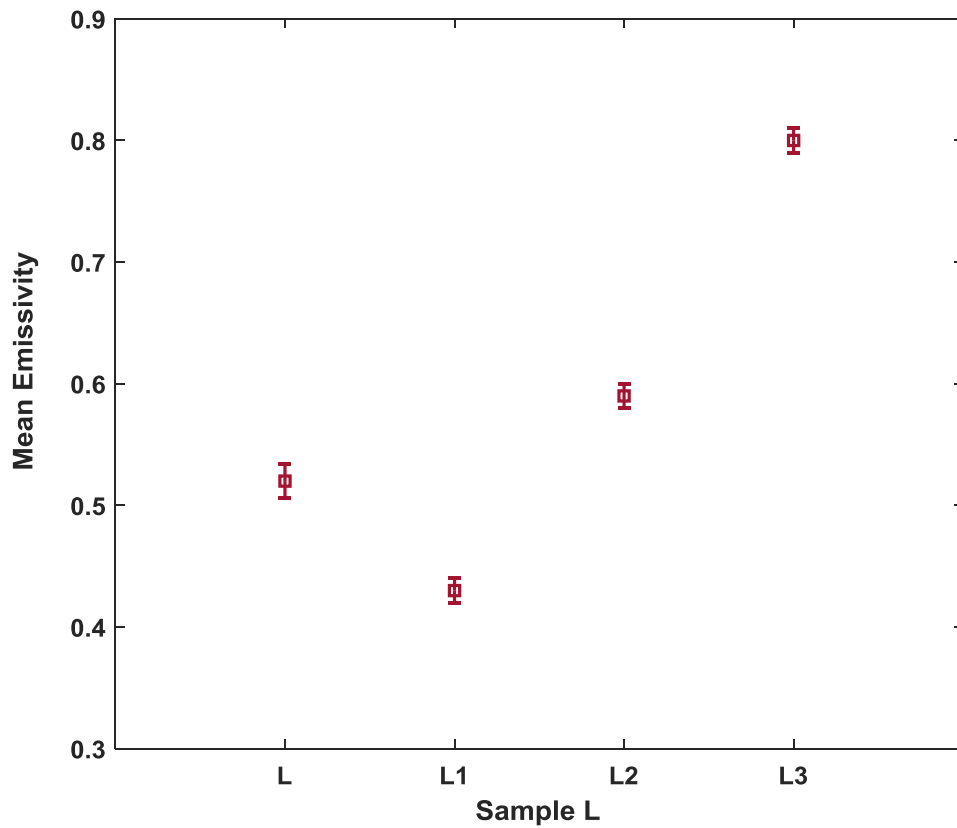


Figure 5.12: Mean emissivity values and standard deviation bars for porcine skin sample before and after different applications of localised heat treatments. Sample L represents the normal skin; L1 represents skin with burns and exudates after 10 seconds of heat treatment, L2 represents skin with burns and without exudates after 60 seconds of extra heat treatment, L3 represents skin with burns and without exudates after 120 seconds of extra heat treatment.

The measurements in Figure 5.12 indicate that the mean emissivity value of the burn-damaged skin with exudates (L1) is lower than the normal skin by  $\sim 0.09$ . Whereas, the mean emissivity values of the burn-damaged skin without exudates and with different burn depth (L2 and L3) are higher by  $\sim 0.07$  and  $0.28$  respectively.

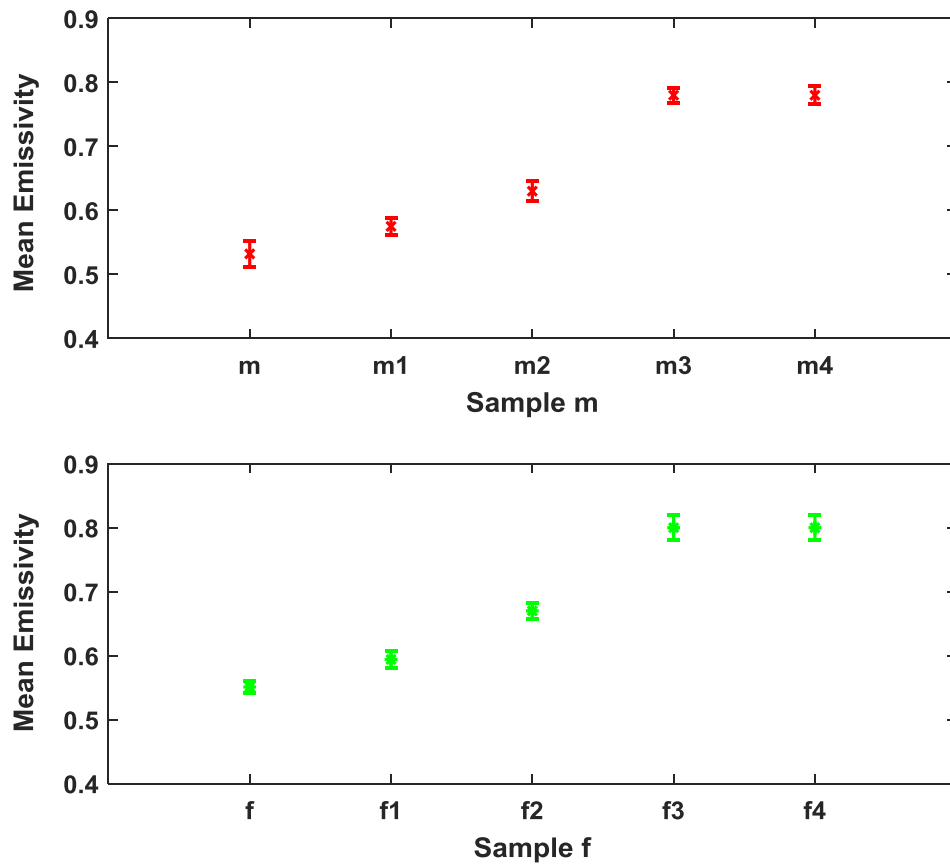


Figure 5.13: Mean emissivity values and standard deviation bars for porcine skin samples before and after different applications of localised heat treatments. Samples m and f represent normal skin; m1 and f1 represent skin with burns after 10 seconds of localised heat treatment, m2 and f2 represent skin with burns after 60 seconds of extra heat treatment, m3 and f3 represent skin with burns after 120 seconds of extra application of heat treatment, and m4 and f4 represent skin with burns after 60 seconds of extra application of heat treatment.

The measurements in Figure 5.13 indicate that the mean emissivity values of burn-damaged skin is higher than that of unburned skin in the range from  $\sim 0.043$  to  $\sim 0.25$ . This is likely to be due to the application of heat that makes the skin drier as the water in the skin is gradually evaporated with the application of heat until the sample contains almost no water as in m3 and f3. Then further heat treatment applied on the sample will not change the emissivity of the sample as in m4 and f4. This behaviour is observed experimentally in the measurements of the two samples presented in Figure 5.13.

## 5.7 Discussion

Measurements of transmission conducted on dressing materials indicate that 80% to 99% of the MMW radiation can propagate through dressing materials with little attenuation (or loss) measured to be in the range of 0.04 dB to 0.969 dB. These measurements indicate that the thickness of the sample and the textiles of the dressings are important factors to be considered as the transmission and the losses of the dressing materials are proportional to those factors.

The measurements conducted on 15 porcine skin samples from the back regions of the animal over the band 80 GHz to 100 GHz indicate that the mean emissivity values of the porcine skin without burns are in the range of 0.52 to 0.55. The measurements of human skin emissivity conducted on the palm of the hand region for a sample of 60 healthy participants in chapter 4 indicate that the mean emissivity values of the human skin for this particular region are ranging from 0.34 to 0.54. This means that the mean emissivity values of the porcine skin samples (back region) are within the range of human skin emissivity measurements of the palm of hand region (thick region). These results confirm that porcine skin is a good phantom model for the human skin.

Measurements of porcine skin samples in Figure 5.8 show that the signature of the skin of the samples A, B, C and D is observed through the 4-layer gauze burn bandage and the light support bandage. The measurements also show that dressing materials increase the mean emissivity values of the skin in the range of 0.01 to 0.02. This increase is due to the increase in the losses and transmission from the skin to air interface since dressing materials enhanced the MMW coupling of energy to the skin and acting as an impedance matching transformer [24].

Measurements of porcine skin samples before and after the applications of cream and water in Figure 5.9 indicate that water and cream reduce the mean emissivity values of the samples in the range of 0.04 to 0.19. This reduction is likely to be increased with the amount of water and cream layer placed on the sample and it also depends on the dielectric properties of the cream and the thickness of the cream layer. This indicates that there is a strong correlation between the emissivity of the skin and the skin water content and the hydration level of the skin. These results are strongly supported by the simulation results of the half space model [124] and indicate that radiometry might be useful for non-invasive diagnosis of skin disease where the disease alter the water content of the skin.

Measurements of porcine skin samples before and after the application of heat treatments in Figure 5.10 indicate that there is a clear signature for the burn that can be detected using the 90 GHz calibrated radiometer. The measurements indicate that the mean emissivity values of the burn-damaged skin are higher than that of unburned skin by 0.044, 0.084, 0.184, and 0.264 for samples X, Y, Z and W and after 10, 60, 120, and 180 seconds of heat treatments applications respectively. This increase in the

mean emissivity is due to the burning process that is removing the water from the skin, thereby reducing the reflectance and increasing the emissivity ( $\eta=1-R$ ). The measurements also show that the signature of the burn is observed through the 6-layers gauze burn bandage and the light support bandage. These results support the knowledge that dressing materials are transparent over the MMW band [3].

Measurements of porcine skin samples before and after different applications of localised heat treatments on the same sample in Figures (5.11 and 5.13) indicate that different application of heat treatments generate different burn depths. The differences in the mean emissivity values between unburned and burn-damaged skin are likely to increase with the degree of the burn, as the water content of the sample significantly decreases and as a result the emissivity increases. These results indicate that radiometry might be used as a non-invasive (non-contact) technique to assess the degree and the depth of the burn.

Measurements of porcine skin sample in Figure 4.12 indicate that the mean emissivity value of the burned skin with exudates is lower than the unburned skin by  $\sim 0.09$ . Whereas, the mean emissivity values of the burned skin without exudates and with different burn depths are higher by  $\sim 0.07$  and  $\sim 0.28$ . The interpretation of this is that burning process cauterises skin resulting in exudates produced around the wound site. These exudates decrease the emissivity of the sample by an amount directly proportional to the amount of exudates produced. However, when all exudates evaporate because of the burning process, the sample emissivity reaches a maximum as there is almost no water remaining. After that, an extra application of heat treatment does not affect the emissivity of the sample, as illustrated in Figure 5.13.

## 5.8 Conclusions

The emissivity of porcine skin samples, with and without burns, were measured experimentally over the band (80-100) GHz using radiometry. The measurements indicate that the mean emissivity value of the burn-damaged skin without exudates is higher than the unburned skin, whereas the mean emissivity value of the burn-damaged skin with exudates is lower than that of unburned skin. This means that the lower emissivities of burn-damaged skin are indicative of the presence of exudates, infection and a non-healing state of the skin, whereas the higher emissivities are indicative of a dry burn, suggesting a full thickness burn (third degree or deep second-degree burn). This indicates that there is a clear signature for the burn that could be used to identify in a non-contact method the status of a burn in a matter of seconds using radiometry.

The measurements in this research confirm that the signature of the burn is observed through two types of dressing materials used in the treatments of burn injuries; gauze burn dressing materials and light support bandage. This means that radiometry might be used as a non-contact technique for monitoring the healing status of the burn wounds under dressing materials.

The measurements also indicate that radiometric sensitivity is sufficient to distinguish between different burn depths as the mean emissivity values of the burn-damaged skin are getting higher after different applications of localised heat treatments. This indicates that radiometry might be used as a non-contact technique to assess the burn depth or the degree of the burn. Research continues in this area to scan images using passive and active MMW technologies as illustrated in chapters 6 and 7.

## Chapter 6

### **Active Millimetre Wave Radar for Sensing and Imaging Through Dressing Materials**

*This chapter discusses the use of a vector network analyser (VNA) to make radar measurements on dressing materials and on a hand support cast. This technique is used to obtain information about the structure of the bandages and used to assess the feasibility of using coherent sources of radiation to penetrate dressing materials having varying moisture content and medicinal creams. The VNA operates in a continuous wave (CW) linear frequency-sweeping mode over the frequency band 15-40 GHz and phase calibration of this enables time-resolved pulsed data to be synthesised. The second part of the measurements investigates the millimetre wave attenuation of different types of medicinal creams used in the treatments of burns and injuries.*

#### **6.1 Technical Background for Radar**

Radio detection and ranging (radar) is an electromagnetic technique for the detection, recognition, and identification of both moving and stationary targets [204, 205]. Although radar was developed initially for the military in the microwave band, there are many commercial civilian applications for air traffic control and remote sensing of the environment [8, 206, 207, 208, 209, 210]. However, in the past few decades, microwave and MMW radar systems have been researched for medical applications such as; early detection of breast cancer [211, 123], measurements of vital signs [212, 213], measurements of heart beating [214], measurements of blood pressure [215, 216], skin cancer detection [56], and brain stroke detection [217].

Based on the number of transmitting and receiving antennas, radar systems are classified into four types and these are: 1) monostatic radar, 2) bistatic radar, 3) array-based radar, and 4) synthetic aperture radar. In a monostatic radar, the transmitter and the receiver are co-located (the same antenna is used for transmitting and receiving the radiation) [67]. However, for a bistatic radar two antennas are used; one for transmitting and the other for receiving the electromagnetic radiation. The separation distance between the two antennas is of the order of the range to the target [205, 218]. Synthetic aperture radar (SAR) is an imaging radar that uses a moving antenna (or a target) to make multiple measurements along the track of a single target. The multiple measurements are processed into an image with a diffraction limited resolution commensurate with the length of the track, having the potential to generate two or three-dimensional images of the target [205].

An array radar (phase array radar) consists multiple transmitting and receiving stationary antennas that fed with phase shift devices that controlled by a computer, and based on the phase difference in the received reflected radiation the system forms an image [219].

In radar, a target object is illuminated by spatially and temporally coherent wave source. The reflections from the target are processed through algorithms into an image [168]. The level of reflected radiation from the target is dependent on the target structure and size. The so-called radar clutter is the return reflections from the environment and all objects which are not the target. The radar system is usually signal to clutter limited in the performance, in contrast to a radiometric system which is signal to noise limited [138, 205, 218]. The radar system has the advantages of controlling the frequency range, the transmitted power level, and the polarisation.

A monostatic radar system illustrated in Figure 6.1 generates a waveform to illuminate the target. The power level of the illumination is adjusted to obtain sufficient reflection return from the target (typically ranging from milliWatts to megawatts, this being application dependent). A power amplifier is used to achieve the appropriate power levels, the power being transmitted and received from the target through an antenna. A duplexer (switch) is used for separating the transmission and the reception modes of the antenna [205].

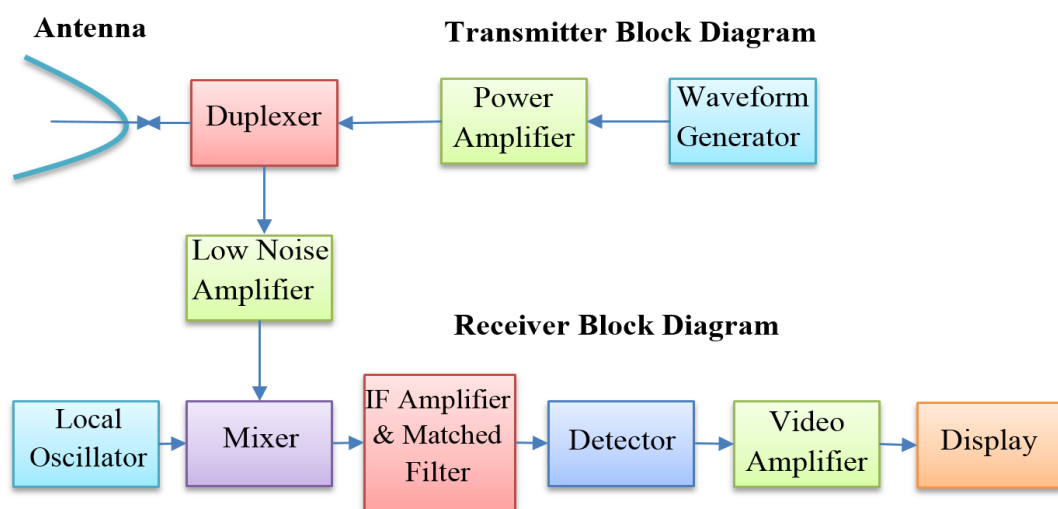


Figure 6.1: A block diagram shows the basic elements of the monostatic radar system [205].

In the receiver mode, the received reflected radiation is a low power signal that requires amplification. To this end, a low noise amplifier is used at the first stage of the receiver, so noise in the system is minimised. In many types of radar systems, the signal is mixed with a local carrier frequency in a mixer; which then generates an intermediate frequency (IF) signal. The signal then enters a matched filter (having a conjugated time-reversed impulse response of the transmit signal) which has the effect of maximising the received signal level. Then the detection decision is made based on

a threshold and a decision criterion [205]. After that, the target location is identified and displayed as illustrated in the receiver block diagram of Figure 6.1.

### 6.1.1 Principle of Operation of a Monostatic Pulsed Radar System

In a monostatic radar, a single antenna transmits a pulse of electromagnetic radiation toward a target. The transmitted radiation interacts with the target; part of the radiation is absorbed or transmitted through the target and the other part is reflected back to the radar system. Then the system uses the reflected radiation to determine the direction and the range of the target [219]. Synchronisation between the transmitter and the receiver is required, and therefore the system should work within a timing frame as illustrated in Figure 6.2. The time counted from the beginning of sending one pulse and starting the next pulse is called the pulse repetition time (PRT), and the number of pulses transmitted per second is measured by means of a pulse repetition frequency (PRF) [219].

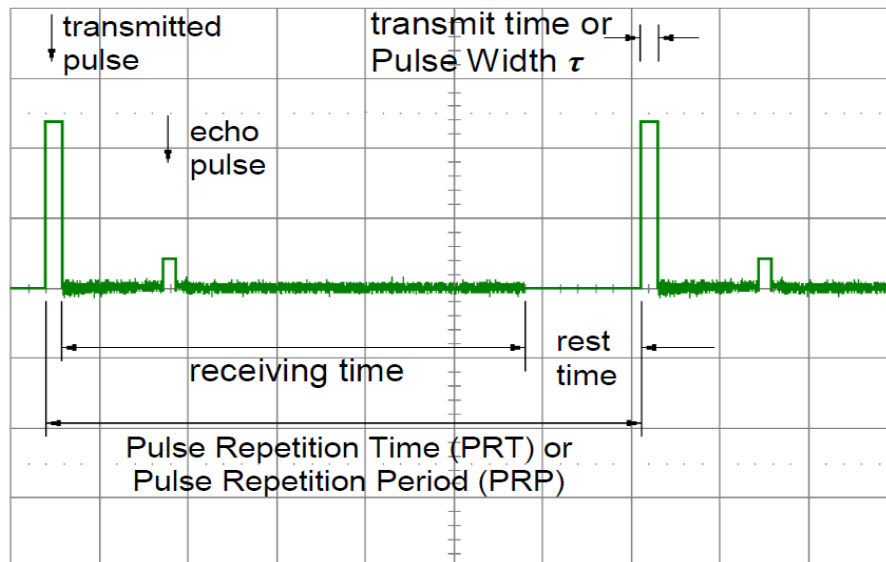


Figure 6.2: Synchronisation between the transmitter and the receiver of the monostatic radar system [219].

### 6.1.2 Radar Range Equation

Consider a monostatic radar system using an isotropic antenna (radiate similar amounts of power in all direction) with a spherical radiation pattern. The average power density of the transmission antenna,  $S_{av}$  in  $W/m^2$  is [204, 205, 219]:

$$S_{av} = \frac{P_t}{4\pi R^2} \quad (6.1)$$

Where,  $P_t$  is the transmitted power in Watts, and  $R$  is the distance to the target measured in meters and it is called the target range.

A more realistic scenario is for a radar to use a directional antenna, in which the average power density becomes [205, 218, 219]:

$$S_D = \frac{GP_t}{4\pi R^2} \quad (6.2)$$

Where  $G$  is the gain of the antenna.

The received power from a target object of the radar system,  $P_r$  in Watts can be expressed in terms of the incident power density (IPD), the effective aperture of the antenna,  $A_e$  in meter square, and the total loss factor in the radar system,  $L_s$ . This equation is best known as a radar range equation and it is given by [218, 219]:

$$P_r = (IPD) \cdot (A_e) \cdot \left(\frac{1}{L_s}\right) = \left(\frac{GP_t}{4\pi R^2} \cdot \frac{\sigma}{4\pi R^2}\right) \cdot \left(\frac{\lambda^2 G}{4\pi}\right) \cdot \left(\frac{1}{L_s}\right) = \frac{P_t \lambda^2 G^2 \sigma}{(4\pi)^3 R^4 L_s} \quad (6.3)$$

Where,  $\lambda$  is the wavelength of the radar signal in meters,  $R$  is the target range in meter, and  $\sigma$  is the radar cross section (RCS) measured in meter square. The effective aperture of the antenna is inversely proportion with the frequency, the higher the frequency the smaller aperture of the antenna [219]. Radar equation indicates that the power received from a given target is inversely proportioned to the fourth power of the range.

The maximum theoretical range of the radar system,  $R_{Max}$  is measured when the power level of the received radiation is goes to the minimum detectable level,  $P_{Min}$ . Below this level, the radar system will not be able to detect the received radiation [205, 218, 219].

$$R_{Max} = \sqrt[4]{\frac{\lambda^2 G^2 P_t \sigma}{(4\pi)^3 L_s P_{Min}}} \quad (6.4)$$

Equation (6.4) indicates that the range of the radar can be increased by either increasing the wavelength of the transmitted radiation, the gain of the antenna, the transmission power level, or by reducing the power level of the minimum detectable signal and this can be achieved by reducing the noise from the system. The RCS is designed based on the physical geometry of the target, the transmitted frequency, and the reflecting surface of the target [219]. Therefore, RCS does not interact significantly in the calculation of the maximum range of the radar system.

The radar system is a combination of electrical components such as antennas, cables, VNA, and computer. Therefore, thermal noise is the main source of noise in this system. This noise can be either internally generated in the radar receiver or it might arise from the atmospheric. The signal to noise ratio (SNR) is an important parameter to consider in the radar system and it can be expressed as [138, 205, 218, 219]:

$$SNR = \frac{P_r}{Noise\ Power} = \left( \frac{P_r}{kT_e B} \right) = \frac{P_t \lambda^2 G^2 \sigma}{(4\pi)^3 R^4 L_s k T_e B} \quad (6.5)$$

Where,  $k$  is Boltzmann's constant ( $1.38 \times 10^{-23} \text{ m}^2 \text{ kg s}^{-2} \text{ K}^{-1}$ ),  $T_e$  is the effective noise temperature of the system in Kelvin, and  $B$  is the bandwidth in Hertz.

### 6.1.3 Radar Clutter

Clutter is defined as those radar echoes returns from everything except the target. The level of these returns are generally larger than that from the target and they are generated by many different objects, to name a few, these would be: ground surface, snow, rain, sea, animals, birds, tall buildings, and other sources. Clutter interferes with the target signal and affects significantly the radar performance. According to the source of clutter, there are three types of clutter and these are [204]:

- Surface clutter (echoes per surface area,  $\sigma^o$ ) is caused mainly from ground and rain reflections and it can be calculated as:

$$\sigma^o = \frac{\sigma_c}{A_c} \quad (6.6)$$

Where,  $\sigma_c$  is the radar cross section for an area,  $A_c$ .

- Volume clutter (echoes per volume,  $\eta$  measured in meter<sup>-1</sup>) is caused from weather and chaff reflections and it can be calculated as:

$$\eta = \frac{\sigma_c}{V_c} \quad (6.7)$$

Where,  $\sigma_c$  is the radar cross section for a volume,  $V_c$ .

- Point clutter is caused from birds, animals, and tall buildings reflections.

The convention in radar is that the first level of signal processing is to reject where possible the clutter in the data so unambiguous information about the target can be obtained. The experimental work conducted in this research was performed indoor in an anechoic region. This minimised the sources of clutter that might interfere with the target echoes and degrades the performance of the radar system.

### **6.1.4 Radar Resolution**

Radar resolution has measured the ability of the radar system to discriminate between two targets that are closely spaced, in either range or bearing. In a radar system, there are two types of resolution; the range resolution, and the spatial angular resolution.

#### **6.1.4.1 Range Resolution**

Range resolution is the smallest distance between the targets that can be resolved. The time delay between the echoes from different targets should be greater than the transmitter pulse width to allow targets to be resolved easily. Otherwise, they are not resolved [125]. Based on the Rayleigh criterion, the theoretical range resolution  $R_r$  can be calculated as shown [204]:

$$R_r = \frac{c}{2 \cdot B} \quad (6.8)$$

Where, B is the bandwidth of the transmitted signal, and c is the speed of the light.

Equation (6.8) indicates that the range resolution of the radar can be enhanced by increasing the bandwidth of the transmitted signal. However, this is limited by many factors such as the antenna, the amplification, and the cost of the components. The limit of the range resolution of the radar system is [204, 218]:

$$R_r \geq \frac{c}{2 \cdot B} \quad (6.9)$$

#### 6.1.4.2 Spatial Angular Resolution

The spatial angular resolution of the radar is defined as the minimum separation in an angle that can be resolved. This is achieved when equal range targets have a separation distance more than the antenna beam width. Therefore, the spatial angular resolution  $A_r$  is determined by the antenna beam width  $\theta$  (which is defined by the -3 dB power point), and the range of the antenna,  $R$  as [204, 205, 218]:

$$A_r \leq 2. R \sin\left(\frac{\theta}{2}\right) \quad (6.10)$$

Equation (6.10) indicates that the spatial angular resolution can be improved by decreasing the beam width of the antenna.

#### 6.1.5 Scattering Parameters and Vector Network Analyser

Scattering parameters are complex amplitudes that can be determined from the incident and the reflected voltage of the network. The scattering parameters of the two-port network in Figure 6.3 are expressed in terms of the incident voltage  $a_1$  and  $a_2$  and the reflected voltage  $b_1$  and  $b_2$  from port 1 and port 2 when they are terminated with a reference matched impedance [140].

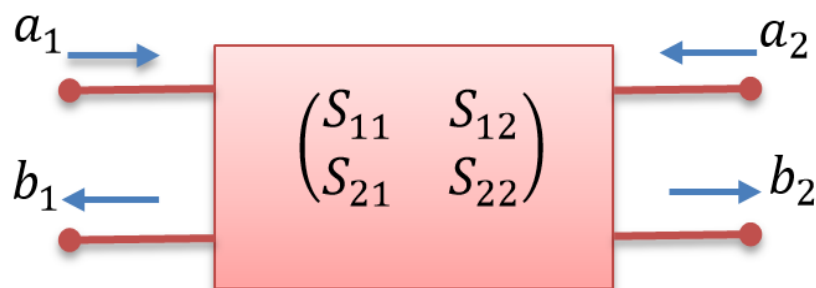


Figure 6.3: Scattering parameters as function of incident and reflected voltage of the two ports network.

The reflected voltages from port 1 and port 2 are [140]:

$$b_1 = S_{11}a_1 + S_{12}a_2 \quad (6.11)$$

$$b_2 = S_{21}a_1 + S_{22}a_2 \quad (6.12)$$

Equations (6.11 and 6.12) can be written in a matrix format (scattering matrix) as:

$$\begin{bmatrix} b_1 \\ b_2 \end{bmatrix} = \begin{bmatrix} S_{11} & S_{12} \\ S_{21} & S_{22} \end{bmatrix} \begin{bmatrix} a_1 \\ a_2 \end{bmatrix} \quad (6.13)$$

The input port reflection coefficient,  $S_{11}$  and the transmission coefficient,  $S_{21}$  are measured when the incident voltage of port 2 is equal to zero ( $a_2 = 0$ ) as [140]:

$$S_{11} = \frac{b_1}{a_1} \quad (6.14)$$

$$S_{21} = \frac{b_2}{a_1} \quad (6.15)$$

The output port reflection coefficient,  $S_{22}$  and the reverse voltage gain,  $S_{12}$  are measured when the incident voltage of port 1 is equal to zero ( $a_1 = 0$ ) as [140]:

$$S_{22} = \frac{b_2}{a_2} \quad (6.16)$$

$$S_{12} = \frac{b_1}{a_2} \quad (6.17)$$

Equations (6.14 to 6.17) indicate that the amplitude of the scattering parameters is determined by the ratio between the reflected voltage and the incident voltage amplitude of the waveform. Whereas, the phase is determined by the phase difference between the reflected and the incident waveform.

A two-port vector network analyser (VNA) illustrated in Figure 6.4, is an instrument used for measuring the magnitude and the phase of the reflection and the transmission coefficients (complex quantities consists of real and imaginary parts) of a two-port network over a range of frequencies. From the S-parameters, the dielectric and the magnetic properties of the materials can also be measured. Moreover, the device can also present the data in real time in either frequency domain or time domain formats [220]. In the course of this research, the VNA is used for measuring the input reflection coefficient ( $S_{11}$ ) of the samples.

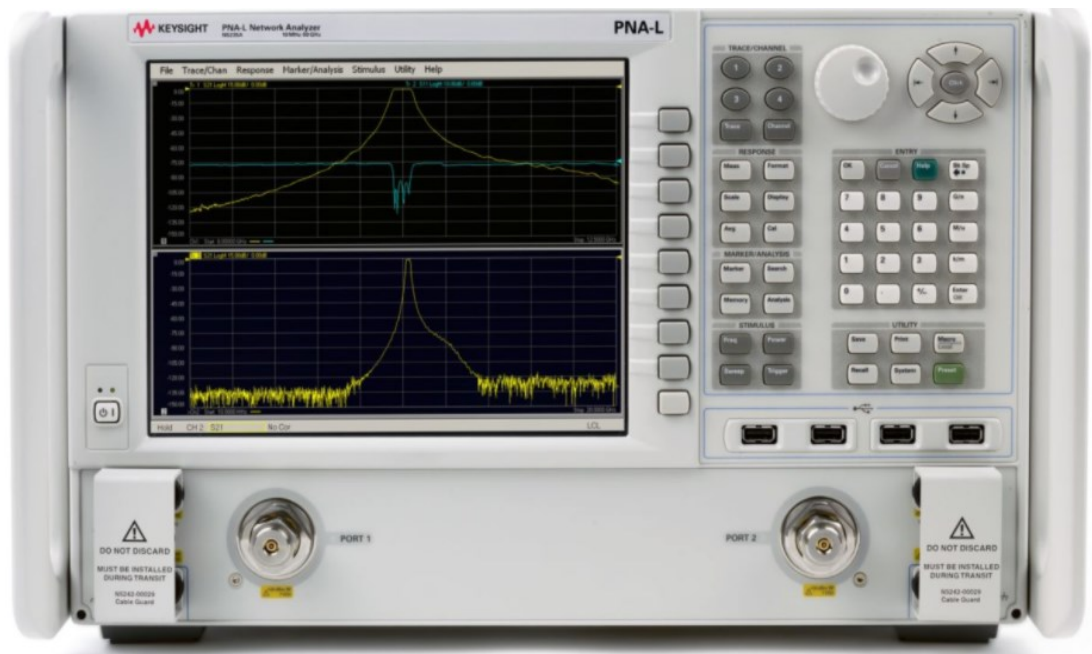


Figure 6.4: Two ports vector network analyser device used for measuring the magnitude and the phase of the scattering parameters.

### 6.1.6 Fourier Transform

Fourier transform is a technique applied on non-periodic finite signals, converting from a time domain to frequency domain and vice versa using an inverse Fourier transform. The transform is used in many applications such as digital signal processing, image processing, convolution, deconvolution, and filtering. The Fourier transform for a non-periodic signal,  $f(t)$  is [221]:

$$F(\omega) = \int_{-\infty}^{+\infty} f(t)e^{-j\omega t} dt \quad (6.18)$$

Where,  $\omega = 2\pi f$  is the angular frequency, measured in rad per second.

The inverse Fourier transform is given by [221]:

$$\mathcal{F}^{-1}\{F(\omega)\} = f(t) = \frac{1}{2\pi} \int_{-\infty}^{+\infty} F(\omega)e^{+j\omega t} d\omega \quad (6.19)$$

The signal representation in time and frequency domains has an inverse relationship. An example of this is the impulse function,  $\delta(t)$  that has zero duration in the time domain and an infinite constant spectrum in the frequency domain as illustrated in Figure 6.5.

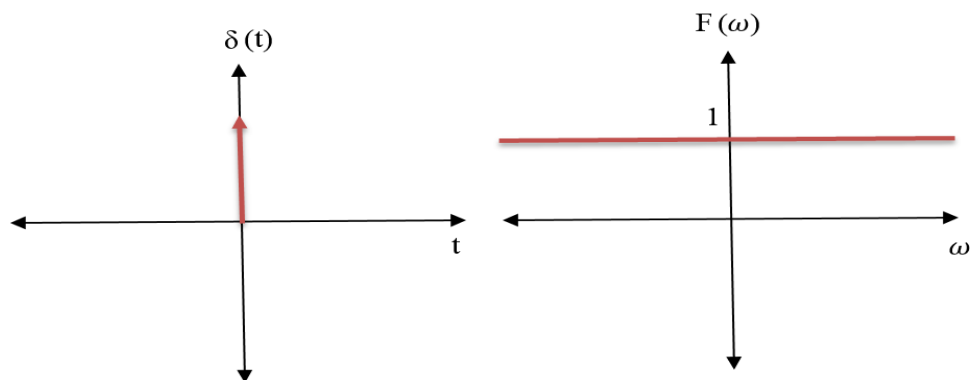


Figure 6.5: Representations of impulse function in both time and frequency domains.

For discrete evenly sampled signals in the time domain, a discrete Fourier transform (DFT) is used to convert the signal from time domain to frequency domain. Whereas, an inverse discrete Fourier transform (IDFT) is used to convert the signal from frequency to time domain as [221]:

$$DFT = X(k) = \sum_{n=0}^{N-1} x(n) \cdot e^{-\frac{j2\pi nk}{N}} \quad 0 \leq k < N \quad (6.20)$$

$$IDFT = x(n) = \frac{1}{N} \sum_{k=0}^{N-1} X(k) \cdot e^{+\frac{j2\pi nk}{N}} \quad 0 \leq n < N \quad (6.21)$$

Where, n and k are the numbers of data points in time and frequency domains.

### **6.1.7 Radar Range**

The line of sight distance between the radar system and the target is defined as the range  $R$ , and it can be measured through the round trip time of the transmitted signal  $\tau$ , the speed of the light  $c$ , and the refractive index of the medium  $n(\omega)$  as [222]:

$$R = \frac{c\tau}{2n(\omega)} \quad (6.22)$$

Using Equation (2.16) in chapter 2, the range can be expressed as a function of the relative complex permittivity as:

$$R = \frac{c\tau}{2\sqrt{\epsilon_r(\omega)}} \quad (6.23)$$

For a low loss material such as dressing materials;  $\epsilon''_r(\omega) \ll 1$ , the range is a function of the real part of the relative complex permittivity as:

$$R = \frac{c\tau}{2\sqrt{\epsilon'_r(\omega)}} \quad (6.24)$$

## **6.2 Experiment 1: Sensing and Imaging Through Dressing Materials**

The objectives of this experiment are highlighted as follows:

- To develop an experimental setup for measuring the propagation path length (PPL) of the dressing materials and the hand support cast using the pulse synthesis radar system operating over the band from 15 GHz to 40 GHz.
- To measure the attenuation effect on MMW radiation of various types of creams use in the treatments of burns and injuries.
- To assess the feasibility of using active MMW radiation to penetrate dressing materials and to provide information about the reflectivity of the metal plate that has been used as a surrogate for the body surface.

### ***6.2.1 Selection of the Frequency Band 15-40 GHz***

The frequency band ranging from 15 GHz to 40 GHz was chosen in this research, as it provides higher penetration capability compared with the higher frequency bands [124, 145]. This is an important factor to consider as the measurements in this chapter are used for measuring the PPL, the thickness of the sample, and the attenuation effect caused from coating the dressing materials with cream. The penetration depth of the millimetre wave radiation in the human skin as a function of frequency is illustrated in Figure 2.2 (chapter 2, section 2.4).

### 6.2.2 Experimental Description

A standard gain pyramid horn antenna with a square aperture (46 mm x 46 mm) and a nominal gain of 20 dBi effective over the band 15 GHz to 40 GHz (Ku, K, and Ka) was located ~ 250 mm from the sample under test (SUT) and was aligned in vertical polarization as illustrated in Figure 6.6.

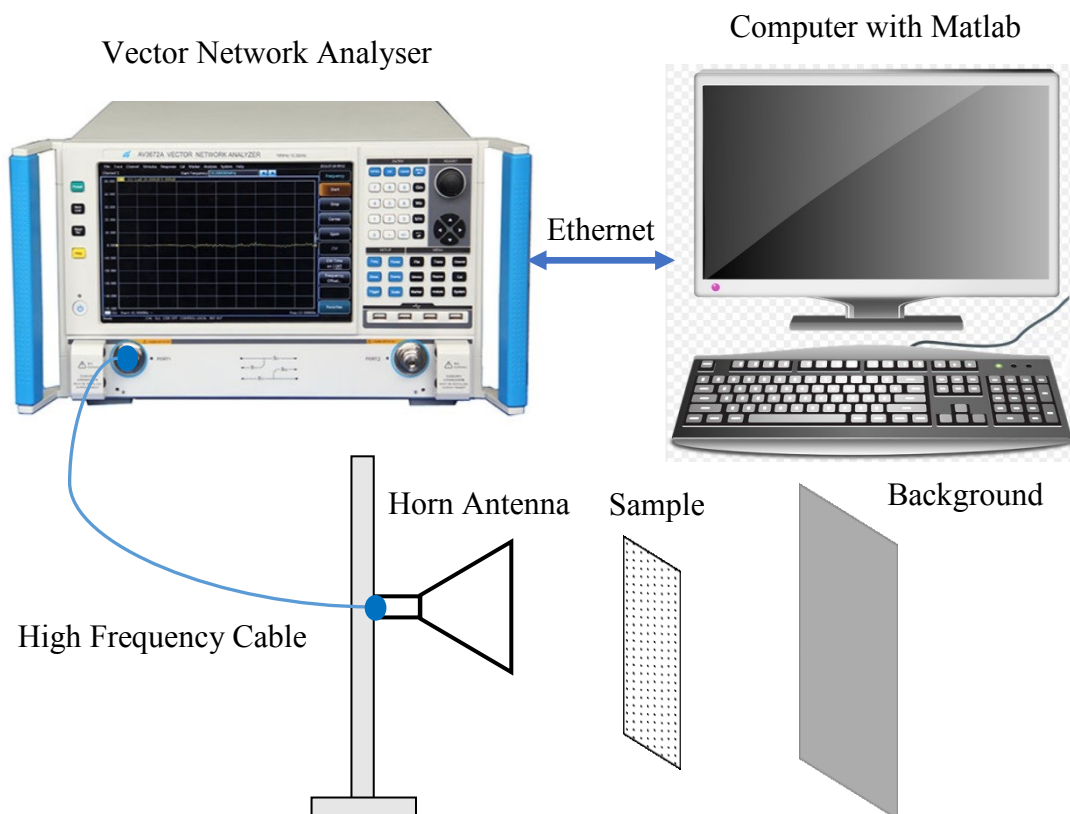


Figure 6.6: Illustration of the experimental apparatus used to make measurements of the propagation path length and the attenuation of the dressing materials using radar.

The antenna was connected through a high-frequency coaxial cable to a vector network analyzer (type: Keysite PNAX VNA, model: N5227A). A large metal plate (length=1200 mm, and width 660 mm) was used as a background and also for calibration purposes. The VNA with an operating frequency band (10 MHz - 67 GHz) was used to illuminate the SUT and was connected to the computer through an Ethernet cable and controlled via a Matlab programme.

The Matlab programme allows the user to determine the start frequency (15 GHz), the end frequency (40 GHz), the number of data points (512), the frequency step size (48.92 MHz), and the transmitted power level (1.0 mW); this power level has been chosen as it is within the radiation safety limits [23]. These parameters result in a theoretical range resolution of 6.0 mm and a bandwidth of 25 GHz. The system was surrounded with a wall of microwave carbon loaded absorbing foam to minimise reflections from other objects in the lab and the data were saved directly to be processed later. The experimental setup in Figure 6.6 was used to conduct measurements on three types of samples:

- Samples with known reflectivity such as a large flat metal plate (100% reflector) [145] and a wall of microwave foam absorber (non-reflective) [149]. These measurements were conducted for calibration purposes.
- Rigid samples such as a hand support cast, a polyethylene cylinder, a polyethylene flat plate, and a wax candle. These measurements were conducted when the sample was located between the horn antenna and the metal plate background.
- Dressing materials in a dry state, wet state, and with cream. These measurements were conducted when the samples were attached directly to the metal plate as the metal plate has been used as a surrogate to the body surface.

### 6.2.3 Methodology of Data Processing

The mono-static radar system in Figure 6.6 was used for measuring: A) the complex reflected signal ( $S_{11}$ ) from the metal plate, B) the internal background signal measured with a microwave foam absorber target and C) the complex reflected signal from the SUT (rigid samples and dressing materials). These particular measurements are selected as it enables calibration to be made quickly, before and after the measurements, thus minimising the effects of systematic errors. The foam absorber calibration measurements were used to subtract any internally reflected radiation, and the metal plate calibration measurement was used to remove the effect of the transmitter and the receiver response "dispersion" by deconvolution. The complex reflected signal for each sample (SUT, metal plate and foam absorber) was measured ten times and averaged at each frequency. The complex reflected signal in the frequency domain was transformed into time domain signal using the Inverse Fast Fourier Transform (IFFT). Zero padding (307 points) was used beyond the measured 0-15 GHz frequency band to aid data interpretation. This methodology together with the distance between two reflection peaks [223] was used to measure the PPL of the samples as illustrated in Equations (6.25 and 6.26). The measured PPL was compared with the actual path length of the sample that obtained using a standard ruler with  $\pm 0.5$  mm absolute uncertainty.

$$PPL = R_2 - R_1 \quad (6.25)$$

By substituting Equation (6.22) into Equation (6.25), the PPL of the sample is:

$$PPL = \frac{c\tau_2}{2n(\omega)} - \frac{c\tau_1}{2n(\omega)} = \frac{c\Delta\tau}{2n(\omega)} = \frac{c\Delta\tau}{2\sqrt{\epsilon_r(\omega)}} \quad (6.26)$$

The following block diagram summarises the methodology of data processing for experiment 1:

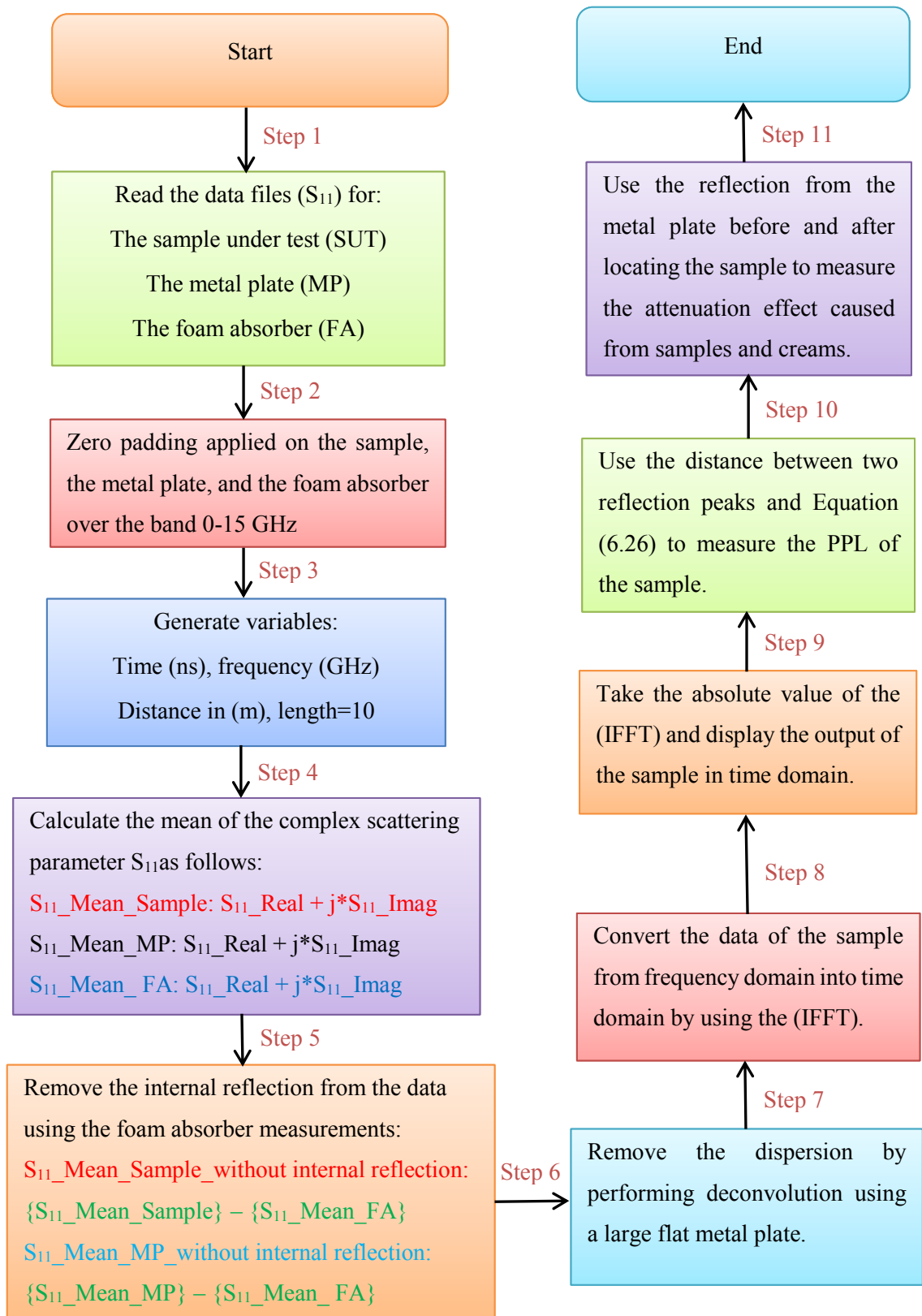


Figure 6.7: A block diagram summarises the methodology of data processing.

#### ***6.2.4 Experimental Results***

The experimental results are divided into four parts; 1) measurements of the spatial resolution of the radar system, 2) calibration measurements applied on a flat metal plate and a wall of microwave carbon loaded foam absorber, 3) measurements of the PPL of the rigid samples, and 4) measurements of the PPL and the attenuation of dressing materials samples.

##### ***6.2.4.1 Radar Spatial Resolution Measurements***

The spatial resolution of the radar was measured experimentally using two flat metal plates; one of the plates was fastened and aligned properly. Whereas, the other plate was movable. Initially, the distance between the two plates was 100 mm and the reflection peaks from the two metal plates were completely resolved on the screen of the VNA. Then the distance between the two plates was reduced by moving the movable metal plate until the two peaks are getting closer to each other's as illustrated in Figure 6.8 (a); this distance was measured to be ~8.0 mm. Then any further movements will combine the two reflection peaks into one reflection peak as illustrated in Figure 6.8 (b). This indicates that the measured spatial resolution of the system is ~8.0 mm. This value is in a good agreement with the theoretical value that indicates a spatial resolution of 6.0 mm using Equation (6.8).

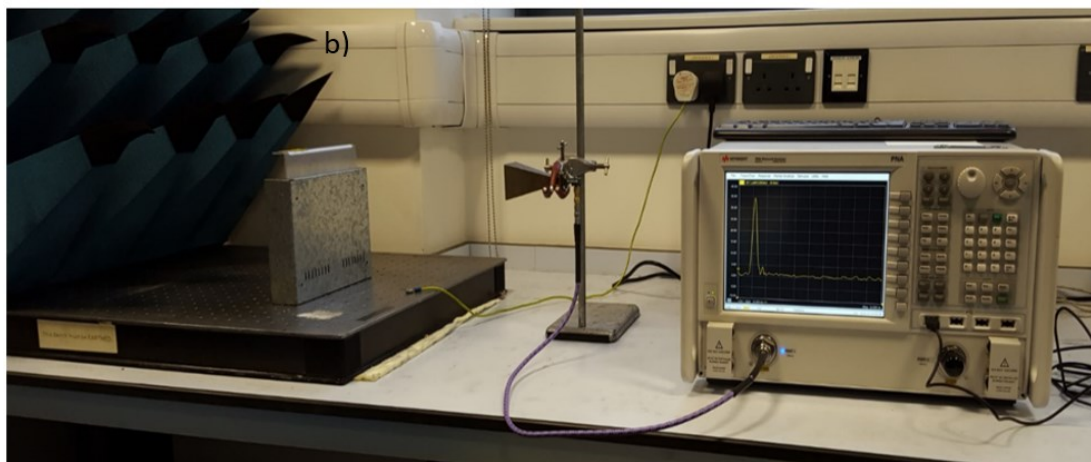
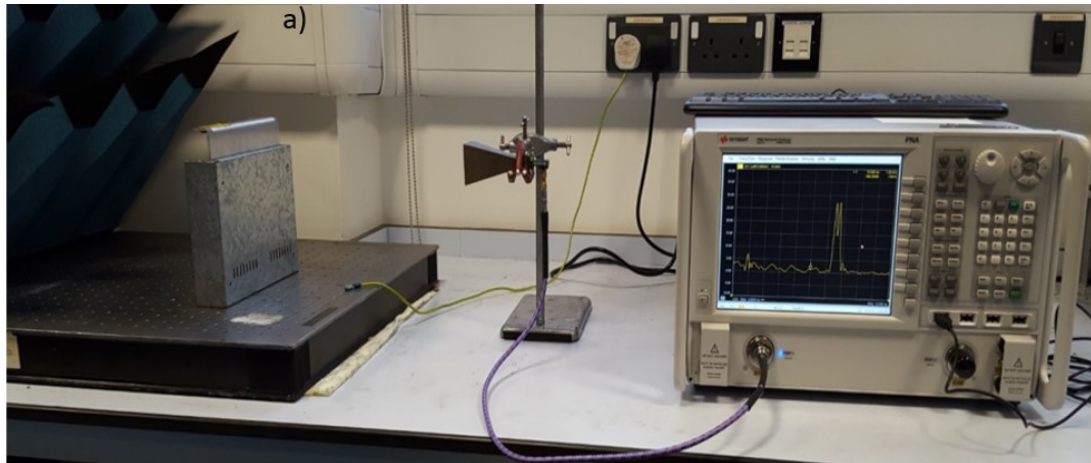


Figure 6.8: The minimum resolvable distance between the two metal plates is  $\sim 8.0$  mm (a) a further decreases in this distance results in a combination of the two peaks into a single peak (b).

Measurements in Figure 6.8 indicate that the measured spatial resolution of the radar system is  $\sim 8.0$  mm. This distance is measured experimentally using a ruler and it is also confirmed by using the distance between two reflection peaks and Equation (6.26).

#### 6.2.4.2 Calibration Measurements

Calibration measurements in this section were conducted on the background that can be either a large flat metal plate or a wall of foam absorber without locating any sample between the horn antenna and the background. The metal plate was aligned properly to obtain the maximum possible reflection and the complex reflected signal ( $S_{11}$ ) was measured ten times and averaged at each data point over the band (15-40) GHz. Then zero padding was performed over the band 0-15 GHz for better data interpretation. Then the complex reflected signal in the frequency domain is transformed into time domain signal using the IFFT as illustrated in Figure 6.9.

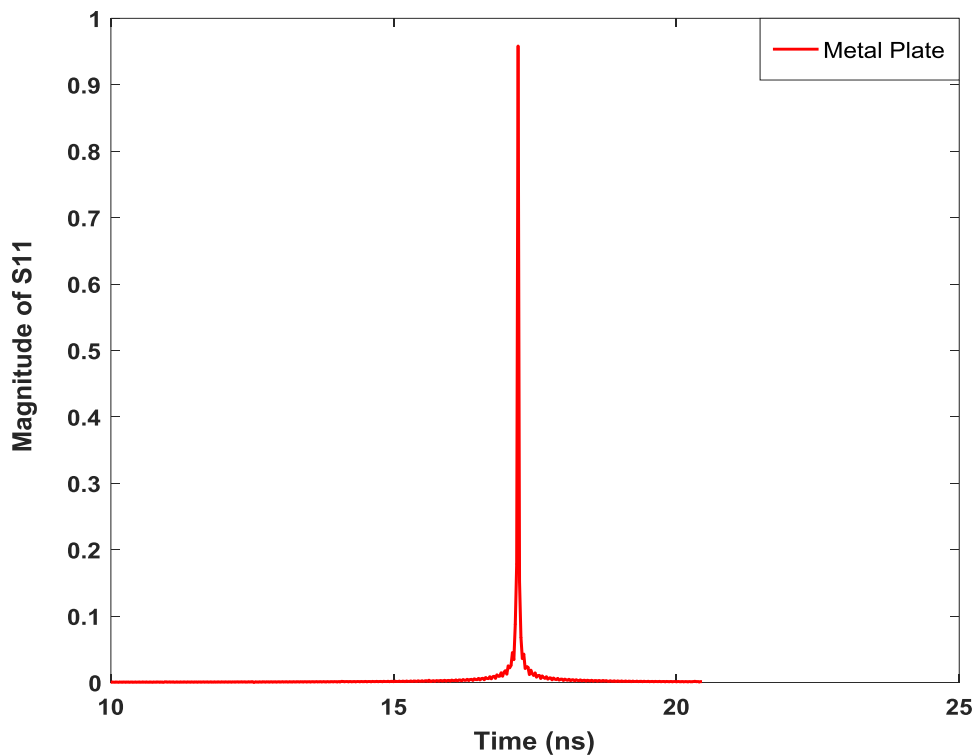


Figure 6.9: The reflected signal from a flat metal plate background (length=1200 mm, and width= 660 mm).

The next calibration measurement was performed on a wall of microwave foam absorber, and the data obtained is illustrated in Figure 6.10.

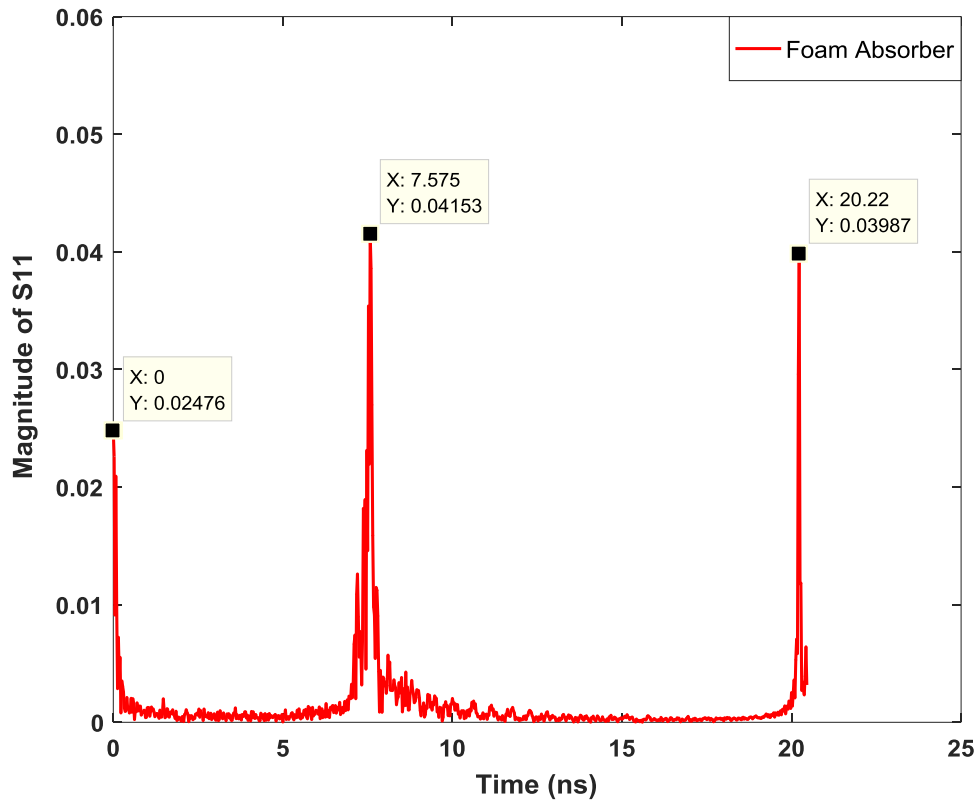


Figure 6.10: The reflected signal from a wall of foam absorber background.

The measurements in Figure 6.10 indicate three reflection peaks in the foam absorbing material caused internally due to mismatch points. The first peak presents the internal reflection from the point of connection between the VNA and the high-frequency cable, the second peak presents reflection from the point of connection between the high-frequency cable and the horn antenna, and the third peak presents reflection from other offsets. The reflectivity measurements applied on the foam absorbing material is used in the next sections to cancel the internal reflection that caused from different offsets and mismatched points. This effect is found in all measurements and it can be removed by subtracting the scattering parameters of the sample from a reference background of microwave foam absorber.

### 6.2.4.3 Propagation Path Length Measurements for Rigid Samples

The measurements presented in this section were conducted on three samples with known PPL and they were: 1) polyethylene cylinder with a 50 mm PPL, 2) polyethylene flat plate with a 10 mm PPL, and 3) wax candle with an 80 mm PPL. These samples are described in details as illustrated in Table 6.1.

Sample	Material	Complex Permittivity	Dimensions (mm)
Cylinder	Polyethylene (HDPE)	$\epsilon_r = 2.26 + i0.00075$ (26-40) GHz [19]	Diameter: 50 mm Length: 160 mm
Flat Plate	Polyethylene (HDPE)	$\epsilon_r = 2.26 + i0.00075$ (26-40) GHz [19]	Length: 200 mm Width: 190 mm Thickness: 10 mm
Wax Candle	Paraffin Wax	$\epsilon_r = 2.3 + i0.00023$ (2-300) GHz [19]	Diameter: 80 mm Length: 290 mm

Table 6.1: Summary of the measured samples dielectric properties and dimensions.

The samples were located between the horn antenna and the metal plate background and the data were processed using the methodology described in Figure 6.7, and the data obtained from different samples are illustrated in Figures (6.11, 6.12, and 6.13):

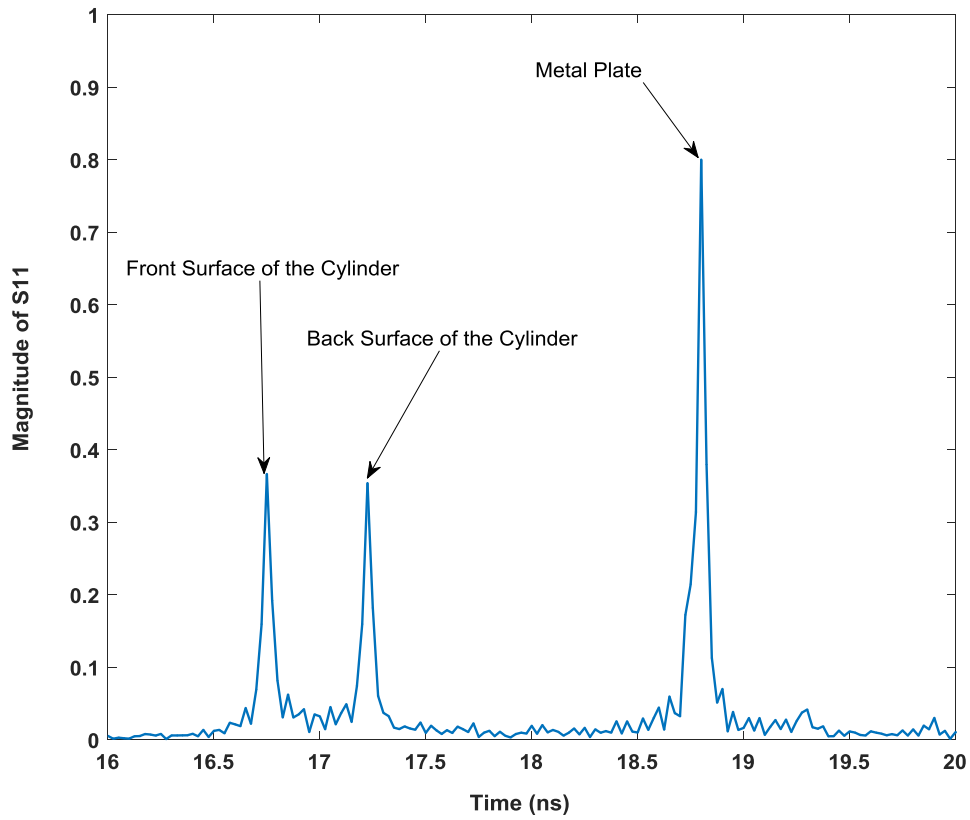


Figure 6.11: The reflected signal from a 50.0 mm thick polyethylene cylinder located in free space between the horn antenna and the metal plate background.

The measurements in Figure 6.11 shows three reflection peaks associated with the cylinder and the metal plate; the first two peaks correspond to the reflections from the front and the back surfaces of the cylinder, whereas the third peak corresponds to the metal plate surface. The PPL of the cylinder is measured using the distance between two reflection peaks [223] and Equation (6.26) as follows:

$$R_1 = \frac{ct_1}{2\sqrt{\epsilon'}} = \frac{3 \times 10^8 \times 16.75 \times 10^{-9}}{2\sqrt{2.26}} = 1.671 \times 10^3 \text{ mm.}$$

$$R_2 = \frac{ct_2}{2\sqrt{\epsilon'}} = \frac{3 \times 10^8 \times 17.22 \times 10^{-9}}{2\sqrt{2.26}} = 1.718 \times 10^3 \text{ mm.}$$

$$PPL = R_2 - R_1 = 47.0 \text{ mm.}$$

The difference between the actual PPL and the measured PPL is calculated to be 3.0 mm. The attenuation in the reflected radiation is measured by comparing the two reflection peaks that are associated with the metal plate before and after locating the sample (cylinder). From the heights of the reflection peaks, the attenuation is estimated as ~20% for a 50.0 mm polyethylene cylinder. The next sample is a flat polyethylene plate and the data obtained from this sample is illustrated in Figure 6.12:

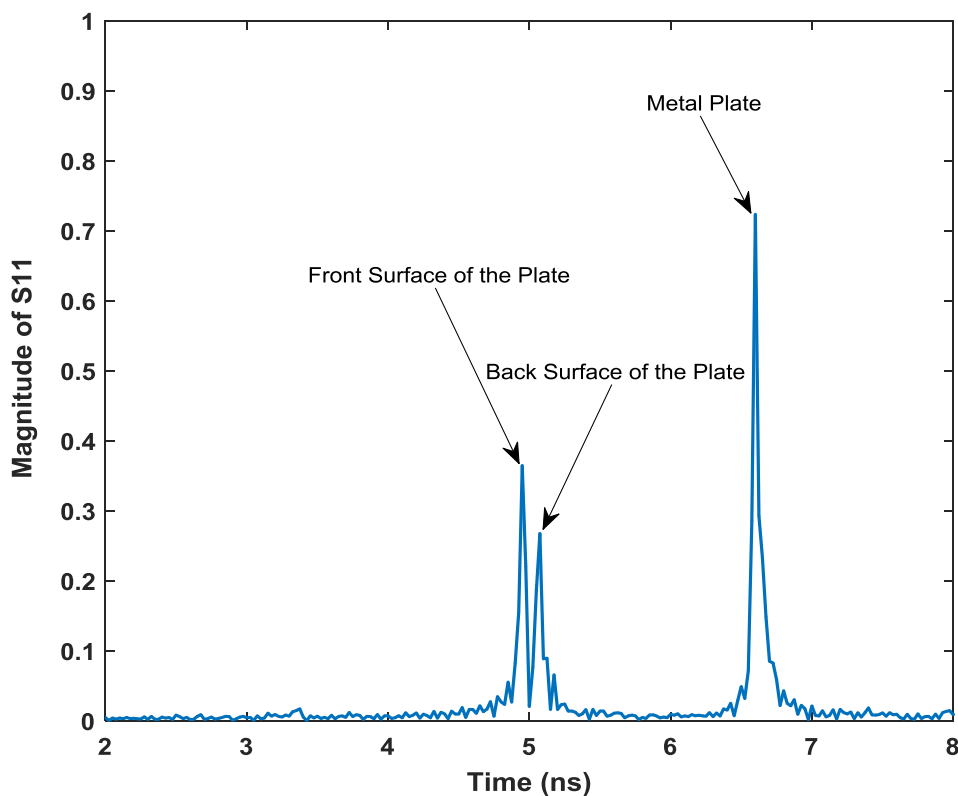


Figure 6.12: The reflected signal from a 10.0 mm thick polyethylene flat plate located in free space between the horn antenna and the metal plate background.

The measurements in Figure 6.12 shows three reflection peaks associated with the flat plate and the metal plate; the first two peaks correspond to the reflections from the front and the back surfaces of the plate, whereas the third peak corresponds to the metal plate surface. The PPL of the plate is measured to be 12.5 mm using the distance

between two reflection peaks and Equation (6.26). The difference between the actual PPL and the measured PPL is 2.5 mm. The attenuation in the metal plate reflected radiation is estimated as ~28% from a 10.0 mm polyethylene plate.

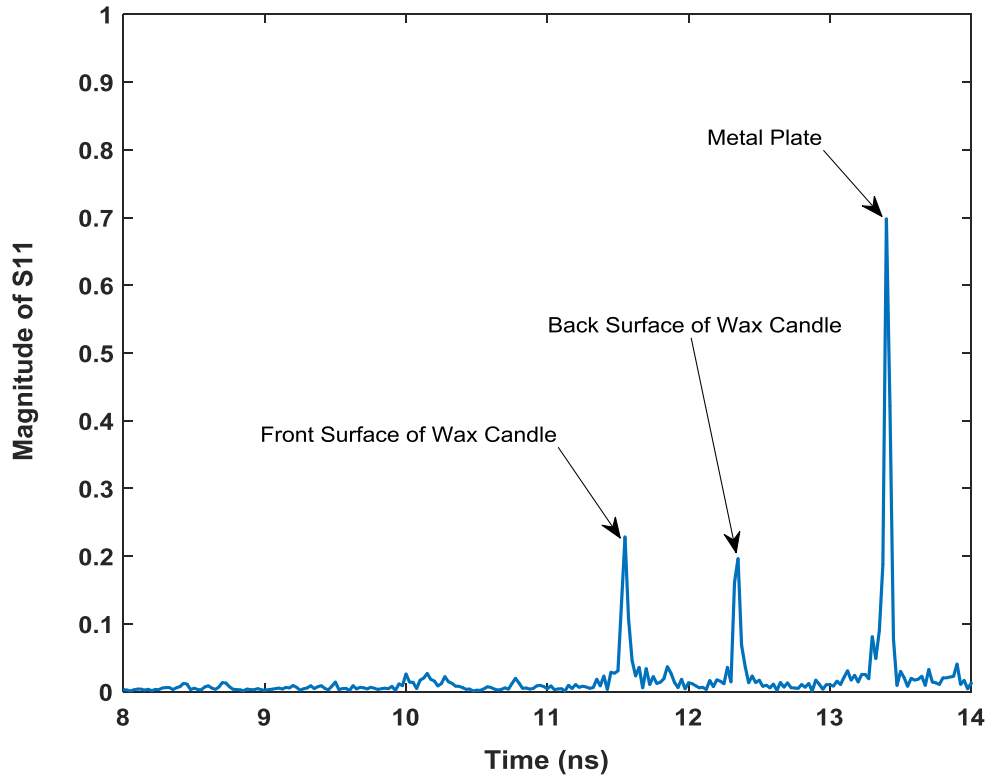


Figure 6.13: The reflected signal from an 80.0 mm thick wax candle located in free space between the horn antenna and the metal plate background.

The measurements in Figure 6.13 shows three reflection peaks associated with the wax candle and the metal plate; the first two peaks correspond to the reflections from the front and the back surfaces of the candle, whereas the third peak corresponds to the metal plate surface. The PPL of the wax candle is measured to be 79.1 mm using the distance between two reflection peaks and Equation (6.26). The difference between the actual PPL and the measured PPL is 0.9 mm. The attenuation in the metal plate reflected radiation is estimated as ~30% from an 80.0 mm wax candle.

#### 6.2.4.4 Measurements Applied on Dressing Materials

The reflectivity measurements presented in this section were conducted on dressing materials and on a hand support cast. The measurements were conducted on dressing materials in different states (dry, wet and with a layer of cream).

##### 6.2.4.4.1 Gauze Burn Dressing Materials in Dry State

A gauze burn bandage with ~10.0 mm thick was located and aligned between the horn antenna and the metal plate. The bandage was in a dry state and removed from protective packaging prior to measurement. The data were processed using the methodology described in Figure 6.7 and the results are illustrated in Figure 6.14.

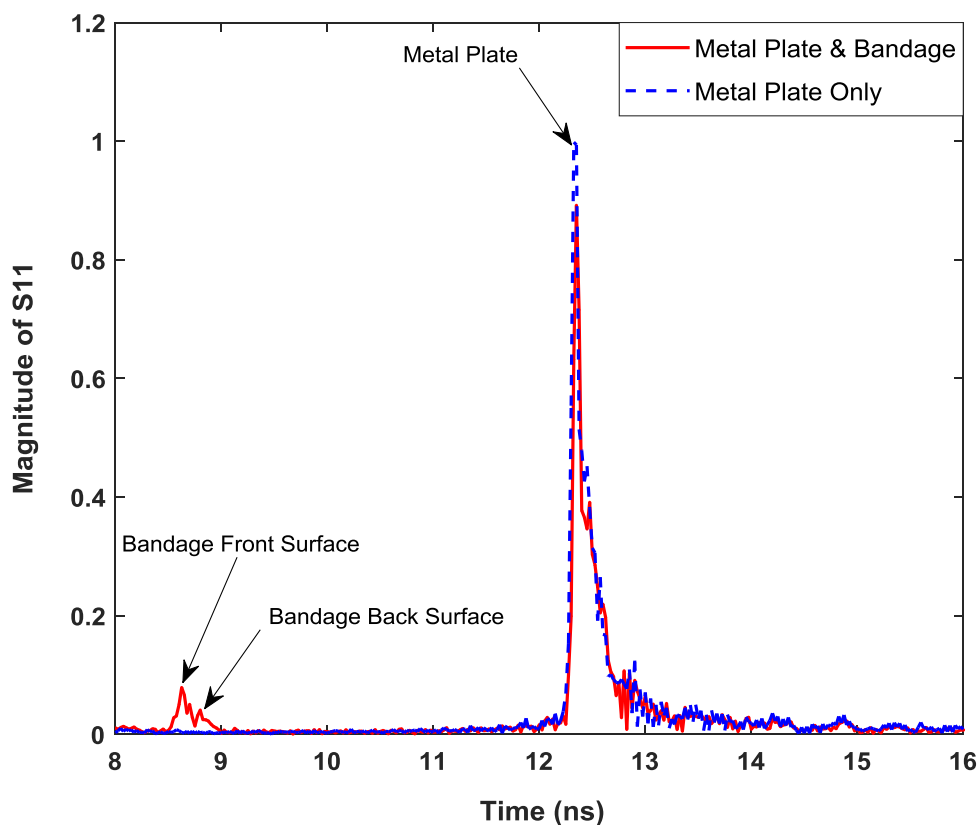


Figure 6.14: The reflected signal from a 10.0 mm thick bandage located in free space between the horn antenna and the metal plate. The solid red line shows the signal from the bandage and the metal plate and the broken blue line when the metal plate only is present.

The measurements in Figure 6.14 indicate that the reflection from the gauze burn bandage is ~10%, compared with the reflection from the metal plate. Although dressing materials are low loss materials, increasing the thickness of dressing materials increases the absorption and causes loss. The attenuation in the reflected radiation is measured by comparing the two reflection peaks that are associated with the metal plate before and after locating the bandage. From the heights of the reflection peaks, the combined attenuation and reflection by the gauze burn bandage is estimated as ~10% for a 10 mm bandage thickness. The PPL of the gauze burn bandage is measured to be ~11.25 mm using the distance between two reflection peaks and Equation (6.26). The difference between the actual and the measured PPL is 1.25 mm.

#### **6.2.4.4.2 Gauze Burn Dressing Materials with Sudocrem**

Dressing materials are used widely on the treatments of injury and burn wounds. These materials are usually used with cream for avoiding friction between the skin and the dressing materials and for healing purposes [125]. This section investigates the feasibility of using active radiation to sense different surfaces attached to the dressing materials and whether it is possible to sense features under these layers.

A ~25.0 mm thick gauze burn bandage is attached to the metal plate and a ~0.5 mm layer of Sudocrem covers the front surface of the bandage. The cream layer was applied on the bandage surface according to the standard medical practice described on the packet of the cream. The cream layer was distributed equally and uniformly on the entire surface of the bandage, and then the measurements were conducted and the data were obtained and processed as shown in Figure.6.15:

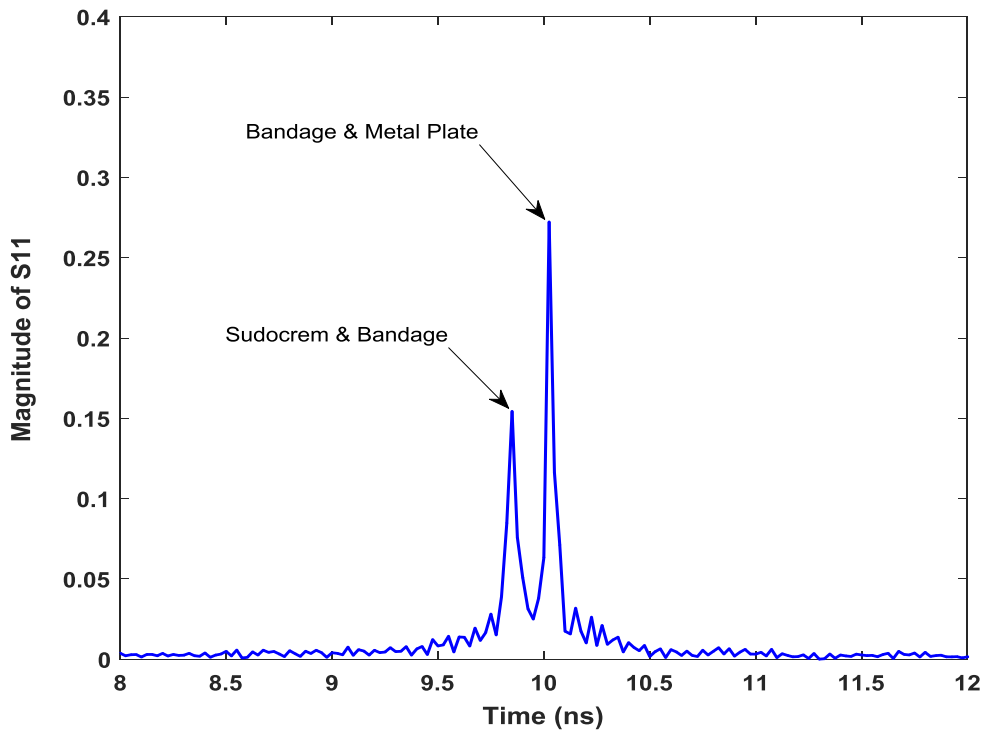


Figure 6.15: The reflected signal from a  $\sim 25.0$  mm thick bandage with Sudocrem. The bandage was attached directly to the metal plate.

The measurements in Figure 6.15 show two reflections peaks; the reflection from the cream and the front surface of the bandage are combined in peak 1, and the reflection from the back surface of the bandage and the metal plate are combined in peak 2. Although the imaging system can't resolve the cream layer attached to the bandage surface itself, this doesn't mean that it can't sense the cream surface. The measured reflection from the front surface of the bandage in a dry state did not exceed  $\sim 10\%$  (see Figure 6.14), whereas when a layer of Sudocrem is attached to the bandage the reflection is increased to  $\sim 16\%$ . The PPL of the bandage is measured to be  $\sim 27.0$  mm from the distance between the two reflection peaks. The difference between the actual PPL and the measured PPL is  $\sim 2.0$  mm. It may be noted that although the metal plate seen through the cream layer has been reduced by a factor of 3, it is still possible to sense features under the cream layer.

#### 6.2.4.4.3 Gauze Burn Dressing Materials with Flamazine Cream

The results obtained with another ~10.0 mm gauze burn bandage coated with a 0.5 mm layer of a different cream Flamazine is illustrated in Figure 6.16.

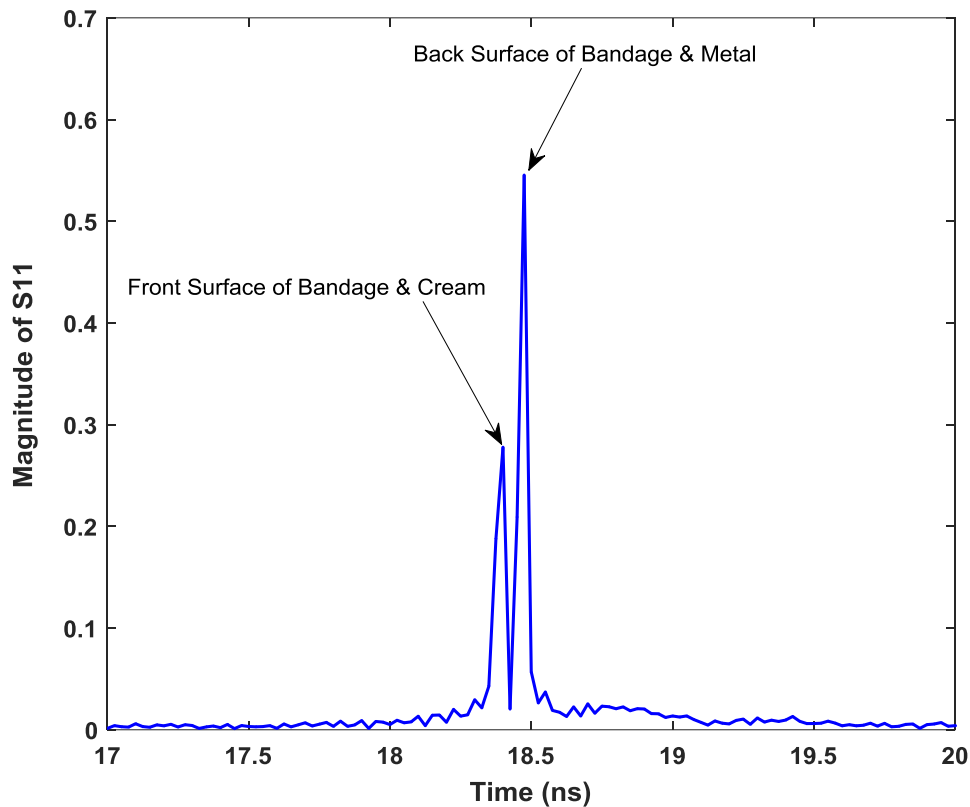


Figure 6.16: The reflected signal from a ~10.0 mm thick bandage coated with Flamazine cream. The bandage was attached directly to the metal plate.

The reflection measurements in Figure 6.16 show that adding a layer of Flamazine cream increases the reflection on the front surface of the bandage in a dry state from ~10% to ~30%. The signal passing through the cream and the bandage and reflected from the metal plate is now 55%. The PPL of the bandage, in this case, is measured to be ~10.5 mm using the distance between two reflection peaks. The difference between the actual PPL and the measured PPL is calculated to be ~0.5 mm.

#### 6.2.4.4 Gauze Burn Dressing Materials with Water

The results obtained from a ~10.0 mm gauze burn bandage in a wet state (bandage with water) is illustrated in Figure 6.17. The percentage of water in the bandage was found to be ~25%. This value was obtained by weighing the bandage before and after the application of water.

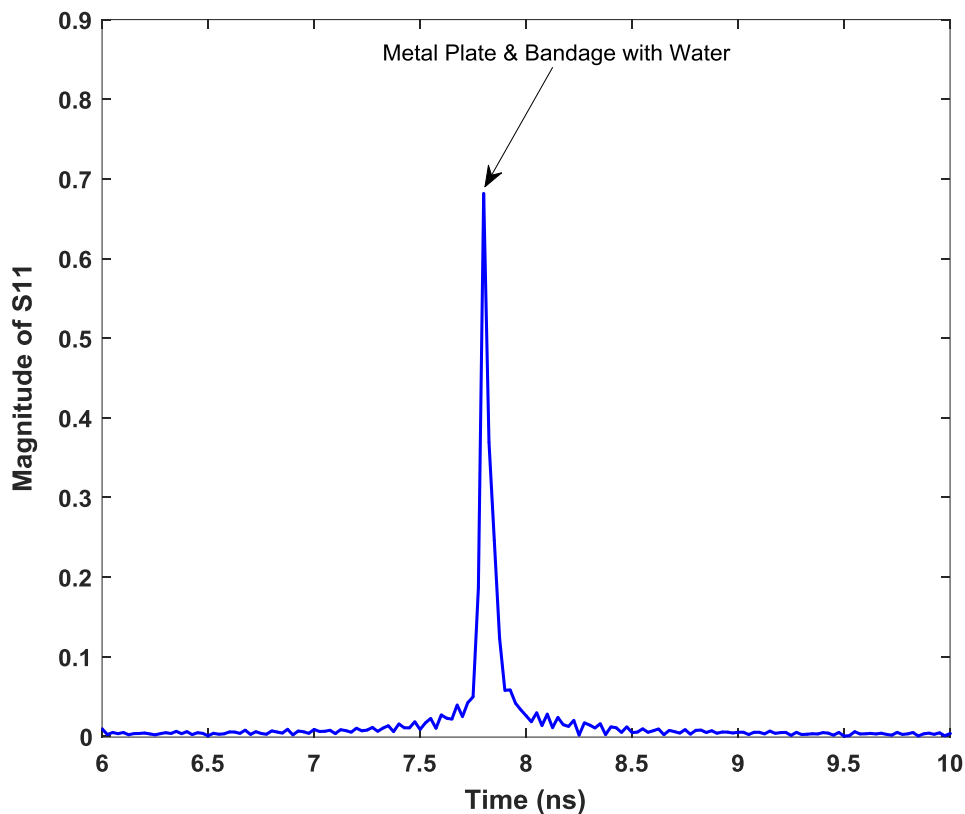


Figure 6.17: The reflected signal from a ~10.0 mm thick wet bandage. The bandage was attached directly to the metal plate.

Reflection measurements in Figure 6.17 show only one reflection peak since MMW radiation is highly absorbed in water [24]. The combined signal reflection from the water in the bandage and that passing through the water and the bandage and reflected from the metal plate is now ~70%. This is higher than the reflection from the water alone 53% [45] so the attenuated reflected radiation from the plate may be estimated

as ~17%. The metal plate seen through the wet bandage has been reduced by a factor of ~6.0. This means that it may still be possible to sense features under wet dressing materials.

#### 6.2.4.4.5 Light Support Bandage with Savlon Cream

A light support bandage with a ~25.0 mm thick was located and aligned between the horn antenna and the metal plate. The bandage was in a dry state and removed from protective packaging prior to measurement. The reflectivity of the bandage is measured to be ~10% in the dry state. After that, the bandage was attached to the metal plate and coated with a 0.5 mm layer of Savlon cream. Then the data were obtained and processed as illustrated in Figure 6.18.

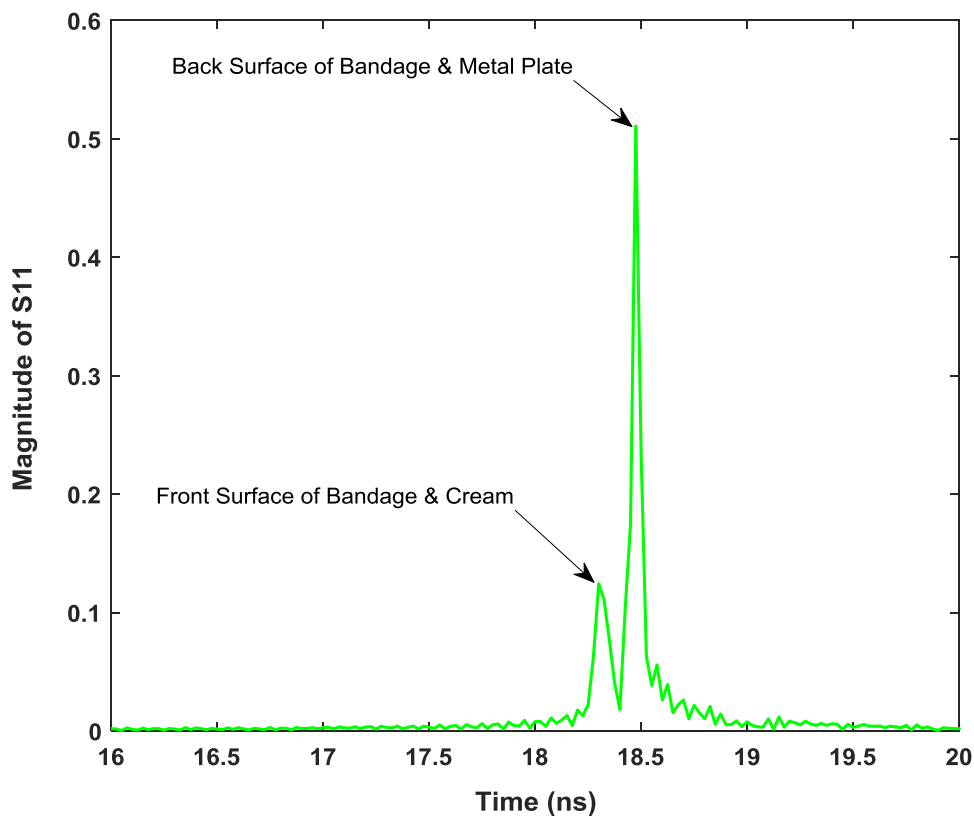


Figure 6.18: The reflected signal from a ~25.0 mm thick light support bandage with Savlon cream. The bandage was attached directly to the metal plate.

The reflection measurements in Figure 6.18 show that adding a layer of Savlon cream increases the reflection on the front surface of the bandage from ~10% in a dry state to ~15%. The signal passing through the cream and bandage and reflected from the metal plate is ~51%. The PPL of the bandage, in this case, is measured to be ~25.5 mm using the distance between two reflection peaks. The difference between the actual and the measured PPL is calculated to be ~0.5 mm.

#### 6.2.4.4.6 Light Support Bandage with Sudocrem

The results obtained from a ~40.0 mm thick light support bandage coated with a 0.5 mm layer of Sudocrem and attached to the metal plate is illustrated in Figure 6.19.

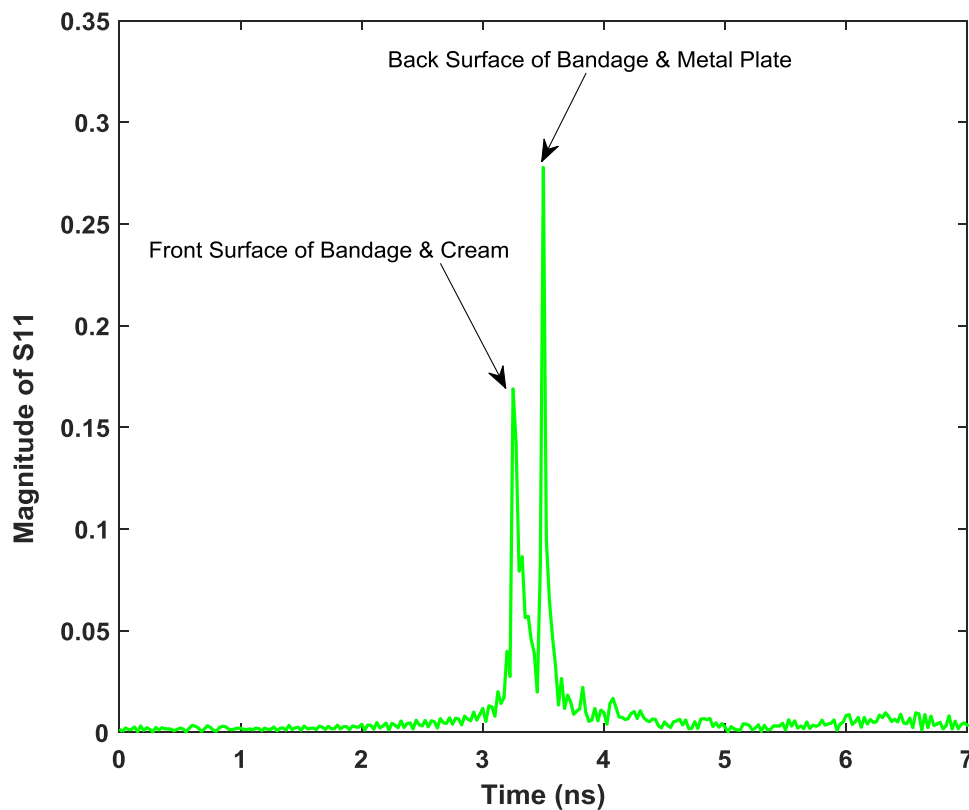


Figure 6.19: The reflected signal from a ~40.0 mm thick light support bandage with Sudocrem. The bandage was attached directly to the metal plate.

The reflection measurements in Figure 6.19 show that adding a layer of Sudocrem increases the reflection of the front surface of the bandage from  $\sim 10\%$  in a dry state to  $\sim 18\%$ . The signal passing through the cream and bandage and reflected from the metal plate is  $28\%$ . The PPL of the bandage, in this case, is measured to be  $\sim 37.5$  mm using the distance between two reflection peaks. The difference between the actual and the measured PPL is  $2.5$  mm.

#### 6.2.4.4.7 Hand Support Cast Sample

A hand cast made of plaster-of-Paris was located and aligned transversely between the horn antenna and the metal plate. The hand cast has a cylindrical tubular shape and dimensions (length  $250$  mm, and diameter  $90$  mm). The results obtained from the hand support cast are illustrated in Figure 6.20.

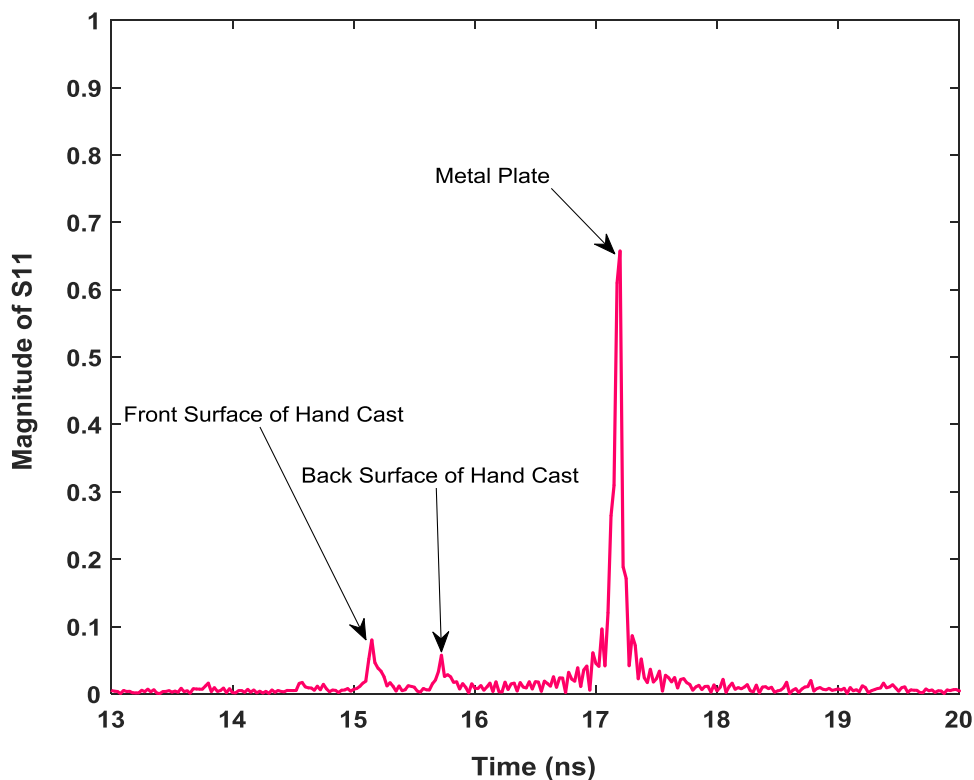


Figure 6.20: The reflected signal from a  $90.0$  mm wide hand cast located in free space between the horn antenna and the metal plate background.

The reflection measurements in Figure 6.20 show three reflection peaks associated with the hand cast and the metal plate; the first two peaks correspond to the reflections from the front and the back surfaces of the hand cast, whereas the third peak corresponds to the metal plate surface, as seen through the cast. Reflection peaks are produced in the time domain resulting from reflections from the surfaces of the sample or discontinuities in dielectric properties. The reduction of the third peak (~35%) compared to the value 1.0 obtained without the cast (see Figure 6.14), is due to reflection and absorption by the cast material. From the distance between two cast peaks, the PPL for the hand cast sample is measured to be ~85.5 mm, close (~4.5 mm) to the actual PPL (90.0 mm).

### 6.2.5 Data Validation

For the purpose of data validation, the PPL measurements were repeated three times in three separate experiments; in each experiment, the measurements were repeated ten times and averaged. The measurements obtained from the three experiments were processed using the methodology described in Figure 6.7. These measurements are summarised in Tables (6.2, 6.3 and 6.4).

Sample	Actual PPL (mm)	$\tau_1$ (ns)	$\tau_2$ (ns)	Measured PPL (mm)	Actual-Measured  PPL in (mm)
Cylinder	50.0	16.75	17.22	47.0	3.0
Flat plate	10.0	4.95	5.075	12.5	2.5
Wax candle	80.0	11.55	12.35	79.1	0.9
Gauze bandage	25.0	9.85	10.03	27.0	2.0
Light support bandage	25.0	18.3	18.47	25.5	0.5
Hand support cast	90.0	15.15	15.72	85.5	4.5

Table 6.2: Propagation path length measurements obtained from experiment 1.

Sample	Actual PPL (mm)	$\tau_1$ (ns)	$\tau_2$ (ns)	Measured PPL (mm)	Actual-Measured  PPL in (mm)
Cylinder	50.0	8.825	9.3	47.9	2.1
Flat plate	10.0	9.15	9.25	10.0	0
Wax candle	80.0	9.15	9.925	77.0	3.0
Gauze bandage	10.0	8.7	8.775	11.25	1.25
Light support bandage	27	10.72	10.87	22.5	4.5
Hand support cast	90.0	9.25	9.825	86.0	4.0

Table 6.3: Propagation path length measurements obtained from experiment 2.

Sample	Actual PPL (mm)	$\tau_1$ (ns)	$\tau_2$ (ns)	Measured PPL (mm)	Actual-Measured  PPL in (mm)
Cylinder	50.0	8.725	9.2	47.4	2.6
Hand support cast	90.0	8.875	9.45	86.3	3.7
Gauze bandage	25.0	9.025	9.175	22.5	2.5
Gauze bandage	30.0	8.625	8.8	26.0	4.0
Light support bandage	37.0	8.7	8.975	41.0	4.0

Table 6.4: Propagation path length measurements obtained from experiment 3.

The measurements in Tables (6.2, 6.3, and 6.4) indicate that the methodology described in Figure 6.7 is sufficient to provide information about the PPL of the dressing materials and the hand support cast as the differences between the actual and the measured PPL for all samples are in the range of 0.0 mm to 4.5 mm. These differences are caused by many factors and these are: 1) the sensitivity to the alignment (or sensitive to the multiple reflections) that arises from the coherence length of the active system (speckle and multipath), and 2) the soft structure of the bandage that might cause variations in the PPL through the bandage during the measurement. During the experimental work, all sources of error were considered as follows:

- All samples were aligned properly; this is achieved by observation of the real-time IFFT displayed on the VNA as the samples were aligned.
- All dressing materials samples were compressed and attached to the metal plate background; this process minimises variation in the sample thickness during the experimental work.
- Cream layer was applied on dressing materials as recommended in the standard medical practice and it was distributed equally and uniformly over the entire surface of the sample.

- Measurements were repeated 10 times in each experiment and the standard deviation in the scattering parameter ( $S_{11}$ ) does not exceed  $\sim 0.0001$ . This indicates that the measurements are consistent.
- The actual PPL of the samples were measured using a ruler with an absolute measurement uncertainty of  $\pm 0.5$  mm (half the smallest division). During the measurements, the samples were placed on a flat and smooth surface (table) and the measurements were conducted five times and averaged.

## **6.3 Experiment 2: Attenuation in Different Types of Cream**

This experiment aims to measure the attenuation of the MMW radiation in different types of cream over the frequency band 15-40 GHz.

### ***6.3.1 Selection of Creams***

In this experiment, the attenuation of the MMW radiation is measured in three types of creams; Flamazine cream, Sudocrem, and Savlon cream. These creams were chosen as they are used in the treatments of burns and injuries. All creams were purchased from the pharmacy (Flamazine cream requires a prescription) and they were opened for the first time directly before the experimental work commenced. By covering metal surfaces with differing thicknesses of creams enabled the attenuations of the creams to be measured directly, which was more accurate than measuring the cream on bandages, as described in the previous sections.

### ***6.3.2 Experimental Description***

The experimental setup used in this part is similar to that in Figure 6.6. However, the sample under test was replaced with a square flat metal plate (length 200 mm, and width 200 mm) and the large metal plate background was replaced with a wall of microwave foam absorber. Initially, the measurements were conducted on a wall of microwave foam absorber background without placing any target object between the horn antenna and the background. This gives the internal reflection between the horn antenna and the high frequency cable (mismatch points); as the microwave foam absorbers are non-reflective [149].

In the next step, the metal plate was located between the horn antenna and the foam absorber background. Then the plate was aligned properly so the maximum possible reflectivity from the metal plate is obtained. The reflected signal from the metal plate target alone (without cream),  $S_{11Metal}$  is measured in the frequency domain as:

$$S_{11Metal} = S_{11Background} + R_{Metal}S_{Metal} \quad (6.27)$$

Where,  $S_{11Background}$  is the reflected signal from the background,  $R_{Metal}$  is the reflectivity of the flat metal plate (100% reflector) and it is approximately  $\sim 1.0$  for perfect reflector [145],  $S_{Metal}$  is the wave form fed to the horn antenna.

After that, the metal plate was coated with cream and the reflectivity measurements were obtained from each type of cream and at different thicknesses (less than 0.5 mm, 0.5 mm, 1.0 mm, and 1.5 mm to 2.0 mm). The reflected signal from the metal plate target coated with cream,  $S_{11Metal\&Cream}$  is:

$$S_{11Metal\&Cream} = S_{11Background} + T_{Cream}R_{Metal}S_{Metal} \quad (6.28)$$

The transmissivity of the cream,  $T_{Cream}$  can be obtained by using Equation (6.27) and Equation (6.28) as:

$$T_{Cream} = \frac{(S_{11Metal\&Cream} - S_{11Background})}{(S_{11Metal} - S_{11Background})} \quad (6.29)$$

The attenuation in the MMW radiation caused from the cream is:

$$Attenuation = 1 - |T_{Cream}| \quad (6.30)$$

During the experimental work, the metal plate was cleaned using dry wipes before changing the type of the cream, and the reflectivity of the metal plate was checked to be maximum (using the VNA internal automatic setup) before coating it with a different cream. The reflectivity measurements for the metal plate were obtained before and after the plate was coated with cream. All the measurements were repeated 10 times (to reduce the random uncertainty) and the data were obtained directly to be processed later. Although, the cream was distributed equally and uniformly on the entire surface of the metal plate. However, the thickness of the cream layer is expected to be the main source of uncertainty in this experiment as it is very difficult to get exactly the same thickness of the cream layer on the entire surface of the metal plate.

### 6.3.3 Methodology of Data Processing

The following block diagram summarised the methodology of data processing for experiment 2:

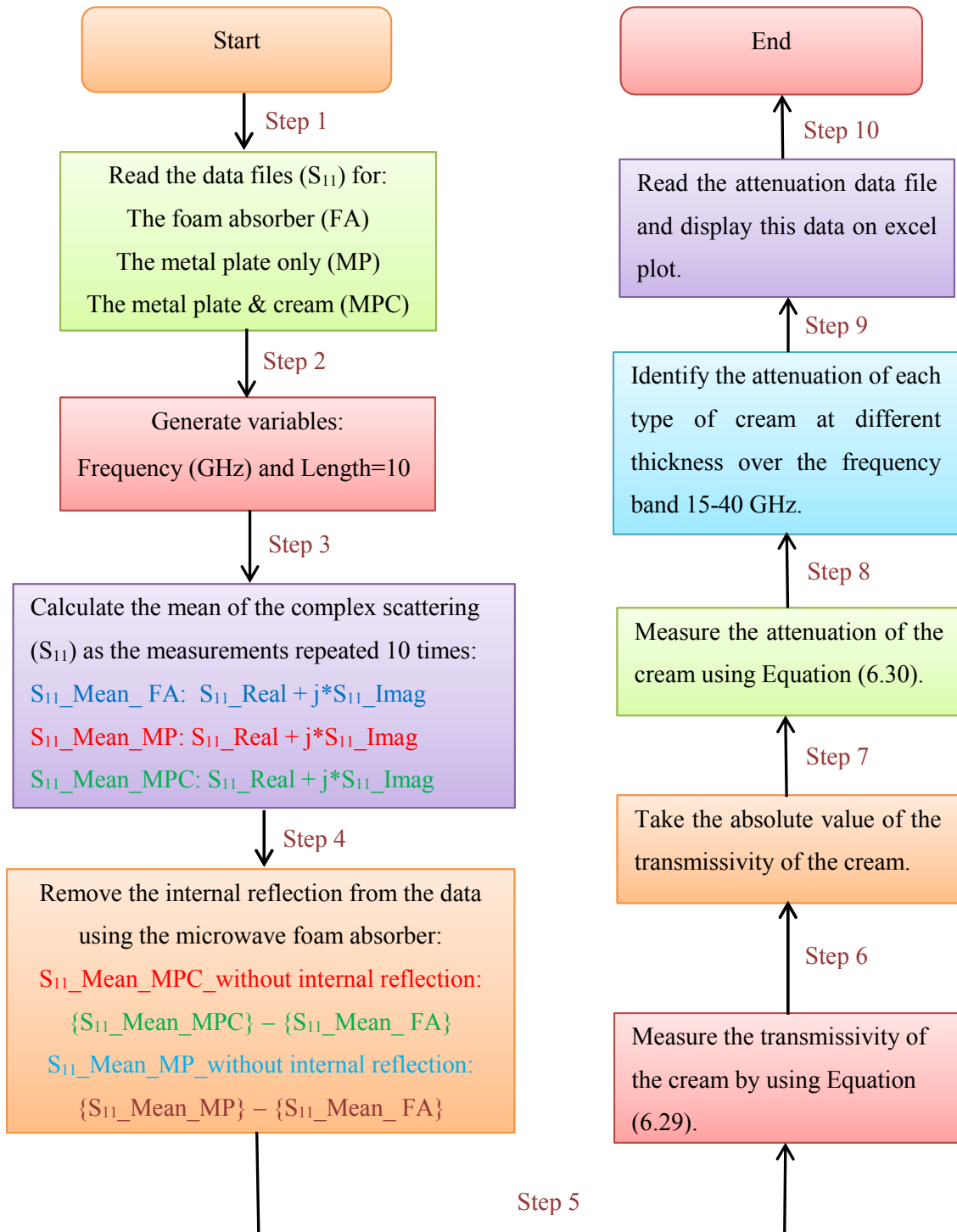


Figure 6.21: A methodology of data processing applied on different types of cream.

### 6.3.4 Experiment 2: Experimental Results

Experimental results in this section present the data obtained from different types of cream used in the treatments of burns and injuries and these are: 1) Flamazine cream, 2) Savlon cream, and 3) Sudocrem.

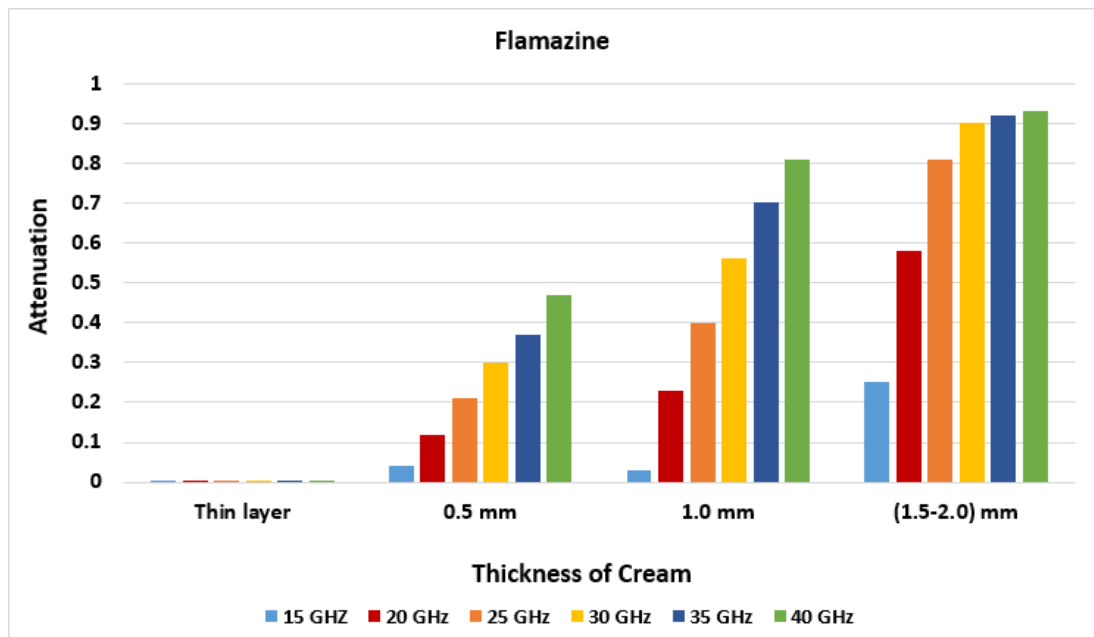


Figure 6.22: The attenuation in the MMW radiation caused by Flamazine cream.

The measurements in Figure 6.22 indicate that the attenuation in the MMW radiation caused by coating the metal plate with Flamazine cream is increased with the thickness of the cream and with the frequency. These results are consistent with the results obtained from Savlon and Sudocrem as illustrated in Figures (6.23 and 6.24). These results confirmed that the attenuation caused by coating the metal plate in cream varies from cream to cream, thickness to thickness, and at different frequencies.

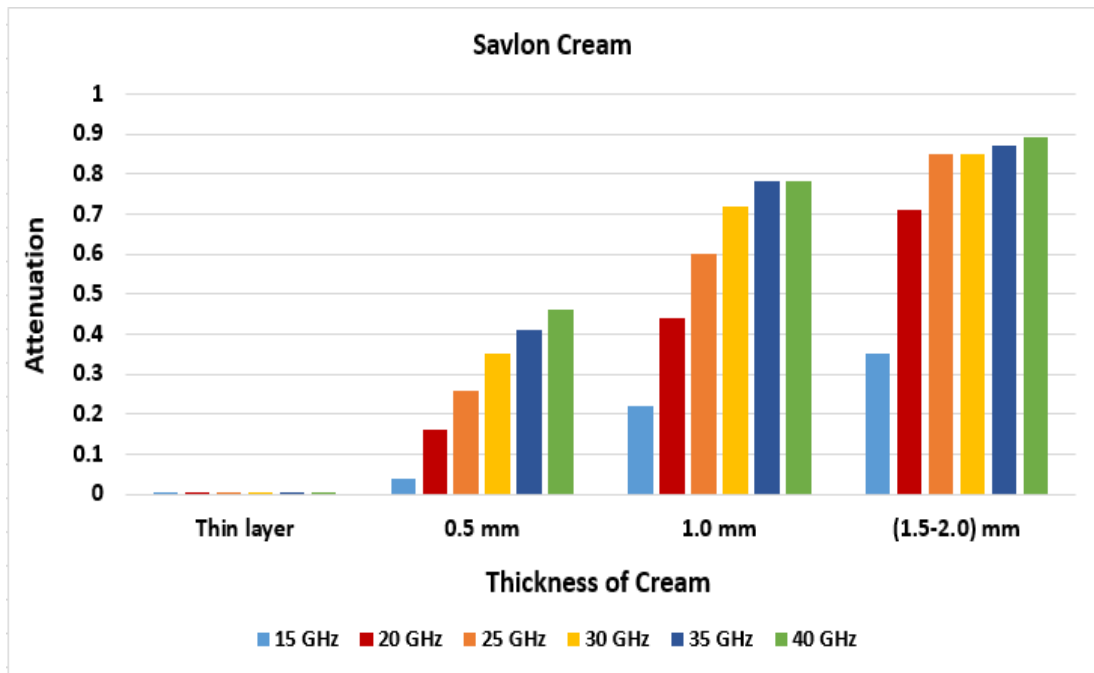


Figure 6.23: The attenuation in the MMW radiation caused by Savlon cream.

The measurements in Figure 6.23 indicate that MMW radiation is attenuated as a result of coating the metal plate with Savlon cream.

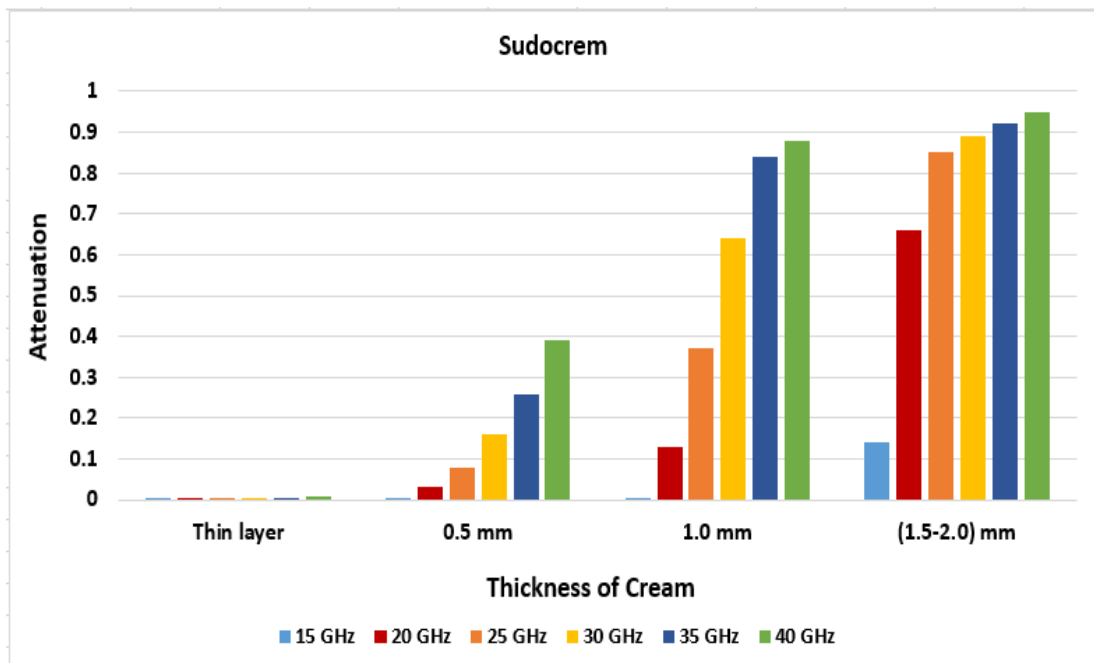


Figure 6.24: The attenuation in the MMW radiation caused by Sudocrem.

Experimental results in Figure 6.24 indicate similar trends to that obtained from Flamazine and Savlon cream. These results confirm that MMW radiation is highly absorbed and attenuated in cream over the frequency band from 15 GHz to 40 GHz.

## 6.4 Discussion

The propagation path length measurements conducted on dressing materials samples and a hand support cast indicate that, the resolved structure from a radar system effective over the band 15 GHz to 40 GHz is capable of providing information about the thickness of the dressing materials samples and the hand support cast using the distance between two reflection peaks. This capability is an advantage to the active imaging system over the passive imaging system that relies on the contrast of the radiation temperature between the target object and the background.

Reflection measurements applied on rigid samples (cylinder, flat plate, wax candle, and hand support cast) show images with three reflection peaks associated with 1) the front surface of the sample, 2) the back surface of the sample, and 3) the metal plate background. These results are reasonable as the separation distance between any two objects was chosen to be greater than the system spatial resolution, measured to be  $\sim 8.0$  mm. Furthermore, the difference between the actual and the measured PPL of the rigid samples was found to be in the range of 0.0 mm to 4.0 mm. This indicates that the experimental methodology is sufficient to provide information about the PPL of the samples.

Reflection measurements performed on dressing materials with cream (gauze burn and light support bandages) show images with two reflection peaks only. These reflections are associated with the front surface of the bandage combined with cream, and the back surface of the bandage combined with the metal plate. The interpretation for this is that the bandages were attached directly to the metal plate that has been used as a surrogate to the body surface, and this means that there is no separation distance between the back surface of the bandage and the metal plate; the system will not be able to resolve the two surfaces.

The measurements performed on Flamazine cream, Savlon cream, and Sudocrem indicate that the attenuation of the cream increases with the frequency and the thickness of the cream layer. Attenuation measurements show also that different cream has different attenuation and this is due to the dielectric properties and the water content that vary from cream to cream. Although the attenuation effect of the cream indicate a limiting factor as it confirms that MMW radiation is highly attenuated especially when the cream layer thickness is increased significantly between 1.5 mm to 2.0 mm. However, reflection measurements performed on dressing materials samples coated with a cream layer and water indicate that it is possible to sense features under the cream and the water as the metal plate is seen through a wet bandage and bandages coated with different types of creams.

## 6.5 Conclusions

A mono-static radar system with 25.0 GHz bandwidth and 8.0 mm spatial resolution was characterised to measure the propagation path length of dressing materials and hand support cast. The system was calibrated using known targets with known reflection properties such as; 1) a large flat metal plate, and 2) a wall of microwave foam absorber. The calibration measurements of the metal plate were used for deconvolution and dispersion compensation. The calibration measurements of the foam absorbing materials were used for internal reflection removal.

In this research, the attenuating effect of bandages and creams applied to burn wounds was measured experimentally. The measurements indicate that adding a cream layer to the bandages increases the reflection. Reflection peaks produce in the time domain result from reflections from the surfaces of the samples and discontinuities in dielectric properties. For in vivo measurements applied on biological tissue; the cream will be absorbed through the skin and this will increase the hydration level of the skin and as a result this makes a clear signature that can be detected and measured using either active or passive system.

The measurements of wet bandages confirm that water is highly reflective and absorbing to MMW radiation. This fact might be useful for identifying a non-healing status of a burn wound, as such a condition results in exudates from the skin.

The measurements indicate that there is a signature for each type of dressing materials and this signature varies with the state of the bandage (dry, wet, and with a layer of cream). These signatures suggested that active MMW radar might be an effective tool for monitoring the wound healing process under dressing materials, without their often-painful removal, and without having direct contact with the human body. The

following chapter demonstrates the feasibility of imaging burns under dressing materials using both passive and active imaging systems.

## Chapter 7

### Passive and Active Millimetre Wave Scanners for Burn Wound Diagnostics

*This chapter presents experimental images obtained from passive (radiometric) and active (radar) scanners measuring human hands and porcine skin samples. In vivo experimental images obtained from the human hands using the passive scanner reveal that passive imaging is capable of sensing surfaces attached to the human hand, and more importantly can detect structural deformations to the body under dressing materials. Experimental images obtained from porcine skin samples using both passive and active scanners reveal that active (15-40) GHz and passive (232-268) GHz millimetre wave imagers can be used for diagnosing burns and for potentially monitoring the healing under dressing materials.*

#### 7.1 Introduction

Imaging for medical applications over the MMW band can be implemented passively (radiometrically), where the natural thermal radiation emitted and reflected by the object is used or actively (radar), where the transmitter provides artificial MMW radiation to illuminate the subject and the image is formed from the reflected radiation [168]. Passive MMW images are free from artefacts such as speckle and glint as the illuminating radiation from the human body and the environment is spatially incoherent [201]. On the other hand, active imaging systems (using a spatially and temporality coherent illumination source) have the advantage of higher penetration capability, enabling probing to greater depths in less transmissive media [171].

Therefore, in this research both active and passive MMW imaging systems are used to assess the feasibility of detecting burns under dressing materials.

## **7.2 Imaging Radiometer**

In general, the main elements of an imaging radiometer are: 1) a high gain antenna, 2) multiple receivers, 3) high-speed scanner, 4) focusing elements such as lenses and mirrors, and 5) data processing software with a display [224].

A single channel radiometer can either be superheterodyne or direct detection receiver. The imaging radiometer consists of multiple independent channels of a single channel receiver. These channels gathering the data to be combined into a single image [224, 225]. The minimum detectable radiation temperature of the radiometer (thermal sensitivity) can be calculated using the radiometer equation (Equation 4.1) that has been discussed in chapter 4.

### **7.2.1 Lenses and Mirrors**

Focusing on elements such as mirrors and lenses are used in an imaging radiometer to achieve high-quality images. In general, mirrors are better at focusing than lenses as they result in fewer optical aberrations [224]. The focal length of a thin lens (thickness  $\ll$  curvature of the lens surface) can be calculated using the distance from the object to the lens,  $d_1$  and the distance from the lens to the image,  $d_2$  as [67]:

$$\frac{1}{f} = \frac{1}{d_1} + \frac{1}{d_2} \quad (7.1)$$

For an imaging system with a single lens. Positive magnification means a virtual image. Whereas, negative magnification means a real inverted image. The magnification factor is defined as the ratio between the sizes of the image to that of the object as [226]:

$$l = -\frac{d_2}{d_1} \quad (7.2)$$

### ***7.2.2 Depth of Field and the Field of View***

The depth of field (DoF) is defined as the span of range over which an object remains in focus. The theoretical DoF can be calculated from the operating wavelength of the system  $\lambda$ , the distance from the imager  $R$ , and the diameter of the aperture lens  $D$ , as [224, 227]:

$$DoF = 4\lambda \left(\frac{R}{D}\right)^2 \quad (7.3)$$

The angular field of view (AFoV) is defined as the angle in degrees through which the optical device can collect electromagnetic radiation as illustrated in Figure 7.1. The captured area of an optical system is directly proportional to the AFoV that can be calculated from the sensor height  $h$ , and the focal length of the optical lens  $f$ , as [228]:

$$AFOV = 2 \tan^{-1}(h/2f) \quad (7.4)$$

The spatial field of view (SFoV) is another important parameter that is measured the maximum size of an object that can be completely observed through an imaging system located at a fixed position. The theoretical spatial field of view in a unit of length can be calculated using the AFoV, and the working distance L as [228]:

$$SFoV = 2L \tan\left(\frac{AFoV}{2}\right) \quad (7.5)$$

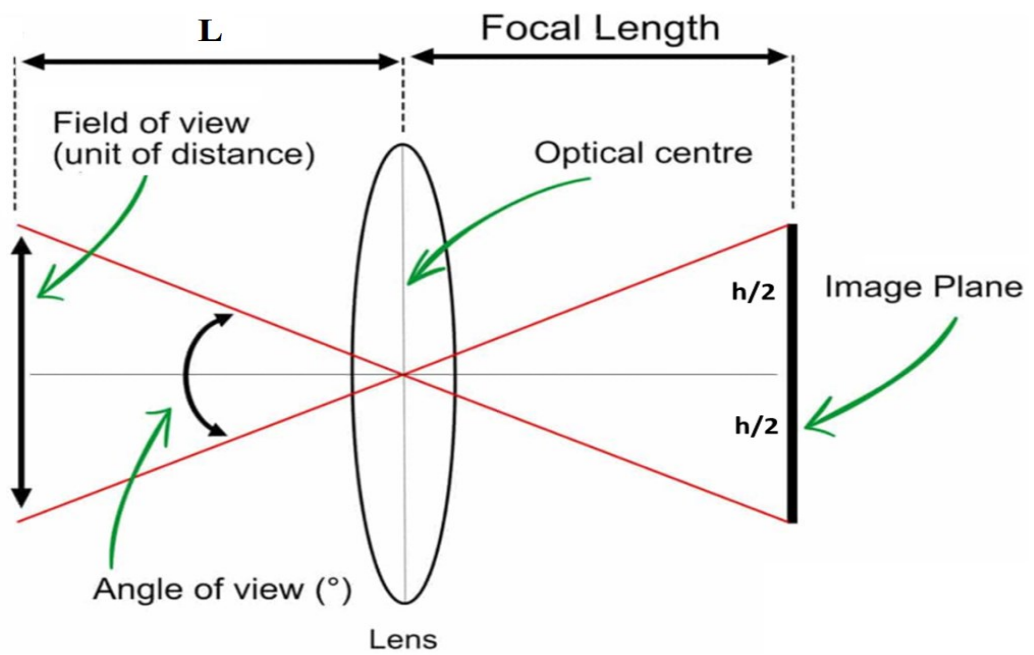


Figure 7.1: Illustration of the field of view and the angle of view for an imaging system [229].

### 7.2.3 Near Field and Far Field Regions

Electromagnetic field regions are classified into three types; 1) reactive near-field region, 2) near-field region (Fresnel), and 3) far-field region (Fraunhofer) as illustrated in Figure 7.2:

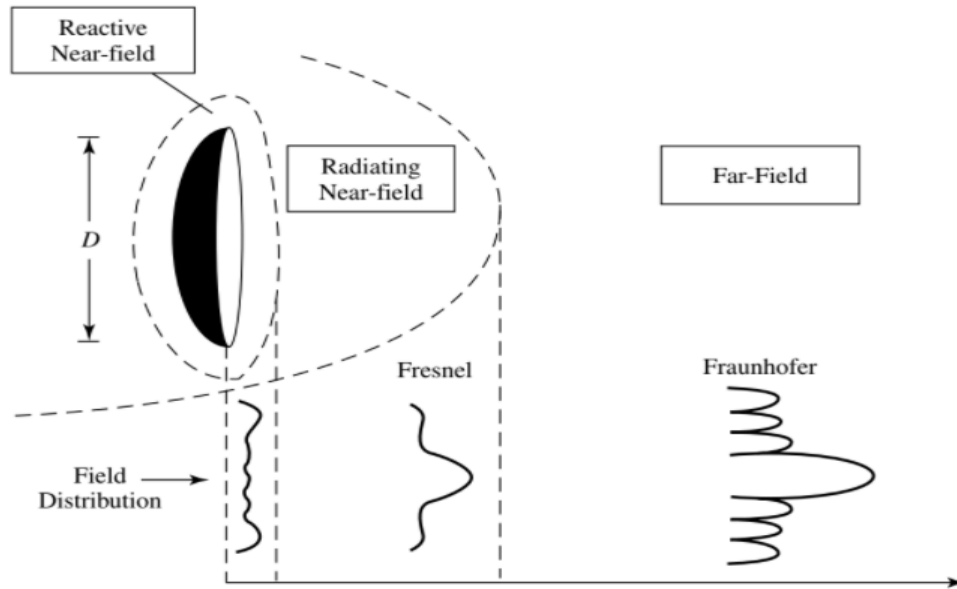


Figure 7.2: Illustration of the near and the far field regions of the EM radiation [230].

The field regions were identified based on the field characteristic and the distance limit that identifies the boundary limits between the three regions. The distance limit between the near field and the far field regions is identified by Fraunhofer [231] as:

$$R_f(\text{near field}) < \frac{2D^2}{\lambda} \quad (7.6)$$

$$R_f(\text{far field}) > \frac{2D^2}{\lambda} \quad (7.7)$$

Where,  $\lambda$  is the wavelength, and  $D$  is the maximum dimension of the antenna. The measurements conducted in this research were performed in the near field zone where the distance from the imager,  $R_f$  is less than  $2D^2/\lambda$ .

## 7.2.4 Diffraction Limits and Resolution

The resolutions limits (angular and spatial) are identified using different assumptions and approaches introduced by Rayleigh [67, 232, 233], Abbe [67, 169, 170], and Sparrow [67]. These approaches are summarised in Figure 7.3:

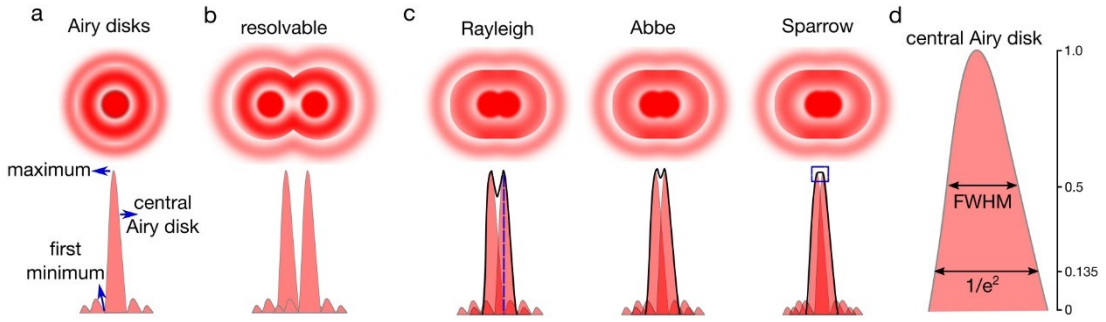


Figure 7.3: Different resolution limits identified by Rayleigh, Abbe, and Sparrow. The resolution limit can also be defined as a full width at half maximum (FWHM) or a  $1/e^2$  width [234].

According to the Rayleigh criterion, the theoretical angular resolution,  $\theta_{\min}$  in radians for an imaging radiometer (incoherent) can be expressed in terms of the system wavelength,  $\lambda$  and the diameter of the aperture lens,  $D$  as [232, 233, 235]:

$$\theta_{\min} = 1.22 \frac{\lambda}{D} \approx \frac{\lambda}{D} \quad (7.8)$$

The wavelength of the dielectric materials  $\lambda$  can be calculated as [67]:

$$\lambda = \frac{\lambda_o}{n} = \frac{\left(\frac{c}{f}\right)}{n} \quad (7.9)$$

Where,  $\lambda_o$  is the wavelength in free space,  $n$  is the refractive index of the dielectric material,  $c$  is the speed of the light, and  $f$  is the operating frequency.

Equation (7.8) indicates that the Rayleigh angular resolution limit can be enhanced either by decreasing the operating wavelength or by increasing the diameter of the aperture. Small wavelengths can be obtained by using higher frequencies and in the MMW band, this generally increases the cost. Large aperture is based on the system and its applications. Therefore, it might not possible to increase the diameter of the aperture [225].

Although, Rayleigh angular resolution limit is well known and it is the same for both coherent and incoherent sources. However, it is not fit for all circumstances and therefore, Sparrow resolution limit is used as an alternative and it can be expressed as [235]:

$$\theta_{\min}(\text{incoherent}) = 0.95 \frac{\lambda}{D} \quad (7.10)$$

$$\theta_{\min}(\text{coherent}) = 1.46 \frac{\lambda}{D} \quad (7.11)$$

The physicist Ernst Abbe identified the microscopic spatial resolution limit for an optical system,  $r_{\min}$  (measured in a unit of length) by using the following formula [169, 170, 235]:

$$r_{\min} = \frac{\lambda}{2D} \approx \frac{\lambda}{2} \quad (7.12)$$

Abbe's resolution limit is proportional to the wavelength, so better resolution are possible at shorter wavelengths. As an example of this, is using the half the wavelength ( $\lambda/2$ ). In this case, the resolution limit of the system becomes ( $\lambda/4$ ). For a non-coherent source, the resolution limit is greater by a factor of two compared to the coherent system [236].

### **7.3 Synthetic Aperture Radar**

Synthetic aperture radar (SAR) is a coherent imaging technique that uses a moving antenna to scan in one or two dimensions, creating two-dimensional (2D) or three-dimensional (3D) images. The spatial resolution can be high as it is commensurate with the length of the scanned baseline. In the SAR imaging system, the radar beam is focused on one patch and the reflected radiation from the target are collected to create a high-resolution image from a large synthetic aperture. This aperture can be obtained from a moving antenna with small physical aperture. The data obtained from SAR imaging system can be processed using either the IFFT algorithm or a SAR algorithm [138, 205, 237].

The SAR image processing algorithms are used to generate high-quality images. In general, the obtained images consist of; desired information, artefacts from signal processing, and unwanted echoes (clutter and speckle). In order to obtain a deeper understanding of these images, it is essential for the user to identify artefacts that manifestations of the technique and that are not present in the target. Effects such as speckle and multipath can generate non-real artefacts and these contribute to clutter in the image. In the experimental work conducted in this research, the measurements were performed indoors, in an anechoic environment. This minimises the multipath reflections and so helps to reduce the clutter. Furthermore, the images obtained in this research are compared with optical photos of the samples, so artefacts in the SAR images can be identified.

The SAR system has the advantage of high penetration capability compared with passive imaging system [171]. This is achieved by having control over the power level and the coherence of the illuminating source. However, the system should provide a balance between the penetration depth and the power level safety limits.

### 7.3.1 Active Imaging Reconstruction Criteria

In the SAR system, the sample is illuminated by spatially and temporally coherent microwave radiation, the complex reflected signal (amplitude and phase) is used to form a focused image using image reconstruction algorithms. Alias-free image reconstruction requires the reflected radiation to be sampled spatially and temporally according to the Nyquist criterion. This can be achieved if the phase shift between any two successive points is less than  $\pi$  in radian. The spatial sampling interval  $\Delta S$ , can be expressed in terms of the operating wavelength  $\lambda$  as [238, 239]:

$$\Delta S < \frac{\lambda}{4} \quad (7.13)$$

Temporally satisfying the Nyquist criterion is governed by sampling in the frequency domain in the VNA. In the frequency domain, the sampling interval is defined by the interval frequency that brings the phase shift between any two successive frequencies to be less than  $2\pi$  radian, as the obtained data consists of real and imaginary part. The frequency sampling interval  $\Delta f$ , then defines the maximum target range,  $d_{max}$  as [238]:

$$\Delta f = \frac{c}{4d_{max}} \quad (7.14)$$

Equation (7.14) can be written in terms of the number of samples  $N$  for a given bandwidth  $BW$  as [238]:

$$N > \frac{2d_{max}}{\left(\frac{c}{2BW}\right)} \quad \text{or} \quad N > \frac{2d_{max}}{\text{Range Resolution}} \quad (7.15)$$

Equation (7.15) indicates that two frequency samples are required per a range resolution. The range resolution of the radar system in dielectric medium  $R$  is:

$$R = \left( \frac{c}{2nBW} \right) \quad (7.16)$$

Where  $n$  is the refractive index of the medium.

### 7.3.2 Cross Range Resolution

For a three-dimensional imaging system, the cross-range resolution in  $x$ ,  $y$ , and  $z$  directions are diffraction limited and they can be identified using polar coordinates as illustrated in Figure 7.4:

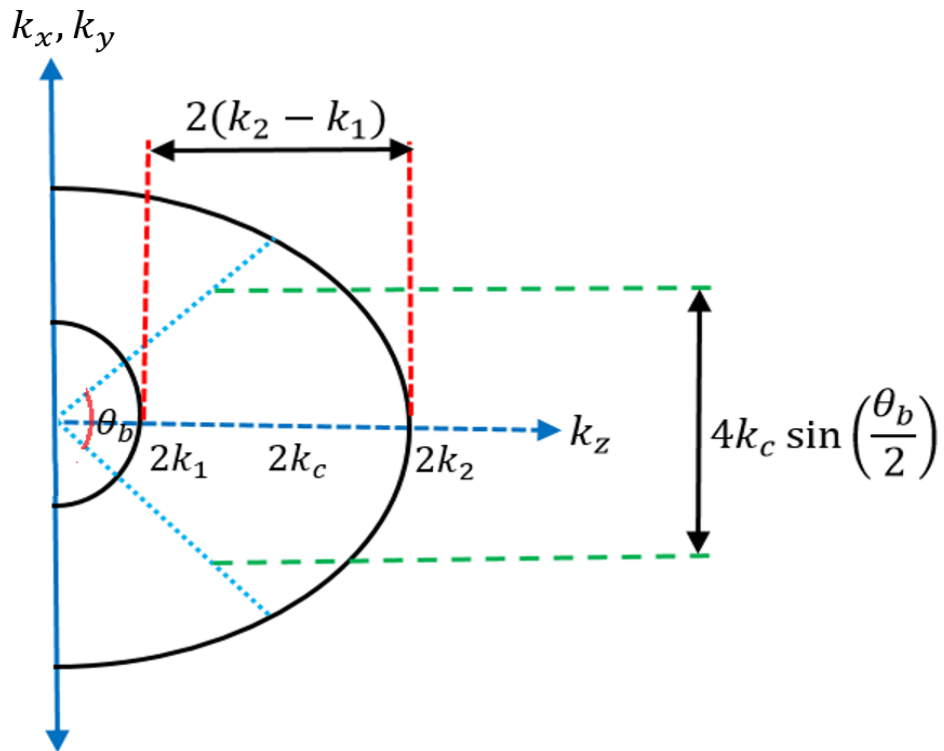


Figure 7.4: illustration of cross range resolutions in  $x$ ,  $y$ , and  $z$  directions in polar coordination [238].

The cross range resolution in the x-direction can be calculated using the wave number at the centre frequency  $\lambda_c$ , and the angle subtended by the aperture  $\theta_b$  as [238]:

$$\delta_x \approx \frac{\lambda_c}{4 \sin\left(\frac{\theta_b}{2}\right)} \quad (7.17)$$

The cross range resolution in the y-direction is approximately similar to that in the x-direction.

$$\delta_x \approx \delta_y \approx \frac{\lambda_c}{4 \sin\left(\frac{\theta_b}{2}\right)} \quad (7.18)$$

The cross range resolution in the z-direction can be expressed in terms of the wavenumbers at the high frequency  $k_2$  and the wavenumber at the low frequency  $k_1$  as [238]:

$$\delta_z \approx \frac{2\pi}{2(k_2 - k_1)} = \frac{c}{2BW} \quad (7.19)$$

Where, BW is the temporal bandwidth of the imaging system.

### 7.3.3 Clutter and Speckle in Radar Imaging

Clutter is defined as anything that is not the target and is usually generated by unwanted echoes returned to the radar system from objects in the scene as illustrated in Figure 7.5; it degrades the quality of the target image and makes it more difficult to interpret. Clutter appears randomly distributed and according to the source of clutter, it is divided into volume and surface distribution clutter [138, 240].

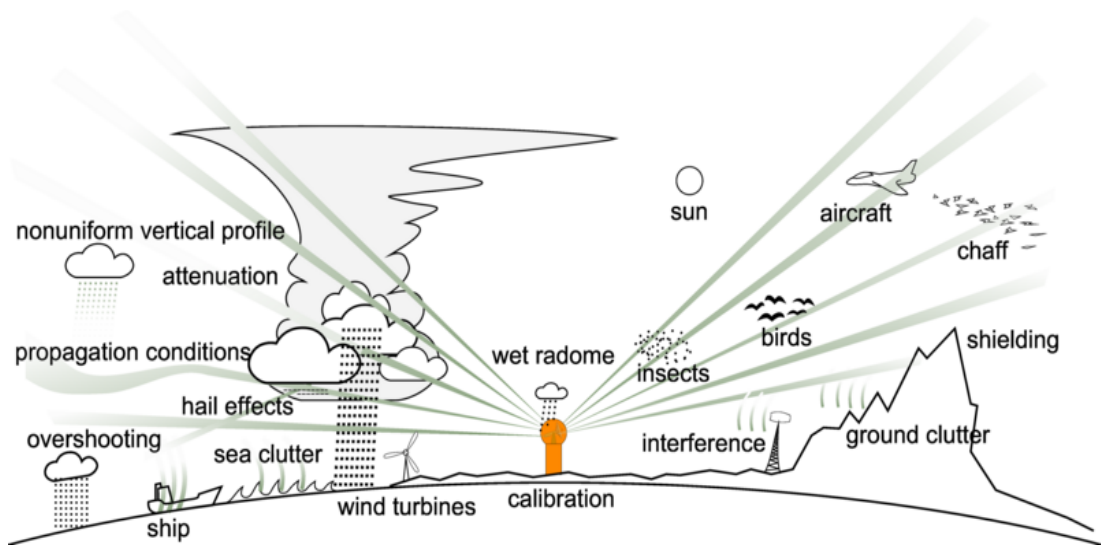


Figure 7.5: Different sources of clutter and anomalies in radar imaging system [241].

Using the radar range equation, the received power  $P_r$  is [240]:

$$P_r = \left( \frac{GP_t}{4\pi R^2} \right) \sigma \left( \frac{\lambda^2 G}{(4\pi)^2 R^2} \right) \cdot \left( \frac{1}{L_s} \right) \quad (7.20)$$

Where,  $\lambda$  is the wavelength of the radar signal in meter,  $R$  is the target range in meter,  $\sigma$  is the radar cross section (RCS) measured in meter square,  $L_s$  is the total loss factor in the radar system,  $G$  is the gain of the transceiver antenna, and  $P_t$  is the transmitted power in Watt.

Clutter echoes contribute to the received power level. Therefore, in the case of volume distribution clutter the received power is [240]:

$$P_r = \left( \frac{GP_t}{4\pi R^2} \right) \cdot (\sigma^c V) \left( \frac{\lambda^2 G}{(4\pi)^2 R^2} \right) \cdot \left( \frac{1}{L_s} \right) \quad (7.21)$$

Where,  $\sigma^c$  is a constant quantity that presents the average volume distributed clutter cross section per unit volume, and  $V$  is the volume of the radar resolution cell and it can be expressed as [240]:

$$V = \left\{ \pi R^2 \left( \frac{\Delta\theta}{4} \right) \left( \frac{\Delta\phi}{2} \right) \right\} \cdot \left( \frac{c\tau}{2} \right) \quad (7.22)$$

Where,  $\Delta\theta$  and  $\Delta\phi$  are represent the half power beamwidth of the main antenna beam in elevation and azimuth directions respectively,  $c$  is the speed of the light, and  $\tau$  is the width of the transmitted pulse.

Equations (7.21 and 7.22) indicate that the volume clutter increases with  $R^2$ . However, in surface clutter the received power is [240]:

$$P_r = \left( \frac{GP_t}{4\pi R^2} \right) \cdot (\sigma^o A) \left( \frac{\lambda^2 G}{(4\pi)^2 R^2} \right) \cdot \left( \frac{1}{L_s} \right) \quad (7.23)$$

Where,  $\sigma^o$  is a constant quantity that represents the average backscatter cross section per unit area of the ground, and  $A$  is the surface area and it can be expressed as [240]:

$$A = (R\Delta\phi) \cdot \left( \frac{c\tau}{2} \right) \quad (7.24)$$

Equations (7.23 and 7.24) indicate that the surface clutter of the radar system is directly proportioned to the radar range  $R$ . Increasing the range of the radar system increases both the volume ( $V \propto R^2$ ) and the surface clutter ( $A \propto R$ ).

In modern radar systems, clutter can be reduced by using matched filters, which through a convolution optimise the signal noise ratio [240].

The unwanted spatial variations of brightness across an image generated using coherent illumination can be caused by speckle; this is a result of constructive and destructive interference from the coherent source. Speckle should not be confused with noise. Speckle is usually most noticeable at limits close to the spatial resolution [138]. In SAR imaging, speckle can influence image interpretation, and therefore speckle filtering algorithms are suggested to be used to reduce the speckle noise and to provide better image interpretation and understanding [242].

## **7.4 Experiment 1: In Vivo Passive Sensing and Imaging Using the ThruVision 250 GHz Imager**

The objectives of this experiment are highlighted as follows:

- To demonstrate the capability of the passive MMW imaging system for monitoring changes in human skin in dry, wet and with cream states under dressing materials.
- To demonstrate the capability of the passive MMW imaging system for detecting missing parts of the human hand under dressing materials.

### ***7.4.1 Frequency Band (232-268) GHz***

The measurements in this research were conducted using a ThruVision passive imager centred ~250 GHz (an existing system in the lab). The frequency band (232-268) GHz is not the optimal band for sensing and imaging through dressing materials, due to the lower penetration capabilities ~0.238 mm [24] and higher absorption compared with the lower frequency bands (30 GHz and 90 GHz). However, the experimental results indicate that the system provides useful information in the measurements of burns under dressing materials. A capability that makes the whole MMW band (30-300) GHz is feasible to be used for the purposes of this research.

### ***7.4.2 Participants***

The measurements in this research were conducted on two healthy participants; female (33 years) and male (36 years) having Asian ethnicity (Middle Eastern) with no history of skin disease.

### 7.4.3 Experimental Setup and Description

A ThruVision passive imager having a centre frequency of 250 GHz and a bandwidth of 36 GHz (type: TS4, manufacturer: Digital Barriers) [243] is used to scan images from the palm of the hand skin with and without dressing materials. These measurements are made when the hand is in the wet and dry state, and with a layer of a medicinal cream applied. The imager is sensitive over the band (232-268) GHz and has a primary lens diameter of 175.0 mm and a measured depth of field of 200 mm. The imager has an operating wavelength of 1.2 mm and a spatial resolution of 5.5 mm. The imager consists of a TS4 unit and a laptop as illustrated in Figure 7.6. The imager requires around 10 minutes of warm-up time. The TS4 unit is connected through an Ethernet cable to a laptop and the data transfer from the TS4 unit to the laptop and vice versa. The images were displayed on the screen of the laptop using a ThruViewer software, and they were saved in screenshots format to be processed later using the Matlab programme.

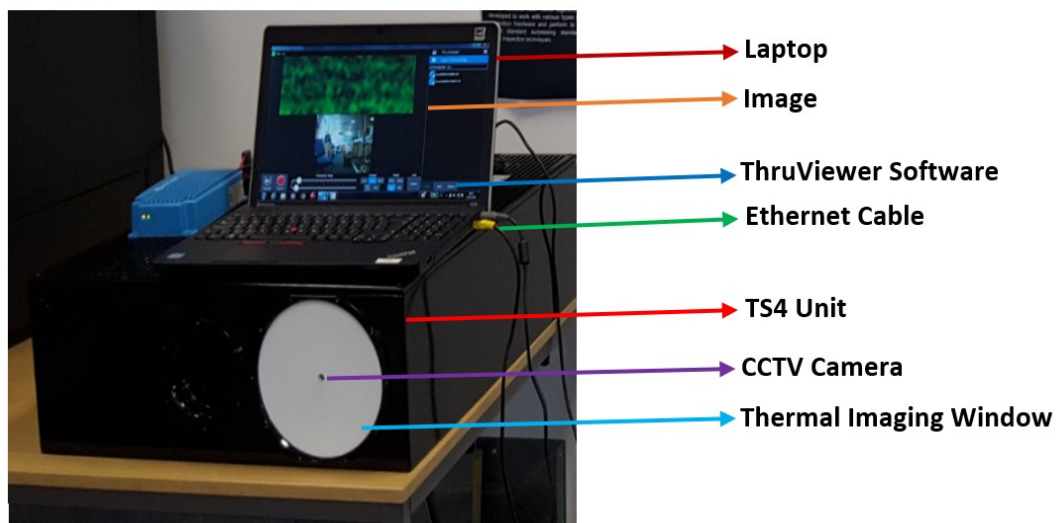


Figure 7.6: A ThruVision 250 GHz passive imager comprises a TS4 unit, a CCTV camera, a thermal imaging window, and a laptop with a ThruViewer software.

#### ***7.4.4 Methodology of Conducting the Experimental Work***

This section discusses different methodologies used for scanning passive images of the palm of the hand skin in vivo with and without the presence of dressing materials in the near-field region. Images were scanned for the skin in normal, wet and with cream states.

##### ***7.4.4.1 Methodology 1: Normal Skin***

The subject hand in the normal state was located over a distance of ~ 800 mm from the imager. This distance was chosen since it is within the depth of field and the range of the imager (range ~1000 mm). The system forms images from the thermal emission (intensity of radiation) emitted from the human hand directly. These images were displayed on the screen of the laptop using a ThruViewer software and they were saved to be processed using the Matlab programme.

In the next step, dressing materials (type: light support bandage) were placed on the hand. Images were then compared with the normal unbandage skin. The thermodynamic temperature of the skin was measured experimentally many times during the experimental work using both an infrared thermometer and a thermocouple.

##### ***7.4.4.2 Methodology 2: Wet Skin***

For wet skin, the palm of the hand was placed inside a bowl of water for ~3.0 seconds (soaking wet) and then methodology 1 was applied to scan images for the wet skin with and without the presence of light support bandage. The temperature of the skin was measured experimentally before and after the application of water.

#### ***7.4.4.3 Methodology 3: Skin with Cream***

For the skin with cream, the hand was placed on a flat table and a thin layer of cream was equally distributed on the palm of the hand skin. Then methodology 1 was applied to scan images for the hand with and without the presence of a light support bandage. The thermodynamic temperature of the skin was measured experimentally before and after the application of the cream.

#### ***7.4.5 Data Processing***

Experimental images obtained via the ThruViewer software [243] were saved as screenshots in portable network graphic format (.png). This format was chosen as it allows the user to access the images without the presence of the ThruViewer software. The images were read using imread function implemented in Matlab programme. Then colour bars were inserted for assigning the thermodynamic temperature of different parts of the images (i.e. skin, background....etc.). The temperature measurements were made during the experimental work using an infrared thermometer. This type of thermometer was chosen as it can provide precise measurements of the surface temperature of the skin.

#### ***7.4.6 Experimental Results***

The measurements obtained from experiment 1 are divided into three parts: 1) measurements of the depth of the field of the imager, 2) measurements obtained from the palm of the hand with skin under normal conditions, in a wet state and with various medicinal creams applied with and without the presence of dressing materials, and 3) measurements obtained from the palm of the hand skin in its normal state with and without dressing materials to identify the missing finger of the hand.

##### ***7.4.6.1 Initial Measurements***

The measurements were conducted indoor in an anechoic environment at a room temperature of  $\sim 22$  °C. The system output was assumed to be linear; as the lower colour in the temperature scale represents the lower temperature (blue) and the higher colour in the temperature scale (red) represents the higher temperature as illustrated in Figure 7.7.

The depth of field of the imager was measured using a cup of hot water having a temperature of  $\sim 70$  °C. Initially, the cup was located close to the imager and then it was moved backward gradually in a straight line until the image of the cup is seen clearly and sharply for the first time as illustrated in Figure 7. 7a. Then the cup was moved further until the point where the image is seen and any further movement after that will affect the image of the cup. The difference in distance between the two measurements indicates that the depth of field of the imager is  $\sim 200$  mm. These measurements were repeated five times and similar results were obtained with a standard deviation of  $\sim 12.5$  mm. These results are closed to the theoretical depth of field result that is calculated to be  $\sim 157$  mm using Equation (7.3).

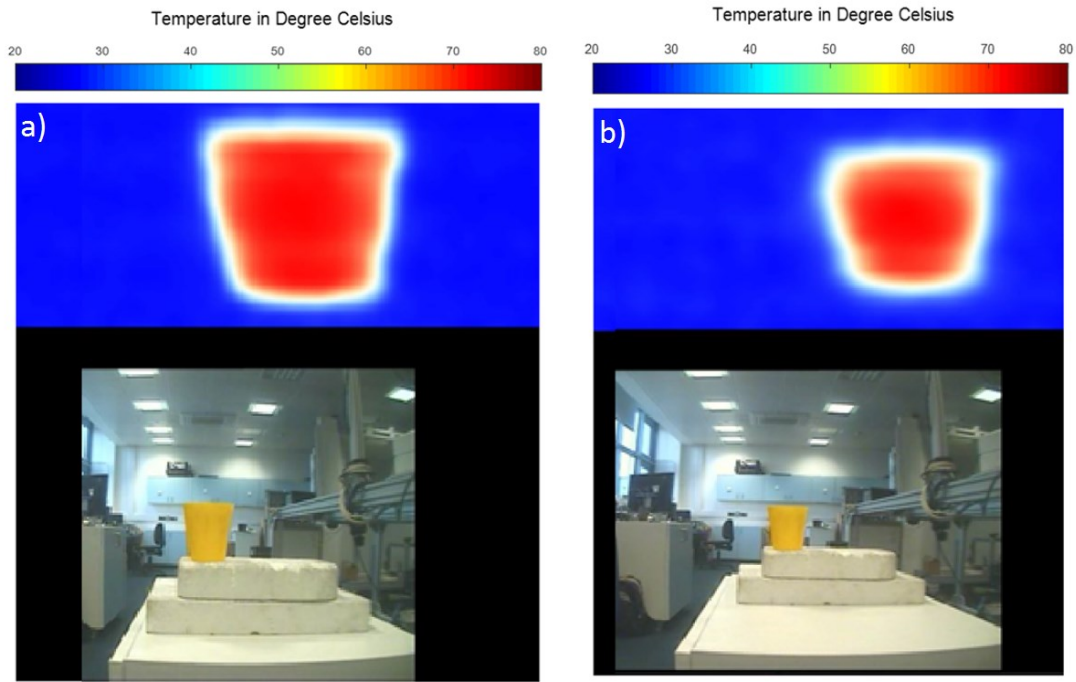


Figure 7.7: Measurements for the depth of the field of the imager using a cup of hot water  $\sim 70$  °C; a) represents an image in the depth of field region, and b) represents an image out the depth of the field region.

#### ***7.4.6.2 Images for the Human Skin at Different States***

A ThruVision passive imager operating over the band 232 GHz to 268 GHz is used for scanning in vivo images for a female participant on the palm of the hand region. The images were taken for the hand in normal, wet, and with cream states with and without dressing materials.

##### **7.4.6.2.1 Normal Skin and Wet Skin**

Measurements of the normal and wet palm of the hand skin were performed using methodology 1 and methodology 2 described in sections 7.4.4.1 and 7.4.4.2 respectively. The images obtained were processed using Matlab programme as illustrated in Figure 7.8.

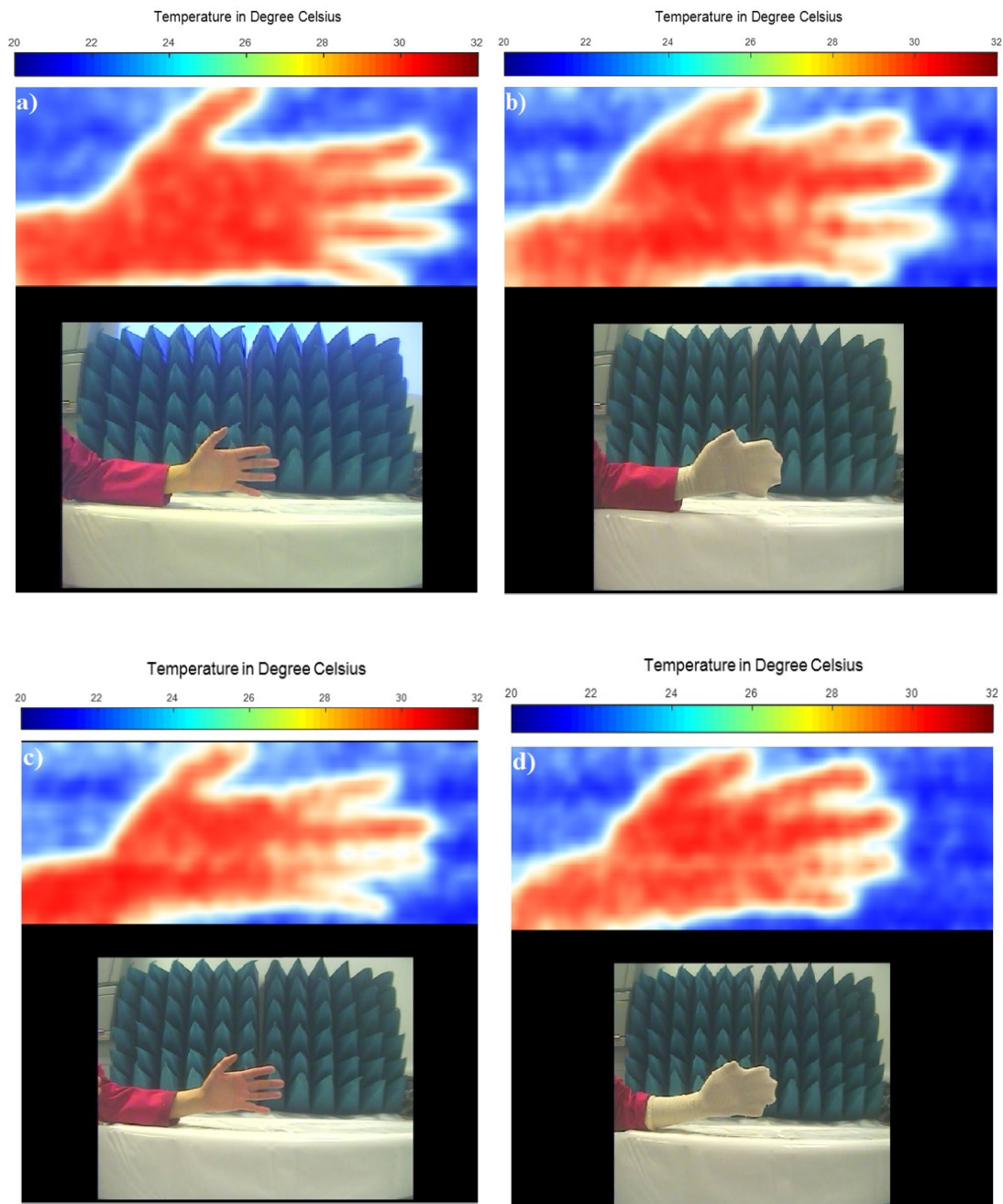


Figure 7.8: MMW images for the palm of the hand skin in normal and wet state for a female participant at 250 GHz; a) represents normal skin without dressing materials, b) represents normal skin with dressing materials, c) represents wet skin without dressing materials, and d) represents wet skin with dressing materials.

The measurements in Figure 7.8 indicates that the human hand can be seen through dressing materials in dry and wet states. The temperature for the palm of the hand skin was measured to be  $\sim 32$  °C in a normal state and the ambient temperature was measured to be  $\sim 22$  °C. Image (a) represents the palm of the hand skin in a normal state, the maximum temperature contrast between the palm of the hand skin and the surrounding background with its effective temperature related with air temperature can be seen effectively in this case. The emissivity and the reflectance for the palm of the hand skin are calculated to be 0.78 and 0.22 respectively. These values are calculated using the dielectric properties of the skin and the half space electromagnetics model [124].

Image (c) represents the palm of the hand skin in a wet state; the thermodynamic temperature for the wet palm of the hand skin was measured to be  $\sim 30$  °C. In this case, the reflectance of the skin increases due to the high dielectric constant of the water in the MMW band [26, 164]. This increase is estimated to be  $\sim 0.15$  [164]. Using the law of conservation of energy, the emissivity of the skin decreases to  $\sim 0.63$  ( $\epsilon=1-R$ ). By comparing image (a) with the image (c), it can be seen that the layer of water can be detected and observed passively.

Image (b) represents the hand in a normal state with dressing material. In this case there is a reduction in the contrast relative to image (a) because of additional absorption from dressing materials and the radiation from the textile materials, but because of the high porosity of the dressing material, the effective temperature is between the air temperature ( $\sim 22$  °C) and the skin temperature ( $\sim 30$  °C). The distribution of the emissivity, in this case, is more uniform compared with the case of wet skin in the image (c).

In the case of wet hand with dressing material, image (d), the image shows a reduction in the contrast relative to the image (b) because of additional water layer present on the palm of the hand skin and this makes the dressing materials partially wet. Therefore, the reflectivity of the hand and dressing materials are higher and this makes a significant reduction in the total emissivity.

#### **7.4.6.2.2 Normal Skin and Skin with Creams**

In medical applications, creams are used widely in the treatments of burns and injury. Therefore, this part presents in vivo images taken for the human skin in a normal state and with cream applied. Two types of creams were used, Savlon and Sudocrem. The measurements were performed using methodology 1 for normal skin (described in section 7.4.4.1) and methodology 3 for the skin with cream (described in section 7.4.4.3). The images obtained from Savlon cream and Sudocrem were processed in the Matlab programme and the results obtained are presented in Figures (7. 9 and 7.10) respectively.

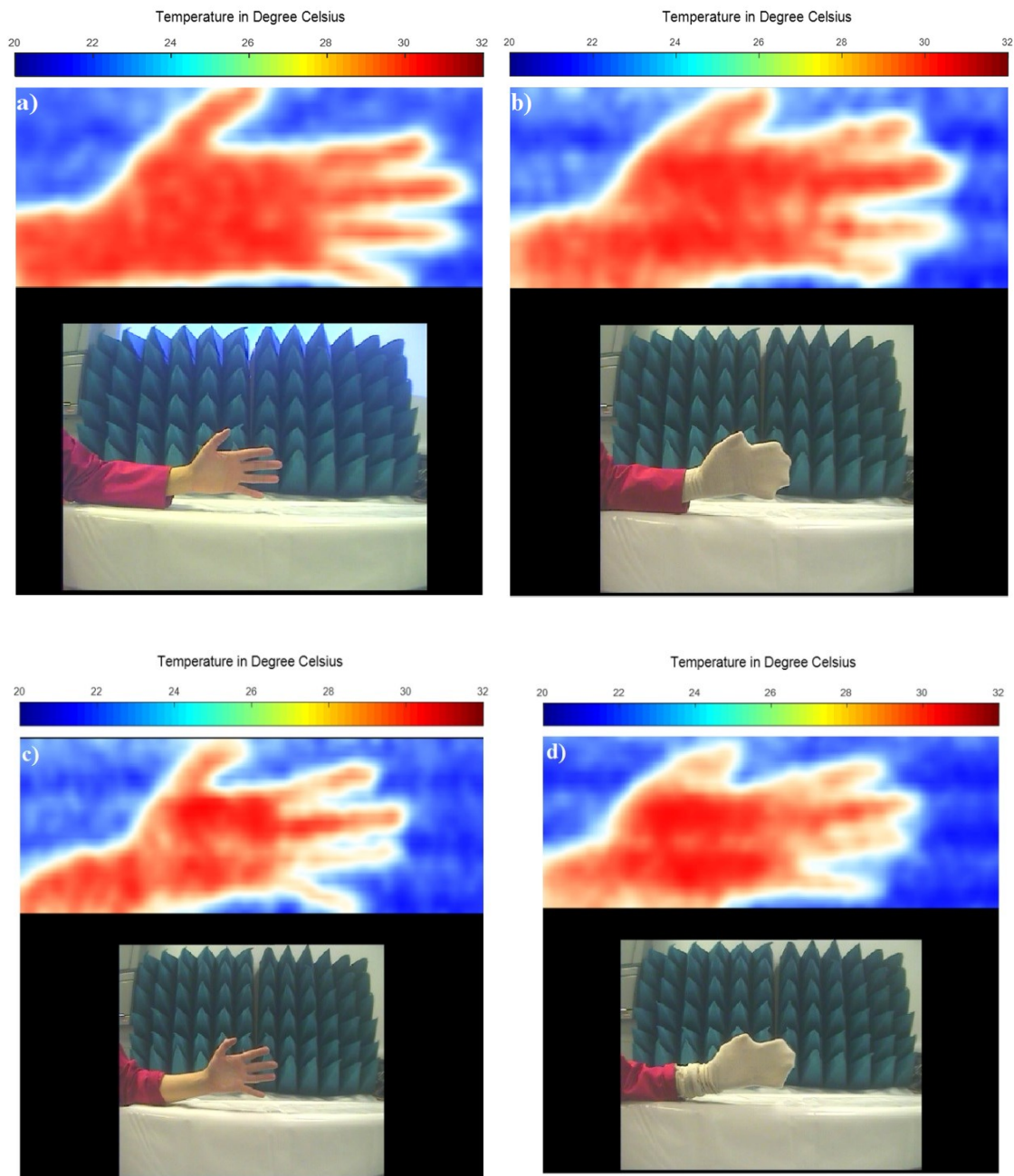


Figure 7.9: MMW images for the palm of the hand skin of a female participant at 250 GHz; a) represents normal skin without dressing materials, b) represents normal skin with dressing materials, c) represents skin with Savlon cream, and d) represents skin with both Savlon cream and dressing materials.

The measurements in Figure 7.9 show that adding a layer of Savlon cream on the skin surface decreases the temperature of the skin by 2.0 °C and increases the reflectivity of the skin significantly. The increase in the reflectivity of the skin is influenced by the water content of the cream, the dielectric properties of the cream, and the thickness of the cream layer as discussed in chapter 6 (section 6.3.4). The measurements also indicate that the human hand can be seen through light support bandage and Savlon cream.

Experimental images obtained from Sudocrem in Figure 7.10 are not dissimilar to those obtained from water and Savlon cream. These measurements confirm that the human hand can be seen through a cream layer and light support bandages. The measurements also show a contrast between normal skin and skin with water and cream. These measurements indicate there is a capability for measuring skin burns and injury under bandages using a passive MMW imager.

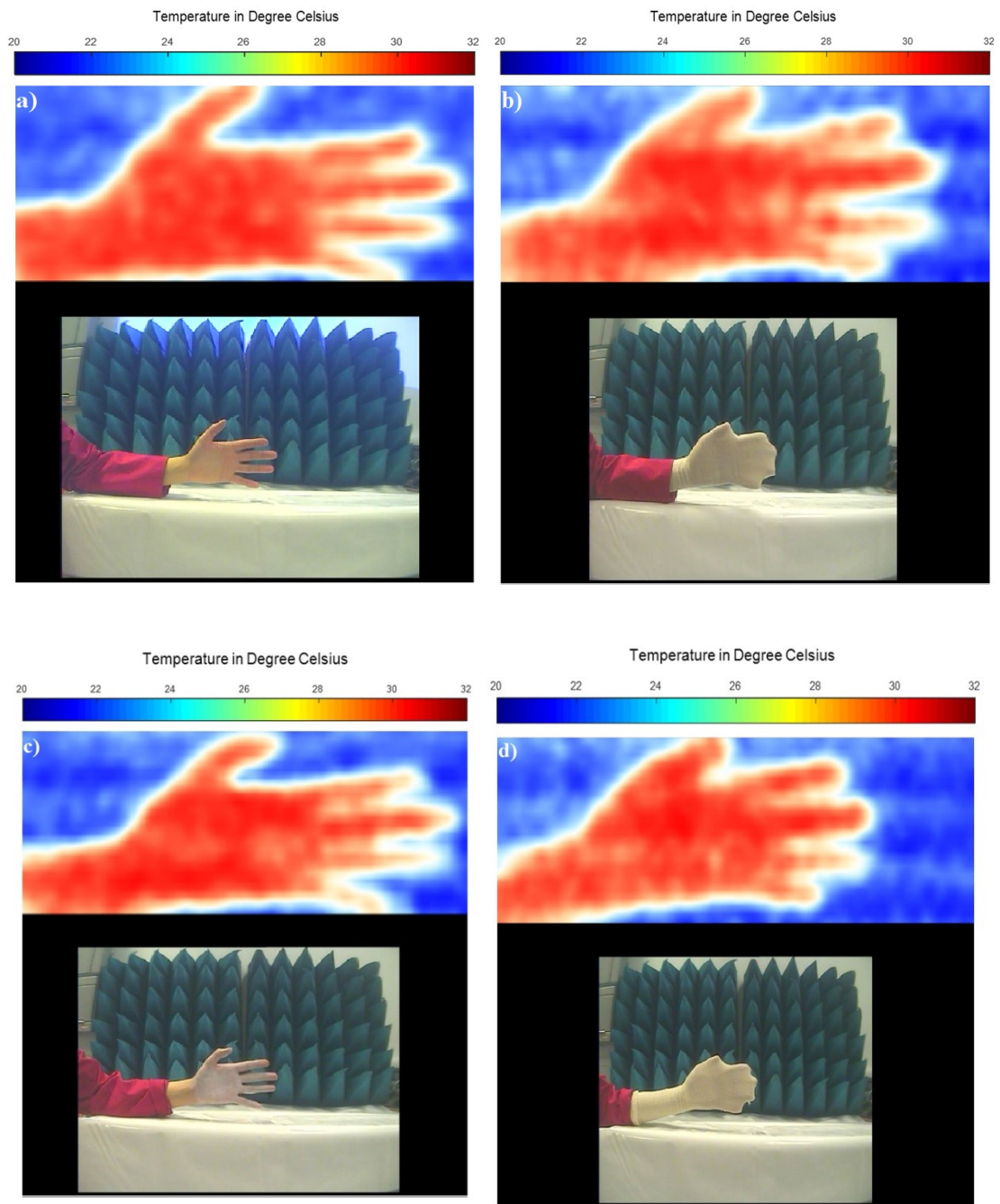


Figure 7.10: MMW images for the palm of hand skin for the female participant at 250 GHz; a) represents normal skin without dressing materials, b) represents normal skin with dressing materials, c) represents skin with Sudocrem, and d) represents skin with both Sudocrem and dressing materials.

### 7.4.6.2.3 Passive Imaging for Detecting Missing Parts

The measurements in this section were conducted on a male participant having a missing finger on his right hand. The measurements were conducted on the hand with and without dressing materials as illustrated in Figure 7.11.

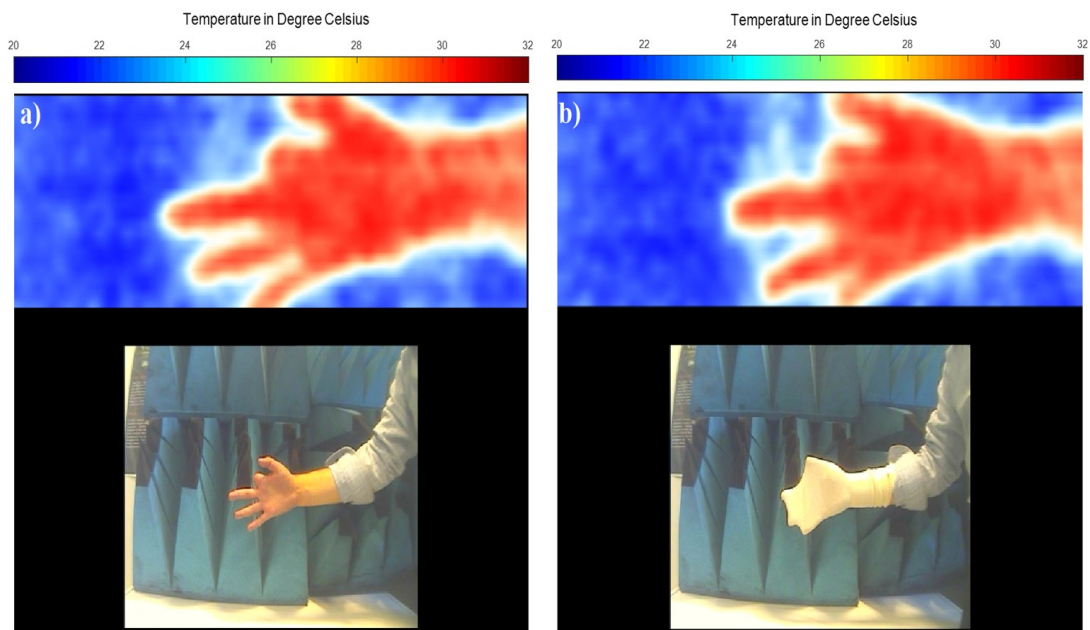


Figure 7.11: MMW images from the palm of the hand skin for a male participant; a) represents the hand without dressing materials, and b) represents the hand with a light support bandage.

The measurements in Figure 7.11 indicate that passive MMW imager can detect a missing finger under dressing materials without the necessity of dressing removal and in non-contact with the human body. These measurements open a new window of research in medical applications; this being the identification of injuries and monitoring of the healing progress of the burn wound.

## **7.5 Experiment 2: Burn Detection Using the ThruVision 250 GHz**

### **Imager**

This experiment aims to scan images for porcine skin samples before and after the application of localised heat treatment with and without the presence of dressing materials using a 250 GHz ThruVision passive imager. The experimental setup for this experimental work is similar to that described in experiment 1 (section 7.4.3).

#### ***7.5.1 Porcine Skin Samples***

Four fresh porcine skin samples were taken from different regions of the animals and measured in this experiment. The study was approved by the ethics committee of Manchester Metropolitan University (ethics reference no: SE1617114C). A copy of the ethical approval is attached in Appendix B.

#### ***7.5.2 Methodologies Applied on Porcine Skin Samples***

This section discusses different methodologies applied on porcine skin samples for scanning images before and after the applications of localised heat treatments with and without the presence of dressing materials.

##### ***7.5.2.1 Methodology 1: Skin without Burns***

The porcine skin sample was located over a digital hotplate (described in chapter 5 in section 5.4.2) and left to be heated and stabilised to 36.0 °C. Then the sample was placed on a white Polystyrene flat plate (length= 400 mm, and width=300 mm). The Polystyrene plate combined with the sample was located vertically over a distance of 800 mm from the passive imager. Images of the skin were obtained using either

screenshots or video recording options from the ThruViewer software. The skin surface temperature of the sample was measured using an infrared thermometer.

In the case of skin with dressing materials, a similar methodology was applied to the sample. However, the dressing materials are located over the sample when the sample was located over the digital hotplate. This means that the thermodynamic temperature of the sample is stabilised to 36.0°C with the presence of different types of dressing materials. This is minimised the variation in the thermodynamic temperature of the skin as a result of adding extra dressing materials layers.

#### ***7.5.2.2 Methodology 2: Skin with Burns***

The sample was located over a digital hotplate and left to be heated and stabilised to 36.0 °C. Then contact burns were applied using a heat control metal plate. The plate was heated to 100 °C and placed directly on the skin surface for a period of 15 seconds with a constant pressure. In this experimental work, single and multiple burns were applied on the sample. Then the sample was placed on a white Polystyrene flat plate. The plate combined with the sample was located vertically over a distance of 800 mm from the passive imager. Images of the skin were obtained using either screenshots or video recording options via the ThruViewer software. The skin surface temperature of the sample was measured using an infrared thermometer.

Then dressing materials were placed on the burn-damaged skin and images were obtained using the methodology described above.

### ***7.5.3 Data Processing***

Experimental images obtained via the ThruViewer software were saved as screenshots in (image.png) format. The images were read using imread function implemented in Matlab programme. Then colour bars were inserted for assigning the thermodynamic temperature of different parts of the images (i.e. skin, burns, and background) and then the images were displayed in the final format.

### ***7.5.4 Porcine Skin Measurements***

Images obtained from this experiment were divided into three parts; 1) images for the skin (unburned skin) with and without the presence of dressing materials, 2) images for the burn-damaged skin without dressing materials, and 3) images for the burn-damaged skin with the presence of dressing materials.

#### ***7.5.4.1 Skin without Burns***

Experimental images for porcine skin sample (length= 140 mm, and width= 110 mm) without burns were performed using methodology 1 described in section 7.5.2.1. The measurements were obtained at a room temperature of  $\sim 22^{\circ}\text{C}$  whilst the skin surface temperature was  $36^{\circ}\text{C}$ . Different types of dressing materials were applied to the skin and images were obtained and processed using Matlab programme as illustrated in Figure 7.12.

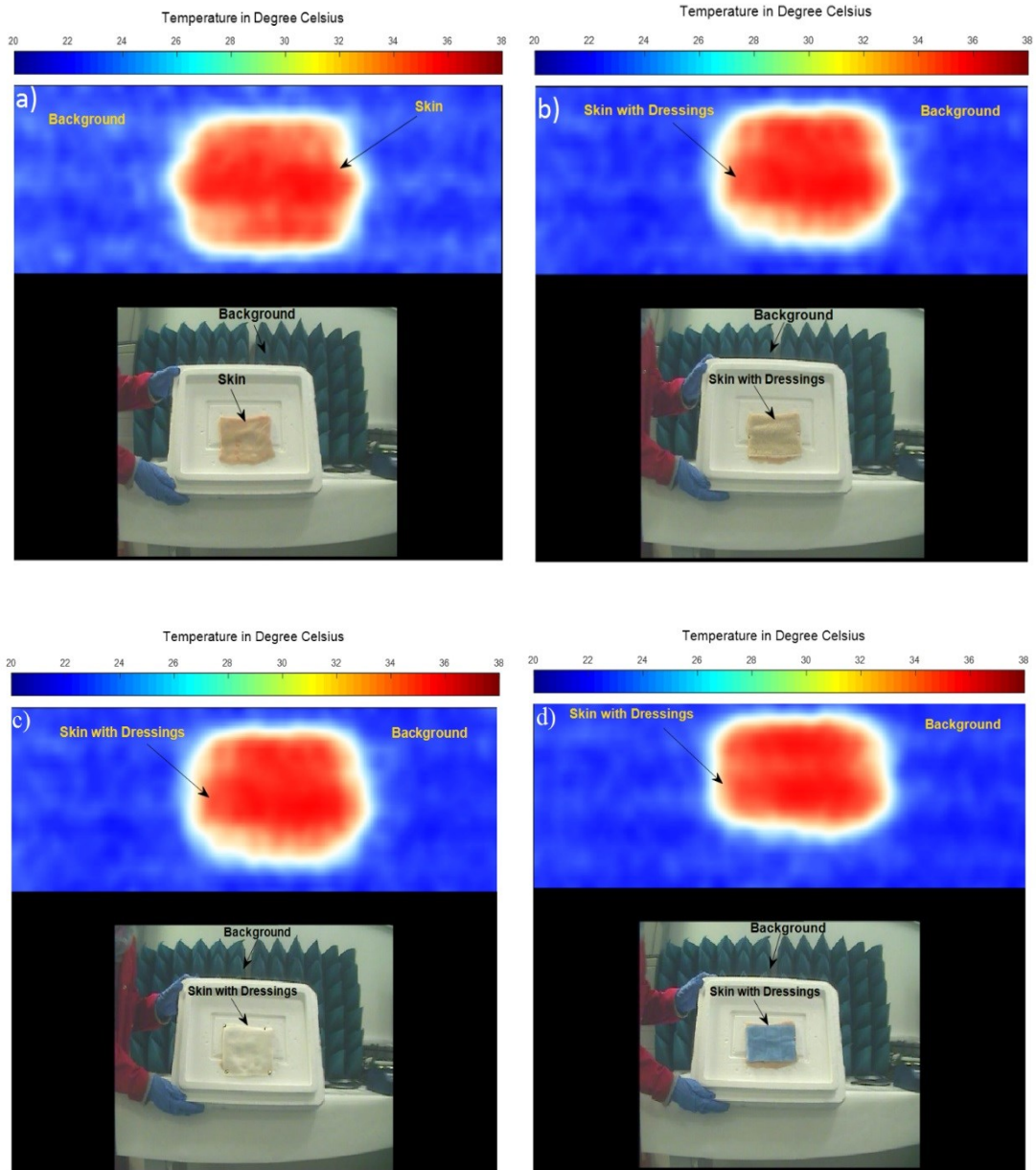


Figure 7.12: MMW images for porcine skin sample at 250 GHz; a) represents the skin without dressings, b) represents the skin with one layer light support bandage, c) represents the skin with 10-layers white gauze burn bandage, and d) represents the skin with 4-layers blue gauze burn bandage.

Experimental images in Figure 7.12 indicate that the skin of the porcine sample is seen through different types of dressing materials having different thicknesses (thin dressings such as a single layer light support bandage in the image (b) and thick dressings such as a 10-layer gauze burn bandage in image (c)).

#### ***7.5.4.2 Skin with Single and Multiple Burns***

Images for porcine skin samples with single and multiple burns were performed using methodology 2 described in section 7.5.2.2. The measurements were applied on two samples; sample 1 (length= 160 mm, and width= 110 mm) and sample 2 (length= 110 mm, and width= 100 mm). Images were obtained at a room temperature of ~22 °C and they were processed using the Matlab programme as illustrated in Figure 7.13.

Images in Figure 7.13 indicate that passive MMW imaging system is capable of detecting burns and identifying the location of the burns (middle or edge) as illustrated in images (a, b, c, and d). The images also indicate that the passive imager is capable of distinguishing between the skin with burns (red colour) and the skin without burns (white or yellow colour). The radiation temperature of the skin is directly proportional to the emissivity of the skin and the thermodynamic temperature of the skin ( $T_R = \epsilon T$ ). Therefore, it is reasonable to assume that the radiation temperature of the skin with burns is equal to the thermodynamics temperature ~60 °C (or 333 K) as the emissivity of the porcine skin with burns is estimated to be ~1.0 at 250 GHz using the half space model [124].

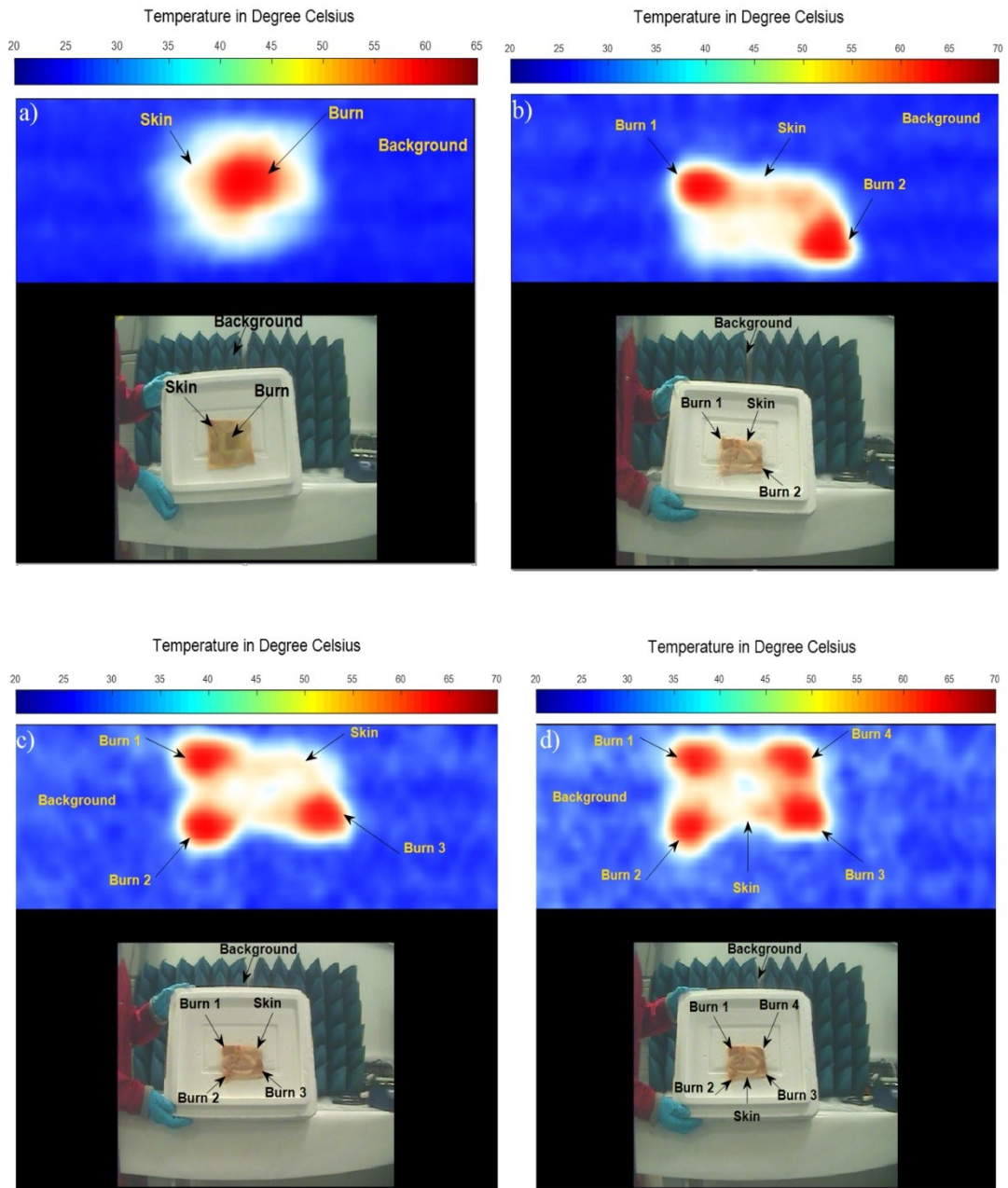


Figure 7.13: MMW images for porcine skin samples at 250 GHz; a) represents the skin with one burn, b) represents the skin with two burns, c) represents the skin with three burns, and d) represents the skin with four burns.

#### ***7.5.4.3 Skin with Burns and Dressing Materials***

Images for porcine skin samples with burns and dressing materials were performed using methodology 2 described in section 7.5.2.2. The measurements were applied on two samples having multiple burns. Images were obtained at a room temperature of  $\sim 22^{\circ}\text{C}$  before and after the dressing materials were placed on the sample as illustrated in Figure 7.14.

Images in Figure 7.14 indicate that thermal burns can be detected and identified under dressing materials without them being removed; as similar images obtained from the samples with dressings compared with those without dressings. The images also indicate that passive imaging systems can distinguish between the unburned skin (white or yellow colour) and the burn-damaged skin (red colour) with the presence of dressing materials. A capability that might be used for monitoring the burn wound healing progress.

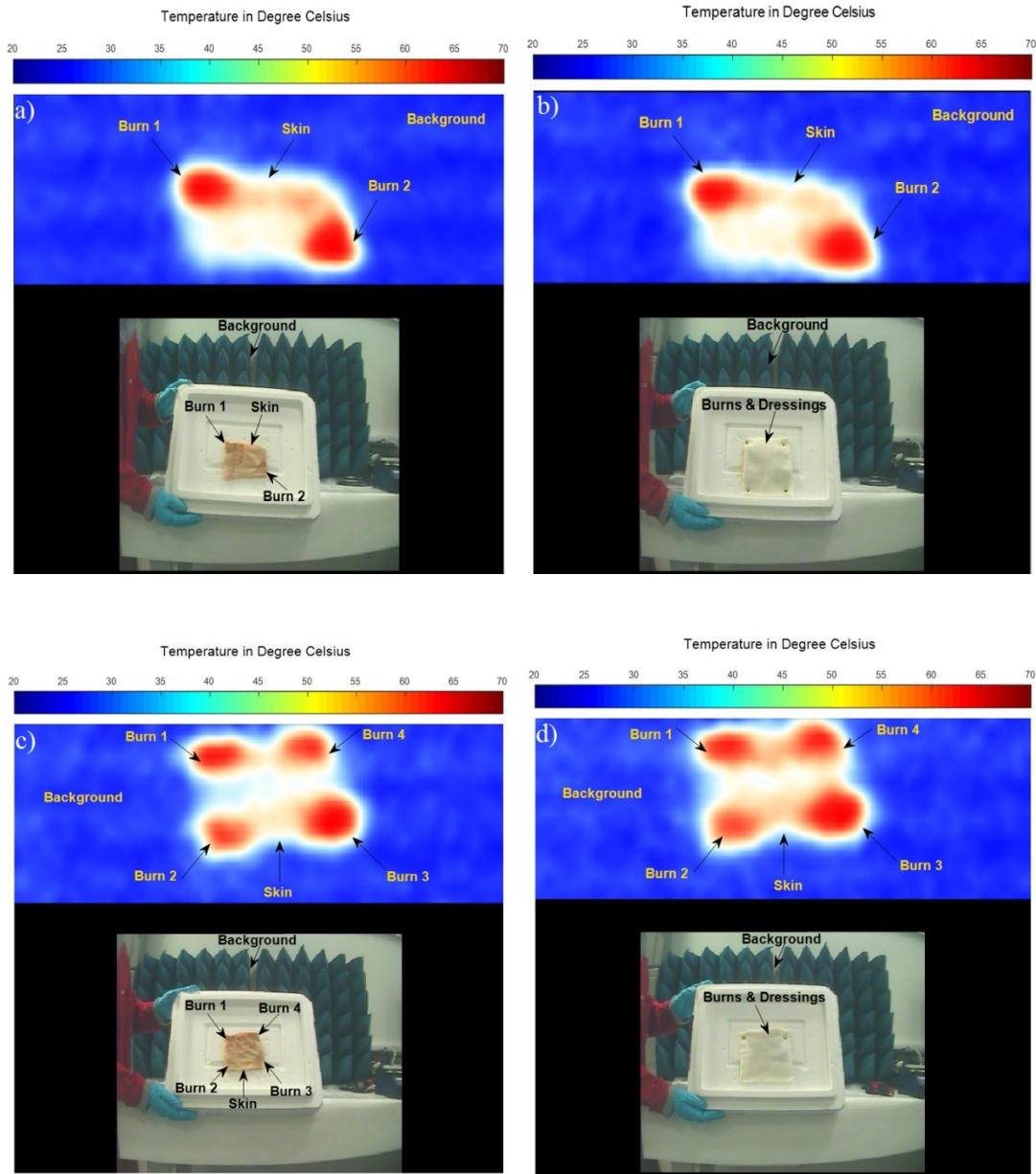


Figure 7.14: MMW images for porcine skin samples at 250 GHz; images in (a) and (c) represent the skin with burns and without dressing materials. Whereas, images in (b) and (d) represent the skin with burns and 10-layer gauze burn dressing materials.

## **7.6 Experiment 3: Burn Wound Diagnostics Using Active**

### **Microwave Scanner**

This experiment aims to assess the feasibility of using the active microwave and MMW scanners to detect burns under dressing materials over the band (15-40) GHz.

#### ***7.6.1 Frequency Band (15-40) GHz***

The active scanner presented in this research is an ideal system for investigating the plane surfaces such as the skin. The scanner effective over the band (15-40) GHz. This band provides wavelengths in the range of 7.5 mm to 20.0 mm and a range resolution of 6.0 mm or less based on the medium. The penetration depth of the radiation over this band is ranging between ~0.7 mm (at 40 GHz) to ~2.0 mm (at 15 GHz) [22]. These characteristics make the active scanner a good candidate to penetrate dressing materials and to detect features of the skin under dressings. The penetration depth of the millimetre wave radiation in the human skin as a function of frequency is illustrated in Figure 2.2 (chapter 2, section 2.4).

#### ***7.6.2 Porcine Skin Samples***

Two fresh porcine skin samples were used for scanning images of the skin with and without the presence of dressing materials and before and after the application of localised heat treatments. The study was approved by the ethics committee of Manchester Metropolitan University (ethics reference no: SE1617114C). A copy of the ethical approval is attached in Appendix B.

### 7.6.3 Experimental Setup

A two-dimensional imaging scanner combined with a Matlab programme was implemented, developed and patented by [208, 244, 245]. The scanner is effective over the band (15-40) GHz and it consists of a VNA that is used to illuminate the sample under test (in this research the skin) with coherent microwave radiation having a transmission power levels less than 1.0 mWatt. The VNA was connected through a high-frequency cable to a K-band horn antenna that is used for transmission and reception purposes (transceiver). The porcine skin sample was placed and aligned on a platform to be scanned. The transceiver horn antenna was moved mechanically to scan an image from the porcine skin sample by using two stepper motors. The motors were controlled via a Matlab programme and the scanner requires ~10 minutes to complete a full scanning cycle from each porcine skin sample. The data (complex scattering parameter  $S_{11}$ ) was obtained directly and saved to be processed later using the SAR algorithm implemented on Matlab by [238]. The front and the bottom view of the active scanner is illustrated in Figure 7.15.

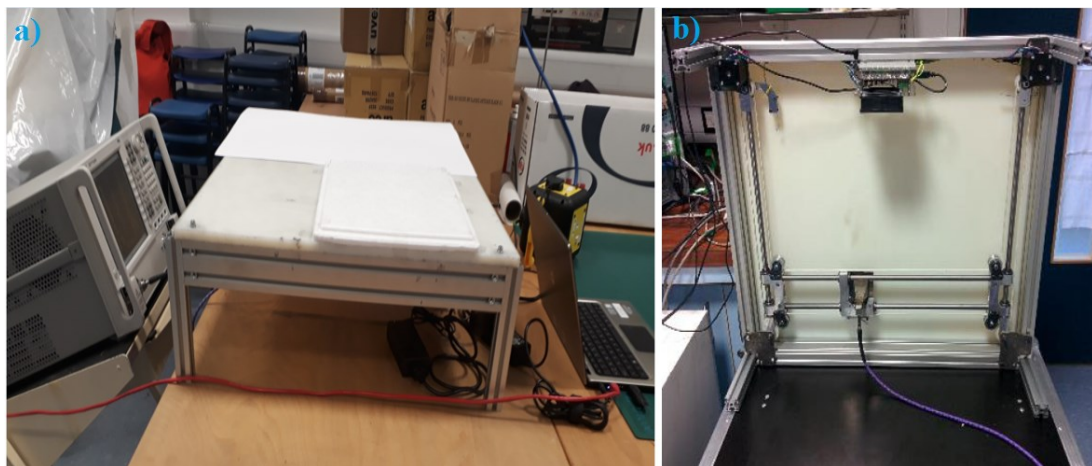


Figure 7.15: The front view of the active microwave scanner (a) and the bottom view of the scanner (b). The scanner has 6.0 mm theoretical range resolution, 25.0 GHz bandwidth, and 256 frequency steps.

#### ***7.6.4 Methodology of Conducting the Measurements***

The complex scattering parameter,  $S_{11}$  for a flat foam background and a flat metal plate was initially measured without locating any skin sample on the scanner as part of a calibration process. These measurements were performed to cancel the internal reflection effect and to deconvolve the antenna response respectively.

A sample of porcine skin was placed and aligned on the platform of the scanner. Initially, images were scanned from the skin without dressing materials. Then a five-layer gauze burn bandage was placed on the skin surface and images were scanned for the skin with dressing materials. After that, a digital hotplate was heated to  $\sim 280$  °C and the middle part of the porcine skin sample was placed in contact with the digital hotplate plate for 3.0 minutes to perform burn. Then the sample with burn was placed and aligned to be scanned. After that, five-layer gauze burn bandage was placed over the skin with burn and images were scanned for the sample with the presence of dressing materials.

### 7.6.5 Data Processing

The following block diagram summarises the methodology of data processing for experiment 3:

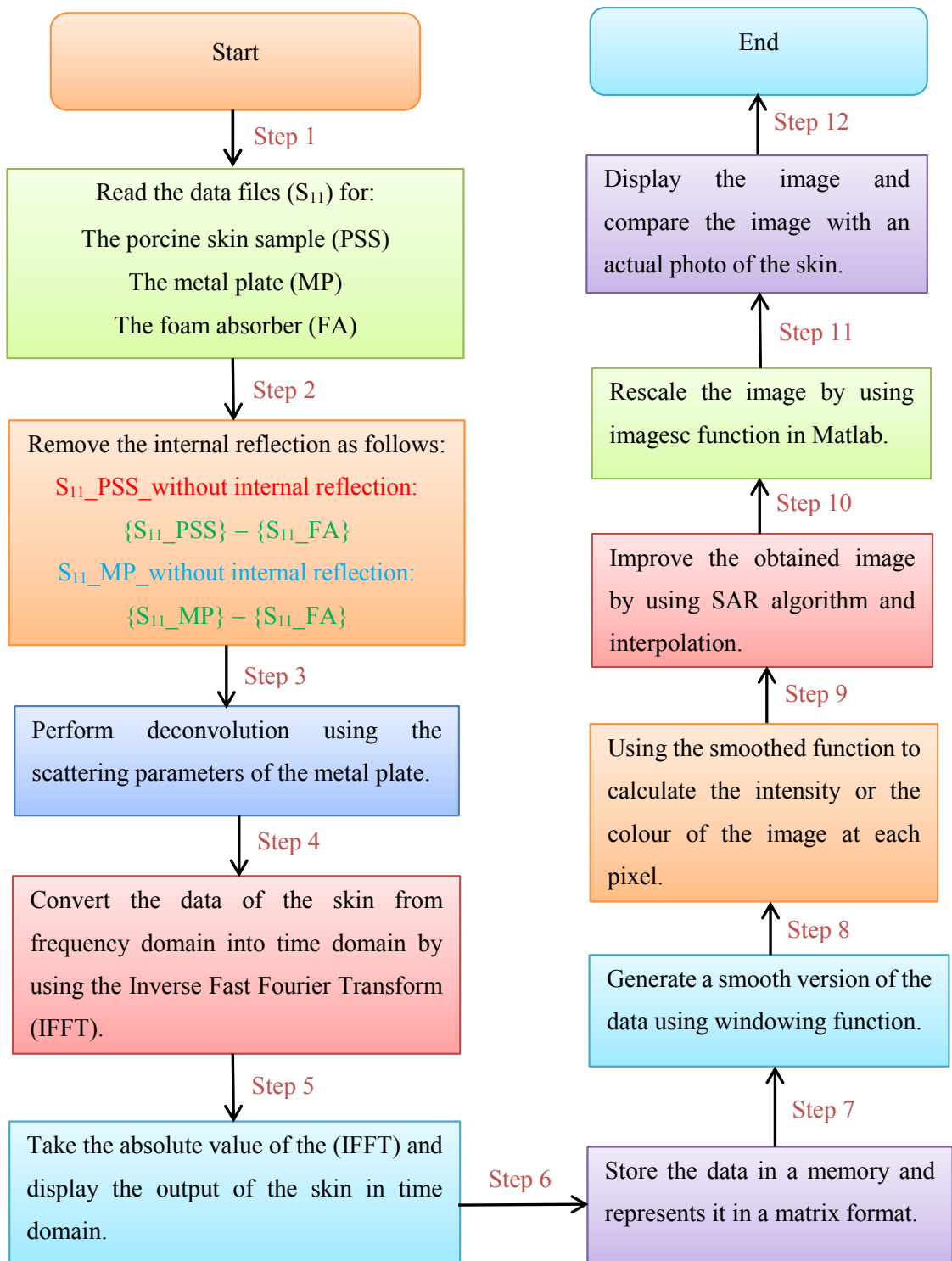


Figure 7.16: A methodology applied to obtain an image from the active scanner [244].

### **7.6.6 Experimental Results**

Images obtained from this experiment (i.e. experiment 3) were divided into four parts:

- Images obtained from the skin without burns and without dressing materials.
- Images obtained from the skin without burns and with dressing materials.
- Images obtained from the skin with burns and without dressing materials.
- Images obtained from the skin with burns and with dressing materials.

#### **7.6.6.1 Skin without Burns**

Experimental images for porcine skin sample (length=90 mm, and width=90 mm) without burns were obtained by using the active microwave scanner and the methodology described in section 7.6.4 and Figure 7.16.

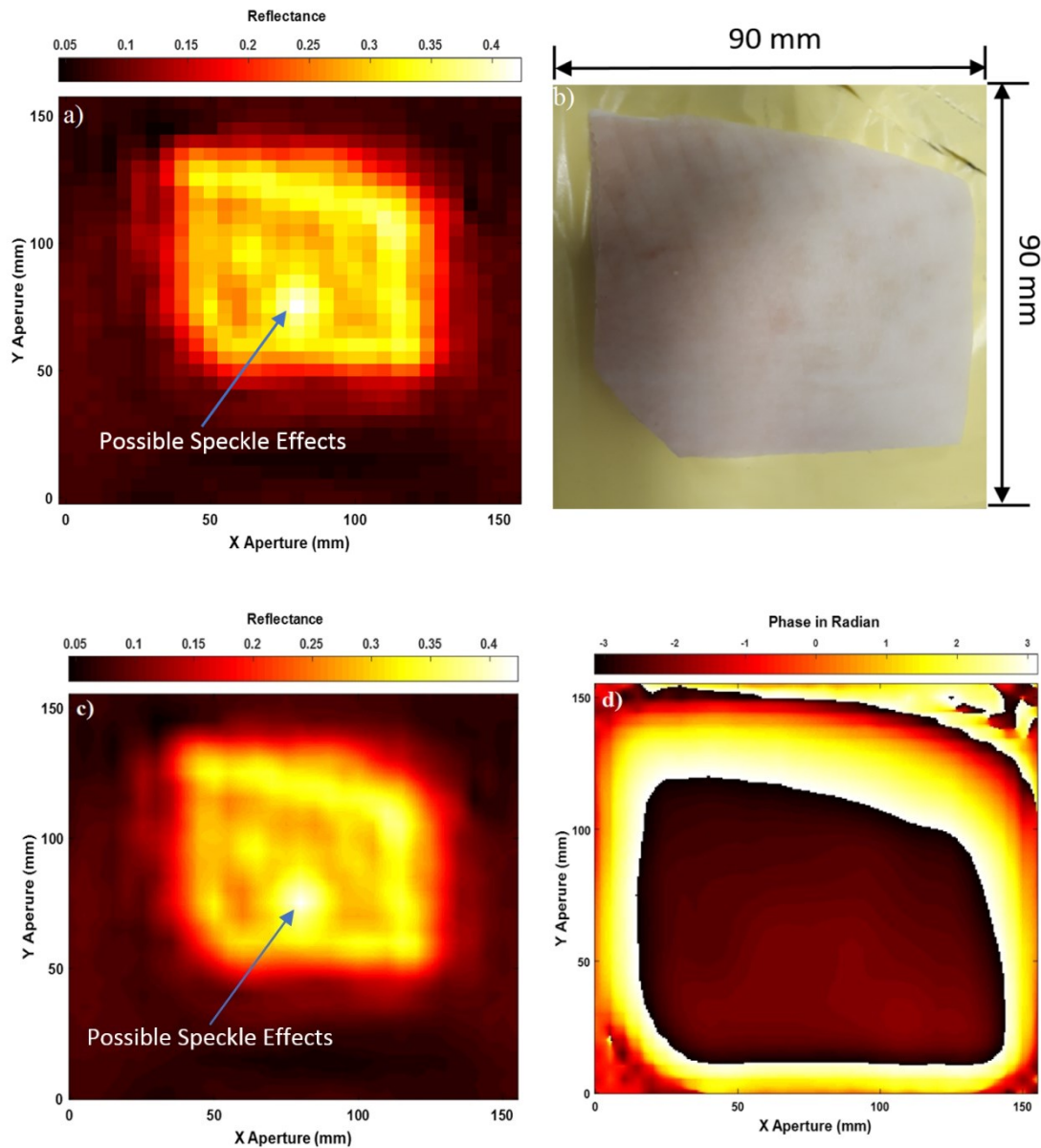


Figure 7.17: Microwave images for unburned skin over the band 15-40 GHz; case (a) represents SAR microwave image 32 x 30 pixels for unburned skin obtained from the amplitude of  $S_{11}$ , (b) represents the sample photo, (c) represents SAR microwave image with interpolation 249 x 233 pixels obtained from the amplitude of  $S_{11}$ , and (d) represents SAR microwave image with interpolation 249 x 233 pixels obtained from the phase of  $S_{11}$ .

Experimental images in Figure 7.17 indicate that active microwave scanner together with SAR algorithm is capable of scanning an image for the skin surface of the porcine skin sample using both amplitude and phase information of the measured scattering parameter  $S_{11}$ . The obtained images from the amplitude measurements in (a) and (c) indicate that interpolation enhances the quality of the images significantly, as features on the skin surface can be seen such as edges, bends, and irregularities in the sample shape. The image obtained from the phase measurements in (d) is not dissimilar from that obtained from the amplitude measurements in (c). The phase image also indicates that the phase is  $\pm\pi$  radian, this is equivalent to  $\pm 180$  degree and this value is an indication of transferring from less condense medium (air) to an optically denser medium (in this case the skin) [67]. These results indicate that the two physical quantities (amplitude and phase) are rich in information.

In an optical system, phase contrast microscopy is a technique for enhancing the contrasts of specimens that are close to transparent. The technique turns the phase shift into intensity so that images become easier to interpret. Therefore, this technique is used to obtain images from in vivo cellular structure [235, 246].

#### ***7.6.6.2 Skin with Dressing Materials***

Experimental images for porcine skin sample (length=90 mm, and width=90 mm) covered with a five-layer gauze burn bandage were obtained by using the active microwave scanner and the methodology described in section 7.6.4 and Figure 7.16.

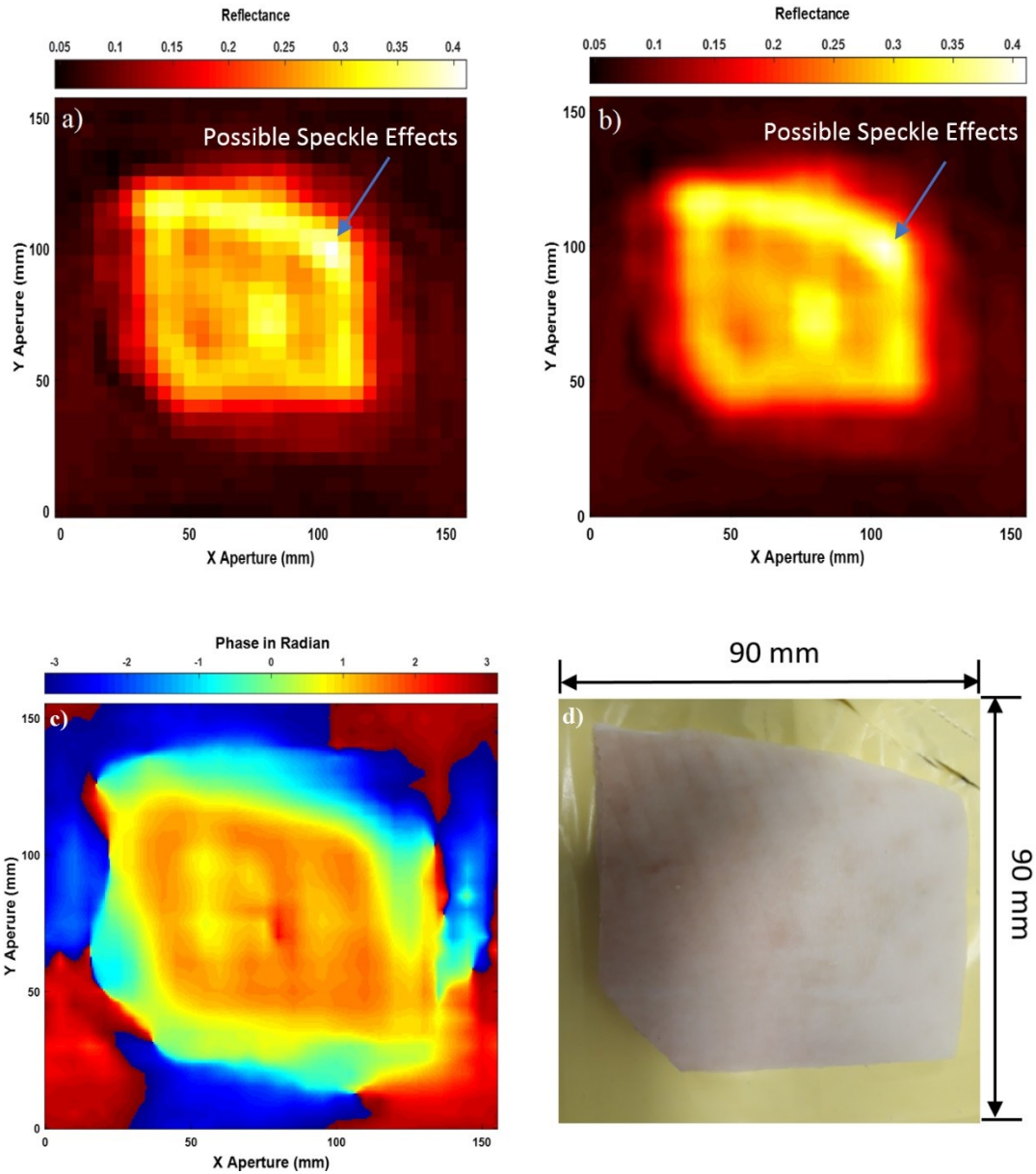


Figure 7.18: Microwave images for the skin with dressing materials over the band 15-40 GHz; case (a) represents SAR microwave image 32 x 30 pixels for the skin with dressings obtained from the amplitude of  $S_{11}$ , (b) represents SAR microwave image with interpolation 249 x 233 pixels obtained from the amplitude of  $S_{11}$ , (c) represents SAR microwave image with interpolation 249 x 233 pixels obtained from the phase of  $S_{11}$ , and (d) represents the skin photo.

Porcine skin images in Figure 7.18 indicate that active microwave radiation is capable of penetrating dressing materials as the skin surface is seen through a five-layer gauze burn bandage in images (a), (b), and (c). This can be observed by comparing the obtained images in (a), (b), and (c) with the photo of the sample before adding the dressing materials in (d). This comparison indicates that dressing materials are completely transparent (transmission in the range of 80% to 99% depending on the thickness of the bandage as discussed in chapter 5) to microwave radiation as the obtained images of the skin with dressing materials show clearly the skin. This indicates that active microwave radiation has a high penetration capability through dressing materials and as a result, this allows the scanner to form high-quality images that show small details in the skin surface of the sample such as edges and irregularities with the presence of dressing materials. The image obtained from the phase measurements in (c) is similar to that obtained from the amplitude measurements in (b).

#### **7.6.6.3 Skin with Burns**

Experimental images for porcine skin sample (length=120 mm, and width=70 mm) with burns were obtained by using the active microwave scanner and the methodology described in section 7.6.4 and Figure 7.16.

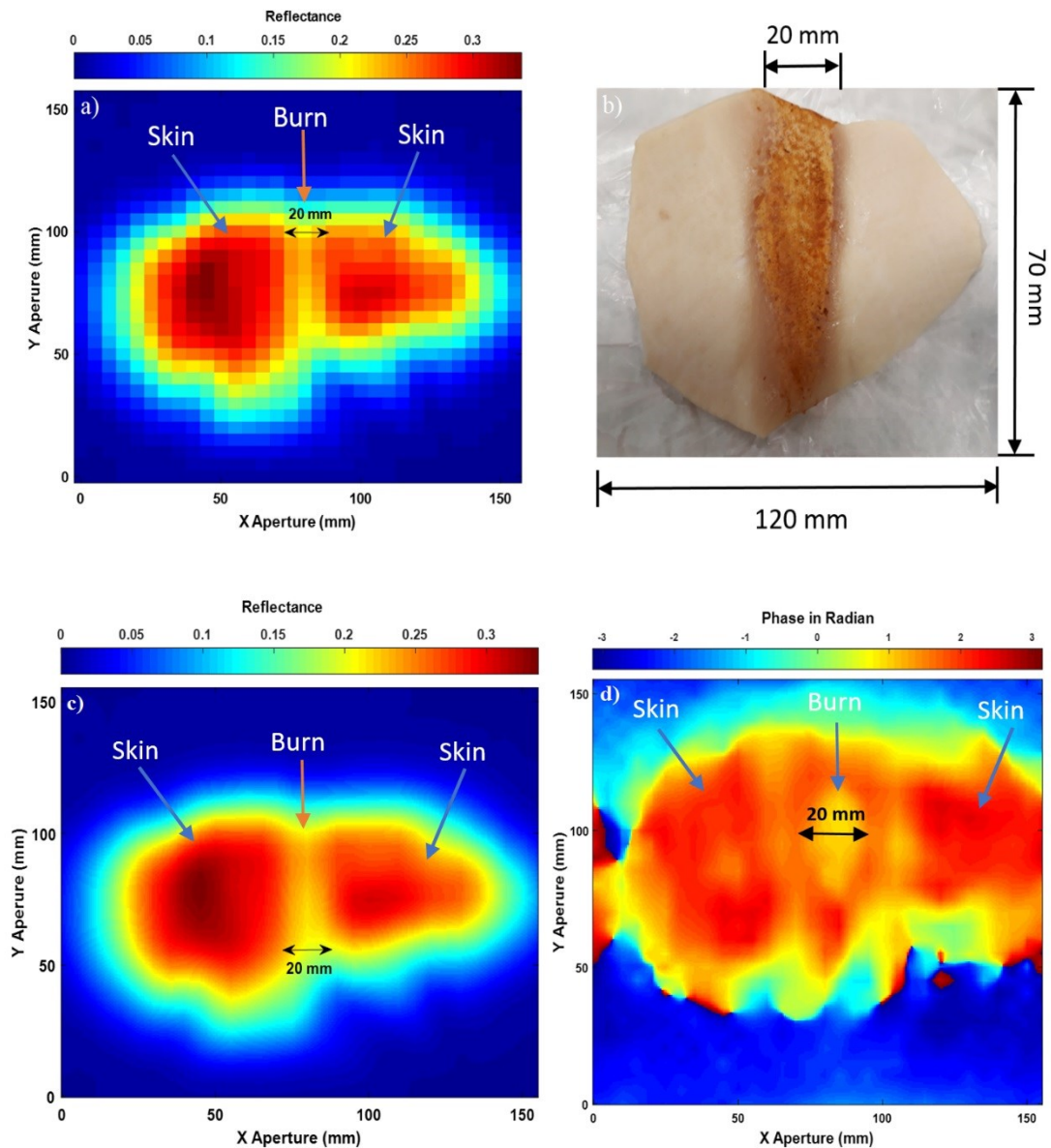


Figure 7.19: Microwave images for burn-damaged skin over the band 15-40 GHz; case (a) represents SAR microwave image 32 x 30 pixels for the skin with burns obtained from the amplitude of  $S_{11}$ , (b) represents the skin with burns photo, (c) represents SAR microwave image with interpolation 249 x 233 pixels for the skin with burns obtained from the amplitude of  $S_{11}$ , and (d) represents SAR microwave image with interpolation 249 x 233 pixels for the skin with burns obtained from the phase of  $S_{11}$ .

Experimental images in Figure 7.19 indicate that active microwave scanner is capable of distinguishing between the skin without burns (red colour) and the burn-damaged skin (yellow colour in the middle region). The mean reflectance of the skin without burns was found to be  $\sim 0.28$ . Whereas, the mean reflectance of the skin with burns was found to be lower by  $\sim 0.08$ . This is due to the burning process that evaporates water from the skin and thereby raising the emissivity of the burn-damaged skin to  $\sim 0.8$ . The scanned images in (a) and (c) show the general shape of the sample and the width of the burn to be  $\sim 20.0$  mm. This value is similar to the measured width of the burn (20.0 mm) that was administered by the localised heat treatment.

The image in Figure 7.19 (d) is obtained from the phase information of the measured scattering parameter  $S_{11}$ . This image looks different compared with the images obtained from the amplitude measurements in (a) and (c), which is perhaps to be expected, as this is measuring a slightly different quantity.

#### ***7.6.6.4 Skin with Burns and Dressing Materials***

Experimental images for porcine skin sample (length=120 mm, and width=70 mm) with burns and a five-layer gauze burn bandage were obtained by using the active microwave scanner and the methodology described in section 7.6.4 and Figure 7.16.

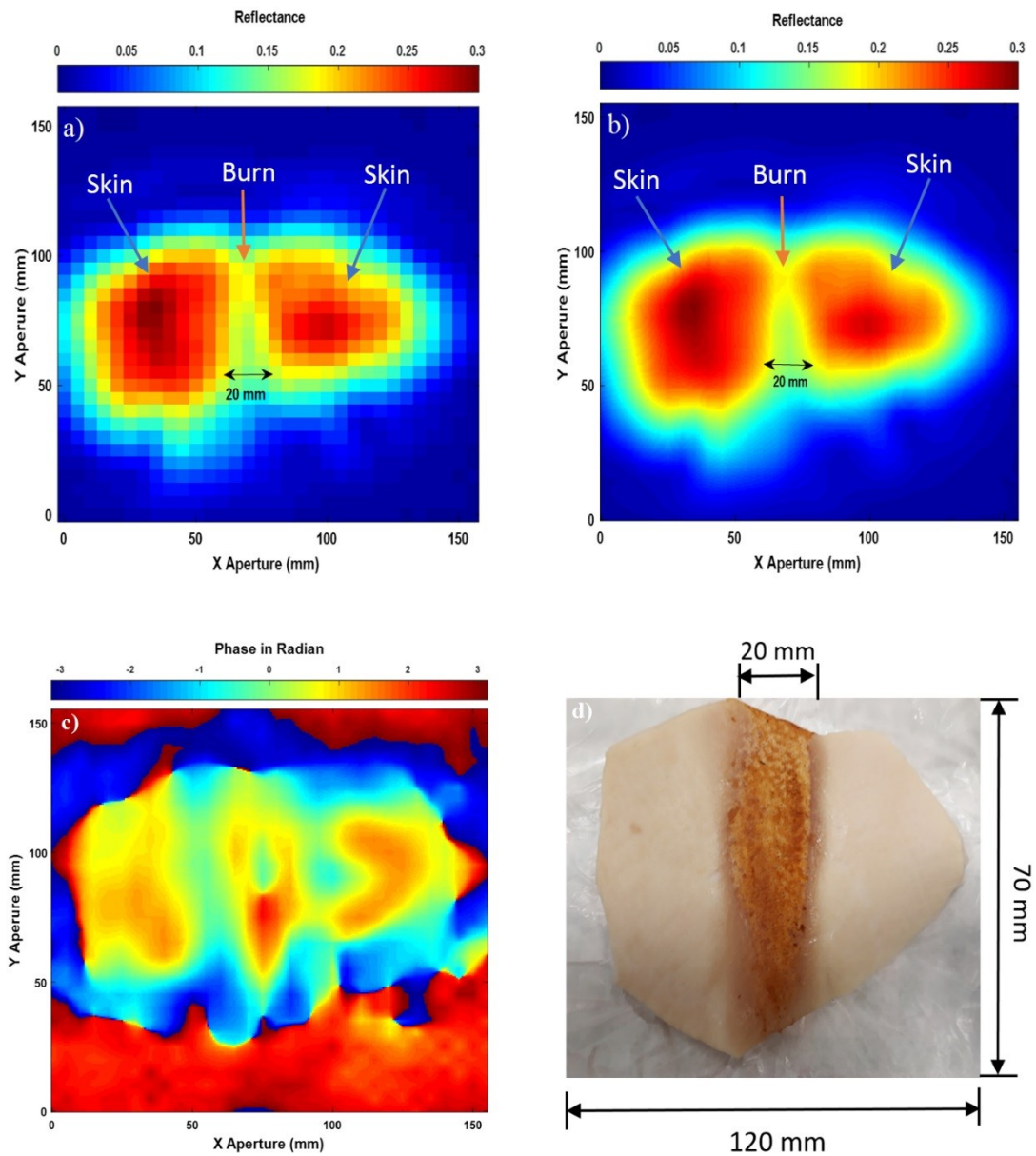


Figure 7.20: Microwave images for the skin with burns and dressing materials over the band 15-40 GHz; case (a) represents SAR microwave image 32 x 30 pixels for the skin with burns and dressings obtained from the amplitude of  $S_{11}$ , (b) represents SAR microwave image with interpolation 249 x 233 pixels obtained from the amplitude of  $S_{11}$ , (c) represents SAR microwave image with interpolation 249 x 233 pixels obtained from the phase of  $S_{11}$ , and (d) represents the skin with burns photo.

Experimental results in Figure 7.20 (a) and (b) indicate that the images obtained from the amplitude measurements of the scattering parameter  $S_{11}$  are capable of detecting burns under a five-layer burn gauze bandage. This is potentially useful as a wound may be monitored without the removal of the protective bandage. The images also provide measurements about the burn width  $\sim 20.0$  mm and they identify clear boundaries and limits between the normal skin and the burn-damaged skin. Furthermore, the images also indicate that adding dressing materials decreases the reflectance of the skin by  $\sim 0.02$ . This can be observed clearly by comparing the reflectance of the images in Figures 7.20 (a) and (b) to that in Figures 7.19 (a) and (c). This is consistent with the fact that dressing materials increase the transmission between the air/skin interface and this increases the emissivity of the skin and as a result decreases the reflectance [3].

Experimental image for burn-damaged skin obtained from the phase measurements in Figure 7.20 (d) is not similar to that obtained from the amplitude measurements in (a) and (b). As amplitude and phase are different physical quantities, it is reasonable to find similarities and differences in the obtained images from those two quantities. The differences in the phase and the amplitude images suggest that there is more information there to be extracted than has already been in this thesis, which could be the subject of future research.

## 7.7 Discussion

The measurements in this chapter present images for the human hands and the porcine skin samples taken from passive and active scanners. The results obtained from these images indicate that it is feasible to detect features of the skin under dressing materials. These features might be burns, water, cream layers, and missing or damaged body parts. These measurements suggest that active and passive microwave and MMW scanners might be efficient tools for monitoring the wound healing progress under dressing materials without the necessity of dressings removal.

The measurements conducted on the palm of the hand skin in normal, wet states, and with cream layers using a 250 GHz ThruVision passive imager indicate that passive images can identify water and cream layers on the human skin with and without the presence of dressing materials, even though the MMW radiation is highly absorbed and attenuated in water [25]. However, measurements confirm that it is possible to form images of the human hand under the cream, water and dressing materials using a passive imaging system. This indicates that the passive imaging system might be used as a non-contact technique for monitoring the wound healing under dressing materials without their painful removal. The technique might be also useful for identifying the signs of infection such as exudates (that consist mainly of water), swelling, and this can be achieved by comparing the image with other images taken at different days (change detection).

Experimental images obtained on the palm of the hand of a male participant using a 250 GHz ThruVision passive imager indicate that the passive imaging system can penetrate dressing materials and provide precise information about different parts of the hand such as the number of fingers and the shape of the parts with the presence of dressing materials. This confirms that passive MMW imaging system is capable of

identifying deformed or missing body parts under dressing materials without the necessity of dressing removal. This capability might allow the system to detect changes on the skin surfaces during the wound healing process.

The measurements conducted on porcine skin samples before and after the application of localised heat treatments with and without the presence of dressing materials indicate that passive imaging system can detect single and multiple burns under dressing materials. The measurements also indicate that the system can distinguish between the unburned skin (white, lower emissivity) and the burn-damaged skin (red, higher emissivity). For in vivo scenarios, it is expected that similar images might be obtained, as there are differences in emissivity values between normal skin and burn-damaged skin [124]. These differences exist in all types of burns and it is expected that these differences are getting significant in serious injuries and burns situations where the removal of dressing materials might be uncomfortable and painful to the patients. These significant differences increase the chance of obtaining good images as the images clearly distinguish between the burn and the unburned skin. It is also expected that the images obtained from a living organism might have different representation based on the degree of the burns and the presence of exudates and infections. As an example of this is the second-degree burn with exudates that is expected to have lower emissivity value compared with unburned skin. In this case, the image will show the normal skin in red colour (higher emissivity) and the burn-damaged skin in white or yellow colour (lower emissivity). However, for the third-degree burn injury it is expected to see the normal skin in white or yellow colour (lower emissivity) and the burn-damaged skin in red colour (higher emissivity).

Images obtained from porcine skin samples using an active microwave scanner operating over the band (15-40) GHz indicate that skin and burns can be detected and observed through dressing materials. The measurements also indicate that there are differences in the reflectance values between unburned and burned damaged skin. This capability means that the active microwave imaging system is feasible for detecting burns and skin conditions.

Images obtained from porcine skin samples using an active microwave scanner indicate that there is useful information in the amplitude and the phase measurements of the scattering parameter  $S_{11}$ .

The measurements in this chapter indicate that the use of both active and passive imaging systems is feasible for detecting features of the skin under dressing materials. An active imaging system has the advantage of higher penetration capabilities that allows assessing the internal structure of the target area of the skin [171]. These capabilities are depending on many factors such as the incident power level, the exposure time limit, the integration time and the noise level. Whereas, the passive imaging system is free from artefacts such as speckle and clutter [201]. The main characteristics of the two imaging systems are summarised as illustrated in Table 7.1.

Key features	Passive imaging system	Active imaging system
Frequency band	232-268 GHz	15-40 GHz
Centre frequency	250 GHz	27.5 GHz
Wavelength	1.2 mm at (250 GHz)	10.9 mm at (27.5 GHz)
Type of radiation	Non-coherent	Coherent
Image is formed based on	Intensity of radiation	Complex Scattering $S_{11}$
Key quantity to measure	Emissivity	Reflectivity
System bandwidth	36.0 GHz	25.0 GHz
Penetration depth	~0.238 mm at 250 GHz	~2.0 mm at 15 GHz
Limitations	A significant contrast in the radiation temperature is required between the burned and the unburned skin to obtain a good image.	Speckle starts to degrade the quality of the images at the resolution limit. The system is sensitive to the alignments.

Table 7.1: Key features and properties of passive and active MMW imaging systems.

## 7.8 Conclusions

In vivo passive images obtained over the band 232 GHz to 268 GHz on the palm of the hand region with and without dressing materials in normal, wet and with cream states indicate that dressing materials are completely transparent (transmission is greater than 80% depending on the thickness of the bandage as discussed and measured in chapter 5) to MMW radiation as thin layer of water, missing part of the hand and shape of the hand are seen through dressing materials.

Passive images obtained on porcine skin samples using the ThruVision imager indicate that single and multiple burns are observed under dressing materials. These results together with the results obtained from the human hand indicate that passive MMW imaging system might be used as a non-contact diagnostic technique for assessing dressed burn wounds as it can detect signs of infection (exudates), burns, disorder, and missing parts under dressing materials.

Active microwave images acquired over the band 15 GHz to 40 GHz on porcine skin samples with and without dressing materials indicate that skin and burns are observed through dressing materials. The images also show that skin with burns has higher reflectance  $\sim 0.05$  compared with that without burns. These results indicate that an active microwave scanner can be used for monitoring the wound healing process under dressing materials.

Experimental images obtained from passive and active imaging systems over different frequency bands demonstrate the potential of the microwave and the MMW radiation for medical applications. Further recommendations and plans for future work will be discussed in the next chapter.

## Chapter 8

### Conclusions and Future Work

*This chapter is a summary of the thesis and plans for future research.*

#### 8.1 Thesis Summary and Conclusions

The research of this thesis is to assess the feasibility of using the microwave and the MMW radiation to detect and assess burn wound under dressing materials. The research falls naturally into five phases for achieving the aim and the objectives of the thesis (discussed in details in chapter 1, section 1.2) and these are detailed below:

- 1) Objective 1: A half space electromagnetic model has been constructed and developed and this has indicated:
  - Simulation results obtained from a half space electromagnetic model indicate differences in emissivity between healthy skin and diseased skin (skin with differing water contents, burn-damaged skin, skin mutated by basal cell carcinoma, dry skin, wet skin, and skin after the application of aqueous gel) are large enough to be measured using active and passive sensors. Such instruments are also capable of making these measurements without making physical contact with the skin. These findings indicate the potential for this band of the electromagnetic spectrum for offering a non-contact method of assessing skin diseases and disorders, which may offer particular benefits in the field of medicine.

2) Objective 2: Single channel radiometers centred at 95 GHz and 90 GHz are calibrated and characterised for measuring the human skin emissivity in vivo. The 95 GHz measurements were of a sample of 30 healthy participants whereas the 90 GHz measurements were of two groups of healthy participants, each consisting of 60 participants. The results are:

- A methodology for measuring the human skin emissivity has been developed and applied. The methodology involves calibrating radiometers and using these to measure radiometric emission, then deriving equations to convert these measurements into emissivities.
- Radiometric measurements show the quantitative variations in the skin emissivity between locations on the arm, gender, individuals, body mass index, different age groups, and ethnicity. The study reveals that these variations are related to the skin thickness, water content, and hydration level of the skin. In general, the lower values of the mean emissivity are a result of measuring particularly thin skin, whereas the higher values of the mean emissivity are results of measuring thick skin.
- Human skin emissivity measurements reveal that there is a signature for the human skin over the MMW band. This finding opens a new window of research in security screening, this being the identification of boundaries and limits for the emissive and reflective properties of different parts of the human body, as a means to anomaly identification.

- 3) Objectives 3: A single channel calibrated radiometer centred at 90 GHz is used to measure the emissivity of 15 fresh porcine skin samples. The measurements were conducted on samples with and without dressing materials and before and after the application of localised heat burns, in which the following outcomes have been achieved:
- Different methodologies have been developed and applied for measuring the emissivity of the porcine skin samples with and without dressing materials and before and after the application of heat treatment.
  - A methodology for measuring the transmission and the attenuation of dressing materials has been developed and applied on different types of dressing materials, having different thicknesses and textiles.
  - Radiometric measurements conducted on porcine skin samples after the application of burns indicate that there is a clear signature of the burn and that it can be detected and observed through dressing materials. The signature indicates that the lower emissivities of burn-damaged skin are indicative of the presence of exudates, infection or a non-healing state of the skin, whereas the higher emissivities are indicative of a dry burn.
  - Experimental results conducted on porcine skin samples indicate that radiometric sensitivity is sufficient to distinguish between different burn depths as the mean emissivity values of the burn-damaged skin are higher after varying doses of localised heat treatment.

4) Objective 4: A vector network analyser has been used to make radar measurements on dressing materials and on a hand support cast. The measurements were conducted on dressing materials having varying moisture contents and various medicinal creams used in the treatments of burns and injuries. The following outcomes have been achieved:

- A development of data processing methodology combined with deconvolution techniques has been introduced and applied on dressing materials samples and the hand support cast. This produced high-quality images with minimum dispersion. These images identify the reflection peaks of the front and the back surface of the samples.
- Radar measurements indicate that MMW radiation penetrates dressing materials samples and can be used to provide information about the propagation path lengths of the samples and the hand support cast, using the distance between two reflection peaks.
- Reflection measurements of dressing material samples coated with a medicinal cream layer and water indicate that it is possible to sense features under the cream and water, as a metal plate could be seen through wet bandage and bandages coated with different types of creams. These signatures suggested that active MMW radar might be an effective tool for monitoring the wound healing process under dressing materials, without their often-painful removal, and without having direct contact with the human body.

5) Objective 5: Experimental images obtained from passive and active scanners have been presented and discussed. The images were obtained from human hands and porcine skin samples in which the following outcomes have been achieved:

- Experimental images obtained from passive and active scanners indicate that it is feasible to detect features of the skin under dressing materials. These features might be burns, water, cream layers, and missing or damaged body parts. These measurements suggest that active and passive microwave and MMW scanners might be used as a non-contact diagnostic technique for assessing dressed burn wounds.
- Images obtained from a passive MMW imager demonstrated measurable changes in emissivity of hands under dressing materials in dry and wet conditions, and also when coated with thin layers of medicinal cream.

The main aim and the objectives of this thesis have been fulfilled through the measurements and the half space electromagnetic model as summarised in Table 8.1:

Thesis objectives	Fulfilled
Develop a model for diagnosing the contrast between natural skin and damaged skin i.e. (skin with burns, skin mutated by basal cell carcinoma, and skin with different water contents).	Chapter 3
Assess the variation in emissivity between individuals and locations on the arm.	Chapter 4
Demonstrate how passive MMW imaging systems can be used for monitoring changes in emissivity under dressing materials.	Chapter 5 and Chapter 7
Determine the feasibility of using active MMW radar systems to penetrate dressing materials and provide information about the propagation path length through dressing materials i.e. (thickness of the dressings).	Chapter 6
Determine the feasibility of sensing and imaging burns under dressing materials using both passive and active imaging systems.	Chapter 5 and Chapter 7

Table 8.1: An overview of the thesis objectives that have been achieved.

## 8.2 Future Work

This thesis has raised a number of key aspects and research ideas that are worthy of further investigation as they have potential for future commercial development with an industrial manufacture and a practitioner as an end-user for medical applications.

Future areas of work are:

- As the half space model identifies the potential of using radiometry as a non-contact technique for non-invasive diagnosis of diseased skin, it is recommended that measurements be made on participants having a range of medical conditions and diseased skin such as eczema, psoriasis, malignancy, and thermal burn. This will demonstrate the potential and the measured signatures of the diseased skin can be compared with the predictions in this thesis. This might be done at a range of frequencies (35 GHz, 60 GHz, 90 GHz, and 120 GHz) the lower frequencies offering greater penetration into the skin and underlying tissue.
- It is recommended that passive and active images are acquired from patients having different degrees of burn injury. These would be analysed to obtain a deeper understanding of the emissivity and the reflectivity of the skin and how these might change between patients and with the severity of the burn injuries. Furthermore, this will allow a comparison to be made between the human skin images and the porcine skin images conducted in this thesis, and this might help in identifying similarities and differences between the human skin and the porcine skin.

- It is recommended that a more sophisticated electromagnetic model of the skin is developed to describe the complex structure of the epidermis and the dermis layers of the skin. This will provide more information about the skin and how different layers of the skin interact with each other in healthy and non-healthy states. This might include using an electromagnetic simulation, structure simulator, and a number of proprietary software products that are currently available.
- It is recommended that further analysis to be made on the active microwave images presented in chapter 7 to determine the level of speckle (an artefact of imaging using a coherent source of radiation). This analysis will help in identifying whether the phase and the amplitude images can provide additional information about the conditions of wounds and skin diseases.

## References

- [1] The Child Accident Prevention Trust, “The costs of burns,” August 2013. [Online]. Available: <http://www.makingthelink.net/tools/costs-child-accidents/costs-burns>. [Accessed 09 July 2018].
- [2] J. R. Sharpe, S. Booth, K. Jubin, N. R. Jordan, D. J. Lawrence-Watt and B. S. Dheansa, “Progression of wound pH during the course of healing in burns,” *Journal of Burn Care & Research*, vol. 34, no. 3, pp. e201-e208, 2013.
- [3] S. W. Harmer, S. Shylo, M. Shah, N. J. Bowring and A. Y. Owda, “On the feasibility of assessing burn wound healing without removal of dressings using radiometric millimetre-wave sensing,” *Progress In Electromagnetics Research M*, vol. 45, pp. 173-183, 2016.
- [4] J. C. Maxwell, A treatise on electricity and magnetism, vol. I, Oxford: Clarendon Press Publisher, 1873.
- [5] J. C. Maxwell, A treatise on electricity and magnetism, vol. II, Oxford: Clarendon Press Publisher, 1873.
- [6] The California State University, “The Electromagnetic Spectrum,” The California State University, 25 January 2018. [Online]. Available: [https://phys.libretexts.org/TextMaps/General\\_Physics\\_TextMaps/Map%3A\\_University\\_Physics\\_\(OpenStax\)/Map%3A\\_University\\_Physics\\_II\\_\(OpenStax\)/16%3A\\_Electromagnetic\\_Waves/16.5%3A\\_The\\_Electromagnetic\\_Spectrum](https://phys.libretexts.org/TextMaps/General_Physics_TextMaps/Map%3A_University_Physics_(OpenStax)/Map%3A_University_Physics_II_(OpenStax)/16%3A_Electromagnetic_Waves/16.5%3A_The_Electromagnetic_Spectrum). [Accessed 01 July 2018].
- [7] R. Appleby, “Passive millimetre-wave imaging and how it differs from terahertz imaging,” *Philosophical Transactions A Mathematical, Physical and Engineering Sciences*, vol. 362, no. 1815, pp. 379-392, 2004.
- [8] S. W. Harmer, N. Bowring, D. Andrews, N. Ddine Rezgui, M. Southgate and S. Smith, “A Review of Nonimaging Stand-Off Concealed Threat Detection with Millimeter-Wave Radar,” *IEEE Microwave Magazine*, vol. 13, no. 1, pp. 160-167, 2012.
- [9] J. Wiltse, “History of millimeter and submillimeter waves,” *Microwave Theory and Techniques, IEEE Transactions*, vol. 32, no. 9, pp. 1118-1127, 1984.
- [10] H. Hertz, *Electric Waves*, 1st ed., London: Macmillan Publisher, 1893.
- [11] P. Lebedew, “Ueber die Dopplbrechung der Strahlen electrischer Kraft,” *Annalen der Physik und Chemie*, vol. 56, no. 9, pp. 1-17, 1895.
- [12] J. C. Bose, On the determination of the wavelength of electric radiation by a diffraction grating, vol. 60, London: Proceedings of the Royal Society, 1897.

- [13] M. Tubiana, "Wilhelm Conrad Röntgen and the discovery of X-rays," *Bulletin Academie Nationale Medicine*, vol. 80, no. 1, pp. 97-108, 1996.
- [14] A. Glagolewa-Arkadiewa, "Short Electromagnetic Waves of Wave-length up to 82 Microns," *Nature*, vol. 113, p. 640, 1924.
- [15] E. F. Nichols and J. D. Tear, "Joining the Infra-Red and Electric Wave Spectra," *Astrophysical Journal*, vol. 61, pp. 17-36, 1923.
- [16] J. P. Rybak, "Nikola Tesla-Scientific Savant," *Popular Electronics*, vol. 16, no. 11, pp. 40-48, 1999.
- [17] T. Maiman, *The Laser Odyssey*, 1st ed., Blaine: The Laser Press Publisher, 2001.
- [18] S. W. Harmer, N. Rezghi, N. Bowring, Z. Luklinska and G. Ren, "Determination of the complex permittivity of textiles and leather in the 14–40 GHz millimetre-wave band using a free-wave transmittance only method," *IET Microwaves, Antennas & Propagation*, vol. 2, no. 6, pp. 606-614, 2008.
- [19] J. W. Lamb, "Miscellaneous data on materials for millimetre and submillimetre optics," *International journal of infrared and millimeter waves*, vol. 17, no. 12, pp. 1997-2034, 1996.
- [20] T. Wang and B. Huang, "Millimeter-wave techniques for 5G mobile communications systems: Challenges, framework and way forward," in *XXXIth URSI General Assembly and Scientific Symposium*, Beijing, 2014.
- [21] P. F. M. Smulders, "Analysis of human skin tissue by millimeter-wave reflectometry," *Skin Research and Technology*, vol. 19, no. 1, pp. e209-e216, 2012.
- [22] T. Wu, T. S. Rappaport and C. M. Collins, "The Human Body and Millimeter-Wave Wireless Communication Systems: Interactions and Implications," in *IEEE International Conference on Communication (ICC)*, London, 2015.
- [23] A. Guraliuc, M. Zhadobov and R. Sauleau, "Dosimetric Aspects Related to the Human Body Exposure to Millimeter Waves," Grant Agreement Number: n°619563, 2014.
- [24] O. P. Gandhi and A. Riazi, "Absorption of millimeter waves by human beings and its biological implications," *Microwave Theory and Techniques, IEEE Transactions*, vol. 34, no. 2, pp. 228-235, 1986.
- [25] M. Zhadobov, N. Chahat, R. Sauleau, C. L. Quement and Y. L. Drean, "Millimeter-wave interactions with the human body: state of knowledge and recent advances," *International Journal of Microwave and Wireless Technologies*, vol. 3, no. 2, pp. 237-247, 2011.
- [26] S. I. Alekseev, A. A. Radzievsky, M. K. Logani and M. C. Ziskin, "Millimeter wave dosimetry of human skin," *Bioelectromagnetics*, vol. 29, no. 1, pp. 65-70, 2008.
- [27] M. Sadiku, *Elements of Electromagnetics*, 4th ed., New York: Oxford University Press Publisher, 2006.

- [28] T. Wu, T. S. Rappaport and C. M. Collins, "Safe for Generations to Come: Considerations of Safety for Millimeter Waves in Wireless Communications," *IEEE Microwave Magazine*, vol. 16, no. 2, pp. 65-84, 2015.
- [29] Z. Xiao, J. Xu and T. Hu , "Research on the Transmissivity of Some Clothing Materials at Millimeter-wave Band," in *2008 International Conference on Microwave and Millimeter Wave Technology*, Nanjing, 2008.
- [30] A. R. Guraliuc, M. Zhadobov, G. Valerio, N. Chahat and R. Sauleau, "Effect of Textile on the Propagation Along the Body at 60 GHz," *IEEE Transactions on Antennas and Propagation*, vol. 62, no. 3, pp. 1489-1494, 2014.
- [31] K. Ali, A. Brizzi, A. Pellegrini, Y. Hao and A. Alomainy , "Investigation of the Effect of Fabric in On-Body Communication Using Finite Difference Time Domain Technique at 60 GHz," in *2012 Loughborough Antennas & Propagation Conference*, Loughborough, 2012.
- [32] F. Gustrau and A. Bahr, "W-band investigation of material parameters, SAR distribution, and thermal response in human tissue," *IEEE Transactions on Microwave Theory and Techniques*, vol. 50, no. 10, pp. 2393-2400, 2002.
- [33] C. M. Alabaster, "The Microwave properties of tissue and other lossy dielectrics," PhD Thesis: Cranfield University, UK, 2004.
- [34] A. Papaioannou and T. Samaras, "Numerical Model of Heat Transfer in the Rabbit Eye Exposed to 60-GHz Millimeter Wave Radiation," *IEEE Transactions on Biomedical Engineering*, vol. 58, no. 9, pp. 2582-2588, 2011.
- [35] A. Karampatzakis and T. Samaras, "Numerical modeling of heat and mass transfer in the human eye under millimeter wave exposure," *Bioelectromagnetics*, vol. 34, no. 4, pp. 291-299, 2013.
- [36] C.-K. Chou, J. D. Andrea and R. Petersen, IEEE Standard for safety levels with respect to human exposure to radio frequency Electromagnetic Fields, 3KHz to 300GHz, USA: Technical Report Published by IEEE Std C 95.1, 2006.
- [37] ICNIRP, "Guidelines for limiting exposure to time-varying electric, magnetic, and electromagnetic fields (up to 300 GHz)," *Health physics*, vol. 74, no. 4, pp. 494-522, 1998.
- [38] Irish Standard EN 50413, "Basic standard on measurement and calculation procedures for human exposure to electric, magnetic and electromagnetic fields (0 Hz – 300 GHz)," Technical Report Published by The National Standard Authority of Ireland (NSAI), Ireland, 2008.
- [39] A. V. Hippel, Dielectric materials and applications, 1st ed., Boston: Artech House Publishers, 1954.
- [40] A. V. Hippel, Dielectrics and Waves, 1st ed., Boston: Artech House Publishers, 1954.

- [41] Rohde & Schwarz, "Measurement of Dielectric Material Properties," Technical Report Published by Rohde & Schwarz, Berlin, 2012.
- [42] O. B. Lubecke, Y. Nikawa, W. Snyder, J. Lin and K. Mizuno , "Novel microwave and millimeter-wave biomedical applications," in *4th International Conference, In Telecommunications in Modern Satellite, Cable and Broadcasting Services*, Yugoslavia, 1999.
- [43] H. Hwang, J. Yim, J. Cho, C. Cheon and Y. Kwon, "110 GHz broadband measurement of permittivity on human epidermis using 1 mm coaxial probe," in *Microwave Symposium Digest, 2003 IEEE MTT-S International*, Philadelphia, 2003.
- [44] N. Chahat, M. Zhadobov, R. Augustine and R. Saulea, "Human skin permittivity models for millimetre-wave range," *Electronics Letters*, vol. 47, no. 7, pp. 427-428, 2011.
- [45] S. I. Alekseev and M. C. Ziskin, "Human skin permittivity determined by millimeter wave reflection measurements," *Bioelectromagnetics*, vol. 28, no. 5, pp. 331-339, 2007.
- [46] C. M. Alabaster, "Permittivity of human skin in millimetre wave band," *Electronics Letters*, vol. 39, no. 21, pp. 1521-1522, 2003.
- [47] H. Zhou, R. M. Narayanan, R. Chandra and I. Balasingham, "Radar for Disease Detection and Monitoring: Detection, Classification, and Assessment," in *Radar for Indoor Monitoring: Detection, Localization and Assessment*, Boca Raton, FL: CRC Press Publisher, 2017, pp. 301-335.
- [48] S. Gabriel, R. W. Lau and C. Gabriel , "The dielectric properties of biological tissues: III. Parametric models for the dielectric spectrum of tissues," *Physics in Medicine & Biology*, vol. 41, no. 11, pp. 2271-2293, 1996.
- [49] K. S. Cole and R. H. Cole, "Dispersion and Absorption in Dielectrics I. Alternating Current Characteristics," *The Journal of Chemical Physics*, vol. 9, no. 4, pp. 341-351, 1941.
- [50] K. S. Cole and R. H. Cole, "Dispersion and Absorption in Dielectrics II. Direct Current Characteristics," *The Journal of Chemical Physics*, vol. 10, no. 2, pp. 98-105, 1942.
- [51] W. D. Hurt, "Multiterm Debye Dispersion Relations for Permittivity of Muscle," *IEEE Transactions on Biomedical Engineering*, vol. 32, no. 1, pp. 60-64, 1985.
- [52] S. Gabriel, R. W. Lau and C. Gabriel , "The dielectric properties of biological tissues: II . Measurements in the frequency range 10 Hz to 20 GHz," *Physics in medicine and biology*, vol. 41, no. 11, pp. 2251-2269, 1996.
- [53] D. K. Ghodgaonkar, O. P. Gandhi and M. F. Iskander, "Complex permittivity of human skin in vivo in the frequency band 26.5-60 GHz," in *Antennas and Propagation Society International Symposium IEEE*, Salt Lake City, 2000.

- [54] S. Kharkovsky, M. T. Ghasr, M. A. Abou-Khousa and R. Zoughi, "Near-field microwave and mm-wave noninvasive diagnosis of human skin," in *IEEE International Workshop on Medical Measurements and Applications*, Cetraro, 2009.
- [55] P. Mehta , K. Chand , D. Narayanswamy , D. G. Beetner, R. Zoughi and W. V. Stoecker, "Microwave Reflectometry as a Novel Diagnostic Tool for Detection of Skin Cancers," *IEEE transactions on instrumentation and measurement*, vol. 55, no. 4, pp. 1309-1316, 2006.
- [56] A. Taeb, S. Gigoyan and S. Safavi-Naeini, "Millimetre-wave waveguide reflectometers for early detection of skin cancer," *IET Microwaves, Antennas & Propagation* , vol. 7, no. 14, pp. 1182-1186, 2013.
- [57] R. Aminzadeh, M. Saviz and A. A. Shishegar, "Dielectric properties estimation of normal and malignant skin tissues at millimeter-wave frequencies using effective medium theory," in *22nd Iranian Conference on Electrical Engineering (ICEE)*, Tehran, 2014.
- [58] E. Pickwell , A. J. Fitzgerald , B. E. Cole , P. F. Taday , R. J. Pye, T. Ha , M. Pepper and V. P. Wallace , "Simulating the response of terahertz radiation to basal cell carcinoma using ex vivo spectroscopy measurements," *Journal of Biomedical Optics*, vol. 10, no. 6, pp. 064021(1-7), 2005.
- [59] E. Pickwell, B. E. Cole, A. J. Fitzgerald, M. Pepper and V. P. Wallace, "In vivo study of human skin using pulsed terahertz radiation," *Physics in Medicine & Biology*, vol. 49, no. 9, pp. 1595-1607, 2004.
- [60] Y. Gao and R. Zoughi, "Millimeter reflectometry as an effective diagnosis tool for skin burn injuries," in *IEEE International Instrumentation and Measurement Technology Conference Proceedings*, Taipei, 2016.
- [61] V. P. Wallace, A. J. Fitzgerald, E. Pickwell, R. J. Pye , P. F. Taday, N. Flanagan and T. Ha, "Terahertz pulsed spectroscopy of human Basal cell carcinoma," *Applied Spectroscopy*, vol. 60, no. 10, pp. 1127-1133, 2006.
- [62] Y. Gao and R. Zoughi, "Millimeter Wave Reflectometry and Imaging for Noninvasive Diagnosis of Skin Burn Injuries," *IEEE Transactions on Instrumentation and Measurement*, vol. 66, no. 1, pp. 77-84, 2017.
- [63] D. Dancila, R. Augustine , F. Töpfer , S. Dudorov, X. Hu , L. Emtestam , L. Tenerz, J. Oberhammer and A. Rydberg, "Millimeter wave silicon micromachined waveguide probe as an aid for skin diagnosis – results of measurements on phantom material with varied water content," *Skin Research and Technology*, vol. 20, no. 1, pp. 116-123, 2014.
- [64] M. Leunig, A. E. Goetz, F. Gamarra, G. Zetterer, K. Messmer and R. K. Jain, "Photodynamic therapy-induced alterations in interstitial fluid pressure, volume

and water content of an amelanotic melanoma in the hamster,” *British journal of cancer*, vol. 69, no. 1, pp. 101-103, 1994.

- [65] R. Siegel and J. Howell, Thermal radiation heat transfer, 4th ed., New York: Taylor & Francis Publisher, 2002.
- [66] M. Fowler and P. Flowers, “Blackbody Radiation Cannot Be Explained Classically,” Chemistry LibreTexts, 23 October 2017. [Online]. Available: [https://chem.libretexts.org/Textbook\\_Maps/Physical\\_and\\_Theoretical\\_Chemistry\\_Textbook\\_Maps/Map%3A\\_Physical\\_Chemistry\\_\(McQuarrie\\_and\\_Simon\)/01%3A\\_A\\_The\\_Dawn\\_of\\_the\\_Quantum\\_Theory/1.1%3A\\_Blackbody\\_Radiation\\_Cannot\\_Be\\_Explained\\_Classically](https://chem.libretexts.org/Textbook_Maps/Physical_and_Theoretical_Chemistry_Textbook_Maps/Map%3A_Physical_Chemistry_(McQuarrie_and_Simon)/01%3A_A_The_Dawn_of_the_Quantum_Theory/1.1%3A_Blackbody_Radiation_Cannot_Be_Explained_Classically). [Accessed 04 July 2018].
- [67] M. Born and E. Wolf, Principles of Optics, 7th ed., Cambridge: Cambridge University Press Publisher, 1999.
- [68] J. C. Weatherall, “Emission from dielectric materials at millimeter wavelengths in passive thermal environments,” in *SPIE Passive Millimeter-Wave Imaging Technology XIII*, Orlando, 2010.
- [69] Z. Zohra and S. W. Lanigan, “Skin: Structure and Function,” in *Dermatology in Clinical Practice*, 1st ed., London, Springer Verlag-London Limited Publisher, 2010, pp. 1-15.
- [70] F. Xu and T. J. Lu, Introduction to Skin Biothermomechanics and Thermal Pain, 1st ed., Berlin: Springer-Verlag Berlin Heidelberg Publisher, 2011.
- [71] Y. Lee and K. Hwang, “Skin thickness of Korean adults,” *Surgical and Radiologic Anatomy*, vol. 24, no. 3-4, pp. 183-189, 2002.
- [72] S. Standring, N. R. Borley, P. Collins, A. R. Crossman and M. A. Gatzoulis, Gray's Anatomy: The Anatomical Basis of Clinical Practice, 40th ed., China: Elsevier Limited Publisher, 2008.
- [73] K. T. Patton and G. A. Thibodeau, Anatomy and Physiology, 8th ed., USA: Elsevier Publisher, 2013.
- [74] F. J. G. Ebling and W. Montagna, “Human skin,” Encyclopædia Britannica, inc., 11 April 2016. [Online]. Available: <https://www.britannica.com/science/human-skin>. [Accessed 20 June 2018].
- [75] S. Knight, Muscle, Bones and Skin, 2nd ed., London: Elsevier Science Limited Publisher, 2003.
- [76] Z. Berzina, “Skin Stories: Charting and Mapping the Skin. Research using analogies of human skin tissue in relation to my textile practice,” PhD Thesis: University of the Arts London, London, 2004.
- [77] N. Y. Z. Chiang and J. Verbov, Dermatology: Handbook for medical students & junior doctors, 2nd ed., UK: British Association of Dermatologists Publisher, 2014.

- [78] C. P. Davis, "Is This Rash Psoriasis?," 15 June 2016. [Online]. Available: [https://www.onhealth.com/content/1/psoriasis\\_rash\\_skin](https://www.onhealth.com/content/1/psoriasis_rash_skin). [Accessed 21 June 2018].
- [79] NHS, "Skin cancer (melanoma)," NHS, 05 May 2017. [Online]. Available: <https://www.nhs.uk/conditions/melanoma-skin-cancer/>. [Accessed 17 August 2018].
- [80] Chicago Burn Injury Attorneys, "Chicago Burn Injury Attorneys Serving Illinois Victims," Chicago Burn Injury Attorneys Serving, January 2018. [Online]. Available: <https://www.rosenfeldinjurylawyers.com/burns.html>. [Accessed 17 August 2018].
- [81] J. Kurk , "The Integumentary System," January 2016. [Online]. Available: <http://slideplayer.com/slide/3478614/>. [Accessed 17 July 2018].
- [82] C. Griffiths , J. Barker, T. Bleiker, R. Chalmers and D. Creamer, Rook's Textbook of Dermatology, 9th ed., Oxford: Wiley-Blackwell Publisher, 2016.
- [83] N. Bajwa, "In vivo terahertz imaging of tissue edema for burn wound and flap assessment," PhD Thesis: University of California, Los Angeles, 2016.
- [84] Z. Seia, L. Musso, S. Palazzini and M. Bertero, "Skin Biopsy Procedures: How and Where to Perform a Proper Biopsy, Skin Biopsy-Perspectives," in *Skin Biopsy*, Shanghai, Intech Publisher, 2011, pp. 1-18.
- [85] R. M. Woodward, V. P. Wallace, B. E. Cole, R. J. Pye, D. D. Arnone, E. H. Linfield and M. Pepper, "Terahertz pulse imaging in reflection geometry of skin tissue using time-domain analysis techniques," in *SPIE Clinical Diagnostic Systems: Technologies and Instrumentation*, San Jose, 2002.
- [86] R. M. Woodward, V. P. Wallace, D. D. Arnone, E. H. Linfield and M. Pepper, "Terahertz Pulsed Imaging of Skin Cancer in the Time and Frequency Domain," *Journal of Biological Physics*, vol. 29, no. 2-3, pp. 257-259, 2003.
- [87] P. Tewari, N. Bajwa, R. S. Singh, M. O. Culjat, W. S. Grundgest, Z. D. Taylor, C. P. Kealey, D. B. Bennett, K. S. Barnett and A. Stojadinovic, "In vivo terahertz imaging of rat skin burns," *Journal of Biomedical Optics*, vol. 17, no. 4, pp. 040503(1-3), 2012.
- [88] Y. Zhao, J. R. Maher, J. Kim, M. A. Selim, H. Levinson and A. Wax, "Evaluation of burn severity in vivo in a mouse model using spectroscopic optical coherence tomography," *Biomedical Optics Express*, vol. 6, no. 9, pp. 3339-3345, 2015.
- [89] S. A. Alawi, M. Kuck, C. Wahrlich, S. Batz, G. McKenzie, J. W. Fluhr, J. Lademann and M. Ulrich, "Optical coherence tomography for presurgical margin assessment of non-melanoma skin cancer – a practical approach," *Experimental Dermatology*, vol. 22, no. 8, pp. 547-551, 2013.
- [90] C. C. Harland, J. C. Bamber, B. A. Gusterson and P. S. Mortimer, "High frequency, high resolution B-scan ultrasound in the assessment of skin tumours," *British Journal of Dermatology*, vol. 128, no. 5, pp. 525-532, 1993.

- [91] B. Partsch, M. Binder, M. Püspök-Schwarz, K. Wolff and H. Pehamberger, "Limitations of high frequency ultrasound in determining the invasiveness of cutaneous malignant melanoma," *Melanoma Research*, vol. 6, no. 5, pp. 395-398, 1996.
- [92] M. I. Liddington and P. G. Shakespeare, "Timing of the thermographic assessment of burns," *Burns*, vol. 22, no. 1, pp. 26-28, 1996.
- [93] Z. D. Taylor, R. S. Singh, D. B. Bennett, P. Tewari, C. P. Kealey, N. Bajwa, M. O. Culjat, A. Stojadinovic, H. Lee, J.-P. Hubschman, E. R. Brown and W. S. Grundfest, "THz Medical Imaging: in vivo Hydration Sensing," *IEEE Transactions on Terahertz Science and Technology*, vol. 1, no. 1, pp. 201-219, 2011.
- [94] B. E. Cole, R. M. Woodward, D. A. Crawley, V. P. Wallace, D. D. Arnone and M. Pepper, "Terahertz imaging and spectroscopy of human skin in vivo," in *SPIE Commercial and Biomedical Applications of Ultrashort Pulse Lasers; Laser Plasma Generation and Diagnostics*, San Jose, 2001.
- [95] S. M. Srinivas, J. F. de Boer, H. Park, K. Keikhanzadeh, H.-e. L. Huang, J. Zhang, W. G. Jung, Z. Chen and J. S. Nelson, "Determination of burn depth by polarization-sensitive optical coherence tomography," *Journal of Biomedical Optics*, vol. 9, no. 1, pp. 207-212, 2004.
- [96] B. H. Park, C. Saxer, S. M. Srinivas, J. S. Nelson and J. F. de Boer, "In vivo burn depth determination by high-speed fiber-based polarization sensitive optical coherence tomography," *Journal of Biomedical Optics*, vol. 6, no. 4, pp. 474-479, 2001.
- [97] K. H. Kim, M. C. Pierce, G. Maguluri, B. H. Park, S. J. Yoon, M. Lydon, R. Sheridan and J. F. de Boer, "In vivo imaging of human burn injuries with polarization-sensitive optical coherence tomography," *Journal of Biomedical Optics*, vol. 17, no. 6, pp. 066012(1-5), 2012.
- [98] A. M. Rollins, M. D. Kulkarni, S. Yazdanfar, R. Ung-arunyawee and J. A. Izatt, "In vivo video rate optical coherence tomography," *Optics Express*, vol. 3, no. 6, pp. 219-229, 1998.
- [99] A. Levine, K. Wang and O. Markowitz, "Optical Coherence Tomography in the Diagnosis of Skin Cancer," *Dermatologic Clinics*, vol. 35, no. 4, pp. 465-488, 2017.
- [100] R. L. Bard, "High-Frequency Ultrasound Examination in the Diagnosis of Skin Cancer," *Dermatologic Clinics*, vol. 35, no. 4, pp. 505-511, 2017.
- [101] M. G. Rippon, K. Springett, R. Walmsley, K. Patrick and S. Millson, "Ultrasound assessment of skin and wound tissue: comparison with histology," *Skin Research and Technology*, vol. 4, no. 3, pp. 147-154, 1998.
- [102] S. C. Gnyawali, K. G. Barki, S. S. Mathew-Steiner, S. Dixith, D. Vanzant, J. Kim, J. L. Dickerson, S. Datta, H. Powell, S. Roy, V. Bergdall and C. K. Sen, "High-

- Resolution Harmonics Ultrasound Imaging for Non-Invasive Characterization of Wound Healing in a Pre-Clinical Swine Model,” *PLoS ONE*, vol. 10, no. 3, pp. 1-19, 2015.
- [103] S. Monstrey, H. Hoeksema, J. Verbelen, A. Pirayesh and P. Blondeel, “Assessment of burn depth and burn wound healing potential,” *Burns*, vol. 34, no. 6, pp. 761-769, 2008.
- [104] M. Dziewonski, “Planimetry of thermograms in diagnosis of burn wounds,” *Scientific Research of the Institute of Mathematics and Computer Science*, vol. 8, no. 1, pp. 33-38, 2009.
- [105] J. Miccio, S. Parikh, X. Marinaro, A. Prasad, S. McClain, A. J. Singer and R. A. F. Clark, “Forward-looking infrared imaging predicts ultimate burn depth in a porcine vertical injury progression model,” *Burns*, vol. 42, no. 2, pp. 397-404, 2016.
- [106] J. Ruminski, M. Kaczmarek, A. Renkielska and A. Nowakowski, “Thermal parametric imaging in the evaluation of skin burn depth,” *IEEE Transactions on Biomedical Engineering*, vol. 54, no. 2, pp. 303-312, 2007.
- [107] H. Essen, J. M. Essen, D. Nuessler, A. Hommes, C. Krebs, N. Fatihi and T. Buzug, “Monitoring of wound healing by millimetre wave imaging,” in *35th International Conference on Infrared, Millimeter, and Terahertz Waves*, Rome, 2010.
- [108] V. P. Wallace, A. J. Fitzgerald, S. Shankar, N. Flanagan, R. Pye, J. Cluff and D. D. Arnone, “Terahertz pulsed imaging of basal cell carcinoma ex vivo and in vivo,” *British Journal of Dermatology*, vol. 151, no. 2, pp. 424-432, 2004.
- [109] M. H. Arbab, D. P. Winebrenner, T. C. Dickey, A. Chen, M. B. Klein and P. D. Mourad, “Terahertz spectroscopy for the assessment of burn injuries in vivo,” *Journal of Biomedical Optics*, vol. 18, no. 7, pp. 077004(1-7), 2013.
- [110] M. H. Arbab, T. C. Dickey, D. P. Winebrenner, A. Chen, M. B. Klein and P. D. Mourad, “Terahertz reflectometry of burn wounds in a rat model,” *Biomedical Optics Express*, vol. 2, no. 8, pp. 2339-2347, 2011.
- [111] N. Bajwa, S. Sung, D. B. Ennis, M. C. Fishbein, B. N. Nowroozi, D. Ruan, A. Maccabi, J. Alger, M. A. S. John, W. S. Grundfest and Z. D. Taylor, “Terahertz Imaging of Cutaneous Edema: Correlation With Magnetic Resonance Imaging in Burn Wounds,” *IEEE Transactions on Biomedical Engineering*, vol. 64, no. 11, pp. 2682-2694, 2017.
- [112] N. Bajwa, B. Nowroozi, J. Garritano, S. Sung, P. Tewari, W. S. Grundfest and Z. Taylor, “An investigation of THz burn wound edema imaging using MRI,” in *39th International Conference on Infrared, Millimeter, and Terahertz waves*, Tucson, 2014.
- [113] D. P. Popescu, L.-P. Choo-Smith, C. Flueraru, Y. Mao, S. Chang, J. Disano, S. Sherif and M. G. Sowa, “Optical coherence tomography: fundamental principles, instrumental designs and biomedical applications,” *Biophysical Reviews*, vol. 3, no. 3, pp. 155-169, 2011.

- [114] G. Lohmann, S. Bohn, K. Müller, R. Trampel and R. Turner, “Image Restoration and Spatial Resolution in 7-Tesla Magnetic Resonance Imaging,” *Magnetic Resonance in Medicine*, vol. 64, no. 1, pp. 15-22, 2010.
- [115] H. J. W. Strutt , “LVIII. On the scattering of light by small particles,” *The London, Edinburgh, and Dublin Philosophical Magazine and Journal of Science*, vol. 41, no. 275, pp. 447-454, 1871.
- [116] J. M. Blackledge, “Scattering Theory,” in *Digital Image Processing Mathematical and Computational Methods*, UK, Woodhead Publishing Series in Electronic and Optical Materials, 2006, pp. 160-197.
- [117] A. Carovac, F. Smajlovic and D. Junuzovic, “Application of Ultrasound in Medicine,” *Acta Informatica Medica*, vol. 19, no. 3, pp. 168-171, 2011.
- [118] H. Alexander and D. L. Miller, “Determining skin thickness with pulsed ultrasound,” *Journal of Investigative Dermatology*, vol. 72, no. 1, pp. 17-19, 1979.
- [119] L. O. Olsen, H. Takiwaki and J. Serup, “High-frequency ultrasound characterization of normal skin. Skin thickness and echographic density of 22 anatomical sites,” *Skin Research and Technology*, vol. 1, no. 2, pp. 74-80, 1995.
- [120] J. A. Brink, P. W. Sheets, K. A. Dines, M. R. Etchison, C. W. Hanke and A. M. Sadove, “Quantitative assessment of burn injury in porcine skin with high-frequency ultrasonic imaging,” *Investigative Radiology*, vol. 21, no. 8, pp. 645-651, 1986.
- [121] S. Iraniha, M. E. Cinat, V. M. VanderKam, A. Boyko, D. Lee, J. Jones and B. M. Achauer, “Determination of Burn Depth With Noncontact Ultrasonography,” *The Journal of Burn Care & Rehabilitation*, vol. 21, no. 4, pp. 333-338, 2000.
- [122] S. Hagness, A. Taflove and J. Bridges, “Three-dimensional FDTD analysis of a pulsed microwave confocal system for breast cancer detection: Design of an antenna-Array element,” *IEEE transactions on antennas and propagations*, vol. 47, no. 5, pp. 783-791, 1999.
- [123] S. Kwon and S. Lee , “Recent Advances in Microwave Imaging for Breast Cancer Detection,” *International Journal of Biomedical Imaging*, vol. 2016, no. 5054912, pp. 1-26, 2016.
- [124] A. Y. Owda, N. Salmon, S. W. Harmer, S. Shylo, N. J. Bowring, N. D. Rezgu and M. Shah, “Millimeter-wave emissivity as a metric for the non-contact diagnosis of human skin conditions,” *Bioelectromagnetics*, vol. 38, no. 7, pp. 559-569, 2017.
- [125] A. Y. Owda, N. Salmon, D. Andrews and N.-D. Rezgui, “Active millimeter-wave radar for sensing and imaging through dressing materials,” in *2017 IEEE SENSORS*, Glasgow, 2017.
- [126] A. Y. Owda, N. Salmon, N.-D. Rezgui and S. Shylo, “Millimetre wave radiometers for medical diagnostics of human skin,” in *2017 IEEE SENSORS*, Glasgow, 2017.

- [127] P. Goldsmith, C.-T. Hsieh, G. Huguenin, J. Kapitzky and E. Moore, "Focal plane imaging systems for millimeter wavelengths," *IEEE Transactions on Microwave Theory and Techniques*, vol. 41, no. 10, pp. 1664-1675, 1993.
- [128] B. Cabane and R. Vuilleumier, "The physics of liquid water," *Elsevier Masson*, vol. 337, no. 1-2, pp. 159-171, 2005.
- [129] F. Grum and R. J. Becherer, *Optical radiation measurements. Volume 1 - radiometry*, New York: Academic Press Publisher, 1979.
- [130] F. T. Ulaby, R. K. Moore and A. K. Fung, *Microwave Remote Sensing: Active and Passive Volume I: Microwave Remote Sensing Fundamentals and Radiometry*, vol. I, London: Artech House Publisher, 1981.
- [131] N. Tamyis, D. K. Ghodgaonkar, M. N. Taib and W. T. Wui, "Dielectric Properties of Human Skin In Vivo in the Frequency Range 20-38 GHz for 42 Healthy Volunteers," in *28th General Assembly of the International Union of Radio Science (URSI)*, New Delhi, 2005.
- [132] S. Sakai, N. Nakagawa, M. Yamanari, A. Miyazawa, Y. Yasuno and M. Matsumoto, "Relationship between dermal birefringence and the skin surface roughness of photoaged human skin," *Journal of Biomedical Optics*, vol. 14, no. 4, pp. 044032 (1-8), 2009.
- [133] C. Gabriel, T. Y. Chan and E. H. Grant, "Admittance models for open ended coaxial probes and their place in dielectric spectroscopy," *Physics in Medicine and Biology*, vol. 39, no. 12, pp. 2183-2200, 1994.
- [134] C. Gabriel and A. Peyman, "Dielectric measurement: error analysis and assessment of uncertainty," *Physics in Medicine and Biology*, vol. 51, no. 23, pp. 6043-6046, 2006.
- [135] K. Sasaki, K. Wake and S. Watanabe, "Development of best fit Cole-Cole parameters for measurement data from biological tissues and organs between 1MHz and 20 GHz," *Radio Science*, vol. 49, no. 7, pp. 459-472, 2014.
- [136] L. Earle, *Dry Skin and Eczema: The best regimes for really effective relief*, 1st ed., London: Hachette Publisher, 2016.
- [137] V. Suntzeff and C. Carruthers, "The water content in the epidermis of mice undergoing carcinogenesis by methylcholanthrene," *Cancer Research*, vol. 6, no. 10, pp. 574-577, 1946.
- [138] W. G. Rees, *Physical Principles of remote sensing*, 3rd ed., New York: Cambridge University Press Publisher, 2013.
- [139] N. A. Salmon, J. R. Borrill and D. G. Gleed, "Absolute temperature stability of passive imaging radiometers," in *SPIE Passive Millimeter-Wave Imaging Technology*, Orlando, 1997.

- [140] D. M. Pozar, *Microwave Engineering*, 4th ed., Hoboken: John Wiley & Sons Publisher, 2011.
- [141] T. M. Brei, "Sure Controls Inc," 6 September 2013. [Online]. Available: <http://www.surecontrols.com/why-calibration-of-your-measuring-instruments-is-important/>. [Accessed 27 March 2018].
- [142] N. Küchler, D. D. Turner , U. Löhnert and S. Crewell, "Calibrating ground-based microwave radiometers: Uncertainty and drifts," *Radio Science*, vol. 51, no. 4, pp. 311-327, 2016.
- [143] G. Maschwitz, U. Löhnert, S. Crewell, T. Rose and D. Turner, "Investigation of ground-based microwave radiometer calibration techniques at 530 hPa," *Atmospheric Measurement Techniques*, vol. 6, no. 10, pp. 2641-2658, 2013.
- [144] D. A. Robertson, D. G. MacFarlane and J. C. G. Lesurf , "Passive subcutaneous body-temperature medical imaging apparatus". United States Patent US7912527B2, 22 March 2011.
- [145] N. A. Salmon, "Outdoor Passive Millimeter-Wave Imaging: Phenomenology and Scene Simulation," *IEEE Transactions on Antennas and Propagation*, vol. 66, no. 2, pp. 897-908, 2018.
- [146] F. Bardati and D. Solimini, "Radiometric sensing of biological layered media," *Radio Science*, vol. 18, no. 6, pp. 1393-1401, 1983.
- [147] C. Wyatt, *Radiometric Calibration: Theory and Methods*, 1st ed., New York: Elsevier Publisher, 1978.
- [148] L. A. Rose, W. E. Asher, S. C. Reising , P. W. Gaiser, K. M. St Germain, D. J. Dowgiallo, K. A. Horgan , G. Farquharson and E. J. Knapp, "Radiometric measurements of the microwave emissivity of foam," *IEEE Transactions on Geoscience and Remote Sensing*, vol. 40, no. 12, pp. 2619-2625, 2002.
- [149] G. Williams, "Microwave emissivity measurements of bubbles and foam," *IEEE Transactions on Geoscience Electronics*, vol. 9, no. 4, pp. 221-224, 1971.
- [150] P. U. Giacomoni, T. Mammone and M. Teri, "Gender-linked differences in human skin," *Journal of Dermatological Science*, vol. 55, no. 3, pp. 144-149, 2009.
- [151] J. Sandby-Møller, T. Poulsen and H. C. Wulf, "Epidermal Thickness at Different Body Sites: Relationship to Age, Gender, Pigmentation, Blood Content, Skin Type and Smoking Habits," *Acta Dermato Venereologica*, vol. 83, no. 6, pp. 410-413, 2003.
- [152] S. Shuster, M. M. Black and E. Mcvitie, "The influence of age and sex on skin thickness, skin collagen and density," *British Journal of Dermatology*, vol. 93, no. 6, pp. 639-643, 1975.
- [153] H. Gray, *Anatomy of the Human Body*, Hiladelphia: Lea & Febiger Publisher, 1981.

- [154] P. F. Millington and R. Wilkinson, *Skin (biological structure and function)*, 1st ed., Cambridge: Cambridge University Press Publisher, 2009.
- [155] J. G. B. Derraik , M. Rademaker, W. S. Cutfield, T. E. Pinto, S. Tregurtha, A. Faherty, J. M. Peart, P. L. Drury and P. L. Hofman, “Effects of Age, Gender, BMI, and Anatomical Site on Skin Thickness in Children and Adults with Diabetes,” *PLoS ONE*, vol. 9, no. 1, pp. 1-6, 2014.
- [156] A. Firooz, B. Sadr, S. Babakoochi, M. Sarraf-Yazdy, F. Fanian, A. Kazerouni-Timsar, M. Nassiri-Kashani, M. M. Naghizadeh and Y. Dowlati, “Variation of biophysical parameters of the skin with age, gender, and body region,” *The Scientific World Journal*, vol. 2012, no. 386936, pp. 1-5, 2012.
- [157] M. Ibrani, L. Ahma and E. Hamiti, “The Age-Dependence of Microwave Dielectric Parameters of Biological Tissues,” in *Microwave Materials Characterization*, London, InTech Publisher, 2012, pp. 140-158.
- [158] K. Robertson and J. L. Rees , “Variation in epidermal morphology in human skin at different body sites as measured by reflectance confocal microscopy,” *Acta Dermato Venereologica*, vol. 90, no. 4, pp. 368-373, 2010.
- [159] N. A. Salmon, L. Kirkham and P. N. Wilkinson, “Characterisation and calibration of a large aperture (1.6 m) ka-band indoor passive millimeter wave,” in *SPIE Millimeter Wave and Terahertz Sensors and Technology V*, Edinburgh, 2012.
- [160] A. S. Jackson, P. R. Stanforth, J. Gagnon, T. Rankinen, A. Leon, D. C. Thirupathi Rao, J. S. Skinner, C. Bouchard and J. H. Wilmore, “The effect of sex, age and race on estimating percentage body fat from body mass index: The Heritage Family Study,” *International Journal of Obesity*, vol. 26, no. 6, pp. 789-796, 2002.
- [161] A. V. Rawlings, “Ethnic skin types: are there differences in skin structure and function?,” *International Journal of Cosmetic Science*, vol. 28, no. 2, pp. 79-93, 2006.
- [162] G. G. Hillebrand, M. J. Levine and K. Shigaki-Miyamoto, “The age dependent changes in skin condition in African Americans, Asian Indians, Caucasians, East Asians and Latinos,” *IFSCC Magazine*, vol. 4, pp. 259-266, 2001.
- [163] K. Sugino, G. Imokawa and H. I. Maibach, “Ethnic difference of varied stratum corneum function in relation to stratum corneum lipids,” *Journal of Dermatological Science*, vol. 6, no. 1, p. 108, 1993.
- [164] S. I. Alekseev, I. Szabo and M. C. Ziskin, “Millimeter wave reflectivity used for measurement of skin hydration with different moisturizers,” *Skin Research and Technology*, vol. 14, no. 4, pp. 390-396, 2008.
- [165] S. Diridollou , V. Vabre , M. Berson , L. Vaillant , D. Black , J. M. Lagarde, J. M. Grégoire , Y. Gall and F. Patat, “Skin ageing: changes of physical properties of human skin in vivo,” *International Journal of Cosmetics Science*, vol. 23, no. 6, pp. 353-362, 2001.

- [166] R. O. Potts , E. M. Buras and D. A. Chrisman , “Changes with age in the moisture content of human skin,” *Journal of Investigative Dermatology*, vol. 82, no. 1, pp. 97-100, 1984.
- [167] N. A. Salmon, “Extended sources near-field processing of experimental aperture synthesis data and application of the Gerchberg method for enhancing radiometric three-dimensional millimetre-wave images in security screening portals,” in *SPIE Europe Security+Defence, Millimetre Wave and Terahertz Sensors and Technology X*, Warsaw, 2017.
- [168] A. Luukanen, R. Appleby , M. Kemp and N. Salmon , “Millimeter-Wave and Terahertz Imaging in Security Applications,” in *Terahertz Spectroscopy and Imaging*, vol. 171, Berlin, Springer Series in Optical Science Publisher, 2012, pp. 491-520.
- [169] E. Abbe, “Beiträge zur Theorie des Mikroskops und der mikroskopischen Wahrnehmung,” *Springer-Verlag*, vol. 9, no. 1, pp. 413-418, 1873.
- [170] E. Abbe, “The Relation of Aperture and Power in the Microscope,” *Journal of the Royal Microscopical Society*, vol. 2, no. 3, pp. 300-309, 1882.
- [171] S. S. Dhillon, M. S. Vitiello, E. H. Linfield, A. G. Davies, M. C. Hoffmann, J. Booske, C. Paoloni, M. Gensch, P. Weightman and G. P. Williams, “The 2017 terahertz science and technology roadmap,” *Journal of Physics D: Applied Physics*, vol. 50, no. 4, pp. 1-49, 2017.
- [172] A. Owda, N.-D. Rezgui and N. Salmon, “Signatures of human skin in the millimeter wave band (80-100) GHz,” in *SPIE Europe Security+Defence, Millimetre Wave and Terahertz Sensors and Technology X*, Warsaw, 2017.
- [173] HM Government, “The United Kingdom’s Strategy for Countering Terrorism,” HM Government, UK, 2018.
- [174] N. Stylianou, I. Buchan and K. W. Dunn, “A review of the international Burn Injury Database (iBID) for England and Wales: descriptive analysis of burn injuries 2003-2011,” *Epidemiology*, vol. 5, no. 2, pp. 1-10, 2014.
- [175] D. M. Jackson, “The Diagnosis of the depth of burning,” *The British Journal of Surgery*, vol. 40, no. 164, pp. 588-596, 1953.
- [176] L. K. Branski, R. Mittermayr, D. N. Herndon, W. B. Norbury, O. E. Masters, M. Hofmann, D. L. Traber, H. Redl and M. G. Jeschke, “A porcine model of full-thickness burn, excision and skin autografting,” *Burns*, vol. 34, no. 8, pp. 1119-1127, 2008.
- [177] W. C. Dewey, “Arrhenius relationships from the molecule and cell to the clinic,” *International Journal of Hyperthermia*, vol. 25, no. 1, pp. 3-20, 2009.
- [178] S. Dhivya, V. V. Padma and E. Santhini, “Wound dressings-a review,” *Biomedicine*, vol. 5, no. 4, pp. 24-28, 2015.
- [179] A. D. Jaskille, J. C. Ramella-Roman, J. W. Shupp, M. H. Jordan and J. C. Jeng, “Critical review of burn depth assessment techniques: part II. Review of laser

- doppler technology,” *Journal of Burn Care & Research*, vol. 31, no. 1, pp. 151-157, 2010.
- [180] Z. Janzekovic , “A new concept in the early excision and immediate grafting of burns,” *Journal of Trauma and Acute Care Surgery*, vol. 10, no. 12, pp. 1103-1108, 1970.
- [181] J. p. Cunha, “MedicineNet.com,” 2016. [Online]. Available: [http://www.medicinenet.com/cuts\\_scrapes\\_and\\_puncture\\_wounds/article.htm](http://www.medicinenet.com/cuts_scrapes_and_puncture_wounds/article.htm). [Accessed 19 August 2018].
- [182] A. D. Jaskille, J. W. Shupp, M. H. Jordan and J. C. Jeng, “Critical Review of Burn Depth Assessment Techniques: Part I. Historical Review,” *Journal of Burn Care & Research*, vol. 30, no. 6, pp. 937-947, 2009.
- [183] D. M. Heimbach, M. A. Afromowitz, L. H. Engrav, J. A. Marvin and B. Perry, “Burn Depth Estimation-Man or Machine,” *Journal of Trauma*, vol. 24, no. 5, pp. 373-378, 1984.
- [184] P. Hlava, J. Moserová and R. Königová , “Validity of clinical assessment of the depth of a thermal injury,” *Acta Chirurgiae Plasticae*, vol. 25, no. 4, pp. 202-208, 1983.
- [185] R. Steiner, K. Kunzi-Rapp and K. Scharffetter-Kochanek, “Optical Coherence Tomography: Clinical Applications in Dermatology,” *Medical Laser Application*, vol. 18, no. 3, pp. 249-259, 2003.
- [186] S. Jiao, W. Yu, G. Stoica and L. V. Wang , “Contrast mechanisms in polarization-sensitive Mueller-matrix optical coherence tomography and application in burn imaging,” *Applied Optics*, vol. 42, no. 25, pp. 5191-5197, 2003.
- [187] M. J. Cobb, Y. Chen, R. A. Underwood, M. L. Usui, J. Olerud and X. Li, “Noninvasive assessment of cutaneous wound healing using ultrahigh-resolution optical coherence tomography,” *Journal of Biomedical Optics*, vol. 11, no. 6, pp. 064002(1-11), 2006.
- [188] M. E. Hackett, “The use of thermography in the assessment of depth of burn and blood supply of flaps, with preliminary reports on its use in Dupuytren's contracture and treatment of varicose ulcers,” *British Journal of Plastic Surgery*, vol. 27, no. 4, pp. 311-317, 1974.
- [189] V. J. Anselmo and B. E. Zawacki, “Effect of evaporative surface cooling on thermographic assessment of burn depth,” *Radiology*, vol. 123, no. 2, pp. 331-332, 1977.
- [190] A. Renkielska, A. Nowakowski, M. Kaczmarek and J. Ruminski, “Burn depths evaluation based on active dynamic IR thermal imaging-a preliminary study,” *Burns*, vol. 32, no. 7, pp. 867-785, 2006.
- [191] A. K. Saxena and G. H. Willital, “Infrared thermography: Experience from a decade of pediatric imaging,” *European Journal of Pediatrics*, vol. 167, no. 7, pp. 757-764, 2008.

- [192] A. M. Kalus, J. Aindow and M. R. Caulfield, "Application of ultrasound in assessing burn depth," *Lancet*, vol. 1, no. 8109, pp. 188-189, 1979.
- [193] P. N. Burns, "The physical principles of Doppler and spectral analysis," *Journal of Clinical Ultrasound*, vol. 15, no. 9, pp. 567-590, 1987.
- [194] K. Waxman, N. Lefcourt and B. Achauer, "Heated laser Doppler flow measurements to determine depth of burn injury," *The American Journal of Surgery*, vol. 157, no. 6, pp. 541-543, 1989.
- [195] C. J. Andrews, M. Kempf, R. Kimble and L. Cuttle, "Development of a Consistent and Reproducible Porcine Scald Burn Model," *PLoS ONE*, vol. 11, no. 9, pp. 1-18, 2016.
- [196] W. Meyer, R. Schwarz and K. Neurand, "The skin of domestic mammals as a model for the human skin, with special reference to the domestic pig," *Current Problems in Dermatology*, vol. 7, pp. 39-52, 1978.
- [197] M. W. Dewhirst, B. L. Viglianti, M. Lora-Michiels, P. J. Hoopes and M. Hanson, "Thermal dose requirement for tissue effect: experimental and clinical findings," in *SPIE Thermal Treatment of Tissue: Energy Delivery and Assessment II*, San Jose, 2003.
- [198] G. M. Gray, R. J. White, R. H. Williams and H. J. Yardley, "Lipid composition of the superficial stratum corneum cells of pig epidermis," *British Journal of Dermatology*, vol. 106, no. 1, pp. 59-63, 1982.
- [199] F. Bardati, V. Brown, M. Ross and P. Tognolatti, "Microwave radiometry for medical thermal imaging: theory and experiment," in *IEEE MTT-S International In Microwave Symposium Digest*, Albuquerque, 1992.
- [200] C. J. Andrews, L. Cuttle and M. J. Simpson, "Quantifying the role of burn temperature, burn duration and skin thickness in an in vivo animal skin model of heat conduction," *International Journal of Heat and Mass Transfer*, vol. 101, pp. 542-549, 2016.
- [201] A. Y. Owda, N. Salmon and N.-D. Rezgui, "Electromagnetic Signatures of Human Skin in the Millimeter Wave Band 80–100 GHz," *Progress In Electromagnetics Research B*, vol. 80, pp. 79-99, 2018.
- [202] T. Log, "Modeling Burns for Pre-Cooled Skin Flame Exposure," *International Journal of Environmental Research and Public Health*, vol. 14, no. 9, pp. 1-13, 2017.
- [203] T. Karacolak, R. Cooper, E. S. Ünlü and E. Topsakal, "Dielectric Properties of Porcine Skin Tissue and In Vivo Testing of Implantable Antennas Using Pigs as Model Animals," *IEEE Antennas and Wireless Propagation Letters*, vol. 11, pp. 1686-1689, 2012.
- [204] S. P. Kingsley and S. Quegan, *Understanding radar systems*, vol. 2, USA: SciTech Publisher, 1999.

- [205] M. Skolnik, Radar handbook, 3rd ed., New York: McGraw Hill Publisher, 2008.
- [206] S. Harmer, D. Andrews, N. Bowring, N. Rezgui and M. Southgate, "Ultra wide band detection of on body concealed weapons using the out of plane polarized late time response," in *SPIE Millimetre Wave and Terahertz Sensors and Technology II*, Berlin, 2009.
- [207] N. J. Bowring, D. O'Reilly, N. A. Salmon, D. A. Andrews, N.-D. Rezgui and S. W. Harmer, "A feasibility study into the screening and imaging of hand luggage for threat items at 35 GHz using an active large aperture (1.6 m) security screening imager," in *SPIE Millimetre Wave and Terahertz Sensors and Technology VI*, Dresden, 2013.
- [208] N. D. Rezgui, N. J. Bowring, D. A. Andrews, S. W. Harmer, M. J. Southgate and D. O'Reilly, "Development of an ultra wide band microwave radar based footwear scanning system," in *SPIE Millimetre Wave and Terahertz Sensors and Technology VI*, Dresden, 2013.
- [209] N. J. Bowring, M. J. Southgate, D. A. Andrews, N. D. Rezgui, S. W. Harmer and D. O'Reilly, "Development of a longer range standoff millimetre wave radar concealed threat detector," in *SPIE Radar Sensor Technology XVII*, Baltimore, 2013.
- [210] E. Blackhurst, N. Salmon and M. Southgate, "Full Polarimetric Millimetre Wave Radar for Stand-off Security Screening," in *SPIE Europe Security+Defence, Millimetre Wave and Terahertz Sensors and Technology X*, Warsaw, 2017.
- [211] M. Klemm, J. A. Leendertz, D. Gibbins, I. J. Craddock, A. Preece and R. Benjamin, "Microwave Radar-Based Differential Breast Cancer Imaging: Imaging in Homogeneous Breast Phantoms and Low Contrast Scenarios," *IEEE Transactions on Antennas and Propagation*, vol. 58, no. 7, pp. 2337-2344, 2010.
- [212] S. Pisa, E. Pittella and E. Piuizzi, "A Survey of Radar Systems for Medical Applications," *IEEE Aerospace and Electronic Systems Magazine*, vol. 31, no. 11, pp. 64-81, 2016.
- [213] E. M. Staderini, "UWB radars in medicine," *IEEE Aerospace and Electronic Systems Magazine*, vol. 17, no. 1, pp. 13-18, 2002.
- [214] A. Vorobyov , E. Daskalaki , C. Hennemann and J.-D. Decotignie, "Human physical condition RF sensing at THz range," in *38th Annual International Conference of the IEEE Engineering in Medicine and Biology Society (EMBC)*, Orlando, 2016.
- [215] Y. Feldman, A. Puzenko, P. Ben Ishai, A. Caduff and A. J. Agranat, "Human Skin as Arrays of Helical Antennas in the Millimeter and Submillimeter Wave Range," *Physical Review Letters*, vol. 100, no. 12, pp. 128102(1-4), 2008.
- [216] Y. Feldman, A. Puzenko, P. Ben Ishai, A. Caduff, I. Davidovich, F. Sakran and A. J. Agranat, "The electromagnetic response of human skin in the millimetre and

submillimetre wave range,” *Physics in Medicine & Biology*, vol. 54, no. 11, pp. 3341-3363, 2009.

- [217] M. Persson, A. Fhager, H. D. Trefná, Y. Yu, T. McKelvey, G. Pegenius, J.-E. Karlsson and M. Elam, “Microwave-Based Stroke Diagnosis Making Global Prehospital Thrombolytic Treatment Possible,” *IEEE Transactions on Biomedical Engineering*, vol. 61, no. 11, pp. 2806-2817, 2014.
- [218] M. I. Skolnik, Introduction to radar systems, 3rd ed., Singapore: McGraw Hill Publisher, 2001.
- [219] C. Wolff, “Radar basics,” radartutorial, 20 December 2009. [Online]. Available: <http://www.radartutorial.eu/02.basics/Pulse%20Radar.en.html>. [Accessed 15 August 2018].
- [220] Keysight Technologies, “PNA microwave network analyzers,” Technical Report Published by Keysight Technologies, USA, 2017.
- [221] B. P. Lathi and Z. Ding, Modern Digital and Analog Communication Systems, 4th ed., USA: Oxford University Press Publisher, 2009.
- [222] S. W. Harmer, N. Bowring, N.-D. Rezgui and D. Andrews, “A comparison of ultra wide band conventional and direct detection radar for concealed human carried explosives detection,” *Progress In Electromagnetics Research*, vol. 39, pp. 37-47, 2013.
- [223] N. Bowring, J. G. Baker, N.-D. Rezgui, M. Southgate and J. F. Alder, “Active millimeter wave detection of concealed layers of dielectric material,” in *SPIE Optics and Photonics in Global Homeland Security III*, Orlando, 2007.
- [224] R. Anderton, “Design of manufacturing concepts for a real time passive millimetre wave imager,” Technical Report Published by University of Reading, UK, 1999.
- [225] Y. Luxin, Z. Tianxu, Z. Sheng, H. Jian and Z. Jianmao , “Study on multichannel passive millimeter-wave radiometer imaging and superresolution,” *International Journal of Infrared and Millimeter Waves*, vol. 27, no. 10, pp. 1403-1414, 2006.
- [226] E. Hecht, Optics, 4th ed., San Francisco: Addison Wesley Publisher, 2002.
- [227] M. Bass, C. DeCusatis, J. Enoch, V. Lakshminarayanan, G. Li, C. Macdonald, V. Mahajan and E. V. Stryland, Handbook of Optics Volume I : Geometrical and Physical Optics, Polarized Light, Components and Instruments, 3rd ed., New York: McGraw-Hill Publisher, 2010.
- [228] Edmund Optics, “Understanding Focal Length and Field of View,” Edmund Optics Ltd, 2018. [Online]. Available: <https://www.edmundoptics.eu/resources/application-notes/imaging/understanding-focal-length-and-field-of-view/>. [Accessed 09 June 2018].
- [229] D. Carr, “Angle of View Vs. Field of View. Is There a Difference and Does it Even Matter?,” Shutter Muse, 5 June 2017. [Online]. Available:

<https://shuttermuse.com/angle-of-view-vs-field-of-view-fov-aov/>. [Accessed 09 June 2018].

- [230] Y. Rahmat-Samii, L. I. Williams and R. G. Yaccarino, "The UCLA bi-polar planar-near-field antenna-measurement and diagnostics range," *IEEE Antennas and Propagation Magazine*, vol. 37, no. 6, pp. 16-35, 1995.
- [231] C. A. Balanis, *Antenna theory analysis and design*, 3rd ed., Hoboken: John Wiley & Sons Publisher, 2005.
- [232] L. Rayleigh, "Investigations in optics, with special reference to the spectroscope," *The London, Edinburgh, and Dublin Philosophical Magazine and Journal of Science*, vol. 8, no. 49, pp. 261-274, 1879.
- [233] L. Rayleigh, "On the Theory of Optical Images, with special reference to the Microscope," *Journal of the Royal Microscopical Society*, vol. 23, no. 4, pp. 474-482, 1903.
- [234] E. Sezgin, "Super-resolution optical microscopy for studying membrane structure and dynamics," *Journal of Physics: Condensed Matter*, vol. 29, no. 27, pp. 1-14, 2017.
- [235] S. G. Lipson, H. Lipson and D. S. Tannhauser, *Optical Physics*, 3rd ed., Cambridge: Cambridge University Press Publisher, 1995.
- [236] C. Cremer and B. R. Masters, "Resolution enhancement techniques in microscopy," *The European Physical Journal H*, vol. 38, no. 3, pp. 281-344, 2013.
- [237] G. W. Stimson, *Introduction to Airborne RADAR*, 2nd ed., USA: SciTech Publisher, 1998.
- [238] D. M. Sheen, D. L. McMakin and T. E. Hall, "Three-dimensional millimeter-wave imaging for concealed weapon detection," *IEEE Transactions on Microwave Theory and Techniques*, vol. 49, no. 9, pp. 1581-1592, 2001.
- [239] D. Sheen, D. McMakin and T. Hall, "Near-field three-dimensional radar imaging techniques and applications," *Applied Optics*, vol. 49, no. 19, pp. E83-E93, 2010.
- [240] D. E. Barrick, "Radar clutter in an air defense system: part 1 clutter physics," Technical Report Published by Battelle Memorial Institute, Ohio, 1968.
- [241] Doxygen, "Anomaly Detection and Removal," 17 September 2015. [Online]. Available: <http://baltrad.fmi.fi/software/rack/doc/rack/html/andrepag.html>. [Accessed 10 June 2018].
- [242] J. S. Lee, L. Jurkevich, P. Dewaele, P. Wambacq and A. Oosterlinck, "Speckle filtering of synthetic aperture radar images: A review," *Remote Sensing Reviews*, vol. 8, no. 4, pp. 313-340, 1994.
- [243] Digital Barriers , "SafeSearch (ThruVision and ThruViewer)," User Manual Published by Digital Barriers Company , UK, 2014.

- [244] N. D. Rezgui, N. Bowring, D. Andrews, S. Harmer , M. J. Southgate and D. O'Reilly, "Scanning Apparatus". United States Patent US 2015/0369756 A1, 24 December 2015.
- [245] N.-D. Rezgui, D. A. Andrews and N. Bowring, "Ultra-wide-band 3D microwave imaging scanner for the detection of concealed weapons," in *SPIE Millimetre Wave and Terahertz Sensors and Technology VIII*, Toulouse, 2015.
- [246] D. B. Murphy, R. Oldfield, S. Schwartz and M. W. Davidson, "Introduction to Phase Contrast Microscopy," Nikon Instruments Inc, 2018. [Online]. Available: <https://www.microscopyu.com/techniques/phase-contrast/introduction-to-phase-contrast-microscopy>. [Accessed 12 June 2018].

# Appendix A: Ethical Approval for Human Skin Emissivity

## Measurements

### A.1 Copy of the Approved Ethics Checklist

#### ETHICS CHECKLIST

This checklist must be completed **before** commencement of **any** research project. This includes projects undertaken by **staff and by students as part of a UG, PGT or PGR programme**. Please attach a Risk Assessment.



Please also refer to the [University's Academic Ethics Procedures](#) and the [University's Guidelines on Good Research Practice](#)

<b>Full name and title of applicant:</b>	Mrs. Amani Yousef Issa Owda	
<b>University Telephone Number:</b>	07 402 939 756	
<b>University Email address:</b>	Amani.Owda@stu.mmu.ac.uk	
<b>Status: (delete as appropriate)</b>	Postgraduate Research Student: Ph.D.	
<b>Department/School/Other Unit:</b>	School of Engineering	
<b>Programme of study (if applicable):</b>	Ph.D.	
<b>Name of DoS/Supervisor/Line manager:</b>	DoS: Dr. Neil Salmon, Second Supervisor: Prof. Nicholas Bowring	
<b>Project Title:</b>	Medical Applications of Microwave and Millimetre-Wave Imaging	
<b>Start &amp; End date of project:</b>	Start date: 1/10/2015-End date: 1/10/2018	
<b>Number of participants (if applicable):</b>	<b>Initial Sample Size: 30 Healthy Participants</b>	
<b>Funding Source:</b>	Internal Ph.D. Studentship	
<b>Brief description of research project activities (300 words max):</b>		
<p>The research activities of this project presented as follows:</p> <ul style="list-style-type: none"> <li>• Stage 1: Passive millimetre-wave imager to be implemented and tested in the lab.</li> <li>• Stage 2: Measurements of human skin in vivo can be taken using the passive imager and calibrated radiometers. The measurements could be either emissivity or reflectivity for forearm, wrist and palm of hand skin or an image of the hand. The measurements will be performed on healthy participants.</li> <li>• Stage 3: Active Millimetre-Wave Imaging system to be implemented and tested in the lab.</li> <li>• Stage 4: Test the capability of the Passive and Active-Millimetre-Wave Imaging system to form an image of the skin under bandages. At this stage, we are aiming to test the capability of Millimetre Wave to penetrate the dielectric material and to look at differences between dry and normal skin. The measurements will be done on at least one of the supervision team and other staff members at the university.</li> </ul>		
<b>Does the project involve NHS patients or resources?</b>		<b>NO</b>
<p>If 'yes' please note that your project may need NHS National Research Ethics Service (NRES) approval. Be aware that research carried out in a NHS trust also requires governance approval.</p> <p>Click <a href="#">here</a> to find out if your research requires NRES approval</p> <p>Click <a href="#">here</a> to visit the National Research Ethics Service website</p> <p>To find out more about Governance Approval in the NHS click <a href="#">here</a></p>		
<b>Does the project require NRES approval?</b>		<b>NO</b>
<p>If yes, has approval been granted by NRES?</p> <p>Attach copy of letter of approval. Approval cannot be granted without a copy of the letter.</p>		

<b>NB Question 2 should only be answered if you have answered YES to Question 1. All other questions are mandatory.</b>	<b>YES</b>	<b>NO</b>
1. Are you are gathering data from people?	<input checked="" type="checkbox"/>	<input type="checkbox"/>
For information on why you need informed consent from your participants please click <a href="#">here</a>		
2. If you are gathering data from people, have you:		
a. attached a participant information sheet explaining your approach to their involvement in your research and maintaining confidentiality of their data?	<input checked="" type="checkbox"/>	<input type="checkbox"/>
b. attached a consent form? (not required for questionnaires)	<input checked="" type="checkbox"/>	<input type="checkbox"/>
Click here to see an example of a <a href="#">participant information sheet</a> and <a href="#">consent form</a>		
3. Are you gathering data from secondary sources such as websites, archive material, and research datasets?	<input checked="" type="checkbox"/>	<input type="checkbox"/>
Click <a href="#">here</a> to find out what ethical issues may exist with secondary data		
4. Have you read the <a href="#">guidance</a> on data protection issues?	<input checked="" type="checkbox"/>	<input type="checkbox"/>
a. Have you considered and addressed data protection issues – relating to storing and disposing of data?	<input checked="" type="checkbox"/>	<input type="checkbox"/>
b. Is this in an auditable form? (can you trace use of the data from collection to disposal)	<input checked="" type="checkbox"/>	<input type="checkbox"/>
5. Have you read the <a href="#">guidance</a> on appropriate research and consent procedures for participants who may be perceived to be vulnerable?	<input checked="" type="checkbox"/>	<input type="checkbox"/>
a. Does your study involve participants who are particularly vulnerable or unable to give informed consent (e.g. children, people with learning disabilities, your own students)?	<input type="checkbox"/>	<input checked="" type="checkbox"/>
6. Will the study require the co-operation of a gatekeeper for initial access to the groups or individuals to be recruited (e.g. students at school, members of self-help group, nursing home residents)?	<input type="checkbox"/>	<input checked="" type="checkbox"/>
Click for an example of a <a href="#">PIS</a> and <a href="#">information about gatekeepers</a>		
7. Will the study involve the use of participants' images or sensitive data (e.g. participants personal details stored electronically, image capture techniques)?	<input type="checkbox"/>	<input checked="" type="checkbox"/>
Click <a href="#">here</a> for guidance on images and sensitive data		
8. Will the study involve discussion of sensitive topics (e.g. sexual activity, drug use)?	<input type="checkbox"/>	<input checked="" type="checkbox"/>
Click <a href="#">here</a> for an advisory distress protocol		
9. Could the study induce psychological stress or anxiety in participants or those associated with the research, however unlikely you think that risk is?	<input type="checkbox"/>	<input checked="" type="checkbox"/>
Click <a href="#">here</a> to read about how to deal with stress and anxiety caused by research procedures		
10. Will blood or tissue samples be obtained from participants?	<input type="checkbox"/>	<input checked="" type="checkbox"/>
Click <a href="#">here</a> to read how the Human Tissue Act might affect your work		
11. Is your research governed by the Ionising Radiation (Medical Exposure) Regulations (IRMER) 2000?	<input type="checkbox"/>	<input checked="" type="checkbox"/>
Click <a href="#">here</a> to learn more about IRMER		
12. Are drugs, placebos or other substances (e.g. food substances, vitamins) to be administered to the study participants or will the study involve invasive, intrusive or potentially harmful procedures of any kind?	<input type="checkbox"/>	<input checked="" type="checkbox"/>
Click <a href="#">here</a> to read about how participants need to be warned of potential risks in this kind of research		
13. Is pain or more than mild discomfort likely to result from the study? Please attach the pain assessment tool you will be using.	<input type="checkbox"/>	<input checked="" type="checkbox"/>





### **A.3 Copy of the Participants Information Sheet**



**Manchester Metropolitan University  
Faculty of Science and Engineering**

**Title of Study:**

**Medical Applications of Microwave and Millimetre-Wave Imaging**

**Researcher Name: Amani Yousef Owda**

## **Participant Information Sheet**

*I would like to invite you to take part in a research study. Before you decide you need to understand, why the research is being done and what it would involve for you. Please take time to read the following information carefully. Ask questions if anything you read is not clear or would like more information. Take time to decide whether or not to take part.*

### **What is the purpose of the study?**

The study aims to measure the human skin emissivity in vivo to assess possible variation in the human skin emissivity between individuals and locations on the hand. The measurements will be taken from different parts of the human hand and forearm such as the palm of the hand, the back of the hand, the dorsal surface of the forearm, the volar side of the forearm, the inner wrist, and the outer wrist.

### **Why have I been invited?**

The study aims to show differences in emissivity between healthy participants (no history of skin diseases or other diseases). Therefore, any healthy participant in the age group 18-70 will be fit for achieving this purpose.

### **Do I have to take part?**

*It is up to you to decide. We will describe the study and go through the information sheet, which we will give to you. We will then ask you to sign a consent form to show you agreed to take part. You are free to withdraw at any time, without giving a reason.*

### **Passive system Experimental measurements:**

- You will be asked to join the lab, the experimenter starting the session by explaining some details associated with the passive system such as the equipments, and how the system is working.
- You will be asked to provide some information such as your age, weight, height, ethnicity, and body mass index. In addition, the weight and the height will be measured in the lab.
- You will be informed that the emissivity measurements should be taken at different parts of your hand and forearm as shown in figure (1.1):

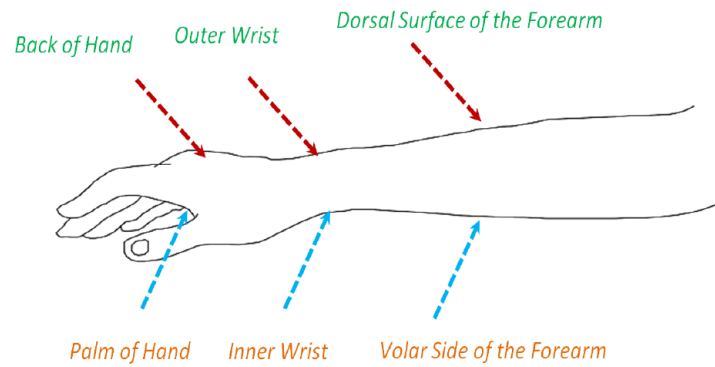


Figure (1.1) Emissivity measurements at different locations on the hand and forearm.

- You will be invited to ask any question before performing the measurements.
- You will be invited to put the target area of the skin in front of the horn antenna of the radiometer as illustrated in figure (1.2), and the experimenter will be measuring the power level of the thermal emission radiated from the target area of your hand and the thermodynamics temperature of the skin using thermometers.

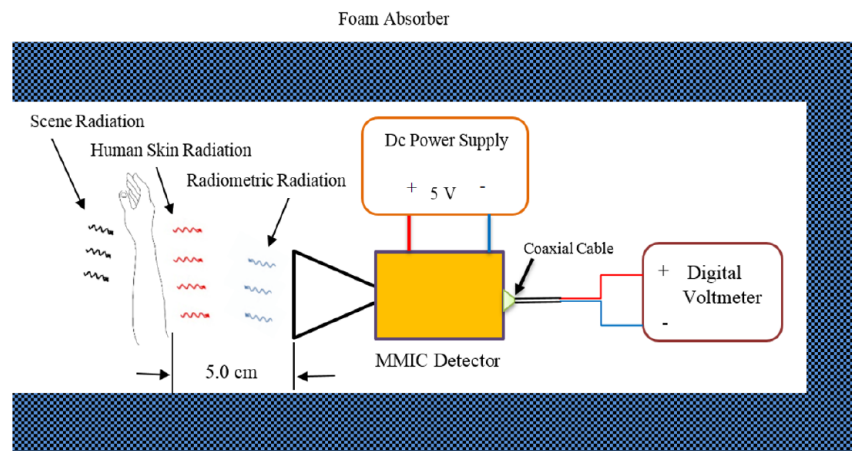


Figure (1.2) Methodology of measuring the human skin emissivity in vivo using a 90 GHz calibrated radiometer.

- You will be informed that, the measurements need to be repeated from 5-10 times for each location.
- You will be informed that, all the emissivity measurements should be taken and saved on the computer.

#### **Data Destroying Policy**

- All information which is collected about you during the course of the research will be kept strictly confidential, and any information about you which leaves the university will have your personal information removed so that you cannot be recognised.
- During the study your numerical score data will be collected on a questionnaire with your personal details stapled onto it. This will be removed and stored separately; a code number will be used to match them if it is required in the future.
- The number ratings you provide and your code number will be stored on a computer spreadsheet, password protected, the personal data sheets will be stored separately in a locked cabinet. These will be in a locked office in an MMU building. Your individual data will be accessible only by the researchers at MMU.
- Six months after publication of first results, identifying personal data will be destroyed. Statistically summarised results will be published and anonymous rating data, which cannot be traced back to you will be stored.

#### **What will I have to do?**

You will be invited to put the target area of your hand in front of the horn antenna of the system presented in figure 1.2 in the previous part.

#### **What are the possible disadvantages and risks of taking part?**

**For the passive system:** The measurements will be taken using radiometers (passive measurements) and therefore there is no risk associated with the experimental work presented in this study, given that the radiometer doesn't exposed the human body to any type of man-made radiation.

#### **What are the possible benefits of taking part?**

There will be no direct benefits to you for taking part in the study.

#### **What if there is a problem?**

In case if any problem happened in the measurements system or during the experimental work, you have the right to decide whether you want to leave or you want to stay longer.

**Will my taking part in the study be kept confidential?**

All your personal details will be treated as confidential with the project team and your identity will be coded. Any published data will not refer to individuals by name.

**Involvement of the General Practitioner/Family Doctor (GP)**

N/A

**What will happen if I don't carry on with the study?**

If you decided to be withdraw from the study that is up to you as a volunteer, but we will keep and possibly use the data collected from you up to your withdrawal.

**What will happen to the results of the research study?**

All your personal details will be treated as confidential with the project team and your identity will be coded. Any published data will not refer to individuals by name. If you wish to obtain a copy of any publications that result from the project, then please write to:

Dr. Neil Salmon  
School of Science and Engineering  
Manchester Metropolitan University  
John Dalton Building  
Manchester, M1 5GD

**Who is organising or sponsoring the research?**

Manchester Metropolitan University, Sensing and Imaging Group, School of Engineering.

**Further information and contact details:**

If you would like further information before deciding whether to take part, please contact: Amani Owda either by phone: 07 402 939 756 or by email: [Amani.owda@stu.mmu.ac.uk](mailto:Amani.owda@stu.mmu.ac.uk)

If you feel that you are not happy or your rights as a participant in this study have been violated, you may write to:

Head of Ethics in the Science and Engineering Faculty

Dr. Nicholas Costen.

Email: [n.costen@mmu.ac.uk](mailto:n.costen@mmu.ac.uk)

Telephone: +44 (0)161 2471490.

Manchester Metropolitan University.

**Finally, thank you!**

Thank you for considering participation in this study.

# Appendix B: Ethical Approval for Porcine Skin

## Measurements

### B.1 Approved Ethic Checklist

#### ETHICS CHECKLIST

This checklist must be completed **before** commencement of **any** research project. This includes projects undertaken by **staff and by students as part of a UG, PGT or PGR programme**. Please attach a Risk Assessment.



Please also refer to the [University's Academic Ethics Procedures](#) and the [University's Guidelines on Good Research Practice](#)

<b>Full name and title of applicant:</b>	Mrs. Amani Yousef Issa Owda
<b>University Telephone Number:</b>	07 402 939 756
<b>University Email address:</b>	Amani.Owda@stu.mmu.ac.uk
<b>Status: (delete as appropriate)</b>	Postgraduate Research Student: Ph.D.
<b>Department/School/Other Unit:</b>	School of Engineering
<b>Programme of study (if applicable):</b>	Ph.D.
<b>Name of DoS/Supervisor/Line manager:</b>	DoS: Dr. Neil Salmon
<b>Project Title:</b>	Medical Applications of Microwave and Millimetre-Wave Imaging
<b>Start &amp; End date of project:</b>	Start date:15/05/2017-End date: 1/12/2017
<b>Number of participants (if applicable):</b>	N/A
<b>Funding Source:</b>	Internal Ph.D. Studentship
<b>Brief description of research project activities (300 words max):</b>	
<p>As porcine skin has similar properties to the human skin in terms of general structure and thickness, it is widely used in medical research as surrogate for human skin. The research project activities will be: 1) purchase samples of porcine skin from an abattoir (preferable a sample from the back region of the animal since it is free from hair follicle and sweat gland; 2) make measurements of the porcine skin in the laboratory, which also involves burn damaging the porcine skin, to assess the effects of the burn on the measurements. In detail the planned activities are:</p> <ul style="list-style-type: none"> <li>• Stage 1: Emissivity measurements on dead animals' skin sample are planned to be taken. The measurements will be applied for the skin in a normal state and after performing the burn. The measurements aim to investigate the capability of the Passive-Millimetre-Wave system to distinguish between skin in normal state and skin with burns.</li> <li>• Stage 2: Scan images for the burn-damaged skin using the ThruVision passive imager with and without the presence of dressing materials, to assess the feasibility of passive millimetre-wave imaging system to detect the burn under dressing material.</li> <li>• Stage 3: Scan an image using Active millimetre wave imaging system might be conducted/ not conducted based on the time and the available resources in the lab.</li> </ul>	

<b>Information about sample handling and disposal:</b>		
<p>1) Porcine skin should be collected from the abattoir in a leak proof container and sealed in a zip lock bag and carried in a cool box. Any packaging should be incinerated after use; the container can be cleaned and reused. Prior arrangements should be made for collection.</p> <p>2) Porcine skin can be either used directly or it can be stored in a fridge for three days only prior to use. After three days the skin need to be disposed of. There are many fridges available and under technicians control for this purpose.</p> <p>3) Used porcine skin will be incinerated via yellow bag biohazard disposal scheme. (SRCL waste collection). Waste collection is every 2 weeks on Thursday. Skin should be frozen in a yellow biohazard bag after use and stored till the next collection date.</p> <p>4) For further information about sample handling, storage and disposal please refer to the risk assessment form that contains all required information in details.</p> <p>5) Fridge and Freezers are available within labs that are labelled from outside with bio-hazard stickers. Following the discussion with the technician they are also agreed to label the fridge and the freezer with bio-hazard stickers.</p>		
<b>Does the project involve NHS patients or resources?</b>		<b>NO</b>
<p>If 'yes' please note that your project may need NHS National Research Ethics Service (NRES) approval. Be aware that research carried out in a NHS trust also requires governance approval.</p> <p>Click <a href="#">here</a> to find out if your research requires NRES approval</p> <p>Click <a href="#">here</a> to visit the National Research Ethics Service website</p> <p>To find out more about Governance Approval in the NHS click <a href="#">here</a></p>		
<b>Does the project require NRES approval?</b>		<b>NO</b>
<p>If yes, has approval been granted by NRES? Attach copy of letter of approval. Approval cannot be granted without a copy of the letter.</p>		

<b>NB Question 2 should only be answered if you have answered YES to Question 1. All other questions are mandatory.</b>			<b>NO</b>
1. Are you are gathering data from people?	<input type="checkbox"/>		<input checked="" type="checkbox"/>
For information on why you need informed consent from your participants please click <a href="#">here</a>			
2. If you are gathering data from people, have you:			

a. attached a participant information sheet explaining your approach to their involvement in your research and maintaining confidentiality of their data?	<input type="checkbox"/>	<input type="checkbox"/>
b. attached a consent form? (not required for questionnaires)	<input type="checkbox"/>	<input type="checkbox"/>
Click <a href="#">here</a> to see an example of a <a href="#">participant information sheet</a> and <a href="#">consent form</a>		
3. Are you gathering data from secondary sources such as websites, archive material, and research datasets?	<input checked="" type="checkbox"/>	<input type="checkbox"/>
Click <a href="#">here</a> to find out what ethical issues may exist with secondary data		
4. Have you read the <a href="#">guidance</a> on data protection issues?	<input checked="" type="checkbox"/>	<input type="checkbox"/>
a. Have you considered and addressed data protection issues – relating to storing and disposing of data?	<input checked="" type="checkbox"/>	<input type="checkbox"/>
b. Is this in an auditable form? (can you trace use of the data from collection to disposal)	<input checked="" type="checkbox"/>	<input type="checkbox"/>
5. Have you read the <a href="#">guidance</a> on appropriate research and consent procedures for participants who may be perceived to be vulnerable?	<input checked="" type="checkbox"/>	<input type="checkbox"/>
a. Does your study involve participants who are particularly vulnerable or unable to give informed consent (e.g. children, people with learning disabilities, your own students)?	<input type="checkbox"/>	<input checked="" type="checkbox"/>
6. Will the study require the co-operation of a gatekeeper for initial access to the groups or individuals to be recruited (e.g. students at school, members of self-help group, nursing home residents)?	<input type="checkbox"/>	<input checked="" type="checkbox"/>
Click <a href="#">for an example of a PIS</a> and <a href="#">information about gatekeepers</a>		
7. Will the study involve the use of participants' images or sensitive data (e.g. participants personal details stored electronically, image capture techniques)?	<input type="checkbox"/>	<input checked="" type="checkbox"/>
Click <a href="#">here</a> for guidance on images and sensitive data		
8. Will the study involve discussion of sensitive topics (e.g. sexual activity, drug use)?	<input type="checkbox"/>	<input checked="" type="checkbox"/>
Click <a href="#">here for an advisory distress protocol</a>		
9. Could the study induce psychological stress or anxiety in participants or those associated with the research, however unlikely you think that risk is?	<input type="checkbox"/>	<input checked="" type="checkbox"/>
Click <a href="#">here to read about how to deal with stress and anxiety caused by research procedures</a>		
10. Will blood or tissue samples be obtained from participants?	<input type="checkbox"/>	<input checked="" type="checkbox"/>
Click <a href="#">here to read how the Human Tissue Act might affect your work</a>		
11. Is your research governed by the Ionising Radiation (Medical Exposure) Regulations (IRMER) 2000?	<input type="checkbox"/>	<input checked="" type="checkbox"/>
Click <a href="#">here</a> to learn more about IRMER		
12. Are drugs, placebos or other substances (e.g. food substances, vitamins) to be administered to the study participants or will the study involve invasive, intrusive or potentially harmful procedures of any kind?	<input type="checkbox"/>	<input checked="" type="checkbox"/>
Click <a href="#">here to read about how participants need to be warned of potential risks in this kind of research</a>		
13. Is pain or more than mild discomfort likely to result from the study? Please attach the pain assessment tool you will be using.	<input type="checkbox"/>	<input checked="" type="checkbox"/>
Click <a href="#">here to read how participants need to be warned of pain or mild discomfort resulting from the study</a> and <a href="#">what do about it.</a>		
14. Will the study involve prolonged or repetitive testing or does it include a physical intervention?	<input type="checkbox"/>	<input checked="" type="checkbox"/>
Click <a href="#">here to discover what constitutes a physical intervention</a> and <a href="#">here to read how any prolonged or repetitive testing needs to managed for participant wellbeing and safety</a>		

15. Will participants to take part in the study without their knowledge and informed consent? If yes, please include a justification.	<input type="checkbox"/>	<input checked="" type="checkbox"/>
<a href="#">Click here to read about situations where research may be carried out without informed consent</a>		
16. Will financial inducements (other than reasonable expenses and compensation for time) be offered to participants?	<input type="checkbox"/>	<input checked="" type="checkbox"/>
<a href="#">Click here to read guidance on payment for participants</a>		
17. Is there an existing relationship between the researcher(s) and the participant(s) that needs to be considered? For instance, a lecturer researching his/her students, or a manager interviewing her/his staff?	<input type="checkbox"/>	<input checked="" type="checkbox"/>
<a href="#">Click here to read guidance on how existing power relationships need to be dealt with in research procedures</a>		
18. Have you undertaken Risk Assessments for each of the procedures that you are undertaking?	<input checked="" type="checkbox"/>	<input type="checkbox"/>
19. Is any of the research activity taking place outside of the UK?	<input type="checkbox"/>	<input checked="" type="checkbox"/>
20. Does your research fit into any of the following security sensitive categories: <ul style="list-style-type: none"> <li>• commissioned by the military</li> <li>• commissioned under an EU security call</li> <li>• involve the acquisition of security clearances</li> <li>• concerns terrorist or extreme groups</li> </ul>	<input type="checkbox"/>	<input checked="" type="checkbox"/>

I understand that if granted, this approval will apply to the current project protocol and timeframe stated. If there are any changes I will be required to review the ethical consideration(s) and this will include completion of a 'Request for Amendment' form.

- I have attached a Risk Assessment
- I have attached an Insurance Checklist

Signature of Applicant: Amani Owda

Date: 10/04/2017

**Independent Approval for the above project is (please check the appropriate box):**

If the applicant has answered **YES** to **ANY** of the questions **5a – 17** then they must complete the [MMU Application for Ethical Approval](#).

**Granted**

I confirm that there are no ethical issues requiring further consideration and the project can commence.

**Not Granted**

I confirm that there are ethical issues requiring further consideration and will refer the project protocol to the Faculty Research Group Officer.



Signature: \_\_\_\_\_ Date: 10.05.2017 (DD/MM/YY)

Print Name: \_\_\_\_\_ Position: \_\_\_\_\_

**Approver: Independent Scrutiniser for UG and PG Taught/ PGRs RD1 Scrutiniser/ Faculty Head of Ethics for staff.**

# Appendix C: Publications and Best Student Award

## Certificate

### C.1: Journal Paper 1:

*Progress In Electromagnetics Research B, Vol. 80, 79–99, 2018*

#### Electromagnetic Signatures of Human Skin in the Millimeter Wave Band 80–100 GHz

Amani Y. Owda\*, Neil Salmon, and Nacer-Ddine Rezgui

**Abstract**—Due to changes in global security requirements attention is turning to new means by which anomalies on the human body might be identified. For security screening systems operating in the millimeter wave band anomalies can be identified by measuring the emissivities of subjects. As the interaction of millimeter waves with the human body is only a fraction of a millimeter into the skin and clothing has a small, but known effect, precise measurement of the emission and reflection of this radiation will allow comparisons with the norm for that region of the body and person category. A technique to measure the human skin emissivity in vivo over the frequency band 80 GHz to 100 GHz is developed and described. The mean emissivity values of the skin of a sample of 60 healthy participants (36 males and 24 females) measured using a 90 GHz calibrated radiometer were found to range from  $0.17 \pm 0.005$  to  $0.68 \pm 0.005$ . The lower values of emissivity are a result of measuring particularly thin skin on the inner wrist, volar side of the forearm, and back of hand, whereas higher values of emissivity are results of measuring thick skin on the outer wrist, dorsal surface of the forearm, and palm of hand. The mean differences in the emissivity between Asian and European male participants were calculated to be in the range of 0.04 to 0.11 over all measurement locations. Experimental measurements of the emissivity for male and female participants having normal and high body mass index indicate that the mean differences in the emissivity are in the range of 0.05 to 0.15 for all measurement locations. These results show the quantitative variations in the skin emissivity between locations, gender, and individuals. The mean differences in the emissivity values between dry and wet skin on the palm of hand and back of hand regions were found to be 0.143 and 0.066 respectively. These results confirm that radiometry can, as a non-contact method, identify surfaces attached to the human skin in tens of seconds. These results indicate a route to machine anomaly detection that may increase the through-put speed, the detection probabilities and reduce the false alarm rates in security screening portals.

### 1. INTRODUCTION

The detection of concealed threats on the human body in transport networks and border crossings poses an international challenge for the development of effective stand-off and portal security screening systems [1, 2]. The millimeter-wave (MMW) band is the region of the electromagnetic spectrum between the microwave and terahertz bands, covering the frequency ranges (30–300) GHz [3, 4]. With a high atmospheric transmission and little attenuation through textile materials and clothing, images can be formed of objects on persons concealed on or under their clothing [5] with high detection probability; a capability which is driving the developments of this security screening technology [6–11]. Imaging applied to security screening applications can either be achieved passively (radiometrically), where the natural thermal radiation emitted and reflected by the object is used or actively (radar), where the transmitter provides artificial MMW radiation to illuminate the subject and the image is formed from

*Received 4 December 2017, Accepted 17 March 2018, Scheduled 30 March 2018*

\* Corresponding author: Amani Y. Owda (amani.owda@stu.mmu.ac.uk).

The authors are with the Manchester Metropolitan University, School of Engineering, Chester Street, Manchester, M1 5GD, United Kingdom.

the reflected radiation [12]. Passive millimeter wave images are free from artefacts such as speckle and glint as the illuminating radiation from the human body is spatially incoherent. This means that all regions of the human body down to the skin can be screened for concealed threats with a technology that potentially generates little or no false alarms [13].

The levels of emissivity and reflectivity are determined by the relative complex permittivity of a medium, and these have been measured for human skin in the microwave and MMW frequency bands at specific frequencies and over limited number of participants and measurement locations by using an open ended coaxial probe in contact with the human body [22, 30, 41–43]. Due to the limited measured data, different theoretical models are often used to predict the relative complex permittivity of the skin, such as the Cole-Cole model and Debye model [43–45]. These studies indicate variations in the relative complex permittivity and the reflectivity of the skin with frequency. However, none of these studies indicates that there is a well validated signature for the human skin over the whole of the MMW frequency band. Therefore, measurement and validation of the human skin signature at the MMW frequency bands is required to bridge this gap.

The key innovation in this work is in recognizing that signatures from the human body enabling regions of the body to be identified as skin (as opposed to concealed threat) are very subtle and then in designing a system to measure and characterize the skin for this purpose. These signature variations from the skin are small (down to tens of milliKelvin), with changes taking place on scale lengths of a centimeter or so. This opportunity has been overlooked until now by the security screening community, as the sensitivities of existing passive millimeter wave imagers are typically in the region of a few Kelvin and with spatial resolutions greater than one centimeter. Consequently, anyone who would have looked would not have observed these subtle effects of the skin. The development of a precisely calibrated radiometer having a radiometric sensitivity of 5.0 mK with a centimeter spatial resolution on the skin has enabled new measurements of the human body to be made, for exploitation in the field of security screening of people.

The main advantages of the technique presented in this paper are: 1) human skin signatures can be measured without exposing the human body to any type of artificial or man-made radiation, 2) radiometric sensitivity is sufficient to identify surfaces attached to the human skin such as liquid, metallic and non-metallic objects. Furthermore, materials intentionally attached to the skin, having dielectric properties identical with human skin (to achieve a false negative in a security screening system), will be identified by their differential radiation temperatures, something which an active system cannot achieve, 3) the measurements can be made in tens of seconds using a non-contact sensor with high precision, and 4) the system is free from artefacts of speckle effects and multipath problems since spatially incoherent emission is used [12, 13].

In Section 2 the experimental work for measuring the human skin emissivity is discussed. This describes the experimental setup and mathematical equations, radiometric calibration, methodology of measuring the human skin emissivity and methodology of data processing. Section 3 presents the experimental results for both genders at different measurement locations on the hand, and emissivity measurements for dry and wet skins, emissivity measurements for participants having Asian and European ethnicities, and emissivity measurements for participants having normal and high body mass indices. Section 4 discusses the implications for security screening. Section 5 discusses all experimental results, and Section 6 presents overall conclusions and recommendations for future work.

## 2. EXPERIMENTAL WORK

This section of the paper contains technical details about the experimental work conducted in this research. An experimental setup, with absolute calibration methodology, is introduced and discussed. A block diagram with detailed information about the methodology of data processing is presented.

### 2.1. Participants

Sixty healthy adult participants (36 males and 24 females) having a variety of ethnicities, ages, and body mass indices were measured in this research project. The participants have ages ranging from 20 to 67 years. The participants have a mean and a standard deviation ( $\pm$ SD) in mass:  $72.5 \pm 13.92$  kg,

and height:  $1.66 \pm 0.099$  m. Male group comprised: 12 Europeans, 12 Asians and 12 others of different ethnicities (American, African . . . etc). The female group consisted of 12 Europeans and 12 Asians. The ethics of the study was approved by the Ethics Committee of Manchester Metropolitan University and a written consent form was obtained from each participant.

## 2.2. Measurement Equipment

A radiometer measures the thermal (Planck) radiation, and for radiation frequencies below the mid-infrared band the intensity of the emission is directly proportional to the temperature of the object, enabling images to be calibrated in degrees Kelvin [14]. The level of thermal emission emitted from human skin can be measured experimentally, applying a linear calibration, using black body emission sources [15]; one at the temperature of the background,  $T_H$  and the other held at a lower temperature,  $T_C$ . For a direct detection radiometer, the system response is assumed to be linear and the output voltage of the receiver for an ambient temperature source calibration  $V_H$  is [15]:

$$V_H = \alpha(T_H + T_N) \quad (1)$$

where,  $\alpha$  is the receiver responsivity measured in  $V/K$ , and  $T_N$  is the receiver noise temperature in K. For the liquid Nitrogen source calibration, the output voltage of the receiver  $V_C$  is [15]:

$$V_C = \alpha(T_C + T_N) \quad (2)$$

and for the human skin target, the output voltage of the receiver  $V_S$  is:

$$V_S = \alpha(T_b + T_N), \quad (3)$$

where,  $T_b$  is the radiation temperature of the human skin given by:

$$T_b = (1 - \eta)T_0 + T_s\eta \quad (4)$$

where the skin has an emissivity of  $\eta$ , a thermodynamic temperature of  $T_s$ , and  $T_0$  is the background illumination temperature [16]. From Eqs. (1) to (4), and equating  $T_0$  to  $T_H$ , the emissivity of the human skin can be expressed as [17]:

$$\eta = \frac{(V_s - V_H)(T_H - T_C)}{(T_s - T_H)(V_H - V_C)} \quad (5)$$

The minimum detectable radiation temperature variation  $\Delta T_{\min}$  for a radiometer is given by the radiometer equation, namely:

$$\Delta T_{\min} = \frac{T_A + T_R}{\sqrt{Bt}} \quad (6)$$

where  $t$  is the post-detection integration time,  $T_R$  the receiver noise temperature,  $B$  the receiver bandwidth, and  $T_A$  the antenna radiation temperature, effectively the radiation temperature of the source in front of the antenna [15]. This constitutes the random uncertainty in the measurements for radiometers of this type.

Although human skin is the largest multifunctional organ in the human body, to date insufficient attention has been paid to human skin signatures over the MMW frequency band for security screening purposes. A number of researchers investigated the electromagnetic response of the human skin over this band for medical purposes only [18–22]. These are useful resources to explore the capabilities for security screening by the identification of anomalies on the human body which may be suggestive of a concealed threat, which is the subject of this paper. Measurement and validation of the emissivity of human skin at MMW frequency bands is an essential requirement, to help assess the feasibility of increasing the detection probabilities and reducing the false alarm rate when screening at, for example, entrances to airport departures lounges [23]. Exploiting this in machine anomaly detection reduces the possibilities for deception in security screening portals [13, 23].

A direct detection radiometer sensitive over the frequency band 80–100 GHz was used for measuring the human skin emissivity of a sample of 60 healthy participants. The measurement equipment comprises: a horn antenna connected to a radiometer (consisting of a two-stage low-noise amplifier (type: monolithic millimeter wave integrated circuit (MMIC) LNA, gain: 20 dB; zero bias diode detector (type: MMIC wideband ZBD, power  $10.0 \mu\text{W}$ ) and buffer amplifier (type: MMIC wideband buffer

amplifier, power: 20 dBm, and voltage: 5.0 V). The radiometer is connected through a coaxial cable to a digital voltmeter and through wires to a DC power supply, as illustrated in Figure 1. The W-band horn antenna (type: AS4341, manufacturer: Atlan Tec RF) has a rectangular aperture ( $30 \times 25 \text{ mm}^2$ ) and a nominal gain of 20 dBi over the frequency band (80–100) GHz. The radiometer (type: MMIC detector, manufacturer: MMIC Solutions) has a rectangular shape and dimensions (length = 70 mm, width = 30 mm, and thickness 15 mm) and a 20 GHz radiation bandwidth and radiometric sensitivity of 5.0 mK. A digital voltmeter (type: digital voltmeter, manufacturer: Keysight Technologies) with a precision of 0.1 mV was used to measure the output voltage level of the thermal emission. This precision is responsible for a systematic measurement uncertainty in the system. The complete system, except for an opening for the subject, was enclosed in an anechoic region, made from carbon loaded absorbing foam. This prevented radiation from external sources, be it from the outdoors or other people in the environment, getting into the system to corrupt signals.

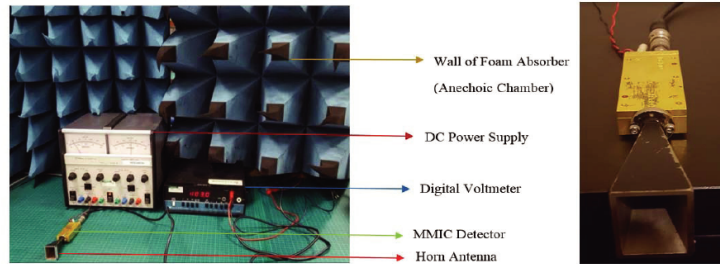


**Figure 1.** The main elements of the experimental work: A horn antenna connected to the MMIC detector. The detector is connected through a coaxial cable to a digital voltmeter and through wires to a DC power supply. A wall of carbon loaded absorbing foam surrounds the system.

### 2.3. Calibration and Initial Measurements

The radiometer was calibrated by comparing the measured data from subjects with the emission levels from known standard sources [24]. The standard sources were carbon loaded foam absorbers at liquid Nitrogen (77 K) and ambient (293 K) temperature, as illustrated in Figure 2. The cold load calibration measurements were taken within 5.0 seconds or less before the liquid Nitrogen evaporated, which is a standard measurement procedure. The carbon foam absorbers (type: Eccosorb AN-73, manufacturer: Laird) had a rectangular shape and dimensions (length = 170 mm, width = 150 mm, and thickness 10 mm). These dimensions were chosen to fill the beam pattern of the horn antenna, thereby minimizing systematic uncertainties. The measured emissivity values of the foam absorbers are greater than 0.99 over the frequency band 80–100 GHz [37–38], thus they behave as good approximations to a black body emitter. The difference in temperature between the hot and the cold load is  $\sim 216 \text{ K}$ , this large difference reducing the systematic uncertainties in the emissivity measurements to a minimum. The calibration Y-factor, defined as the ratio of receiver output when measuring the hot black body source to that measuring the cold source, was 1.408. These measurements were taken from ten experiments and repeated 5–10 times at each experiment, the calibration measurements were repeated 5–10 times and they were consistent. This indicates that the radiometer had a good long-term measurement stability.

The amount of self-emission reflected back from subjects was investigated by placing a metal plate perpendicular to the beam a distance 1.0 cm from the horn antenna beam. The mean level of self-emission reflected back from the metal plate (100% reflective surface) was measured to be in the range of 294–295 K with a standard deviation of  $\pm 1.0 \text{ K}$ . These results show that the radiation temperature from the metal plate is approximately the same as the ambient temperature, meaning there is no spurious emission from the radiometer or glint effects to corrupt measurements [25].

It is a well-known fact that the fluorescent lighting generates a low level (few Kelvin) of MMW radiation, modulated at 100 Hz, double the frequency of the mains electricity supply [25]. Millimeter-

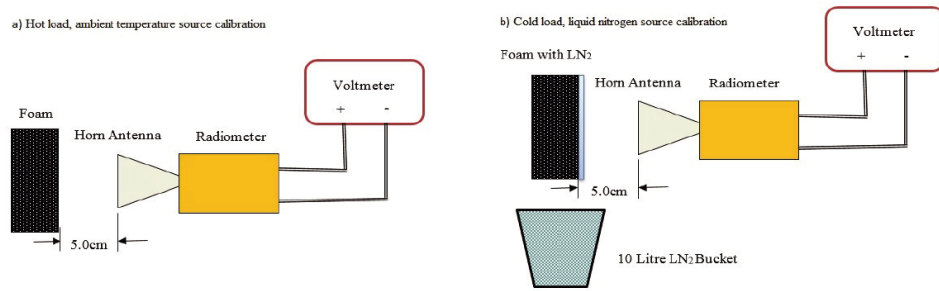


Figure 2. Ambient temperature and liquid Nitrogen calibration sources.

Wave emission emitted from a fluorescent light located  $\sim 5.0$  cm from the horn antenna (where the measurements are conducted) was found to increase the radiation temperature measured by the radiometer by an amount 62–74 K; a mean value of 67.5 K with a standard deviation of  $\pm 4.0$  K. When the fluorescent light was located directly in the beam of the horn antenna (where the maximum increase in radiation temperature is observed), the radiation temperature was found to increase by an amount 80–100 K; a mean value of 84.3 K with a standard deviation of  $\pm 8.0$  K. For this reason, all fluorescent lights were turned off in the laboratory during the measurements.

#### 2.4. Methodology for Measuring the Human Skin Emissivity

The horn antenna was located at a distance  $\sim 5.0$  cm from three different radiation sources: 1) ambient temperature source calibration (see Figure 2(a)), 2) liquid Nitrogen source calibration (see Figure 2(b)) and 3) the human skin (see Figure 3). The distance 5.0 cm has been chosen as an optimal distance for an existing measurements system. This distance is chosen for convenience, to minimize the chances of subjects accidentally touching and moving the measurement apparatus. A greater distance between the measured subject and the horn antenna would lead to measurements having poorer spatial resolution. A digital voltmeter with 0.1 mV resolution was used to measure the output voltage for the target area of the skin and the calibration sources, and an infrared thermometer with absolute accuracy  $0.01^\circ\text{C}$  was used to measure the skin surface temperature, and the thermodynamics temperature of the calibration sources. Error propagation through Eq. (5) indicates that the systematic uncertainty is  $\pm 0.005$ , whereas error propagation from Eq. (6) indicates that the random error in the minimum detectable radiation temperature is 5.0 mK.

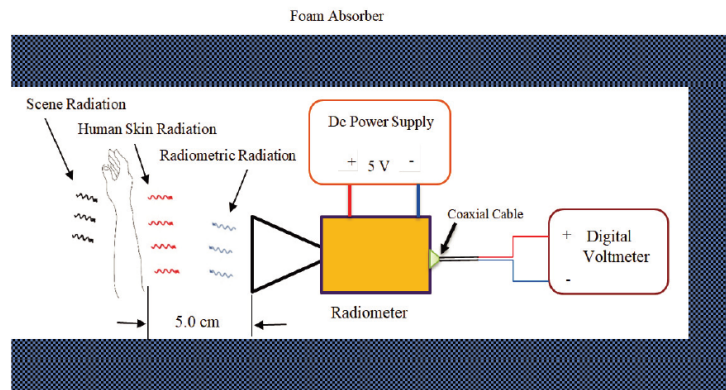
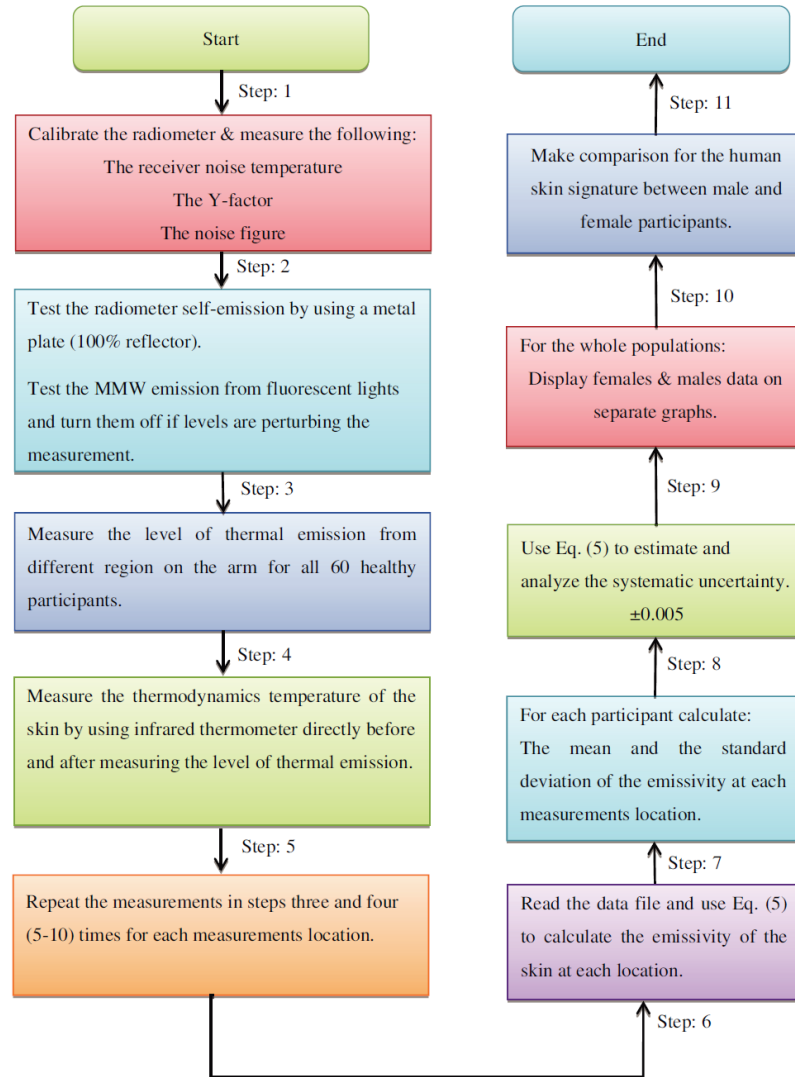


Figure 3. Experimental measurements for human skin emissivity.

The following block diagram summarizes the methodology and the statistical analysis for human skin emissivity measurement:



**Figure 4.** Methodology of data processing and statistical analysis.

### 3. EXPERIMENTAL RESULTS

Emissivity measurements were performed on 60 healthy participants over the frequency band 80 GHz–100 GHz. The measurements were made at six locations on the body and these were: 1) palm of hand, 2) back of hand, 3) inner wrist, 4) outer wrist, 5) volar side of the forearm, and 6) dorsal surface of the forearm as illustrated in Figure 5. These locations were chosen to provide variations in skin thickness and water content.

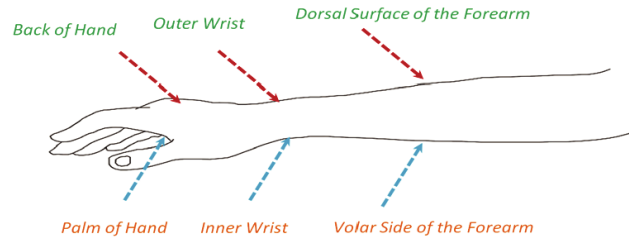


**Figure 5.** Six locations on the arm where the emissivity of the human skin was measured.

### 3.1. Male Skin Signatures

The measurements in Figures 6, 7 and 8 represent the mean emissivity for 36 male participants, with error bars representing the systematic uncertainty. The measurements show variation in emissivity between individuals and locations on the arm. These variations are due to the differences in skin thickness and the number of blood vessels (which raises the water content) which varies from one location to another and between individuals [26, 27]. The emissivity from males was found to range from 0.18 to 0.68, with mean ( $\mu$ ) and standard deviation ( $\sigma$ ) for all measurement locations being 0.401 and 0.0865 respectively. In general, lower values of emissivity are a result of measuring particularly thin skin on the inner wrist, back of hand, and volar side of the forearm [27], whereas higher values of emissivity are results of measuring thick skin on the outer wrist, palm of hand, and dorsal surface of the forearm [28]. Error propagation analysis through Eq. (5) indicates that the experimental measurements uncertainty is  $\pm 0.005$ . Table 1 shows the mean, the standard deviation, and the standard error in the mean ( $\sigma/\sqrt{n}$ , where  $n$  is the number of participants) for a sample of 36 male participants at the six measurements locations presented in Figures 6, 7, and 8:

**Table 1.** Statistical analysis for emissivity measurements performed on a sample of 36 males.

Location	Mean Emissivity	Standard Deviation	Standard Error in the Mean
Outer Wrist	0.396	0.0606	0.0101
Inner Wrist	0.343	0.0639	0.0106
Palm of Hand	0.451	0.0997	0.0166
Back of Hand	0.385	0.0844	0.0140
Dorsal Surface	0.449	0.0778	0.0129
Volar Side	0.381	0.0725	0.0121

Experimental measurements in Figures 6, 7, and 8 indicate differences in the mean emissivity values between the thicker skin regions of the hand (the outer wrist, the palm of the hand and the dorsal surface of the forearm) and the thinner skin regions of the hand (the inner wrist, the back of the hand and the volar side of the forearm) for all male participants. Statistical analysis on a sample of 36 male participants indicates that the mean differences in the emissivity values between the outer and the inner wrist, the palm of the hand and the back of the hand, and the dorsal and the volar regions are: 0.0529, 0.0658 and 0.0675 with a sample standard deviation in the differences of 0.0345, 0.0531 and 0.0319 respectively. These differences are due to the skin thickness and water content (blood vessels) that varies with location and between individuals [26, 27]. The thinner skin regions with blood vessels closed to the skin surface makes the skin more reflective and this results in higher reflectance ( $R$ ) and lower emissivity ( $\eta = 1 - R$ ).

Although the emissivity measurements in Figures 6, 7, and 8 suggest possible trends related to the age of the participants, it is still too early to draw conclusions as the numbers of participants in each age category are too small. Therefore, it is recommended that further measurements needed to be conducted to address variation in emissivity with age.

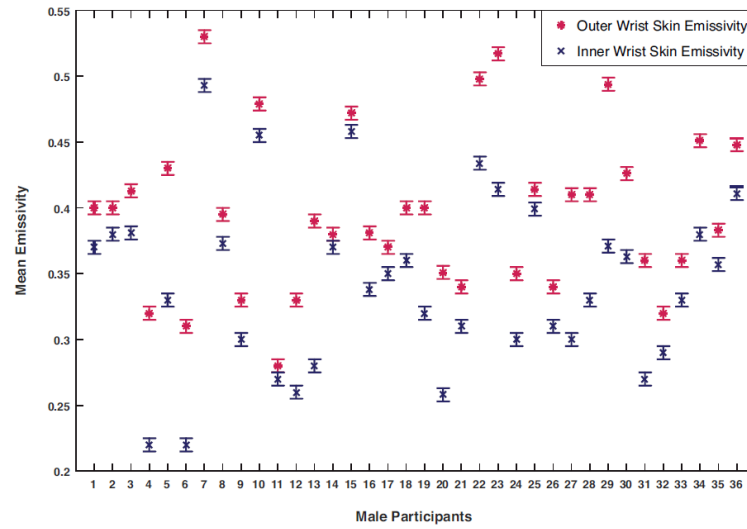


**Figure 6.** Mean emissivity for inner and outer wrist skin for a sample of 36 male participants. The participants' ages are as follows: 1) 20, 2) 20, 3) 21, 4) 22, 5) 22, 6) 22, 7) 23, 8) 23, 9) 23, 10) 24, 11) 24, 12) 25, 13) 26, 14) 26, 15) 26, 16) 26, 17) 27, 18) 28, 19) 29, 20) 29, 21) 30, 22) 31, 23) 31, 24) 32, 25) 34, 26) 35, 27) 37, 28) 37, 29) 40, 30) 40, 31) 42, 32) 42, 33) 45, 34) 52, 35) 58, 36) 67.

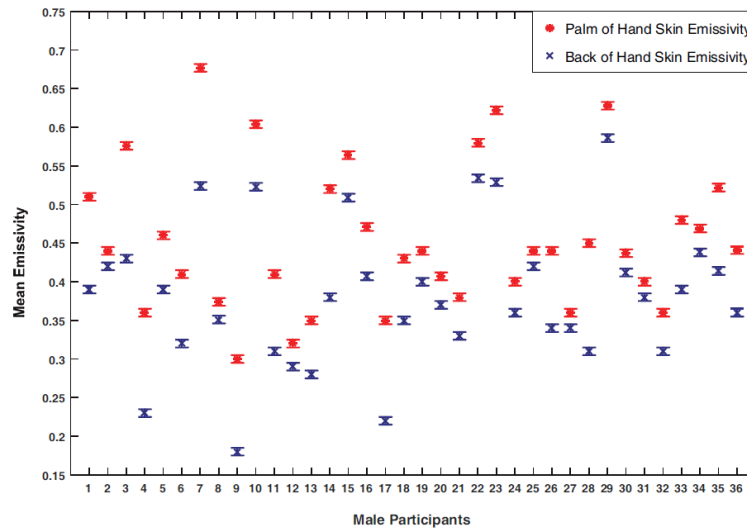


**Figure 7.** Mean emissivity for palm of hand and back of hand skin for a sample of 36 male participants. The participants' ages are as in Figure 6.

### 3.2. Female Skin Signatures

The measurements in Figures 9, 10 and 11 represent the mean emissivity for 24 female participants, with error bars representing the systematic uncertainty. The mean emissivity of the samples over all measurement locations is 0.383 with a standard deviation of 0.0839 and experimental measurement

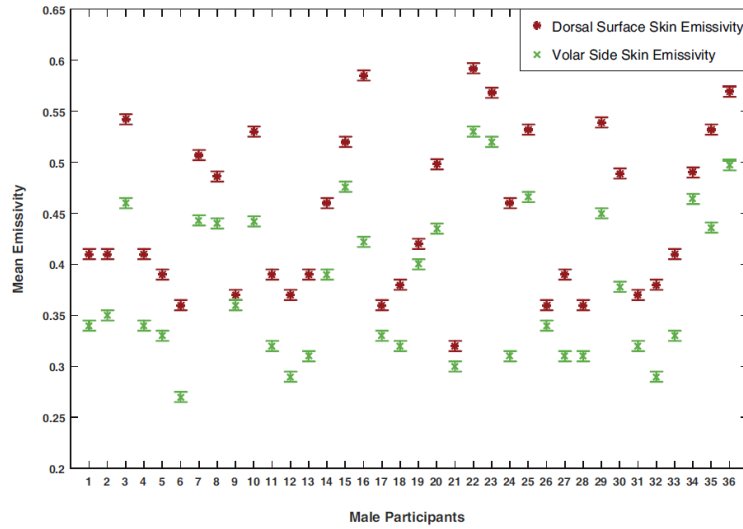


**Figure 8.** Mean emissivity for dorsal surface and volar side for a sample of 36 male participants. The participants’ ages are as in Figure 6.

uncertainty of  $\pm 0.005$ . Table 2 shows the mean, the standard deviation, and the standard error in the mean for a sample of 24 female participants at six measurement locations:

**Table 2.** Statistical analysis for emissivity measurements performed on a sample of 24 females.

Location	Mean Emissivity	Standard Deviation	Standard Error in the Mean
Outer Wrist	0.378	0.0654	0.0134
Inner Wrist	0.313	0.0620	0.0127
Palm of Hand	0.430	0.0951	0.0194
Back of Hand	0.371	0.0865	0.0177
Dorsal Surface	0.438	0.0659	0.0135
Volar Side	0.365	0.0549	0.0112

The measurements in Figures 9, 10 and 11 show a similar trend to that of the males in terms of differences in the mean emissivity values between the thicker skin region and the thinner skin region. Statistical analysis on a sample of 24 female participants indicates that the mean differences in the emissivity values between the outer and the inner wrist, the palm of the hand and the back of the hand, and the dorsal and the volar regions are: 0.0646, 0.0589 and 0.0729 with a sample standard deviation in the differences of 0.0394, 0.0375 and 0.0449, respectively.

### 3.3. Male and Female Skin Signatures in Dry and Wet States

In security screening, the radiometric sensitivity should be sufficient to sense different surfaces attached to the human skin such as liquid and metallic objects. With a metallic object MMW radiation has a clear signature, and this can be identified by using either active or passive MMW imaging systems. However, for the materials intentionally attached to the skin and having dielectric properties identical with human skin, a passive system can identify this anomaly by measuring radiation temperature of

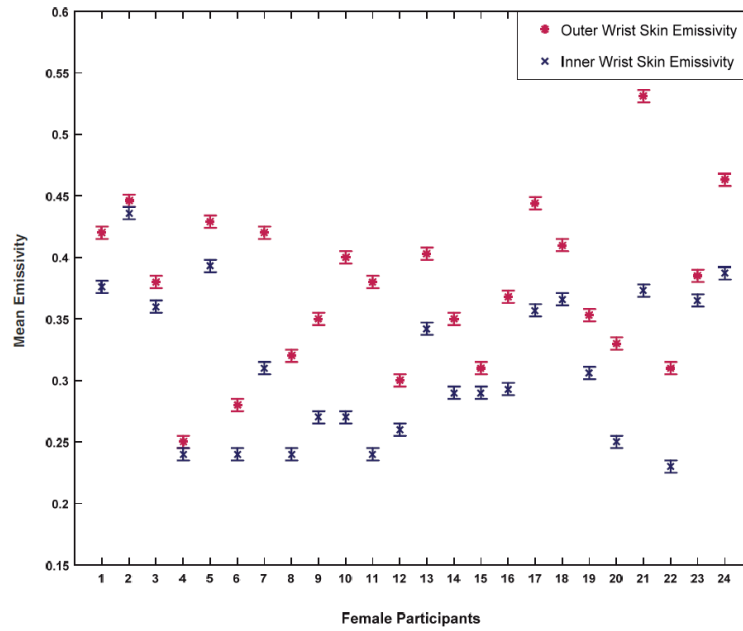


**Figure 9.** Mean emissivity for inner and outer wrist skin for a sample of 24 female participants. The participants' ages are as follows: 1) 22, 2) 23, 3) 23, 4) 24, 5) 24, 6) 24, 7) 25, 8) 26, 9) 27, 10) 29, 11) 29, 12) 30, 13) 31, 14) 32, 15) 32, 16) 33, 17) 33, 18) 35, 19) 36, 20) 42, 21) 44, 22) 45, 23) 45, 24) 54.

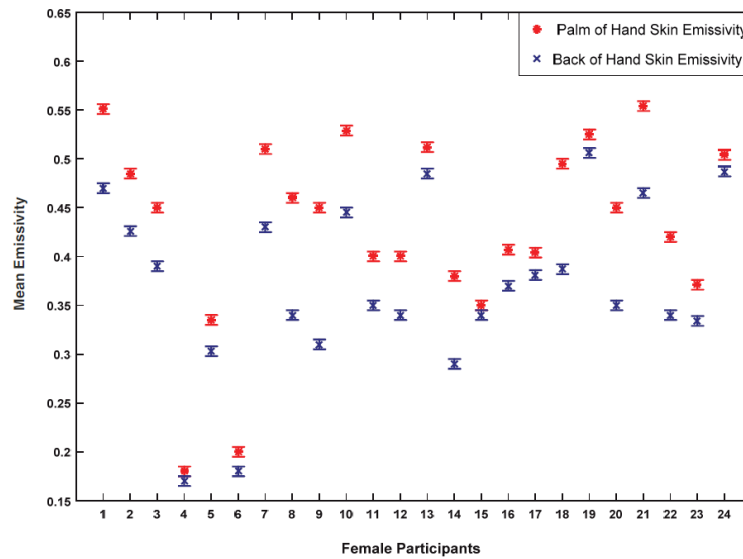


**Figure 10.** Mean emissivity for palm of hand and back of hand skin for a sample of 24 female participants. The participants' ages are as in Figure 9.

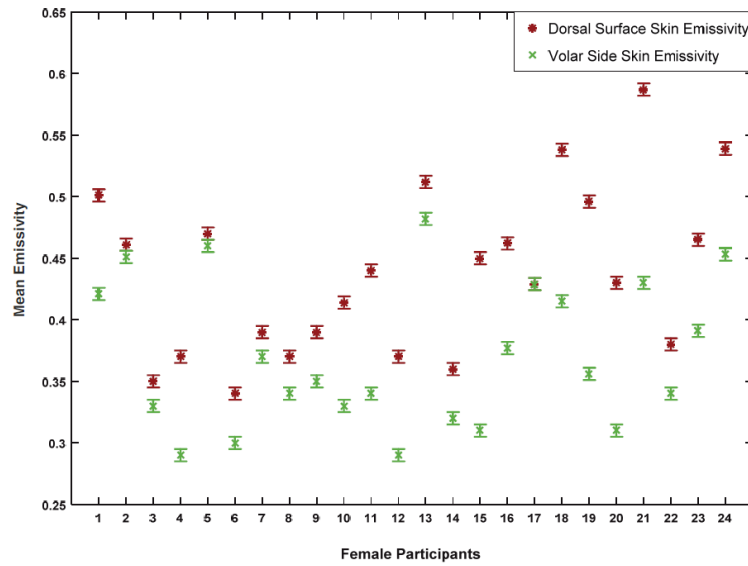


**Figure 11.** Mean emissivity for dorsal surface and volar side for a sample of 24 male participants. The participants' ages are as in Figure 9.

the skin, whereas an active system will not be able to do this as it only measured reflectivity. It is a known fact that the electromagnetic properties of water dominate the electromagnetic properties of the skin over the MMW bands [29]. Therefore, this experiment investigates the ability of the radiometer to identify and sense water (H<sub>2</sub>O) on the skin surface. The experiments were performed on 16 participants (10 males and 6 females) and on two measurement locations; the palm of the hand and the back of the hand skin. The methodology for measuring the emissivity of wet skin can be summarized as follows:

- 1) the target area of the skin was placed in a bowl of water for one minute, 2) then the hand was located on a flat surface (table) with the measurement location facing upwards for a period of 2–4 minutes until the water is absorbed, 3) then wet skin was wiped using clean and dried wipes, and 4) then the measurements were taken and repeated 5 times directly, the mean emissivity values of the palm of the hand and the back of the hand skin before and after the application of water are illustrated in Figures 12 and 13. Wet skin in this sense describes skin which has been saturated with water, but contains no surface water.

Emissivity measurements in Figure 12 for normal and wet palm of hand skin indicate differences in the mean emissivity between dry and wet skins. Statistical analysis on the data indicates that the mean difference in emissivity for the palm of the hand skin before and after wetting with water is  $\sim 0.143$  with a sample standard deviation of  $\sim 0.07$ , generating a standard error in the mean of 0.0175. These differences are due to the water that increases the hydration level of the skin and this makes the reflectance of the skin higher and the emissivity of the skin lower [30].

Experiment measurements in Figure 13 for normal and wet back of hand skin indicate differences in the mean emissivity between dry and wet back of hand skins. Statistical analysis on the data indicates that the mean difference in emissivity for back of hand skin before and after wetting with water is  $\sim 0.066$  with a sample standard deviation of  $\sim 0.046$ , generating a standard error in the mean of 0.0115. This difference is less than that of the palm of the hand skin. The thick Stratum Corneum (SC) layer on the palm of the hand region can retain water and this makes the hydration level for the palm of hand skin in wet state significantly higher than that of normal state [30], and therefore the difference between the palm of the hand skin in wet and normal states is more significant compared with the back of the hand region. Furthermore, the thickness and the ability of the SC layer to retain water vary from

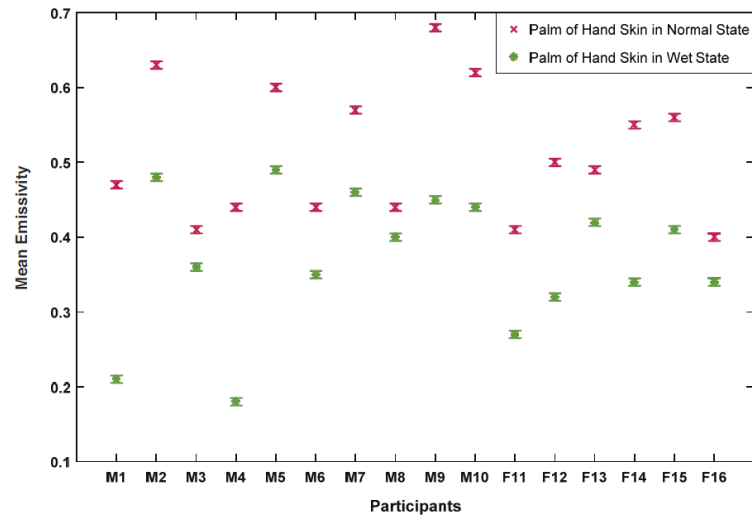


**Figure 12.** Emissivity measurements for normal and wet palm of hand skin performed on 10 males (M) and 6 females (F).

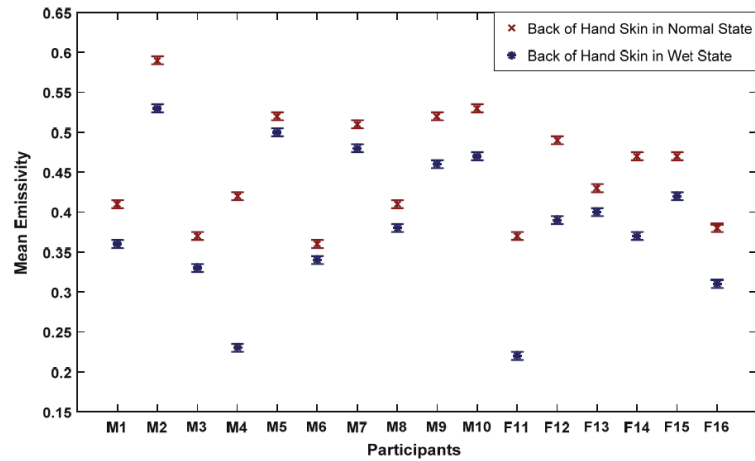


**Figure 13.** Emissivity measurements for dry and wet back of hand skins performed on 10 males (M) and 6 females (F).

person to person and therefore the differences between wet and normal skin vary between individuals and locations on the body.

### 3.4. Comparison between Male and Female Skin Signatures

Measurements of human skin emissivity of 36 male and 24 female healthy participants are presented in Table 3. The measurements show that the average of male participants' emissivity is higher than the average of the female participants' emissivity. This is consistent with the fact that male skin is thicker

than that of female skin for all ages [31–33]. This can be supported with the measurements presented in Figures 6 to 11. The measurements show that emissivity is high in the locations where the skin is thick such as; the palm of the hand, the dorsal surface of the forearm, and the outer wrist skin, and it is low in the locations where the skin is thin and the blood vessels are closer to the skin surface such as; the inner wrist, the volar side of the forearm and the back of the hand skin. These measurements show strong correlation between human skin emissivity, skin thickness and water content. This opens a new window of research in security screening, this being the identification of boundaries and limits for the emissive and reflective properties of different parts of the human body, as a means to anomaly identification.

**Table 3.** Mean emissivity values for male and female participants on all measurements locations.

Location	Mean Emissivity (Males)	SD (Males)	Mean Emissivity (Females)	SD (Females)
Outer Wrist	0.396	0.0606	0.378	0.0654
Inner Wrist	0.343	0.0639	0.313	0.0620
Palm of Hand	0.451	0.0997	0.430	0.0951
Back of Hand	0.385	0.0844	0.371	0.0865
Dorsal Surface	0.449	0.0778	0.438	0.0659
Volar Side	0.381	0.0725	0.365	0.0549

### 3.5. Skin Signature for Male and Female Participants Having European and Asian Ethnicities

The measurements presented in this section of the paper are from 48 participants from two different ethnicities; European and Asian from both genders (24 male (12 European and 12 Asian), and 24 female (12 European and 12 Asian)). The measurements in Figures 14 and 15 represent the mean emissivity for male and female groups with error bars representing the systematic uncertainty.

Experimental measurements in Figure 14 indicate that the mean emissivity for the sample of Asian males is lower than that of European males at all measurement locations. The mean values of the differences in emissivity between Asian and European males were calculated to be  $\sim 0.04$  for the inner wrist and the outer wrist locations,  $\sim 0.085$  for palm of hand, back of hand and volar side locations, and  $\sim 0.11$  for the dorsal surface location. These differences are likely to arise due to Asian skin being thinner than that of European skin and hydration levels and the water contents of the Asian skin being higher than that of European skin [34–36]. This makes Asian skin more reflective compared to European skin and as a result the mean emissivity of Asian participants is lower than that of European participants at all measurement locations. The standard deviations in the emissivity measurements for Asian and European male participants are summarized in Table 4 as follows:

**Table 4.** Standard deviation for Asian and European male participants at six measurement locations.

Location	SD for Asian Males	SD for European Males
Palm of Hand	$\pm 0.081$	$\pm 0.080$
Back of Hand	$\pm 0.089$	$\pm 0.073$
Inner Wrist	$\pm 0.047$	$\pm 0.074$
Outer Wrist	$\pm 0.054$	$\pm 0.064$
Volar Side of Forearm	$\pm 0.041$	$\pm 0.081$
Dorsal Surface of Forearm	$\pm 0.051$	$\pm 0.068$

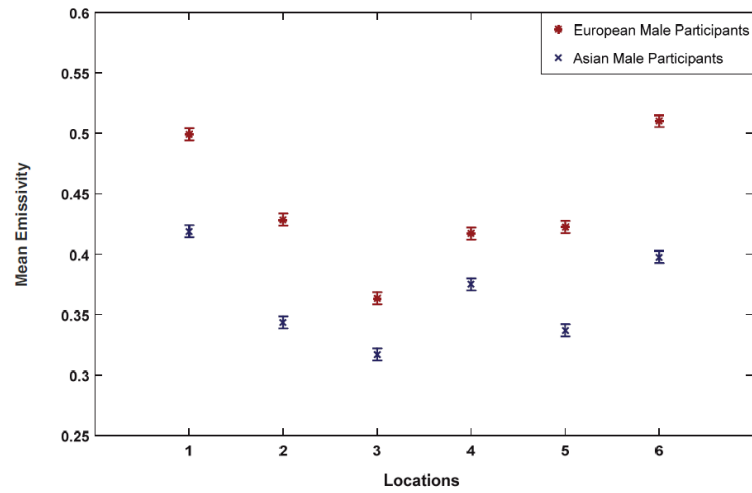


**Figure 14.** Mean emissivity of 24 male participants having Asian and European ethnicities at six locations: 1) palm of hand, 2) back of hand, 3) inner wrist, 4) outer wrist, 5) volar side, and 6) dorsal surface of the forearm.

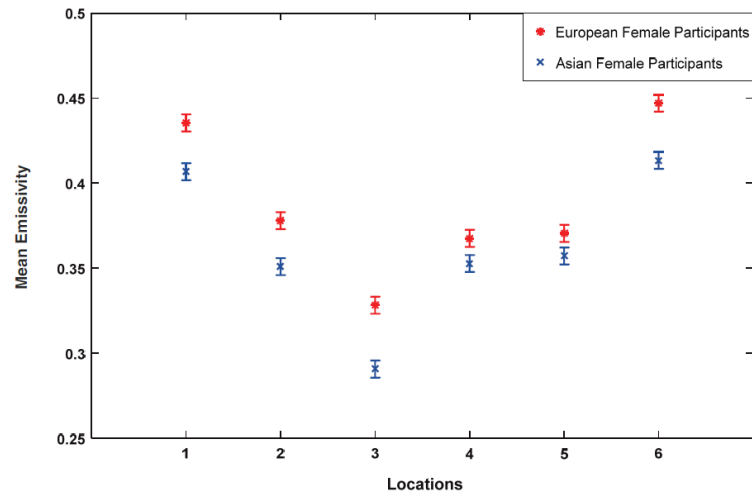


**Figure 15.** Mean emissivity of 24 female participants having Asian and European ethnicities at six measurements locations identified in Figure 14.

The measurements in Figure 15 indicate that there are differences in the mean emissivity values of skin between the Asian and European female samples, the measurements showing a similar trend to that of the males. However, the mean differences in the emissivity values between the two female groups were calculated to be in the range of 0.014 to 0.038 for all measurements locations. These differences are lower than that of the male groups. The standard deviation for Asian and European female groups is calculated and summarized in Table 5.

**Table 5.** Standard deviation for Asian and European female participants at six locations.

Location	SD for Asian Females	SD for European Females
Palm of Hand	$\pm 0.072$	$\pm 0.103$
Back of Hand	$\pm 0.065$	$\pm 0.097$
Inner Wrist	$\pm 0.054$	$\pm 0.065$
Outer Wrist	$\pm 0.045$	$\pm 0.048$
Volar Side	$\pm 0.053$	$\pm 0.054$
Dorsal Surface	$\pm 0.050$	$\pm 0.060$

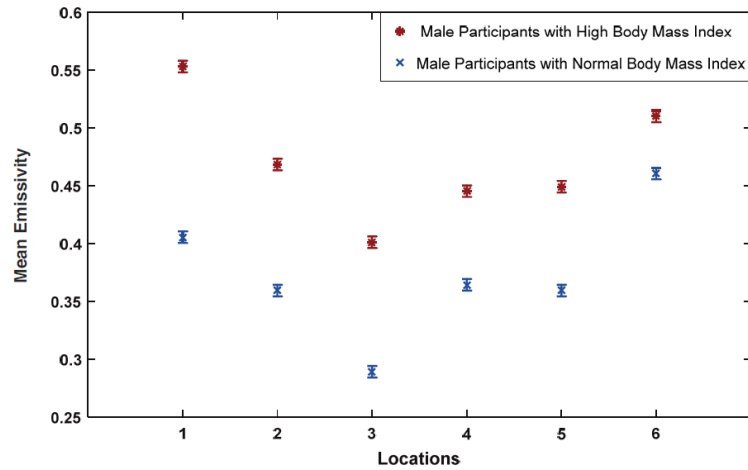


**Figure 16.** Mean emissivity for a sample of 10 male participants having normal and high body mass index on: 1) palm of hand, 2) back of hand, 3) inner wrist, 4) outer wrist, 5) volar side, and 6) dorsal surface of the forearm.

### 3.6. Skin Signature for Male and Female Having Normal and High Body Mass Index

Human skin becomes thicker with increasing body mass index (BMI) for both genders at any age [39], so variability in the emissivity of the skin from suitably selected participants was investigated. The measurements were performed on 20 participants (10 males and 10 females) having normal and high body mass index. For the purpose of this study, participants with BMI ranging between (18.5–24.9) kg/m<sup>2</sup> were classified as having normal BMI, whereas participants with BMI ranging between (25.0–29.9) kg/m<sup>2</sup> were classified as having high BMI [40]. Experimental measurements of the mean emissivity values of males with high and normal BMI are shown in Figure 16, with similar plots for females shown in Figure 17, with the corresponding values of the standard deviations shown in Tables 6 and 7.

Experimental measurements of the skin emissivity of males indicate that those with high BMI have on average an emissivity  $\sim 0.0981$  higher than those with normal BMI, with the differences in the mean emissivity values across the different locations varying from  $\sim 0.05$  to  $\sim 0.15$ . These differences are consistent with the fact that human skin is getting thicker with increasing the BMI [39], a consequence of this being that blood vessels are further from the surface of the skin.

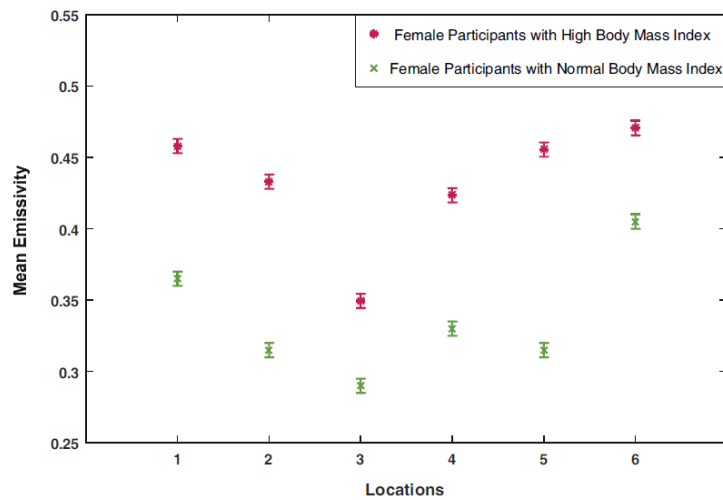
Experimental measurements of skin emissivity of females indicate that those with high BMI have on average an emissivity  $\sim 0.095$  higher than those with normal BMI, with the differences in the mean emissivity values across the different arm locations varying from  $\sim 0.06$  to  $\sim 0.14$ , a result similar to the

**Table 6.** Standard deviation for 10 male participants having normal and high body mass index.

Location	Standard Deviation for Males with Normal BMI	Standard Deviation for Males with High BMI
Palm of Hand	$\pm 0.039$	$\pm 0.049$
Back of Hand	$\pm 0.043$	$\pm 0.069$
Inner Wrist	$\pm 0.028$	$\pm 0.046$
Outer Wrist	$\pm 0.0136$	$\pm 0.064$
Volar Side of Forearm	$\pm 0.0567$	$\pm 0.077$
Dorsal Surface of Forearm	$\pm 0.078$	$\pm 0.067$

**Table 7.** Standard deviation for 10 female participants having normal and high body mass index.

Location	Standard Deviation for Female with Normal (BMI)	Standard Deviation for Female with High (BMI)
Palm of Hand	$\pm 0.015$	$\pm 0.054$
Back of Hand	$\pm 0.025$	$\pm 0.052$
Inner Wrist	$\pm 0.005$	$\pm 0.008$
Outer Wrist	$\pm 0.02$	$\pm 0.021$
Volar Side of Forearm	$\pm 0.005$	$\pm 0.027$
Dorsal Surface of Forearm	$\pm 0.045$	$\pm 0.042$

**Figure 17.** Mean emissivity for a sample of 10 female participants having normal and high body mass index at six measurement locations identified in Figure 16.

male group. However, the measurements of male emissivity indicate a larger scatter, this being 0.29 and 0.553 for those of normal and high BMI respectively. The corresponding scatter in the female group is 0.29 and 0.47 for normal and high BMI individuals. As with previous measurements these also indicate that the mean emissivity of males is  $\sim 0.038$  higher than those of females.

#### 4. IMPLICATIONS FOR SECURITY SCREENING

The implications of having model emissivities for different regions of the human body and different genders, ethnicities, body mass index and age groups, is that security screening of persons can become more of an automated process. As radiometry is used in the estimation of emissivity, any attempts at deception, by substituting a human skin surrogate over the body will be recognised as it will not fit the expected characteristics. This is because the emissivity is derived from the amount of radiation emitted by the body, not just from its reflection properties. This means that skin surrogates will be recognised even if they have exactly the same electrical properties as human skin. An active (coherent wave) illumination system will not have this capability, as it measures reflectivity directly. In a walk-through portal screening system a machine would process in a matter of second the radiometric measured emissivity from all regions of the human body together with a profile of the individual derived from gender, age and ethnicity. In a stand-off, crowd-surveillance or check-point screening scenario a similar process would take place, using emission data available from perhaps only one side of a subject.

#### 5. DISCUSSION

Human skin signature for a sample of 60 participants over the frequency band 80–100 GHz indicates that there is a scatter in emissivity measurements over a range 0.17 to 0.68, and this is much greater than the experimental measurement uncertainty of  $\pm 0.005$ . The measurements show that the levels of thermal emission (emissivity and reflectance) vary consistently over different regions of the hand and forearm, with age, gender, body mass index and ethnicity. In general, the lower values of the mean emissivity are a result of measuring particularly thin skin on the inner wrist, volar side and back of hand, whereas higher values of mean emissivity are results of measuring thick skin on the outer wrist, dorsal surface and palm of hand. The measurements also show variation in emissivity from person to person, and at different locations on the human body. Estimating the sample mean emissivity values for the 36 males and 24 females separately for all measurement locations indicates that the difference between male and female emissivity is  $\sim 0.02$ . This finding is consistent with the skin of males being thicker than that of females [31–33].

Experimental measurements of the differences in the emissivity between dry and wet skins on the palm of hand and back of hand regions indicate that radiometric sensitivity over the frequency band 80–100 GHz is sufficient to sense surfaces attached to the human skin. The measurements show a clear signature between normal skin and skin with water and this signature varies from person to person and between regions on the human body. The differences between wet and normal palm of hand skin are more significant than that of back of hand skin, and this is due to the thick (SC) layer that can retain water and make the hydration level for the palm of hand skin significantly higher in a wet state compared with a normal state. These results confirm that radiometry can identify surfaces attached to the human skin in tens of seconds and in the absence of any contact with or pat-down search of non-contact with the human body.

Experimental measurements of the mean emissivity of a sample of 24 male participants having Asian and European ethnicities show that the mean emissivity of male participants having Asian ethnicity is lower than that of male participants having European ethnicity over all measurement locations. The mean differences in emissivity values between Asian and European male participants were calculated to be in the range of 0.04 to 0.11. These differences are likely to be due to higher hydration level and thinner skin of Asian male participants [34–36].

Experimental measurements of the mean emissivity of a sample of 24 female participants having Asian and European ethnicities show that the mean emissivity of female participants having Asian ethnicity is lower than that of female participants having European ethnicity over all measurement locations. The mean differences in emissivity values between Asian and European female participants were calculated to be in the range of 0.014 to 0.038. Again, it is likely that these differences are due to thinner skin and higher hydration levels of female participants having Asian ethnicity compared with Europeans [34–36].

Experimental measurements of the mean emissivity of male and female groups having normal and high body mass index show that male and female groups with high BMI have higher mean emissivity

at all measurement locations compared with those having normal BMI. The mean differences in the emissivity values between the two male groups are calculated to be in the range of 0.05 to 0.15 for all measurement locations, these differences are also similar between the two females group. These results confirm that there are strong correlations between the skin thickness, the body mass index and the emissivity of the skin over the millimeter-wave frequency band (80–100) GHz for both genders.

It is recommended that further measurements are made on larger and more varied groups of individuals and overall body regions to provide statistics about the emissive and reflective properties of the human skin. This might be done on the skin directly and also on regions covered with clothing at ranges of frequencies over the millimeter wave frequency bands, the lower frequencies offering greater penetration into layers of clothing and down to the skin. The higher frequencies offer higher resolution. This will lead to greater understanding of human skin signature at the MMW frequency bands. When this is done, expected emissivity values can be identified at each location on the human body and these values can be compared with the measured emissivity from a template ensemble of recognised responses on an automated basis at security screening portals. Any deviation from the norm might identify anomalies. This will increase the detection probabilities, reduce the false alarm rate, and ensure high throughputs at entrances to future airport departure lounges and transport networks. An overview of the statistical analysis for the differences in the mean emissivity values between different locations and groups are summarized in Table 8:

**Table 8.** Overview of the statistical analysis for the human skin measured emissivity values.

Locations or Group	Differences in Emissivity $\pm$ SD Males Participants	Differences in Emissivity $\pm$ SD Females Participants
Palm and Back of Hand	0.0658 $\pm$ 0.0531	0.0589 $\pm$ 0.0375
Inner Wrist and Outer Wrist	0.0529 $\pm$ 0.0345	0.0646 $\pm$ 0.0394
Dorsal Surface and Volar Side	0.0675 $\pm$ 0.0319	0.0729 $\pm$ 0.0449
Dry and Wet Palm of Hand	0.148 $\pm$ 0.074	0.135 $\pm$ 0.054
Dry and Wet Back of Hand	0.056 $\pm$ 0.045	0.0833 $\pm$ 0.039
Normal and High BMI	Differences Range: 0.05–0.15 SD for Normal BMI: $\pm$ 0.0704 SD for High BMI: $\pm$ 0.0797 For All Six Locations	Differences Range: 0.06 to 0.14 SD for Normal BMI: $\pm$ 0.0446 SD for High BMI: $\pm$ 0.0549 For All Six Locations
Asian and European Participants	Differences: 0.04–0.11 SD for Asian: $\pm$ 0.0726 SD for European: $\pm$ 0.098 For All Locations	Differences: 0.014–0.038 SD for Asian: $\pm$ 0.0723 SD for European: $\pm$ 0.0875 For All Locations

## 6. CONCLUSIONS

A radiometer effective over the frequency band 80–100 GHz has been investigated and characterized for measuring the human skin signature of a sample of 60 healthy participants. The system was calibrated absolutely using liquid Nitrogen and ambient temperature sources. These measurements were used to characterize self-emission and millimeter wave radiation from a metal plate and fluorescent lights. The mean level of the self-emission reflected back from a metal plate was typically  $\pm$ 1.0 K above the background. Millimeter-wave emission emitted from a fluorescent light was found to increase the radiation temperature of the radiometer in the range of 62–74 K with a standard deviation of  $\pm$ 4.0 K.

Radiometric measurements made on a sample of 60 participants show that the mean emissivity of human skin varies from 0.17 to 0.68 over the 80 GHz to 100 GHz band. These variations are due to the differing water content and skin thicknesses of the participants. Statistical analysis on the data indicates that the mean emissivity of males over all measurements locations is higher than that of females by  $\sim$ 0.02. This supports the knowledge that on average the skin of males is thicker than that of females [31–33].

Experimental measurements of a sample of 36 male participants indicate that the mean differences in the emissivity values between the palm of hand and back of hand, the dorsal and volar regions of the forearm, and the inner and the outer wrist locations are: 0.0658, 0.0675 and 0.0529 with a sample standard deviation of 0.0531, 0.0319 and 0.0345 respectively. For female participants, the sample mean of the differences in the emissivity values between thinner and thicker skin regions were found to be: 0.0589, 0.0729 and 0.0646 respectively with a standard deviation of 0.0375, 0.0449, and 0.0394. These measurements indicate differences in the mean emissivity between the thinner and the thicker skin regions.

Experimental measurements of a sample of 16 participants (10 males and 6 females) indicate that the mean differences in the emissivity values between the normal and the wet palm of hand, and the normal and the wet back of hand skin are 0.143, and 0.066 with a sample standard deviation of 0.07, and 0.046, respectively. This indicates strong correlation between the human skin emissivity and the hydration level of the skin.

Experimental measurements of a sample of 48 male and female participants having Asian and European ethnicities indicate that the mean emissivity of the Asian sample of participant is lower than that of European sample of participants at all measurement locations, and this is due to the thinner skin and higher hydration levels of the skin of Asians.

Experimental measurements of a sample of 20 healthy participants from both genders having normal and high body mass index show that the group of participants with high BMI have higher mean emissivity values at all measurement locations than those having normal BMI. These measurements confirm a strong correlation between the human skin emissivity and the BMI, the latter being directly proportional to the skin thickness.

Research continues in this area to understand the signature of the human skin in the millimeter wave frequency bands and to design a full-body imaging security portal with machine anomaly detection for rapid walk-through, high-probability of detection, low false alarm rate screening.

## REFERENCES

1. Zheng, C., X. Yao, A. Hu, and J. Miao, "A passive millimeter-wave imager used for concealed weapon detection," *Progress In Electromagnetics Research B*, Vol. 46, 379–397, 2013.
2. Yang, B.-H., Z.-P. Li, C. Zheng, J. Zhang, X.-X. Yao, A.-Y. Hu, and J.-G. Miao, "Design of a passive millimeter-wave imager used for concealed weapon detection BHU-2D-U," *WSEAS Transactions on Circuits and Systems*, Vol. 13, 94–103, 2014.
3. Appleby, R., "Passive millimetre-wave imaging and how it differs from terahertz imaging," *Philos. Trans. A Math. Phys. Eng. Sci.*, Vol. 362, 379–392, 2004, doi:10.1098/rsta.2003.1323
4. Harmer, S. W., N. Bowring, D. Andrews, N. D. Rezgui, M. Southgate, and S. Smith, "A review of nonimaging stand-off concealed threat detection with millimeter-wave radar," *IEEE Microwave Magazine*, Vol. 13, 160–167, 2012, doi:10.1109/MMM.2011.2174125.
5. Sheen, D. M., D. L. McMakin, and T. E. Hall, "Cylindrical millimeter-wave imaging technique for concealed weapon detection," *Proc. SPIE*, Vol. 3240, 0000, 1998, doi:10.1117/12.300061.
6. Salmon, N. A., "Experimental results and simulations from aperture synthesis three-dimensional radiometric imaging," *Proc. SPIE*, Vol. 9993, 99930B, 2016, doi:10.1117/12.2231696.
7. Salmon, N. A., "3-D radiometric aperture synthesis imaging," *IEEE Transactions on Microwave Theory and Technology*, Vol. 63, 3579–3587, 2015, doi:10.1109/TMTT.2015.2481413.
8. Rezgui, N.-D., D. A. Andrews, and N. J. Bowring, "Ultra wide band 3D microwave imaging scanner for the detection of concealed weapons," *Proc. SPIE*, Vol. 9651, 965108, 2015, doi:10.1117/12.2197581.
9. Blackhurst, E., N. Salmon, and M. Southgate, "Full polarimetric millimetre wave radar for stand-off security screening," *Proc. SPIE*, Vol. 10439, 1043906, 2017, doi:10.1117/12.2282564.
10. Ahmed, S. S., A. Schiessl, F. Gumbmann, M. Tiebout, S. Methfessel, and L.-P. Schmidt, "Advanced microwave imaging," *IEEE Microwave Magazine*, Vol. 13, 26–43, 2012, doi:10.1109/MMM.2012.2205772.

11. Ahmed, S. S., O. Ostwald, and L.-P. Schmidt, "Automatic detection of concealed dielectric objects for personnel imaging," *Proc. IEEE MTT-S International Microwave Workshop on Wireless Sensing, Local Positioning, and RFID*, 1–4, 2009, doi:10.1109/IMWS2.2009.5307899.
12. Luukanen, A., R. Appleby, M. Kemp, and N. Salmon, *Millimeter-Wave and Terahertz Imaging in Security Applications*, Vol. 171, Springer, Berlin, Heidelberg, 2012.
13. Salmon, N. A., "Extended sources near-field processing of experimental aperture synthesis data and application of the Gerchberg method for enhancing radiometric three-dimensional millimetre-wave images in security," *Proc. SPIE*, Vol. 10439, 1043905, 2017, doi:10.1117/12.2282563.
14. Salmon, N. A., J. R. Borrill, and D. G. Glee, "Absolute temperature stability of passive imaging radiometers," *Proc. SPIE*, Vol. 3064, 110–120, 1997, doi:10.1117/12.277072.
15. Pozar, D. M., *Microwave Engineering*, 4th edition, John Wiley & Sons, Hoboken, New Jersey, 2011.
16. Bardati, F. and D. Solimini, "Radiometric sensing of biological layered media," *Radio Science*, Vol. 18, 1393–140, 1983, doi:10.1029/RS018i006p01393.
17. Owda, A. Y., N. A. Salmon, N.-D. Rezgui, and S. Shylo, "Millimetre wave radiometers for medical diagnostics of human skin," *Proc. IEEE Sensors*, 1–3, 2017.
18. Harmer, S. W., S. Shylo, M. Shah, N. J. Bowring, and A. Y. Owda, "On the feasibility of assessing burn wound healing without removal of dressings using radiometric millimetre-wave sensing," *Progress In Electromagnetics Research M*, Vol. 45, 173–183, 2016.
19. Owda, A. Y., N. Salmon, S. W. Harmer, S. Shylo, N. J. Bowring, N. D. Rezgui, and M. Shah, "Millimeter-wave emissivity as a metric for the non-contact diagnosis of human skin conditions," *Bioelectromagnetics*, Vol. 38, 559–569, 2017, doi:10.1002/bem.22074.
20. Feldman, Y., A. Puzenko, P. Ben Ishai, A. Caduff, and A. J. Agranat, "Human skin as arrays of helical antennas in the millimeter and submillimeter wave range," *Physical Review Letters*, Vol. 100, 128102, 2008, doi:https://doi.org/10.1103/PhysRevLett.100.128102.
21. Feldman, Y., A. Puzenko, P. Ben Ishai, A. Caduff, I. Davidovich, F. Sakran, and A. J. Agranat, "The electromagnetic response of human skin in the millimetre and submillimetre wave range," *Physics in Medicine & Biology*, Vol. 54, 3341–3363, 2009, doi:https://doi.org/10.1088/0031-9155/54/11/005.
22. Smulders, P. M. F., "Analysis of human skin tissue by millimeter-wave reflectometry," *Skin Research and Technology*, Vol. 19, e209–e216, 2012, doi:10.1111/j.1600-0846.2012.00629.x.
23. Owda, A. Y., N.-D. Rezgui, and N. A. Salmon, "Signatures of human skin in the millimetre wave band (80–100) GHz," *Proc. SPIE*, Vol. 10439, 1043904, 2017, doi:10.1117/12.2292046.
24. K uchler, N., D. D. Turner, U. L ohnert, and S. Crewell, "Calibrating ground-based microwave radiometers: Uncertainty and drifts," *Radio Science*, Vol. 51, 311–327, 2016, doi:10.1002/2015RS005826.
25. Salmon, N. A., L. Kirkham, and P. N. Wilkinson, "Characterisation and calibration of a large aperture (1.6 m) ka-band indoor passive millimeter wave security screening imager," *Proc. SPIE*, Vol. 8544, 854408, 2012, doi:10.1117/12.999278.
26. Lee, Y. and K. Hwang, "Skin thickness of Korean adults," *Surgical and Radiologic Anatomy*, Vol. 24, 183–189, 2002, doi:10.1007/s00276-002-0034-5.
27. Gray, H., *Anatomy of the Human Body*, Lea & Febiger, Philadelphia, Pennsylvania, 1981.
28. McGrath, J. A. and J. Uitto, *Rook's Textbook of Dermatology*, 9th edition, Wiley-Blackwell, Oxford, UK, 2016.
29. Zhadobov, M., N. Chahat, R. Sauleau, C. L. Quement, and Y. L. Drean, "Millimeter-wave interactions with the human body: State of knowledge and recent advances," *International Journal of Microwave and Wireless Technologies*, Vol. 3, 237–247, 2011, doi:https://doi.org/10.1017/S1759078711000122.
30. Alekseev, S. I., I. Szabo, and M. C. Ziskin, "Millimeter wave reflectivity used for measurement of skin hydration with different moisturizers," *Skin Research and Technology*, Vol. 14, 390–396, 2008, doi:10.1111/j.1600-0846.2008.00319.x.

31. Giacomoni, P. U., T. Mammone, and M. Teri, "Gender-linked differences in human skin," *Journal of Dermatological Science*, Vol. 55, 144–149, 2009, doi: <https://doi.org/10.1016/j.jdermsci.2009.06.001>.
32. Sandby-Møller, J., T. Poulsen, and H. C. Wulf, "Epidermal thickness at different body sites: relationship to age, gender, pigmentation, blood content, skin type and smoking habits," *Acta Derm Venereol*, Vol. 83, 410–413, 2003, doi:10.1080/00015550310015419.
33. Shuster, S., M. M. Black, and E. Mcvitie, "The influence of age and sex on skin thickness, skin collagen and density," *Br. J. Dermatol.*, Vol. 93, 639–643, 1975, doi:10.1111/j.1365-2133.1975.tb05113.x.
34. Rawlings, A. V., "Ethnic skin types: Are there differences in skin structure and function?," *International Journal of Cosmetic Science*, Vol. 28, 79–93, 2006, doi:10.1111/j.1467-2494.2006.00302.x.
35. Sugino, K., G. Imokawa, and H. I. Maibach, "Ethnic difference of varied stratum corneum function in relation to stratum corneum lipids," *Journal of Dermatological Science*, Vol. 6, 108, 1993, doi: [https://doi.org/10.1016/0923-1811\(93\)91343-S](https://doi.org/10.1016/0923-1811(93)91343-S).
36. Hillebrand, G. G., M. J. Levine, and K. Shigaki-Miyamoto, "The age dependent changes in skin condition in African Americans, Asian Indians, Caucasians, East Asians & Latinos," *IFSCC Magazine*, Vol. 4, 259–266, 2001.
37. Williams, G. F., "Microwave emissivity measurements of bubbles and foam," *IEEE Trans. Geosci. Elect.*, Vol. 9, 221–224, 1971, doi: 10.1109/TGE.1971.271504.
38. Rose, L. A., W. E. Asher, S. C. Reising, P. W. Gaiser, K. M. St Germain, D. J. Dowgiallo, K. A. Horgan, G. Farquharson, and E. J. Knapp., "Radiometric measurements of the microwave emissivity of foam," *IEEE Trans. Geosci. Remote Sens.*, Vol. 40, 2619–2625, 2002, doi: 10.1109/TGRS.2002.807006.
39. Derraik, J. G. B., M. Rademaker, W. S. Cutfield, T. E. Pinto, S. Tregurtha, A. Faherty, J. M. Peart, P.L. Drury, and P. L. Hofman, "Effects of age, gender, BMI, and anatomical site on skin thickness in children and adults with diabetes," *PLoS ONE*, Vol. 9, e86637, 2014, doi: <https://doi.org/10.1371/journal.pone.0086637>.
40. Jackson, A. S., P. R. Stanforth, J. Gagnon, T. Rankinen, A. S. Leon, D. C. Rao, J. S. Skinner, C. Bouchard, and J. H. Wilmore, "The effect of sex, age and race on estimating percentage body fat from body mass index: The Heritage Family Study," *International Journal of Obesity*, Vol. 26, 789–796, 2002, doi:10.1038/sj.ijo.0802006.
41. Alekseev, S. I. and M. C. Ziskin, "Human skin permittivity determined by millimeter wave reflection measurements," *Bioelectromagnetics*, Vol. 28, 331–339, 2007, doi: 10.1002/bem.20308.
42. Egot-Lemaire, S. J.-P. and M. C. Ziskin, "Dielectric properties of human skin at an acupuncture point in the 50–75 GHz frequency range. A pilot study," *Bioelectromagnetics*, Vol. 32, 360–366, 2011, doi: 10.1002/bem.20650.
43. Gabriel, S., R. W. Lau, and C. Gabriel, "The dielectric properties of biological tissues: III. Parametric models for the dielectric spectrum of tissues," *Physics in Medicine and Biology*, Vol. 41, 2271–2293, 1996.
44. Gabriel, S., R. W. Lau, and C. Gabriel, "The dielectric properties of biological tissues: II. Measurements in the frequency range 10Hz to 20 GHz," *Physics in Medicine and Biology*, Vol. 41, 2251–2269, 1996.
45. Wallace V. P., J. Fitzgerald, S. Shankar, N. Flanagan, R. Pye, J. Cluff, and D. D. Arnone, "Terahertz pulsed imaging of basal cell carcinoma ex vivo and in vivo," *British Journal Dermatology*, Vol. 151, 424–432, 2004, doi:10.1111/j.1365-2133.2004.06129.x.

## Millimeter-Wave Emissivity as a Metric for the Non-Contact Diagnosis of Human Skin Conditions

Amani Yousef Owda,<sup>1\*</sup> Neil Salmon,<sup>1</sup> Stuart William Harmer,<sup>2</sup> Sergiy Shylo,<sup>3</sup> Nicholas John Bowring,<sup>1</sup> Nacer Ddine Rezgui,<sup>1</sup> and Mamta Shah<sup>4</sup>

<sup>1</sup>Manchester Metropolitan University, Manchester, United Kingdom

<sup>2</sup>University of Chichester, Chichester, United Kingdom

<sup>3</sup>Usikov Institute of Radiophysics and Electronics National Academy of Sciences of Ukraine, Kharkiv, Ukraine

<sup>4</sup>Royal Manchester Children's Hospital, Manchester, United Kingdom

A half-space electromagnetic model of human skin over the band 30–300 GHz was constructed and used to model radiometric emissivity. The model showed that the radiometric emissivity rose from 0.4 to 0.8 over this band, with emission being localized to a layer approximately one millimeter deep in the skin. Simulations of skin with differing water contents associated with psoriasis, eczema, malignancy, and thermal burn wounds indicated radiometry could be used as a non-contact technique to detect and monitor these conditions. The skin emissivity of a sample of 30 healthy volunteers, measured using a 95 GHz radiometer, was found to range from 0.2 to 0.7, and the experimental measurement uncertainty was  $\pm 0.002$ . Men on average were found to have an emissivity 0.046 higher than those of women, a measurement consistent with men having thicker skin than women. The regions of outer wrist and dorsal forearm, where skin is thicker, had emissivities 0.06–0.08 higher than the inner wrist and volar forearms where skin is generally thinner. Recommendations are made to develop a more sophisticated model of the skin and to collect larger data sets to obtain a deeper understanding of the signatures of human skin in the millimeter wave band. *Bioelectromagnetics*. 38:559–569, 2017. © 2017 The Authors. *Bioelectromagnetics* published by Wiley Periodicals, Inc.

**Keywords:** permittivity; eczema; malignant lesions; vascularization; burns

### INTRODUCTION

Skin is the largest organ of the human body, playing important roles in temperature and water regulation. In contact with the environment, it suffers a variety of damage: cancer arising from exposure to UV radiation; thermal burns from sources of heat; psoriasis and eczema from exposure to chemicals, and through allergies. However, in response to this damage, the skin presents signatures that can be measured using non-contact millimeter wave sensors that could indicate the type and degree of the damage. This paper begins to explore those opportunities. Radiation in the millimeter wave band [Wiltse, 1984; Goldsmith et al., 1993] (30–300GHz) is ideally suited to measurement of the skin as it interacts strongly and only with the human body's skin layers [Gandhi and Riazi, 1986; Alekseev and Ziskin, 2007; Zhadobov et al., 2011; Smulders, 2012], thus enabling the potential for highly localized measurements. Furthermore, as the method presented in this paper does not involve artificial man-made sources of radiation, only

naturally present millimeter wave emission from the environment is required. There are no health perception issues, such as those associated with ionizing radiation of x-rays and gamma rays [Smulders, 2012].

This is an open access article under the terms of the Creative Commons Attribution License, which permits use, distribution and reproduction in any medium, provided the original work is properly cited.

Grant sponsors: Manchester Metropolitan University; Engineering and Physical Sciences Research Council (EPSRC).

Conflicts of interest: None.

\*Correspondence to: Amani Yousef Owda, School of Engineering, Manchester Metropolitan University, Manchester M1 5GD, United Kingdom. E-mail: amani.owda@stu.mmu.ac.uk

Received for review 7 October 2016; Accepted 20 July 2017

DOI: 10.1002/bem.22074  
Published online 24 August 2017 in Wiley Online Library (wileyonlinelibrary.com).

Millimeter wave sensors are operable in vivo and through medical dressings that are transparent to millimeter wave radiation, allowing diagnosis without their painful removal [Harmer et al., 2016].

It is well known that the level of water in human skin changes as a result of damage. Water levels rise as a result of vascularization around tumors and exudates from burns, while levels fall as a result of eczema or psoriasis [Griffiths et al., 2016]. Conveniently, the water molecule has a very high dipole moment, resulting in high dielectric permittivity in the millimeter wave band, which generates a large signature that can be measured using sensors in this band [Gandhi and Riazi, 1986; Alekseev and Ziskin, 2007; Zhadobov et al., 2011]. Furthermore, the permittivity changes with frequency over the band meaning lower frequencies can probe deeper skin layers, while higher frequencies can measure surface skin.

Human skin is made of three layers: the epidermis (outer layer), dermis (inner layer), and hypodermis (fat layer) [Alekseev and Ziskin, 2007]. The thickness of the epidermis layer is on average  $\sim 0.1$  mm, but it can be up to 0.7 mm on the palms of the hand. The thickness of the dermis layer varies over the body, but it is generally between 1.0 mm and 2.0 mm [Meema et al., 1964; Alekseev and Ziskin, 2007].

A convenient metric to describe the condition of human skin is emissivity, as this can be measured relatively easily using active (i.e., radar) and passive techniques [Grum and Becherer, 1979; Ulaby et al., 1981; Siegel and Howell, 2002]. A half-space electromagnetic model of the human skin was therefore developed to determine the emissivity of healthy skin and skin having a variety of medical conditions. The reflection coefficients for healthy skin and skin with second degree burns over the band 26.5–40 GHz were taken from Gao and Zoughi [2017] with open-ended coaxial probe data from Alekseev and Ziskin [2007], Egot-Lemaire and Ziskin [2011], and Smulders [2012]. Permittivity data were used from the parametric models such as the Cole-Cole model and Debye model [Gabriel et al., 1996a,b; Wallace et al., 2004]. Permittivity data of the healthy skin and skin with basal cell carcinoma (BCC) were calculated in the frequency band 100–300 GHz using a two-pole Debye model [Pickwell et al., 2004; Wallace et al., 2004; Pickwell et al., 2005].

Over the past few decades, technology in the millimeter wave band has shown steady and consistent development with an increasing number of applications. A wide variety of devices (sources, detectors, and mixers) have become available, enabling novel system architecture of imagers, non-imaging sensors, radiometers and radars to be developed. As an

*Bioelectromagnetics*

imaging sensor, these systems can deliver spatial resolutions of less than the wavelength, which in the millimeter wave band is down to about 1.0 mm. The instrument chosen to measure the emissivity of skin reported in this paper was a 95 GHz radiometer. This frequency was chosen as indications [Smulders, 2012] are that radiation at this frequency interacts mostly with the top 0.4 mm layer of the skin, so it is ideally suited to the measurements of the epidermis and dermis. The emissivity of skin in wrist and forearm areas of 30 volunteers was measured and analyzed and compared with models.

## MATERIALS AND METHODS

### Human Skin Emissivity Model

A simple half-space electromagnetic model was constructed to determine the emissivity of human skin directly from measurements or simulations of either the relative complex permittivity or complex reflectivity of human tissue. In the half-space model, one half is a semi-infinite layer of air, and the other half is a semi-infinite layer of skin, as shown in Figure 1.

Both layers are isotropic and homogenous and can be described by the relative complex permittivity values. Conservation of electromagnetic energy in the model gives the relationship between reflectance  $R$ , transmittance  $T$ , and emissivity  $\eta$  at the skin surface as:

$$R + T + \eta = 1. \quad (1)$$

The relationship between reflectance and reflectivity (fraction of incident complex field amplitude reflected),  $\Gamma$ , can be expressed as:

$$R = |\Gamma|^2 \quad (2)$$

The relationship between transmittance and transmissivity (fraction of complex field amplitude transmitted),  $t$ , can be expressed as:

$$T = |t|^2 \quad (3)$$

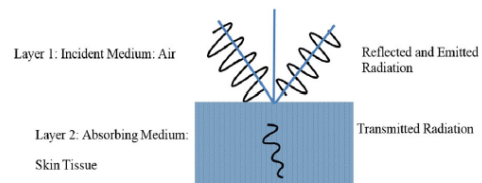


Fig. 1. Half-space electromagnetic model.

In this model, it is assumed that skin is a specular reflector, which is reasonable, as the surface roughness of skin is considerably less than the wavelength of radiation. Therefore, in this half-space model the normal and parallel polarization reflectivities of skin can be determined by the Fresnel equations [Born and Wolf, 1999] which are:

$$\Gamma_n = \frac{\sqrt{\epsilon_1} \cos(\theta_i) - \sqrt{\epsilon_2} \cos(\theta_t)}{\sqrt{\epsilon_1} \cos(\theta_i) + \sqrt{\epsilon_2} \cos(\theta_t)} \quad (4)$$

$$\Gamma_p = \frac{\sqrt{\epsilon_2} \cos(\theta_i) - \sqrt{\epsilon_1} \cos(\theta_t)}{\sqrt{\epsilon_2} \cos(\theta_i) + \sqrt{\epsilon_1} \cos(\theta_t)} \quad (5)$$

where  $\theta_i$  is the angle of incidence,  $\theta_t$  is the angle of transmission,  $\epsilon_1$  is the relative complex permittivity of medium 1, and  $\epsilon_2$  is the relative complex permittivity of medium 2.

The normal and parallel polarization transmissivities (likewise from the Fresnel equations) are:

$$t_n = \frac{2\sqrt{\epsilon_1} \cos(\theta_i)}{\sqrt{\epsilon_1} \cos(\theta_i) + \sqrt{\epsilon_2} \cos(\theta_t)} \quad (6)$$

$$t_p = \frac{2\sqrt{\epsilon_1} \cos(\theta_i)}{\sqrt{\epsilon_2} \cos(\theta_i) + \sqrt{\epsilon_1} \cos(\theta_t)}. \quad (7)$$

The penetration depth of the millimeter wave radiation in the human skin (defined as the distance over which the transmitted power reduces to a fraction of  $1/e^2$ ) is 0.782–0.23 mm over the frequency band 30–300 GHz [Gandhi and Riazi, 1986], and this is confirmed by simulations performed by the authors and presented in this paper. The short penetration depth is mainly due to the attenuating effects of water in the human body [Alekseev et al., 2008]. A consequence of this is that an accurate electromagnetic model of the skin may be realized without knowledge of deeper tissue properties. This property also enables highly localized measurements to be made of skin which cannot be obtained in the visible region of the spectrum, and so potentially constitutes the basis for a new diagnostic tool.

For an object that transmits no radiation ( $T=0$ ), the emissivity is equal to the fraction of the incident radiation that is absorbed, which becomes  $(1-R)$  as indicated by Equation (1). In a half-space model, therefore, the emissivity can be calculated by integrating  $(1-R)$  over the air-side hemisphere. The reflectance is a function of the polarization and the angle of incidence, and thus integration over all angles and polarization states is required to calculate the emissivity. As the illumination is isotropic and the

received wave is plane, the measurements are performed in the near field zone, where the distance to the receiver (described in Experimental Method section) is 1.0 cm. The power incident over an area,  $dS$ , of skin is:

$$dP_{\text{incident}} = IdS \int_{2\pi} \cos(\theta) d\Omega \quad (8)$$

where  $d\Omega$  is the solid angle that defines the direction of propagation of the radiation relative to the normal to the area  $dS$ , and  $I$  is the power density from the incident isotropic sources in units of watts per unit area, per steradian. Integration over the air-side hemisphere gives:

$$dP_{\text{incident}} = I\pi dS \quad (9)$$

The fraction of this incident power absorbed by the skin is then

$$\begin{aligned} dP_{\text{absorbed}} &= IdS \int_{2\pi} (1 - R(\theta)) \cos(\theta) d\Omega \\ &= I\pi dS \left( 1 - \int_0^{\pi/2} R(\theta) \sin(2\theta) d\theta \right) \end{aligned} \quad (10)$$

The emissivity  $\eta$  is the fraction of the incident radiation that is absorbed; hence, from Equations (9) and (10) this is:

$$\eta = 1 - \int_0^{\pi/2} R(\theta) \sin(2\theta) d\theta. \quad (11)$$

In the case of unpolarized sources, the reflectance  $R(\theta)$  must be replaced by the average of the normal and parallel polarization reflectances.

$$R(\theta) = \frac{1}{2} [(Rn(\theta) + Rp(\theta))] \quad (12)$$

Equation (11) provides a relationship between the emissivity and the complex permittivity of the sample. The integral in Equation (11) is not easily evaluated analytically and so a numerical approach, implemented in Matlab, was used to compute emissivity values. Equations (1) to (12) were evaluated numerically using an algorithm developed by the authors in the language of Matlab.

The uncertainties in the simulated emissivity values can be determined by error propagation of uncertainties in the relative complex permittivity values through Equations (1) to (12). Given the uncertainty in the permittivity from the single relaxation Debye model is  $\pm 0.05$  [Gabriel et al., 1994; Gabriel et al., 1996a; Gabriel and Peyman, 2006; Sasaki et al., 2014],

error propagation indicates the uncertainty in the emissivity of skin is  $\pm 0.006$ , unless otherwise stated; this is the case throughout the paper. With typical values of emissivity ranging from 0.4 to 0.75, this indicates a precision of less than  $\sim 1.5\%$ .

**Experimental Method to Measure Human Skin Emissivity**

Human skin emissivity can be measured using a radiometer [Harmer et al., 2016]. The output of such a device is a voltage  $V$  in volts, expressed as:

$$V = \alpha(T_b + T_N) \tag{13}$$

where  $T_b$  is the radiation temperature of the source (in this case the skin) expressed in Kelvin,  $\alpha$  is the receiver responsivity (in Volts per Kelvin), and  $T_N$  the receiver noise temperature (also in Kelvin). However, the radiation temperature of the source can also be expressed in terms of the source emissivity  $\eta$ , skin thermodynamic (or physical) temperature  $T_s$ , and background illumination radiation temperature  $T_0$  [Bardati and Solimini, 1983]:

$$T_b = (1 - \eta)T_0 + T_s\eta \tag{14}$$

Calibration of this radiometer can be done using two black body radiator sources, one at a low temperature  $T_C$  and the other at a high temperature  $T_H$  [Wyatt, 1978; Ulaby et al., 1981; Pozar, 2011]. This process calibrates the receiver responsivity and receiver noise temperature, both of which are assumed to be constant; or alternatively, the system response is assumed to be linear. If the measurements are done indoors and in an anechoic environment (where there is no radiometric emission from people or lower emissions from outdoors), the low temperature calibration source can be a foam absorber at ambient temperature  $T_C$ . Under these circumstances, the voltage output when measuring the low temperature calibration source becomes:

$$V_C = \alpha(T_C + T_N) \tag{15}$$

and when measuring the high temperature calibration source it is:

$$V_H = \alpha(T_H + T_N) \tag{16}$$

From this calibration procedure the receiver responsivity is:

$$\alpha = \frac{(V_H - V_C)}{(T_H - T_C)} \tag{17}$$

and the emissivity from Equation (14) becomes:

$$\eta = \frac{(V - V_C)(T_H - T_C)}{(V_H - V_C)(T_S - T_C)} \tag{18}$$

A radiometer sensitive at 95 GHz was used for the measurements of human skin. The equipment for measurement and calibration comprised: a horn antenna connected through a circulator to a radiometer, two pieces of carbon-loaded foam absorbers acting as hot and cold calibration sources (carbon loaded foam absorber type: Eccosorb AN-73, Laird, Geel, Belgium), and the subject tissue to be measured, as illustrated in Figure 2.

The radiometer is essentially a low noise, high gain amplifier, followed by a detector, with sufficient sensitivity to detect the thermal (Planck) emission from ambient temperature sources over the frequency band (94–96 GHz). Radiometers have the performance metric of noise temperature measured in Kelvin; the lower the figure the more sensitive the system. The particular radiometer used for this research was purchased from Millitech (Direct Detector Radiometer, Northampton, MA). Its noise temperature was measured in the course of our research to be 453.7 K, which represents a good performance for this application.

A circulator operating over the frequency band (94–96 GHz) was purchased from ELVA-1 Microwave Handelsbolag (CR-10/95/2, Furulund, Sweden). The circulator was placed between the horn antenna

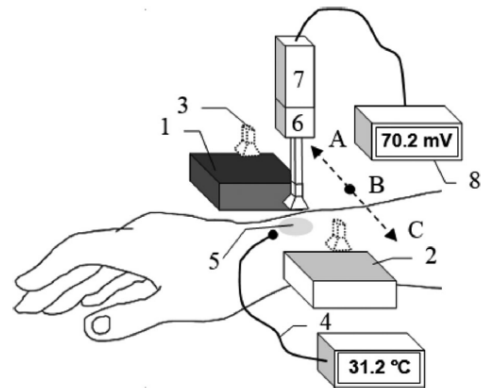


Fig. 2. In the experimental set-up radiometric emission at 95 GHz is collected by a moveable horn antenna (3) at positions: A to measure a hot calibration source (1), B to measure skin (5), and C to measure cold calibration source (2). A thermocouple (4) is used to measure thermodynamic temperature of skin, a digital voltmeter (8) is used to measure output voltage of calibration sources and skin. The horn antenna connected through a waveguide circulator (6) to a radiometer (7) that consists of low noise amplifier and detector.

and receiver. This device prevents radiation that has passed into the radiometer from being reflected back out of the system, which may be reflected from the subject back into the radiometer. Its function in the system was to minimize the effects of spurious signals that would otherwise arise from these retro-reflections. In trials to identify spurious signals, by reflecting emissions from the radiometer back into the receiver, none were found.

The complete system, except for an opening for the subject to be measured, was enclosed in an anechoic region made by surrounding the majority of the radiometer and antenna with carbon-loaded absorbing foam. This prevented radiation from external sources, be it from the outdoors or other people in the environment, getting into the system to corrupt signals.

A horn antenna has a rectangular aperture ( $20 \times 15 \text{ mm}^2$ ) and a nominal gain of 20 dBi, effective over the frequency band (90–100) GHz. The horn antenna was purchased from Flann Microwave (27240-20, Cornwall, United Kingdom). During the experiment, the horn antenna was moved laterally by hand to measure emission from the subject and from the hot and cold calibration sources in relatively quick succession. It typically takes about 1.0 min to complete this measurement process, allowing for a settling time, which minimizes systematic errors associated with drift. The horn antenna during these measurements was located approximately  $\sim 1.0 \text{ cm}$  away from the sources, and the antenna beam pattern on the skin was approximately 20 mm across. The hot calibration source was stabilized at a temperature of  $53.8^\circ\text{C}$  with a precision that was smaller than a fraction of a degree by using a Peltier plate heater/cooling device from European Thermodynamics (APH-241-14-11-E, Leicestershire, United Kingdom). The cold calibration source remained at the ambient temperature of  $23.0^\circ\text{C}$ , as maintained by the building central heating system. The carbon loaded foam absorbers had emissivity values greater than 0.99 in this frequency band, thus they behaved as good approximations to a black body emitter.

Regions of the human body measured by this method were areas on the wrist and forearm. A standard thermocouple from Leaton Tech (L812, Shenzhen, China) was used to measure the skin surface temperature in these regions directly, before and after the measurement. The temperature was indicated via a digital readout with a  $\pm 0.5^\circ\text{C}$  absolute measurement uncertainty and  $0.1^\circ\text{C}$  step size. An infrared thermometer from Maplin (N85FR, Manchester, United Kingdom) was used to measure the thermodynamic temperatures of the calibration

sources and had an absolute measurement uncertainty of  $\pm 1.5^\circ\text{C}$ . The devices were cross-calibrated by measuring the temperature of the same source, so the relative uncertainty of the measurement was much smaller, typically less than  $0.1^\circ\text{C}$ . Typical voltage measurements were up to 100 mV with a precision of 0.1 mV. Error propagation through Equation (18) indicates the uncertainty on the measured emissivity is  $\pm 0.002$ .

## SIMULATION RESULTS

### Simulations of Human Skin Emissivity

Simulations of human skin emissivity were made with the half-space model and compared to the results of an existing three-layer model [Harmer et al., 2016], then used to predict emissivity signatures for skin with differing water contents, burned damaged skin, and skin mutated by basal cell carcinoma.

### Model Comparison: Half-Space Versus Three-Layer Model

The half-space model described above (Equations 2–11) is a relatively simple model used to describe the emissivity of human skin. In this first simulation a comparison was made between this model and the more complex three-layer model comprising: a semi-infinite layer of air, 1.44 mm layer of skin, and a semi-infinite layer of fat. The relative complex permittivity of skin was calculated from measurement of reflection coefficients of skin [Dancila et al., 2014], while the relative complex permittivity of fat tissue was calculated using Gabriel model [Gabriel et al., 1996a]. Comparison between the two models was made for skin with three different water contents, namely 50%, 75%, and 95%, and results presented over the frequency band of 30–100 GHz are in Figure 3. These results indicate that emissivity rises with frequency and falls with skin water content. The comparison shows that the results for the half-space model are exactly the same as those for the three-layer model.

### Skin With Differing Water Contents (Psoriasis, Normal Healthy Skin, and Malignancy)

The simulations of the emissivity of in vivo skin for the three different water contents, 50%, 75%, and 95%, shown in Figure 3, correspond to water contents that are representative of dry skin, normal healthy skin, and skin with malignant lesions, respectively [Suntzeff and Carruthers, 1946; Leunig et al., 1994; Alekseev and Ziskin, 2007; Earle, 2016]. The emissivity of skin with a 95% water content is lower by  $\sim 0.12$  than that

*Bioelectromagnetics*

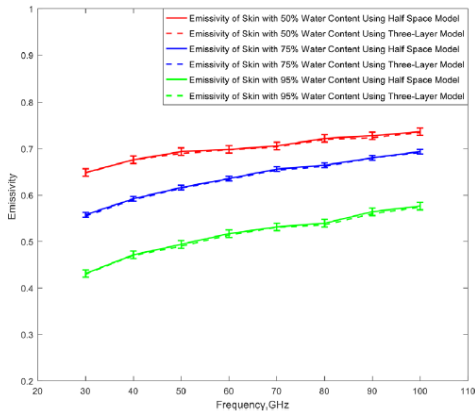


Fig. 3. Simulations of the emissivity of human skin for the half-space and three-layer model show how increasing water content lowers emissivity.

of normal healthy skin with a water content of 75%. Properties and characteristics of skin with differing water contents are summarized in Table 1.

**Skin After the Application of Aqueous Gel (30–100 GHz)**

In this simulation, a comparison was made between the emissivity of normal healthy skin and skin after the application of an aqueous gel (a mixture that consists mainly of water with a thickener, such as ultrasound scan gel). This simulation used the relative complex permittivity of in vivo skin [Gabriel et al., 1996a]. The simulated emissivity rose over the frequency band from 30 GHz to 100 GHz, as shown in Figure 4, indicating emissivity is less for moistened skin, on average over the band by about 0.016. At 100 GHz this difference in emissivity rose to ~0.025, with error propagation analysis indicating the uncertainty was ±0.0011. Aqueous gel can be used to

achieve good contact between open-ended coaxial probes and the human skin. Adding gel to the human skin increases the hydration level of the stratum corneum layer of skin and reduces the inhomogeneity of skin [Gabriel et al., 1996a; Gabriel and Peyman, 2006]. This better contact between the probe and skin reduced the systematic uncertainties in the dielectric permittivity measurements arising from the otherwise variable coupling between the probe and skin. Furthermore, the gel that consists mainly of water could be used in measurements of the dielectric properties of skin in wet state, as it can stay adhered to the skin surface longer than water. There are ethical issues associated with performing measurements on patients [Harmer et al., 2016], making the moistened skin a convenient in vivo model for damaged skin, where the damage affects the water content of the skin.

**Wet and Dry Human Skin Samples (90–100 GHz)**

In this simulation a comparison was made between the emissivity of wet and dry skin samples taken from a human cadaver. The wet samples were taken from a 10% formaldehyde solution, rinsed in water and then measured, whereas the dry samples were dried for a 4.0 h period prior to the measurements [Alabaster, 2003]. Measurements of the relative complex permittivity were made over the frequency band 90–100 GHz [Alabaster, 2003] using free-space method of the transmission and reflection coefficients, and these measurements were taken and used in the half-space model to calculate the emissivity values of wet and dry skin; they are presented in Figure 5. The figure shows higher emissivity values for dry skin, with the difference being ~0.09 ± 0.009 across the band.

**Comparison of Skin Emissivity With the Harmer Model**

Emissivity calculated using the half-space model presented here has been compared with other methods

TABLE 1. Characteristics of Skin With Differing Water Contents

Parameters	Skin type	References
Skin with 50% water content		
Skin condition	Dry: eczema and psoriasis	Earle [2016]
Complex permittivity	6.86-j3.33 at 100 GHz	Dancila et al. [2014]
Return loss (S11)	-9.22 dB at 100 GHz	Dancila et al. [2014]
Skin with 75% water content		
Skin condition	Healthy skin	Alekseev and Ziskin [2007]
Complex permittivity	7.34-j5.71 at 100 GHz	Dancila et al. [2014]
Return loss (S11)	-8.59 dB at 100 GHz	Dancila et al. [2014]
Skin with 95% water content		
Skin condition	Skin with malignant lesion	Leunig et al. [1994]
Complex permittivity	7.55-j13.72 at 100 GHz	Dancila et al. [2014]
Return loss (S11)	-5.81 dB at 100 GHz	Dancila et al. [2014]

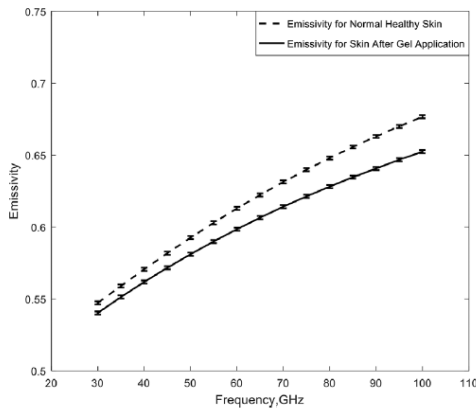


Fig. 4. The simulated emissivity of healthy skin before and after it has been moistened by the application of an aqueous gel.

[Harmer et al., 2016]. The comparison, shown in Table 2, shows a consistent rise in emissivity with frequency, with values from this model presented here being 2.0% lower. This difference may be accounted for by the two slightly different ways in which the total reflectance is calculated. The study in this paper is a refinement on the Harmer model, integrating emission over the air-side hemisphere, which includes reflectance at all angles from normal to glancing incidence, whereas Harmer assumes a plane wave normal to the skin surface. In the Harmer model [Harmer et al., 2016], human skin was assumed to be a lossy dielectric material and the reflection from inner layers was neglected. In this model, the relative

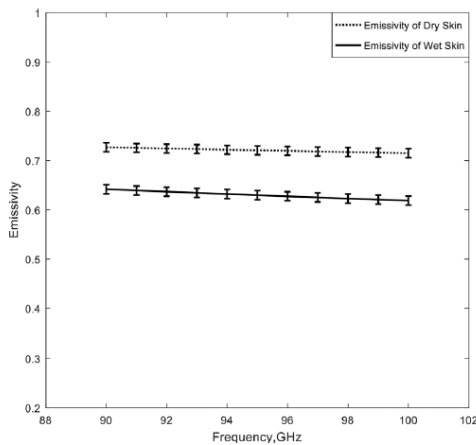


Fig. 5. Simulations of the emissivities of samples of dry and wet human skin.

complex permittivity measurements over the frequency band 30–37 GHz were used and converted to emissivity.

**Burned and Unburned Porcine Skin Samples**

Simulation of the emissivity of burned and unburned skin was made using the complex reflection coefficient measurements over the frequency band 30–40 GHz [Gao and Zoughi, 2017], and the results are shown in Figure 6. In these experiments burn damage was induced in porcine skin samples after the animals had been slaughtered [Gao and Zoughi, 2017]. The simulations show a rise in emissivity with frequency and that the burned skin had an emissivity ~0.05 higher than that of unburned skin. The absolute uncertainty is estimated to be ±0.005 from error propagation analysis.

**Skin With Basal Cell Carcinoma**

The relative complex permittivity of healthy skin and skin with BCC was calculated in the frequency band 100–300 GHz using a two pole Debye model [Pickwell et al., 2004; Wallace et al., 2004; Pickwell et al., 2005]. The parameters of the model were extracted from measurements performed on five patients. From the relative complex permittivity data, the emissivity of healthy skin and skin with basal cell carcinoma was calculated using the model discussed in section two and Equation (11); results are shown in Figure 7.

The simulations indicate emissivity rises with frequency and that the emissivity of skin with basal cell carcinoma was ~0.03 lower than that of normal healthy skin. The uncertainties in the simulated emissivity values over the frequency band were ±0.0016 (100–140 GHz), ±0.002 (150–220 GHz), and ±0.003 (230–300 GHz), estimated by error propagation analysis.

Other studies of skin with BCC using in vivo reflectivity measurements [Taeb et al., 2013] have estimated the relative permittivity to be 15.0-j20.5 at 42 GHz, and that of healthy skin to be 11.5-j14.3. Using these permittivity values in the above half-space model gives emissivity values of 0.52 and 0.57 for skin with BCC and healthy skin, respectively.

**EXPERIMENTAL RESULTS**

**Measurements of Human Skin Emissivity**

Measurements of human skin emissivity of 12 female and 18 male healthy volunteers (having a variety of ethnicities and ages) were made at four measurement locations on the body, which were: 1)

*Bioelectromagnetics*

**TABLE 2. Simulated Emissivity of Skin Over the 30–37 GHz Spectral Region**

Frequency (GHz)	Simulated emissivity from Harmer et al. [2016]	Simulated emissivity from the half-space model of this paper
30	0.61	0.59
31	0.62	0.61
32	0.63	0.61
33	0.64	0.62
34	0.65	0.62
35	0.66	0.63
36	0.67	0.64
37	0.68	0.65

inner wrist, 2) outer wrist, 3) dorsal surface of the forearm, and 4) volar side of the forearm; these are presented in Figure 8a and b). The mean emissivity over the sample of 30 volunteers was 0.413 and standard deviation in the sample was 0.091, for a measurement uncertainty of  $\pm 0.002$ . Upon closer inspection, trends can be seen in these data related to gender and thickness of the skin layers for different regions of the body.

Statistical analysis on the data indicates that females have a sample mean ( $\mu$ ) emissivity of 0.3846 with a sample standard deviation ( $\sigma$ ) of 0.0877, generating a standard error in the mean ( $\sigma/\sqrt{n}$ , where  $n$  is the number of samples) of 0.0253. This is considerably larger than the estimated experimental uncertainty in the measurements of  $\pm 0.002$ . Males have a sample mean emissivity of 0.431 with a sample standard deviation of 0.0878, generating a standard error in the mean of 0.0207. The sample means of the

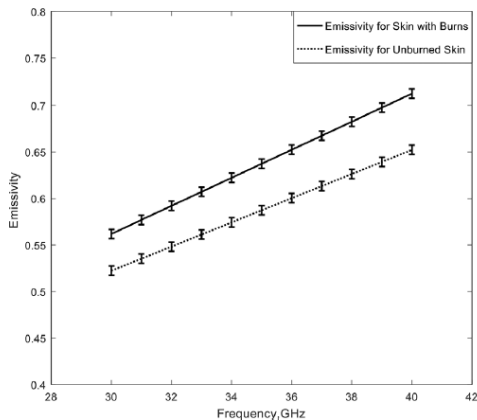


**Fig. 6. Simulations of the emissivities of unburned and second-degree burn damaged porcine skin samples.**

*Bioelectromagnetics*

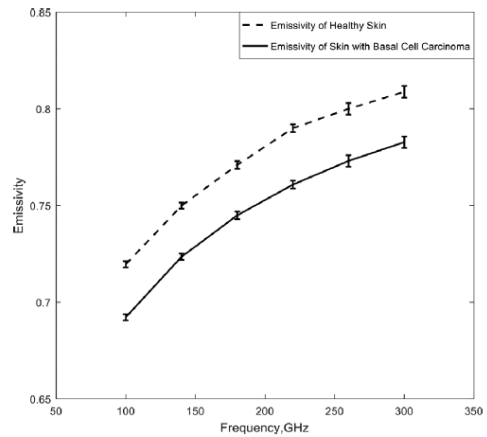


**Fig. 7. Simulations of the emissivities of healthy skin and skin with basal cell carcinoma.**

emissivity values of the male participants are higher by 0.0464 than those of the female participants, a difference of approximately twice the standard error. This indicates that there are consistent differences in the emissivity values of the skin between females and males.

The sample mean (over all 30 volunteers) of the differences in emissivity values between the inner and outer wrist locations is 0.06 with a sample standard deviation of 0.035, generating an error in the mean of 0.0064. This difference is 9.3 times the standard error, indicating statistically significant differences between the emissivity of the inner and outer wrist locations.

The sample mean of the differences in the emissivity values between the dorsal and volar side of the forearm is 0.08 with a sample standard deviation of 0.041, generating an error in the mean of 0.0075. This difference is 10.7 times the standard error, indicating statistically significant differences between the emissivity of dorsal and volar side of the forearm.

**DISCUSSION**

As simulated emissivities from the half-space and three-layer model of human skin (Fig. 3) were identical (within simulation uncertainty), radiation from the skin must originate from the layer no deeper than  $\sim 1.44$  mm, as that was the upper layer skin thickness in the three-layer model. This is consistent with the statement from Gandhi and Riazi [1986] that radiation over the band 30–300 GHz is absorbed within a distance of 0.782–0.238 mm from the surface of the skin. It also means that the simulations in this

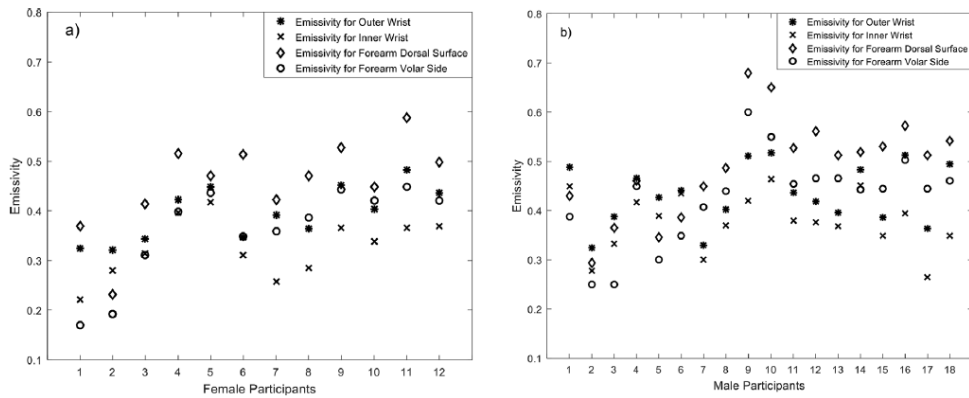


Fig. 8. Emissivity of human skin measured at 95 GHz from 12 female (a) and 18 male (b) volunteers at four different locations on the body.

paper (using the simpler half-space model) are sufficient to describe the electromagnetic behavior of human skin over the frequency band 30–300 GHz. These simulations also show a rise in the emissivity of skin with frequency, which is a behavior that directly results from the decrease in magnitude of relative complex permittivity of water over this frequency band. As with other authors [Zhadobov et al., 2011; Smulders, 2012], we conclude that the water content of skin dominates its electromagnetic behavior in the millimeter-wave band.

Simulations of the emissivity of human skin over the 30–100 GHz band (Fig. 4) before and after the application of an aqueous gel indicate the gel reduced emissivity at all frequencies on average over the band by  $\sim 0.016$ . Simulations of samples of wet and dry human skin indicated emissivity over the band 90–100 GHz was lower for wet skin than for dry skin by  $\sim 0.09$  (Fig. 5). The lower value for wet skin was consistent with the high relative permittivity of water resulting in higher reflectance, and therefore lower emissivity.

Simulations of the emissivity of porcine skin indicate that the burned samples had an emissivity 0.05 higher than unburned samples (Fig. 6). The interpretation here is that the burning process removes water from the skin, thereby reducing the reflectance and increasing emissivity. For living organisms, however, a burn would result in exudates (mainly water) being introduced around the wound which would reduce the emissivity of the wound site. Knowledge of this and the transparency of bandages in the millimeter wave region has led [Harmer et al., 2016] to investigate of the feasibility of using millimeter waves to monitor wound healing under bandages.

Simulations of the emissivity of skin with varying water contents (50%, 75%, and 95% in Fig. 3) over the band 30–100 GHz show that emissivity rises with frequency, but falls with skin water content. This is due to the electromagnetic properties of water dominating the electromagnetic properties of skin, providing a potentially viable, non-contact method to assist in the diagnosis of medical conditions where the skin water content is affected, such as psoriasis, eczema, and malignancy [Hagness et al., 1999; Mehta et al., 2006].

Simulations of the emissivity of human skin with basal cell carcinoma over the band 100–300 GHz indicate values were 0.03 lower than that of healthy tissue (Fig. 7). This is consistent with the interpretation that malignancy increases local vascularization, which through increased blood flow, raises the water content of tissue resulting in reduced emissivity at the site. This indicates potential opportunities of the technique for initial detection of malignancy in basal cells, which may not easily be observed in the visible band of the spectrum due to opacity of the epidermis.

Experimental measurements of the emissivity at 95 GHz from the wrists and arms of 30 volunteers indicate that there was a scatter over a range 0.2–0.7, and this was much greater than the experimental measurement uncertainty of  $\pm 0.002$ . Estimating the sample mean emissivity values for the 18 males and 12 females separately indicates that the difference between male and female emissivity is twice the sample standard error in the mean (Fig. 8). This finding is consistent with the skin of males being thicker than that of females [Derraik et al., 2014].

Experimental measurements of the differences in emissivity values between the inner and outer wrist,

and between the dorsal and volar regions of the forearm of all 30 volunteers indicate a difference approximately 10 times the standard error of the measurement. This large difference is likely to be due to much thicker skin on the outer wrist and dorsal area of the forearm. The thinner skin on the inner wrist and volar regions [Gray, 1918] means that radiation is more readily reflected from the blood vessels [Millington and Wilkinson, 2009], and this reduces emissivity.

Simulated emissivities from the half-space model show that radiometric emissivity rose from 0.4 to 0.8 over the frequency band 30–300 GHz, with emission being localized to a layer 1.0 mm deep in the skin. At 95 GHz the emissivity of healthy skin was simulated to be in the range 0.66–0.68, as shown in Figures 3 and 4. For comparison, the emissivity from a sample of 30 healthy volunteers, presented in Figure 8, was measured to range from 0.2 to 0.7, with the mean and standard deviation being 0.413 and 0.091, respectively. The lower values of emissivity are results of measuring particularly thin skin on the inner wrist area, whereas higher values of emissivity are results of measuring thick skin on the dorsal surface area. The spread in the emissivities also indicates the variability from person to person. The simulated emissivity values of healthy skin are in agreement with the measured values, and also in agreement with the simulations from the Harmer model [Harmer et al., 2016], as illustrated in Table 2.

The measurements indicate that differences in emissivities between thicker regions of skin (on the outer wrist and dorsal forearm) and thinner regions of skin (on the inner wrist and volar forearm) are in the range from 0.06 to 0.08. However, simulations indicate a larger variation than this for unhealthy skin, as indicated in Figures 3 and 5. It is therefore recommended that further measurements be made of the skin of participants having a range of medical conditions such as psoriasis, eczema, malignancy, and thermal burn, to better understand the effects of these conditions on emissivity.

Generally, it is recommended that further measurements be made on larger and more varied groups of individuals to study how emissivity varies with gender, age, ethnicity, and state of health. This might be done at a range of frequencies, the lower frequencies offering greater penetration into the skin and underlying tissue. It is further recommended that a more sophisticated electromagnetic model of the skin be developed to describe the complex structure of the epidermis and dermis, which might include using an electromagnetic simulation tool [Feldman et al., 2009], so that greater understanding

*Bioelectromagnetics*

can be made of the interpretation of future measurements.

## CONCLUSIONS

A half-space electromagnetic model showed that emissivity of human skin rose from 0.4 to 0.8 over the 30–300 GHz band, and this behavior was consistent with the fall in the magnitude of the dielectric permittivity of water over this region. Simulations showed that the emissivity of the skin varied with water content, and this could be used as a metric to detect and monitor malignancy, eczema, psoriasis, and burn healing in skin. Simulations indicated that interaction of the millimeter waves was in the region from the skin surface to  $\sim 1.0$  mm below the surface, with greater (or less) penetration at the lower (or higher) frequencies over the 30–300 GHz band, suggesting opportunities for highly localized and selective skin layer measurements.

Radiometric measurements made on a sample of 30 volunteers at 95 GHz were consistent with the simulations presented. The measurements showed that on average the emissivity of men was higher than that of women by  $\sim 0.0464$ , with standard error of the mean 0.0207 and experimental uncertainty  $\pm 0.002$ . This supports the knowledge that on average the skin of men is thicker than that of women [Derraik et al., 2014]. Measurements also show that the emissivity of thick layers of skin in the human body, such as the outer wrist and dorsal forearm, was higher than those of the inner wrist and volar forearm by about 0.06–0.08, this difference being approximately 10 standard errors. Again, the higher emissivity is indicative of thicker skin.

These measurements indicate the emissivity of human skin in the millimeter wave band is rich in information about skin and that these measurements can be made in tens of seconds by a non-contact sensor with high precision. Simulations indicate this richness could be potentially exploited for the diagnosis of a range of medical conditions. Research continues in this area to understand in detail how and why emissivity varies over a much broader sample of the population of healthy volunteers and patients.

## REFERENCES

- Alabaster CM. 2003. Permittivity of human skin in millimetre wave band. *Elec Lett* 39:1521–1522.
- Alekseev SI, Radzievsky AA, Ziskin MC. 2008. Millimetre wave dosimetry of human skin. *Bioelectromagnetics* 29:65–70.
- Alekseev SI, Ziskin MC. 2007. Human skin permittivity determined by millimeter wave reflection measurements. *Bioelectromagnetics* 28:331–339.

- Bardati F, Solimini D. 1983. Radiometric sensing of biological layered media. *Radio Sci* 18:1393–1401.
- Born M, Wolf E. 1999. *Principles of Optics*. Cambridge, United Kingdom: Cambridge University Press. pp 24–74.
- Dancila D, Augustine R, Topfer F, Dudorov S, Hu X, Emestam L, Tenerz L, Oberhammer J, Rydberg A. 2014. Millimeter wave silicon micromachined waveguide probe as an aid for skin diagnosis—results of measurements on phantom material with varied water content. *Skin Res Technol* 20:116–123.
- Derraik JGB, Rademaker M, Cutfield WS, Pinto TE, Tregurtha S, Faherty A, Peart JM, Drury PL, Hofman PL. 2014. Effects of age, gender, BMI, and anatomical site on skin thickness in children and adults with diabetes. *PLoS ONE* 9:e86637.
- Earle L. 2016. *Dry Skin and Eczema: The Best Regimes for Really Effective Relief*. London, United Kingdom: Hachette. pp 5–50.
- Egot-Lemaire SJ-P, Ziskin MC. 2011. Dielectric properties of human skin at an acupuncture point in the 50-75 GHz frequency range. A pilot study. *Bioelectromagnetics* 32:360–366.
- Feldman Y, Puzenko A, Ishai PB, Caduff A, Davidovich I, Sakran F, Agranat AJ. 2009. The electromagnetic response of human skin in the millimetre and submillimetre wave range. *Phys Med Biol* 54:3341–3363.
- Gabriel C, Chan TY, Grant EH. 1994. Admittance models for open ended coaxial probes and their place in dielectric spectroscopy. *Phys Med Biol* 39:2183–2200.
- Gabriel C, Peyman A. 2006. Dielectric measurement: Error analysis and assessment of uncertainty. *Phys Med Biol* 51:6043–6046.
- Gabriel S, Lau RW, Gabriel C. 1996a. The dielectric properties of biological tissues: III. Parametric models for the dielectric spectrum of tissues. *Phys Med Biol* 41:2271–2293.
- Gabriel S, Lau RW, Gabriel C. 1996b. The dielectric properties of biological tissues: II. Measurements in the frequency range 10 Hz to 20 GHz. *Phys Med Biol* 41:2251–2269.
- Gandhi OP, Riaz A. 1986. Absorption of millimeter waves by human beings and its biological implications. *IEEE Trans Microw Theory Tech* 34:228–235.
- Gao Y, Zoughi R. 2017. Millimeter wave reflectometry and imaging for noninvasive diagnosis of skin burn injuries. *IEEE Trans Instrument Measure* 66:77–84.
- Goldsmith PF, Hsieh C-T, Huguenin GR, Kapitzky J, Moore EL. 1993. Focal plane imaging systems for millimeter wavelengths. *IEEE Trans Microw Theory Tech* 41:1664–1675.
- Gray H. 1918. *Anatomy of the Human Body*. Philadelphia, Pennsylvania: Lea & Febiger. pp 1320–1330.
- Griffiths C, Barker J, Bleiker T, Chalmers R, Creamer D. 2016. *Rook's Textbook of Dermatology*. Oxford, United Kingdom: Wiley-Blackwell. pp 50–300.
- Grum F, Becherer RJ. 1979. *Optical Radiation Measurements. Volume 1—Radiometry*. New York, New York: Academic Press. pp 40–100.
- Hagness SC, Taflove A, Bridges JE. 1999. Three-dimensional FDTD analysis of a pulsed microwave confocal system for breast cancer detection: Design of an antenna—Array element. *IEEE Trans Antennas Propag* 47:783–791.
- Harmer SW, Shylo S, Shah M, Bowring NJ, Owda AY. 2016. On the feasibility of assessing burn wound healing without removal of dressings using radiometric millimetre-wave sensing. *Prog Electromagn Res* 45:173–183.
- Leunig M, Goetz AE, Gamarra F, Zetterer G, Messmer K, Jain RK. 1994. Photodynamic therapy-induced alterations in interstitial fluid pressure, volume and water content of an amelanotic melanoma in the hamster. *Br J Cancer* 69:101–103.
- Meema HE, Sheppard RH, Rapoport A. 1964. Roentgenographic visualization and measurement of skin thickness and its diagnostic application in acromegaly. *Radiology* 82:411–417.
- Mehta P, Chand K, Narayanswamy D, Beetner DG, Zoughi R, Stoecker WV. 2006. Microwave reflectometry as a novel diagnostic tool for detection of skin cancers. *IEEE Trans Instrument Measure* 55:1309–1316.
- Millington PF, Wilkinson R. 2009. *Skin (Biological Structure and Function)*. Cambridge, United Kingdom: Cambridge University Press. pp 48–80.
- Pickwell E, Cole BE, Fitzgerald AJ, Pepper M, Wallace VP. 2004. In vivo study of human skin using pulsed terahertz radiation. *Phys Med Biol* 49:1595–1607.
- Pickwell E, Fitzgerald AJ, Cole BE, Taday PF, Pye RJ, Ha T, Pepper M, Wallace VP. 2005. Simulating the response of terahertz radiation to basal cell carcinoma using ex vivo spectroscopy measurements. *J Biomed Opt* 10:21.
- Pozar DM. 2011. *Microwave Engineering*. Hoboken, New Jersey: John Wiley & Sons. pp 497–511.
- Sasaki K, Wake K, Watanabe S. 2014. Development of best fit Cole-Cole parameters for measurement data from biological tissues and organs between 1 MHz and 20 GHz. *Radio Sci* 49:459–472.
- Siegel R, Howell JR. 2002. *Thermal Radiation Heat Transfer*. New York, New York: Taylor & Francis. pp 1–30.
- Smulders PFM. 2012. Analysis of human skin tissue by millimetre-wave reflectometry. *Skin Res Technol* 19:e209–e216.
- Suntzeff V, Carruthers C. 1946. The water content in the epidermis of mice undergoing carcinogenesis by methylcholanthrene. *Cancer Res* 6:574–577.
- Taeb A, Gigoyan S, Safavi-Naeini S. 2013. Millimetre-wave waveguide reflectometers for early detection of skin cancer. *IET Microw Antennas Propag* 7:1182–1186.
- Ulaby FT, Moore RK, Fung AK. 1981. *Microwave Remote Sensing: Active and Passive. Volume I: Microwave Remote Sensing Fundamentals and Radiometry*. London, United Kingdom: Artech House. pp 1282–1450.
- Wallace VP, Fitzgerald J, Shankar S, Flanagan N, Pye R, Cluff J, Arnone DD. 2004. Terahertz pulsed imaging of basal cell carcinoma ex vivo and in vivo. *Br J Dermatol* 151:424–432.
- Wiltse JC. 1984. History of millimeter and submillimeter waves. *IEEE Trans Microw Theory Tech* 32:1118–1127.
- Wyatt CL. 1978. *Radiometric Calibration: Theory and Methods*. New York, New York: Elsevier. pp 67–76.
- Zhadobov M, Chahat N, Sauleau R, Quement CL, Drean YL. 2011. Millimeter-wave interactions with the human body: State of knowledge and recent advances. *Int J Microw Wirel Technol* 3:237–247.

### C.3: Journal Paper 3:

*Progress In Electromagnetics Research M*, Vol. 45, 173–183, 2016

## On the Feasibility of Assessing Burn Wound Healing without Removal of Dressings Using Radiometric Millimetre-Wave Sensing

Stuart W. Harmer<sup>1, \*</sup>, Sergiy Shylo<sup>2</sup>, Mamta Shah<sup>3</sup>,  
Nicholas J. Bowring<sup>1</sup>, and Amani Y. Owda<sup>1</sup>

**Abstract**—The authors present transmission data, taken at Ka (36 GHz) and W (95 GHz) bands in the millimetre-wave region of the electromagnetic spectrum, for various dressing materials used in the treatment and management of burn wounds. The results show that such materials are highly transparent (typically > 90% transmission) and, in their dry state, will permit the sensing of the surface of the skin through the thick layers (> 2 cm) of different dressings typically applied in medical treatment of burn wounds. Furthermore, the authors present emissivity data, taken at the same frequency bands, for different regions of human skin on the arm and for samples of chicken flesh with and without skin and before and after localised heat treatment. In vivo human skin has a lower emissivity than chicken flesh samples, 0.3–0.5 compared to 0.6–0.7. However, changes in surface emissivity of chicken samples caused by the short-term application of heat are observable through dressing materials, indicating the feasibility of a millimetre-wave imaging to map changes in tissue emissivity for monitoring the state of burn wounds (and possibly other wounds) non-invasively and without necessitating the removal of the wound dressings.

### 1. INTRODUCTION

Burns are a very common cause of injury with over a quarter of a million people requiring treatment a year in the UK and costing millions of dollars p.a. [1]. Globally, this figure is far greater. The majority of these burn wounds are partial thickness burns with a potential for spontaneous wound healing from the appendage remnants in the depths of the dermis and surrounding undamaged skin.

The current management of burn wounds requires that the dressings are removed regularly for inspection of the progress of wound healing as well as to detect signs of wound infection. This inevitably causes pain, discomfort and anxiety for the patients, particularly for children. In addition, it also causes distress to the parents/carers and the frequent visits to hospital results in loss of person-hours from work. Furthermore, frequent exposure and handling of the wounds for washing during dressing changes could potentially cause damage to the neo-epithelium covering the wound bed and increase the risk of infection. Although millimetre-wave has been suggested and as a contact probe to assist in the diagnosis of skin cancers [2–8] and there are techniques which utilise infra-red, thermal imagery to assess the wound [9], these require the wound to be exposed. Currently, there are no tools which could assess the state of the healing burn wound without removing the dressings. The materials are layered as follows: the primary dressing, the secondary absorbent layers and the retention layers. A technique that could penetrate dressings and identify the healing status of wounds would be extremely beneficial to both patients and healthcare professionals by reducing the pain, anxiety and distress caused by wound dressing changes as well as reduce healthcare interventional time.

*Received 5 November 2015, Accepted 17 December 2015, Scheduled 5 January 2016*

\* Corresponding author: Stuart William Harmer (swharmer@gmail.com).

<sup>1</sup> School of Engineering, Manchester Metropolitan University, England. <sup>2</sup> Usikov Institute of Radiophysics and Electronics National Academy of Sciences of Ukraine, Kharkiv 61085, Ukraine. <sup>3</sup> NHS, Manchester Department of Plastic Surgery, Royal Manchester Children's Hospital, Oxford Road, Manchester M13 9PT, England.

Several other clinical scenarios would also benefit from such a tool. Patients who have sustained fractures will require plaster casts for prolonged periods of time. Often these patients may also have cutaneous wounds which would require periodic inspection for wound healing status. This inevitably requires the plaster cast to be removed or a window placed in the cast overlying the wound. The mechanics of this interfere with the healing of the underlying fractured bone. Hence, if a system were available to inspect the healing state of the wound through the plaster cast and the dressings, it would be possible to reduce the frequency of plaster cast changes. Another group of patients to benefit would be patients who have relatively clean venous leg ulcers with minimal exudates requiring prolonged compression bandages.

## 2. MILLIMETRE WAVE RADIOMETRY

The millimetre-wave (MMW) region of the electromagnetic spectrum lies between 30 GHz and 300 GHz, and perhaps, its best known applications are in security screening [10–13], remote sensing [14–16], automotive radar [17, 18] and communications [19]. When applied to security screening, MMW devices are classified according to whether they transmit artificial MMW radiation, which reflects from the scene being imaged, or, whether they receive only thermally emitted radiation from the scene. The former systems are termed ‘active’ and the latter ‘passive’, or radiometric [20]. For both passive and active MMW imagings, it is the electromagnetic properties of textile materials that permit effective imaging of objects concealed under layers of clothing. The complex permittivity of textiles is such that clothing materials (natural and synthetic) are highly transparent [21], allowing differences in the electromagnetic properties of objects (for example, a handgun, knife, explosive material or narcotics) in the MMW band to be observed against the human body. Considerable data are available concerning the phenomenology of millimetre-wave imaging, especially relating to security screening of people [22–24].

Due to their construction, dressing materials used in the treatment of burns and other wounds share similar properties to clothing and because these dressing materials are attached externally to the human body, and the imaging of wounds through dressing materials is a similar problem to security screening. The phenomenology of the wound site is quite different from the phenomenology of most concealed objects of interest, such as metallic weapons, which provide a high contrast in the image due to the large difference in the emissivity and reflectance of metal compared to the human body. The contrast between the undamaged and damaged tissues at a wound site is likely to be smaller and consequently will make imaging of the extent of the wound more difficult than locating a concealed weapon. Although wounds, especially those with infection, may present a higher thermodynamic temperature than healthy tissue, reliance on thermodynamic temperature alone is likely to provide a rather limited tool. For example, a burn, which is healing without infection but is producing excessive scar tissue may not present any thermodynamic temperature contrast. A better approach is to utilise the likely changes in the emissivity between damaged and undamaged tissues. These changes may well result from the altered tissue structure of the wound site. The advantage of this approach over one, which simply maps the thermodynamic temperature, is that the extent of the wound may also be monitored, permitting the healing process to be monitored with recourse to visual inspection. Measurement would be relative, for example, by comparing the brightness temperature of a known area of undamaged skin under the dressing material in close proximity to the wound, and the effects of external factors, such as temperature, humidity and patient perspiration, may be mitigated.

Active MMW imaging is sensitive to alignment and gives an image in which the contrast is due to the differing reflectance in the scene [25]. The sensitivity to alignment is due to the reflectance being dependent on angle of incidence. A small difference in the alignment of a reflecting surface can result in significant differences in the received, reflected radiation and is a common and unwanted phenomenon in active MMW imaging for security screening [20]. Although there is expected to be a difference in the reflectance between undamaged and damaged skins in the MMW band, the sensitivity to alignment may make imaging the wound difficult in practice. Radiometric imaging is better suited for the proposed task as there is no such sensitivity to alignment because skin and dressing materials scatter and radiate nearly isotropically. Radiometric contrast is due to the differences in the brightness temperature (the product of thermodynamic temperature and emissivity) between the wound and undamaged skin.

The receiver output signal,  $U$ , is composed of the received power and noise power, which is

made up of two components, one from the antenna and the other from the receiver. In the MMW band, the emitted radiation is proportional (with constant of proportionality  $a$ ) to the product of the thermodynamic temperature of the emitter and the emissivity of the surface, and this quantity is the ‘brightness temperature’  $T'$  and is given by,

$$U = a(T' + T_N) \tag{1}$$

The noise temperature is given by

$$T_N = \left[ \frac{1}{\eta_a} - 1 \right] T_a + \frac{(NF - 1)}{\eta_a} T_0 \tag{2}$$

where,  $\eta_a$  is the antenna efficiency,  $T_a$  the temperature of the antenna,  $NF$  the noise figure of the receiver and  $T_0$  the ambient temperature. The brightness temperature of the sample,  $T'$ , is dependent upon the electromagnetic properties of the materials that comprise the sample and their thermodynamic temperatures. The dressed wound may be approximately modelled with a planar three-layer system, as shown in Figure 1. The brightness temperature of the sample is determined by the external radiation, which is reflected from the sample; the radiation which is transmitted from the skin, through the dressing, and subsequently received and the radiation which is emitted from the dressing layer itself and then received. In the ideal case ( $\eta_a = 1$  and  $NF = 1$ ) the receiver noise temperature is equal to that of the surroundings,  $T_0$ , this receiver noise radiation is reflected from the sample and contributes to the received signal (see [26] for further information).

$$T' = T_0 R(1 - f) + T_N Rf + T_D A + T_S \varepsilon \tag{3}$$

where,  $T_D$  and  $T_S$  are the temperatures of the dressing layer and wound/skin, respectively.  $R$  is the reflectance of the dressed wound,  $A$  the absorptance (emissivity) of the dressing layer and  $\varepsilon$  the emissivity of the wound/skin. The parameter  $f$  is the fraction of the total radiation blocked from being reflected from the sample by the antenna, and the value of  $f$  depends upon the antenna and its proximity to the sample. Conservation of energy for the system is expressed as,

$$1 = R + A + \varepsilon \tag{4}$$

Using Eq. (3) for an ideal receiver, with  $T_N = T_0$  (which may be realised by placing a waveguide circulator between the antenna and receiver) and for very low loss dressing materials,  $A \approx 0$ , Eq. (3) is simplified to,

$$T' \approx T_0(1 - \varepsilon) + T_S \varepsilon \tag{5}$$

The receiver output (Eq. (1)) can be written in terms of the 3-layer system’s brightness temperature (Eq. (3)) as,

$$U \approx a(T_0(1 - \varepsilon) + T_S \varepsilon + T_N) \tag{6}$$

Determination of the emissivity is realised by means of a two point (linear) calibration with ‘hot’ and ‘cold’ black bodies; one at ambient temperature,  $T_0$  and the other held at a higher temperature,  $T_H$ . From Eqs. (1) and (6), these measurements give,

$$U_H = a(T_H + T_N) \tag{7}$$

$$U_C = a(T_0 + T_N) \tag{8}$$

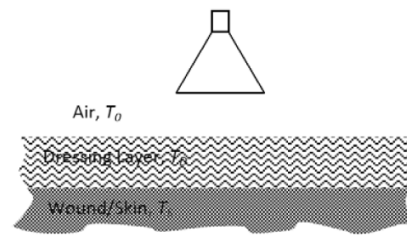


Figure 1. The model of the dressed wound, comprising three layers (air, dressing and the wound/skin).

Subtraction of Eqs. (7) and (8) provides the constant of proportionality,  $a$ , as,

$$a = \frac{U_H - U_C}{T_H - T_0} \quad (9)$$

The value of  $aT_N$  may be determined directly from either Eq. (7) or Eq. (8) as,

$$aT_N = U_H - aT_H \quad (10)$$

So that the emissivity of an unknown sample may be determined using Eqs. (6), (7) and (10) as,

$$\varepsilon \approx \frac{(U - U_C)(T_H - T_0)}{(U_H - U_C)(T_S - T_0)} \quad (11)$$

The thermodynamic temperature of the sample,  $T_S$ , is required in Eq. (11) to compute the emissivity and is measured using suitable probes. Since the temperature may well vary over the wound site, a thermodynamic temperature map,  $T_S(x, y)$ , is required to obtain an emissivity map  $\varepsilon(x, y)$ . However, with current dressings this is not feasible. Because the images have an absolute brightness temperature scale, due to the two-point calibration process, the calculation of emissivity (by measurement of the skin's thermodynamic temperature) is unnecessary in a practical system, and the brightness temperature will show relative variations in the surface of the wound. Furthermore, multiple images, taken different times, will provide information on the wound healing process by measuring the change in size and shape of the wound and may be able to reveal the incidence of infection or other disease process.

The largest error is likely to be that of measuring the temperature of the skin, and the error due to noise can be reduced by increasing the integration time during which the sensor receives radiation from the area under observation [20]. The relative error in emissivity,  $\Delta\varepsilon$ , associated with measurement error of the temperature of the skin,  $\Delta T_S$ , is,

$$\left| \frac{\Delta\varepsilon}{\varepsilon} \right| \approx \left| \frac{\Delta T_S}{T_0 - T_S} \right| \quad (12)$$

Therefore, a low contrast between ambient and skin temperature will increase the error in the emissivity measurement, and uncertainty in skin/wound temperature will translate into uncertainty in the permittivity. This is likely to be the limiting factor in determining emissivity since it may not be practicable to accurately measure the temperature of the surface of the skin/wound under the dressing at or lower than the spatial resolution of the imaging system. With an error of 1 K in skin temperature and a difference between background and skin temperatures of  $\sim 10$  K the relative error in permittivity is  $\sim 0.05$ .

### 3. EXPERIMENTAL DESCRIPTION

The horn antenna may be located in three regions: 'hot' black body, 'cold' black body or SUT, see Figure 2. The first two regions are used to provide a calibration, as outlined in Section 2. The third region contains the SUT, and the output of the receiver may be used, in conjunction with the calibration data, to obtain the emissivity or loss of the SUT. The horn antenna is fixed in the laboratory, and the other equipment is placed upon a movable cart, which travels on rails, thereby permitting the system to be calibrated prior to examining the SUT. The receiver output signal is registered by digital data acquisition. A W-band waveguide circulator is placed between horn antenna and receiver input, so that noise radiation emitted from the antenna to the SUT is the same in intensity as background radiation with air temperature  $T_0$ . Dressing materials are placed directly onto the SUT when required. An electric heating element is used to heat the SUT to a desired bulk temperature, and temperature probes are used to measure the bulk and surface temperatures of the SUT. This information along with the calibration allows the emissivity of the SUT to be calculated using Eq. (11). The parameters for the experimental apparatus are given in Table 1.

### 4. RESULTS & DISCUSSION

Although it is very well known that MMW radiation is minimally attenuated in textiles used in clothing, with the exception of leather [21] and [27], investigation of the transparency of medical dressing materials

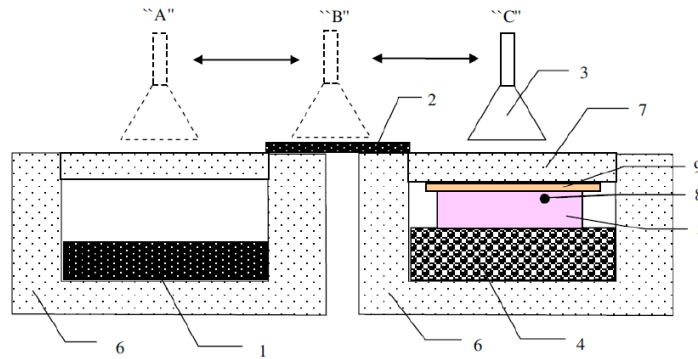


**Figure 2.** The main elements are: 1 — ‘Hot’ black body emitter (carbon loaded foam) at a temperature  $\sim 54\text{C}$ ; 2 — ‘Cold’ black body emitter in thermodynamic equilibrium with air temperature  $\sim 20\text{C}$ ; 3 — Horn antenna of the measuring radiometer; this can be located in 3 regions — A, or B, or C; 4 — Electric heating element; 5 — Sample Under Test (SUT); 6 — Insulating chamber  $20 \times 20 \times 10 \text{ cm}$  (polystyrene foam); 7 — Radio transparent window (polystyrene foam); 8 — sensor for mean temperature of a sample tissue indication; 9 — Dressing materials placed over the SUT (when required).

**Table 1.** System Parameters.

Parameter	Value	Remarks
<i>Radiometric system</i>		
Centre frequency ( $f_0$ )	95 GHz	
High frequency band	$\pm 1 \text{ GHz}$	relative to ( $f_0$ )
Temperature sensitivity	0.2 K	
Integration time	1 s	
Aperture size of the receiving horn antenna ( $E \times H$ ), $\text{mm}^2$	$15 \times 20 \text{ mm}^2$	
<i>Hot Load</i>		
Reflection coefficient	-20 dB	at W band
Emissivity	0.99	at W band
Viewing angles	$\pm 60^\circ$	relative to the normal to the plane of the radiotransparent window
Average operating temperature	$+54^\circ\text{C}$ (327 K)	corresponds to brightness of output radiation
Temperature variation	$\pm 1.5 \text{ K}$	

used in the treatment of burn injuries was undertaken, as there is little available information for these materials in the literature. Measurements to determine the emissivity, or loss, for the dressing samples listed in Table 2 were made at W-band (95 GHz centre frequency) and Ka-band (36.6 GHz centre frequency), and these measurements are based on Eq. (11). The skin is now replaced by the hot calibration load (i.e., the dressing material is placed directly onto the hot calibration load),  $T_S = T_H$ , so that, for dressing materials alone,

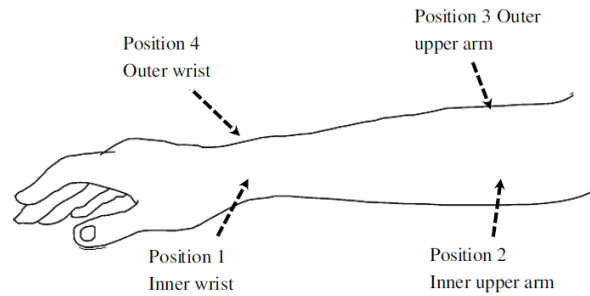
$$\varepsilon \approx \frac{(U - U_C)}{(U_H - U_C)} \tag{13}$$

Here, the ambient temperature was  $\sim 25\text{C}$ , and the hot calibration load had a temperature of  $\sim 54\text{C}$ .

It may be seen that the losses at Ka and W bands are not dissimilar; this could be due to the large

**Table 2.** Transmission of MMW, at Ka and W bands, through dressings used in the treatment of burn injuries.

Dressing Type	Sample number	Transmission %		Loss (dB)		Comments
		Ka-band	W-band	Ka-band	W-band	
Gauze	1	96.4	94.0	0.16	0.26	All dressings are dry and removed from protective packaging prior to measurement. The air temperature was $\sim 25^{\circ}\text{C}$ during measurements. 6 layers of gauze are used in the measurements
Light Support Bandage Type 2 (BP cotton stretch, 10 cm $\times$ 4.5 m)	2	95.2	93.8	0.21	0.28	1 layer used
Light Support Bandage Type 2 (BP cotton stretch, 10 cm $\times$ 4.5 m)	3	91.9	88.9	0.36	0.51	2 layers used
Light Support Bandage Type 2 (BP cotton stretch, 10 cm $\times$ 4.5 m)	4	86.6	82.5	0.62	0.84	3 layers used
Elasticated stocking bandage	5	94.7	88.6	0.23	0.82	2 layers used (in practice, only one layer will be present in patients)
Non-adherent Clear Wound Dressing (Tefla <sup>TM</sup> )	6	100	100	0	0	1 layer used
Temporary Wound Dressing (Biobrane <sup>®</sup> )	7	100	100	0	0	1 layer used

**Figure 3.** Four positions on the lower arm where emissivity of human skin at W-band was measured on eight uninjured volunteers. Each position was measured several times and the mean and standard deviation of the results are given presented in Figure 4.

scale porosity of the samples, especially samples 1–4, which may cause more scattering at Ka band (where structure size is  $\sim$  wavelength) than at W-band (where structure size is  $>$  wavelength). Sample 5 (without the stretching of fabric) has a smaller scale structure and therefore results in more loss at

W band. Ka-band measurements of the emissivity of chicken tissue (breast) heated to a temperature of  $\sim 37\text{C}$  with give values of 0.31 and 0.36 for undressed and dressed samples. The dressings applied were four layers of burns gauze and one layer of Light Support Bandage Type 2. There is some increase in emissivity associated with the application of dressing materials, but this increase is within the error of the measurement.

To assess the feasibility of measuring changes in emissivity at W-band, eight uninjured volunteers were measured at four points on their lower arm, see Figure 3. This will allow an assessment of the expected range of permittivity values of the human skin on the arm and the likely variation from person to person.

In the uninjured skin there is variation in emissivity from location to location of the lower arm, and this variation is likely to be similar across other parts of the body. The variation is quite large for persons 5, 6 and 7, probably due to greater presence of subcutaneous fat in these people. The variation (standard deviation) calculated by taking multiple measurements is 0.027 for person one and 0.082 for person seven. Variations in emissivity are important because the emissivity map will change between points on the skin to a greater or lesser degree. These changes may prevent useful imagery of wounds if the variations are larger or commensurate to the changes in emissivity which result from the wound. However, with a burn or other wound the change in emissivity between uninjured and damaged tissue is expected to be a well-defined interface taking place over distances of  $\sim 1\text{ cm}$ , whereas changes due to variations in composition of healthy tissue are expected to be less localised, taking place over distances of  $\sim 10\text{ cm}$ .

Assessing the likely changes in emissivity of human skin which has suffered from burn injury requires patients who have burn injuries. A simpler, though less specific, experiment was to select a biological tissue from a dead animal and use this as a ‘phantom’ for living human tissue. Chicken (breast and leg tissue, with and without skin) was selected for this purpose. The chicken samples were raised to human body temperature  $\sim 37\text{C}$  and their emissivities measured at W band in the MMW spectrum. The dressing materials, four layers of burns gauze and one layer of Light Support Bandage Type 2 (BP cotton stretch), were applied, and their effect on the emissivity is seen to be small in both Ka and W bands (see Figure 5).

Multiple measurements were taken for each case (A, B, C and D), and the mean and standard deviation of these are presented Figure 5. Firstly, the emissivity of the chicken samples is about two times larger at W-band ( $\sim 0.6$ ) than at Ka-band ( $\sim 0.3$ ), so W-band measurement will likely be more sensitive and offer a higher spatial resolution in imaging due to the shorter wavelength. The additional losses in dressing materials at W-band are not so great as to reduce contrast, so W-band would seem to be preferable to Ka band in all respects except, perhaps, the higher cost of components required to build imaging systems.

The effects of skin on the tissue samples are observable, comparing A and B in Figure 5. The presence of skin reduces the emissivity which is consistent with the presence of subcutaneous fat having

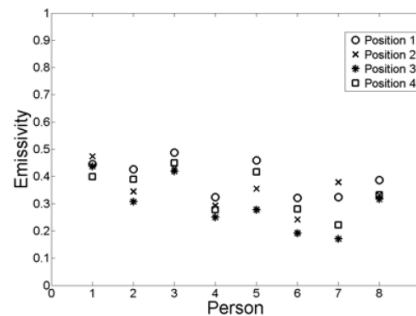


**Figure 4.** Mean values of the measured emissivity for of eight people at four different points on their lower arms. The people’s gender and age is as follows: 1) M, 62; 2) M, 23; 3) M, 61; 4) M, 65; 5) M, 67; 6) F, 55; 7) F, 58; 8) M, 61.

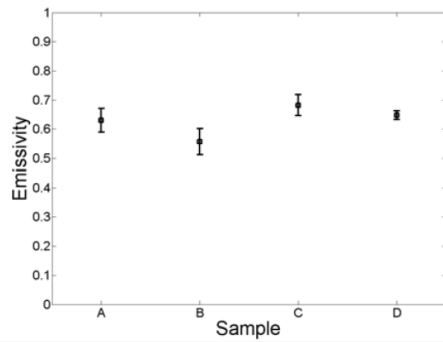


**Figure 5.** Measured values of emissivity and standard deviation bars for chicken samples at  $\sim 37^{\circ}\text{C}$ . The samples are: A, tissue without skin and without dressing materials; B, tissue with skin and without dressing materials; C, tissue without skin but with dressing materials and D, tissue with skin and dressing materials.

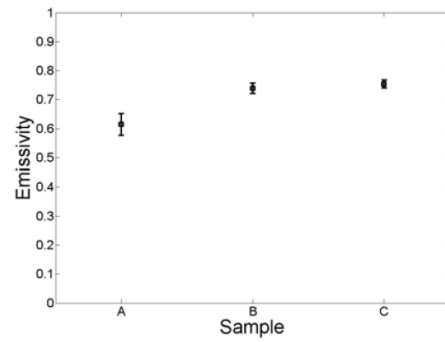


**Figure 6.** Samples of chicken tissue with skin which have undergone high temperature heating with air at  $200^{\circ}\text{C}$ . Sample A, control without heating; B, heat treatment applied for 60s; C, heat treatment applied to sample twice. The samples are measured without dressing materials. The standard deviation calculated from multiple measurements is displayed as error bars.

**Table 3.** Electromagnetic measurements of human skin in the millimetre wave band for medical diagnosis.

Type of the Skin	Measured Quantity	Reference
Skin Cancer	Complex Permittivity at 20–70 GHz	[28]
Healthy Skin and Burn Wounds	Complex permittivity at 30–40 GHz	[29]
Healthy Skin	Complex Permittivity and Emissivity at 20–36 GHz	[30]
Dry Skin	Complex Permittivity at 57–76 GHz	[23]

a higher reflectance than tissue without fat. The effects of dressings (see C and D in Figure 5) slightly increase the emissivity, due to increased losses and increased transmission from the skin to air by virtue of reducing the discontinuity in impedance at the skin/air interface. However, the lower emissivity of the sample with skin is still seen through the dressing materials. The chicken tissue samples have a significantly higher emissivity than in-vivo human skin (about 50% larger) and therefore is not an accurate phantom. Furthermore, the response of living tissue to burn injuries is different from that of the non-living samples. However, alteration of the sample emissivity by application of localised heat demonstrated that changes in the surface and near surface layers of biological tissue were measurable through wound dressing materials.

A chicken tissue sample with skin was exposed to hot air ( $200^{\circ}\text{C}$ ) for 60s to alter the surface material by denaturing proteins in the tissue, and the sample was then allowed to cool and maintained at body temperature by electrical heating. The emissivity was measured, without dressing materials, before exposure to heat, after one exposure to heat and then again after a second exposure to heat, see Figure 6. Application of heat increases the emissivity of the sample from 0.593 to 0.724, and a second application leaves the emissivity almost unchanged.

The application of millimetre wave to medical screening for burns and skin cancer is summarised in Table 3. In most articles in this field, the complex permittivity is the measured quantity; for passive imaging, the emissivity is more useful. Significant differences in complex permittivity between healthy and diseased or damaged skin do not necessarily imply commensurate differences in emissivity.

## 5. CONCLUSION

Dressings used in the medical management of burn injuries were measured for losses at two commonly used bands in the MMW spectrum, Ka and W-bands. Both bands have low attenuation in all dressing materials tested, in the unused state, allowing for the possibility that the healing process of such wounds may be monitored without recourse to removing the dressing, as current medical practice.

The emissivity of samples of chicken, with and without skin, was measured to ascertain whether these would make mimic living human tissue. Although the chicken samples have a higher emissivity than living human skin and tissue, the capability to measure the effect of localised alteration to the emissivity of chicken samples was observed. Chicken samples were heated with hot air for a short period of time, and the emissivity of the samples was measured before and after such treatment. Heat treatment produces an increase in the emissivity of chicken samples of  $\sim 25\%$  by altering the chemistry and structure of the surface and near surface tissue, and this change is observable through the dressing materials used in the management of burn injuries, allowing the size of the ‘damaged’ area to be observed.

Measurements of the variation in emissivity of human skin on the lower arm show significant variation from person to person and, more importantly, significant variation at different positions on the arm of individuals. These variations in emissivity are similar in magnitude to those produced by the localised high temperature heating of the chicken sample. However, these natural variations occur over longer length scales than would be the case for a localised wound site, so the edges of wounds are likely to be observable through the typical dressing materials applied to burn injuries. Changes in ambient conditions such as temperature and humidity and variations in the skin due to perspiration or surface temperatures will alter the mean brightness temperature of the scene but the contrast between damaged and undamaged skin will likely be preserved. In this way, a time series of images taken on different days will present different mean brightness temperatures, but the edges and features of the wound should remain observable due to relative differences in brightness temperature. The most likely serious limitation will be the deposition of biological matter from the wound into the dressing materials. These exudates may prevent effective measurement of the wound’s emissivity, although there may be a correlation between exudate depositions and the state of the wound, and so the technique could still provide useful information on the state of the wound without necessitating removal of the entire dressing.

## REFERENCES

1. The Child Accident Prevention Trust (CAPT), “The costs of burns,” *Working Together for Safer Children*, Aug. 2013, Available: <http://www.makingthelink.net/tools/costs-child-accidents/costs-burns>, Accessed: Sep. 12, 2015.
2. Arbab, M. H., T. C. Dickey, D. P. Winebrenner, A. Chen, M. B. Klein, and P. D. Mourad, “Terahertz reflectometry of burn wounds in a rat model,” *Biomedical Optics Express*, Vol. 2, No. 8, 2339–2347, Aug. 2011.
3. Smulders, P. F. M., “Analysis of human skin tissue by millimeter-wave reflectometry,” *Skin Research and Technology*, Vol. 19, No. 1, 209–216, Apr. 2012, DOI: 10.1111/j.1600-0846.2012.00629.x.
4. Kharkovsky, S., M. T. Ghasr, M. A. Abou-Khousa, and R. Zoughi, “Near-field microwave and mm-wave noninvasive diagnosis of human skin,” *International Workshop on Medical Measurements and Applications*, 5–7, Italy, May 2009.
5. Siegel, P. H., “Terahertz technology in biology and medicine,” *IEEE Transactions on Microwave Theory and Techniques*, Vol. 52, No. 10, 2438–2447, Oct. 2004.
6. Essen, H., J. M. Essen, D. Nuessler, A. Hommes, C. Krebs, N. Fatihi, and T. Buzug, “Monitoring of wound healing by millimetre wave imaging,” *35th International Conference on Infrared, Millimeter, and Terahertz Waves*, 1–2, Sep. 2010.
7. Siegel, P. H., “Microwave symposium digest,” *IEEE MTT-S International*, Vol. 3, 1575–1578, Jun. 2004, ISSN: 0149-645X, Print ISBN: 0-7803-8331-1 INSPEC, Accession Number: 8058048, DOI:10.1109/MWSYM.2004.1338880.

8. Bardati, F., V. J. Brown, M. P. Ross, and P. Tognolatti, "Microwave radiometry for medical thermal imaging: Theory and experiment," *IEEE MTT-S International in Microwave Symposium Digest*, Vol. 3, 1287–1290, Jun. 1992, ISSN: 0149-645X, Print ISBN: 0-7803-0611-2 INSPEC, Accession Number: 4296960, DOI: 10.1109/MWSYM.
9. Dziejowski, M., "Planimetry of thermograms in diagnosis of burn wounds," *Scientific Research of the Institute of Mathematics and Computer Science*, Vol. 8, No. 1, 33–38, 2009.
10. Federici, J. F., B. Schulkin, F. Huang, D. Gary, R. Barat, F. Oliveira, and D. Zimdars, "THz imaging and sensing for security applications — Explosives, weapons and drugs," *Semiconductor Science and Technology*, Vol. 20, No. 7, S266–S280, Jun. 2005.
11. Appleby, R. and R. N. Anderton, "Millimeter-wave and submillimeter-wave imaging for security and surveillance," *IEEE Publisher*, Vol. 95, No. 8, 1683–1690, Aug. 2007, ISSN: 0018-9219 INSPEC, Accession Number: 9633436, DOI:10.1109/JPROC.2007.898832.
12. Sheen, D. M., D. L. McMakin, and T. E. Hall, "Three-dimensional millimeter-wave imaging for concealed weapon detection," *IEEE Transactions on Microwave Theory and Techniques*, Vol. 49, No. 9, 1581–1592, Sep. 2001.
13. Oka, S., H. Togo, N. Kukutsu, and T. Nagatsuma, "Latest trends in millimeter-wave imaging technology," *Progress In Electromagnetics Research Letters*, Vol. 1, 197–204, 2008.
14. Nashashibi, A. Y., K. Sarabandi, P. Frantzis, R. D. De Roo, and F. T. Ulaby, "An ultrafast wide-band millimeter-wave (mmw) polarimetric radar for remote sensing applications," *IEEE Transactions on Geoscience and Remote Sensing*, Vol. 40, No. 8, 1777–1786, Aug. 2002, ISSN: 0196-2892 INSPEC, Accession Number: 7416289, DOI:10.1109/TGRS.2002.802462.
15. Appleby, R., R. N. Anderton, N. H. Thomson, and J. W. Jack, "The design of a real-time 94-GHz passive millimetre-wave imager for helicopter operations," *Passive Millimetre-wave and Terahertz Imaging and Technology*, Vol. 5619, 38–46, Dec. 2004, DOI:10.1117/12.581336, Available: <http://dx.doi.org/10.1117/12.581336>, Accessed: Sep. 13, 2015.
16. Coward, P. and R. Appleby, "Comparison of passive millimeter-wave and IR imagery in a nautical environment," *Passive Millimeter-wave Imaging Technology XII*, Vol. 7309, No. 730904, Apr. 2009, DOI:10.1117/12.819852, Available: <http://dx.doi.org/10.1117/12.819852>, Accessed: Sep. 13, 2015.
17. Hasch, J., E. Topak, R. Schnabel, T. Zwick, R. Weigel, and C. Waldschmid, "Millimeter-wave technology for automotive radar sensors in the 77 GHz frequency band," *IEEE Transactions on Microwave Theory and Techniques*, Vol. 60, No. 3, 845–860, Mar. 2012, ISSN: 0018-9480 INSPEC, Accession Number: 12571080, DOI:10.1109/TMTT.2011.2178427.
18. Wengerl, J., "Automotive mm-wave radar: Status and trends in system design and technology," *Automotive Radar and Navigation Techniques, IEE Colloquium. IET*, Ref. No. 1998/230, 1–7, 1998, INSPEC, Accession Number: 5877493, DOI:10.1049/ic:19980188.
19. Pi, Z. and F. Khan, "An introduction to millimeter-wave mobile broadband systems," *IEEE Communications Magazine*, Vol. 49, No. 6, 101–107, Jun. 2011, ISSN: 0163-6804 INSPEC, Accession Number: 12036181, DOI:10.1109/MCOM.2011.5783993.
20. Kemp, M. C., "Millimetre wave and terahertz technology for the detection of concealed threats: A review," *Optics and Photonics for Counterterrorism and Crime Fighting II*, Vol. 6402, Sep. 2006, DOI:10.1117/12.692612, Available: <http://dx.doi.org/10.1117/12.692612>, Accessed: Sep. 14, 2015.
21. Lamb, J. W., "Miscellaneous data on materials for millimetre and submillimetre optics," *International Journal of Infrared and Millimeter Waves*, Vol. 17, No. 12, 1997–2034, Dec. 1996.
22. Alekseev, S. I. and M. C. Ziskin, "Human skin permittivity determined by millimeter wave reflection measurements," *Bioelectromagnetics*, Vol. 28, No. 5, 331–339, Jul. 2007, DOI: 10.1002/bem.20308, Available: <http://onlinelibrary.wiley.com/>, Accessed: Sep. 14, 2015.
23. Alabaster, C. M., "The microwave properties of tissue and other lossy dielectrics," PhD Thesis, Cranfield University, Mar. 2004.
24. Zastrow, E., S. K. Davis, M. Lazebnik, F. Kelcz, B. D. Van Veen, and S. C. Hagness, "Development of anatomically realistic numerical breast phantoms with accurate dielectric properties for modeling microwave interactions with the human breast," *IEEE Transactions on Biomedical Engineering*, Vol. 55, No. 12, 2792–2800, Dec. 2008.

25. Harmer, S. W., N. Bowring, D. Andrews, N. D. Rezgui, M. Southgate, and S. Smith, "A review of nonimaging stand-off concealed threat detection with millimeter-wave radar," *IEEE Microwave Magazine*, Vol. 13, No. 1, 160–167, Feb. 2012, ISSN: 1527-3342 INSPEC, Accession Number: 12479283, DOI:10.1109/MMM.2011.2174125.
26. Bardati, F. and D. Solimini, "Radiometric sensing of biological layered media," *Radio Science*, Vol. 18, No. 6, 1393–1401, Dec. 1983, DOI: 10.1029/RS018i006p01393.
27. Harmer, S. W., N. Rezgui, N. Bowring, Z. Luklinska, and G. Ren, "Determination of the complex permittivity of textiles and leather in the 14–40 GHz millimetre-wave band using a free-wave transmittance only method," *IET Microwaves, Antennas & Propagation*, Vol. 2, No. 6, 606–614, Sep. 2008, ISSN: 1751-8725 INSPEC, Accession Number: 10158942, DOI:10.1049/iet-map:20070235.
28. Aminzadeh, R., M. Saviz, and A. A. Shishegar, "Dielectric properties estimation of normal and malignant skin tissues at millimeter-wave frequencies using effective medium theory," *22nd Iranian Conference on Electrical Engineering (ICEE), 2014*, 1657–1661, IEEE, May 2014.
29. Olga, B. L., Y. Nikawa, W. Snyder, J. Lin, and K. Mizuno, "Novel microwave and millimeter-wave biomedical applications," *4th International Conference on Telecommunications in Modern Satellite, Cable and Broadcasting Services, 1999*, Vol. 1, 186–193, IEEE, Oct. 1999.
30. Tamyis, N. M., D. K. Ghodgaonkar, M. N. Taib, and W. T. Wui, "Dielectric properties of human skin in vivo in the frequency range 20–38 GHz for 42 healthy volunteers," *Proc. of the 28th URSI General Assembly*, 2005.

# Active Millimeter-Wave Radar for Sensing and Imaging Through Dressing Materials

Amani Yousef Owda, Neil Salmon, David Andrews, and Nacer Ddine Rezgui

Dep. Electrical and Electronic Engineering, Manchester Metropolitan University, Manchester, United Kingdom

Email: Amani.owda@stu.mmu.ac.uk, n.salmon@mmu.ac.uk, david.andrews@mmu.ac.uk, n.rezgui@mmu.ac.uk

**Abstract**—A radar system is used to obtain information about the structure of dressing materials and hand support cast. The system is used also to assess the feasibility of using active radiation to penetrate dressing materials at different state (dry, wet and with cream) and provide information about the metal plate under the dressing. A comparison is made between the resolved structure of the samples from a pulse synthesis direct detection radar system that operates over the frequency band 15–40 GHz and the actual dimensions of the samples. Based on the results obtained, the authors suggest that active millimeter-wave imaging might be used as a non-contact technique for monitoring the wound healing under dressing materials without necessity of dressing removal.

**Keywords**—active sensing; bandages; refractive index; dielectric permittivity; millimeter wave.

## I. INTRODUCTION

In Radar, which is best known in security screening and remote sensing [1], the target object is illuminated by a coherent microwave source, and based on the reflected radiation from the target object the system can form an image. The line of sight distance between the Radar system and the target object or range  $R$ , can be measured through the round trip time  $T$  of the transmitted signal, the speed of the light  $c$ , and the refractive index  $n$  (where  $n=1$  in vacuum), as shown in (1). A key figure of merit in Radar is the range resolution (the smallest distance between the targets at which they are resolved into separate targets) [2] and this is related to the bandwidth of the system  $BW$ , as illustrated in (2). The thickness of the sample  $d$  can be measured experimentally using the distance between two reflection peaks [3], as expressed in (3).

$$R = c * T / 2n \quad (1)$$

$$\Delta R_s \geq c / (2n * BW) \quad (2)$$

$$d = R_2 - R_1 = c * (T_2 - T_1) / 2n \quad (3)$$

The millimeter-wave (MMW) band is the electromagnetic region between the microwave frequency band, and the terahertz frequency band and it covers the frequency band (30–300) GHz. Because electromagnetic radiation at microwave and MMW frequencies can propagate through typical dressing materials with little attenuation, these bands of the electromagnetic spectrum are promising for assessing bandaged wounds [4]. The transparency of bandages in the MMW region has led [5] to investigate using active MMW radiation to monitor wound healing under a plaster and a

gypsum cast in contact with the human body. Currently visual inspection is the current protocol for monitoring the wound healing and this requires the removal of dressing layers, which can cause medical problems, be uncomfortable or painful to the patient [4]. Up-to-date there are no methods successfully assess the wound healing progress without removing dressing materials. A technique that could penetrate dressings and identify the healing status of wounds would be extremely beneficial, and therefore this paper aims to help assess the feasibility of using active MMW Radar to monitor wound healing in non-contact with the human body, by measuring the attenuating effect of bandages and creams, which are applied to cover the wounds.

## II. EXPERIMENTAL SETUP

### A. Experimental Description

A standard Ka-band horn antenna with a square aperture ( $46 \times 46 \text{ mm}^2$ ) and nominal gain of 20 dBi over the frequency band (15–40) GHz was located  $\sim 250 \text{ mm}$  from the sample under test (SUT) and was aligned in vertical polarization. As illustrated in Fig. 1, the antenna was connected through a high frequency cable to the vector network analyser (VNA). A large metal plate (length=1200 mm, and width 660 mm) was used as a background and also used for calibration purposes. A VNA with an operating frequency band (10 MHz–67 GHz) was used to illuminate the SUT and was connected to the computer through Ethernet cable and controlled via a Matlab program. The program allows the user to determine the start frequency (15 GHz), the end frequency (40 GHz), the number of data points (512), and the transmitted power level (1.6 mW); these parameters result in a range resolution 6.0 mm and bandwidth 25 GHz. The system was surrounded with absorbent foam material to minimise reflections from other objects in the lab and the data were saved directly to be processed later.

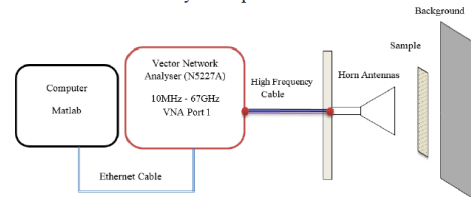


Fig. 1. Experimental setup for an active millimetre wave imaging system.

Manchester Metropolitan University's Internal Investment and Innovation Fund and Engineering and Physical Sciences Research Council (EPSRC) have funded this work.

### B. Methodology of Data Processing

A mono-static radar system (transmitter and receiver are co-located) in Fig. 1 was utilised for measuring: A) the complex reflected signal ( $S_{11}$ ) from the metal plate, B) the internal background signal measured with a microwave foam absorber target and C) the complex reflected signal from the sample under test. These particular measurements are selected as it enables calibration to be made quickly, before and after the measurements, thus minimising the effects of systematic errors. The foam absorber calibration measurements were used to subtract any internal reflected radiation, and the metal plate calibration measurement was used to remove the effect of transmitter and receiver response “dispersion” by de-convolution. The complex reflected signal for each sample (SUT, metal plate and foam absorber) were measured ten times and averaged at each frequency. The complex reflected signal in the frequency domain was transformed into time domain signal using the Inverse Fast Fourier Transform (IFFT). Zero padding was utilised beyond the measured 0-15 GHz frequency band to aid data interpretation. This methodology together with (1) and (3) was used to calculate the optical path length of the samples. The measured optical path length was compared with the actual path length of the sample that obtained using a standard ruler with  $\pm 0.5$  mm absolute uncertainty.

## III. RESULTS AND DISCUSSION

### A. Hand Support Cast Sample

A hand cast made of plaster-of-Paris was located and aligned transversely between the horn antenna and the metal plate. The hand cast has a cylindrical tubular shape and dimensions (length 250 mm, and diameter 90 mm). Fig. 2 shows three reflection peaks associated with the hand cast and the metal plate; the first two peaks correspond to the reflections from the front and the back surfaces of the hand cast, whereas the third peak corresponds to the metal plate surface, as seen through the cast. Reflection peaks are produced in the time domain resulting from reflections from the surfaces of the sample or discontinuities in dielectric properties. The reduction of the third peak ( $\sim 35\%$ ) compared to the value 1.0 obtained without the cast (see Fig. 3), is due to reflection and absorption by the cast material. The conversion between the time domain and the optical path length in free space was performed using (1). From the distance between two cast peaks ( $d = R_2 - R_1$ ), the optical path length for the hand cast sample was measured to be  $\sim 85.5$  mm, close ( $\sim 4.5$  mm) to the actual optical path length (90 mm).

### B. Gauze Burn Dressing Materials in Dry State

A gauze burn bandage with  $\sim 10$  mm thick was located and aligned between the horn antenna and the metal plate. The bandage was in dry state and removed from protective packaging prior to measurement. As illustrated in Fig. 3. The reflection from the gauze burn bandage is  $\sim 10\%$ , compared with the reflection from the metal plate. Although, dressing materials are low loss materials, increasing the thickness of dressing materials increases the absorption and causes loss. The attenuation in the reflected radiation is measured by comparing the two reflection peaks that associated with the metal plate

before and after locating the bandage. From the heights of the reflection peaks, the combined attenuation and reflection by the gauze burn bandage is estimated as  $\sim 10\%$  for a 10 mm bandage thickness.

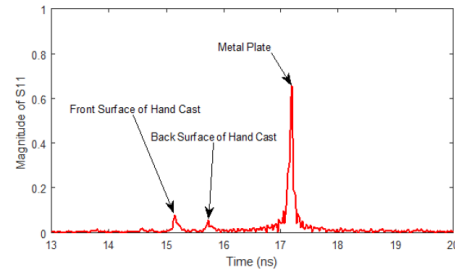


Fig. 2. Image displaying the reflected signal from a 90 mm wide hand cast located in free space between the horn antenna and the metal plate.

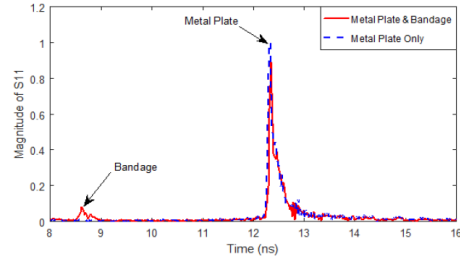


Fig. 3. Image displaying the reflected signal from a 10 mm thick bandage located in free space between the horn antenna and the metal plate. The solid red line shows the signal from the bandage and the metal plate and the broken blue line when the metal plate only is present.

### C. Gauze Burn Dressing Materials with Sudocrem

Dressing materials are used widely on the treatments of injury and burn wounds. These materials are usually used with cream for avoiding friction between the skin and the dressing materials and for healing purposes. This section investigates the feasibility of using active radiation to sense different surfaces attached to the dressing materials and whether it is possible to sense features under these layers. A gauze burn bandage  $\sim 25$  mm thick is attached to the metal plate and a thin layer of Sudocrem is attached directly to the front surface of the bandage; the complex reflected signal in frequency domain is transformed into a time domain signal using the Inverse Fast Fourier Transform (IFFT) and the result obtained is illustrated in Fig. 4. The results show two reflections peaks; the reflection from the cream and the front surface of the bandage is combined in peak 1, and the reflection from the back surface of the bandage and the metal plate is combined in peak 2. Although the imaging system can't resolve the cream layer attached to the bandage surface itself, this doesn't mean that it can't sense the cream surface. The measured reflection from the front surface of the bandage in dry state did not exceed  $\sim 10\%$  (see Fig. 2), whereas when a layer of Sudocrem is attached to the bandage the reflection is increased to  $\sim 16\%$ . The optical path length of the

bandage is measured to be  $\sim 27$  mm from the distance between the two peaks. The difference between the actual path length and the measured path length is  $\sim 2.0$  mm. It may be noted that although the metal plate seen through the cream layer has been reduced by a factor of 3, it is still possible to sense features under the cream layer.

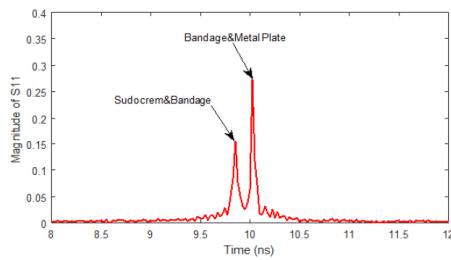


Fig. 4. Image displaying the reflected signal from a  $\sim 25$  mm thick bandage with Sudocrem.

#### D. Gauze Burn Dressing Materials with Flamazine Cream

The results obtained with another  $\sim 10$  mm bandage coated with a thin layer of a different cream Flamazine is illustrated in Fig. 5. The measurements show that, adding a layer of Flamazine cream increases the reflection of the front surface of the bandage from  $\sim 10\%$  in dry state to  $\sim 30\%$ . The signal passing through the cream and bandage and reflected from the metal plate is now  $55\%$ . The optical path length of the bandage in this case is measured to be  $\sim 9.5$  mm using the distance between two peaks and (3). The difference between the actual path length and the measured path length is calculated to be  $\sim 0.5$  mm.

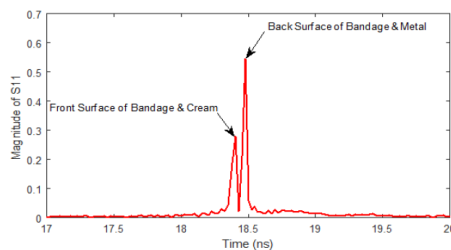


Fig. 5. Image displaying the reflected signal from a  $\sim 10$  mm thick bandage coated with Flamazine cream.

#### E. Gauze Burn Dressing Materials with Water

The results obtained from  $\sim 10$  mm wet bandage (bandage with water) is illustrated in Fig. 6. The bandage was attached directly with the metal plate and the results obtained show only one reflection peak since MMW radiation is highly absorbed in water [2]. The combined signal from reflection from the water in the bandage and that passing through the water and the bandage and reflected from the metal plate is now  $\sim 70\%$ . This is higher than reflection from water alone ( $55\%$ ), so the attenuated reflected radiation from the plate may be estimated

as  $\sim 15\%$ . The metal plate seen through the wet bandage has been reduced by a factor of  $\sim 7$ . This means that it may still be possible to sense features under wet dressing materials.

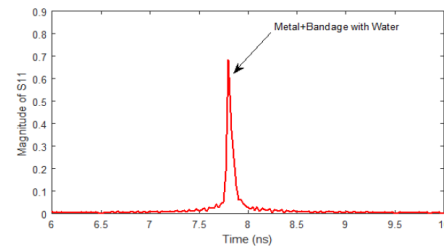


Fig. 6. Image showing the reflected signal from a  $\sim 10$  mm thick wet bandage.

#### IV. CONCLUSION

Active millimetre wave Radar can provide precise information about the optical path length of the dressing materials and hand support cast (as in Fig. 2) and more importantly, it can penetrate the dressing materials and provide information about the metal plate under the dressing materials. Adding a cream layer to the bandages has a clear signature on the level of reflected radiation. This signature is based on the thickness of the cream layer and the dielectric properties of the cream as illustrated in Figs. 4 and 5. Millimetre wave radiation is highly absorbed with water and as a result, there is only a single reflection peak associated with wet dressing materials as illustrated in Fig. 6. The results obtained in this paper show that active millimetre wave Radar might be an efficient tool for monitoring the wound healing under dressing materials without their often-painful removal and in non-contact with the human body. In this paper, metal plate has been used a surrogate to the body surface and therefore, it is recommended that further measurements be made on human body or animals tissue to study the effect of wound size, exudates and cream layer.

#### REFERENCES

- [1] N. A. Salmon, "3-D radiometric aperture synthesis imaging," IEEE Transactions on Microwave Theory and Technology, vol. 63, pp. 3579-3587, 2015.
- [2] S. W. Hamer, N. J. Bowring, N. D. Rezzgui, D. Andrews, "A comparison of ultra wide band conventional and direct detection radar for concealed human carried explosives detection," Progress In Electromagnetics Research, vol. 39, pp. 37-47, 2013.
- [3] N. J. Bowring, J. G. Baker, N. D. Rezzgui, M. Southgate, J. F. Alder, "Active millimeter wave detection of concealed layers of dielectric material," Proc. SPIE 6540, Optics and Photonics in Global Homeland Security III, 65401M, pp. 37-47, 2007.
- [4] S. W. Hamer, S. Shylo, M. Shah, N. J. Bowring, A.Y.Owda, "On the feasibility of assessing burn wound healing without removal of dressings using radiometric millimetre-wave sensing," Progress In Electromagnetics Research, vol. 45, pp. 173-183, 2016.
- [5] H. Essen, J. M. Essen, D. Nuessler, A. Hommes, C. Krebs, N. Fatihi, T. Buzug, "Monitoring of wound healing by millimetre wave imaging," 35th International Conference on Infrared, Millimeter, and Terahertz Waves, 2010.

# Millimetre Wave Radiometers for Medical Diagnostics of Human Skin

Amani Yousef Owda<sup>1</sup>, Neil Salmon<sup>1</sup>, Nacer Ddine Rezgui<sup>1</sup>, and Sergiy Shylo<sup>2</sup>

<sup>1</sup>Dep. Electrical and Electronic Engineering, Manchester Metropolitan University, Manchester, United Kingdom

<sup>2</sup>Usikov Institute of Radiophysics and Electronics National Academy of Sciences of Ukraine, Kharkiv, Ukraine

Email: amaniabubaha@gmail.com, n.salmon@mmu.ac.uk, n.rezgui@mmu.ac.uk, shilo@ire.kharkov.ua

**Abstract**—A technique to measure the human skin emissivity in vivo is described for the frequency band 80-100 GHz. Emissivity measurements were performed on 60 participants, 35 males and 25 females, with ages ranging from 20 to 60 years. Results show that the emissivity of males is higher than that of females. The study suggests a trend in the emissivities with age and gender, which might be due to variations of skin thickness and water content. As non-contact screening is desirable in medical applications, passive millimeter-wave sensing could be a means of achieving this in the diagnosis of skin disease or damage, where the disease/damage alters the water content or the skin thickness.

**Keywords**—radiometric; emissivity; millimeter wave.

## I. INTRODUCTION

Over the past few decades, millimetre wave technology has shown a steady and consistent development, with a wide variety of devices and system architectures (imaging, non-imaging, radiometers and radars) becoming available. As an imaging sensor, these systems can deliver spatial resolutions down to around half of the wavelength of the radiation used, ~1.0 mm for the millimetre wave band. This property enables highly localized, non-contact measurements to be made just below the skin surface, a capability not available in the visible spectrum. A convenient metric to describe the condition of human skin is the emissivity [1], this being defined as the ratio of the level of thermal electromagnetic (Planck) radiation to that level from a thermal blackbody source at the same thermodynamic temperature [2]. Many studies reveal strong correlation between skin dielectric properties, skin thickness, water content and hydration level, all of which vary with age, gender and body site [3-5]. However, to date the potential for medical diagnostics using this information has not been exploited, possibly because insufficient attention has been paid to experimental detail. This study redresses this balance by analyzing the emissivity of skin at different regions of the human body, for subjects of different gender, ethnicity and age, over the frequency band (80-100) GHz.

## II. EXPERIMENTAL SETUP

### A. Radiometric Calibration and Emissivity Measurements

A radiometer operating over the frequency band 80-100 GHz was used to measure the human skin emissivity. The

equipment for measurement and calibration comprises: a horn antenna connected to Millimeter-Wave Monolithic Integrated Circuit (MMIC) detector, two pieces of carbon loaded foam absorbers acting as hot and cold calibration sources, a digital voltmeter and the subject tissue to be measured, as illustrated in Fig. 1. The horn antenna has a rectangular aperture (3x2.5 cm<sup>2</sup>) and a nominal gain of 20 dBi over the frequency band (80-100) GHz. The MMIC detector consists of a two-stage low-noise amplifier (LNA), zero bias detector and buffer amplifier. The radiometer is calibrated by measuring emissions from the hot and cold sources [1, 6] at respective temperatures of  $T_H$  and  $T_C$ .

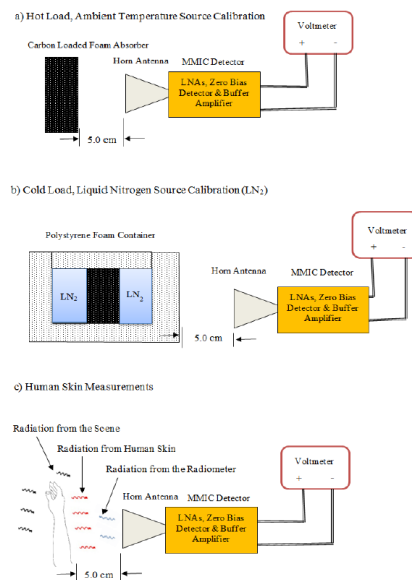


Fig. 1. Experimental setup for human skin emissivity measurements.

Manchester Metropolitan University's Internal Investment and Innovation Fund and Engineering and Physical Sciences Research Council (EPSRC) have funded this work.

The horn antenna may be located at a distance (~5.0 cm) from three different radiation sources: 1) “Hot” black body, a piece of carbon loaded foam absorber with  $T_H=T_{\text{ambient}}=293$  K, 2) “Cold” black body, a piece of carbon loaded foam absorber is dipped in the liquid nitrogen with  $T_C=77$  K and 3) the human skin. The system response is assumed to be linear, since the measurements are done indoors and in an anechoic environment. The output of the receiver for “Hot” black body, Fig. 1a, can be expressed as [1, 6]:

$$V_H = \alpha(T_H + T_N) \quad (1)$$

Where,  $T_H$  is the hot load temperature in K,  $\alpha$  is the receiver responsivity in V/K, and  $T_N$  is the receiver noise temperature in K. For the “Cold” black body, the output of the receiver, Fig. 1b, is [1, 6]:

$$V_C = \alpha(T_C + T_N) \quad (2)$$

The radiation temperature of the skin can be expressed in terms of the skin emissivity  $\eta$ , the skin thermodynamic temperature  $T_s$ , and the background illumination temperature  $T_0$  [6]:

$$T_b = (1 - \eta)T_0 + T_s\eta \quad (3)$$

From (1) to (3), and identifying  $T_0$  with  $T_H$ , the measured emissivity of the human skin can be expressed as:

$$\eta = \frac{(V_s - V_H)(T_H - T_C)}{(T_s - T_H)(V_H - V_C)} \quad (4)$$

A digital voltmeter with 0.1 mV resolutions was used to measure the output voltage for the target area of the skin,  $V_s$ , and an infrared thermometer with absolute accuracy 0.01 °C was used to measure the skin surface temperature,  $T_s$ .

### III. RESULTS AND DISCUSSION

The objective of these experiments is to study how the emissivity of the human skin varies with age and gender. The measurements were performed on 60 healthy participants; 35 males and 25 females. Participants were divided into four age groups: 20-30, 30-40, 40-50, and 50-60. There were 5-10 subjects in each group.

#### A. Radiometric Calibration Results

The calibration Y-factor, defined as the ratio of receiver output when measuring the hot black body source, to that measuring the cold source was 1.408. This gives a receiver noise temperature of 453.7 K.

#### B. Male Emissivity Measurements

The measurements in Figs. 2, and 3 represent the mean emissivities for the male groups, with error bars representing the standard error in the mean (SEM). The measurements show significant and consistent variations in emissivity at different locations of the hand for different age groups. Emissivity for dorsal surface and outer wrist positions are higher than volar side and inner wrist positions. Skin on volar side and inner wrist is

thin and smooth [7], and as a result, the blood vessels are closer to the skin surface. This increases the reflectivity of the skin and makes the emissivity lower as a result of conservation of energy [6, 8]. However, the skin on the dorsal surface of the forearm and outer wrist is thick and dense [7] and this makes the skin reflectivity lower and as a result skin emissivity increases. The results also suggest two age-related trends: 1) a possible slight decrease in the emissivity in the age groups between 20-40 years. This decrease is consistent with the fact that male skin thickness decreases gradually with the age [3, 8]. 2) An increase in the emissivity in the age groups between 40-60 years. This increase is consistent with the fact that water content and skin hydration level decrease with the age [4, 5] and this makes aged skin drier compared with young skin [3]. The statistical analysis of the male samples shows that the sample mean ( $\mu$ ) of the differences in the emissivities between the dorsal and volar side of the forearm is 0.0675 with a sample standard deviation ( $\sigma$ ) of 0.0319, whereas the sample mean of the differences in the emissivities between the inner and outer wrist is 0.0535 with a sample standard deviation of 0.0336. These results indicating a very consistent difference between the emissivity of different location on the body. Error propagation through (4) indicates the uncertainty on the measured emissivity is  $\pm 0.002$ .

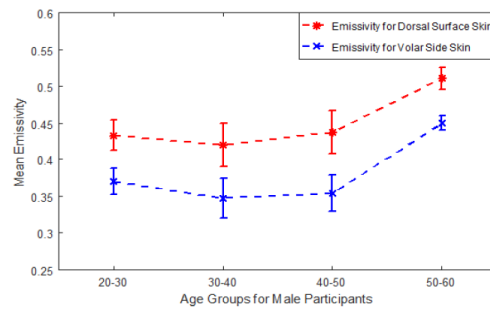


Fig. 2. Dorsal surface and volar side emissivity measurements for 35 male, with standard error in the mean (SEM  $\leq 0.029$ ) for each age group.

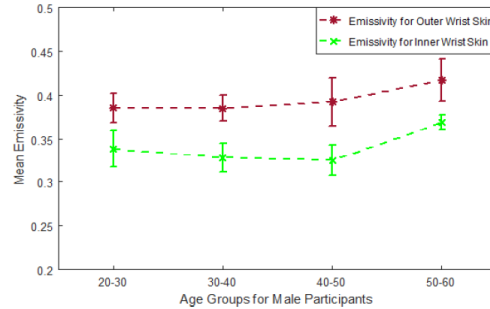


Fig. 3. Outer and inner wrist emissivity for 35 male, with standard error in the mean (SEM  $\leq 0.027$ ) for each age group.

### C. Females Emissivity Measurements

The measurements in Figs. 4 and 5 show that emissivity of the dorsal surface skin is higher than that of the volar side and emissivity of the outer wrist is higher than that of the inner wrist for all female groups. The measurements also suggest two age-related trends: 1) relatively unchanged emissivity in the age groups 20-50 years with slight increase in dorsal surface skin emissivity. 2) Significant decreases in the emissivity in the age group 50-60 years. These trends are consistent with the fact that females skin maintain the same thickness up to the age of 50 and then beyond this the skin thickness gets significantly thinner, probably due to decreased oestrogen levels after menopause [3]. The statistical analysis of the female sample shows that, the sample mean of the differences in the emissivities between the dorsal surface and the volar side locations is 0.0678 with a sample standard deviation of 0.0439, whereas the sample mean of the differences in the emissivities between the inner and outer wrist location is 0.0645 with a standard deviation of 0.0387.

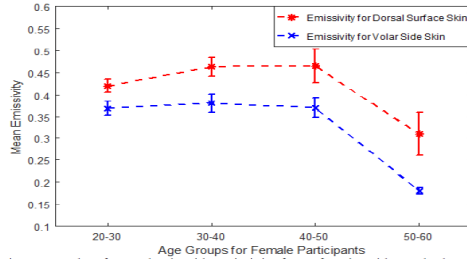


Fig. 4. Dorsal surface and volar side emissivity for 25 female, with standard error in the mean ( $SEM \leq 0.038$ ) for each age group.

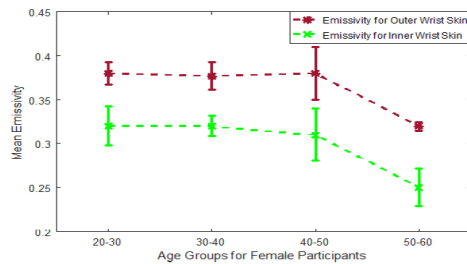


Fig. 5. Outer and inner wrist emissivity for 25 female, with standard error in the mean ( $SEM \leq 0.04$ ) for each age group.

### D. Comparison Between Males and Females Emissivity

The measurements in Fig. 6 show that, when averaged over all age groups, the emissivity of males is higher than that of females in all positions with a difference in the standard error in the mean of approximately 0.02. This result is consistent with the fact that the skin of men is thicker than that of women [3, 8]. Furthermore, the measurements show that for both genders, the emissivity is higher in the locations where the skin is thick, and it is lower in the locations where the skin is thin. The emissivity measurements in this paper are consistent with [6].

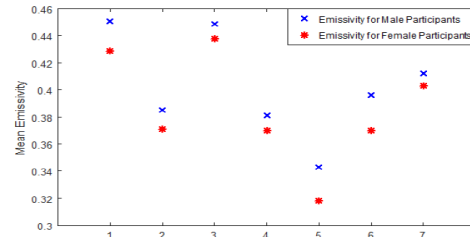


Fig. 6. Mean emissivity for all participants at different locations on the hand: 1) palm of hand 2) back of hand 3) dorsal surface of the forearm 4) volar side of the forearm 5) inner wrist 6) outer wrist and 7) elbow.

### E. Exploitation in Medical Applications

As human skin emissivity shows strong correlation with skin thickness and water contents, this indicates that radiometry could be used as a non-contact technique to detect and monitor skin conditions such as psoriasis, eczema, malignancy and burn wounds.

Although measurements presented here are made using a single channel radiometer, an exploitation route might consider the development arrays of antennas to make measurements on larger skin areas or perhaps the whole of the human body in tens of seconds.

### IV. CONCLUSION

The measurements show variations in emissivity between skin location, gender and age group. The results indicate that the emissivity of human skin in the millimeter wave band is rich in information and this could potentially be exploited for the diagnosis of a range of medical conditions.

### REFERENCES

- [1] F. T. Ulaby, R. K. Moore, A. K. Fung, Microwave remote sensing: active and passive, volume I: microwave remote sensing fundamentals and radiometry, United Kingdom: Artech House, 1981, pp.1282-1450.
- [2] F. Grum, R. J. Becherer, Optical radiation measurements. Volume 1 – radiometry, New York: Academic Press, 1979, pp. 40-100.
- [3] S. Diridollou, V. Vabre, M. Berson, L. Vaillant, D. Black, J. M. Lagarde, J. M. Grégoire, Y. Gall, F. Patat, "Skin ageing: changes of physical properties of human skin in vivo," International Journal of Cosmetics Science., vol. 23, pp. 353-362, 2001.
- [4] A. Firooz, B. Sadr, S. Babakoochi, M. S. Yazdy, F. Fanian, A. K. Timsar, M. N. Kashani, M. M. Naghizadeh, Y. Dowlati, "Variation of biophysical parameters of the skin with age, gender, and body region," The Scientific World Journal., vol. 2012, pp. 1-5, 2012.
- [5] R. O. Potts, E. M. Buras, D. A. Chrisman, "Changes with age in the moisture content of human skin," J Invest Dermatol., vol. 82, pp. 97-100, 1984.
- [6] S. W. Hamer, S. Shylo, M. Shah, N. J. Bowring, A.Y.Owda, "On the feasibility of assessing burn wound healing without removal of dressings using radiometric millimetre-wave sensing," Progress In Electromagnetics Research., vol. 45, pp. 173-183, 2016.
- [7] H. Gray, Anatomy of the human body. Philadelphia: Lea & Febiger, 1981, pp. 100-450.
- [8] P. F. Millington, R. Wilkinson. Skin (biological structure and function). United Kingdom: Cambridge University Press, 2009, pp. 48-80.

# PROCEEDINGS OF SPIE

[SPIDigitalLibrary.org/conference-proceedings-of-spie](https://spiedigitallibrary.org/conference-proceedings-of-spie)

## Signatures of human skin in the millimetre wave band (80-100) GHz

Amani Y. Owda, Nacer-Ddine Rezgui, Neil A. Salmon

**SPIE.**

Downloaded From: <https://www.spiedigitallibrary.org/conference-proceedings-of-spie> on 10/12/2017 Terms of Use: <https://spiedigitallibrary.spie.org/ss/TermsOfUse.aspx>

## Signatures of human skin in the millimetre wave band (80-100) GHz

Amani Y. Owda\*, Nacer-Ddine Rezgui, Neil A. Salmon  
School of Engineering, Manchester Metropolitan University, M1 5GD, United Kingdom

### ABSTRACT

With the performance of millimeter wave security screening imagers improving (reduced speckle, greater sensitivity, and better spatial resolution) attention is turning to identification of anomalies which appear on the human body. Key to this identification is the understanding of how the emissive and reflective properties vary over the human body and between different categories of people, defined by age and gender for example. As the interaction of millimetre waves with the human body is only a fraction of a millimetre into the skin, precise measurement of the emission and reflection of this radiation will allow comparisons with the norm for that region of the body and person category. On an automated basis at security screening portals, this will increase detection probabilities and reduce false alarm rates, ensuring high throughputs at entrances to future airport departure lounges and transport networks.

A technique to measure the human skin emissivity in vivo over the frequency band 80 GHz to 100 GHz is described. The emissivities of the skin of a sample of 60 healthy participants (36 males and 24 females) measured using a 90 GHz calibrated radiometer was found to range from  $0.17 \pm 0.002$  to  $0.68 \pm 0.002$ . The radiometric measurements were made at four locations on the arm, namely: palm of hand, back of hand, dorsal surface of the forearm, and volar side of the forearm, where the water content and the skin thickness are known to be different. These measurements show significant variation in emissivity from person to person and, more importantly, significant variation at different locations on the arms of individuals. Males were found to have an emissivity 0.03 higher than those of females. The emissivity of the back of the hand, where the skin is thinner and the blood vessels are closer to the skin surface, was found to be lower by 0.0681 than the emissivity of the palm of the hand, where the skin is thicker. The measurements also show that the emissivity of the volar side location where the blood vessels are closer to the skin surface is lower by 0.0677 than the emissivity of the dorsal surface location. The measured differences agree with those differences estimated by a half space electromagnetic model of the interaction and can be interpreted in terms of the differing water contents and skin thickness of those regions of the body.

**Keywords:** security screening, emissivity, millimetre waves, permittivity, skin thickness, water content.

### 1. INTRODUCTION

As passive millimetre wave imaging is free from artefacts such as speckle and sensitivity to the alignment, it provides a means to screen people for concealed threats through the clothing down to the skin, for all regions of the human body [1]. In this paper, attention is turning to identification of anomalies, which appear on the human body and can be identified by measuring the signature of the human skin at the millimeter wave frequency band. Measurement and validation of the emissivity of human skin at MMW frequency bands is an essential requirement, to help assess the feasibility of increasing the detection probabilities and reducing the false alarm rate when screening at entrances to airport departures areas. The main advantages of the passive millimeter wave imaging system are: 1) human skin signature can be measured without exposing the human body to any type of radiation, 2) radiometric sensitivity is sufficient to sense different surfaces attached to the human skin such as liquid and metallic objects, and 3) the measurements and processing of data can be made in tens of seconds by using a non-contact sensor with high precision in which this will minimise the systematic uncertainty.

\*amaniabubaha@gmail.com; Manchester Metropolitan University; mobile number +44 7402 939 756.

Millimetre Wave and Terahertz Sensors and Technology X, edited by Neil A. Salmon,  
Sherif Sayed Ahmed, Proc. of SPIE Vol. 10439, 1043904 · © 2017 SPIE  
CCC code: 0277-786X/17/\$18 · doi: 10.1117/12.2292046

Proc. of SPIE Vol. 10439 1043904-1

Downloaded From: <https://www.spiedigitallibrary.org/conference-proceedings-of-spie> on 10/12/2017 Terms of Use: <https://spiedigitallibrary.org/ss/TermsOfUse.aspx>

## 2. THE SYSTEM

### 2.1 Experimental setup

A radiometer sensitive over the frequency band 80-100 GHz was used for measuring the human skin emissivity in vivo. The experimental setup for measurement comprises; a horn antenna connected to a radiometer that consists of a two-stage low-noise amplifier (LNA), zero bias detector and buffer amplifier. The radiometer is connected through coaxial cable to a digital voltmeter and through wires to a DC power supply, as illustrated in Figure 1. The horn antenna has a rectangular aperture ( $30 \times 25 \text{ mm}^2$ ) and a nominal gain of 20 dBi over the frequency band (80-100) GHz.

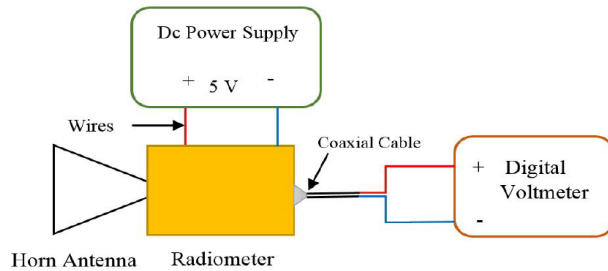


Figure 1. Experimental setup for measuring the human skin emissivity over the frequency band from 80 GHz to 100 GHz

### 2.2 Radiometric calibration and testing

The radiometer was calibrated using liquid nitrogen and ambient temperature sources, as illustrated in Figure 2. The horn antenna of the radiometer may be placed at distance ( $\sim 5.0 \text{ cm}$ ) from two different radiation sources located in the same plane: "Hot" black body (ambient temperature source calibration). A piece of carbon loaded foam absorber with  $T_H = T_{\text{ambient}} = 293 \text{ K}$ , and "Cold" black body (liquid nitrogen source calibration). A piece of carbon loaded foam absorber was dipped in liquid nitrogen at  $T_C = 77 \text{ K}$ . The cold load calibration measurements were taken within 5 seconds or less before the liquid nitrogen evaporates. Foam absorbers had a rectangular shape and emissivity values greater than 0.99 over the frequency band 80-100 GHz, thus they behave as good approximations to a black body emitter. The difference in temperature between the hot and the cold load is  $\sim 216 \text{ K}$ . This large difference is important to provide an accurate calibration. The calibration Y-factor, defined as the ratio of receiver output when measuring the hot black body source, to that measuring the cold source was 1.408. This gives a receiver noise temperature of 453.7 K and noise figure of 2.55. These measurements were taken from ten separate experiments and at each experiment, the calibration measurements were repeated 5-10 times so the device was stable and the measurements were consistent.

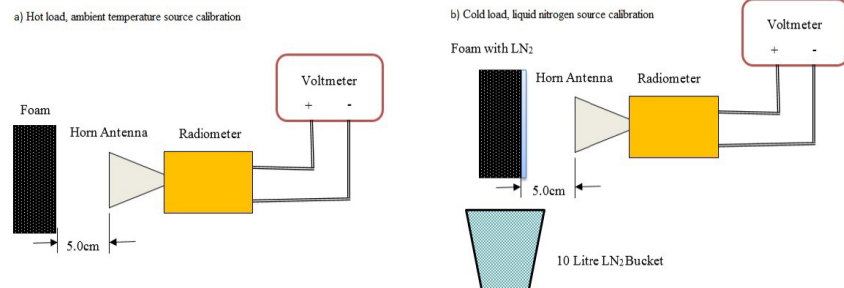


Figure 2. Radiometric calibration using ambient temperature source (hot load) and liquid nitrogen source (cold load)

The amount of self-emission reflected back from subjects was investigated by moving a metal plate in a distance 1.0 cm from the horn antenna beam. The mean level of self-emission reflected back from the metal plate (100% reflective surface) was measured to be in the range of 294-295 K with standard deviation  $\pm 1.0$  K. The results presented show that the radiation temperature from the metal plate is approximately the same as the ambient temperature, and therefore no parasitic signals were identified when emission from the receiver was reflected back into the system by a normal incidence metal reflector placed directly in front of the horn antenna.

Millimeter-Wave emission emitted from a fluorescent light located 5.0 cm from the horn antenna was found to increase the radiation temperature measured by the radiometer by an amount 62-74 K; a mean value of 67.5 K with a standard deviation of  $\pm 4.0$  K. When the fluorescent light was located directly in the beam of the horn antenna, the radiation temperature was found to increase by an amount 80-100 K; a mean value of 84.3 K with a standard deviation of  $\pm 8.0$  K. This effect was cancelled during the experimental work by turning off all the fluorescent light in the lab [2].

### 3. METHODOLOGY OF MEASURING HUMAN SKIN EMISSIVITY

The complete system except for an opening for the subject to be measured (skin) was enclosed in an anechoic region made by surrounding the majority of the radiometer and antenna with carbon loaded absorbing foam, as illustrated in Figure 3. This prevented radiation from external sources, be it from the outdoors or other people in the environment, getting into the system to corrupt signals.

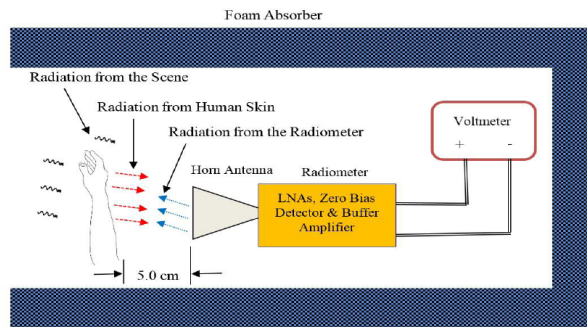


Figure 3. Experimental description for in vivo radiometric emissivity measurements performed on human hand

The target area of the skin was located 5.0 cm from the horn antenna of the radiometer, and the measurements were done indoors in an anechoic environment, and therefore the system response is assumed to be linear. Under these circumstances, the output voltage when measuring the liquid nitrogen and ambient temperature calibration sources can be expressed in terms of the receiver noise temperature  $T_N$  in K, and the receiver responsivity,  $\alpha$  in V/K [3]:

$$V_C = \alpha(T_C + T_N) \quad (1)$$

$$V_H = \alpha(T_H + T_N) \quad (2)$$

From Equations (1) and (2) the receiver responsivity,  $\alpha$ , and the emissivity of the skin,  $\eta$ , are [3]:

$$\alpha = \frac{(V_H - V_C)}{(T_H - T_C)} \quad (3)$$

$$\eta = \frac{(V_S - V_H)(T_H - T_C)}{(V_H - V_C)(T_S - T_H)} \quad (4)$$

An infrared thermometer with an absolute measurement uncertainty of  $\pm 1.5\text{ }^\circ\text{C}$  was used to measure the thermodynamic temperatures of the skin,  $T_s$  directly before and after the measurements. A digital voltmeter with a precision of 0.1 mV was used to measure the output voltage for the target area of the skin;  $V_s$ . Error propagation through Equation (4) indicates the uncertainty on the measured emissivity is  $\pm 0.002$ .

#### 4. RESULTS

The objective of these experiments is to study how the signature of the human skin varies between individuals, gender and locations over the frequency band 80-100 GHz. Emissivity measurements were performed on 60 healthy participants; 36 males and 24 females having a variety of ethnicities, ages, and body mass index. The measurements were made at four locations on the body and these were: 1) palm of hand, 2) back of hand, 3) dorsal surface of the forearm, and 4) volar side of the forearm. These locations were chosen due to variation in skin thickness and water content.

##### 4.1 Male emissivity measurements

Measurements of human skin emissivity of a sample of 36 male participants are presented in Figure 4. The measurements show variation in emissivity between individuals and locations on the arm. These variations are due to the skin thickness and blood vessels (water content) that varies from location to location across the human body and between individuals [4]. The emissivity from male sample was found to range from  $0.18 \pm 0.002$  to  $0.68 \pm 0.002$ , with mean ( $\mu$ ) and standard deviation ( $\sigma$ ) for all measurements location being 0.416 and 0.091 respectively. In general, lower values of emissivity are results of measuring particularly thin skin on the volar side and back of hand [5], whereas higher values of emissivity are results of measuring thick skin on the dorsal surface and palm of hand [6].

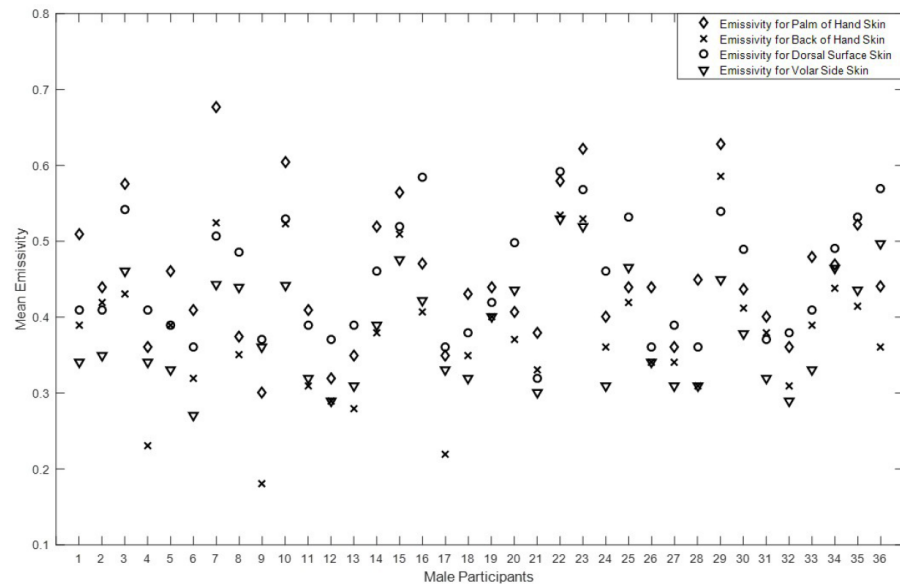


Figure 4. Radiometric emissivity measurements for 36 male participants performed over the frequency band 80-100 GHz

The measurements indicate the differences in emissivities between thicker regions of skin (dorsal forearm and palm of hand) and thinner regions of skin (volar forearm and back of hand) are in the range from 0.068 to 0.074 with a sample standard deviation in the range of 0.032 to 0.041 respectively. These results show a clear signature for the human skin emissivity at the millimeter wave frequency band (80-100) GHz. The presented signature might be useful for identifying anomalies on the human body by comparing the measured emissivity of the subject area of the skin with the standard values of the population (mean emissivity  $\pm$  standard deviation), so any value much higher or much lower than the standard values might identify anomalies.

#### 4.2 Female emissivity measurements

Measurements of human skin emissivity in a sample of 24 female participants are presented in Figure 5. Emissivity for the dorsal surface and palm of hand skin are higher than volar side and back of hand skin. Variation in emissivity between individuals and locations on the hand are consistent with the variations in male participants. However, female emissivity was found to be lower than that of male in the range from  $0.17 \pm 0.002$  to  $0.587 \pm 0.002$ , with mean and standard deviation for all measurement locations being 0.383 and 0.0839 respectively. The measurements also indicate the differences in emissivity values between thicker regions of skin and thinner regions of skin are in the range from 0.0597 to 0.0679 with a sample standard deviation in the range of 0.0358 to 0.0439.

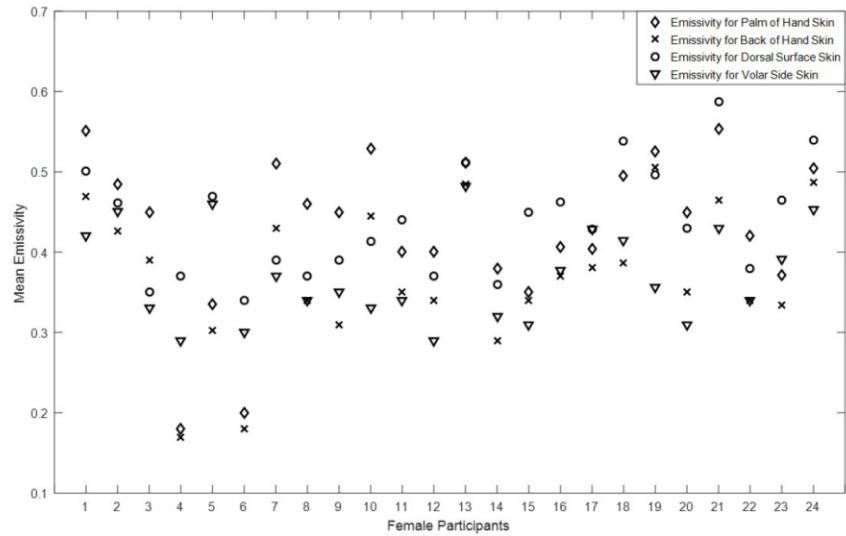


Figure 5. Emissivity measurements for 24 female participants performed over the frequency band 80-100 GHz

### 4.3 Comparison between male and female emissivity

Experimental measurements of human skin emissivity of 36 male and 24 female healthy participants are presented in Table 1. The measurements show that emissivities of male participants are higher than that of female participants at all locations on the arm. This finding is consistent with the fact that male skin is thicker than that of female skin [7]. Estimating the sample mean emissivity values for the male and female participants separately indicates the difference between male and female emissivity is  $\sim 0.03$ . This difference is  $\sim 15$  times the systematic measurement uncertainty ( $\pm 0.002$ ) indicating a significant difference in the emissivity between male and female participants. Furthermore, the measurements show that for both genders, the emissivity is higher in the locations where the skin is thick: dorsal surface of the forearm and palm of hand [6], and it is lower in the locations where the skin is thin: volar side of the forearm and back of hand skin [5]. These measurements show strong correlation between human skin emissivity and skin thickness.

Table 1. Comparison in emissivity, between male and female participants at four locations on the arm.

Location	Mean Emissivity Male	Standard Deviation (M)	Mean Emissivity Female	Standard Deviation (F)
Palm of Hand	0.4511	0.0997	0.4293	0.0924
Back of Hand	0.3853	0.0844	0.3712	0.0847
Dorsal Surface	0.4486	0.0778	0.4381	0.0646
Volar Side	0.3811	0.0725	0.3702	0.0566
All Locations	0.416	0.091	0.383	0.0839

## 5. DISCUSSION

Human skin signature over the frequency band 80-100 GHz indicate that there is a scatter in emissivity measurements over a range 0.17 to 0.68, and this is much greater than the experimental measurement uncertainty of  $\pm 0.002$ . Human skin emissivity measurements in Figures 4 and 5 show variations in emissivity from person to person, and at different locations on the human body. Estimating the sample mean emissivity values for the 36 males and 24 females separately for all measurements locations indicates the difference between male and female emissivity is  $\sim 0.03$ . This finding is consistent with the skin of males being thicker than that of females [7]. Experimental measurements of the differences in the emissivity values between the palm of hand and back of hand skin, and between the dorsal and volar regions of the forearm of all 60 participants indicate that the difference in emissivity can be up to 0.074. This large difference is likely to be due to the much thicker skin on the palm of hand and dorsal area of the forearm. The presence of the blood vessels on the volar forearm and the back of hand locations make the skin more reflective, and as a result human skin emissivity decreases and this results in a significant difference in the emissivity between thinner and thicker skin regions on the body.

Skin thickness and water content are strongly dominating the level of thermal emission emitted from the human body at the millimeter-wave band, and therefore it is recommended for security screening purposes that further measurements are made on larger and more varied groups of individuals, to study how the emissivity varies overall the human body and between individuals. When this is done, expected emissivity values can be identified at each location on the human body and these values can be compared with the measured emissivity from a template ensemble of recognised responses on an automated basis at security screening portals. Any deviation from the norm might identify anomalies. This will increase detection probabilities and reduce false alarm rates in the security screening of people.

Emissivity measurements in this paper are in agreement with the emissivity measurements presented in [4]. These measurements indicate that forearm skin emissivity varies in the range of 0.17 to 0.5. This range is in agreement with the range of the measured emissivity in this paper (0.17 to 0.68). Emissivity measurements in this paper are also in agreement with the simulated emissivities of the half-space model [8].

## 6. CONCLUSIONS

A radiometer effective over the frequency band 80-100 GHz has been investigated and characterised for measuring the human skin signature of a sample of 60 participants. The system was calibrated using liquid nitrogen and ambient temperature sources. These measurements were used to characterise self-emission and millimeter wave radiation from metal plate and fluorescent lights. The mean level of self-emission reflected back from the metal plate was typically  $\pm 1.0$  K above the background. Millimeter-Wave emission emitted from fluorescent light was found to increase the radiation temperature of the radiometer in the range of 62-74 K with standard deviation of  $\pm 4.0$  K.

Radiometric measurements made on a sample of 60 participants show that the emissivity of human skin varies from 0.17 to 0.68 over the 80 GHz to 100 GHz band. Measurements show that the emissivity of the skin varies with the water content and skin thickness. The measurements show that the emissivity of males is higher than that of females by  $-0.03$ . This supports the knowledge that on average the skin of males is thicker than that of females [7]. Measurements also show the emissivity of thick layers of skin in the human body, such as the palm of the hand and the dorsal forearm was higher than those of the back of the hand and the volar forearm by about 0.0597 to 0.068 for both genders.

Research continues in this area to understand the signature of the human skin at the millimeter wave frequency band to increase detection probabilities and reduce false alarm rates, so ensuring high throughputs at entrances to future airport departure lounges.

## 7. FUTURE WORK

It is recommended that further measurements be made on larger and more varied groups of individuals overall body regions to provide statistics about the emissivity of the human skin. This might be done at a range of frequencies over the millimeter wave frequency bands, the lower frequencies offering greater penetration into under layers of clothing and down to the skin. Whereas, the higher frequencies offering higher resolution. This will lead to greater understanding of human skin signature at the MMW frequency bands and it might be useful for increasing the detection probabilities and reducing the false alarm rate at security screening portals.

## REFERENCES

- [1] Salmon, N.A. "Experimental results and simulations from aperture synthesis three-dimensional radiometric imaging", SPIE Millimeter Wave and Terahertz Sensors and Technology IX, SPIE proc. vol. 9993, doi: 10.1117/12.2231696, Edinburgh, September, (2016).
- [2] Salmon, N.A. "Characterisation and calibration of a large aperture (1.6 m) ka-band indoor passive millimeter wave security screening imager", SPIE Millimeter Wave and Terahertz Sensors and Technology V, SPIE proc. vol. 8544, doi: 10.1117/12.999278, Edinburgh, September, (2012).
- [3] Pozar D.M., [Microwave Engineering], John Wiley & Sons Publisher, New Jersey & Hoboken, 497-511 (2011).
- [4] Harmer, S.W., Shylo, S., Shah, M., Bowring, N.J. and Owda, A.Y., "On the feasibility of assessing burn wound healing without removal of dressings using radiometric millimeter-wave sensing." Progress In Electromagnetics Research. Papers 45,173-183 (2016).
- [5] Gray, H., [Anatomy of the Human Body], Lea & Febiger Publisher, United States & Philadelphia, 1320-1330 (1918).
- [6] Millington, P.F., Wilkinson, R., [Skin (Biological Structure and Function)], Cambridge University Press Publisher, United Kingdom & Cambridge, 48-80 (2009).
- [7] Diridollou, S., Vabre, V., Berson, M., Vaillant, L., Black, D., Lagarde, J.M., Grégoire, J.M., Gall, Y. and Patat, F., "Skin ageing: changes of physical properties of human skin in vivo," International Journal of Cosmetics Science. Papers 23, 353-362 (2001).
- [8] Owda, A.Y., Salmon, N.A., Harmer, S.W., Shylo, S., Bowring, N.J., Rezgui, N.D. and Shah, M., "Millimeter-Wave Emissivity as a Metric for the Non-Contact Diagnosis of Human Skin Conditions", Journal of Bioelectromagnetics, vol. 38, issue, 7, pp. 559-569 (2017).

## On the feasibility of monitoring the wound healing under dressing materials using non-contact active millimetre wave imaging system

AY Owda<sup>1</sup>, N Salmon<sup>1</sup>

<sup>1</sup> *Sensing and Imaging Group, School of Science and Engineering, Manchester Metropolitan University, Manchester*

**INTRODUCTION:** In England and Wales, around 3750 people are admitted to hospital annually with burn and scald injuries<sup>1</sup>. Current assessment and monitoring of wound healing is through visual inspection, necessitating the removal of dressing materials. The removal of dressing layers can cause medical problems, be uncomfortable or painful to the patient. Currently, there are no tools which could assess the state of the healing burn wound without removing the dressings. Because electromagnetic radiation at microwave and millimeter wave frequencies can propagate through typical dressing materials with little attenuation, these bands of the electromagnetic spectrum are promising for assessing bandaged wounds<sup>2</sup>. In this paper the concepts of Active Millimeter Wave Imaging (AMMWI) is developed for assessing the feasibility of active radiation to monitor the wound healing under dressing materials in non-contact with the human body.

**METHODS:** A standard Pyramid Ka-band horn antenna with 20dB gain was aligned in vertical polarisation. The antenna was connected with the vector network analyser (VNA) via high frequency cable. The VNA is used to illuminate the sample under test (SUT) and it is control via PC and Matlab program. The SUT was located between the horn antenna and the background. Large metal plate was used as a background and it was utilised for calibration purposes. The lab was covered with absorbent foam material to minimise the reflection from other objects in the lab. The VNA sends a pulse of electromagnetic radiations to the SUT. When the radiations hitting the SUT, the radiations will be reflected from the front and the back surface of the sample and also there will be reflected radiations from the background. The complex reflected signal in frequency domain is transformed into time domain signal using the Inverse Fast Fourier Transform (IFFT) and from the distance between the front and the back surface of the reflected radiations; the optical path length of the SUT is calculated as follows:

$$d = R_2 - R_1 = c(t_2 - t_1)/2 \quad (1)$$

Where,  $c$  is the speed of the light, and  $t$  is the round trip time for the front and the back surface of the reflected radiations.

**RESULTS:** Figure 1a shows three reflections peak associated with the hand cast sample that made of plaster of paris. The reflection peaks produce in the time domain resulting from reflections from the surfaces of the hand cast and discontinuities in dielectric properties. Using equation (1) the optical path length for the hand cast is ~8.55 cm. The difference between the actual (9.0 cm) and the measured optical path length is ~0.45 cm.

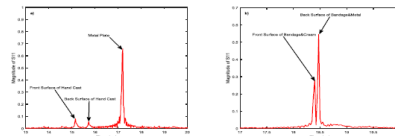


Fig. 1a : Image display the reflected signal from 9.0 cm width hand cast located in free space between the horn antenna and the metal plate. Fig. 1b Image display reflected signal from ~1.0 cm thick gauze burn bandage with Flamazine cream, the bandage was attached directly with the metal plate. In both cases 512 data points are used and the VNA operates over the frequency band (15-40) GHz with 6.0mm spatial resolution.

Figure 1b shows two reflection peaks associated with gauze burn bandage with Flamazine cream layer. The back surface of the bandage was attached directly with the metal plate, and there was no separation between the cream and the front surface of the bandage, and therefore the reflection from the cream layer and the front surface of the bandage is combined in peak1, and the reflection from the back surface of the bandage and the metal plate is combined in peak 2. The measured reflection from the front surface of the bandage in dry state was ~10%, whereas when a layer of cream was attached to the bandage the reflection increases to ~30%, as illustrated in figure 2b. The measured optical path length of the bandage is 0.95 cm. The difference between the actual and the measured optical path length is ~0.05 cm, the uncertainty in the measurements is likely to be from the sensitivity to the alignments and it is estimated to be ~0.6 cm.

**DISCUSSION & CONCLUSIONS:** The results obtained from different samples and various types of cream that used in the treatments of the burn wound show that AMMWI can provide precise information about the structure of dressing materials and more importantly it can sense different surfaces attached to the dressing materials. As non-contact screening is often desirable in medical applications, AMMWI might be an efficient tool for monitoring the wound healing under dressing materials.

**REFERENCES:** S.W. Harmer, S. Shylo, M. Shah, et al (2016) *on the feasibility of assessing burn wound healing without removal of dressings using radiometric millimetre-wave sensing*. PIER 45:173-183. <sup>2</sup>H. Essen, J. M. Essen, D. Nuessler, et al (2010) *Monitoring of wound healing by millimetre wave imaging*. 35th International Conference on Infrared, Millimeter, and Terahertz Waves.

## **C.8 Short Abstract 1:**

### **Assessment of Human Skin Emissivity using Passive Millimetre-Wave Sensing**

#### **(Oral Presentation)**

**Sensing & Imaging Group, School of Engineering, Manchester Metropolitan University,  
John Dalton Building, Chester Street, M1 5GD, United Kingdom.**

**Authors:** Amani Yousef Owda (Amani.Owda@stu.mmu.ac.uk), and Dr. Neil Salmon (n.salmon@mmu.ac.uk)

**Keywords:** Millimetre-Wave, Skin thickness, Water Content, Emissivity, Reflectivity.

#### **Abstract**

Over the past few decades technology in the millimetre wave band has shown a steady and consistent development and increased usage, with a wide variety of devices and system architectures (imaging, non-imaging, radiometers and radars) sensors becoming available. As an imaging sensor, these systems can deliver spatial resolutions of less than the wavelength, which in the millimetre wave band is down to about 1.0 mm. This property enables highly localised measurements to be made of skin which cannot be seen in the visible region of the spectrum. A convenient metric to describe the condition of human skin is the emissivity. Many studies reveal strong correlation between skin dielectric properties, skin thickness, water content and hydration level with age, gender and body site. This study is aiming to assess variation in emissivity between different body sites, age groups and genders over the frequency band (80-100) GHz to obtain a deeper understanding of the signatures of human skin in the millimetre wave frequency band.

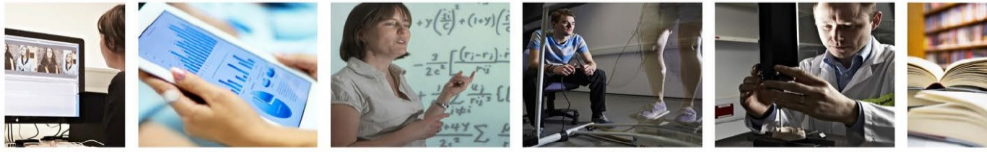
In this paper a technique to measure the human skin emissivity in vivo is described over the frequency band 80-100 GHz. Emissivity measurements were performed on 60 participants, 35 males and 25 females ranging in age 20-60 years. Results show that emissivity of males higher than that of females. The study also confirm variation trend of emissivity with age for both genders. The results suggest that variation in emissivity over the age is due to variation on skin thickness and water content.

## C.9 Short Abstract 2:

The University for  
**World-Class Professionals**



Manchester  
Metropolitan  
University



**9th Manchester Metropolitan University  
Postgraduate Research Conference 2017**



**Changing Lives**  
22nd February 2017

Student Union  
Manchester Metropolitan University

### **Active Millimetre-Wave Imaging for Monitoring the Wound Healing Progress**

Amani Owda, Neil Salmon

Visual inspection is the current protocol for monitoring the wound healing progress. This protocol gives an excellent indicator about the state of the wound and the healing progress, and more importantly, it can detect signs of infections such as exudates, redness, swelling, heat, functionality of the infected part and pus draining (Cunha, 2016). However, visual inspection requires the removal of dressing layers, this practice consumes time, money and it could be unsafe in serious burn and injury situations, and it can cause medical problems, be uncomfortable or painful to the patient and increase the chance of infection (Harmer et al., 2016). Active Millimetre-wave scanner is another approach that has been tried by (Essen et al., 2010). The scanner is designed to probe under plaster and gypsum cast and it is capable to monitor the healing of the scars and sutured wound under cast at 94 GHz. The results obtained from the scanner are strongly supported that millimetre-wave (MMW) can be used for monitoring the wound healing progress. Currently, there are no tools, which could assess the state of the healing burn wound without removing the dressings. A technique that could penetrate dressings and identify the healing status of wounds would be extremely beneficial to both patients and healthcare professionals.

This research is aiming to assess the feasibility of the active millimetre-wave imaging system to monitor the wound healing progress. Two types of measurements are performed on dressing materials; optical path length and surface sensing. The results obtained show that active imaging system can penetrate dressing materials and it can provide information about the optical path length of the sample. Furthermore, the experimental work shows that active millimetre-wave imaging system is capable to sense different surfaces attached to the bandage such as water and cream layer.

## C.10 Short Abstract 3:

### Millimetre-Wave Radiometer in Medical Applications

Sensing & Imaging Group, School of Engineering, Manchester Metropolitan University,  
John Dalton Building, Chester Street, M1 5GD, United Kingdom.

**Authors:** Amani Yousef Owda, Dr. Stuart William Harmer and Prof. Nicholas John Bowring

**Emails:** amani.owda@stu.mmu.ac.uk, S.Harmer@mmu.ac.uk, N.Bowring@mmu.ac.uk

**Keywords:** Millimetre-Wave, Emissivity, Skin model.

#### Abstract

Human skin covers around 95% of the human body and it plays an important role in temperature and water level regulation. However, human skin is sensitive to external and internal variations [1] and it can be damaged or broken by mechanical, electrical and thermal traumas. The current treatments of assessing and monitoring wound healing is through visual inspection, necessitating the removal of dressing materials used to assist in the wound healing process. The removal of dressing layers can have undesirable effects, such as increasing the probability of infection [2].

Open-ended coaxial probes have been used for measuring the complex dielectric permittivity of healthy skin and skin with second-degree burns [3]. The relative complex permittivity is easily measured using a suitable coaxial probe. This probe must be in contact with the sample under measurement. This requirement prevents use in scenarios where contact is not desirable or not possible. Electromagnetic radiation at Microwave and Millimetre-Wave frequencies can propagate through typical dressing materials with little attenuation and is non-ionising [4]; these bands of the electromagnetic spectrum are promising for assessing wounds through dressing materials.

As non-contact screening is often desirable in medical applications and since coaxial probes are unable to provide measurements over large areas without being repeatedly placed in contact with the skin, a radiometric approach is a more appropriate solution. Therefore, two-layer skin model is implemented in this work for predicting the emissivity of healthy skin and damage skin, the simulation results show that, emissivity of healthy skin is 57% and emissivity of second degree burn skin is 56%. There is a more significant difference, 5% to 10% in the emissivity between healthy skin and skin with malignant lesions. These differences in emissivity are due to different water that affected strongly the human skin emissivity. The experimental work in the lab shows that, dressing materials reduce the reflectivity of the skin and as a result, human skin emissivity is increased. Based on the presented results the authors conclude passive Microwave/Millimetre-Wave (MMW) sensing may be used for non-contact diagnosis of skin disease and for monitoring the wound healing under bandages.

#### References:

- [1] Kharkovsky, S., Ghasr, M.T., Abou-Khousa, M.A. and Zoughi, R., 2009, May. Near-field microwave and mm-wave noninvasive diagnosis of human skin. In *Medical Measurements and Applications, 2009. MeMeA 2009. IEEE International Workshop*. pp. 5-7.
- [2] Harmer, S.W., Shylo, S., Shah, M., Bowring, N. J., and Owda, A. Y., 2016. "On the feasibility of assessing burn wound healing without removal of dressings using radiometric millimetre-wave sensing." *Progress In Electromagnetics Research M*, Vol. 45, pp.173-183.
- [3] Boric-Lubecke, O., Nikawa, Y., Snyder, W., Lin, J. and Mizuno, K., 1999. Novel microwave and millimeter-wave biomedical applications. In *Telecommunications in Modern Satellite, Cable and Broadcasting Services, 1999. 4th International Conference on*, Vol. 1, pp.186-193.
- [4] Essen, H., Essen, J.M., Nuessler, D., Hommes, A., Krebs, C., Fatihi, N. and Buzug, T., 2010. Monitoring of wound healing by millimetre wave imaging. In *35th International Conference on Infrared, Millimeter, and Terahertz Waves*.

## C.11 Best Student Paper Award:

---

**SPIE.** SECURITY+  
DEFENCE

BEST STUDENT PAPER  
WINNERS

---

**AMANI YOUSEF  
OWDA**

Manchester Metropolitan Univ. (United Kingdom)



---

For Paper title:

**Signatures of human skin in the millimetre wave band  
(80-100) GHz** (10439-15)

Presented at:

Millimetre Wave and Terahertz Sensors and Technology

Presented by:

**Ric Schleijpen**, TNO Defence, Security and Safety, Netherlands

**Karin Stein**, Fraunhofer-Institut für Optronik, Systemtechnik und  
Bildauswertung, Germany

2017 Symposium Chairs

C.12 Writing in Met Scientist Magazine:

31|50

Manchester Metropolitan University

Issue 7 October 2016

Beneficiation of Contaminated Land for Metal Recovery



Medical applications of microwave and millimetre-wave imaging



Congestion in a big data world



Origami Chips



# Met Scientist

# Medical applications of microwave and millimetre-wave imaging



Amani Owda  
Amani.Owda@stu.mmu.ac.uk

Beyond the blue sky, I have a dream to contribute to the future. I have had dreams since my childhood to become a builder, architect, initiator, accomplisher, creator, designer, inventor, writer and an engineer; finally I will become a scientist! In my current research, I am very proud to work with Dr Neil Salmon and Professor Nicholas Bowring in the area of sensing and imaging. Our research is investigating the feasibility of using radiation in the microwave/millimetre-wave region for non-invasive monitoring of wound healing under dressing materials.

Skin covers 95% of the human body; this organ is sensitive to external and internal variations and it can be damaged or broken through many causes that may be electrical, mechanical, environmental, biological, chemical and thermal in nature. In England and Wales, around 3750 people are admitted to hospital annually with burn and scald injuries. The current treatment of assessing and monitoring the wound involves the removal of dressing materials. In medicine, there are many techniques used for examining the surface area of burn wounds such as: the rule of hands, the rule of fives, the Wallace rule of nine and the so-called chessboard diagram expansion method. The first three of these methods give an approximate estimation of the surface area of the burn wound, whilst the last method gives an accurate estimation of the surface area. Although these methods are efficient, they do not provide sufficiently detailed information about the wound healing progress. Currently, the only way to do this well is by visual inspection and this requires the removal of dressing layers, which can cause medical problems, be uncomfortable and painful to the patient and increase

the chance of infection. In some cases, it can also damage the layer of skin that covers the wound bed.

Our research develops the concepts of using active, Millimetre-Wave (MMW) devices to probe wound conditions under dressings. This scanner has the potential to monitor wound healing under a plaster and gypsum cast. However, low speed is one of the limitations of this scanner. Passive millimetre-wave reflectometry is a second possible in vivo technique for monitoring wound healing, measuring predominantly the water content in human skin, which can be used to determine hydration levels. This technique determines the reflection coefficient of human skin at different places and at different frequencies. Furthermore, recent studies of microwave and MMW reflectometry used an open-ended rectangular wave-guide probe to measure the dielectric properties of human skin at the different frequency bands. These measurements rely on close skin contact and this is another major limitation of current concepts. Currently there are no methods that successfully assess the burn wound healing process without removing dressing materials, which is why it is important to develop this MMW technique.



Through our research we have conducted a number of experiments to test the effectiveness of the passive and the active Millimetre-Wave imaging systems. For the passive system, emissivity measurements were performed on eight healthy volunteers and for the active system, two types of measurements were performed: sample thickness and surface sensing measurements. The results obtained from the passive and the active systems are promising for monitoring the wound healing under dressing materials. In the coming year further work such as scanning an image will be conducted.

## Appendix D: Matlab Codes

### %% Matlab Code 1 for the Metal Plate %%

```
%% Read the data from the excel file (Metal.xlsx), the file
consists of 512 frequency sweep (step size 49 MHz over the band
15GHz-40GHz) and 307 zero padding points inserted over the band
0-15GHz %%

data=xlsread('Metal.xlsx');

%% Identify how many times each data point is measured %%

Length=10;

%% Identify the frequency (column 1 in the excel file)

freq=data(:,1)*1e6;

%% Identify the time limits in Nano-Seconds%%
Time=0:0.025:20.45;

%% Identify the real part of the scattering parameter S11 %%

S11_Real_Metal=data(:,2:11);

%% Identify the imaginary part of the scattering parameter S11

S11_Imaginary_Metal=data(:,12:21);

%%Find the mean value of the real part of S11%%

mean_real_Metal=(data(:,2)+data(:,3)+data(:,4)+data(:,5)+data(:,6)
)+data(:,7)+data(:,8)+data(:,9)+data(:,10)+data(:,11))/Length;

%% Find the mean value of the imaginary part of S11%%

mean_imaginary_Metal=(data(:,12)+data(:,13)+data(:,14)+data(:,
15)+data(:,16)+data(:,17)+data(:,18)+data(:,19)+data(:,20)+
data(:,21))/Length;

%% Data for the foam Absorber %%%

data1=xlsread('FoamAbsorber.xlsx');

%% Identify the real part of the scattering parameter S11 %%

S11_Real_Absorber=data1(:,2:11);

%% Identify the imaginary part of the scattering parameter S11

S11_Imaginary_Absorber=data1(:,12:21);
```

```

%%Find the mean value of the real part of S11 for the foam %%
mean_real_Absorber=(data1(:,2)+data1(:,3)+data1(:,4)+data1(:,5)
)+data1(:,6)+data1(:,7)+data1(:,8)+data1(:,9)+data1(:,10)+data
1(:,11))/Length;

%% Find the mean value of the imaginary part of S11 for foam
mean_imaginary_Absorber=(data1(:,12)+data1(:,13)+data1(:,14)+
data1(:,15)+data1(:,16)+data1(:,17)+data1(:,18)+data1(:,19)+
data1(:,20)+data1(:,21))/Length;

%% S11 for the Metal plate without Internal Reflection (WIR)%%
S11_Real_WIR=mean_real_Metal-mean_real_Absorber;
S11_Imaginary_WIR=mean_imaginary_Metal-mean_imaginary_Absorber;
A=S11_Real_WIR+i*S11_Imaginary_WIR;
%%%%%%%%%%%%%%%%%%%%%%%%%%%%%%%%%%%%%%%%%%%%%%%%%%%%%%%%%%%%%%%%%%%%%%%%
%% Frequency domain plot %%

% D=abs(A)

% plot(freq,D)

% xlabel('Frequency, (GHz)')

% ylabel('Magnitude of S11')

%%%%%%%%%%%%%%%%%%%%%%%%%%%%%%%%%%%%%%%%%%%%%%%%%%%%%%%%%%%%%%%%%%%%%%%%

%% Time Domain Plot %%

%% Perform the Deconvolution %%

B=A./A;

W=exp(6*pi*freq*1.09e-9*i);

Z=B.*W;

%%Perform the Inverse Fast Fourier Transform to convert the
data from frequency domain into time domain%%

C=ifft(Z);

%% Plot the Magnitude of S11 versus the Time %%

plot (Time,abs(C),'r')

xlabel('Time (ns)')

ylabel('Magnitude of S11')

%%%%%%%%%%%%%%%%%%%%%%%%%%%%%%%%%%%%%%%%%%%%%%%%%%%%%%%%%%%%%%%%%%%%%%%% End %%%%%%%%%%%%%%%%%%%%%%%%%%%%%%%%%%%%%%%%%%%%%%%%%%%%%%%%%%%%%%%%%%%%%%%%%

```

**%% Matlab Code 2 for the Sample under Test %%**

```
%% Read the data for the sample, metal plate and foam absorber
%% Each file consists of 512 frequency sweep (step size 49 MHz
over the band 15 GHz-40 GHz)and 307 zero padding points inserted
over the band 0-15 GHz %%
```

```
data=xlsread('Sample.xlsx');
```

```
data1=xlsread('FoamAbsorber.xlsx');
```

```
data2=xlsread('Metal.xlsx');
```

```
%% Identify how many times each data point is measured
```

```
Length=10;
```

```
%% Identify the frequency (column 1 in the excel file)
```

```
f=data(:,1)*1e6;
```

```
%% Identify the time limits in Nano-Seconds%%
```

```
Time=0:0.025:20.45
```

```
%% Identify the real part of S11 for the sample
```

```
S11_Real_Sample=data(:,2:11);
```

```
%% Identify the imaginary part of S11 for the sample
```

```
S11_Imaginary_Sample=data(:,12:21);
```

```
%%Find the mean of the real part of S11 for the sample
```

```
mean_real_Sample=(data(:,2)+data(:,3)+data(:,4)+data(:,5)+data(:,
6)+data(:,7)+data(:,8)+data(:,9)+data(:,10)+data(:,11))/Length;
```

```
%%Find the mean of the imaginary part of S11%%
```

```
mean_imaginary_Sample=(data(:,12)+data(:,13)+data(:,14)+
data(:,15)+data(:,16)+data(:,17)+data(:,18)+data(:,19)+
data(:,20)+data(:,21))/Length;
```

```
%%%%%%%%%% Foam Absorber %%%%%%%%%%%
```

```
%% Identify the real part of S11 for the Foam
```

```
S11_Real_Foam_Absorber=data1(:,2:11);
```

```
%% Identify the imaginary part of S11 for the Foam
```

```
S11_Imaginary_Foam_Absorber=data1(:,12:21);
```

```
%%Find the mean of the real part of S11 for the Foam
```

```

mean_real_Foam_Absorber=(data1(:,2)+data1(:,3)+data1(:,4)+data
1(:,5)+data1(:,6)+data1(:,7)+data1(:,8)+data1(:,9)+data1(:,10)
+data1(:,11))/Length;

%%Find the mean of the imaginary part of S11 for the Foam

mean_imaginary_Foam_Absorber=(data1(:,12)+data1(:,13)+data1(:,
14)+data1(:,15)+data1(:,16)+data1(:,17)+data1(:,18)+data1(:,19
)+data1(:,20)+data1(:,21))/Length;

%%%%%%%%%%%%%%%%%%%%%%%%%%%%%%%%%%%%%%%%%%%%%%%%%%%%%%%%%%%%%%%%%%%%%%%% Metal Plate %%%%%%%%%
%% Identify the real part of S11 for the Metal Plate

S11_Real_Metal=data2(:,2:11);

%% Identify the imaginary part of S11 for the Metal Plate

S11_Imaginary_Metal=data2(:,12:21);

%%Find the mean of the real part of S11 for the Metal Plate

mean_real_Metal=(data2(:,2)+data2(:,3)+data2(:,4)+data2(:,5)+
data2(:,6)+data2(:,7)+data2(:,8)+data2(:,9)+data2(:,10)+data2(
(:,11))/Length;

%%Find the mean of the imaginary part of S11 for the Metal

mean_imaginary_Metal=(data2(:,12)+data2(:,13)+data2(:,14)+data
2(:,15)+data2(:,16)+data2(:,17)+data2(:,18)+data2(:,19)+data2(
(:,20)+data2(:,21))/Length;

%%% S11 for the sample without internal reflection (WIR)%%

S11_Sample_real_WIR=mean_real_Sample-mean_real_Foam_Absorber;

S11_Sample_imaginary_WIR=mean_imaginary_Sample-
mean_imaginary_Foam_Absorber;

A=S11_Sample_real_WIR+i*S11_Sample_imaginary_WIR;

%%% S11 for the Metal without internal reflection (WIR)%%

S11_Real_Metal_WIR=mean_real_Metal-mean_real_Foam_Absorber;

S11_Imaginary_Metal_WIR=mean_imaginary_Metal-
mean_imaginary_Foam_Absorber;

A1=S11_Real_Metal_WIR+i*S11_Imaginary_Metal_WIR;

%% Perform the Deconvolution %%

W=A./A1;

B=exp(-2*pi*f*5e-9*i);

```

```

Z=W.*B

%%Perform the Inverse Fast Fourier Transform to convert the
data from frequency domain into time domain%%

C=ifft(Z);

%% Plot the Magnitude of S11 versus the Time %%

plot (Time,abs(C),'r')

xlabel('Time (ns)')

ylabel('Magnitude of S11')

%%%%%%%%%%%%%%%%%%%%%%%%%%%%%%%%%%%%%%%%%%%%%%%%%%%%%%%%%%%%%%%%%%%%%%%% End %%%%%%%%%

```